

**A Thesis Submitted for the Degree of PhD at the University of Warwick**

**Permanent WRAP URL:**

<http://wrap.warwick.ac.uk/89711>

**Copyright and reuse:**

This thesis is made available online and is protected by original copyright.

Please scroll down to view the document itself.

Please refer to the repository record for this item for information to help you to cite it.

Our policy information is available from the repository home page.

For more information, please contact the WRAP Team at: [wrap@warwick.ac.uk](mailto:wrap@warwick.ac.uk)

**Zinc on the Move:  
Insights Towards Understanding Zinc  
Homeostasis in the Open Ocean  
Cyanobacterium *Synechococcus* sp.  
WH8102**

By

Amira Zahir Ksibe

A thesis submitted for the fulfilment of the degree of  
Doctor of Philosophy in Chemistry

THE UNIVERSITY OF  
WARWICK

Department of Chemistry and School of Life Sciences

February 2017

# Table of Contents

<b>Table of Contents</b> .....	<b>i</b>
<b>List of Figures</b> .....	<b>viii</b>
<b>List of Tables</b> .....	<b>xiii</b>
<b>Acknowledgments</b> .....	<b>xiv</b>
<b>Declaration</b> .....	<b>xv</b>
<b>Dedications</b> .....	<b>xvi</b>
<b>Abstract</b> .....	<b>xvii</b>
<b>List of Abbreviations</b> .....	<b>xix</b>
<b>Amino Acid Abbreviations</b> .....	<b>xxii</b>
<b>Chapter 1 General Introduction</b> .....	<b>1</b>
1.1 Zinc Hypothesis in the Open Ocean .....	1
1.1.1 Evidence Points to Bioactive Zinc Cycles.....	2
1.1.2 Properties of Organic Zinc Ligands .....	4
1.2 Elemental Composition of Life .....	5
1.3 Metal Cofactors in Biology .....	7
1.4 Zinc in Biological Systems.....	8
1.4.1 Zinc is Impressive.....	9
1.5 Systems for Zinc Homeostasis .....	11
1.6 Families of Zinc Transporters .....	14
1.6.1 Efflux Transporters.....	14
1.6.2 Uptake Transporters .....	16
1.6.2.1 High-affinity Uptake Systems .....	16
1.6.2.2 Low-affinity Uptake Systems .....	18
1.7 Zinc Responsive Transcription Regulators.....	20
1.7.1 The Fur Family of Metal Sensing Proteins.....	20
1.7.2 Zinc Uptake Regulators: The Zur Sensor .....	26
1.7.2.1 Metal Sites in Zur Proteins .....	27

1.7.3 The Functions of Zur .....	29
1.7.3.1 Zur as a Repressor .....	29
1.7.3.2 Zur as an Activator .....	30
1.8 Zincophores: Molecules whose Time Has Come .....	31
1.9 Metals in Cyanobacteria .....	34
1.9.1 Zinc Homeostasis in Cyanobacteria .....	35
1.9.1.1 The Zinc Uptake Regulator, Zur in Cyanobacteria .....	36
1.10 Research Motivation and Aims .....	40
<b>Chapter 2 General Materials and Experimental Methods .....</b>	<b>43</b>
2.1 Chemicals and Reagents .....	43
2.2 Media, Bacterial Growth and Incubation Conditions .....	43
2.2.1 Cyanobacterial Media and Growth Conditions .....	43
2.2.2 Contamination Plates .....	45
2.3 Analysis of Culture Supernatant .....	46
2.3.1 Cell Pre-concentration and Ligand Extraction Procedures .....	46
2.3.2 Chromatography Analysis .....	48
2.4 Physiological Methods .....	49
2.4.1 Flow Cytometry .....	49
2.4.2 Growth Rate Analysis .....	50
2.4.3 Chlorophyll <i>a</i> Extraction .....	50
2.5 Identification of Proteins using MALDI-TOF .....	51
2.5.1 Sample Preparation .....	51
2.5.2 Band Preparation and Destaining .....	51
2.5.3 Peptide Mass Fingerprinting (PMF) .....	53
2.5.4 Data Interpretation and Database Searching .....	53
2.6 Molecular Biology Procedures .....	53
2.6.1 Genomic DNA Extraction from <i>Synechococcus</i> sp. WH8102 .....	53
2.6.2 Synthetic <i>synw_2401</i> gene .....	54
2.6.3 Gene Amplification by PCR .....	55
2.6.4 Agarose Gel Electrophoresis .....	56
2.6.5 Purification of PCR Product .....	56
2.6.6 Gene Cloning into the TOPO <sup>®</sup> vector .....	57

2.6.7 Transformation of Competent Cells and Plasmid Purification.....	57
2.7 Overproduction and Purification of Zur Protein .....	58
2.7.1 Production of Recombinant Zur Protein.....	58
2.7.2 Immobilized Metal Affinity Chromatography .....	59
2.7.3 TEV Protease Purification .....	60
2.8 Protein Identification .....	61
2.8.1 SDS-polyacrylamide Gel Electrophoresis .....	61
2.8.2 Native Polyacrylamide Gel Electrophoresis (NP-AGE) .....	61
2.8.3 Detection of Protein by Western Blotting .....	61
2.9 Estimation of Zur Protein Concentration .....	62
2.9.1 Ellman's Test, Thiol Quantification .....	62
2.9.2 Inductively Coupled Plasma-Optical Emission Spectroscopy .....	63
2.10 Protein Biophysical Techniques .....	63
2.10.1 Electrospray Ionization Mass Spectrometry (ESI-MS).....	63
2.10.2 Circular Dichroism (CD) Spectroscopy .....	64
2.10.3 Nuclear Magnetic Resonance (NMR) Spectroscopy.....	64
2.10.3.1 1D <sup>1</sup> H-NMR Spectroscopy .....	64
2.10.3.2 2D Heteronuclear NMR Spectroscopy .....	65
2.11 Monitoring Protein Conformational Changes .....	66
2.12 pH Titrations.....	66
2.13 Electrophoretic Mobility Shift Assays (EMSA).....	67
2.14 Homology Modelling and Validation.....	68
<b>Chapter 3 Toward Novel Zinc Complexing Ligands in the Marine Cyanobacterium</b> <b><i>Synechococcus</i> sp. WH8102 .....</b>	<b>69</b>
3.1 Introduction .....	69
3.2 Detection of Trace Metals by ICP-MS .....	71
3.3 A Zincophore Detection by UHPLC/Q-TOF-MS .....	73
3.4 Zincophore Detection by HPLC .....	78
3.5 Summary and Conclusion.....	84

<b>Chapter 4 Growth and Proteomic Changes in <i>Synechococcus</i> sp. WH8102 under Zinc Depleted and Replete Conditions .....</b>	<b>85</b>
4.1 Introduction .....	85
4.2 Growth Characteristics of <i>Synechococcus</i> sp. WH8102 .....	86
4.2.1 Specific Growth Rates .....	88
4.2.2 Chlorophyll <i>a</i> Concentration .....	89
4.3 Proteomics Analysis .....	91
4.3.1 1D-SDS-PAGE Profiles .....	91
4.3.2 Protein Identification by MALDI-TOF Mass Spectrometry .....	92
4.4 Discussion.....	97
4.4.1 Growth Characteristics .....	97
4.4.2 Preliminary Proteomics Analyses.....	98
4.4.2.1 The ATP-dependent Clp Protease, Hsp 100, ATP-binding Subunit ClpB.....	98
4.4.2.2 Fructose-1,6-bisphosphate Aldolase.....	101
4.4.2.3 ABC Transporter, Substrate Binding Protein, Phosphate.....	103
4.5 Summary and Conclusion.....	105
<b>Chapter 5 Cloning, Expression, Purification and Identification of the Zinc Uptake Regulator (Zur) Protein from <i>Synechococcus</i> sp. WH8102.....</b>	<b>108</b>
5.1 Introduction .....	108
5.2 Flow Chart for this Study .....	109
5.3 Optimised <i>synw_2401</i> Nucleotide Sequence.....	111
5.4 Cloning of the Synthetic Gene <i>sync_2401</i> .....	112
5.4.1 Amplification of <i>synw_2401</i> Gene by PCR .....	112
5.4.2 Cloning of Target Gene using the TOPO Cloning System .....	113
5.4.2.1 Why pET151/D-TOPO@.....	113
5.4.3 Identifying Positive Colonies by PCR and DNA Sequencing.....	115
5.5 Over-expression of <i>Synechococcus</i> sp. WH8102 Zur protein.....	116
5.5.1 Over-expression using BL21 Star <sup>TM</sup> (DE3) and Rosetta <sup>TM</sup> 2(DE3)pLysS .....	116
5.5.2 Over-expression of Zur protein using Takara system .....	119
5.5.2.1 Over-expression of Zur using pG-Tf2 in MagicMedia <sup>TM</sup> .....	122
5.5.2.2 Overexpression of Zur using pG-Tf2 in LB Medium .....	123
5.5.3 Western Blotting Confirmation of Over-expressed Zur Protein .....	126

5.6 Purification of <i>Synechococcus</i> sp. WH8102 Zur Protein .....	127
5.6.1 Immobilized Metal Affinity Chromatography .....	127
5.6.2 Cleaving the Zur Protein with TEV Protease .....	131
5.7 Characterization of Zur Protein .....	133
5.7.1 Mass Spectrometry under Denaturing Conditions: Apo-Zur .....	133
5.7.2 Determination of Protein Concentration .....	134
5.7.3 Molar Extinction Coefficient.....	136
5.7.4 Native ESI Mass Spectrometry of Zur Protein.....	137
5.7.5 Influence of Freezing on SynZur.....	140
5.7.6 Circular Dichroism Spectroscopy.....	143
5.8 Summary and Conclusions .....	147
<b>Chapter 6 Towards the Three Dimensional Structure of Zur Protein from <i>Synechococcus</i></b>	
<b>sp. WH8102 .....</b>	<b>148</b>
6.1 Introduction .....	148
6.2 Nuclear Magnetic Resonance (NMR) Spectroscopy.....	149
6.3 Optimization of Conditions for NMR .....	153
6.3.1 Effect of Temperature on SynZur.....	154
6.3.2 Effect of Salt on SynZur.....	157
6.4 Two Dimensional NMR Spectroscopy.....	160
6.4.1 Transverse Relaxation-optimized Spectroscopy (TROSY).....	161
6.4.1.1 Technical Background for TROSY NMR.....	162
6.4.2 Impact of TROSY on [ <sup>1</sup> H, <sup>15</sup> N] HSQC Spectra for SynZur.....	164
6.5 3D Structural Prediction for SynZur .....	166
6.5.1 Structure Validation.....	168
6.6 Summary and Conclusion.....	173
<b>Chapter 7 Monitoring Protein Conformational Changes and Dynamic Studies.....</b>	<b>174</b>
7.1 Introduction .....	174
7.2 Observations of Zinc Release from SynZur .....	175
7.2.1 Competition Reactions with EDTA.....	175
7.2.1.1 Competition Reaction using UV-Visible Spectroscopy .....	176
7.2.1.2 Competition Reaction using CD Spectroscopy .....	177

7.2.1.2.1 Prediction of Secondary Structure Fractions .....	180
7.2.1.3 Competition Reaction using ESI-MS .....	182
7.2.1.4 Competition Reaction using 1D <sup>1</sup> H NMR .....	194
7.2.1.5 Competition Reaction using [ <sup>1</sup> H, <sup>15</sup> N] TROSY.....	199
7.2.1.5.1 Chemical Shift Perturbation .....	199
7.2.2 Re-addition of Zinc Ions to the Zn <sub>1</sub> Zur Species .....	207
7.2.3 Hydrogen Ions as a Probe for SynZur Protein.....	215
7.2.3.1 Reactivity with Hydrogen Ions using UV-Visible Spectroscopy .....	216
7.2.3.2 Reactivity with Hydrogen Ions using CD .....	217
7.2.3.2 Reactivity with Hydrogen Ions by NMR.....	219
7.2.3.3 Reactivity with Hydrogen Ions using ESI-MS .....	221
7.3 Summary and Conclusion.....	226
<b>Chapter 8 Identification of Target Genes for the SynZur Protein .....</b>	<b>229</b>
8.1 Introduction .....	229
8.2 Correcting the Start Codon for <i>synw_0971</i> .....	232
8.3 Transcription Factor Elements, -10 and -35 .....	234
8.4 Electrophoretic Mobility Shift Assays (EMSA).....	236
8.4.1 Detection Limit in EMSA .....	237
8.4.2 Zinc-loaded SynZur Binds Specifically to its Promoters .....	238
8.4.3 EDTA-Treated SynZur .....	243
8.5 Defining the Recognition Motif .....	252
8.5.1 (6-1-6) Motif.....	252
8.5.2 Purine-N-N-N-N-Pyrimidine Motif.....	255
8.6 Why does ZnuABC System 1 ( <i>synw_2481</i> ) Lack a Zur Box? .....	259
8.7 Why does <i>smtA</i> Promoter ( <i>synw_0359</i> ) have a Zur Box? .....	260
8.7.1 SynZur May Repress <i>smtA</i> at High Levels of Zn(II) .....	263
8.7.2 SynZur May Activate <i>smtA</i> at High Levels of Zn(II).....	264
8.7.2.1 SynZur as a Transcriptional Activator of <i>smtA</i> .....	267
8.9 Summary and Conclusion.....	270
<b>Chapter 9 General Discussion, Recommendations and Conclusions .....</b>	<b>272</b>
9.1 Introduction .....	272

9.2 Key Findings .....	275
9.3 Recommendations .....	280
9.4 Conclusions .....	282
<b>Bibliography.....</b>	<b>283</b>
<b>Appendices .....</b>	<b>Error! Bookmark not defined.</b>

# List of Figures

Figure 1.01 Dissolved zinc (II) speciation vs. depth. ....	4
Figure 1.02 The periodic table highlighting the essential elements of life.....	6
Figure 1.03 Competitiveness according to the Irving–Williams series and bioavailability are correlated.....	10
Figure 1.04 Zinc homeostasis system in bacteria. ....	12
Figure 1.05 Types of efflux transporter.....	15
Figure 1.06 Transporters involved in metal uptake. ....	18
Figure 1.07 Members of the Fur family sensors.....	21
Figure 1.08 Crystal structures of Fur family proteins. ....	22
Figure 1.09 Crystal structures of members of the Fur family. ....	23
Figure 1.10 Sequential alignment of characterized Fur family proteins. ....	24
Figure 1.11 Allosteric structural changes in PerR from <i>Bacillus subtilis</i> . ....	25
Figure 1.12 Crystal structure of the EcZur dimer binding to the <i>znuABC</i> promoter.....	26
Figure 1.13 Zinc-binding sites in Zur proteins. ....	28
Figure 1.14 Structures of EDDS and EDTA. ....	32
Figure 1.15 Predicted structure of coelibactin from <i>Streptomyces coelicolor</i> . ....	33
Figure 1.16 <i>Anabaena</i> sp. PCC 7120 $\Delta$ <i>zur</i> phenotype under zinc deplete conditions. ....	37
Figure 1.17 Phylogenetic relationship among Fur-like proteins from marine cyanobacteria. .	38
Figure 1.18 Structural features of Zur proteins. ....	39
Figure 1.19 Sequence logo for Zur boxes in cyanobacteria. ....	40
Figure 2.01 Schematic diagram describing protein In-gel tryptic digestion. 52	
Figure 2.02 Map of pMA-T vector with <i>synw_2401</i> gene. ....	55
Figure 3.01 ICP-MS analysis of trace metals from SPE extracts.....	73
Figure 3.02 Total ion chromatograms of SPE extracts using UHPLC/Q-TOF-MS.....	74
Figure 3.03 Zinc isotope distributions.....	74
Figure 3.04 Mass spectra for SPE extracts with a retention time of 15.7-22.0 min.....	75
Figure 3.05 Modelling zinc isotope distributions for the hypothetical formula $C_{17}H_{37}N_5O_3Zn$ . .....	76
Figure 3.06 UHPLC/Q-TOF-MS spectra. ....	77
Figure 3.07 HPLC spectra for the fraction eluted with 50:50 methanol: water. ....	79
Figure 3.08 Schematic illustration of mechanisms of metal uptake across the outer membrane. .....	81

Figure 3.09 Hypothesised model of zinc transport through the outer membrane of <i>Synechococcus</i> sp. WH8102.....	83
Figure 4.01 Growth curves of <i>Synechococcus</i> sp. WH8102.....	87
Figure 4.02 Growth (number of cells) of <i>Synechococcus</i> sp. WH8102.....	87
Figure 4.03 Growth curves of <i>Synechococcus</i> sp. WH8102 for 7 days. ....	88
Figure 4.04 Specific growth rates for <i>Synechococcus</i> sp. WH8102.....	89
Figure 4.05 Time course of chlorophyll a ( <i>Chl a</i> ).....	90
Figure 4.06 SDS-PAGE profiles of whole-cell lysates of <i>Synechococcus</i> sp. WH8102. ....	92
Figure 4.07 Analysis of proteins in Mascot software.....	94
Figure 4.08 MALDI-MS spectrum for some identified peptides for fructose-1,6 bisphosphate aldolase. ....	95
Figure 4.09 MALDI-MS spectrum for some identified peptides for ABC transporter, substrate binding protein, phosphate. ....	96
Figure 4.10 Models for the mechanisms of Clp/Hsp100 proteins.....	99
Figure 4.11 Structural features of Class II FBPA proteins.....	102
Figure 4.12 Sequential alignment for FBPA. ....	103
Figure 4.13 Hypothetical modelling of expression of FBPA protein under Zur protein. ....	106
Figure 5.01 General steps of cloning, over-expression and characterisations of the <i>Synechococcus</i> sp. WH8102 Zur protein, encoded by the <i>synw_2401</i> gene.....	110
Figure 5.02 Modified <i>synw_2401</i> gene sequence for <i>Synechococcus</i> sp. WH8102.....	111
Figure 5.03 Amplification of <i>synw_2401</i> gene using two different thermostable proofreading polymerases. ....	112
Figure 5.04 TOPO vector mechanisms.....	114
Figure 5.05 PCR products for positive colonies.....	115
Figure 5.06 Model of protein folding in the cytosol with the assistant of chaperones.....	121
Figure 5.07 A map of chaperon plasmid pG-Tf2. ....	122
Figure 5.08 Over-expression of the <i>Synechococcus</i> sp. WH8102 Zur protein using the Takara system at 37°C using silver staining.....	124
Figure 5.09 Over-expression of the <i>Synechococcus</i> sp. WH8102 Zur protein using the Takara system at 30°C using silver staining.....	125
Figure 5.10 Western blotting of the putative Zur protein.....	126
Figure 5.11 Partial structure of IDA resin charged with Ni <sup>2+</sup> . ....	128
Figure 5.12 The elution profile of crude extract proteins from the Ni-IMAC column. ....	129
Figure 5.13 SDS-PAGE analysis of protein fractions collected from the Ni-IMAC column.....	130
Figure 5.14 SDS-PAGE analysis of the cleaved His <sub>6</sub> -tag from the Zur protein. ....	132

Figure 5.15 Identification of the non-native Zur protein by ESI-MS.....	134
Figure 5.16 <i>Synechococcus</i> sp. WH8102 Zur protein amino acid in black with six additional amino acids (GIDPFT) in red resulting from sub-cloning. ....	134
Figure 5.17 ESI-MS analyses of the native state of SynZur. ....	137
Figure 5.18 Non-denaturing PAGE analysis of the SynZur protein.....	139
Figure 5.19 Influence of freezing on SynZur charge state distribution.....	141
Figure 5.20 Influence of freezing on selected monomer/dimer charge states for SynZur. ....	142
Figure 5.21 Schematic diagram showing the vertically linearly polarized light (left panel) and horizontally linearly polarized light (right panel).....	144
Figure 5.22 Schematic diagram showing the left-hand circularly polarised light (left panel) and right-hand circularly polarised light (right panel). ....	145
Figure 5.23 The CD spectra of protein structural elements with the secondary structure conformation.....	145
Figure 5.24 Circular dichroism analyses of the <i>Synechococcus</i> sp. WH8102 Zur protein. ...	146
Figure 6.01 Quantum model of NMR visualising the two spin states.....	150
Figure 6.02 Distribution of spin $\frac{1}{2}$ nuclei in the absence and in the present of the external magnetic field ( $B_0$ ).....	150
Figure 6.03 A spin precessing about the magnetic field in the absence and presence of radio frequency (RF) pulse. ....	151
Figure 6.04 One-dimensional $^1\text{H}$ NMR spectrum of <i>Synechococcus</i> sp. WH8102 Zur.....	152
Figure 6.05 Stacked plot of 1D $^1\text{H}$ NMR spectra at various temperatures for SynZur. ....	155
Figure 6.06 Stacked plot of 1D $^1\text{H}$ NMR spectra for SynZur at different salt concentration. ....	158
Figure 6.07 Structure of amino acid chains with NMR active nuclei in ( $^1\text{H}$ , $^{15}\text{N}$ ) HSQC experiment. ....	161
Figure 6.08 Impact of protein size and rotational correlation on linewidths in 1D $^1\text{H}$ NMR spectra.....	162
Figure 6.09 Contour plots of [ $^1\text{H}$ , $^{15}\text{N}$ ] correlation spectra for an example $^1\text{H}$ , $^{15}\text{N}$ spin system. ....	163
Figure 6.10 Contour plots of [ $^1\text{H}$ , $^{15}\text{N}$ ] correlation spectra for SynZur.....	165
Figure 6.11 Two 3D structural predictions for the SynZur protein.....	167
Figure 6.12 Superimposition of SynWH_Zur1 with three known Zur proteins.....	170
Figure 6.13 Structural features for SynZur monomer form.....	172
Figure 6.14 Electrostatic potential map of the predicted SynZur protein. ....	173
Figure 7.01 Monitoring the competition reaction of SynZur with EDTA using UV-Visible spectroscopy. ....	177

Figure 7.02 Monitoring the competition reaction of SynZur with EDTA using CD spectroscopy. .....	179
Figure 7.03 Estimation of secondary structure fractions for SynZur. ....	181
Figure 7.04 Monitoring the competition reaction of SynZur using ESI-MS. ....	184
Figure 7.05 The speciation of the +15 charge state from monomeric SynZur during the competition reaction with EDTA. ....	186
Figure 7.06 The speciation of the +19 charge state of dimeric SynZur during the competition reaction with EDTA.....	188
Figure 7.07 Monitoring the competition reaction of SynZur with EDTA using ESI-MS.....	190
Figure 7.08 Electrostatic potential map of the predicted SynZur protein. ....	193
Figure 7.09 Monitoring the competition reaction of SynZur using 1D <sup>1</sup> H NMR. ....	195
Figure 7.10 Stacked plot of the EDTA time course with SynZur. ....	198
Figure 7.11 Description of chemical shift perturbations in slow and fast exchange rate.....	200
Figure 7.12 Monitoring the competition reaction of SynZur using 2D [ <sup>1</sup> H, <sup>15</sup> N] HSQC-TROSY spectroscopy. ....	201
Figure 7.13 Overlay of 2D [ <sup>1</sup> H, <sup>15</sup> N] HSQC-TROSY for SynZur during the EDTA time course. .....	203
Figure 7.14 Chemical shift perturbation, close-up, of [ <sup>1</sup> H, <sup>15</sup> N] HSQC-TROSY spectra for SynZur during the EDTA time course.....	204
Figure 7.15 Overlay of [ <sup>1</sup> H, <sup>15</sup> N] HSQC-TROSY before and after EDTA incubation. ....	206
Figure 7.16 Stacked plot of the 1D <sup>1</sup> H NMR spectra for SynZur before and after EDTA treatment, as well as after zinc ion re-addition.....	208
Figure 7.17 Re-addition of zinc ions to the EDTA-treated SynZur, Zn <sub>1</sub> Zur species. ....	210
Figure 7.18 +15 charge state of the SynZur monomer before EDTA treatment, after EDTA treatment, and after zinc ion re-addition.....	212
Figure 7.19 +19 charge state of the SynZur dimer before EDTA treatment, after EDTA treatment, and after zinc ion re-addition.....	213
Figure 7.20 Influence of pH on SynZur using UV-Visible spectroscopy. ....	217
Figure 7.21 Influence of pH on SynZur using CD spectroscopy. ....	218
Figure 7.22 Monitoring the influence of pH on SynZur by 1D <sup>1</sup> H NMR. ....	220
Figure 7.23 Monitoring the influence of pH on SynZur using ESI-MS.....	222
Figure 7.24 The speciation of the +15 charge state for monomeric SynZur during pH titration. .....	224
Figure 7.25 The speciation of the +19 charge state for dimeric Zur during pH titration. ....	225
Figure 8.01 The Zn(II)-uptake transporter, ZnuABC system.....	230

Figure 8.02 Zur boxes in <i>Synechococcus</i> sp. WH8102. ....	231
Figure 8.03 Analysis of the signal peptide sequence in <i>synw_0971</i> . ....	234
Figure 8.04 The upstream region of the <i>znuABC</i> transporter and <i>smtA</i> genes. ....	235
Figure 8.05 Principles of electrophoretic mobility shift assay. ....	237
Figure 8.06 Determining the detection limit for a DNA probe using SYBR-Green dye. ....	238
Figure 8.07 Titration of the <i>znuA</i> , <i>znuC</i> and <i>smtA</i> upstream DNA fragments with the SynZur protein. ....	239
Figure 8.08 Binding affinity curve for <i>Zur-P<sub>znuA</sub></i> . ....	241
Figure 8.09 Titration of <i>ntcA</i> , <i>znuA</i> from system 1 and zur promoter regions with the SynZur protein. ....	242
Figure 8.10 Titration of the <i>znuA</i> and <i>znuC</i> promoters with EDTA-treated SynZur. ....	244
Figure 8.11 Binding affinity curve for <i>SynZur-P<sub>znuA</sub></i> . ....	245
Figure 8.12 Effects of Zn(II) and EDTA on <i>SynZur-znuA</i> and <i>SynZur-znuC</i> complexes. ....	246
Figure 8.13 Titration of the <i>smtA</i> promoter with EDTA-treated SynZur, in the presence of both Zn(II) and EDTA. ....	248
Figure 8.14 Binding affinity curve and Hill plot for <i>SynZur-P<sub>smtA</sub></i> . ....	250
Figure 8.15 Sequential alignment of SynZur with other Zur proteins. ....	251
Figure 8.16 Comparison of models explaining the Fur box consensus sequence. ....	253
Figure 8.17 Motifs prediction for Zur boxes in cyanobacteria. ....	254
Figure 8.18 Sequence logo representation for RNNNNY motifs. ....	257
Figure 8.19 Model of one and two SynZur dimers bound to a Zur box. ....	258
Figure 8.20 Multiple sequence alignments for SmtA/BmtAs from cyanobacteria. ....	261
Figure 8.21 A schematic representation of the Holo-enzyme for RNA polymerase. ....	267
Figure 8.22 Hypothetical mechanism for SynZur as an activator for the <i>smtA</i> promoter. ....	269
Figure 9.01 Allosteric structural changes in SynZur in low levels of Zn(II). ....	278

# List of Tables

Table 2.01 Anhydrous and hydrous salts used to prepare Aquil* medium.....	44
Table 2.02 Macronutrients and micronutrients added to Aquil* medium. ....	44
Table 2.03 Instrument conditions and measurement parameters in ICP-MS.....	47
Table 2.04 Source conditions for UHPLC/Q-TOF-MS. ....	48
Table 2.05 Ion transfer conditions for UHPLC/Q-TOF-MS. ....	49
Table 2.06 Gradient elution for HPLC. ....	49
Table 2.07 Forward and reverse primers of <i>synw_2401</i> gene. ....	56
Table 2.08 T7 Forward and reverse primers.....	58
Table 2.09 Conditions and techniques used for monitoring the competition reaction of the SynZur with EDTA. ....	66
Table 2.10 Conditions and techniques used for monitoring the pH titration of the SynZur. ...	67
Table 2.11 List of primer sequences for amplification of different promoters of <i>Synechococcus</i> sp. WH8102.....	68
Table 4.01 Identification of proteins in three bands.....	93
Table 5.01 Summary of Zur protein over-expression in BL21 Star <sup>TM</sup> (DE3) and Rosetta <sup>TM</sup> 2(DE3) pLysS strains. ....	118
Table 5.02 Comparison of three different techniques for the determination of protein concentration .....	135
Table 5.03 The mass differences for the observed species for SynZur protein. ....	138
Table 5.04 Estimation of secondary structure proportions for SynZur using different algorithms. ....	147
Table 8.01 Zur boxes in <i>Synechococcus</i> sp. WH8102 with their sequences, location, (6-1-6) motif, and [(6-1-6) <sub>2</sub> ] motifs. ....	255

# Acknowledgments

First of all, I am most grateful to ALLAH almighty for the protection and blessing throughout the duration of my doctoral course and writing up thesis.

I am deeply thankful to my supervisor Dr. Claudia Blindauer for her supervision, objective criticisms, patient review and many helpful comments at crucial times, especially during the writing up stage. At the same time, I am very grateful to my second supervisor Prof. David Scanlan who has been very interested in my work and did not hesitate in providing me with his technical support, feedback and helpful comments whenever needed.

Most importantly, I am very indebted to my family; my husband Dr. Said El-Hassan and my daughter Malak El-Hassan, for believing in me, motivating me and supporting me. I am short of words to thank Dr. El-Hassan for being there for me whenever I needed him and to appreciate all his efforts in giving me continuous insights regarding scientific assistance and IT presentation of my work. I also remain eternally grateful to my parents, brothers and sisters for all their enormous love, inspiration and prayers.

I am thankful to all my colleagues and fellows in the Blindauer and Scanlan groups for the help and assistance they made to my research: Dr. Maria Tareen, Dr. Hasan Tanvir Imam, Dr Rahman Pour, Dr. Branko Rihtman, Dr. Joseph Christie-Oleza, Dr. Rich Puxty, Dr. Andrew Millard, and Mrs. Julie Scanlan. Special thanks for Dr. James Barnett for his advice and nice discussion. I also would like to extend my thanks to all people who gave me training to perform my experiments: Mrs. Ann Smith, Dr. Lijiang Song, Dr. Ivan Prokes, Mr. Phil Aston. I would like to extend great thanks to all my friends who were with me and supported me, especially Dr. Zeina Rihawi and Dr. Kifaya Al Qaddume.

Finally, I gratefully acknowledge the Ministry of Higher Education, Syria, and the University of Warwick, UK, for providing the financial support of this research study.

# Declaration

I, Amira Zahir Ksibe, confirm that this thesis is original and my own work and the use of all materials from other sources has been properly and fully acknowledged. The described work has never been submitted or published in this University nor any other University for any qualification. The work was carried out between 2012 and 2016 by the author under the direct supervision of Dr. Claudia Blindauer, Department of Chemistry, and Prof. David Scanlan, School of Life Sciences, Warwick University.

Name: **Amira Zahir Ksibe**

Signature: ...*A. KSIBE*.....

Date: February 2017

## Publications during this Study

**Zhu, Y., A. Z. Ksibe, H. Schäfer, C. A. Blindauer, T. D. H. Bugg and Y. Chen.** 2016. O<sub>2</sub>-independent demethylation of trimethylamine *N*-oxide by Tdm of *Methylocella silvestris*. *FEBS J.*

**Barnett, J. P, A. Millard, A. Z. Ksibe, D. J. Scanlan, R. Schmid and C. A. Blindauer.** 2012. Mining genomes of marine cyanobacteria for elements of zinc homeostasis. *Front. Microbiol.* **3**:142.

## **Dedications**

Dedicated to my dearest husband Dr. SAID El-Hassan, beloved daughters Yomna and Malak El-Hassan and my Parents; Zahir Ksibe and Yanal Alnshiwati, for their love and ever-lasting encouragement.

# Abstract

Since the discovery of zinc as an essential element for living organisms including humans, animals, plants, fungi and bacteria, much has been learnt about zinc in biological systems, ranging from its effects at the whole organism level, including the uptake/efflux of zinc, identification of important zinc-regulator proteins, down to structural, thermodynamic, and kinetic details of zinc–protein interactions. One of the most exciting fields to work on, currently, is understanding the importance of zinc “on the move” – in particular the “acquisition and homeostasis” of this micronutrient element by the organisms. In this wider context, zinc homeostasis by open ocean cyanobacteria, which occupy variable ecosystems with an erratic nutrient supply, has become of recent interest.

In an attempt to resolve how open ocean cyanobacteria persist in regions where the zinc concentration is thought to be limited, we hypothesised that the cyanobacterium *Synechococcus* sp. WH8102 might provide an extracellular zinc scavenger for the acquisition of this essential element. Therefore, the current study developed a method to isolate and purify the putative biogenic zinc-binding ligand (zincophore) using polystyrene-divinylbenzene resin and liquid chromatographies. However, it seems likely *Synechococcus* sp. WH8102 produce ligands that can bind to zinc only under zinc-depleted conditions. Then, we performed zinc limitation and repletion experiments on axenic cultures of marine *Synechococcus* sp. WH8102, and data determined that this strain mounted an adaptive response for zinc under depleted and replete conditions, resulting in the induction and/or repression of a number of proteins.

As a homologue to the Fur family, Zur from *Synechococcus* sp. WH8102 was sub-cloned and purified in the absence of zinc ions in the cultures. *Synechococcus* sp. WH8102 Zur protein at neutral pH (~pH 7.8), in mass spectrometry, presented as a mixture of species including a monomer with two zinc ions bound  $Zn_2Zur$ , a dimer with four zinc ions bound, and another

well folded  $Zn_4Zur_2$  dimer. The complementary technique, ICP-OES, confirmed that the zinc binding stoichiometry was in agreement with mass spectrometric findings,  $2.1 \pm 0.2$  Zn(II) ions per monomer.

Mimicking a drop in available cellular zinc as may be expected in zinc-deplete conditions, it was found that only one of the two metal ions bound per monomer was removed by EDTA from *Synechococcus* sp. WH8102 Zur protein, giving  $0.9 \pm 0.3$  Zn(II) atoms per monomer, with shifting in the monomer/dimer equilibrium toward  $Zn_1Zur$  species. No large difference in the secondary structure between the metallo-species of the SynZur protein was found in CD spectroscopy. Moreover, *Synechococcus* sp. WH8102 Zur protein was found to behave in a similar manner to previously studied Fur family proteins, where zinc removal from the sensory site is fully reversible and has the ability to re-establish a (2:1) Zn(II):protein ratio in less than 15 min with  $1.9 \pm 0.4$  Zn(II) atoms per monomer. Similarly, *Synechococcus* sp. WH8102 Zur was found to act as a transcriptional factor in the presence of zinc ions and bind specifically to 23 AT-rich DNA sequence. The “free” cytosolic zinc concentrations that Zur protein trigger transcription of *znuABC* and *smtA* found to be in femtomolar range  $\sim 1.78 \times 10^{-15}$ , with the dissociation constant  $\sim 62.65 \pm 1.47$  nM and  $61.76 \pm 2.42$  nM for *Zur-P<sub>znuA</sub>* promoter and *SynZur-P<sub>smtA</sub>* promoter, respectively.

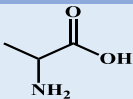
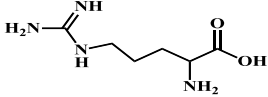
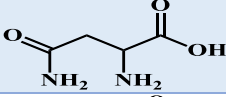
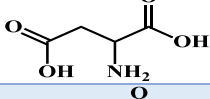
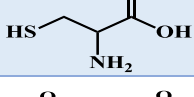
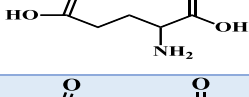
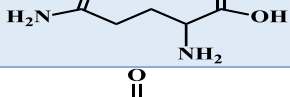
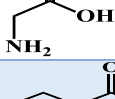
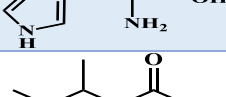
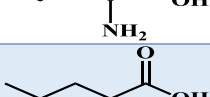
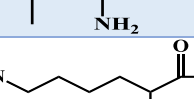
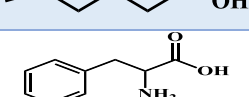
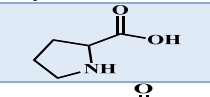
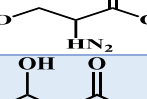
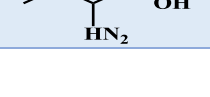
# List of Abbreviations

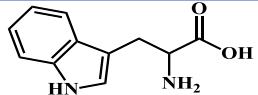
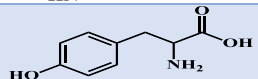
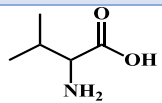
ASW	Artificial seawater
ABC	Adenosine triphosphate-binding cassette
ATP	Adenosine tri-phosphate
ADP	Adenosine di-phosphate
Bp	Base pair
Bs	<i>Bacillus subtilis</i>
CD	Circular dichroism
Cd	Cadmium
CDF	Cation diffusion facilitator
Co	Cobalt
Cu	Copper
Cm	Centimetre
Da	Dalton
DNA	Deoxyribonucleic acid
dNTP	Deoxyribonucleotide triphosphate
DTNB	5,5'-dithiobis-(2-nitrobenzoic acid)
DTT	Dithiothreitol
<i>E. coli</i>	<i>Escherichia coli</i>
e.g.	For example
EDTA	Ethylenediaminetetraacetic acid
EDDA	Ethylenediamine diortho-hydroxyphenyl acetic acid
EMSA	Electrophoretic mobility shift assay
ESI	Electrospray ionisation
Fe	Iron
FPLC	Fast protein liquid chromatography
Fur	Ferric uptake regulator
G	Gram(s)
H <sup>+</sup>	Proton
HPLC	High performance liquid chromatography
Hrs	Hours
HSQC	Heteronuclear signal quantum coherence
H-T-H	Helix-Turn-Helix
ICP-MS	Inductively coupled plasma mass spectrometry
ICP-OES	Inductively coupled plasma optical emission spectroscopy
IPTG	Isopropyl-beta-D-thiogalactopyranoside
Irr	Iron-responsive regulator
kDa	Kilo- Dalton
Kg	Kilo gram(s)
L	Litre(s)
LB	Luria-Bertani medium or liquid broth

M	Molar
M	Meter(s)
<i>m/z</i>	Mass over charge
MP	Metalloprotein
Mb	Megabases
MncA	Mn-binding protein
m <sup>2</sup>	Square meter
MALDI	Matrix assisted laser desorption ionisation
mg	Milligram(s)
min	Minute(s)
mL	Millilitre(s)
mm	Millimetre(s)
Mn	Manganese
Mo	Molybdenum
MS	Mass spectrometry
MS/MS	Tandem mass spectrometry
MT	Metallothionein
Mur	Manganese uptake regulator
Mt	<i>Mycobacterium tuberculosis</i>
NaCl	Sodium chloride
Ni	Nickel
nM	Nanomolar
NMR	Nuclear magnetic resonance
N-terminal	Amino-terminal
Nur	Nickel uptake regulator
NRPS	Non-ribosomal peptide synthesis
OD	Optical density
ORF	Open reading frame
PCR	Polymerase chain reaction
PDB	Protein data bank
ppm	Parts per million
Pa	<i>Pseudomonas aeruginosa</i>
rpm	Revolutions per minute
PMSF	Phenylmethanesulfonyl fluoride
RND	Resistance nodulation division
Sec	Seconds
RF	Radio frequency
SDS-PAGE	Sodium dodecyl sulfate polyacrylamide gel electrophoresis
Sc	<i>Streptomyces coelicolor</i>
Syn	<i>Synechococcus</i> sp. WH8102
UV	Ultra violet
V	Volts

Vis	Visible
Vc	Vibrio cholera
vol	Volume
wt	Weight
Xcc	<i>Xanthomonas campestris pathovar campestris</i>
Zn	Zinc
Zip	Zinc like protein
Zur	Zinc uptake regulator
Mg	Microgram(s)
$\mu\text{m}$	Micrometer
$\times g$	Times gravity

# Amino Acid Abbreviations

1 little code	3 little code	Residue	Mono-isotopic mass	Structure*
A	Ala	Alanine C <sub>3</sub> H <sub>5</sub> NO	71.037114	
R	Arg	Arginine C <sub>6</sub> H <sub>12</sub> N <sub>4</sub> O	156.101111	
N	Asn	Asparagine C <sub>4</sub> H <sub>6</sub> N <sub>2</sub> O <sub>2</sub>	114.042927	
D	Asp	Aspartic acid C <sub>4</sub> H <sub>5</sub> NO <sub>3</sub>	115.026943	
C	Cys	Cysteine C <sub>3</sub> H <sub>5</sub> NOS	103.009185	
E	Glu	Glutamic acid C <sub>5</sub> H <sub>7</sub> NO <sub>3</sub>	129.042593	
Q	Gln	Glutamine C <sub>5</sub> H <sub>8</sub> N <sub>2</sub> O <sub>2</sub>	128.058578	
G	Gly	Glycine C <sub>2</sub> H <sub>3</sub> NO	57.021464	
H	His	Histidine C <sub>6</sub> H <sub>7</sub> N <sub>3</sub> O	137.058912	
I	Ile	Isoleucine C <sub>6</sub> H <sub>11</sub> NO	113.084064	
L	Leu	Leucine C <sub>6</sub> H <sub>11</sub> NO	113.084064	
K	Lys	Lysine C <sub>6</sub> H <sub>12</sub> N <sub>2</sub> O	128.094963	
M	Met	Methionine C <sub>5</sub> H <sub>9</sub> NOS	131.040485	
F	Phe	Phenylalanine C <sub>9</sub> H <sub>9</sub> NO	147.068414	
P	Pro	Proline C <sub>5</sub> H <sub>7</sub> NO	97.052764	
S	Ser	Serine C <sub>3</sub> H <sub>5</sub> NO <sub>2</sub>	87.032028	
T	Thr	Threonine C <sub>4</sub> H <sub>7</sub> NO <sub>2</sub>	101.047679	

<b>W</b>	Trp	Tryptophan C <sub>11</sub> H <sub>10</sub> N <sub>2</sub> O	186.079313	
<b>Y</b>	Tyr	Tyrosine C <sub>9</sub> H <sub>9</sub> NO <sub>2</sub>	163.06332	
<b>V</b>	Val	Valine C <sub>5</sub> H <sub>9</sub> NO	99.068414	

\* All amino acid structures were prepared in ChemDraw software.

# Chapter 1

## General Introduction

---

### 1.1 Zinc Hypothesis in the Open Ocean

A little over a hundred years ago Forchhammer (1862) elegantly defined the scope of marine chemistry where he stated, “The quantity of the different elements in seawater is not proportional to the quantity of elements which river water pours into seawater, but are inversely proportional to the ease which these elements in seawater are made insoluble by general chemical or organo-chemical actions in the sea” (Forchhammer, 1862). Since that time researchers from varied branches of marine science have undertaken the task of deciphering this puzzle (Goldberg, 1963; Bruland & Lohan, 2006).

One of the most striking themes of marine chemistry has not only been to present metal ions as essential elements, but also to recognise the changing concentration of these elements over the life of the earth. These changes led, for instance, to the “iron hypothesis” (Neilands, 1981; Martin & Fitzwater, 1988; Martin *et al.*, 1994), and the “zinc hypothesis” (Morel *et al.*, 1994).

As an example, a study in 1996 indicated that zinc levels in the oceans during the glacial periods were at least 36 times higher than those today and suggested that this change was the result of increasing levels of wind-blown dust (Hong *et al.*, 1996). These changes in zinc levels will

affect the “biological pump<sup>1</sup>” in the ocean, particularly marine microbial community structure. In addition, a study by Sigman and Boyle (2000) showed that the concentration of carbon dioxide in the atmosphere and in the Arctic ice-core was lower during the Ice Age than it is today.

Various lines of evidence have recently suggested a link between nutrient availability or utilisation and the “biological pump” (Sigman & Boyle, 2000). In particular, zinc and carbon co-limitation in marine phytoplankton has been postulated (Hong *et al.*, 1996). However, zinc ions, in common with other trace elements, cannot exist alone in seawater, so the trace elements may exist as free solvated ions, or associated with inorganic and organic ligands.

### 1.1.1 Evidence Points to Bioactive Zinc Cycles

One of the most important discoveries in marine chemistry is that the oceans have remarkably low concentrations of many elements that occur at nanomolar ( $10^{-9}$  M) to picomolar ( $10^{-12}$  M) levels in the upper water column (Bruland *et al.*, 1991). Some of them are required to fulfil a vast array of enzymatic reactions carried out by marine organisms, including bacterioplankton, phytoplankton, fungi and macroalgae (Singh & Singh, 1987; Sunda *et al.*, 2005; Saito & Goepfert, 2008). In contrast to their low concentration in the upper water column, at depth there are much higher concentrations of many of these metals, including iron, copper, cadmium, nickel (Morel *et al.*, 2006), zinc and cobalt (Sunda & Huntsman, 1995).

The development of voltammetric techniques, such as differential pulse cathodic stripping voltammetry (DPCSV) and differential pulse anodic stripping voltammetry (DPASV) have provided a powerful tool for measuring zinc speciation at low concentrations in the marine environment.

---

<sup>1</sup> The biological pump is the process by which CO<sub>2</sub> from the atmosphere is fixed by phytoplankton.

In numerous studies (Bruland, 1989; Bruland *et al.*, 1991; Bruland & Lohan, 2006), it has been observed that organic complexes dominate the speciation of dissolved zinc (~98%), which may suggest a biological influence.

In the central North Pacific, the total concentration of dissolved<sup>2</sup> zinc varies from close to 0.1 nM in surface waters (Bruland, 1989; Jakuba *et al.*, 2012) to 3 nM at a depth of 500 m (Bruland, 1989) and 8 nM at 1500 m (Nienhuis, 1981) (Figure 1.01A), with inorganic zinc ranging from 2 pM in surface waters to 2 nM at 500 m (Bruland, 1989). The concentration of free Zn(II) varies from values close to  $10^{-11.8}$  M at depths shallower than 200 m to  $10^{-8.6}$  M at 600 m (Bruland *et al.*, 1991) (Figure 1.01B), while the concentration of zinc-specific organic ligands was measured to be 1.2 nM at the surface water in the central North Pacific (Bruland, 1989) (Figure 1.01C).

Another study by Jakuba and colleagues found that the total dissolved zinc across the subarctic North Pacific and across the Bering Sea ranged from 0.10 nM to 1.15 nM, the concentration of free Zn(II) varied from 2 to 7 pM and the concentration of zinc-specific organic ligands varied from 1.1 to 3.6 nM in the near-surface waters. However, in the westernmost station in the North Pacific, the concentration of free Zn(II) was 33 pM (Jakuba *et al.*, 2012).

Moving to the north-eastern part of the Atlantic Ocean, it was found that total zinc concentrations ranged from 0.3 nM in surface waters to 2 nM at a depth of 2000 m (Ellwood & Van den Berg, 2000) or 0.08 to 1.3 nM (Jakuba *et al.*, 2008b) (Figure 1.01A), while the concentration of zinc-specific organic ligands was 0.4 to 2.5 nM (Ellwood & Van den Berg, 2000). Zinc organic speciation was also studied in the Sargasso Sea where *Synechococcus* sp. WH8102 is dominated (Jakuba *et al.*, 2008a).

---

<sup>2</sup> Total dissolved metal concentration is composed of free metal ion (free solvated ions), inorganic complexes and organic complexes.

In Manila Bay, it was found that the total concentration of dissolved zinc ranged from 2.48 to 147.43 nM with 50% of total dissolved zinc being organically bound (Velasquez *et al.*, 2002).

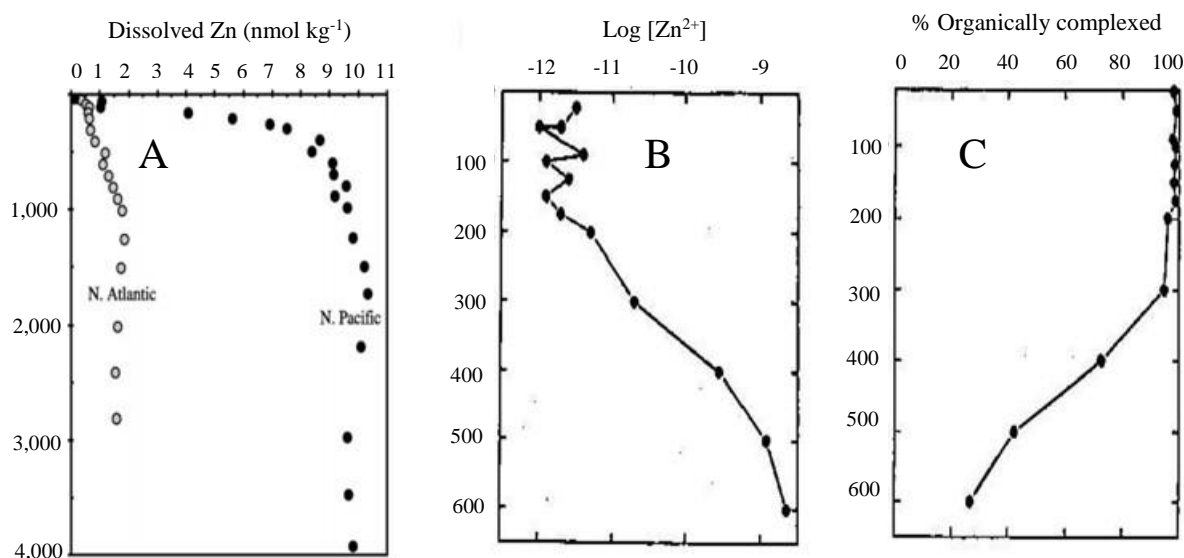


**Figure 1.01 Dissolved zinc (II) speciation vs. depth.**

(A) Vertical concentration profiles of dissolved zinc in the North Atlantic Oceans (○) and in the North Pacific (●) (Bruland & Lohan, 2006); (B) Log concentration values of free Zn(II) ion in the central North Pacific (Bruland, 1989); (C) Concentrations of Zn-complexing organic ligands in the central North Pacific (Bruland, 1989).

The vertical distribution of total dissolved Zn(II) is depleted at the surface by biological activity and biogenic particles, and concentrations increase with depth (Bruland, 1989) (Figure 1.01), which indicates that the organisms presented in the area utilise this element and produce the organic speciation. However, the source of the Zn-organic complexes is at present unconfirmed, although it is thought to be derived from phytoplankton, both autotrophic and heterotrophic.

### 1.1.2 Properties of Organic Zinc Ligands

Two classes of zinc binding ligands have so far been identified in seawater: strong ligands, in the following labelled L<sub>1</sub>, and weak ligands, labelled L<sub>2</sub> (Table 1.01).

By studying zinc ligand concentrations in the River Scheldt Estuary, the presence of two ligands was noted at concentrations between 22 and 220 nM (Van den Berg *et al.*, 1987). In Narragansett Bay, the Zn-binding ligand concentrations varied from 48 to 11 nM, with a relatively uniform conditional stability constant of 9.0 (Kozelka & Bruland 1998).

**Table 1.01 Properties of marine zinc binding ligands.**

Name of place	Type of class <sup>~</sup>	Stability constants	Concentration <sup>*</sup> nM	References
Central North Pacific	strong class	$K_{ZnL1} = 10^{11}$	1.2	(Bruland, 1989; Bruland <i>et al.</i> , 1991)
North-east Pacific	strong class	$K_{ZnL1} = 10^{10.3-11.2}$	1.60-2.22	(Donat & Bruland, 1990 )
North Pacific	strong class	$K_{ZnL1} = 10^{9.3-11.0}$	1.1 - 3.6	(Jakuba <i>et al.</i> , 2012).
North Atlantic	weak class	$K_{ZnL1} = 10^{9.8-10.5}$	0.9 - 1.5	(Jakuba <i>et al.</i> , 2008a)
Atlantic sector of the Southern Ocean	weak class	$K_{ZnL2} = 10^{8.7-9.12}$	3.2	(Baars & Croot, 2011)
East of New Zealand	weak class	$K_{ZnL2} = 10^{9.8-10.28}$	1 - 2.5	(Ellwood, 2004).

<sup>~</sup>Type of zinc-binding ligands. <sup>\*</sup> Concentration of zinc-binding ligands at the surface of seawater.

The important point from the literature mentioned above is that the existence of these ligands is undisputed, but that despite overwhelming evidence of their existence, almost nothing is known about their chemical identity, their stability, or their origin.

## 1.2 Elemental Composition of Life

Living cells are consummate experimentalists; over the course of several billion years of evolution, single-celled life-forms learned to exploit a wide variety of niches that often differed mainly in the availability of the “elements of life” (Merchant & Helmann, 2012).

Bearing in mind that life on earth has developed in equilibrium with the hydrosphere and the lithosphere, all the elements of life are necessary for performing essential functions (Andreini



### 1.3 Metal Cofactors in Biology

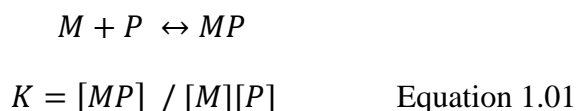
Owing to the fact that amino acids and proteins alone are insufficient to perform all the reactions needed for life, it is not surprising that living beings have evolved the capacity to use metal ions as key to many biological processes (Bertini *et al.*, 2007; Andreini *et al.*, 2009).

Increasing information on the role of metal ions in biology led to estimates that 30% or more of proteins in most organisms contain at least one metal ion (Waldron & Robinson, 2009; Shin *et al.*, 2011). Such metal ions are called “metal cofactors” (Outten & O'Halloran, 2001; Bertini *et al.*, 2007; Waldron & Robinson, 2009), which are defined as catalytic structures, and regulatory cofactors (Maret, 2013).

In the case of structural and regulatory cofactors, binding certain metal ions may reduce the number of accessible conformations of a given polypeptide chain, stabilizing the protein structure (Bertini *et al.*, 2007; Dennis, 2007), which includes hydrogen bonds, ion pairs, van der Waals contacts and cross-links (Bertini *et al.*, 2007). Stabilization of domains by metal ions may be more common in intracellular proteins, owing to the reducing environment of the cell which limits the presence of disulfides as common stabilizing cross-links (Dennis, 2007; Hudek *et al.*, 2013b).

Metal cofactors which are essential for enzymatic catalysis include Fe, Cu, and Zn. For example, the redox couples Fe(II)/Fe(III) and Cu(I)/Cu(II) play critical roles as cofactors in electron transfer reactions and in the catalysis of redox actions (Bertini *et al.*, 2007). The Zn(II) ion can act as a Lewis acid to produce a bound nucleophilic Zn-OH moiety from water around neutral pH (Bertini *et al.*, 2007). These properties have rendered these metal ions indispensable in living organisms (Lyons & Eide, 2007).

Often, these metals associate strongly with proteins and form so-called metalloproteins (Bertini *et al.*, 2007). The affinity between the metal ion and the protein can be expressed as Equation 1.01:



Where  $K$  is the equilibrium binding constant between the metal ion  $M$ , and the polypeptide chain  $P$ , to form the metalloprotein,  $MP$ . The thermodynamic stability of such adducts is often very high and  $K$  can have values greater than  $\sim 10^8 \text{ M}^{-1}$ , compared to non-transition metal ions such as  $\text{Na(I)}$ ,  $\text{K(I)}$  or  $\text{Mg(II)}$ , which form much weaker complexes (Bertini *et al.*, 2007).

The selective co-ordination environments of metalloproteins are clearly a contributory factor, but insufficient on its own to control the concentration of free metal inside the cells. An astonishing discovery within the last few years has postulated the presence of metal homeostatic systems, which ensure that cells contain sufficient ions of each metal to satisfy the requirements of metalloproteins, while avoiding any excess that would otherwise compete for inappropriate (adventitious) sites (Cavet *et al.*, 2003). Metal selectivity ‘within the homeostatic proteins’ (metal sensors, metal transporters, sequestration proteins and metallochaperones) is paramount.

## 1.4 Zinc in Biological Systems

Zinc might be considered a relatively inconspicuous trace element compared to iron and copper. Owing to its filled  $d$  shell in the only accessible oxidation state,  $\text{Zn(II)}$ , zinc is not strictly a transition element and is sometimes referred to as a post- or ‘honorary’ transition metal (Lennartson, 2014). For the same reason, simple zinc compounds are colourless. Unlike copper and iron,  $\text{Zn(II)}$  is not redox-active.  $\text{Zn(0)}$  and  $\text{Zn(II)}$  are well known, but  $\text{Zn(I)}$  species are rare, and calculations have recently confirmed that a stable zinc(III) compound will never be seen (Lennartson, 2014).

However, Zn(II) has not received as much interest as many other elements. For these reasons, the question arose if “zinc is a boring element?” due to its straightforward and “predictable” chemistry.

### 1.4.1 Zinc is Impressive

The old image about the boring character of element 30, zinc, is not the right picture. Element 30 is fascinating because of its rich biological chemistry. Since its discovery as an essential element for fungi, animals, humans, plants and bacteria, including the discovery in 1939 of the first enzyme shown to require zinc for its activity, much has been learned about zinc in biological systems (Blindauer, 2015). Recent bioinformatic approaches have found that proteins containing zinc are represented to the extent of about 9% in eukaryotes and 5% to 6% in prokaryotes (Andreini *et al.*, 2006; Andreini *et al.*, 2009).

Zinc plays a critical role in a wide variety of biochemical processes. For example, it is a cofactor required for the function of over 300 different enzymes from all six enzyme classes (Gaither & Eide, 2001), including RNA polymerase, alkaline phosphatase, alcohol dehydrogenase, Cu/Zn superoxide dismutase and carbonic anhydrase (Guerinot, 2000; Lennartson, 2014; Blindauer, 2015).

Remarkably, zinc plays a pivotal role in biological systems for four major reasons. Firstly, the borderline hardness of Zn(II) ions allows it to coordinate to a variety of potential side-chain ligands, including histidine, cysteine and carboxylates (Dennis, 2007). Secondly, Zn(II) can form four-, five-, or even six-coordinate complexes and the lack of any ligand-field stabilization for Zn(II) permits conversion between these various coordination states (Glusker *et al.*, 1999; Dennis, 2007). Thirdly, Zn(II) is resistant to redox changing and is unable to generate radicals. Finally, it is the most abundant metal ion on the earth after iron. Therefore, a combination of these effects makes it possible to regard Zn(II) as a structural metal ion (Dennis, 2007).

Owing to the importance of Zn(II) in biological systems, it seems that virtually all organisms have elaborate mechanisms to control its levels and distribution (Zhao & Eide, 1996; Outten & O'Halloran, 2001; Hantke, 2005; Barnett *et al.*, 2012). Total cellular concentrations are typically in the high micromolar range (Outten & O'Halloran, 2001). However, various lines of evidence have indicated that “free” cytosolic zinc concentrations are extremely low, falling into the femtomolar (Outten & O'Halloran, 2001) to the picomolar (Braymer & Giedroc, 2014) range.

The apparent need for the narrow range of tolerable zinc concentrations initially puzzled some researchers, as there seems to have been a widespread belief that zinc was not particularly toxic to cells.

However, free zinc ions in sub-micromolar range are surprisingly toxic (Bozym *et al.*, 2010). The deleterious effects of Zn(II) may be the result of its high affinity to proteins. Chelating binding affinities of Zn(II) for a given ligand are generally higher than for earlier first-row divalent transition metals (except Cu(II)), a trend known as the “Irving–Williams” series for divalent ions (Figure 1.03) (Irving and Williams, 1953).

Due to its high affinity for binding sites in proteins, zinc is able to out-compete the less competitive metal ions in the first-row, as demonstrated with cytochrome *c* oxidase (Shin *et al.*, 2007) and the Mn-binding protein MncA (Tottey *et al.*, 2008). Moreover, higher concentration of zinc can also block important thiols (Patzner & Hantke, 2000; Andreini *et al.*, 2006; Waldron & Robinson, 2009) and suppress copper and iron absorption. Due to these properties, the intracellular zinc level must be precisely regulated for optimal survival.

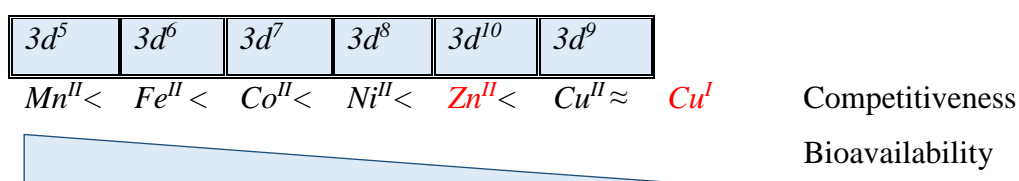


**Figure 1.03 Competitiveness according to the Irving–Williams series and bioavailability are correlated.** Adapted from (Braymer & Giedroc, 2014).

In summary, zinc can be a double-edged sword, and it is not surprising that cells have evolved homeostatic systems that can control the level of “free” cytosolic zinc (Outten & O'Halloran, 2001).

## 1.5 Systems for Zinc Homeostasis

Given the important role of zinc in biological processes, within the last decade, major insights into zinc homeostasis in bacteria have been gained (Hantke, 2005; Barnett *et al.*, 2014; Braymer & Giedroc, 2014). A number of lines of evidence over the past decade have confirmed that zinc homeostasis in bacteria is maintained by means of a small number of critical processes, including zinc transporters and zinc-dependent transcription factors, also termed zinc sensor proteins (Figure 1.04) (Liu *et al.*, 2004; Blindauer, 2015). Fluxes of zinc into and out of bacteria depend in the first instance on the level of expression of the membrane-bound transporters which is regulated by specific transcription factors.

Under conditions of zinc depletion, Zn(II) uptake regulators have a low affinity for their DNA operator sequence in the de-metalled state<sup>3</sup> (Figure 1.04A). This leads to de-repression, which then allows the expression of genes involved in zinc import. At the same time, Zn(II) efflux regulators have high affinity for their DNA operator in the absence of Zn(II) and repress efflux genes. This response allows the cell to maintain the number of zinc atom, “free zinc”, in the cytoplasm (Figure 1.04A). Movement of Zn(II) to selected proteins may involve the action of zinc chaperones such as COG0523 and metallothioneins (Barnett *et al.*, 2012).

---

<sup>3</sup> The de-metalled state is the state after releasing zinc from the sensory site(s) in the regulator. It is named in some papers as the apo state.



On the other hand, under zinc-replete conditions (Figure 1.04B), the uptake regulators are metallated<sup>4</sup> and bind with high affinity to their DNA operator, thereby repressing genes involved in zinc import. In the presence of Zn(II), the efflux regulators dissociate from their operator sequence, or become transcriptional activators, in the Zn(II)-bound state, resulting in the transcription of genes involved in zinc export (Braymer & Giedroc, 2014). Zinc speciation in the cytoplasm is believed to involve Zn-requiring metalloproteins and possibly zinc chaperones (Braymer & Giedroc, 2014).

Several types of zinc-specific regulators have been discovered in the last few years, including members of the ferric uptake regulator (Fur) family (Zur) (Shin *et al.*, 2007; Gilston *et al.*, 2014) and of the MarR/SlyA family (AdcR) (Reyes-Caballero *et al.*, 2010; Guerra *et al.*, 2011; Sanson *et al.*, 2015) for zinc import, and members of the MerR (ZntR) and ArsR/SmtB families (Morby *et al.*, 1993; Kondrat *et al.*, 2013), (CzcA) (Goldberg *et al.*, 1999), and (ZiaR) (Thelwell *et al.*, 1998) for zinc export.

Usually the regulators sensing zinc excess trigger the expression of proteins involved in efflux (*e.g.* P-type ATPases, CDF proteins, RND proteins) (Klein & Lewinson, 2011) or sequestration (metallothioneins), whereas regulators for zinc depletion mediate enhanced expression of uptake transporters (ZnuABC and AdcABC systems, porins, ZIP, and Ribosomal proteins), putative chaperones, and proteins that reduce cellular zinc requirements (Kallifidas *et al.*, 2010; Gilston *et al.*, 2014; Blindauer, 2015).

The following two sections provide an overview for some of these families. Specific examples of the zinc-transporters and zinc regulator proteins are presented.

---

<sup>4</sup> Metallated state is the state where zinc is bound to the sensory site in the regulators.

## 1.6 Families of Zinc Transporters

Bacteria have evolved a number of transport mechanisms to detoxify and to maintain metal homeostasis. These are of two types, export/efflux and import/uptake.

### 1.6.1 Efflux Transporters

Based on the types of transporters, research has identified three types of membrane-embedded efflux transporters, including P-type ATPases, CDF (Cation Diffusion Facilitator) and RND (Resistance Nodulation Division) proteins, that participate in metal translocation across cell membranes (Figure 1.05) (Klein & Lewinson, 2011). All of these proteins are induced by high zinc concentrations and play a major role in zinc resistance.

RND transporters consist of multiple subunits spanning the inner membrane, the periplasm, and the outer membrane (Kim *et al.*, 2011). Metal ions can enter the translocation pathway either in the cytoplasm or in the periplasm (Kim *et al.*, 2011; Klein & Lewinson, 2011). They utilize the energetically downhill movement of protons across the inner membrane ( $\Delta\mu\text{H}^+$ ) to drive metal efflux from the cytosol and the periplasm to the cell exterior (Klein & Lewinson, 2011).

P-type ATPases are monomers powered by ATP to catalyze metal efflux from the cytosol, across the inner membrane, to the periplasm. A similar task is performed by the dimeric CDF transporters (Palmiter & Huang, 2004; Eide, 2006) which utilize the energy of  $\Delta\mu\text{H}^+$  to drive metal efflux across the inner membrane to the periplasm (Klein & Lewinson, 2011).

Several examples of zinc-transporting P-type ATPases have been recently described, including ZntA in *E. coli* (Rensing *et al.*, 1997; Banci *et al.*, 2002), Bxa1 in the cyanobacterium *Oscillatoria brevis* (Liu *et al.*, 2004), ZiaA in *Synechocystis* PCC 6803 (Thelwell *et al.*, 1998), and CadA in *B. subtilis* (Gaballa *et al.*, 2002).

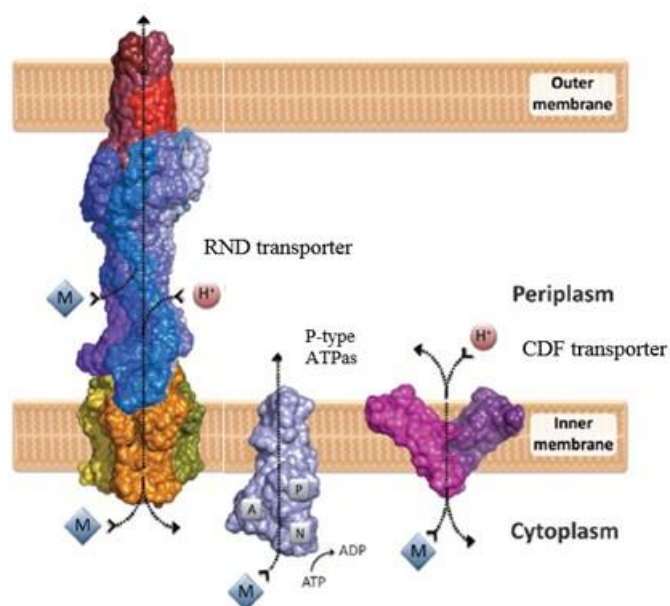


**Figure 1.05 Types of efflux transporter.**

Three types of transporter participate in metal efflux in bacteria. The arrows indicate the directionality of transporting the transition metals. From left to right: RND transporter traverses both the inner and outer membranes. P-type ATPases and CDF transporters efflux metal across the inner membrane to the periplasm. Taken from (Klein & Lewinson, 2011).

In addition, several members of the RND family have been found, such as *CusCBA* of *E. coli* and *GesABC* of *Salmonella* (Conroy *et al.*, 2010), *CzcCBA* and *ZncCBA* from *Cupriavidus metallidurans* (De Angelis *et al.*, 2010; Pak *et al.*, 2013), and *CzcCB2A* from *Ralstonia* sp. CH34 (Goldberg *et al.*, 1999) and *Streptococcus pneumoniae* (Jacobsen *et al.*, 2011; Cheryl *et al.*, 2014). Zinc transport in the CDF family has been reported for YiiP (Lu & Fu, 2007), and ZitB (Grass *et al.*, 2001; Anton *et al.*, 2004) in *E. coli*.

Although at least some of these transporters have been established as zinc efflux proteins, it should be noted that they have also been shown to transport lead, nickel, cobalt, copper, cadmium and magnesium (Hou & Mitra, 2003; Anton *et al.*, 2004; Neis, 2007; Hudek *et al.*, 2013a).

## 1.6.2 Uptake Transporters

Due to the importance of zinc as a component of many proteins, in particular DNA polymerases, proteases and ribosomal proteins, most bacteria must have effective systems for zinc uptake. Such zinc transporters include systems with either high or low affinity for zinc.

### 1.6.2.1 High-affinity Uptake Systems

Striking examples of high affinity<sup>5</sup> uptake systems are the ABC transporters. ABC stands for adenosine triphosphate-binding cassette. In general, ABC transporters utilise the energy released by ATP binding, ATP hydrolysis and ADP-P<sub>i</sub> release to transport substrates vectorially across cell membranes.

Members of the ABC transporter family transport a variety of substrates (Linton & Higgins, 2007), with members belonging to cluster 9 of the family mainly transporting zinc. Such high affinity zinc uptake systems have been identified in almost all bacterial species (Hantke, 2005).

In many bacteria, their high-affinity zinc uptake system is encoded by the *znuABC* genes and consists of the ZnuB channel, the ZnuC ATPase component, which provides the energy necessary for ion transport through the inner membrane, and ZnuA, a soluble protein that captures Zn(II) in the periplasm with high efficiency and delivers it to ZnuB (Patzner and Hantke, 1998). The ZnuABC transporters have been studied in a number of bacteria, including *Synechococcus* sp. PCC7942 (Phung *et al.*, 1994), *Nostoc punctiforme* (Hudek *et al.*, 2013a), *E. coli* (Patzner & Hantke, 1998; Chandra *et al.*, 2007), *Streptococcus pneumoniae* (Dintilhac & Claverys, 1997), *Salmonella enterica* (Campoy *et al.*, 2002) and *Yersinia pestis* (Desrosiers *et al.*, 2010).

---

<sup>5</sup> High affinity system whereas the mutation of this operon can inhibit the growth of the cell and upregulated with sensor protein.

A related zinc uptake system (AdcABC/ZitSPQ) has also been characterized in *Streptococcus pneumoniae* (Panina *et al.*, 2003; Reyes-Caballero *et al.*, 2010; Sanson *et al.*, 2015) and some other Gram-positive bacteria, where AdcA is distinguished by a histidine-rich region that may constitute a metal (Zn) binding site that shows clear sequence and structural homology with ZnuA (Panina *et al.*, 2003).

ABC transporters can play a variety of physiological roles, not only in transporting small ions, but also in transporting large polypeptides (Linton & Higgins, 2007; Lebrette *et al.*, 2015). ABC transporters are embedded in the inner membrane, and by interaction with their cognate substrate-binding proteins, outer membrane receptors and the ExbB/ExbD/TonB system, they participate in metal uptake through the outer membrane, the periplasm, and the inner membrane, delivering transition metals to the cytoplasm (Figure 1.06) (Klein & Lewinson, 2011).

Outer membrane receptors related to zinc uptake have been found in several bacteria, and one family are the “ZnuD” proteins. A number of ZnuDs have been discovered and characterized during the last few years, including one each in *Neisseria gonorrhoeae* (Stork *et al.*, 2010) and *Neisseria meningitidis* (Pawlik *et al.*, 2012), two in *Acinetobacter baumannii* (Hood *et al.*, 2012) and four in *Pseudomonas protegens* PF-5 (Lim *et al.*, 2013).

ZnuD, belonging to the TonB-dependent receptor family, is a receptor protein which is up-regulated under Zn-limiting conditions. ZnuD can bind free zinc and transport it into the periplasm by diffusion. On the other hand, ZnuD can additionally recognize a complexed form of zinc and transport it into the periplasm using the TonB system (Stork *et al.*, 2010; Hood *et al.*, 2012).

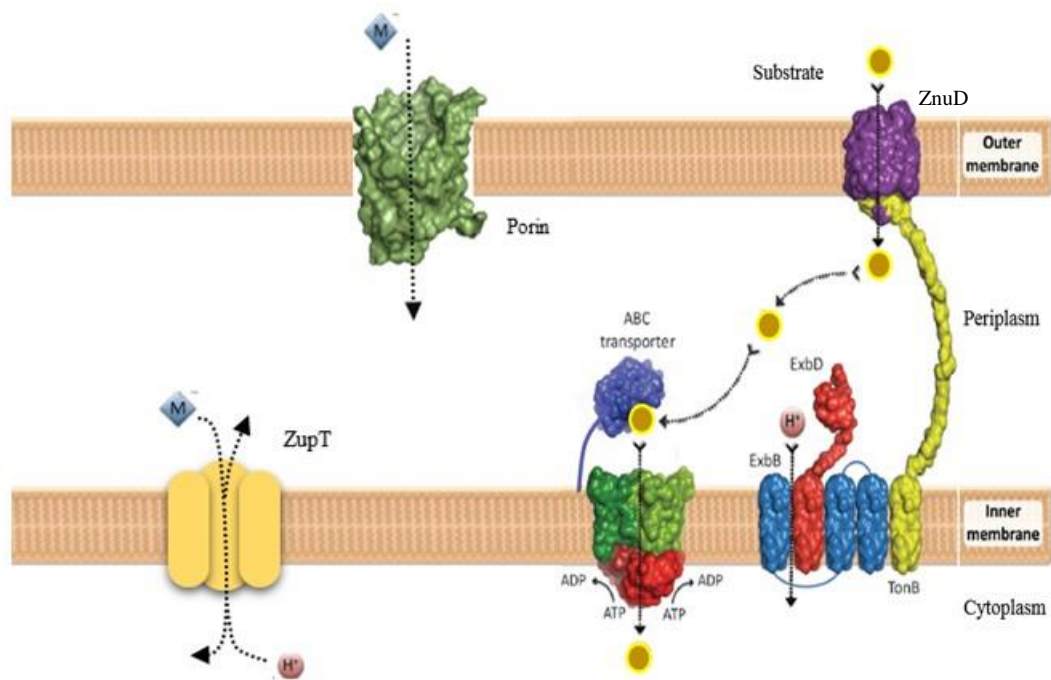


**Figure 1.06 Transporters involved in metal uptake.**

Three types of transporters participate in metal uptake in bacteria. Arrows indicate the directionality of transport. From left to right: ZupT, a zinc uptake protein with low affinity is embedded in the inner membrane. An outer membrane protein porin, is embedded in the outer membrane. An ABC uptake system with high affinity is embedded in the inner membrane with the energy-transducing ExbB/ExbD/TonB complex and outer membrane transporter, receptor. Partly adapted from (Klein & Lewinson, 2011).

Another type of outer membrane transporter are porin proteins, which mediate the diffusion of nutrients and ions into cells (MacDiarmid *et al.*, 2000; Blindauer, 2015) (Figure 1.06). Some porins, including one from the marine cyanobacterium *Synechococcus* sp. WH8102, has been shown to be upregulated by zinc deprivation (Barnett *et al.*, 2014), suggesting they may play a role in zinc uptake.

### 1.6.2.2 Low-affinity Uptake Systems

Zinc permease transporters, described as ZIP (Zrt-like proteins), are named after the first member of the family identified as Zrt1 from *Saccharomyces cerevisiae* (Zhao & Eide, 1996).

ZIP proteins occur in a number of types: subfamilies I and II, GufA subfamilies and LIV-1 subfamilies. Many members of ZIP subfamilies I and II are involved in zinc import (MacDiarmid *et al.*, 2000; Gaither & Eide, 2001) into the cytosol, either from the extracellular space or from organelles. Some ZIP proteins are shown to be constitutively expressed, such as *Zrt1* and *Zrt2* in the yeast *S. cerevisiae* (MacDiarmid *et al.*, 2000), and are inducible by zinc limitation.

The transporter ZupT, formerly *ygiE*, has been identified in *E. coli* (Grass *et al.*, 2002; Taudte & Grass, 2010), guided by similarities to the eukaryotic zinc transporters of the ZIP (Zrt-like proteins) family (Gaither & Eide, 2001). However, the ZupT transporter has a lower affinity for zinc than *ZnuABC* (Grass *et al.*, 2002). The substrate specificity for *E. coli* ZupT shows a broad metal specificity, but displays a clear preference for zinc over other divalent metals (Grass *et al.*, 2002; Taudte & Grass, 2010). The detailed transport mechanism of this protein family remains to be determined. ZupT, like members of the CDF family, depends on the proton motive force to energize zinc import (Gaither & Eide, 2001; Cerasi *et al.*, 2014).

It should be noted that most bacteria have developed both uptake and efflux transporters and many of them have developed two types of uptake/efflux transporters at the same time to deal with the fluctuation of zinc metal in their environment. For instance, *Streptococcus pneumoniae* has both an ABC uptake transporter (Panina *et al.*, 2003; Reyes-Caballero *et al.*, 2010; Sanson *et al.*, 2015) and a *Czc* efflux transporter (Jacobsen *et al.*, 2011; Cheryl *et al.*, 2014). Another example is found in *E. coli*, which has two *ZnuABC* systems for uptake (Patzer & Hantke, 1998; 2000) and *ZntA* for efflux (Patzer & Hantke, 1998; Brocklehurst *et al.*, 1999). A similar example has also been found in *B. subtilis*, which has *ZnuABC* for zinc uptake (Gabriel *et al.*, 2008), and *CadA* (Gaballa *et al.*, 2002) for zinc efflux.

A number of lines of evidence have indicated that the expression of these transporters is regulated through zinc-responsive transcriptional regulators discovered in the last few years.

## 1.7 Zinc Responsive Transcription Regulators

In the last few years, studies have shown that zinc sensing in bacteria is carried out by regulators of several different families, including SmtB/ArsR, MerR, TetR, MarR and the Fur family (Ma *et al.*, 2009). These proteins function as dimeric transcription factors that bind to palindromic DNA sequences in the promoters of regulated genes (Ma *et al.*, 2009). The following section focuses on Fur family proteins.

### 1.7.1 The Fur Family of Metal Sensing Proteins

The Fur “ferric uptake repressor” family of proteins is widespread within bacteria, with around 800 homologs represented in different databases (Lee & Helmann, 2007). Members of the Fur family function as repressors by binding to DNA targets that overlap promoter sequences, thus blocking access of the RNA polymerase (Lucarelli *et al.*, 2007; Ma *et al.*, 2009; Napolitano *et al.*, 2012; Pérard *et al.*, 2016). The Fur family includes proteins that, despite showing broad sequence similarity and a similar composition of structural domains, are diverse enough to respond to distinct stimuli.

This family includes members such as Zur (Outten & O'Halloran, 2001; Shin *et al.*, 2011; Gilston *et al.*, 2014), Fur (Pohl *et al.*, 2003; Sheikh & Taylor, 2009; Pérard *et al.*, 2016), Nur (Ahn *et al.*, 2006; An *et al.*, 2009), and Mur (Diaz-Mireles *et al.*, 2004; Bellini & Hemmings, 2006; Green *et al.*, 2013), which sense specific divalent metals (Zn, Fe, Ni and Mn, respectively) (Figure 1.07). Also included are PerR (Traoré *et al.*, 2006; Giedroc, 2009; Jacquamet *et al.*, 2009) and Irr (Hamza *et al.*, 1998; Anderson *et al.*, 2011) which sense cytoplasmic peroxides and heme, respectively.

Mur	Fur		Nur		Zur
Mn	Fe	Co	Ni	Cu	Zn

**Figure 1.07 Members of the Fur family sensors.**

The Fur family have members that sense different metal ions, including: Fur for Fe; Zur for Zn; Mur for Mn; and Nur for Ni.

Since 2003, a number of crystal structures of metal-bound Fur regulators have been reported, including proteins from *Pseudomonas aeruginosa* (PaFur) (Pohl *et al.*, 2003) and *Vibrio cholerae* (VcFur) (Sheikh & Taylor, 2009), *Mycobacterium tuberculosis* (MtZur) (Lucarelli *et al.*, 2007), *Streptomyces coelicolor* (ScZur) (Shin *et al.*, 2011) and (ScNur) (Ahn *et al.*, 2006), *E. coli* ( EcZur) (Gilston *et al.*, 2014) and *Bacillus subtilis* (BsPerR) (Jacquamet *et al.*, 2009).

Structural analysis of these proteins has revealed that they are homodimeric (Lucarelli *et al.*, 2007; An *et al.*, 2009; Jacquamet *et al.*, 2009; Sheikh & Taylor, 2009; Ma *et al.*, 2011; Shin *et al.*, 2011; Gilston *et al.*, 2014) (Figure 1.08A), and that each monomer consists of an N-terminal DNA binding (DB) domain, a C-terminal dimerization (D) domain, and a hinge loop between the two (Figure 1.08B).

Their homodimeric nature allows DNA interactions mainly with palindromic or pseudo-palindromic regions, where a ‘recognition helix’ from a winged helix-turn helix motif is located in the major groove of the oligonucleotide and is critical for specificity (Huffman & Brennan, 2002).

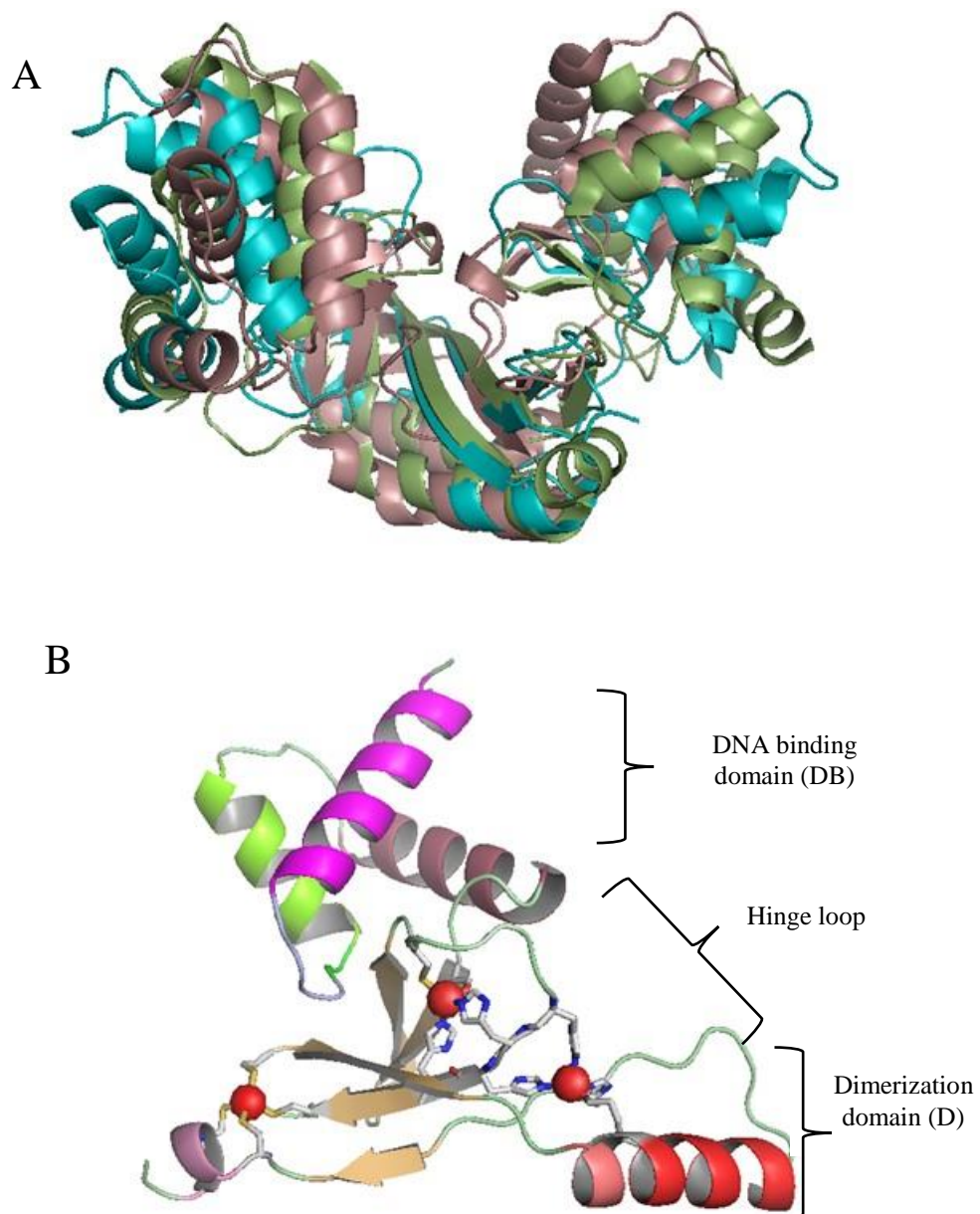


**Figure 1.08 Crystal structures of Fur family proteins.**

(A) Ribbons representing three Fur family proteins as homodimers with a superposition of the C-terminal dimerization domain, including Nur from *S. coelicolor* ((Ahn *et al.*, 2006); pdb 3EYY, salmon), Zur from *E. coli* ((Gilston *et al.*, 2014); pdb 4MTE, green) and PerR from *B. subtilis* ((Jacquamet *et al.*, 2009); pdb 3F8N, cyan). (B) One monomer of Zur from *S. coelicolor* ((Shin *et al.*, 2011); pdb 3MWM) reveals DNA binding domain and a dimerization domain containing a hinge loop.

The winged helix domain is formed by  $\alpha\alpha\alpha\beta\beta\beta$  secondary structure elements (Figure 1.09A) such as in (PaFur) (Pohl *et al.*, 2003), (VcFur) (Sheikh & Taylor, 2009), (BsPerR) (Jacquamet *et al.*, 2009), (EcZur) (Gilston *et al.*, 2014) and (ScNur) (Ahn *et al.*, 2006) or  $\alpha\alpha\beta\beta\beta$

secondary structure elements (Figure 1.09B) such as in (MtZur) (Lucarelli *et al.*, 2007) and (ScZur) (Shin *et al.*, 2011).

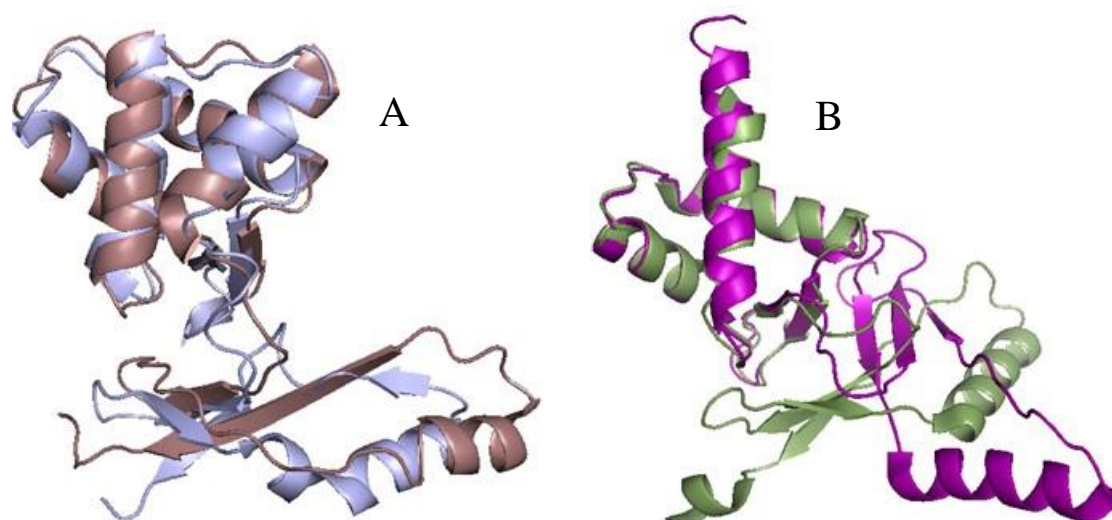


**Figure 1.09 Crystal structures of members of the Fur family.**

Ribbons represent the superposition of the winged helix DNA binding domains for (A)  $\alpha\alpha\alpha\beta\beta\beta$  and (B)  $\alpha\alpha\alpha\beta\beta\beta$  fold. (A) Nur from *S. coelicolor* (Ahn *et al.*, 2006); pdb 3EYY, cyan) and PerR from *B. subtilis* ((Jacquamet *et al.*, 2009); pdb 3F8N, salmon). (B) Zur from *S. coelicolor* ((Shin *et al.*, 2011); pdb 3MWM, green) and Zur from *M. tuberculosis* ((Lucarelli *et al.*, 2007), pdb 2O03, purple) .

These proteins usually exhibit two or three metal-binding sites (Figure 1.10). One site lies in the inter-domain hinge-loop region. The other site is in the D-domain, constructed by four conserved cysteines near the C-terminus. Alternatively, a site at the surface of the D-domain pointing toward the hinge region is present (Figure1.08B).

Our understanding of the mechanism of Fur family proteins was significantly advanced by the determination of the crystal structure of *Bacillus subtilis* PerR (Traoré *et al.*, 2006; Jacquamet *et al.*, 2009). In *B. subtilis* most peroxide-inducible oxidative stress genes are regulated by a metal-dependent repressor, PerR, a “redox sensing” transcriptional regulator (Lee & Helmann, 2006; Jacquamet *et al.*, 2009). PerR is a homodimer protein which contains two binding sites, zinc in its structural site and Mn or Fe in a regulatory site in each monomer, which may work as PerR-Zn-Mn or PerR-Zn-Fe.



Reaction of PerR-Zn-Fe with low levels of hydrogen peroxide ( $H_2O_2$ ) leads to oxidation of two His residues, thereby leading to de-repression (Lee & Helmann, 2006). Structural comparison between inactive apo-PerR-Zn (Traoré *et al.*, 2006) and metallated active forms PerR-Zn-Mn (Jacquamet *et al.*, 2009) of BsPerR suggested that regulatory metal binding caused the DB-domains to swing around the hinge region with respect to the D-domain, from an open (swung-out) to a closed (converged) conformation (Traoré *et al.*, 2006; Jacquamet *et al.*, 2009) (Figure 1.11). This process leads to a model that the rearrangement of DB domains by binding a regulatory metal in the hinge region is responsible for the allosteric transition of all Fur family regulators from the inactive open conformation to the active closed conformation (Giedroc, 2009).

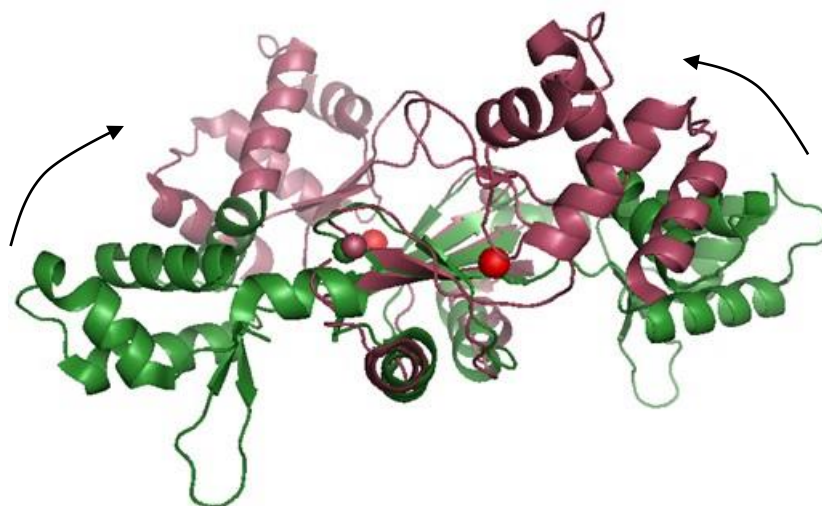


**Figure 1.11 Allosteric structural changes in PerR from *Bacillus subtilis*.**

Ribbon representation of the PerR-Zn-apo and PerR-Zn-Mn crystal structures in *B. subtilis*. Superposition of the dimer structures of PerR-Zn-apo ((Traoré *et al.*, 2006); pdb 2FE3, green) and PerR-Zn-Mn ((Jacquamet *et al.*, 2009); pdb 3F8N, maroon). The structural Zn(II) ions are in green or maroon and the Mn(II) regulatory ions are in red. Allosteric structural changes induced by the binding of regulatory Mn(II) to the sensory site.

Moving to the member of the Fur family that is of most interest to the current project, the Zur protein will be discussed in greater detail in the following sections.

## 1.7.2 Zinc Uptake Regulators: The Zur Sensor

Research on zinc sensor proteins has burgeoned in the past few decades and significant progress has been made regarding 3-dimensional structures. Zur proteins, zinc uptake regulators that sense Zn(II), have 4-coordinate sites formed by mixtures of Cys, His, Glu, and Asp.

Early studies clearly indicated that Zur proteins exhibited sensitivity at femtomolar levels,  $\sim 2.0 (\pm 0.1) \times 10^{-16}$  M, of free intracellular zinc (Outten & O'Halloran, 2001; Gabriel *et al.*, 2008) and regulate the high-affinity zinc uptake system, *znuABC* (Patzner & Hantke, 2000; Gilston *et al.*, 2014).

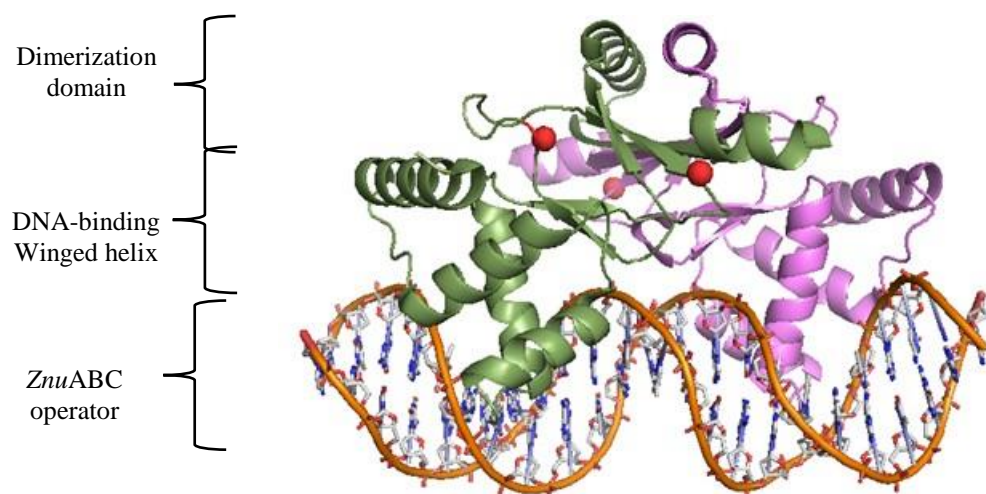


**Figure 1.12 Crystal structure of the EcZur dimer binding to the *znuABC* promoter**

The winged helix-turn-helix motif of Zur located in the major groove of its recognition sequence in the *znuABC* promoter from *E. coli* ((Gilston *et al.*, 2014); pdb 4MTE). The two monomers are highlighted as green and pink ribbons, DNA strands are shown in orange, and zinc ions as red spheres.

Zur proteins, like all members of the Fur family proteins, are homodimeric DNA-binding proteins with two functional domains: a DNA-binding domain with a winged helix-turn-helix (wHTH) motif and a dimerization domain. The zinc-sensing sites are located in the inter-domain region of Zur, and metal occupancy produces conformational changes that enable DNA binding. When sufficient zinc is available, the metallated form of Zur binds operator sequences

in Zur-regulated promoters, resulting in repression of gene expression (Figure 1.12) (Guerra *et al.*, 2011).

### 1.7.2.1 Metal Sites in Zur Proteins

Metal population in Zur sensors seems to be problematic, and as a consequence there is some controversy regarding the stoichiometry as well as the role of the various sites.

Shin and colleagues clarified the structure of the Zur protein from *S. coelicolor*, with three zinc sites per monomer, using X-ray crystallography (Shin *et al.*, 2011). In the same study (Shin *et al.*, 2011), they found that two of the metal ions were in the dimerization domain, and one was located in the hinge region between the dimerization and the DNA binding domain. Each of the metal sites exhibited different structural and chemical environments, depending on its functional role. Site 1 is tetrahedrally coordinated to a cluster of sulfur ligands as follows: Cys-90 and Cys-93 from the dimerization domain and Cys-130 and Cys-133 located at the C terminus (Figure 1.13A). This corresponds to a structural zinc site that is also present in many other Fur family proteins.

In contrast, site 2 is formed by Asp-65, Cys-79, His-85, and His-87 (Figure 1.13A). This site occupies a strategic position in the protein structure, since it is coordinated by two amino acids from the DNA binding domain (Asp-65 and Cys-79) and two from the dimerization domain (His-85 and His-87). Site 3 is located in the core of the dimerization domain. Here, the Zn(II) ion is tetrahedrally coordinated by three histidines (His-84, His-86, and His-122) and one glutamate (Glu-105) (Figure 1.13A). All three sites are essentially conserved in *Streptomyces coelicolor* (Shin *et al.*, 2011), *Bacillus subtilis* (Ma *et al.*, 2011) and *Mycobacterium tuberculosis* (Lucarelli *et al.*, 2007) (Figure 1.10).

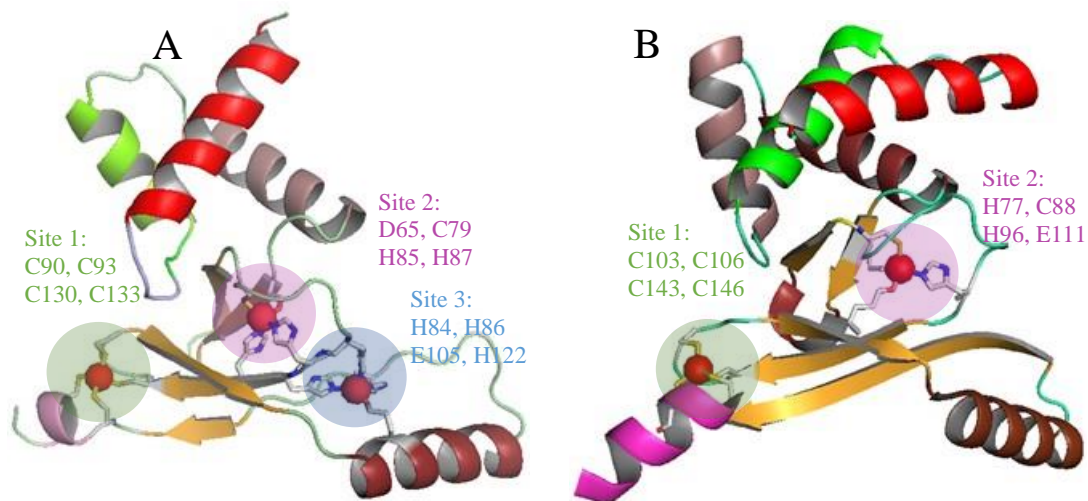


### Figure 1.13 Zinc-binding sites in Zur proteins.

(A) Ribbon represents the crystal structure of Zur from *S. coelicolor* ((Shin *et al.*, 2011); pdb 3MWM) which presents three binding sites. (B) Ribbons represent the crystal structure of Zur from *E. coli* ((Gilston *et al.*, 2014); pdb 4MTE) which presents two binding sites. The zinc-binding sites are highlighted in green (site 1: structural ZnCys<sub>4</sub> site), pink (site 2: sensory site) and cyan (site 3). The colours presented in this figure are the same colours also used in the alignment picture (Figure 1.10).

Another example from *E. coli*, EcZur reveals two distinct Zn(II) binding sites in each monomer: Zn(II) in the structural site 1 is bound to four sulfur atoms from Cys-103, Cys-106, Cys-143, and Cys-146 and the Zn(II) in site 2 is bound by the residues His-77, Cys-88, His-96, and Glu-111 (Gilston *et al.*, 2014) (Figure 1.13B).

In all examples quoted there is an agreement that site 2 plays the critical role as the major sensory site and site 3 is less clear (Barnett *et al.*, 2012). The structural ZnCys<sub>4</sub> site 1 is always populated while a sensory site readily binds and releases zinc (Tottey *et al.*, 2012).

Based on the availability of Zn(II) to bind to the sensory site, Zur containing only one Zn(II) ion per monomer (Zur:Zn<sub>1</sub>, with Zn(II) exclusively in the structural Cys<sub>4</sub> site) does not bind DNA. In the presence of excess Zn(II), Zur (presumably Zur<sub>2</sub>:Zn<sub>4</sub> for *E. coli* and either Zur<sub>2</sub>:Zn<sub>4</sub> or Zur<sub>2</sub>:Zn<sub>6</sub> for other members) can bind to the *znu* promoter and sterically hinders the binding of RNA polymerase (Outten & O'Halloran, 2001).

Recently, the different phenotypes of  $\Delta zur$  mutants have been studied (Shin *et al.*, 2007). It was reported that  $\Delta zur$  mutant from *Streptomyces coelicolor* A3 grew more slowly and reached lower plateau values than wild-type cells (Shin *et al.*, 2007). Growth was significantly retarded on plates, and very small numbers of spores and quantities of the blue antibiotic pigment, actinorhodin, were observed. Based on a similar observation, Sein-Echaluce and co-workers demonstrated that a  $\Delta zur$  mutant displayed a distinct phenotype in *Anabaena* sp. PCC 7120 (Sein-Echaluce *et al.*, 2014).

Phenotypic differences in  $\Delta zur$  mutants demonstrate the importance of the Zur protein, not only in regulating *ZnuABC* but probably other genes as well.

### 1.7.3 The Functions of Zur

#### 1.7.3.1 Zur as a Repressor

Evidence has been reported that, in addition to repressing *znuABC*, Zur can also repress a number of genes encoding homologues of ribosomal proteins (Panina *et al.*, 2003; Gilston *et al.*, 2014). For example, the genetic response to zinc starvation/limitation in *B. subtilis* includes not only the de-repression of its high-affinity zinc uptake system, an ABC transporter encoded by the *ycdHI-yceA* operon (Gaballa *et al.*, 2002), but also that of three genes (*ytiA*, *rpmGC*, and *yhzA*) encoding paralogues of ribosomal proteins (Panina *et al.*, 2003).

Under depletion conditions, the *ytiA* gene (a non-zinc-containing L31 paralog, C<sup>-</sup>) is de-repressed and the newly synthesized YtiA replaces RpmE (zinc-containing ribosomal protein L31, CxxC motif, C<sup>+</sup>) (Akanuma *et al.*, 2006). Similar data have been expressed for *Streptomyces coelicolor* (Shin *et al.*, 2007) and for *M. tuberculosis* (Prisic *et al.*, 2015). Since ribosomes are highly abundant in rapidly growing cells, the presence of two or three zinc-

containing ribosomal proteins represents a large reservoir of zinc, and this may in fact account for the majority of intracellular zinc (Lee & Helmann, 2007; Shin *et al.*, 2007).

Another observation was made with *E. coli* K-12, in which the Zur regulon includes the *znuABC* zinc uptake gene cluster, in addition to genes encoding a pair of ribosomal proteins (L31p and L36p) and a periplasmic zinc trafficking protein (ZinT) (Hantke, 2005; Gilston *et al.*, 2014). These three cellular processes, zinc importer systems, ribosomal proteins and periplasmic scavenging proteins, contribute to zinc homeostasis in *E. coli*.

A further study by Kallifidas and colleagues found that Zur from *Streptomyces coelicolor* controls a cluster of genes predicted to direct synthesis of an uncharacterized siderophore-related non-ribosomally encoded peptide designated coelibactin (Kallifidas *et al.*, 2010). They reported that disruption of a key coelibactin biosynthetic gene suppressed the Zur sporulation phenotype, suggesting that deregulation of coelibactin synthesis inhibits sporulation, and that coelibactin might be a zinc-chelating compound (Kallifidas *et al.*, 2010) – a “zincophore” (see Section 1.8).

### **1.7.3.2 Zur as an Activator**

Research by Huang and colleagues has suggested a new function for the Zur protein. They demonstrated *in vivo* and *in vitro* that in addition to acting as a repressor of Zn(II) uptake systems and other genes, Zur in the bacterial phytopathogen *Xanthomonas campestris pathovar campestris* (Xcc) acts as an activator of a Zn(II) efflux pump (Huang *et al.*, 2008). Xcc Zur binds to a canonical zur-box with ~30-bp AT-rich sequence in the promoters of the genes encoding putative Zn(II) uptake systems, but also to a 59-bp GC-rich sequence with a 20-bp inverted repeat overlapping the promoter's –35 to –10 sequence of the gene encoding a Zn(II) export system (Huang *et al.*, 2008).

A similar observation was made by Teramoto and colleagues, who discovered that Zur from *Corynebacterium glutamicum* can also activate the cation diffusion facilitator (*zrf*) and the metal-translocating P-type ATPase (*zra*) with two Zur boxes, each one overlaps by 21 bp the putative -35 region of both the *zrf* and *zra* promoters (Teramoto *et al.*, 2012).

In another example, from *Anabaena* sp. PCC 7120, Zur was shown to bind to *isiA* at high concentration of zinc, and to *petE* at lower concentration of zinc (Napolitano *et al.*, 2012). This may mean that Zur can work as a repressor for *isiA* and may act as activator for *petE*. The proteins IsiA and PetE are involved in iron and copper homeostasis, respectively.

Like Fur, Zur may thus function as a global regulator, not only to control zinc ion uptake, but also zinc ion storage and mobilization (Lee & Helmann, 2007; Kallifidas *et al.*, 2010).

Despite the progress made in understanding the structure, mechanism and selectivity of zinc sensor proteins and uptake/efflux transporters, many questions remain as to the ways in which organisms integrate these complex zinc-specific systems to achieve zinc homeostasis, particularly under the conditions of vanishingly small concentrations of “free” zinc thought to exist in the environment of some cells, such as in the open ocean.

## 1.8 Zincophores: Molecules whose Time Has Come

A zincophore - a zinc-binding ligand involved in zinc uptake- was first studied and reported in early 1997 (Zwicker *et al.*, 1997). They noted that growing *Amycolatopsis orientalis* under zinc-limiting conditions, the bacterium was able to produce [S,S] ethylenediamine disuccinic acid (EDDS)<sup>6</sup>, which has structural and functional similarities to EDTA (Figure 1.14) (Zwicker *et al.*, 1997). It is possible that *A. orientalis* uses EDDS as a zincophore to satisfy its Zn(II) demands (Hantke, 2001a).

---

<sup>6</sup> EDDS is a cation chelator isomeric to EDTA.

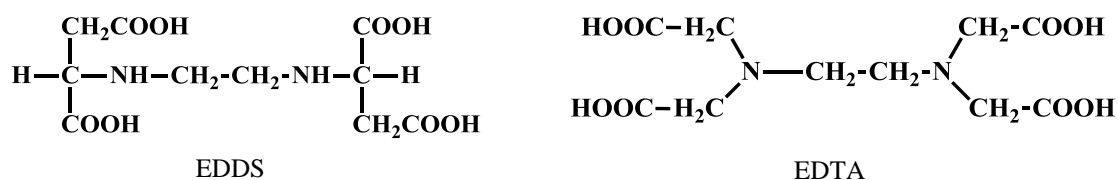


**Figure 1.14 Structures of EDDS and EDTA.**

Taken from (Zwicker et al. 1997).

Napolitano and colleagues (2012) studied zinc homeostasis in *Anabaena*, a genus of filamentous cyanobacterium. These authors mentioned that *Anabaena* might synthesise and excrete a zinc binding ligand a “zincophore”, reminiscent of siderophores<sup>7</sup> for iron (Reid *et al.*, 1993; Holt *et al.*, 2005; Martin *et al.*, 2006) or chalkophores<sup>8</sup> for copper (Kim *et al.*, 2004; Rosenzweig & Balasubramanian, 2008).

Moving from marine organisms to pathogenic microorganisms, there is another fascinating mention of zincophores (Citiulo *et al.*, 2012). In this study it was reported that the fungus *Candida albicans*<sup>9</sup> secretes a scavenger protein, the pH-regulated antigen1 (Pra1), which sequesters zinc from host cells. The Pra1 protein then reassociates with the fungal cell membrane transporter ZRT1, that encodes a high affinity zinc transporter to acquire this essential metal (Citiulo *et al.*, 2012). Although the suffix “-phore” is normally related to small molecules, not proteins, this is the first report of a zinc scavenger protein that has been dubbed a zincophore.

---

<sup>7</sup> Siderophores (Greek: "iron carrier") are small, high-affinity iron chelating compounds secreted by microorganisms

<sup>8</sup> Chalkophore (Greek: "copper carrier") are small, high-affinity copper chelating compounds secreted by microorganisms

<sup>9</sup> *Candida albicans* is one of the few fungal species of the normal human microbiome.

In 2002, a new type of siderophore, coelibactin A3 (2), was reported from *Streptomyces coelicolor* by analysis of the NRPS<sup>10</sup> proteins (Figure 1.15A) (Bentley *et al.*, 2002). However, based on the analysis of known siderophore structures, the structure of this type of siderophore is not expected to possess a strong affinity for Fe(III) (Hider & Kong, 2010). Later Kallifidas and colleagues (2010) reported that the zinc-responsive regulator, Zur, controls expression of the coelibactin gene cluster in *Streptomyces coelicolor*. In 2012, Zhao and co-workers suggested that the reduction in the terminal ring of coelibactin (Figure 1.15A) generates a coelibactin candidate (Figure 1.15B) which will bind zinc under physiological conditions in a bidentate mode, utilising the terminal carboxylate and the nitrogen of the adjacent heterocyclic ring (Zhao *et al.*, 2012). In this study, Zhao and his co-workers suggested that coelibactin, a putative NRPS product, is a zincophore which is a new class of biogenic zinc-binding ligands. (Zhao *et al.*, 2012).

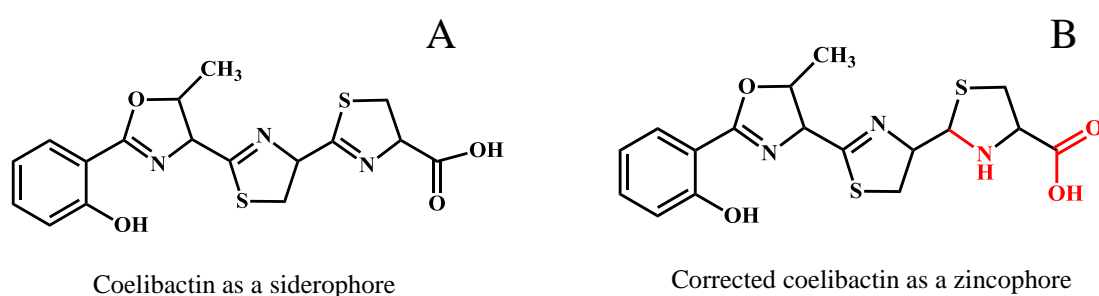


**Figure 1.15 Predicted structure of coelibactin from *Streptomyces coelicolor*.**

(A) Coelibactin as a siderophore (Bentley *et al.*, 2002); (B) Corrected coelibactin as a zincophore (Zhao *et al.*, 2012).

<sup>10</sup> NRPS: Non-ribosomal peptide synthesis.

## 1.9 Metals in Cyanobacteria

Cyanobacteria are part of the phytoplankton<sup>11</sup>, colloquially also called blue-green algae. They are a major phylum of the superkingdom bacteria, and acquire their name from the bluish pigment phycocyanin (Scanlan *et al.*, 2009), although they can display many different colours. Without these organisms, life on this planet would be very different, as they are not only the first organisms to develop oxygenic photosynthesis, but are also the ancestors of plant chloroplasts (Blindauer, 2008; Nies, 2012). The numerically dominant cyanobacteria in open ocean waters are the unicellular genera *Synechococcus* and *Prochlorococcus* (see Appendix A. Figure A.01) which contribute significantly to marine CO<sub>2</sub> fixation (Jardillier *et al.*, 2010).

These cyanobacteria have efficiently changed the biogeochemistry of our planet. The evolution and accumulation of oxygen in the atmosphere has dramatically changed the solubility of metal-ion compounds. Whilst Fe(II) was quite abundant before oxygen was present, copper and zinc were locked up in sparingly soluble sulfides. After O<sub>2</sub> accumulated, Fe(II) was oxidised to Fe(III), leading to precipitation of Fe(OH)<sub>3</sub> (and subsequently Fe<sub>2</sub>O<sub>3</sub>), sulfide (S<sup>2-</sup>) was oxidised to sulfate, and both copper and zinc sulfates have good solubility.

Metal requirements in cyanobacteria are higher than in most other prokaryotes, largely due to the requirements for photosynthesis (Shcolnick & Keren, 2006; Hudek *et al.*, 2013b). For example, in *Synechocystis* sp. PCC6803 (Foster *et al.*, 2012), manganese for the oxygen evolving water-splitting enzyme, 22 atoms of iron/pair for the two photosystems, copper for plastocyanin, zinc in carbonic anhydrase to liberate CO<sub>2</sub> for fixation in carboxysomes (So & Espie, 1998) and cobalt for cyanocobalamin are needed. Nickel is used by a bidirectional hydrogenase which can generate dihydrogen gas to remove surplus reducing potential from the

---

<sup>11</sup> Phytoplankton are autotrophic components of the plankton, and generally photosynthetic organisms. This name is derived from the Greek words phyto (plant) and plankton (wanderer or drifter).

light reactions of photosynthesis (Foster *et al.*, 2012), urease and a Ni-dependent superoxide dismutase.

Similar to other organisms, there is a need for cyanobacteria to regulate intracellular metal levels, in which an excess of any metal will cause toxicity while a deficiency will cause stress, leading to reduced growth rates and cell death (Hudek *et al.*, 2013b). As a consequence, cyanobacteria have developed efficient strategies for metal export/uptake and regulation (Shcolnick & Keren, 2006).

### **1.9.1 Zinc Homeostasis in Cyanobacteria**

At concentrations observed in the open ocean (see Section 1.1.1), zinc is not toxic to cyanobacteria. Based on the relationship between zinc concentrations in surface waters and the zinc requirements of marine cyanobacteria, it may be suggested that zinc could be an important selective force acting on cyanobacteria. It ultimately may affect the structure of cyanobacterial communities (Brand *et al.*, 1983; Bruland, 1989) and their ability to fix CO<sub>2</sub> from seawater *via* the carbonic anhydrase enzyme (So & Espie, 1998). For instance, by analysing genomes of cyanobacteria, it has been found that all analysed cyanobacterial genomes contain genes encoding proteins that are predicted to bind zinc ions (Blindauer, 2008).

Genome-mining approaches have identified genes that are strong candidates for potentially requiring zinc, such as carboxysomal carbonic anhydrases, as well as proteins involved in uptake (ABC-type zinc uptake systems) and in the intracellular handling of zinc (metallothioneins and putative COG0523 metallochaperones) (Blindauer, 2008; Barnett *et al.*, 2012). A number of other enzymes in cyanobacteria are also predicted to require zinc for their function, including for example DNA ligase and alkaline phosphatase (Palenik *et al.*, 2003).

Like other bacteria, it was found that zinc homeostasis in cyanobacteria is based on export and uptake systems, which are controlled by their own regulators such as SmtB/ZiaR and Zur (Linton & Higgins, 2007; Barnett *et al.*, 2012; Hudek *et al.*, 2013a; Hudek *et al.*, 2013b). Given the almost complete absence of SmtB/ZiaR homologues in marine cyanobacteria (Blindauer, 2008), only Zur will be reviewed in the following.

### 1.9.1.1 The Zinc Uptake Regulator, Zur in Cyanobacteria

To date, the only zinc-specific metalloregulatory protein from cyanobacteria known to deal with zinc at low levels is the Zur regulator with its regulation of *znuABC* systems and others.

In the freshwater cyanobacterium *Synechocystis* sp. PCC6803, a high affinity zinc-specific ABC transporter, *ZnuABC*, has been identified for the active uptake of zinc from the periplasm (Cavet *et al.*, 2003).

In 2012, researchers working with *Synechocystis* sp. PCC6803 isolated and purified Zur that bind to the promoter located between *slr2043* (*ZnuA*) and *sll1937* (*Zur*) which indicates that Zur can regulate the expression of the *znuABC* system and itself (Tottey *et al.*, 2012).

As recently as 2014, (metallo-)proteomic approaches revealed not only the presence of several zinc-binding proteins, but also demonstrated increased expression of SYNW2224 a putative outer-membrane porin, during the growth of *Synechococcus* sp. WH8102 under zinc-depleted conditions (Barnett *et al.*, 2014).

Bioinformatic and expression analyses of genes mediating zinc homeostasis in *Nostoc punctiforme* (Hudek *et al.*, 2009) have revealed several genes involved in Zn(II) uptake (i) a predicted divalent heavy-metal cation transporter, which is a putative ZIP; ii) Zur, the zinc uptake regulation protein; and (iii) a putative *ZnuABC* system including an ATPase component.

In the same study (Hudek *et al.*, 2009), it was noticed that exposure of *Nostoc punctiforme* cells to 22  $\mu$ M zinc led to the reduction in *zip*, *znuC*, and *zur* expression.

It was found that *Anabaena* sp. PCC 7120 contains FurB (*all2473*) identified as a Zur protein (Nies, 2012). It was also found that dozens of genes that are under Zur control including: two TonB-dependent receptor genes (*alr3242* and *alr4028-4029*) and two further genes (*all4727* and *all4726*) which might be required to provide an export pathway for a possible zinc-chelating substance (a zincophore) (Napolitano *et al.*, 2012). A  $\Delta zur$  deletion mutant in *Anabaena* sp. PCC 7120 showed a change in phenotype, including alterations in septum morphology and the organization of the outermost cell layers, among other features (Sein-Echaluze *et al.*, 2014). Scanning electron microscopy (SEM) analyses showed that  $\Delta zur$  cells displayed a different shape and appeared to be connected by narrower septa, and were also different in culture sedimentation (Sein-Echaluze *et al.*, 2014) (Figure 1.16).

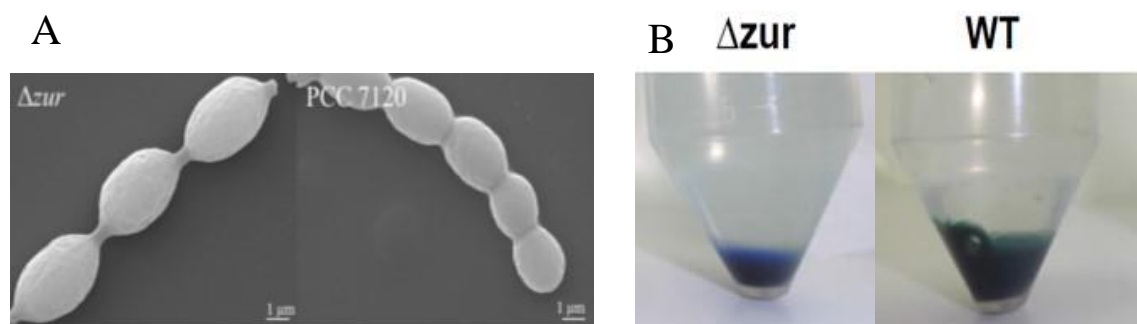


**Figure 1.16** *Anabaena* sp. PCC 7120  $\Delta zur$  phenotype under zinc deplete conditions.

Analyses of cell surface and culture sedimentation of *Anabaena* sp. PCC 7120 in  $\Delta zur$  and in WT. (A) SEM photographs from exponentially growing cultures, and (B) Sedimentation of the strains indicating changes in the phenotype under zinc deplete conditions. Taken from (Sein-Echaluze *et al.*, 2014).

BLAST searches in the genomes of marine cyanobacteria have retrieved members of the COG0735 family, which corresponds to the Fur family (Barnett *et al.*, 2012). In the same study the Fur family of proteins from marine cyanobacteria clustered into four distinct groups, and

through comparison with *Synechocystis* Zur and Fur, suggested that one branch corresponds to ‘Zurs’, light purple bubble (Figure 1.17).

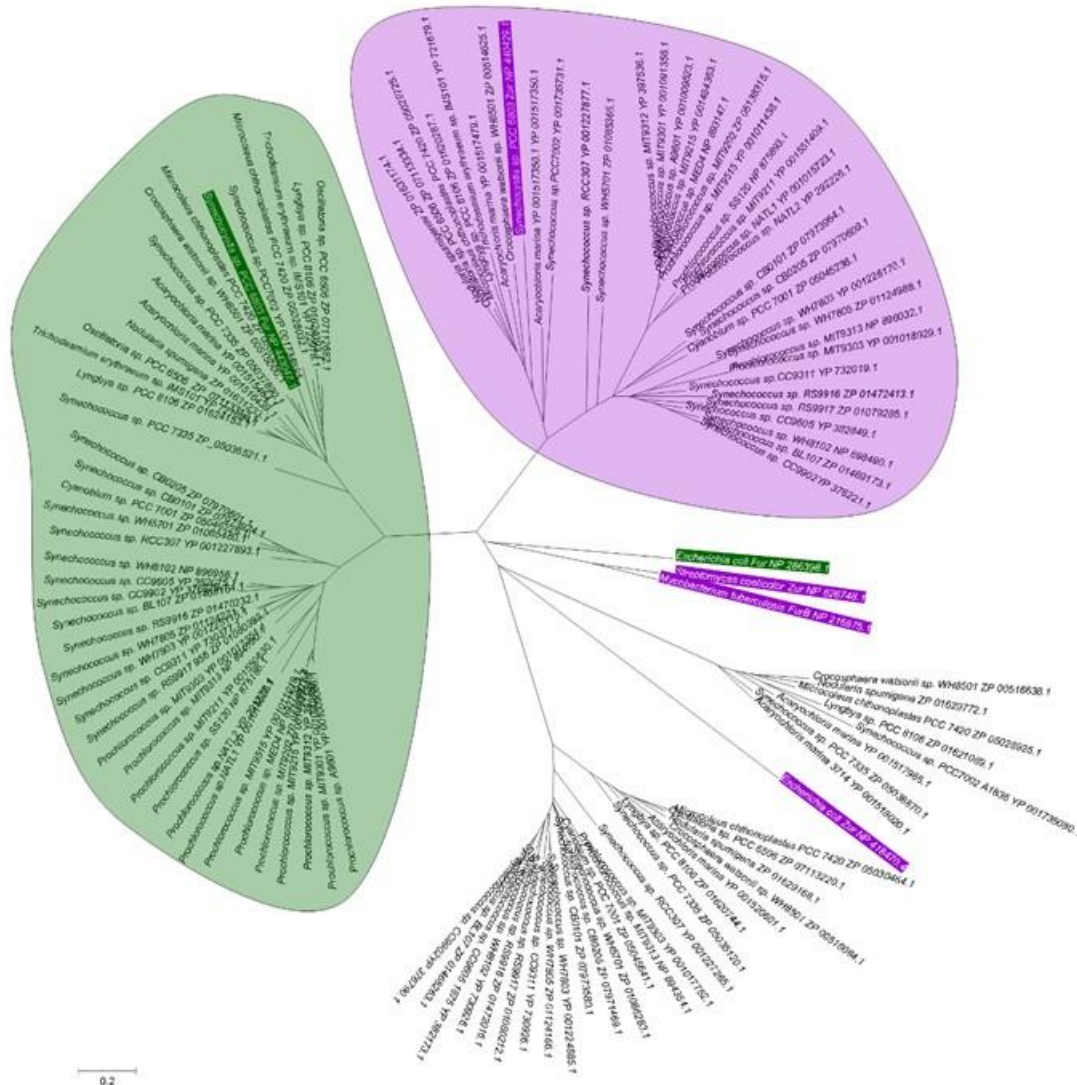


**Figure 1.17 Phylogenetic relationship among Fur-like proteins from marine cyanobacteria.**

Sequences are labelled with species and protein accession number; four clear branches were found. Inclusion of *Synechocystis* Zur and Fur allows the suggestion that the branches containing these sequences correspond to zinc-responsive (light purple bubble) and iron-responsive (light green bubble) regulators. Adapted from (Barnett *et al.*, 2012).

Sequence comparisons between Zur proteins from cyanobacteria and known structurally characterised Fur family proteins show that an equivalent of site 2 cannot be identified in the cyanobacterial Zur homologs, nor are all residues of site 3 the same as in structurally

characterized Zur proteins (Figure 1.18A) (Barnett *et al.*, 2012). We have constructed a homology model of the representative from *Prochlorococcus* sp. SS120 (CCMP1375). The model obtained (Figure 1.18B and B1) suggests, in concordance with the sequence analysis, that the cyanobacterial Zurs may contain a variation of site 3, comprising Asp-80, His-82, Cys-98, and His-118. Thus, the predicted zinc-sensing site is in a location corresponding to site 3, but has a ligand set that is similar to that of site 2, which may suggest that the zinc-binding affinity of this site is also closer to that of site 2 (Barnett *et al.*, 2012).

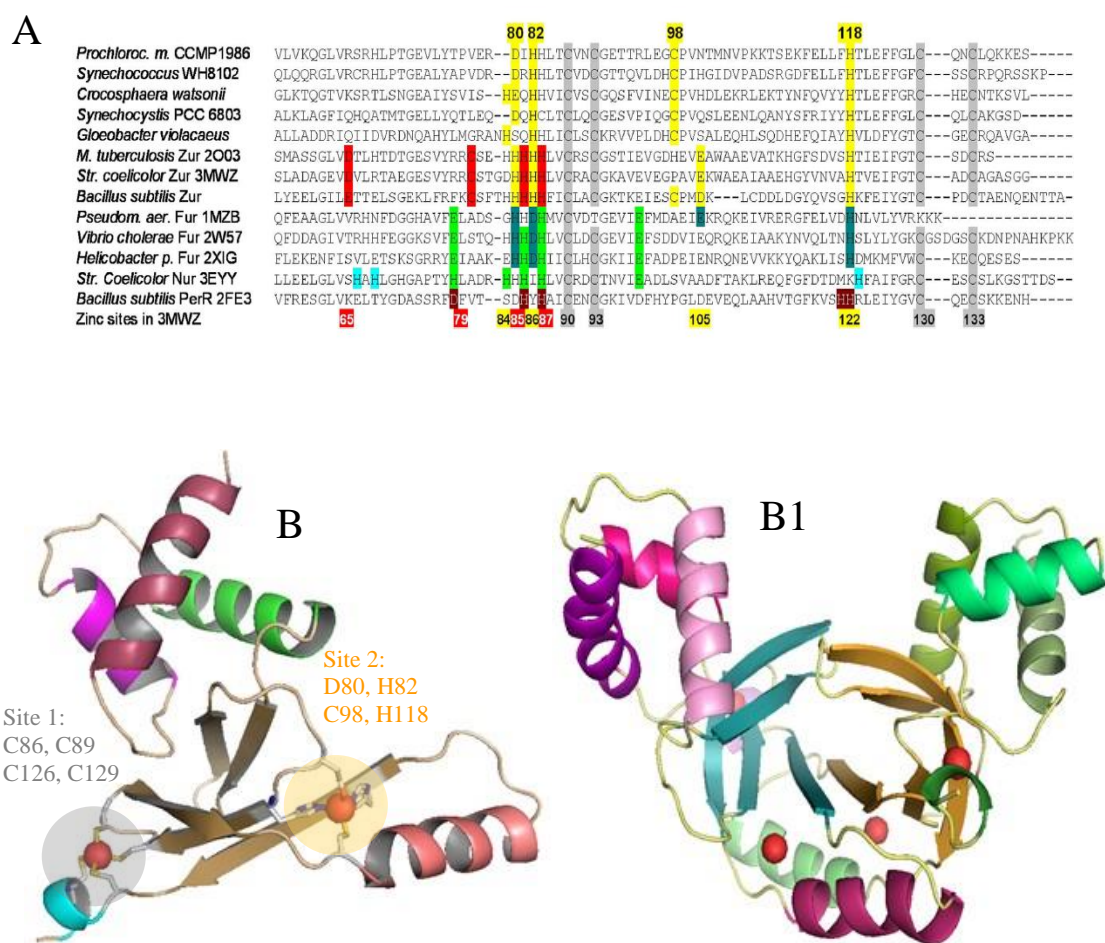


**Figure 1.18 Structural features of Zur proteins.**

(A) Portion of a sequential alignment of structurally characterized Fur-family proteins from various bacteria together with selected sequences from cyanobacteria. The three zinc-binding sites are highlighted in grey (site1, structural site), red and green (site 2, major sensory site), and yellow and cyan (site 3). The consensus sensory site 2 is clearly not present in cyanobacterial sequences, but a variation of site 3, highlighted in yellow, can be discerned. (B) Homology model for Pro1502, a predicted Zur protein from *Prochlorococcus marinus* sp. CCPM1375 and a monomer with two binding sites, B, and as a dimer with four binding sites, B1. Adapted from (Barnett *et al.*, 2012).

Several advances in the area of identifying Zur regulons have been made recently. In 2010, Novichkov and co-workers predicted the Zur boxes from cyanobacteria with 23 bp in the RegPrecise database (Novichkov *et al.*, 2009) (Figure 1.19).



**Figure 1.19 Sequence logo for Zur boxes in cyanobacteria.**

Consensus sequence deposited in the RegPrecise database (Novichkov *et al.*, 2009), using 75 sequences from the genomes of *Synechococcus* sp. PCC7002, *Synechocystis* sp. PCC6803, *Cyanothece* sp. ATCC51142, *Cyanothece* sp. PCC8801, *Cyanothece* sp. PCC7425, *Microcystis aeruginosa* NIES-843, *Nostoc* sp. PCC7120, *Trichodesmium erythraeum* IMS101, *Synechococcus elongatus* PCC7942, *Prochlorococcus marinus* str. MIT9313, *Synechococcus* sp. JA-3-3Ab, *Synechococcus* sp. WH8102, *Gloeobacter violaceus* PCC7421 and *Thermosynechococcus elongatus* BP-1.

Unfortunately no crystal structure of a Zur protein from any cyanobacterium has, so far, been elucidated. In conclusion, although cyanobacteria are at the root of what life and marine trace metal chemistry are like today, their zinc requirements require further study.

## 1.10 Research Motivation and Aims

*Synechococcus* sp. WH8102 is an open ocean cyanobacterium isolated in March 1981 from the North Atlantic Ocean, specifically the Sargasso Sea, and belongs to the subcluster 5.1 A, Clade III of marine *Synechococcus* (Waterbury *et al.*, 1986) (see Appendix A Figure A.01). The size of the genome of this strain is 2.43 (Mb) and the number of protein-coding genes is 2,519 (Palenik *et al.*, 2003; Scanlan *et al.*, 2009), while the size of this strain is 1  $\mu\text{m}$ . These bacteria possess a unique type of swimming motility by propelling themselves in seawater at speeds of up to 25 mm/sec without any external organelle or flagella.

Clade III marine *Synechococcus* members, of which *Synechococcus* sp. WH8102 is one strain, are prominent components of the marine biosphere being especially abundant in oligotrophic regions of the world's oceans (Zwirgmaier *et al.*, 2008). The strain is obligately marine, having elevated growth requirements not only for Na(I), but also for Cl<sup>-</sup>, Mg(II) and Ca(II); it has the ability to acquire major nutrients and trace metals at submicromolar concentrations (*e.g.* P, Fe and Zn) found in the oligotrophic open seas.

This strain has been studied under zinc limitation conditions and found to be perfectly adapted to such conditions (Barnett *et al.*, 2014). The use of immobilised zinc affinity chromatography (Zn(II)-IMAC) has enabled the capture and detection of a number of proteins with a potential function in zinc metabolism. Apart from the detection of a predicted periplasmic zinc-binding protein (ZnuA), along with several other periplasmic binding proteins, the most significant finding concerns two predicted porins with zinc-binding affinity, novel candidates for mediating zinc uptake across the outer membrane (Barnett *et al.*, 2014).

Moreover, genomic analysis of *Synechococcus* sp. WH8102 led to the identification of two Fur homologs named Fur (SYNW0865) and Zur (SYNW2401), according to CyanoBase (<http://genome.kazusa.or.jp/cyanobase>).

However, I believe that the bacterium *Synechococcus* sp. WH8102, isolated from Sargasso Sea where zinc organic speciation is dominated and zinc ion is limited (Jakuba *et al.*, 2008a), possesses effective mechanisms both for zinc acquisition and zinc homeostasis that require further study, due to the interesting in the global warming whereas affecting the growth of this bacterium will decrease the carbon fixation and this will lead to increase in the temperature of the universe.

The specific objectives of my PhD study can be summarised as follows:

1. To investigate whether the model marine cyanobacterium *Synechococcus* sp. WH8102 produces ligands that bind to zinc when grown in laboratory culture using an artificial seawater medium. To develop a method for the extraction of such ligands from the culture supernatants of *Synechococcus* sp. WH8102 strain (Chapter 3).
2. To assess whether *Synechococcus* sp. WH8102 can respond to zinc depletion and excess conditions and if so, identify increased or decreased protein expression under those conditions using proteomic approaches (Chapter 4).
3. To express and characterise the Zur transcriptional regulator from *Synechococcus* sp. WH8102 in the presence and absence of Zn(II), *via* protein over-expression in *E. coli* (Chapter 5).
4. To investigate the three dimensional structure of the Zur protein (Chapter 6).
5. To study the effects of zinc release on structure and dynamics of the Zur protein (Chapter 7).
6. To investigate the function of the Zur protein from *Synechococcus* sp. WH8102 by carrying out binding assays to predicted *zur* boxes in the promoter regions of *znuABC* and *smtA* (Chapter 8).

# Chapter 2

## General Materials and Experimental Methods

---

### 2.1 Chemicals and Reagents

All chemicals, microbiological media and reagents used in this study, unless otherwise stated, were purchased from Sigma-Aldrich (Gillingham, Dorset, UK) and Fisher Scientific (Loughborough, Leicestershire, UK). The chemicals were of the highest grade available for use in analytical or chemical biology studies and used without any further purification.

For preparing all reagents and rinsing glassware, ultrapure water obtained from a Milli-Q water purification system (Milli-Q-Millipore, Ultra-Pure, UK) was used.

Highly purified HNO<sub>3</sub> was prepared by sub-boiling quartz distillation of reagent nitric acid (Sigma, Aldrich, UK), then the purified HNO<sub>3</sub> was diluted with Milli-Q water as required.

### 2.2 Media, Bacterial Growth and Incubation Conditions

#### 2.2.1 Cyanobacterial Media and Growth Conditions

Axenic cultures of *Synechococcus* sp. WH8102 originally isolated from the Sargasso Sea in the North Atlantic Ocean, which were kindly supplied by co-supervisor Prof. David Scanlan

(University of Warwick, School of Life Sciences). These bacteria were grown in artificial seawater medium, prepared according to the recipe for Aquil<sup>\*12</sup> medium (Sunda *et al.*, 2005).

**Table 2.01 Anhydrous and hydrous salts used to prepare Aquil<sup>\*</sup> medium.**

Component	Final concentration (M)
Anhydrous salts	
NaCl	$4.20 \times 10^{-1}$
Na <sub>2</sub> SO <sub>4</sub>	$2.88 \times 10^{-2}$
KCl	$9.39 \times 10^{-3}$
NaHCO <sub>3</sub>	$2.38 \times 10^{-3}$
KBr	$8.40 \times 10^{-4}$
H <sub>3</sub> BO <sub>3</sub>	$4.85 \times 10^{-5}$
NaF	$7.15 \times 10^{-5}$
Hydrous salts	
MgCl <sub>2</sub> •6H <sub>2</sub> O	$5.46 \times 10^{-2}$
CaCl <sub>2</sub> •2H <sub>2</sub> O	$1.05 \times 10^{-2}$
SrCl <sub>2</sub> •6H <sub>2</sub> O	$6.38 \times 10^{-5}$

**Table 2.02 Macronutrients and micronutrients added to Aquil<sup>\*</sup> medium.**

Component	Final concentration (M)
NaH <sub>2</sub> PO <sub>4</sub> •H <sub>2</sub> O	$1 \times 10^{-4}$
NaNO <sub>3</sub>	$1 \times 10^{-3}$
EDTA (pH= 8.0)	$1 \times 10^{-4}$
FeCl <sub>3</sub>	$1 \times 10^{-6}$
ZnSO <sub>4</sub> •7H <sub>2</sub> O	$8 \times 10^{-8}$ or $2 \times 10^{-6}$
MnCl <sub>2</sub> •4H <sub>2</sub> O	$1.2 \times 10^{-7}$
CoCl <sub>2</sub> •6H <sub>2</sub> O	$5 \times 10^{-8}$
Na <sub>2</sub> MoO <sub>4</sub> •2H <sub>2</sub> O	$1 \times 10^{-7}$
Na <sub>2</sub> SeO <sub>3</sub> •5H <sub>2</sub> O	$1 \times 10^{-8}$
NiCl <sub>2</sub> •6H <sub>2</sub> O	$1 \times 10^{-8}$
HEPES (pH= 8.0)	$2 \times 10^{-8}$

Briefly, an artificial seawater medium used in this study, Aquil<sup>\*</sup> medium, was prepared according to Sunda *et al.* (2005) and modified by adding different concentrations of zinc ions to the medium. A mineral solution of Aquil<sup>\*</sup> medium was made by dissolving of the anhydrous salts (Table 2.01) in 600 mL of Milli-Q water. Next, the hydrous salts ingredients was diluted

<sup>12</sup> Aquil<sup>\*</sup> medium is a new version of the Aquil medium (Sunda *et al.*, 2005).

to 300 mL (Table 2.01). Then both of medium solutions were mixed and the total volume made up to 1 L and sterilised by autoclaving at 121°C for 20 min. Finally, macronutrients and micronutrients (Table 2.02) were added to the final volume of 1 L broth medium.

To produce standardised bacterium inoculum, axenic cultures of *Synechococcus* sp. WH8102 was grown in 50 mL of Aquil\* medium using 200 mL Erlenmeyer conical flasks, acid washed. The axenic culture flasks were incubated at 20°C under continuous light, at an intensity of 10  $\mu\text{E m}^{-2} \text{s}^{-1}$ , on a constant rotary shaker (INFORS Multitron, UK) at 140 rpm.

For all experiments, the bacterium growth of *Synechococcus* sp. WH8102 in Aquil\* medium was monitored by estimating the optical density (OD) every two days at 750 nm in 1 cm plastic cuvettes (semi-micro disposable polystyrene 1.6 mL capacity, 10 mm light path, Fisher Scientific, UK) and a Shimadzu UV-160U spectrophotometer using 1 mL of culture. Sterile Aquil\* medium was used as a blank. The OD was measured at 750 nm because it has been shown to linearly relate to cell abundance for pico-cyanobacteria (Wilhelm & Trick, 1995; Henley & Yin, 1998).

EDTA was added to the growth Aquil\* medium to buffer any metal present and to chelate any toxic metals (Zhou & Wangersky, 1989; Sunda *et al.*, 2005; Wiramanaden *et al.*, 2008). Two different growth conditions were chosen, including: replete (2  $\mu\text{M}$ ) and depleted (80 nM) of zinc ions in the medium. This corresponds to ca. 400 pM and 16 pM free Zn(II), respectively (estimated using the “Species” module of the SCD database, Sourby Old Farm, UK).

### 2.2.2 Contamination Plates

Contamination plates were used for the detection of heterotrophic contamination in *Synechococcus* sp. WH8102 cultures. To check this, Aquil\* medium prepared in 500 ml Milli-Q water and similar 500 ml Milli-Q water supplemented with 0.15% (w/v) yeast extract and

1.5% (w/v) Bacto-agar. These basal medium solutions were autoclaved separately, cooled to 55 °C and then mixed thoroughly before pouring in the petri plates. Solid agar-plates were streaked with *Synechococcus* sp. WH8102 culture and half of the plates were covered with aluminium foil to prevent the light. The others half of plates were sealed with Parafilm and kept under constant light on the bench.

## 2.3 Analysis of Culture Supernatant

### 2.3.1 Cell Pre-concentration and Ligand Extraction Procedures

Briefly, 1 L of *Synechococcus* sp. WH8102 culture was prepared and grown in Aquil\* medium as described in Section 2.2.1. After 35-40 days, when the culture reached an OD<sup>13</sup><sub>750</sub> of ca 0.3, bacterial biomass from 1 L was harvested by centrifugation (Avanti™ J-25 Centrifuge, Beckman Coulter, UK) at 6,000 × g for 20 min to pellet the cells. In addition, *Synechococcus* sp. WH8102 was completely removed from the collected supernatant by using a filter membrane (GSWP with a pore-size of 0.22 µm) assisted by a vacuum system (Fisher brand, Filter FB- 70155).

Ligands were extracted from culture supernatants by using a polystyrene-divinylbenzene SPE cartridge (Strata™XL-100 µm Polymeric reverse phase, 2 g× 20 mL, Phenomenex, UK) as described previously (McCormack *et al.*, 2003). Briefly, after loading 1L of culture supernatant, the cartridge was washed with 50:50 (v/v) methanol/water to eliminate salts and then the metal-binding ligands and free-metal ligands (organic complexes) were eluted with 50 mL of 1:20:80 (v/v/v) formic acid/water/methanol in the first experiment. For the second experiment, the SPE cartridge was first washed with 11.2 mM ammonium bicarbonate to eliminate salts and then the

---

<sup>13</sup> OD<sub>750</sub> the optical density measured using a spectrophotometer adjusted at 750 nm absorbance wavelength.

putative organic complexes were eluted with the following solvents including: 50:50 (v/v) methanol/water; and 1:20:80 (v/v/v) formic acid/water/methanol.

In order to remove the solvents from the eluted solutions obtained by the SPE cartridge, a rotary evaporator (Buchi- UK) was used at 60°C for 20 min. After that the eluted solutions were blown down under nitrogen and put in the freeze dryer (VirTis-benchtop K-Ulc-Mode) at a pressure of 111 µBar, condenser -69.8 °C and ambient temperature (21.2°C) overnight. During these procedures, it was observed that there were yellow solid materials, graduating from light yellow to dark yellow, formed in the culture supernatant flasks. When 1.5 mL of 3% (v/v) HNO<sub>3</sub> was added to each flask, all yellow solid materials were dissolved and disappeared.

**Table 2.03 Instrument conditions and measurement parameters in ICP-MS.**

Instrument type	Agilent Technologies - 7500 Series	Sample matrix	3% (v/v) Nitric acid
Torch	Fassel-type	Isotopes of interest	<sup>56</sup> Fe, <sup>57</sup> Fe, <sup>59</sup> Co, <sup>60</sup> Ni, <sup>63</sup> Cu, <sup>65</sup> Cu, <sup>66</sup> Zn, <sup>111</sup> Cd, <sup>95</sup> Mo, <sup>55</sup> Mn.
Spray chamber	Quartz Double Pass	Internal standard	<sup>166</sup> Er
Nebuliser	Glass concentric expansion	Sample time (s)	0.30 -0.45
Cones standard	Ni sampler and skimmer	Runs	3
Radio frequency power (W)	1551	Gas collision mode	No
Cool water (L min <sup>-1</sup> )	1-1.5	Auxiliary Ar gas flow (L min <sup>-1</sup> )	0.90
Plasma Ar gas flow (L.min <sup>-1</sup> )	15	Nebuliser pump (rpm)	0.20

The metals binding to ligands (organic complexes) eluted from the culture supernatant and uncultured medium by using a polystyrene-divinylbenzene SPE cartridge, were analysed by using an Agilent Technologies -7500 Series ICP-MS. The matrix effects and instrumental drift in the ICP-MS measurements were corrected by the internal standard <sup>166</sup>Er and the instrument was calibrated by using external standards <sup>56</sup>Fe, <sup>57</sup>Fe, <sup>59</sup>Co, <sup>60</sup>Ni, <sup>63</sup>Cu, <sup>65</sup>Cu, <sup>66</sup>Zn, <sup>111</sup>Cd, <sup>95</sup>Mo and <sup>55</sup>Mn. The instrument operating conditions for ICP-MS are summarised in Table 2.03. The

calibration curves for each isotope were drawn with excellent linearity for each isotope (see Appendix B, Figure B.01).

### 2.3.2 Chromatography Analysis

Once a successful SPE cartridge (polystyrene-divinylbenzene) resin was chosen, the same steps as in Section 2.3.1 were followed. Three samples including culture supernatant, uncultured medium and culture supernatant after adding excess/plenty of zinc were passed through the SPE cartridge to separate and concentrate the free-metal ligands and metal-binding ligands (organic complexes). Each time a 200  $\mu\text{L}$  eluted solution was submitted to the UHPLC/Q-TOF-MS instrument.

LC-MS analysis was carried out using a Dionex 3000RS UHPLC coupled with a Bruker MaXis Q-TOF mass spectrometer. A Sigma Ascentis Express column (C18, 150 $\times$ 2.1mm, 2.7 $\mu\text{m}$ ) was also used. Mobile phases consisted of solution A (water with 0.1% formic acid) and solution B (methanol with 0.1% formic acid). A gradient of 5% B to 100% B in 15 min was employed with a flow rate at 0.2 mL min<sup>-1</sup>. UV was set to 210 nm. Subsequently, an isocratic elution with 100% of B solution for 20 min was employed at the same flow rate, 0.2 mL min<sup>-1</sup>. The mass spectrometer was operated in electrospray positive mode with a scan range 50-2.000 m/z. Source conditions are given in Table 2.04 and the ion transfer conditions are summarised in Table 2.05. In the beginning of each run, calibration was done with sodium formate (10 mM) through a loop injection of 20  $\mu\text{L}$  of standard solution.

**Table 2.04 Source conditions for UHPLC/Q-TOF-MS.**

End plate offset	-500V
Capillary	-4500V
Nebuliser gas (N <sub>2</sub> )	1.6 bar
Dry gas (N <sub>2</sub> )	8 mL.min <sup>-1</sup>
Dry temperature	180°C.

**Table 2.05 Ion transfer conditions for UHPLC/Q-TOF-MS.**

Ion funnel RF	200 Vpp	Ion cooler RF	50-350 Vpp
Multiple RF	200 Vpp	Collision RF	600 Vpp
Quadruple low mass	55 m/z	Pre-pulse storage time set	1 $\mu$ s
Collision energy	5.0 ev	Transfer time set	121 $\mu$ s

For analytical HPLC, three samples of culture supernatant (80 nM Zn(II)), culture supernatant after adding excess zinc, and culture supernatant (2  $\mu$ M Zn(II)) were passed through the SPE cartridge and 500  $\mu$ L eluted solution was submitted to the HPLC instrument.

Analytical HPLC runs were conducted on an Agilent 1100 series HPLC quaternary pump. Samples were loaded onto a Phenomenex Gemini-NX column (C18, 4.60 $\times$ 250, 5 $\mu$ m, 100 $\text{\AA}$ ). The flow rate was 1  $\mu$ L min<sup>-1</sup> and the injection volume was 50  $\mu$ L. Mobile phases consisted of two solutions: solution A (water with 0.1% TFA) and solution B (methanol with 0.1% TFA) with gradient and isocratic elutions (Table 2.06) and the UV was set to 210, 220 and 400 nm.

**Table 2.06 Gradient elution for HPLC.**

Time (min)	20	10	10	20
Solvent (B)	15-50	50-75	75-100	100

## 2.4 Physiological Methods

### 2.4.1 Flow Cytometry

Flow cytometry BD FACScan™ (BD Biosciences) was used to count *Synechococcus* cell number per 1 mL of Aquil\* medium. Same volume of Aquil\* medium without bacterium was used as a control. Prior to analysis, *Synechococcus* sp. WH8102 cultures were diluted (1:100) prior to analysis, and when the OD<sub>750</sub> was larger than 0.05, the cultures were diluted by (1:1,000).

Fluidics settings were set to a pre-run for 5 min and stabilised for 5 min and the samples were loaded for 1 min. The machine was cleaned before and between samples by loading bleach solution, Milli-Q water, and subsequently sterile Aquil\* medium as a blank.

## 2.4.2 Growth Rate Analysis

Specific growth rates ( $\mu$ ,  $d^{-1}$ ) were calculated according to Henley and Yin (1998) where the specific growth rates were calculated as the slopes of linear regressions of  $\ln$  (cell density) versus day number for individual cultures over the range of linearity (Equation 2.01).

$$\mu_{\max} = \frac{\ln (M1/M2 )}{(T2 - T1)} \quad \text{Equation 2.01}$$

Where  $\mu_{\max}$  is the specific growth rate, M1 and M2 are the cell number at times T1 and T2, respectively.

## 2.4.3 Chlorophyll $a$ Extraction

The amount of chlorophyll  $a$  was calculated according to Ritchie (2006) using Equation 2.02.

$$\text{Chl } a \text{ ( mg. ml}^{-1}\text{)} = (-8.0962 \times A_{652} + 16.5169 \times A_{665})(\pm 0.04696) \quad \text{Equation 2.02}$$

1 mL *Synechococcus* sp. WH8102 cell culture was harvested by centrifuging at  $13,000 \times g$  for 10 min at room temperature and 900  $\mu\text{L}$  supernatant was discarded. Then the remaining 100  $\mu\text{L}$  were resuspended in 900  $\mu\text{L}$  methanol and incubated at  $60^\circ\text{C}$  for 60 min. The extract was then centrifuged at  $13,000 \times g$  for 10 min at room temperature. Later the cell density at  $\text{OD}_{652}$  and  $\text{OD}_{665}$  were measured against a blank of 1:9 of Aquil\* medium: methanol.

## 2.5 Identification of Proteins using MALDI-TOF

### 2.5.1 Sample Preparation

1 L *Synechococcus* sp. WH8102 culture was grown as described in Section 2.2.1. When the culture reached an OD<sub>750</sub> of *ca* 0.3 (between 35- 40 days), the bacterial cells were harvested by centrifugation (Avanti™ J-25 Centrifuge, Beckman Coulter) at 6,000×g for 30 min. Cell pellets were resuspended in 20 ml cell lysis buffer (20 mM Tris-HCl, pH 8.0). A complete protease inhibitor cocktail tablet (EDTA-free), Roche, was added to the buffer before using to inhibit protease activity and maximise protein yields.

To facilitate cell lysis, cells were sonicated at amplitude 40-50 (Ultrasonic Processor SONICS-Vibra cell) for 2 × 30 sec, then samples were centrifuged at 13,000 × g for 5 min. The supernatant was then transferred to a fresh tube and stored on ice until analysis.

In each sample, the concentration of proteins was calculated by using the Bradford assay (Bradford, 1976). Equal protein concentrations from each sample were resolved by SDS-PAGE (Sodium Dodecyl Sulfate Polyacrylamide, Mini-Protean® TGX™ precast gels (4-15 %) (BioRad, UK)). The electrophoresis was run at 180 mV using a Mini-Protean® tetra, UK system (GeneFlow, BioRad) with a running buffer (25 mM Tris, 192 mM Glycine, 0.1% SDS, (BioRad)) for 30 min. For detection of proteins on SDS-PAGE, Coomassie staining was used.

### 2.5.2 Band Preparation and Destaining

Protein spots of interest were excised from 1D gels by cutting the band into 2×2 mm pieces with a spot picker or a scalpel. The gel plugs were dislodged with an intact pipette tip into microcentrifuge tubes for storage and processing (Figure 2.01). An In-Gel tryptic Digestion kit (Thermo Scientific, UK) was used to digest proteins in the excised bands from SDS-PAGE gels

as follows. Briefly, 200  $\mu\text{L}$  of destaining solution was added to the gel pieces and the sample was incubated at 37°C for 30 min. Then the destaining solution was removed and discarded.

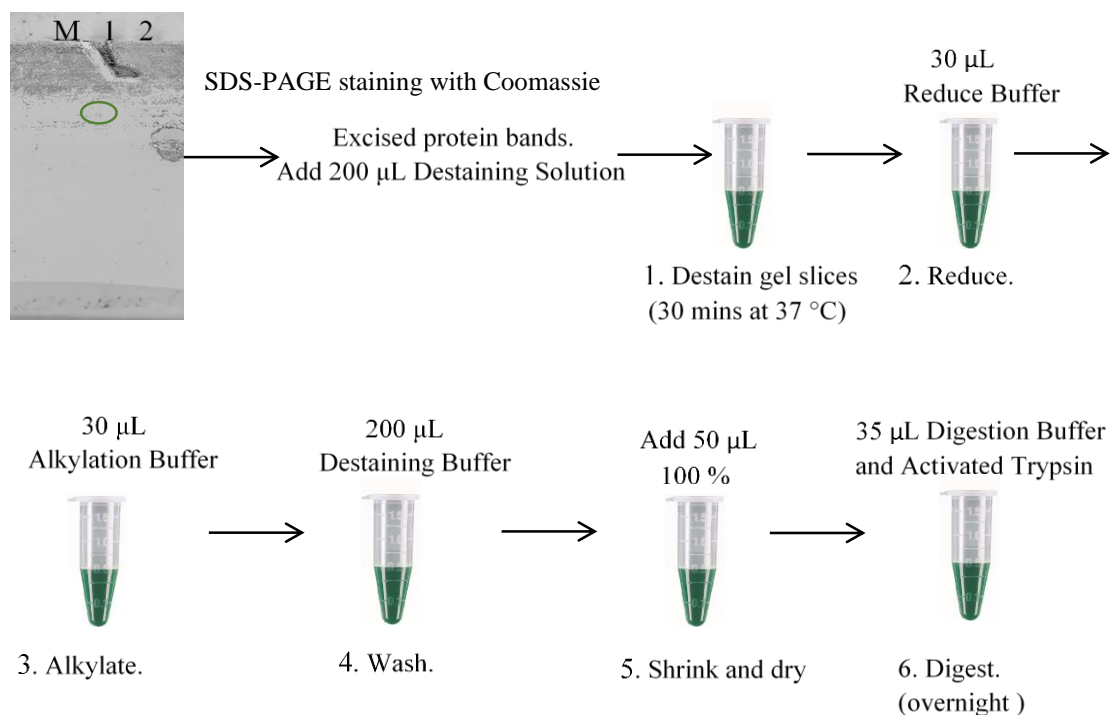


**Figure 2.01 Schematic diagram describing protein In-gel tryptic digestion.**

30  $\mu\text{L}$  reducing buffer was added to the sample and incubated at room temperature for 10 min. Subsequently the reducing buffer was removed and discarded. 30  $\mu\text{L}$  alkylation buffer was then added to the sample and the sample was incubated at room temperature for 40 min. After that the alkylation buffer was removed and discarded then the sample was washed with 200  $\mu\text{L}$  destaining buffer and incubated at 37°C for 15 min on the shaker.

Gel pieces were shrunk by adding 50  $\mu\text{L}$  acetonitrile, then the sample was incubated at room temperature for 15 min. After removing the acetonitrile and drying the gel pieces in the air for 10 min, the gel pieces were swollen by adding 10  $\mu\text{L}$  active Trypsin and incubated for 15 min at room temperature. 25  $\mu\text{L}$  digestion buffer was added to the tube and the sample was then incubated at 30°C overnight.

### 2.5.3 Peptide Mass Fingerprinting (PMF)

An aliquot of each protease digest was added to  $\alpha$ -Cyano-4-hydroxycinnamic acid (CHCA), and the sample was spotted onto a Bruker Scout 384™ MALDI target plate and exposed to air-drying.

A mass range of up to 4,000 m/z was scanned for peptides. The optimised range was set between 1,000 and 4,000 m/z. The laser intensity was optimised with the range being from 12 to 23 kHz laser power. A total of 6 to 8 shots were acquired in each spot before proceeding to the next spot. Spectra were externally calibrated with sodium formate.

### 2.5.4 Data Interpretation and Database Searching

Peptide mass matching and protein identification searches were performed against a comprehensive nonredundant protein sequence database. No limitations on protein molecular weights or species of origin were imposed. Database searching used a peptide mass map at the Matrix Science Ltd. server (<http://www.matrixscience.com/>) using Mascot software. All complete and partial peptide sequences obtained by PredictSequence were used for MS BLAST searching of uniprot (<http://www.uniprot.org/>) and cyanorak (<http://application.sb-roscoff.fr/cyanorak/>) databases.

## 2.6 Molecular Biology Procedures

### 2.6.1 Genomic DNA Extraction from *Synechococcus* sp. WH8102

Total genomic DNA from *Synechococcus* sp. WH8102 was extracted by using a method modified from Murray and Thompson (1980). Briefly, 2 L *Synechococcus* sp. WH8102 culture was harvested by centrifugation at  $6000 \times g$  for 20 min at 4°C. The supernatant was removed

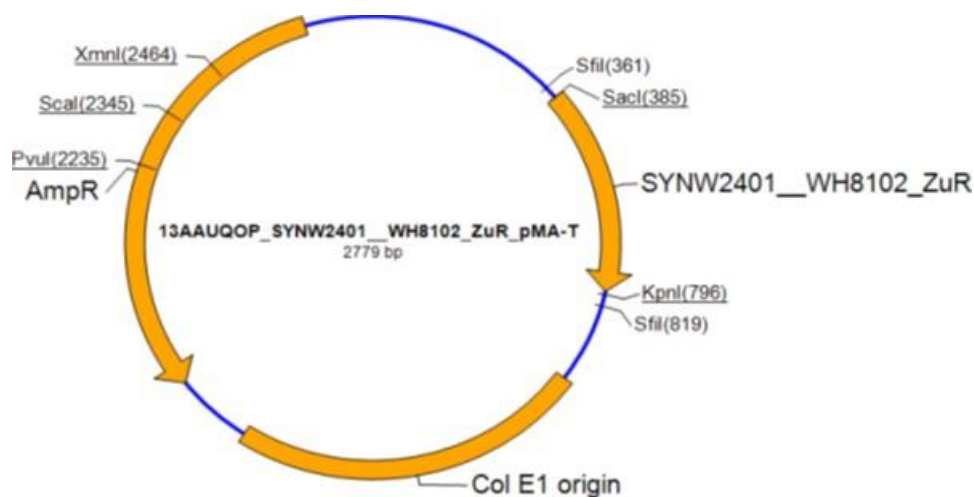
and the pellet was collected and resuspended in 500  $\mu$ L TE buffer containing (10 mM Tris-HCl, 1 mM disodium EDTA, 0.5% (w/v) SDS, pH=8.0), then the mixture was incubated at 65°C for 1 hour. Later, the mixture was transferred to a 1.5 mL Eppendorf tube and an equal volume of phenol was added, mixed and left for 5 min at room temperature. The mixture was centrifuged at  $13,000 \times g$  for 10 min.

The supernatant was transferred into a fresh Eppendorf tube and an equal volume of phenol:chloroform (24:1 v/v) was added, mixed and left at room temperature for 5 min, and then centrifuged at  $13,000 \times g$  for 5 min. Later the aqueous layer was extracted and mixed with an equal volume of phenol:chloroform:isoamylalcohol (25:24:1 v/v/v) and left for 5 min at room temperature, followed by further centrifugation for 5 min as above.

The aqueous layer was transferred to a new Eppendorf tube and an excess of 100% (v/v) ethanol was added. The mixture then was incubated at -20°C and followed by centrifugation at  $13,000 \times g$  for 30 min at 4°C to pellet the DNA before washing by adding 100  $\mu$ L 70 % (v/v) ethanol and centrifugation for 20 min at  $13,000 \times g$  at 4°C. The genomic DNA was then air-dried and resuspended in nuclease-free water. The concentration of DNA was measured by NanoDrop (ND-1000 UV-Vis Spectrophotometer, UK) and frozen at -20°C until further use.

### **2.6.2 Synthetic *synw\_2401* gene**

The synthetic gene *synw\_2401* was optimised by Gene Art<sup>®</sup> company and cloned into pMA-T at the SfiI restriction enzyme site (Figure 2.02).



Vector backbone : pMA-T  
 Designation : *E. coli* K12 (dam+dcn+tonA)  
 Gene size : 405 bp  
 Cloning site : SfiI

**Figure 2.02** Map of pMA-T vector with *synw\_2401* gene.

### 2.6.3 Gene Amplification by PCR

Polymerase chain reaction (PCR) was carried out to amplify the target gene, *synw\_2401*, in a total reaction volume of 25  $\mu$ L. Two DNA polymerases were used, Platinum<sup>®</sup>*Pfx* DNA polymerase (Invitrogen) and KAPA HiFi DNA polymerase (Kapa Biosystems).

Each PCR reaction contained 15-30 ng template DNA, 1  $\mu$ L of each diluted forward and reverse primer, 1  $\mu$ L dNTPs (from a 12.5 mM stock, Invitrogen), 0.5  $\mu$ L Mg<sub>2</sub>SO<sub>4</sub> (from a 50 mM stock, Invitrogen) for Platinum<sup>®</sup>*Pfx* DNA polymerase or without MgCl<sub>2</sub> for KAPA HiFi polymerase. 2.5  $\mu$ L 10 $\times$  *Pfx* amplification buffer and 0.2  $\mu$ L of Platinum<sup>®</sup>*Pfx* DNA polymerase or 5  $\mu$ L KAPA HiFi DNA polymerase and 0.5  $\mu$ L KAPA HiFi DNA polymerase were added and made up to 25  $\mu$ L with sterilized Milli-Q water.

Primers used in PCR reactions were designed as shown in Table 2.07. The *synw\_2401* forward primer was designed to be very specific, where a CACC overhang was added to a 20-base single-stranded oligonucleotide for cloning into the pET151/D-TOPO<sup>®</sup> vector.

**Table 2.07 Forward and reverse primers of *synw\_2401* gene.**

<i>synw_2401</i> F	5'-CAC CAT GAC CGG TAG CAG TCC GGC-3'
<i>synw_2401</i> R	5'-TTA CGG TTT GCT GCT ACG CT-3'

PCR reactions were performed on a Biometra T gradient T3000 Thermocycler. The general reaction cycle consisted of an initial denaturation step at 95°C for 2 min, followed by denaturation at 95°C for 20 sec and annealing at 55-67.5°C as required by the primers set for 45 sec and extension at 72°C for 1 min. Then the reaction was finished with a 1 min final extension step at 72°C and kept at 4°C until use.

## 2.6.4 Agarose Gel Electrophoresis

Agarose gel electrophoresis was used to analyse the size of DNA fragments. Gels were prepared with UltraPure™ agarose (Invitrogen, life technique) in 1×TBE buffer (Tris Base, Borate, 0.5 M EDTA, pH 8). A final concentration of 4 µL GelRed (Nucleic Acid Gel Stain, 10,000 × in water, Biotium) was added to the gel.

Samples and appropriate DNA size markers (100-bp DNA ladder, Invitrogen) were gently mixed with 6×DNA Loading Dye (Fermentas) before loaded onto the gel. Agarose gels were run in 1×TBE buffer using an electrophoresis PowerPac™ Basic (BioRad) at a constant voltage of 120 V.

## 2.6.5 Purification of PCR Product

A PCR clean-up system (Promega, USA) was used to purify the DNA fragments amplified from PCR reactions. The DNA band of interest was excised from the gel in a dark room under UV light and the gel slice placed in a 1.5 mL microcentrifuge tube. 10 µL membrane binding

solution per 10 mg of gel slice was added to the gel slice. Then the microcentrifuge tube was vortexed and incubated at 65°C until the gel slice was completely dissolved.

The dissolved gel mixture was transferred to the mini-column assembly and incubated at room temperature for 1 min and centrifuged at  $13,000 \times g$  for 1 min. Then the flow through was discarded and the mini-column was reinserted into the collection tube. 700  $\mu\text{L}$  membrane wash solution was added to the mini-column, centrifuged at  $13,000 \times g$  for 1 min and the flow through was discarded. The previous step was repeated by adding 500  $\mu\text{L}$  membrane wash solution and centrifuged at  $13,000 \times g$  for 5 min. The pure PCR product was eluted with nuclease-free water and the concentration was measured using a NanoDrop (ND-1000 UV-Vis Spectrophotometer, UK).

### 2.6.6 Gene Cloning into the TOPO<sup>®</sup> vector

The pET151/D-TOPO<sup>®</sup> vector was used to clone the target gene *synw\_2401* as an insert using the TOPO cloning kit purchased from Invitrogen. Purified PCR product (Section 2.6.5) was mixed gently with the pET151/D-TOPO<sup>®</sup> vector and incubated for 5 min at room temperature (22-23°C), after that the reaction mixture was placed on ice for further transformation.

### 2.6.7 Transformation of Competent Cells and Plasmid Purification

3  $\mu\text{L}$  of the TOPO<sup>®</sup> cloning reaction was added directly to *E. coli* competent cells including: One Shot<sup>®</sup> TOPO10, and DH5 $\alpha$ . The mixture was incubated on ice for 30 min, followed by heat-shocking the cells at 42°C for 45 sec. After that the tubes were transferred immediately to ice for 2 min. Finally, 250  $\mu\text{L}$  of room temperature S.O.C medium (2% tryptone, 0.5% yeast extract, 10 mM NaCl, 2.5 mM KCl, 10 mM MgCl<sub>2</sub>, 10 mM MgSO<sub>4</sub>, and 20 mM glucose) was added to the mixture and incubated at 37°C for 1 hour. Then 25-200  $\mu\text{L}$  from each transformation was spread on a pre-warmed selective plate (0.05 mg mL<sup>-1</sup> ampicillin) and

incubated overnight at 37°C. Next day, 10 colonies were picked up and cultured in LB medium containing the ampicillin antibiotic (0.05 mg mL<sup>-1</sup>).

**Table 2.08 T7 Forward and reverse primers.**

<b>T7-F</b>	5'-TAA TAC GAC TCA CTA TAG GG -3'
<b>T7-R</b>	5'-TAG TTA TTG CTC AGC GGT GG -3'

Plasmids from the successfully grown cells were purified using the QIAprep®Spin Miniprep Kit (QIAGEN, Sample & Assay Technologies). The template DNA was mixed with 5 pmol of primers T7-forward and T7-reverse (Table 2.08) to confirm the presence of the correct orientation of *synw\_2401*.

PCR products were subsequently sequenced by GATC Lightrun sequencing service (GATC Biotech, Konstanz, Germany) and analysed using SeqMan software. The correct plasmid construct was transformed into BL21 Star™ (DE3) (ThermoFisher), Rosetta™ 2(DE3) pLysS (Novagen) and the Takara strain (BL21 cells containing the pG-Tf2 plasmid, Takara Bio Inc).

## 2.7 Overproduction and Purification of Zur Protein

### 2.7.1 Production of Recombinant Zur Protein

For overnight cultures at 37°C, a single *E. coli* colony, containing the synthetic gene *synw\_2401* cloned into the pET151/D-TOPO® vector, was picked to inoculate 10 mL LB containing 0.05 mg mL<sup>-1</sup> ampicillin for the BL21 Star™(DE3) and Rosetta™2(DE3)pLysS strains, and additionally, 0.0175 mg mL<sup>-1</sup> chloramphenicol for the Takara strain containing the pG-Tf2 plasmid. The overnight culture of the respective strain was used to inoculate 200 mL LB medium containing 0.05 mg mL<sup>-1</sup> ampicillin for the BL21 Star™(DE3) and Rosetta™2(DE3)pLysS strains, and 0.0175 mg mL<sup>-1</sup> chloramphenicol as well as 0.002 µg mL<sup>-1</sup>

tetracycline for the Takara strain, and these were incubated at 30°C and 37°C on shaker at 180 rpm. When the cell concentration reached  $OD_{600} = 0.8$  for BL21 Star™(DE3) or Rosetta™ 2(DE3)pLysS, and an  $OD_{600}=0.5$  for the Takara strain, IPTG (isopropyl-beta-D-thiogalactopyranoside, Fermentas) was added to the culture at final concentrations of 0.3 mM, 0.5 mM and 0.7 mM, and the cultures were further incubated at 30°C for 6 h. Cells were harvested by centrifugation at  $4,000 \times g$  for 20 min at 4°C .

Auto-induction medium (MagicMedia™, Invitrogen, Life Technologies) was also used to check the expression of the Zur protein using the Takara strain. The overnight culture was used to inoculate 200 mL MagicMedia™ containing  $0.05 \text{ mg mL}^{-1}$  ampicillin,  $0.0175 \text{ mg mL}^{-1}$  chloramphenicol, and  $0.002 \text{ } \mu\text{g mL}^{-1}$  tetracycline. Bacterial cells were incubated at 30°C and 37°C on rotary shaker at 180 rpm overnight. All protein pellets were centrifuged and stored at -80°C for further use.

For the production of labelled protein, 10 mL of starter culture was added to the  $^{15}\text{N}$  labelled minimal medium (M9) (12.8 g  $\text{Na}_2\text{HPO}_4$ , 3 g  $\text{KH}_2\text{PO}_4$ , 0.5 g NaCl, 1 mM  $\text{MgSO}_4 \cdot 7\text{H}_2\text{O}$ , 0.1 mM  $\text{CaCl}_2 \cdot 2\text{H}_2\text{O}$ ,  $7.5 \text{ } \mu\text{g/ml}$   $\text{FeSO}_4 \cdot 7\text{H}_2\text{O}$ ,  $0.5 \text{ } \mu\text{g/mL}$  Thiamine and 1 g  $^{15}\text{NH}_4\text{Cl}$  in 1 L) and incubated at 30°C. When the cell concentration reached  $OD_{600}= 0.5$ , the cells were induced with 0.5 mM IPTG and allowed to grow for 6 hours at 180 rpm. Finally, the cell pellets were harvested and stored at -80°C for further use.

### **2.7.2 Immobilized Metal Affinity Chromatography**

2 g cells (wet weight) were re-suspended in 4 mL lysis buffer (50 mM  $\text{NaH}_2\text{PO}_4$ , 300 mM NaCl, 10 mM imidazole) with  $1 \text{ mg mL}^{-1}$  lysozyme (from egg white, Merck) and 1 mM PMSF phenylmethylsulfonyl fluoride, protease inhibitor, and cells were sonicated at amplitude 40-50 (Ultrasonic Processor SONICS- Vibra cell) for  $4 \times 30$  sec. The cell lysate was centrifuged at  $4000 \times g$  for 20 min at 4°C for separation from cell debris.

Purification of the Zur protein from *Syenchococcus* sp. WH8102 was carried out by immobilised metal affinity chromatography (5 ml IMAC column, HiTrap Chelating HP, GE Healthcare) using a FPLC AKTApurifier system (Amersham Biosciences) including a UPC-900 monitor, P-900 sample pump, and Frac-950 fraction collector. The cell extract was loaded onto the IMAC column equilibrated with washing buffer (50 mM NaH<sub>2</sub>PO<sub>4</sub>, 300 mM NaCl, 20 mM imidazole). Protein was eluted using elution buffer (50 mM NaH<sub>2</sub>PO<sub>4</sub>, 300 mM NaCl, 250 mM imidazole) gradient for 30 min and isocratic for another 30 min. The protein elution was monitored by absorbance 220 nm and 280 nm for peptide bonds and aromatic groups, respectively. Fractions were collected and analyzed by SDS-PAGE. Fractions containing the Zur protein were kept for further incubation with TEV protease.

### 2.7.3 TEV Protease Purification

10 mL overnight culture of *E. coli* BL21 (DE3) CodonPlus-RIL cells (Stratagene, La Jolla, CA, USA) was used to inoculate 200 mL LB medium with 0.05 mg ml<sup>-1</sup> ampicillin and incubated at 37°C on rotary shaker 180 rpm. When the cell concentration reached OD<sub>600</sub>=0.8, IPTG was added to the culture at a final concentration of 0.5 mM, and the culture was further incubated at 15°C overnight. Cells were harvested by centrifugation at 4°C for 20 min at 4000 × g.

1 g cells (wet weight) was re-suspended in 4 mL lysis buffer (50 mM NaH<sub>2</sub>PO<sub>4</sub>, 300 mM NaCl, 10 mM imidazole) containing 1 mg mL<sup>-1</sup> lysozyme (from egg white, Merck) and 1 mM PMSF and cells were sonicated for 3 min. The cell lysate was centrifuged at 4000 × g for 20 min at 4°C, and the clear supernatant was passed through HisPur Ni-NTA resin (Fisher Scientific, UK). TEV protease was eluted with elution buffer (50 mM NaH<sub>2</sub>PO<sub>4</sub>, 300 mM NaCl, 250 mM imidazole). The purification step was repeated twice and the protein was analysed by SDS-PAGE.

Purified Zur protein from *Synechococcus* sp. WH8102, was incubated overnight with purified TEV protease at a ratio of 2:1 for His<sub>6</sub>-tag cleaving. On the second day, a second IMAC run was carried out to obtain a pure and cleaved Zur protein, which, having lost the His<sub>6</sub>-tag.

## **2.8 Protein Identification**

### **2.8.1 SDS-polyacrylamide Gel Electrophoresis**

SDS-PAGE was performed using mini-Protean TGX precast 4–15% gels (BioRad, UK) and using standard protocols. Prior to gel loading, samples were mixed with an equal volume of gel loading buffer and heated to 95°C for 5 min. 10 µL sample was loaded per lane except where otherwise stated. Gels were stained using Coomassie brilliant blue R-250 (National Diagnostics, USA) or silver nitrate (Sigma-Aldrich).

### **2.8.2 Native Polyacrylamide Gel Electrophoresis (NP-AGE)**

Before loading the sample, a mini-Protean TGX precast 4–15% gel (BioRad, UK) was run only with water at a fixed voltage (150 V) for 30 min to remove the detergent. Then the purified protein was mixed with native sample buffer (250 mM Tris base, 0.0185% Coomassie R-250, 0.00625% Phenol Red, 10% glycerol, pH 8.7) and loaded on the water-treated precast 4–15% gel. Electrophoresis was achieved at a fixed voltage of 150 V for 120 min in the native running buffer (50 mM Tris base, 50 mM MOPS, 0.0375% SDS, pH 7.4).

### **2.8.3 Detection of Protein by Western Blotting**

Western blotting was used to transfer proteins from SDS-PAGE gels onto PVDF (Polyvinylidene difluoride) membranes and was performed using a semi-dry blotting apparatus

(BioRad). The apparatus was used exactly as instructed by manufacturer. Briefly, two sheets of Whatman paper soaked in transfer buffer were placed onto the positive electrode.

The PVDF membrane was also soaked in a towbin transfer buffer (25 mM Tris, 192 mM glycine, and 20% methanol) (Towbin *et al.*, 1979), and placed over the Whatman papers and then the gel was placed on the top. Finally, another two sheets of Whatman paper was soaked in transfer buffer and placed over the gel. The transfer of proteins was achieved using a current of 150 mA over a 1 hour period.

After the transfer of protein from acrylamide gels to the PVDF membrane, the membrane was blocked to prevent non-specific binding of antibodies using 5% (w/v) dried milk solution. The PVDF membrane was subsequently placed into another container containing monoclonal antibody (Mouse Anti-Histidine TAG: ALK.PHOS, AbD Serotec). After 1 hour, the membrane was washed and the detection of protein was performed using chromogenic substrate detection reagents containing nitro-blue tetrazolium and 5-bromo-4-chloro-3'-indolyphosphate (Invitrogen).

## **2.9 Estimation of Zur Protein Concentration**

### **2.9.1 Ellman's Test, Thiol Quantification**

The concentration of recombinant Zur protein from *Synechococcus* sp. WH8102 was estimated using a modified method for quantitation of free thiols, based on Ellman's reagent, DNTB (5,5-dithio-bis-(2-nitrobenzoic acid)) (Ellman, 1958). Different concentrations (0, 2.5, 10, 13.3, 26.7, 40 and 53.3  $\mu$ M) of cysteine solution were prepared in 2.6 ml Tris buffer (0.1 M, pH 7.05) with 200  $\mu$ L DNTB (2.5 mM in 50 mM ammonium acetate, pH 5.0, 1 mM EDTA). The absorbance was then recorded by Biomate 3 spectrophotometer (Fisher Scientific) at 412 nm.

10-200  $\mu\text{L}$  protein samples were prepared in the same way as for standards with allowing the reaction to proceed as above for 20-40 min before measuring the absorbance at 412 nm. The thiol concentration was determined from the calibration curve obtained from the standard readings. The protein concentration was divided by seven, the number of cysteines residues present in Zur protein sequence.

## **2.9.2 Inductively Coupled Plasma-Optical Emission Spectroscopy**

Metal specificity and stoichiometry of the target protein was analysed by Inductively Coupled Plasma-Optical Emission Spectroscopy (ICP-OES) (Perkin-Elmer Optima 5300DV, PerkinElmer, UK). The metals content of protein (S, Zn, Cu, Cd, Ni and Co) were determined by measuring S at (180.669 and 181.975 nm), Zn at (206.200 and 213.857 nm), Cu at (327.393 and 324.752), Cd at (228.802 and 214.440 nm), Ni at (231.604 and 232.003), Fe at (238.204 and 259.939 nm) and Co at (230.786 and 228.616 nm). Each sample was analysed using three replicate readings, with a washing time of 60 sec. The conditions for plasma operating were: Argon flow rate  $13.0 \text{ L min}^{-1}$ , auxiliary gas flow rate  $0.2 \text{ L min}^{-1}$ , nebuliser flow rate  $0.8 \text{ L min}^{-1}$  and RF power at 13000 W. The ICP-OES data were analysed using WinLab 32 software; data were divided by the appropriate atomic mass for each element. The protein concentration was obtained by dividing the sulfur concentration by the total number of sulfur atoms in the protein (S=10). Subsequently, the ratio of metal to protein was calculated.

## **2.10 Protein Biophysical Techniques**

### **2.10.1 Electrospray Ionization Mass Spectrometry (ESI-MS)**

ESI-MS was employed to identify the target protein and study metal release kinetics. A protein sample (90  $\mu\text{L}$ , in 10 mM ammonium bicarbonate, pH 7.8) was mixed with 10% (v/v) methanol

(Sigma, 99.8%) to record native protein mass spectra, Zn(II)-loaded Zur protein from *Synechococcus* sp. WH8102. Formic acid (2% v/v final concentration) was added to the protein sample to obtain the apo form, Zn(II)-free Zur. Samples were injected into a Bruker Daltonics MicroTOF (Bremen, Germany) fitted with an electrospray ionization source.

The spectrometer was operated in positive mode with the following parameters: flow rate 4  $\mu\text{L min}^{-1}$ , range (300 - 5000 m/z), temperature 195°C, nebulizer 0.6 Bar, capillary exit 100 V, skimmer (1) 50V, skimmer (2) 25.2 V, hexapole (1) 24.2 V, hexapole (2) 22.4 V, hexapole (RF) 450 V, dry-gas 4.5 L  $\text{min}^{-1}$  and detector TOF 2300V.

## **2.10.2 Circular Dichroism (CD) Spectroscopy**

Circular dichroism spectroscopy for the purified protein samples was performed using a Jasco J-815 spectropolarimeter (Jasco UK, Great Dunmow, UK) with 1 mm path length quartz cuvettes (Starna, Optiglass Ltd, UK).

Protein samples were prepared in 5 mM Tris buffer at pH 7.8 with a final concentration of 25.9-30  $\mu\text{M}$ . Spectra were recorded in the range 190 to 300 nm, with 2 nm band width, 100 nm  $\text{min}^{-1}$  scanning speed and 8 averaging scans.

## **2.10.3 Nuclear Magnetic Resonance (NMR) Spectroscopy**

### **2.10.3.1 1D $^1\text{H}$ -NMR Spectroscopy**

Protein samples were prepared in 20 mM ammonium bicarbonate at different pH, different temperature, and different NaCl concentrations (as discussed in Results). 1D  $^1\text{H}$  NMR spectroscopy was carried out using a Bruker Avance 700 Ultrashield spectrometer mounted with a cryoprobe operating at 700.24 MHz, and using excitation sculpting with gradients for water suppression (Hwang & Shaka, 1995). The spectra were recorded with 16 k complex data

points, 128 scans and a spectral width of 15.9 ppm. 1D  $^1\text{H}$  NMR data were processed using TopSpin 3.2 software.

### 2.10.3.2 2D Heteronuclear NMR Spectroscopy

#### $[^1\text{H}, ^{15}\text{N}]$ HSQC

A  $^{15}\text{N}$  labelled protein sample (see Section 2.7.1) prepared in 20 mM ammonium bicarbonate, 10%  $\text{D}_2\text{O}$ , 150 mM NaCl, and 308 K was used to record 2D  $[^1\text{H}, ^{15}\text{N}]$  heteronuclear single quantum coherence (HSQC) spectrum with 8 k data points in F2 ( $^1\text{H}$ ) and 128 increments in F1 ( $^{15}\text{N}$ ). The spectrum was acquired with a spectral width of 16 ppm in F2 and 40 ppm in F1 dimensions over 16 scans with a  $^1J_{\text{NH}}$  coupling constant of 90 Hz. The raw data were Fourier transformed into  $2048 \times 512$  data points in the F2 $\times$ F1 dimensions. The pulse program was hsqcetf3gpsi2.

#### $[^1\text{H}, ^{15}\text{N}]$ TROSY

For the 2D  $[^1\text{H}, ^{15}\text{N}]$  transverse relaxation optimized spectroscopy (TROSY), the spectra were recorded with 8 k data points in F2 ( $^1\text{H}$ ) and 256 increments in F1 ( $^{15}\text{N}$ ). The spectra were acquired with a spectral width of 16 ppm in F2 and 25 ppm in F1 dimensions, and the raw data were Fourier transformed into  $2048 \times 512$  data points in the F2 $\times$ F1 dimensions. For the EDTA reaction, the spectra were done using 40 increments in F1 with 32 scans for the lower resolution, while for the higher resolution the spectra were recorded with 128 increments in F1 and 64 scans. The pulse program was trosytf3gpsi2.

2D NMR recorded spectra were processed using Sparkly v3.106 by transferring the data from TopSpin 3.2 software.

## 2.11 Monitoring Protein Conformational Changes

Different concentrations of Zn(II)-loaded Zur protein, determined using ICP-OES, in different buffers (Table 2.09) were incubated with 2 equivalents, 4 equivalents, and 10 equivalents of EDTA. The protein samples were then measured using different techniques (Table 2.09).

**Table 2.09 Conditions and techniques used for monitoring the competition reaction of the SynZur with EDTA.**

Purpose	Protein concentration	Buffer	EDTA Concentration	Instrument
UV-Visible	12.4 $\mu$ M	1 mM Tris-Cl, pH~7.8	24.8 $\mu$ M, 29.6 $\mu$ M, and 124 $\mu$ M	Varian Cary 50 spectrophotometer
UV circular dichroism	25.9 $\mu$ M	5 mM Tris-Cl, pH~7.8	51.8 $\mu$ M, 103.6 $\mu$ M, and 259 $\mu$ M	Jasco J-815 spectropolarimeter
ESI-MS spectrometry	32 $\mu$ M	10 mM $\text{NH}_4\text{HCO}_3$ , pH= 7.8, 10 % MeOH	64 $\mu$ M	Bruker MicroTOF mass spectrometer
1D NMR spectroscopy	600 $\mu$ M	20 mM $\text{NH}_4\text{HCO}_3$ , 10% $\text{D}_2\text{O}$ , pH~7.4, 308 K	1.2 mM	Bruker Avance 700 NMR spectrometer
2D NMR spectroscopy	450 $\mu$ M	20 mM $\text{NH}_4\text{HCO}_3$ , 10% $\text{D}_2\text{O}$ , 308 K, 150 mM NaCl, pH~6.2	900 $\mu$ M	Bruker Avance 700 NMR spectrometer

## 2.12 pH Titrations

Samples at different concentrations of Zn(II)-loaded Zur in different buffers (Table 2.10) were adjusted to a range of pH values, between 8.1 and 2.71, using either acetic acid or hydrochloric acid to lower the pH. The protein samples were then left to equilibrate for 10-15 min at room temperature before recording spectra using different techniques (Table 2.10).

**Table 2.10 Conditions and techniques used for monitoring the pH titration of the SynZur.**

Purpose	Protein concentration	Buffer	pH range	Instrument
UV-Visible	5.2 $\mu$ M	1 mM Tris-Cl	7.8 to 3.1	Varian Cary 50 spectrophotometer
UV circular dichroism	25.9 $\mu$ M	5 mM Tris-Cl	7.8 to 2.71	Jasco J-815 spectropolarimeter
ESI-MS spectrometry	35 $\mu$ M	10 mM $\text{NH}_4\text{HCO}_3$ , 10 % MeOH	8.01 to 4.2	Bruker MicroTOF mass spectrometer
1D NMR spectroscopy	600 $\mu$ M	20 mM $\text{NH}_4\text{HCO}_3$ , 10% $\text{D}_2\text{O}$ , 150 mM NaCl, 308 K	8.1 to 3.60	Bruker Avance 700 NMR spectrometer

## 2.13 Electrophoretic Mobility Shift Assays (EMSA)

PCR amplicons (5 ng) for different promoters (Table 2.11), using DNA extracted from *Synechococcus* sp. WH8102 as template (see Section 2.6.1), were incubated at 23°C for 20-30 min with different concentrations of purified Zn(II)-loaded Zur protein (0-100  $\mu$ M) in the binding buffer (20 mM Tris, 50 mM KCl, 100  $\mu$ g mL<sup>-1</sup> bovine serum albumin, 5% (v/v) glycerol, and 3 mM spermidine).

After the incubation, samples were resolved on a 6% polyacrylamide gel cast and run at -4°C in TAE buffer (40 mM Tris-acetate, 1 mM EDTA) with 1 mM  $\text{MgCl}_2$ . Subsequently, the gels were stained with SYBR-Green (Amersham) and scanned using a phosphorimager (Fuji FLA-5000) at 473 nm emission.

For EDTA-treated Zur protein, Zn(II)-loaded Zur, was incubated with 2 equivalents of EDTA overnight. On the second day, the incubated protein was desalted using PD-10 columns (Sephadex G-25, GE Healthcare) to remove free EDTA and Zn(II)-EDTA. All experiments for EDTA-treated Zur protein were run as described above by using an anaerobic workstation (Don

Whitley Scientific, UK). All images were analysed using ImageReader V3.0 and Aida/2D Densitometry software.

**Table 2.11 List of primer sequences for amplification of different promoters of *Synechococcus* sp. WH8102.**

Target gene	Forward sequence	Reverse sequence	Amplicon length
<i>zur</i> ( <i>synw_2401</i> )	5' CAGCAGCGACAGCGCAGGG 3'	5' GGAACCAGTCATGGCATCAGAA 3'	175-bp
<i>znuC</i> ( <i>synw_0970</i> )	5' TGATGTCACACAGGGTTCCA 3'	5' CTTGATGGACGAATGCGGTT 3'	246-bp
<i>znuA</i> ( <i>synw_0971</i> )	5' GAGATTCTGGCTGCTAGATG 3'	5' GTTCCATCCACAGCCACAAC 3'	256-bp
<i>smtA</i> ( <i>synw_0359</i> )	5' AACGTAACACCACTGATCGG 3'	5' GCACATTTGATTGCTGTAGACATTT 3'	250-bp
<i>znuA</i> ( <i>synw_2481</i> )	5' TGCCGTGCTCTTCTCTCAAG 3'	5' CGAGCCAGTAGCCCACTTAC 3'	250-bp
<i>ntcA</i> ( <i>synw_0275</i> )	5' CACCCTCAGCCGCTCCGAAC 3'	5' TGAAACCACTGCTGGCCACCAT 3'	201-bp

## 2.14 Homology Modelling and Validation

3D homology modelling was performed using the I-TASSER server, an internet service system (Zhang, 2008; Roy *et al.*, 2010). i3Drefine software (Bhattacharya & Cheng, 2013) was used to refine the final structure. Plausible models of the Zur protein obtained from the I-TASSER server were verified using the Structural Analysis and Verification Server (SAVES) to evaluate its stereo-chemical quality (<http://services.mbi.ucla.edu/SAVES/>). All figures prepared in this study were generated using PyMOL software (DeLano, 2007).

# Chapter 3

## Toward Novel Zinc Complexing Ligands in the Marine Cyanobacterium *Synechococcus* sp. WH8102

---

### 3.1 Introduction

Life expanded over all the oceans from the tropics to the poles and from surface waters down to the abyssal depth. It is not surprising that life should endure and thrive up to the present day in the oceans, and organic compounds may have conditioned the marine environments where the prerequisites for life were absent (Duursma & Dawson, 1981). However, the story of organic compounds in the oceans is almost as old as the sea itself (Duursma & Dawson, 1981).

There are of course thousands of organic compounds that originate from organisms, and of these, an even tinier fraction will be “ligands”, fractions that have metal-binding ability. However discovery of metal-binding ligands produced by phytoplankton in seawater has burgeoned in the past two decades (Okujo *et al.*, 1994; Moffett & Brand, 1996), and the study of these ligands has become an important topic for analysis.

The ability of cyanobacteria to assimilate essential nutrients from their environments is critical for growth. Cyanobacteria are known to survive in zinc-deficient environments, but the ways in which they acquire Zn(II) and acclimate are not completely understood (Napolitano *et al.*,

2012; Barnett *et al.*, 2014). Recent studies indicate that there is a high abundance of zinc-binding ligands in surface waters of the North Atlantic, especially in the Sargasso Sea (Jakuba *et al.*, 2008a), where oligotrophic cyanobacteria like the model strain *Synechococcus* sp. WH8102 can dominate (Waterbury *et al.*, 1986; Zwirgmaier *et al.*, 2008).

The ability of *Synechococcus* sp. WH8102 to grow at low zinc concentrations and maintain cellular zinc homeostasis suggests that this bacterium has extremely efficient zinc uptake mechanisms capable of scavenging zinc even from deplete medium (Barnett *et al.*, 2014). However, mechanisms for metal ion uptake in marine cyanobacteria are only partially understood. Genes for DNA-binding metal sensor proteins of the Fur family are predicted to be present in all available genomes, as are ABC transporters for iron and zinc (Blindauer, 2008; Scanlan *et al.*, 2009). However, little is known regarding transport of metal ions across the outer membrane. Considering Zn(II) must be bio-accumulated by a factor of at least  $10^5$ , it follows that uptake mechanisms, including transport across the outer membrane, must be highly efficient (Barnett *et al.*, 2014).

Here, we hypothesises that analogous to siderophore-mediated iron acquisition (Holt *et al.*, 2005; Matthijs *et al.*, 2016) and chalkophore-mediated copper acquisition systems (Yoon *et al.*, 2010; Yoon *et al.*, 2011), *Synechococcus* sp. WH8102 might utilise (a) zinc-binding ligand(s) zincophore(s), extracellular zinc scavengers, for acquiring zinc ions from the marine environment.

For this purpose, a method was developed to isolate and characterise biogenic zinc-binding ligand(s) zincophore(s) that may be produced by the cyanobacterium *Synechococcus* sp. WH8102. Isolation of putative ligands was carried out using solid-phase extraction and liquid chromatographies.

## 3.2 Detection of Trace Metals by ICP-MS

In order to investigate if *Synechococcus* sp. WH8102, grown in zinc-depleted medium (see Section 2.2.1), can produce a zinc-binding organic ligand (designated a zincophore), polystyrene-divinylbenzene solid phase extraction (SPE cartridge) was used to extract any potential metal ligands along with other organic compounds (see Section 2.3.1). Solid phase extraction is a method of sample preparation that concentrates and purifies organic compounds from solution by sorption onto a disposable solid phase cartridge, followed by elution of these compounds using several solvents. However, the mechanism of separation in this technique is depending on hydrophobic and hydrophilic interactions. The main reasons for choosing this solid phase extraction approach were as follows: (i) polystyrene-divinylbenzene has previously been shown to extract metal-binding ligands from seawater (Wiramanaden *et al.*, 2008), (ii) there is a high recovery of metal-binding ligands from this type of solid phase extraction cartridge (Wiramanaden *et al.*, 2008).

*Synechococcus* sp. WH8102 was grown in an artificial seawater medium based on Aquil<sup>\*</sup> media supplemented with 80 nM zinc (zinc-deplete medium) (see Section 2.2.1). An EDTA-based buffer system was used to control the trace metal concentration in the medium. In general, the reaction of zinc with EDTA is given in Equation 3.01:



Where  $\text{EDTA}^{4-}$  represents the nominally free ligand, while  $\text{Zn}^{2+}$  represents the labile pool of dissolved inorganic zinc species or “free zinc”.

Eventually, the rates of chelate formation and dissociation equal one another, and the concentrations of the reacting species no longer change with time (Sunda *et al.*, 2005). Under

this equilibrium condition, the concentrations of the various reacting species ( $[\text{Zn}^{2+}]$ ,  $[\text{EDTA}^{4-}]$  and  $[\text{ZnEDTA}^{2-}]$ ) are related to one another by Equation 3.02:

$$K'_{\text{ZnEDTA}} = [\text{ZnEDTA}^{2-}]/([\text{Zn}^{2+}][\text{EDTA}^{4-}]) \quad \text{Equation 3.02}$$

Where  $K'_{\text{ZnEDTA}}$  is the conditional stability constant for the formation of the Zn-EDTA chelate. At equilibrium, virtually all of the zinc is present as biologically un-reactive Zn-EDTA chelates, and only ~1 in 6,500 zinc atoms is present as reactive  $\text{Zn}^{2+}$  species, “free zinc” (Sunda *et al.*, 2005). For example in the present case, at a total zinc concentration of 80 nM, the equilibrium concentration of biologically available inorganic zinc species is only 16 pM, estimated using the “Species” module of the SCD database considering the total concentration for all metals present in the medium, which is similar to zinc concentration found in natural open ocean surface waters which vary from 2 to 33 pM (Jakuba *et al.*, 2012).

If all of the existing inorganic zinc species were removed by *Synechococcus* sp. WH8102, the system would automatically readjust to its original state by the dissociation of an equivalent amount of Zn-EDTA chelate. This dissociation would remove only 1/6,500 of the chelated zinc, and thus, would not affect the equilibrium  $\text{Zn}^{2+}$  concentration (Sunda *et al.*, 2005). Therefore, the system is well buffered with respect to changes in dissolved inorganic zinc species.

In a first step to study whether *Synechococcus* sp. WH8102 produces ligands that may bind to zinc or not, ICP-MS was performed to detect the trace metals binding to ligands in the culture supernatant (culture grown with cells), and uncultured medium<sup>14</sup> (control medium, medium without cells). Ligands and metal complexes were captured on SPE cartridges, followed by elution with (1:20:80 v/v/v) formic acid: water: methanol (see Section 2.3.1).

---

<sup>14</sup> Uncultured medium was run as a control to confirm a biological origin for the metal-binding compounds present in the culture supernatant and to exclude any contamination in our work.

After extraction of the putative metal-binding ligands using a SPE cartridge, 3% (v/v) nitric acid was used for dilutions, because of the solubility of the nitrates as well as the relative freedom from chemical and spectral interferences (Figure 3.01).

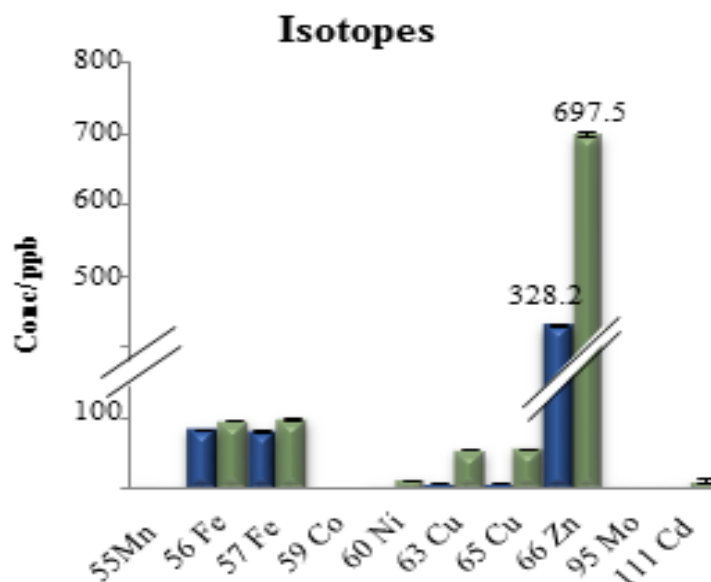


**Figure 3.01 ICP-MS analysis of trace metals from SPE extracts.**

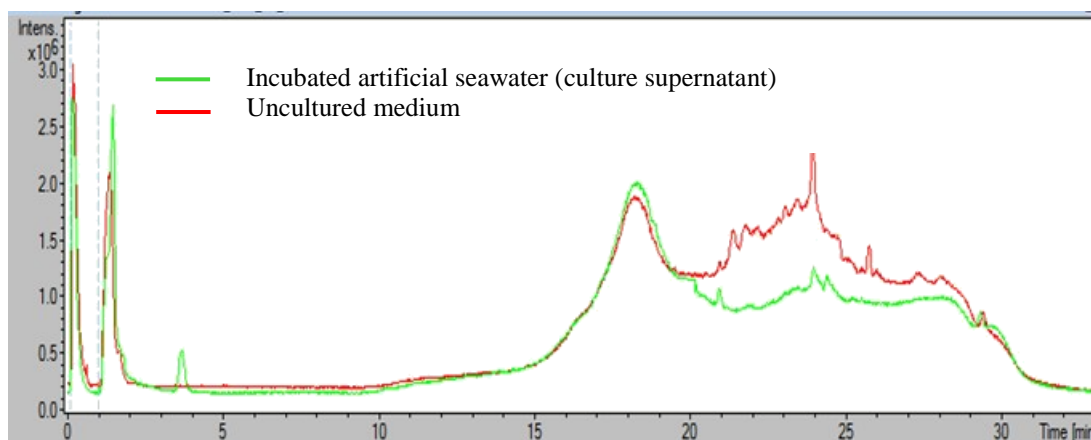
Column charts show the trace metals in ppb after growing *Synechococcus* sp. WH8102 in Aquil\* medium with 80 nM zinc and eluting the metal-complexes from a SPE cartridge using (20:80:1) water: methanol: formic acid. Green bars are culture supernatant and blue bars uncultured medium. The error bars indicate standard error of the mean between three biological replicates.

Figure 3.01 shows that there are differences indeed between culture supernatant and uncultured medium, especially for zinc, which may indicate the presence of a zincophore(s) or zinc bound ligand(s) produced by *Synechococcus* sp. WH8102.

### 3.3 A Zincophore Detection by UHPLC/Q-TOF-MS

To get more insights into the zinc binding ligands that may be produced by *Synechococcus* sp. WH8102, UHPLC/Q-TOF-MS (Ultra High Performance Liquid Chromatography coupled with Quadrupole Time-of-Flight) was performed. Two samples were run in the same conditions: culture supernatant and uncultured medium containing 80 nM zinc in the medium. Metal

complexes were eluted from the SPE cartridge using (20:80:1) water: methanol: formic acid and the SPE extracts were run on the UHPLC/Q-TOF-MS (Figure 3.02).



**Figure 3.02 Total ion chromatograms of SPE extracts using UHPLC/Q-TOF-MS.**

Extractions from two samples, including culture supernatant (green) and uncultured medium (red), were extracted using a Strata-SPE cartridge and the products were analysed on a Dionex 3000RS UHPLC coupled with a Bruker MaXis Q-TOF mass spectrometer.

The reason for using UHPLC/Q-TOF-MS was to enable analysis of isotopic distributions indicative of zinc-containing molecules that may give evidence of zinc complexes. In general, zinc has distinguishable five stable isotopes  $^{64}\text{Zn}$ ,  $^{66}\text{Zn}$ ,  $^{67}\text{Zn}$ ,  $^{68}\text{Zn}$  and  $^{70}\text{Zn}$  with abundance 48.63: 27.90: 4.10: 18.75: 0.62 (Figure 3.03).

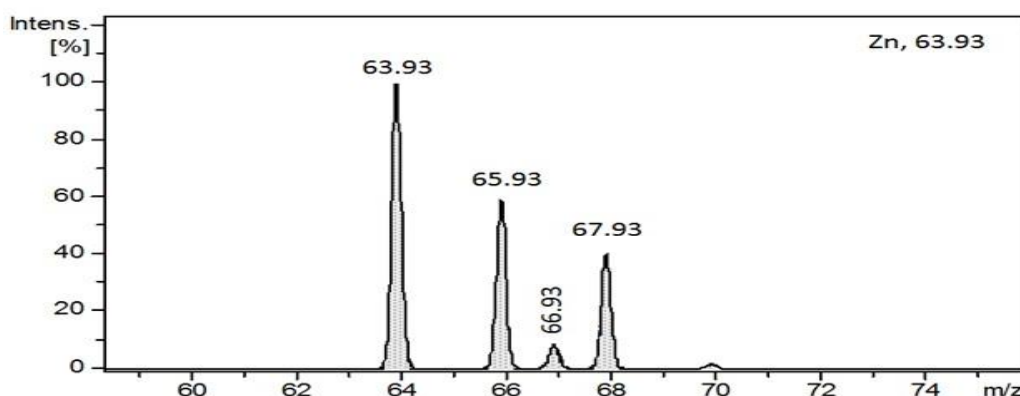


**Figure 3.03 Zinc isotope distributions.**

Focusing on the peak with a retention time between 16 to 22 min (Figure 3.02), it was noticed that there was a compound at 423.27 m/z produced by *Synechococcus* sp. WH8102 in Aquil\* medium supplemented with 80 nM zinc with characteristics expected for zinc isotopes (Figure 3.04A).

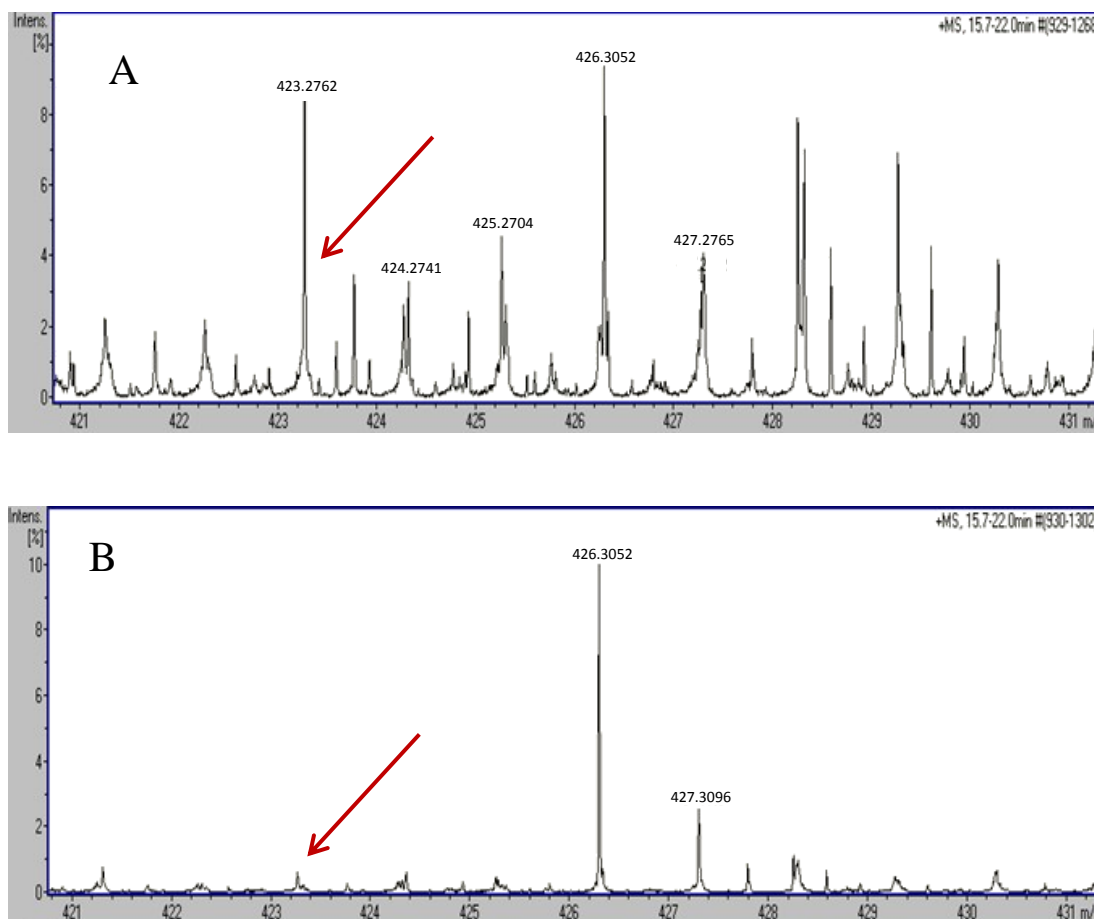


**Figure 3.04 Mass spectra for SPE extracts with a retention time of 15.7-22.0 min.**

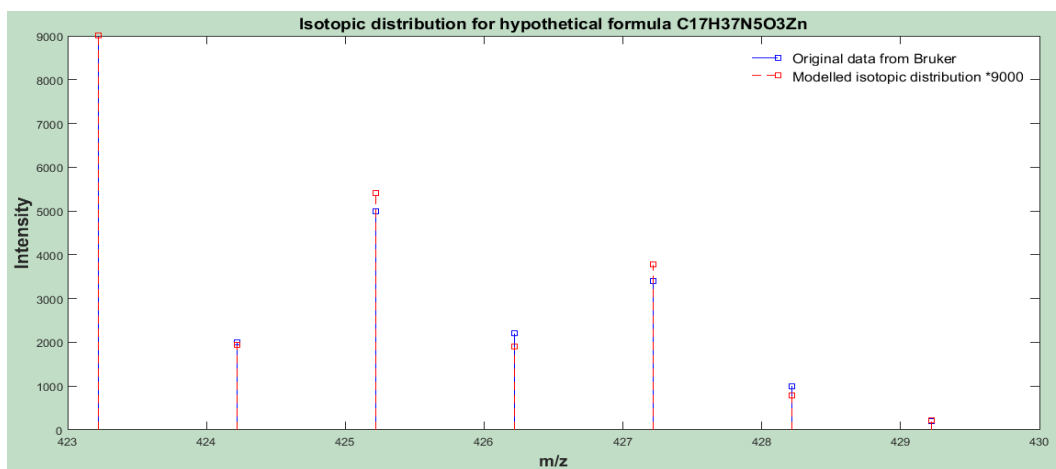
Mass spectra for the 423.27m/z compound present in the culture supernatant (A), and in absence of the 423.27m/z compound in an uncultured medium (B) within the retention time of 15.7-22 min. Red Arrow indicates the presence and absence of 423.27m/z compound.

Figure 3.04A shows there is an isotope distribution at 423.27, 425.27, 426.27, 427.27 m/z and 424.27 for  $^{13}\text{C}$ . This distribution was found only in the culture supernatant (Figure 3.04A) and did not appear in the uncultured medium (Figure 3.04B). In addition, this compound was seen before at the same elution time when *Synechococcus* sp. WH8102 was grown in Pro99 medium which is based on natural seawater (see Appendix C, Figure C.01) (Ksibe, 2011). However, the

intensity of this molecule was highly abundant following growth of *Synechococcus* sp. WH8102 in Pro99 medium containing natural seawater i.e. after culturing, while the presence of this compound in Aquil\* medium was very low. Even so, it is possible that this molecule is produced by *Synechococcus* sp. WH8102.

Data analysis in the Bruker DataAnalysis program was used to predict a formula for this compound; it was found that  $C_{17}H_{37}N_5O_3Zn$  with charge state +1 and 89% score was the best formula.

The original data from the Bruker DataAnalysis program were compared with the modelled isotopic distribution from the isotopident program, an online service, in MATLAB software for the hypothetical formula  $C_{17}H_{37}N_5O_3Zn$  to check the agreement between experimental and theoretical data (Figure 3.05).



**Figure 3.05 Modelling zinc isotope distributions for the hypothetical formula  $C_{17}H_{37}N_5O_3Zn$ .**

Comparison of the original data from the Bruker DataAnalysis program (blue) with the theoretically calculated data from the isotopident program (red) for the  $C_{17}H_{37}N_5O_3Zn$  formula. The graph was prepared in MATLAB.

In the previous chromatograms (Figure 3.02), a peak at 3.8 min was conspicuously present only after culturing. In order to test whether this compound may interact with zinc, the culture supernatant was supplemented with an excess of zinc prior to applying it to SPE. When the ion

chromatogram was derived from the culture supernatant containing excess zinc, the small peak at 3.8 min, present only in the culture supernatant, disappeared (Figure 3.06A). The mass spectrum for the peak of interest (POI) contained a number of peaks with the following masses: 123.11 m/z, 239.11 m/z, 350.17 m/z, 372.17 m/z, 388.18 m/z and 721.34 m/z with the most intense mass at 239.11 m/z (Figure 3.06B).

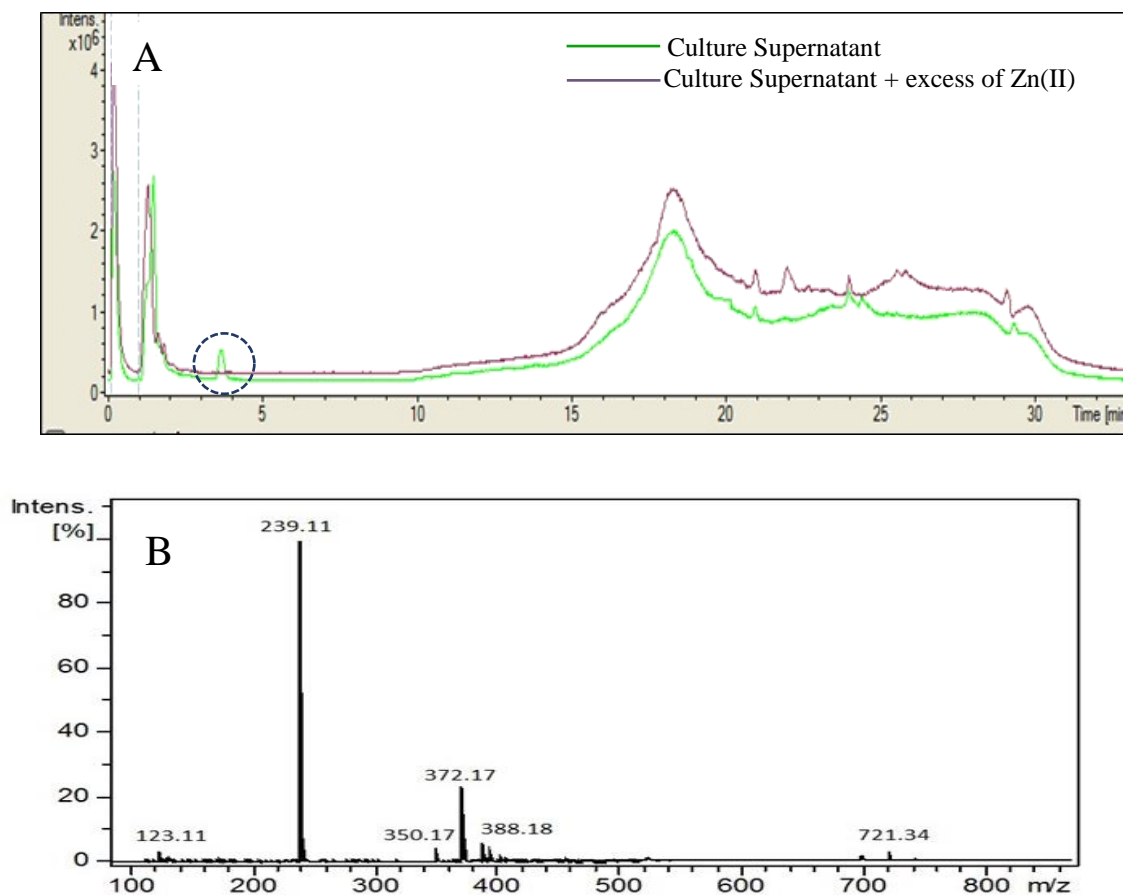


**Figure 3.06 UHPLC/Q-TOF-MS spectra.**

(A) Total ion chromatogram of two samples including culture supernatant (green) and culture supernatant after adding an excess of zinc (purple) in UHPLC/Q-TOF-MS. (B) Mass spectrum for peak of interest (POI) at 3.8 min.

However, it was difficult to predict a plausible formula for 721.34 m/z and 239.11 m/z in Bruker software, so 388.18 was chosen and a predicted formula for this mass was  $C_{20}H_{24}N_2O_2S_2$  with (-0.5 ppm) mean error and 92% score. Searching in the ChemSpider online service, approximately 920 possible formulae were found for this theoretical formula. The suggested

formula is not unreasonable for a potential zincophore; for example, coelibactin from *Streptomyces coelicolor* which acts as a zincophore has the formula  $C_{17}H_{17}N_3O_4S_2$  (Kallifidas *et al.*, 2010). However, a comprehensive identification of the compound from *Synechococcus* sp. WH8102 will require a very large biomass that would allow isolation of sufficient quantities for characterisation.

Our data shows that *Synechococcus* sp. WH8102 might produce more than one kind of ligand under zinc deplete conditions. However, this is not surprising given it has been reported that several bacteria can produce more than one siderophore (Kano *et al.*, 2003; Holt *et al.*, 2005; Martin *et al.*, 2006), so this might also be the case for zincophores.

Due to the difficulty of using the fractions from UHPLC analysis, a further set of experiments was carried out using analytical HPLC with UV-Vis detection at 220 nm.

### **3.4 Zincophore Detection by HPLC**

In the previous experiments and during washing the SPE cartridge with 50:50 water: methanol (see Section 2.3.1), it was noted that there were yellow solids in the washing fraction. Therefore a new experiment was designed by washing the SPE initially with aqueous ammonium bicarbonate (see Section 2.3.1). Then the putative ligands were extracted from the SPE cartridge using two solutions including: 50:50 (v/v) water: methanol (designated here as fraction 1), and 1:20:80 (v/v/v) formic acid: water: methanol (designated here as fraction 2). Fractions were then submitted to HPLC instead of UHPLC that differs in the size of particles filled into the column. Particle sizes of 2.7  $\mu\text{m}$  were used for UHPLC with higher pressure, while 5  $\mu\text{m}$  ones were used for analytical HPLC with lower pressure.

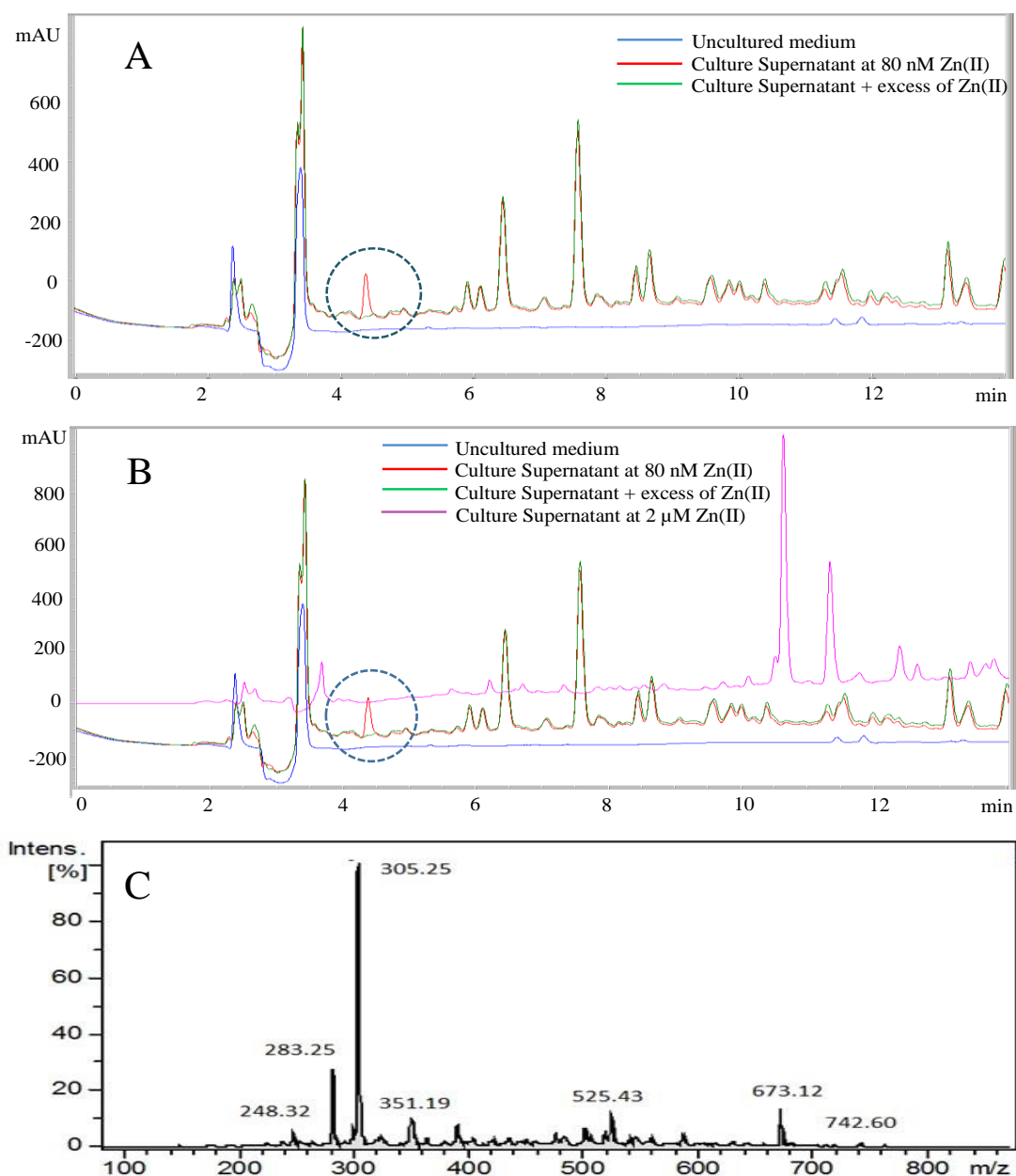


**Figure 3.07 HPLC spectra for the fraction eluted with 50:50 methanol: water.**

(A) HPLC chromatograms at 220 nm for eluted fractions from a SPE cartridge using (50:50) methanol:water from three samples after pre-concentration on a SPE cartridge including uncultured medium (Blue), culture supernatant (Red), and culture supernatant after adding excess zinc (Green) where *Synechococcus* sp. WH8102 was grown in 80 nM Zn(II) supplemented medium. (B) Comparing the HPLC spectra for eluent fractions including uncultured medium (Blue), culture supernatant (Red), culture supernatant after adding excess of zinc (Green) whereas *Synechococcus* sp. WH8102 was grown at 80 nM of Zn(II) in the cultures, and culture supernatant (Pink) where *Synechococcus* sp. WH8102 was grown at 2 μM of Zn(II) in its culture. All chromatograms were conducted on an Agilent 1100 series HPLC quaternary pump. (C) Mass spectrum for peak of interest (POI) at 4.3 min that is expected to be a zinc free-ligand.

Once again (Figure 3.07), three samples were analysed by chromatography under the same conditions and included culture supernatant, uncultured medium and culture supernatant after adding excess zinc. For fraction (1), eluted with 50:50 (v/v) water: methanol, it was noted that there was a small peak at 4.3 min which disappeared after adding excess zinc ions (Figure 3.07A), in the same range for the peak observed in the UHPLC-MS experiments. However, this peak vanished due to interaction between this compound with zinc ions and is subsequently not captured on a C18 column or the retention time is changed. Moreover, in this experiment, no difference in the samples was found in fraction (2) eluted with 1:20:80 (v/v/v) formic acid: water: methanol.

To check whether *Synechococcus* sp. WH8102 can produce the same compound at 4.3 min in zinc replete medium (i.e. at higher zinc concentration in the medium), *Synechococcus* sp. WH8102 was grown in the presence of 2  $\mu$ M Zn(II) supplemented medium where a theoretical “free zinc” concentration is 400 pM, estimated using the “Species” module of the SCD database considering all metals presenting in the medium. Interestingly, the peak at 4.3 min was present only after culturing *Synechococcus* sp. WH8102 in zinc-deplete medium but not in zinc-replete medium (Figure 3.07B).

The putative zinc free ligand eluting at 4.3 min was collected and subjected to mass spectrometry to partially characterise this compound (Figure 3.07C). The mass spectrum for the interesting peak shows a number of peaks at the following masses 283.25 m/z, 305.25 m/z, 351.19 m/z, 525.43 m/z, 673.12 m/z and 742.60 m/z with the most intense mass at 305.25 m/z. Comparing Figures 3.06C with 3.07C indicates that there is not much agreement between the two mass spectra obtained but the spectrum is still in the same range  $\sim$  720 m/z.

However, no further information could be gleaned, except that we know that these compounds are produced by *Synechococcus* sp. WH8102 under zinc deplete conditions, and that addition of zinc to culture supernatants leads to the removal of these peaks from the chromatograms.

Unfortunately, due to the low amount of this compound obtained from 4-5 litres of culture supernatant and the relatively long growth rate of this strain (60-70 days for 4 liters), no further experiments were achieved.

Three mechanisms for the uptake of metals from metal-organic ligands (ML) have been proposed for phytoplankton cells (Figure 3.08): 1) the intact ML metal complex may be transported into the cell, as is the case with siderophores and chalkophores; 2) the inorganic metal concentration in the vicinity of the cell may be increased by dissociation of the ML; or 3) the ML metal complex may be able to form a transient ternary complex XML (Aristilde *et al.*, 2012). The latter can occur if ML delivers M to a metal uptake molecule, X, thus transferring M directly to the cell (Aristilde *et al.*, 2012) (Figure 3.08).

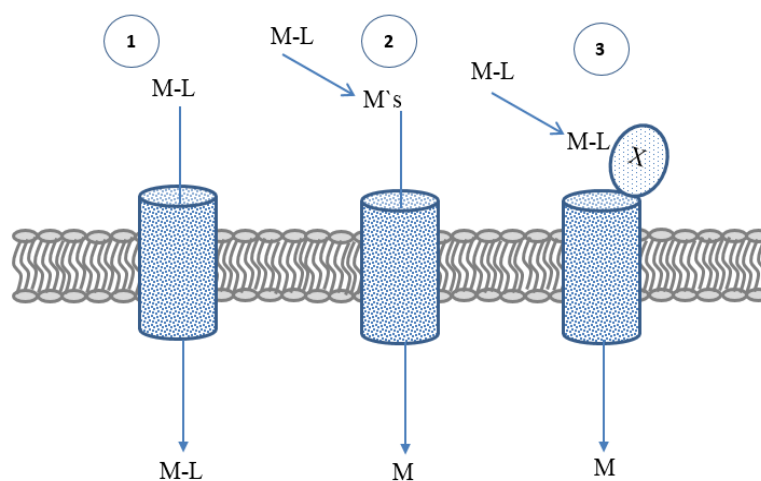


**Figure 3.08 Schematic illustration of mechanisms of metal uptake across the outer membrane.**

Metal uptake mechanisms at the cell surface, where (L) is an organic ligand, (M's) is inorganic metal or free ion and M is the free metal. Adapted from (Aristilde *et al.*, 2012).

Very little is known about zinc uptake across the outer membrane. It seems often to have been assumed that Zn(II) enters the periplasm by diffusion along a concentration gradient through non-specific porins. However, this will only be suitable for zinc-replete conditions, but not for

zinc-deplete conditions, especially when the exterior free Zn(II) levels are extremely low, as in the open ocean.

Recently, the zinc-uptake protein, ZnuD, was described in several bacteria (see Section 1.6.2.1) as an outer-membrane protein. A scavenger protein a “zincophore”, the pH-regulated antigen 1 (Pra1), which sequesters zinc was also reported (see Section 1.8).

Zinc homeostasis in the cyanobacterium *Anabaena* sp. PCC7120 also highlights the ability of this bacterium to adapt to zinc deplete conditions by synthesising a zinc chelator or “zincophore” (Napolitano *et al.*, 2012; Nies, 2012).

*Synechococcus* sp. WH8102 has recently been studied following growth under zinc depleted conditions (Barnett *et al.*, 2014). Immobilised zinc affinity chromatography (Zn(II)- IMAC) enabled the capture and detection of several proteins with potential functions in zinc metabolism, such as ZnuA (SYNW2481) and two outer membrane proteins (SYNW2224 and SYNW2227) (Barnett *et al.*, 2014). SYNW2224 and SYNW2227 belong to a family of cyanobacterial porins (CBP) with the hypothesis that these porins transport simple inorganic ions but not organic ligands.

Therefore our first hypothesis regarding zinc transport through the outer membrane of *Synechococcus* sp. WH8102 is that a zincophore binds to one of the above-mentioned porin proteins (e.g. SYNW2224) but the porin transport only the zinc ion (i.e. not the metal-ligand complex) into *Synechococcus* sp. WH8102 (Figure 3.09A). SYNW2224 shows a 16-stranded  $\beta$ -barrel, and a N-terminal S-layer homology domain, connected by a long amphipathic helix (Barnett *et al.*, 2014). However, no defined metal binding sites are found in SYNW2224 (Barnett *et al.*, 2014) suggesting that the porin may bind to a Zn(II)-zincophore complex rather than naked metal ions.

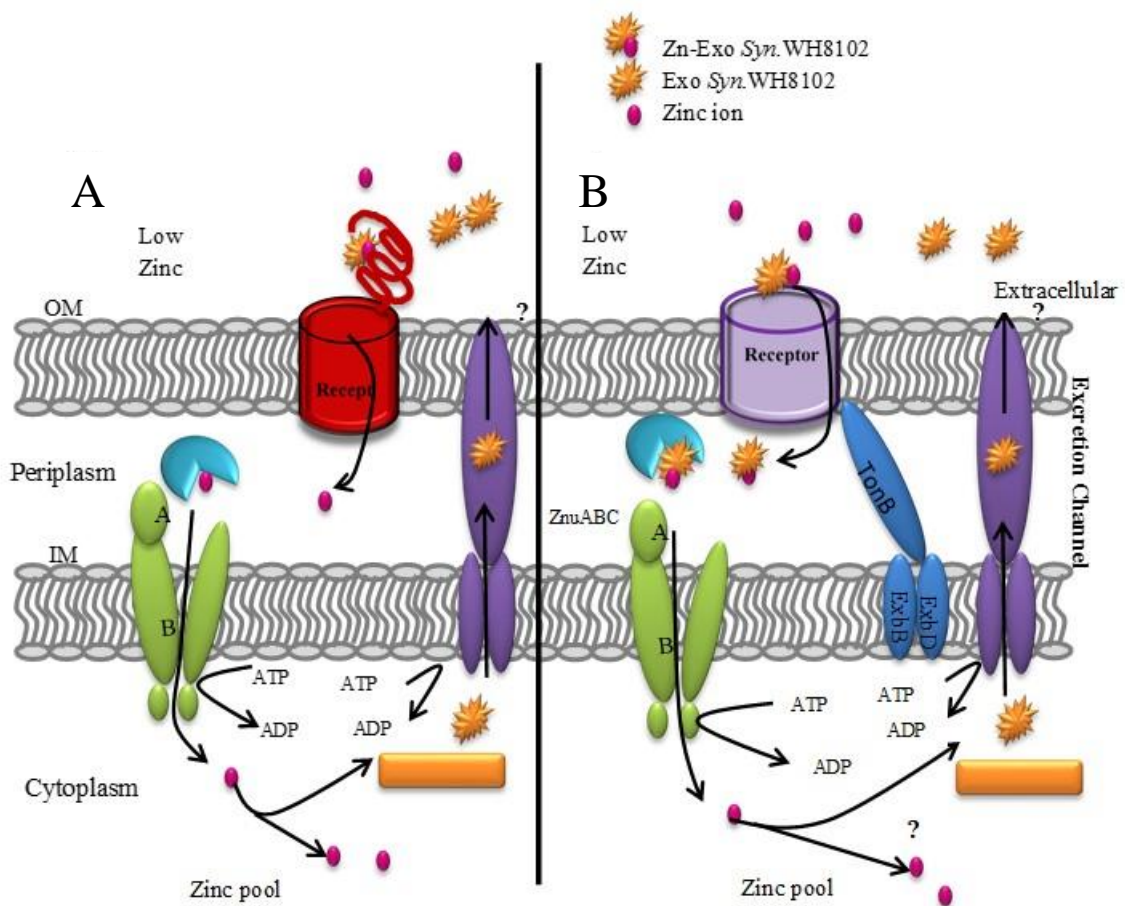


**Figure 3.09 Hypothesised model of zinc transport through the outer membrane of *Synechococcus* sp. WH8102.**

Under zinc-deplete conditions, *Synechococcus* sp. WH8102 may compensate for low zinc levels by producing zincophores (orange starbursts) which could scavenge zinc ions (pink dots) and form Zn(II)-zincophore complexes. Uptake of zinc ions by *Synechococcus* sp. WH8102 may require binding of the Zn(II)-zincophore complex to a porin protein and transferring only the zinc ions through the outer membrane (A) or the Zn(II)-zincophore complex may bind to an unknown receptor and transfer the complex through the outer membrane using e.g. TonB-dependent receptors (B). Subsequently, the ZnuABC transporter system could be used for zinc transport across the inner membrane.

Hence, the second hypothesis is that zinc is transported into the *Synechococcus* sp. WH8102 as a Zn(II)-zincophore complex (Figure 3.09B). This option typically involves TonB-dependent receptors, which actively transport their substrates (i.e. under consumption of ATP). However, it is known that most marine *Synechococcus* strains lack these TonB-dependent receptors (Palenik *et al.*, 2003; Scanlan *et al.*, 2009) suggesting a novel mechanism and preventing identification of such receptors merely using bioinformatics or even they do not exist.

### 3.5 Summary and Conclusion

Bioinformatic studies of cyanobacterial strains, the dominant photosynthetic organisms in oligotrophic regions of the world's oceans, strongly point towards dedicated networks for zinc uptake and utilisation. However, an absolute requirement of marine cyanobacteria for zinc has not been demonstrated conclusively (Blindauer, 2008; 2015).

Here, we used the oligotrophic open-ocean strain *Synechococcus* sp. WH8102 as a model cyanobacterium to study the potential production of zinc ligands or zincophores following growth under zinc-depleted conditions.

Solid phase extraction with liquid chromatography were effective methods in detecting a putative zincophore. Using UHPLC/Q-TOF-MS, a compound with characteristics expected for a zinc ligand was detected following culturing *Synechococcus* sp. WH8102 in Aquil\* medium with a mass of 423.27 m/z and a predicted formula  $C_{17}H_{37}N_5O_3Zn$ . Additionally, a zinc-free ligand, which disappeared after adding zinc, was found at 3.8 min in the total ion chromatogram.

Using analytical HPLC, a zinc-free ligand located at 4.3 min in the total ion chromatogram was detected in the culture supernatants of *Synechococcus* sp. WH8102 following growth in zinc-depleted medium. However, the compound at 4.3 min was produced by *Synechococcus* sp. WH8102 under zinc depleted medium (80 nM of Zn(II)), and was not found under zinc replete medium (2  $\mu$ M of Zn(II)).

Unfortunately, due to low amounts of this compound being recovered from culture supernatants, even when using 4-5 litre culture volumes, no further characterisation of these molecules could be achieved.

# Chapter 4

## Growth and Proteomic Changes in *Synechococcus* sp. WH8102 under Zinc Depleted and Replete Conditions

---

### 4.1 Introduction

Analysis of the genome of *Synechococcus* sp. WH8102 revealed some of the ways that these organisms have adapted to their largely oligotrophic environment, in comparison to freshwater cyanobacteria such as *Synechocystis* sp. PCC6803 or *Synechococcus* sp. PCC7942. In addition, this strain has a reduced regulatory machinery consistent with the fact that the open ocean constitutes a far more constant and buffered environment than fresh water (Palenik *et al.*, 2003). However, *Synechococcus* sp. WH8102 possesses a large number of ABC family efflux transporters (Palenik *et al.*, 2003), especially efflux pumps for metals (SYNW1472 and SYNW0900) suggesting that this strain type, despite living in extremely oligotrophic conditions, may still find themselves in the position of needing to export “toxins” or some metal that may fluctuate in its environment (Palenik *et al.*, 2003).

However, our knowledge of zinc-dependent gene regulation in this strain is patchy and fragmented. In an effort to resolve how open ocean *Synechococcus* sp. WH8102 persists in

regions where zinc concentrations are thought to be depleted, this strain was grown in zinc-depleted and replete conditions. The cells were allowed to grow over 35-40 days in Aquil\* media supplemented with (80 nM and 2  $\mu$ M) zinc, and cells from two cultures harvested for comparative proteomics using MALDI-MS technique.

## 4.2 Growth Characteristics of *Synechococcus* sp. WH8102

To investigate if zinc concentration may affect the growth of *Synechococcus* sp. WH8102 in an artificial seawater medium based on Aquil\* media, two cultures were supplemented with either 80 nM (zinc-depleted medium) or 2  $\mu$ M (designated here as “replete” medium) (see Section 2.2.1).

The free Zn(II) concentrations in open ocean surface waters vary from 2 to 33 pM (Jakuba *et al.*, 2012). The “free zinc” concentration in our depleted medium (16 pM) is not dissimilar to those that *Synechococcus* sp. WH8102 might encounter in its natural habitat, close to oligotrophic level. The “free zinc” concentration in our “replete” medium (400 pM) is out of this range. However, it was previously reported that the “free zinc” concentration 1000 pM in the media is toxic with 500 pM is partially toxic to this strain (Chu, 2013).

By monitoring the optical density (OD) at 750 nm to get the cell density as well as the chlorophyll content, a growth curve was plotted for each condition. As shown in Figure 4.01, bi-phasic growth was observed with a faster growth rate in the first 200 hours and a slower growth rate subsequently for both cultures. At the same time, it was observed that there is a difference between 1-3 days (24-72 hours) by a reduction in the growth curve for the 80 nM cultures compared to that for 2  $\mu$ M cultures (Figure 4.01). Our results show that *Synechococcus* sp. WH8102 appears to be able to adapt to its environment at these two conditions (Figure 4.01).

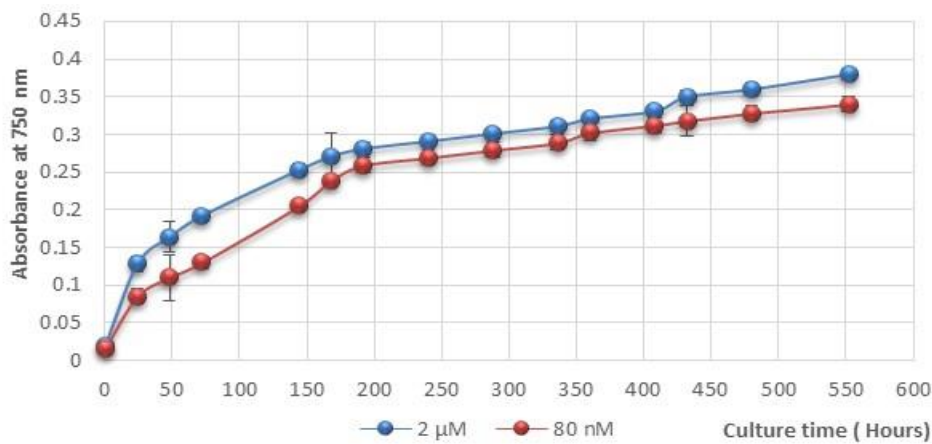


**Figure 4.01 Growth curves of *Synechococcus* sp. WH8102.**

*Synechococcus* sp. WH8102 was grown with two concentrations of zinc in the media (80 nM and 2 μM). Growth was monitored by the absorbance at 750 nm; Blue line: Growth in Aquil\* medium (containing 2 μM zinc); Red line: Growth in Aquil\* medium (containing 80 nM). The error bars indicate standard error of the mean between two biological replicates.

However, another growth curve was followed by monitoring cell abundance number using flow cytometry as a proxy for growth under these two conditions (see Section 2.4.1). A small difference in cell abundance was detected for the 80 nM cultures just before 3 days and this difference started decreasing progressively with time (Figure 4.02).

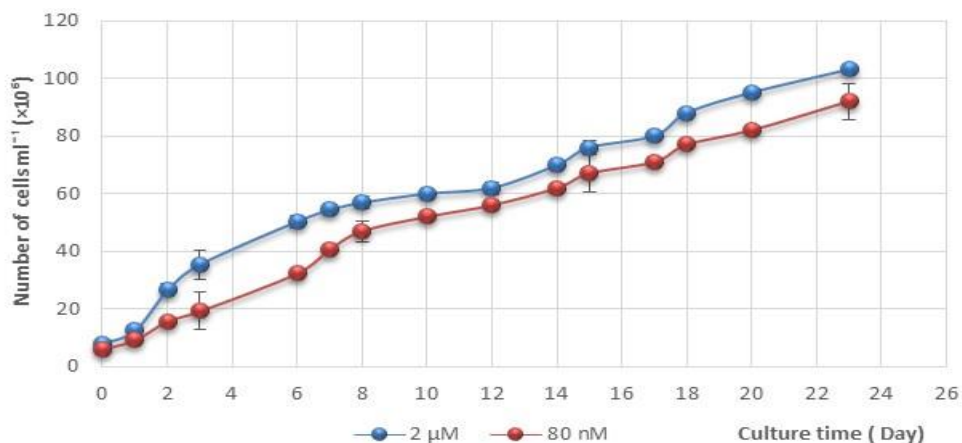


**Figure 4.02 Growth (number of cells) of *Synechococcus* sp. WH8102.**

*Synechococcus* sp. WH8102 was grown with two concentrations of zinc in the media (80 nM and 2 μM). Growth was monitoring as the number of cells in 1 ml counted using flow cytometry; Blue line: Growth in Aquil\* medium (containing 2 μM zinc); Red line: Growth in Aquil\* medium (containing 80 nM). The error bars indicate standard error of the mean between two biological replicates.

By looking in more detail at the growth curve for the first 7 days (Figure 4.03), it was noticed that there was a plateau at 2 days for cells grown in 80 nM cultures but this was later recovered at day 7.

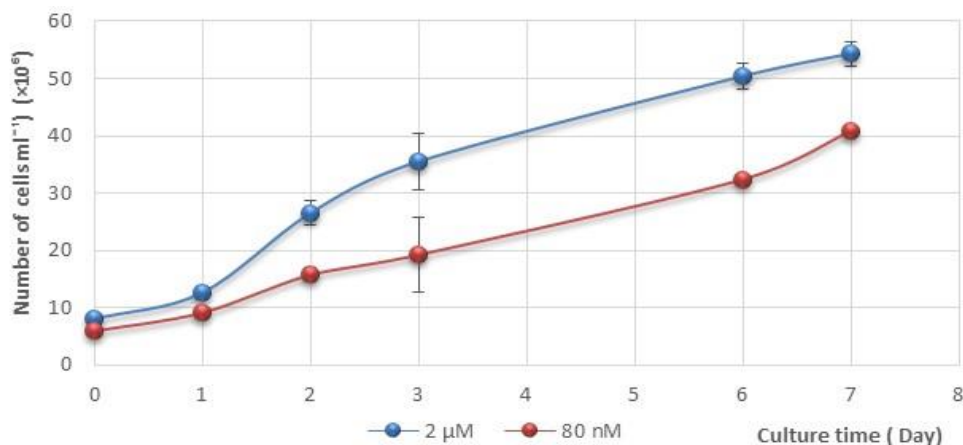


**Figure 4.03 Growth curves of *Synechococcus* sp. WH8102 for 7 days.**

Representative growth curves of *Synechococcus* sp. WH8102 for 7 days with two concentrations of zinc in the media (80 nM and 2 μM). Growth was monitored as the number of cells in 1 ml counted using flow cytometry; Blue line: Growth in Aquil\* medium (containing 2 μM zinc); Red line: Growth in Aquil\* medium (containing 80 nM). The error bars indicate standard error of the mean between two biological replicates.

### 4.2.1 Specific Growth Rates

Specific growth rates ( $\mu_{\max}$ ) during time ( $d^{-1}$ ) were calculated as the slopes of linear regressions of  $\ln(\text{cell density})$  versus day number for individual cultures over the range of linearity (see Section 2.4.2).

Analysing the specific growth rate for *Synechococcus* sp. WH8102 in two cultures (80 nM and 2 μM) for time point  $t = 8-14$  days, where  $R^2$  was 0.9294 and 0.9988 for 80 nM and 2 μM respectively, it was noticed that there was a small difference between the two conditions, but this was not significant (Figure 4.04B). It was observed however that there was a clear difference between 80 nM and 2 μM at time point  $t = 2-7$  days, where  $R^2$  was 0.9544 and 0.9898 for 80 nM and 2 μM respectively (Figure 4.04A).

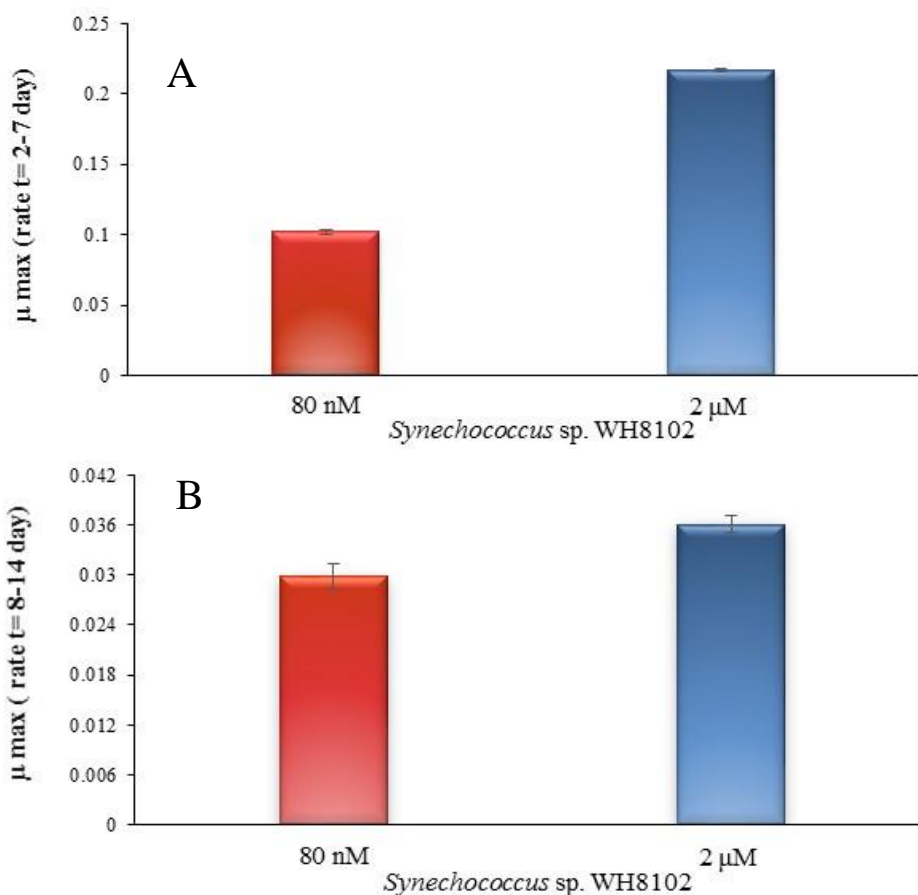


**Figure 4.04 Specific growth rates for *Synechococcus* sp. WH8102.**

Comparison of specific growth rates for *Synechococcus* sp. WH8102 in two cultures (80 nM and 2  $\mu$ M) at (A) time point t = 2-7 day and (B) time point t = 8-14 day. Error Bars indicate standard error of the mean between two biological replicates.

From these results it can be concluded that the *Synechococcus* sp. WH8102 was not significantly affected at concentration of 2  $\mu$ M, but that growth at 80 nM Zn(II) was initially slower, and recovered later.

#### 4.2.2 Chlorophyll *a* Concentration

Marine unicellular cyanobacteria are responsible for an estimated 20–40% of chlorophyll biomass and carbon fixation in the oceans (Palenik *et al.*, 2003) and zinc plays an important role in carbonic anhydrase and carbon fixation. Therefore, the amount of chlorophyll *a* in two cultures was calculated to check if there was any difference in these cultures.

The chlorophyll *a* content of the 80 nM and 2  $\mu$ M cultures was monitored by methanol extraction and the amount of chlorophyll *a* was calculated according to Ritchie (2006) (see Section 2.4.3).

Figure 4.05 shows a small difference in the chlorophyll *a* level in the first 7 days between the 80 nM and 2  $\mu$ M cultures.

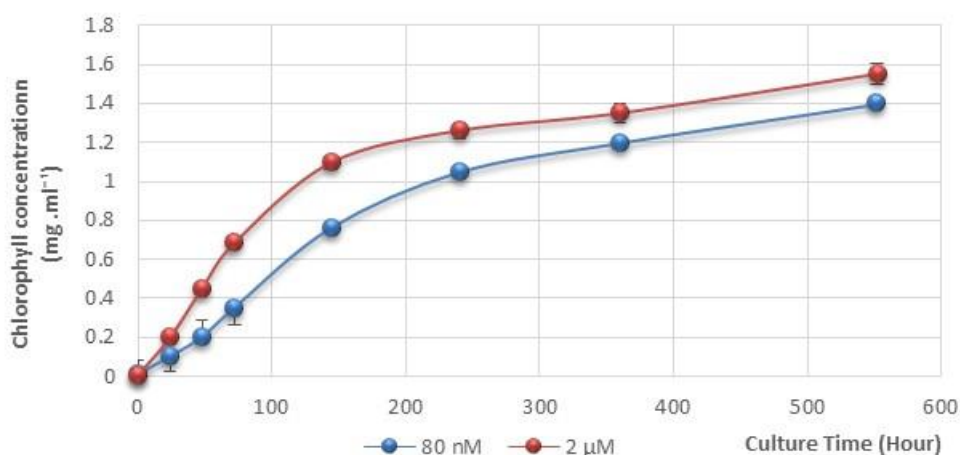


**Figure 4.05 Time course of chlorophyll *a* (*Chl a*).**

Time course of chlorophyll *a* content for *Synechococcus* sp. WH8102 measured by spectrophotometric technique and calculated according to Ritchie (2006). Blue line: Growth in Aquil\* medium (containing 2  $\mu$ M zinc); Red line: Growth in Aquil\* medium (containing 80 nM). The error bars indicate standard error between two biological replicates.

Considerable evidence from the time course suggests the presence of slight differences between the two cultures in the first 7 days. However, these cells look like they can adapt to their environment during later stages.

Several questions arise from this part of study what are the adaptations that *Synechococcus* sp. WH8102 undergoes? Is there any difference in protein expression data between these two conditions? Can this strain repress or de-repress the expression of any proteins that can help them to adapt to these two conditions?

## 4.3 Proteomics Analysis

Comparative proteomics aims to systematically and quantitatively compare two or more proteomes to assess static or perturbation-induced changes in protein profiles. At present, no single technique in a one-step operation can provide the identification and quantification of all proteins in a complex system, such as soluble and insoluble cell extracts. So concerted approaches are required, including sample preparation, protein or peptide separation, mass spectrometric analysis, as well as bio-informatic tools for database search and quantification.

In order to study any obvious changes in protein expression, whole-cell lysates from cultures grown at 80 nM and 2  $\mu$ M were separated on SDS gels, and bands for differentially expressed proteins were excised, in-gel digested (see Section 2.5). Then the proteins were analysed by peptide mass-mapping by matrix-assisted laser desorption/ ionisation (MALDI) time-of-flight (TOF) mass spectrometry and Mascot peptide mass fingerprint software (see Section 2.5).

### 4.3.1 1D-SDS-PAGE Profiles

Protein comparisons between two *Synechococcus* sp. WH8102 cultures grown at 80 nM or 2  $\mu$ M zinc, were performed using 1D SDS-PAGE with Coomassie staining (Figure 4.06). From the SDS-PAGE profile it was observed that there was one protein which is downregulated in the 2  $\mu$ M culture, while there were two proteins up-regulated in the 2  $\mu$ M culture (Figure 4.06).

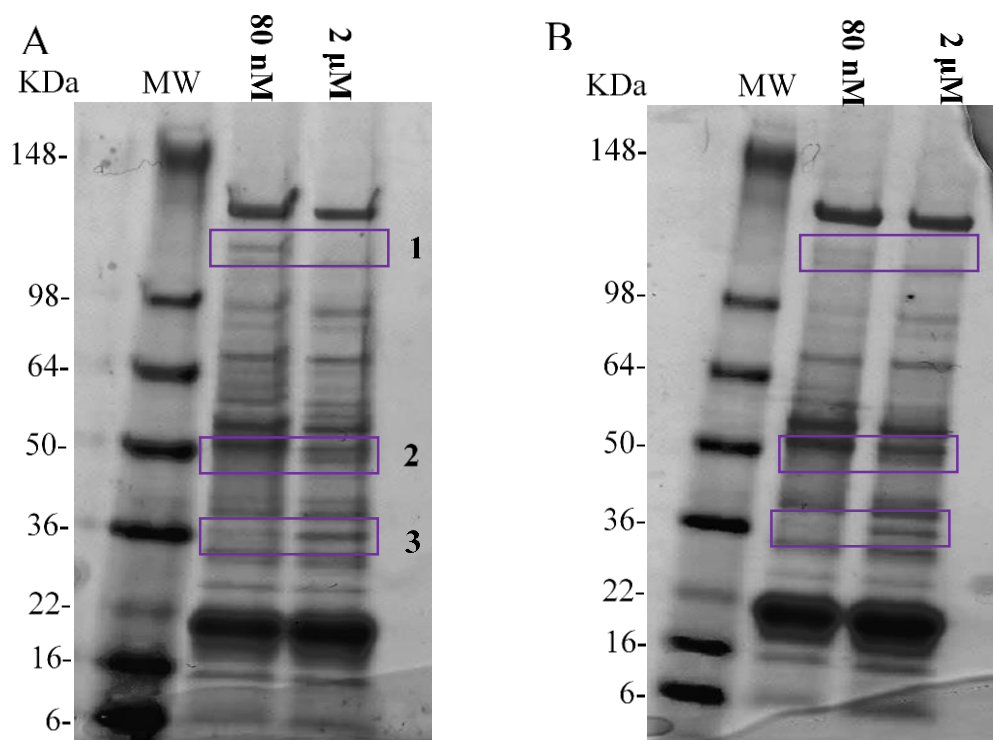


**Figure 4.06 SDS-PAGE profiles of whole-cell lysates of *Synechococcus* sp. WH8102.**

*Synechococcus* sp. WH8102 was grown in Aquil\* medium supplemented with two concentrations of zinc (80 nM and 2 µM). Proteins showing a marked difference in expression are boxed. (A) Lysate with 80 µg of protein per lane; (B) Duplicated experiment with 40 µg of protein per lane.

### 4.3.2 Protein Identification by MALDI-TOF Mass Spectrometry

The bands displaying differential protein intensity were excised and subjected to In-gel digestion with trypsin<sup>15</sup>, and the peptides analysed by MALDI-TOF (see Section 2.5).

The MALDI-MS spectra for bands 1, 2 and 3 were interrogated using Mascot 2.1 (Matrix Science, Boston, MA) for searching against the NCBI database using Bacteria-Other bacteria taxonomy.

---

<sup>15</sup> Trypsin is a serine protease that specifically cleaves peptide bonds at the carboxyl side of lysine and arginine residues.

**Table 4.01 Identification of proteins in three bands.**

<b>Band</b>	<b>MOWSE<sup>16</sup> Score</b>	<b>Peptide Matches</b>	<b>Sequence Coverage %</b>	<b>Protein Mass KDa</b>	<b>Locus tag</b>
<b>1</b>	225	30	32	99.782	Synw_2346
<b>2</b>	78	8	26	38.728	Synw_0791
<b>3</b>	91	10	35	33.861	Synw_1018

The protein in band 1 (less abundant at 2  $\mu$ M zinc) matched ATP-dependent Clp protease, Hsp 100, ATP-binding subunit ClpB [*Synechococcus* sp. WH8102] with a MOWSE score of 225, while the protein in band 2 (less abundant at 80 nM zinc) is fructose-1,6-bisphosphate aldolase [*Synechococcus* sp. WH8102] with score 78, and the protein in band 3 (less abundant at 80 nM zinc) is the substrate-binding protein of a phosphate-ABC transporter, [*Synechococcus* sp. WH8102] with score 91<sup>16</sup> (Table 4.02 and Figure 4.07).

---

<sup>16</sup> MOWSE, MOlecular Weight SEarch, is a method for identification of proteins from the molecular weight of peptides created by proteolytic digestion and measured with mass spectrometry.

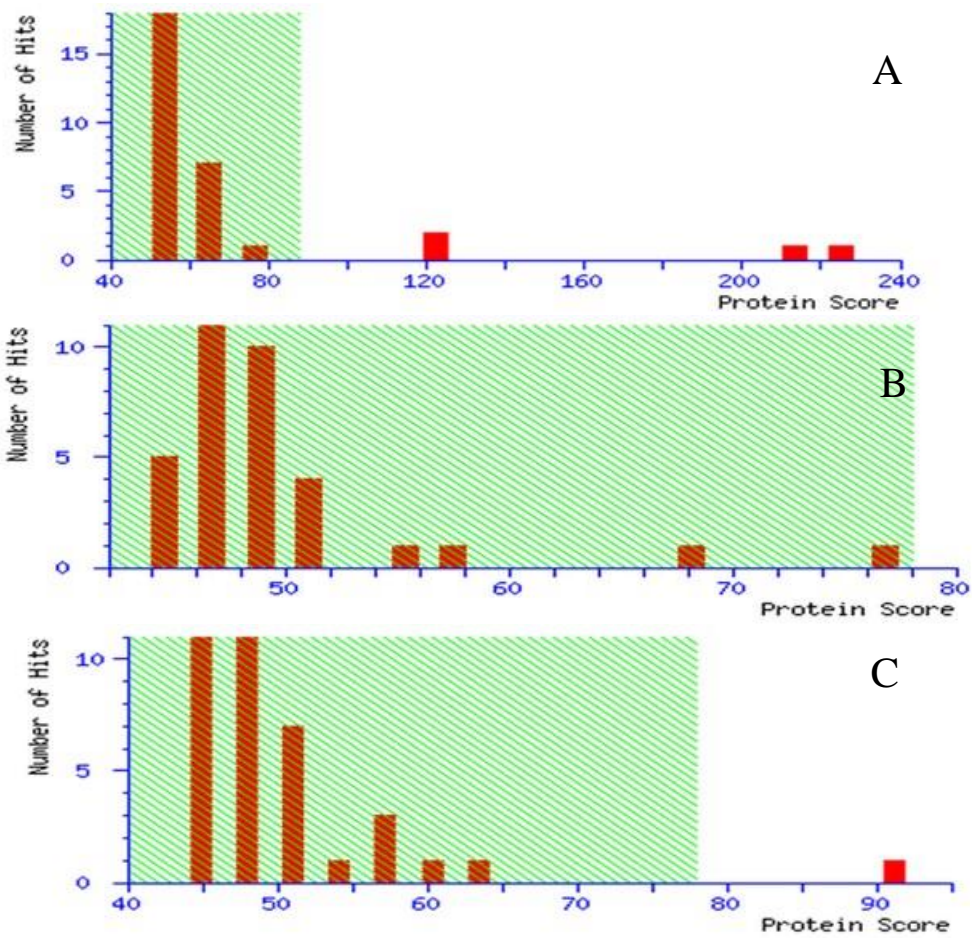


**Figure 4.07 Analysis of proteins in Mascot software.**

(A) Mascot Score Histogram for protein ATP-dependent Clp protease, Hsp 100, ATP-binding subunit ClpB, where protein score greater than 88 are significant ( $p < 0.05$ ), and the score of protein in band 1 was 225; (B) Mascot Score Histogram for protein fructose-1,6-bisphosphate aldolase, where protein score greater than 78 are significant ( $p < 0.05$ ), and the score of protein in band 2 was 78; (C) Mascot Score Histogram for protein substrate-binding protein of a phosphate-ABC transporter, where protein score greater than 78 are significant ( $p < 0.05$ ), and the score of protein in band 3 was 91.

Once the proteins were identified, it was possible to assign some peptides in the original MALDI-MS spectra, which are shown for fructose-1,6-bisphosphate aldolase (Figure 4.08 and see Appendix D, Table D.01), and for ABC transporter, substrate binding protein, phosphate (Figure 4.09 and see Appendix D, Table D.02).

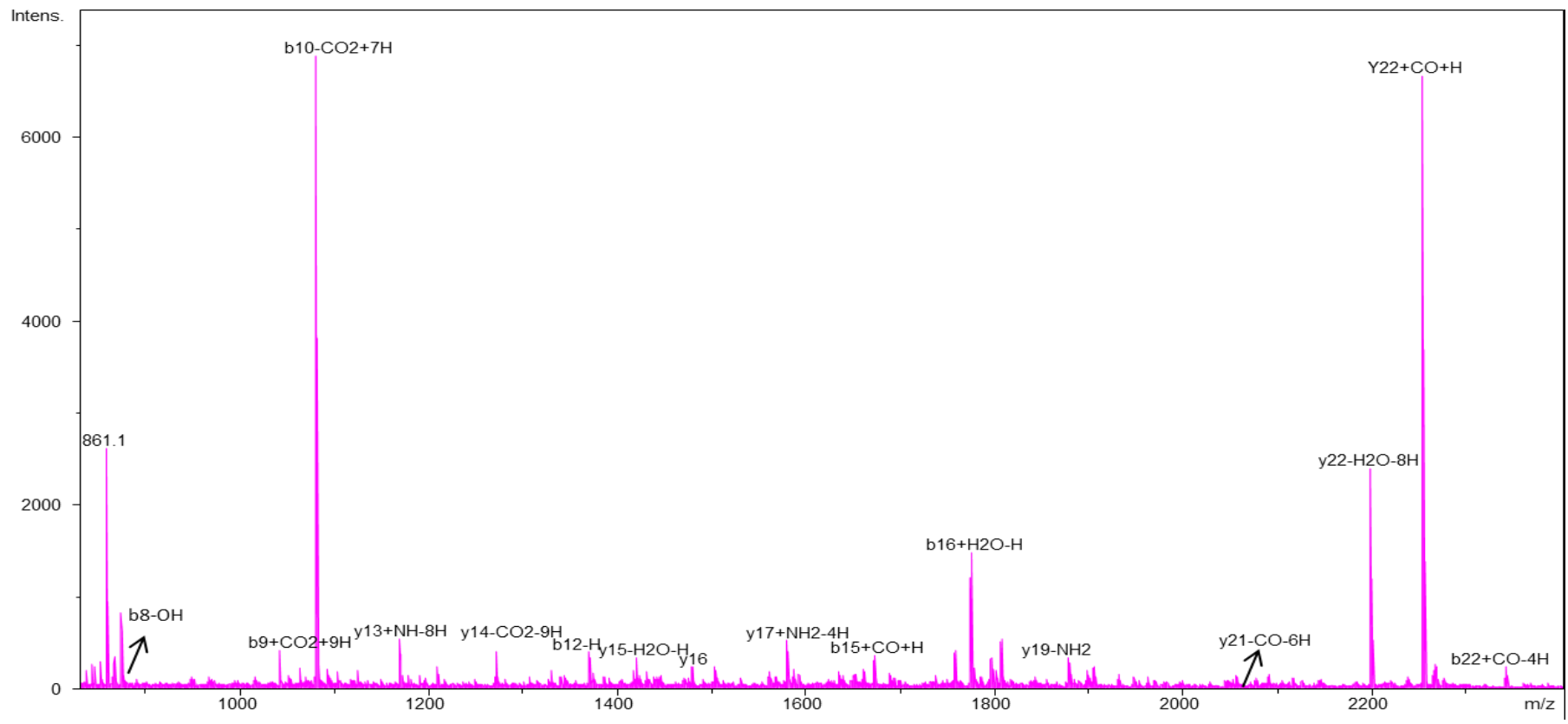


**Figure 4.08 MALDI-MS spectrum for some identified peptides for fractose-1,6 bisphosphate aldolase.**

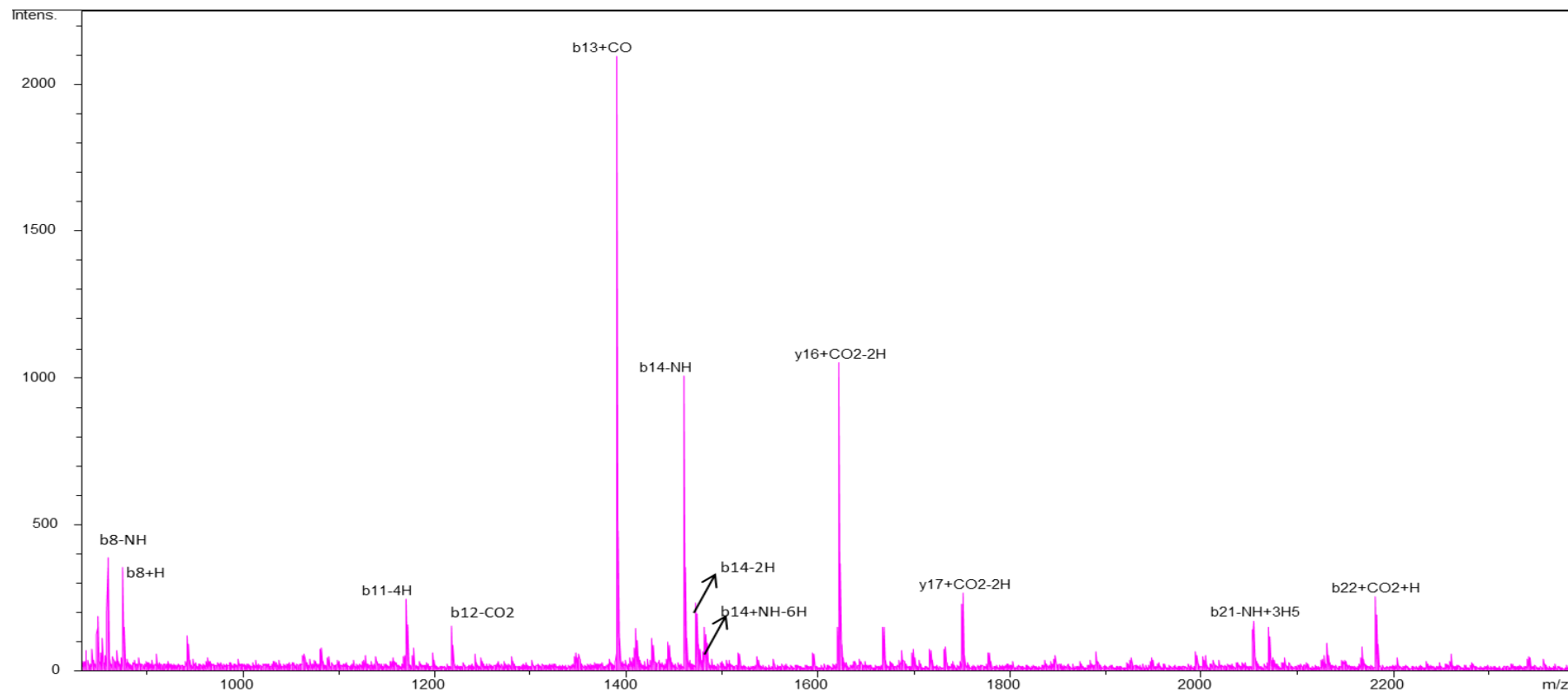


**Figure 4.09 MALDI-MS spectrum for some identified peptides for ABC transporter, substrate binding protein, phosphate.**

## 4.4 Discussion

### 4.4.1 Growth Characteristics

It was previously stated that a concentration of 80 nM zinc in *Synechpococcus* sp. WH8102 medium corresponds to 'replete' condition (Barnett *et al.*, 2014). However, in this study, we define zero zinc as 'starvation', 80 nM zinc as 'depletion', and 2  $\mu$ M zinc as replete conditions. A consideration of 2  $\mu$ M zinc, containing 400 pM "free zinc", as replete condition was based on the fact that presence of 1000 pM "free zinc" in *Synechococcus* sp. WH8102 culture was toxic, while presence of 500 pM "free zinc" in the culture was partially toxic and led to reduced growth for *Synechococcus* sp. WH8102 (Chu, 2013).

During growth of *Synechococcus* sp. WH8102 in zinc depleted or replete conditions, the initial growth rates were slightly different with a noticeable reduction in growth rate in zinc depleted medium. In contrast, previous experiments in our group did not indicate a difference in growth rate or final cell yield between cultures grown at 80 nM and 0 nM (Barnett *et al.*, 2014).

The ability of this strain to cope equally well in starvation media (0 nM added zinc) (Barnett *et al.*, 2014), depletion media (80 nM), and repletion/"zinc-rich" media (2  $\mu$ M) may indicate the following; (i) *Synechococcus* sp. WH8102 has no absolute requirement for zinc. However, based on our genome-mining work (Barnett *et al.*, 2012) as well as biochemical evidence for the expression and zinc-binding ability of proteins involved in zinc homeostasis in *Synechococcus* sp. WH8102, this hypothesis can be rejected; (ii) *Synechococcus* sp. WH8102 has a highly effective system for zinc uptake, and indeed, this has also been confirmed recently (Cox & Saito, 2013; Barnett *et al.*, 2014).

The fact that the strain also copes well with levels of zinc that are significantly higher than those typically found in its natural environment may indicate that this strain has also mechanisms to

cope with a certain degree of zinc excess. The bacterial metallothionein (which is regulated by the Zur zinc sensor; see Chapter 8) may play a role here.

## 4.4.2 Preliminary Proteomics Analyses

### 4.4.2.1 The ATP-dependent Clp Protease, Hsp 100, ATP-binding Subunit ClpB

The ATP-dependent Clp protease, Hsp 100, ATP-binding subunit ClpB<sup>17</sup> protein identified under zinc depletion conditions (band 1 in Figure 4.06), is part of the Clp family comprising a functionally diverse range of proteins that includes Hsp (heat-shock protein) representatives.

Clp/Hsp100 proteins are members of the AAA<sup>+</sup><sup>18</sup> family of ATPase proteins that have now been identified as molecular chaperones.<sup>19</sup> They are hexameric protein machines that have a multiplicity of functions such as folding of newly synthesised proteins, refolding and reactivation of unfolded and misfolded proteins (Figure 4.10A), assembly and disassembly of macromolecular protein structures, and targeting abnormal and inactive proteins for degradation (Sanchez *et al.*, 1992; Clarke, 1996; Schelin *et al.*, 2002; Doyle & Wickner, 2009; Shah *et al.*, 2014).

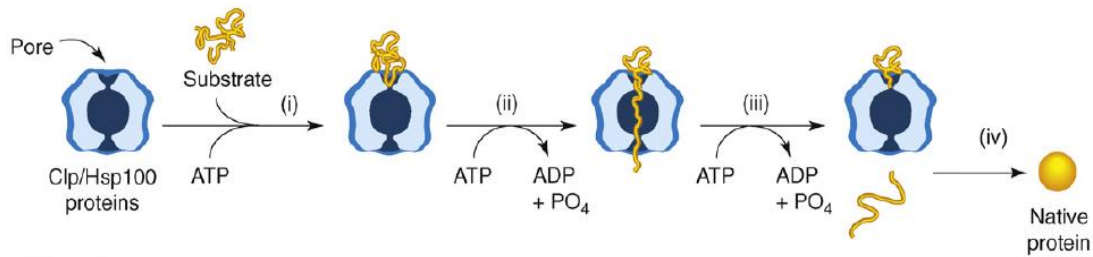
---

<sup>17</sup> ClpB: Caseinolytic peptidase B protein homologue.

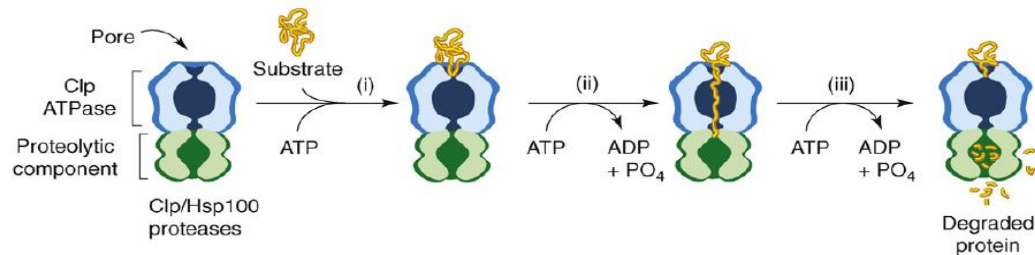
<sup>18</sup> AAA or AAA+: ATPases associated with various cellular activities.

<sup>19</sup> Molecular chaperones are vital contributors to cell homeostasis during stress conditions. Without an effective system constantly controlling and monitoring protein quality, many cellular processes would eventually cease, leading ultimately to cell death.

A) Protein remodelling by Clp/Hsp 100 proteins



B) Protein degradation by Clp/Hsp 100 proteins in association with a proteolytic component



C) Disaggregation by Clp/Hsp in combination with the Hsp/DnaK Chaperon component

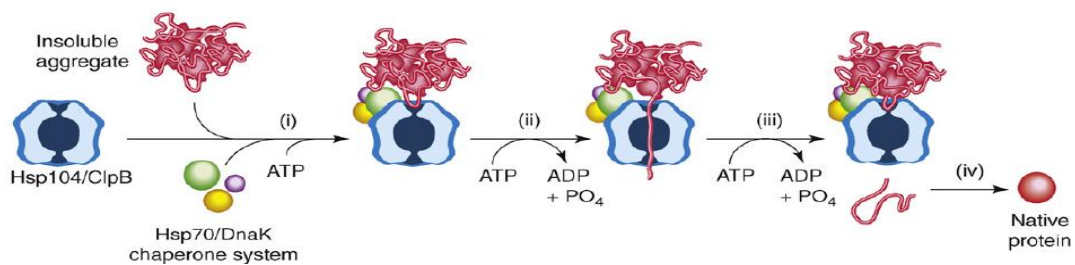


**Figure 4.10 Models for the mechanisms of Clp/Hsp100 proteins.**

(A) Protein remodelling by Clp/Hsp100 proteins. Substrates, such as specific proteins, multimeric proteins and small aggregates, interact *via* unstructured regions containing recognition motifs with Clp/Hsp100 proteins. Substrates are unfolded by forcible translocation through the central channel of Clp/Hsp100 proteins using the energy of ATP hydrolysis. The unfolded polypeptides are released and refold spontaneously. (B) Protein degradation by Clp/Hsp100 proteins in association with a proteolytic component. Clp/Hsp100 proteins associate with a partner peptidase and recognises, unfolds and translocates substrate polypeptides progressively into the chamber of the proteolytic component where degradation occurs. (C) Disaggregation by Hsp104 and ClpB in combination with the Hsp70/DnaK system (another molecular chaperone). Hsp70/DnaK chaperone system is likely to assist in presenting substrates to Hsp104/ClpB and might additionally coordinate ATP hydrolysis by Hsp104/ClpB, then remove polypeptides from the aggregate by forcible translocation of the polypeptides through their central channels and release the unfolded polypeptides to refold spontaneously. Adapted from (Doyle & Wickner, 2009).

Some, but not all, Clp/Hsp proteins associate with proteolytic components forming compartmentalised ATP-dependent proteases (Schelin *et al.*, 2002; Doyle & Wickner, 2009)

that help in effectively degrading the rising levels of faulty proteins that cannot be preserved or repaired by molecular chaperones (Figure 4.10B) (Clarke, 1996). Interestingly, sometimes Clp/Hsp combine with another chaperone system that helps the unfolded protein to refold (Figure 4.10C).

Clp/Hsp proteins are heat shock proteins that are induced under conditions of heat stress (Sanchez & Lindquist, 1990). Moreover, Clp/Hsp proteins can protect cells against a variety of stresses under many physiological conditions (Parsell *et al.*, 1994).

The Clp/Hsp100 protein family consists of at least five different proteins (ClpA, B, C, X and Y) that can be grouped into two general categories (Doyle & Wickner, 2009). Of the three proteins, ClpB is the most widespread being found in almost all organisms studied (Clarke, 1996).

ClpB is found in both prokaryotes and eukaryotes and in each case is primarily a stress-inducible protein (Sanchez *et al.*, 1992; Clarke, 1996). However, early studies showed that ClpB was detectable under conditions of extreme thermal stress, such as in *Saccharomyces cerevisiae* (Sanchez & Lindquist, 1990). Later in the same bacteria, this protein was found to play a critical importance role in tolerance to ethanol, sodium arsenite and long-term storage in the cold, and also found to be expressed under high levels of acetate (Sanchez *et al.*, 1992). ClpB has been shown to facilitate the resolubilisation of heat-denatured luciferase protein from insoluble aggregates in *Vibrio harveyi* (Parsell *et al.*, 1994).

In the freshwater cyanobacterium *Synechocystis* sp. PCC6803, ClpB protein is up-regulated as a response to heat stress where the level of this protein was elevated after incubation of cells at 44°C for 60 min (Suzuki *et al.*, 2006). Additionally, this protein was also up-regulated under phosphate stress in *Synechocystis* sp. PCC6803 (Fuszard *et al.*, 2013). Furthermore, ClpB protein in *Synechococcus* sp. PCC7942 do not respond to high temperatures or other stresses

such as cold, high light or oxidation, suggesting that there are other functions which are unknown to this family yet (Schelin *et al.*, 2002).

The importance of Clp/Hsp proteins under adverse growth conditions has been clearly demonstrated by their capacity to protect proteins from thermal denaturation and resolubilise inactive protein aggregates. However, at least in some cyanobacteria, this protein is not a heat shock protein, but rather responds to nutrient deprivation, e.g. phosphate stress. In *Synechococcus* sp. WH8102, ClpB was more abundant at low zinc concentrations which may indicate that at low zinc concentrations there are more unfolded proteins that require chaperone activity to be induced.

Despite a wealth of information about Clp proteins, however, many questions still remain, especially concerning their precise function in cyanobacteria.

#### 4.4.2.2 Fructose-1,6-bisphosphate Aldolase

Fructose-1,6-bisphosphate aldolase (FBPA) catalyses the reversible cleavage of D-fructose 1,6-bisphosphate (FBP) to dihydroxyacetone phosphate (DHAP) and D-glyceraldehyde 3-phosphate (G3P) (Berry & Marshall, 1993; Cooper *et al.*, 1996; Galkin *et al.*, 2009; Pegan *et al.*, 2009).

Two evolutionarily and mechanistically unrelated classes of these enzymes exist, designated as class I (which employs an active site lysine in Schiff base<sup>20</sup> formation) and class II (which employs a Zn (II)co-factor) (Berry & Marshall, 1993; Galkin *et al.*, 2009; Pegan *et al.*, 2009).

The class II aldolase enzyme is homodimeric/tetrameric (Figure 4.11A) and its active site

---

<sup>20</sup> Schiff base, synonymous with azomethine, is a compound with a functional group that contains a carbon-nitrogen double bond with the nitrogen atom connected to an aryl or alkyl group. These bases have the general formula  $R^1R^2C=NR^3$ , where R is an organic side chain.

contains a zinc ion that is utilised in the catalytic mechanism (Galkin *et al.*, 2007; Pegan *et al.*, 2013).

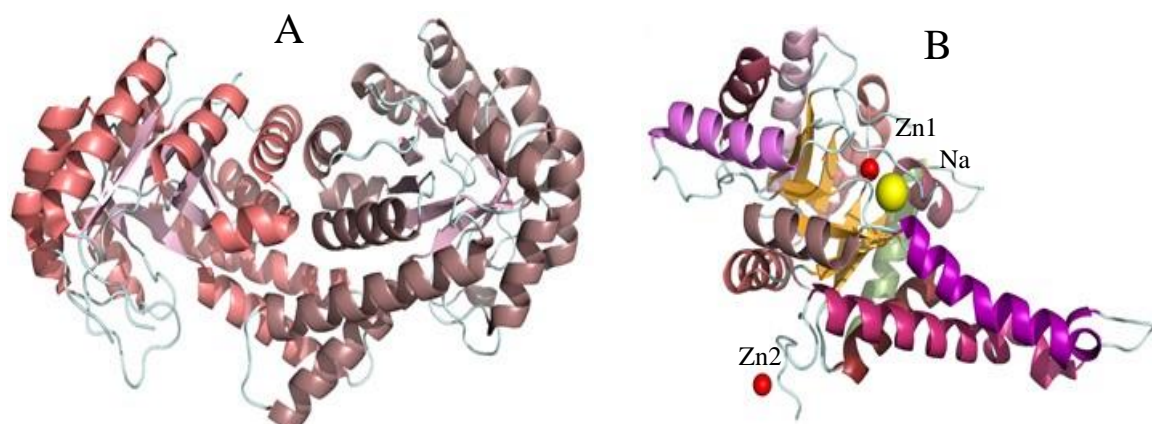


**Figure 4.11 Structural features of Class II FBPA proteins.**

(A) Ribbons represent the FBPA protein as a homodimer *Bacillus anthracis* (pdb 3Q94). (B) Ribbons represent one monomer of the FBPA protein from *M. tuberculosis* (pdb 3ELF) with one sodium in yellow and two zinc cations in red (Pegan *et al.*, 2009).

Early investigation about the nature of the zinc-binding site(s) in the Class II aldolases has suggested involvement of 3 His and 1 Cys residue (Berry & Marshall, 1993), and a more recent crystallographic investigation identified two zinc ions per monomer (Pegan *et al.*, 2013). One of the two zinc cations (Zn1) is located within the active site bound to 3 His residues and one water molecule whereas the other zinc ion (Zn2) is located at a crystal contact between two monomers (Pegan *et al.*, 2013) (Figure 4.11B), and hence probably physiologically not relevant.

Moreover, it was reported that this enzyme is necessary for the survival of *Giardia lamblia* (Galkin *et al.*, 2007) and cyanobacteria (Rogers *et al.*, 2007) under optimal laboratory growth conditions. Sequential alignment between FBPA from *M. tuberculosis* and FBPA from *Synechococcus* sp. WH8102 shows that the 3 His, zinc-binding residues, are conserved (Figure 4.12).

FBPA-Syn	MALVP---LRLLLDHAENGYGIPAFNVNMLEQVQAIMEAADETDSPVILQASRGARNYA	57
FBPA-MT	MPIATPEVYAEMLGQAKQNSYAFPAINCTSSSETVNAAIKGFADAGSDGIIQFSTGGAEFG	60
FBPA-Syn	GEIFLRHLILAATE-----TYPHIPVVMHQDIGNAPDTCYSAaing-----	98
FBPA-MT	SGLGVKDMVTGAVALAEFTHVIAAKYP-VNVALHTDH-CPKDKLDSYVRPLLAISAQRVS	118
FBPA-Syn	-----FTSVMMDGSLEADAKTPASYEYNVAVTKQVVDFAHSVGVSVEGELGCLGSLETG	152
FBPA-MT	KGGNPLFQSHMWDGS-----AVPIDENLAIAQELLKAAAAAKIILEIEIGVVGGEEDG	171
FBPA-Syn	KGEA--EDGHGFEGELSKDMLLTDPAEADFVAKTKCDALAIAGTSHGAYK---FTRKP	207
FBPA-MT	VANEINEKLYTSPGDFEKTIEALGAGEHGKYL-----LAATFGNVHGVYKPGNVKLRP	224
FBPA-Syn	----TGEVLAISRIAEIHKAIPNTHLVMHGSSSVPQEWLEMINKHGGAIPEITYGVPVEEI	263
FBPA-MT	DILAQQQQVAAAKLGLPADAKP-FDFVFHGGSS-----GSLKSEI	262
FBPA-Syn	QEGIRNGVRKVNIDTDNRLAFTAAVR-----EAAMADPANFDRHFNKPKARK	310
FBPA-MT	EEALRYGVVKNVDTDTQYAFTRPIAGHMFTNYDGVLKVDGEVGVKVKVYDPRSYLKKAEA	322
FBPA-Syn	YMKQVCLDRYQQFWAAGNASKIQQQTINYAGLYAKGALDPKAAVAA	357
FBPA-MT	SMSQRVVQACNDLHCAGKSLTH-----	344

**Figure 4.12 Sequential alignment for FBPA.**

Sequential alignment for fructose-1,6-bisphosphate aldolase from *Synechococcus* sp. WH8102, FBPA-Syn, and from *M. tuberculosis* FBPA-MT.

It can be concluded that fructose-1,6-bisphosphate aldolase Class II is a zinc-dependent enzyme in *Synechococcus* sp. WH8102. It may be hypothesised that lack of zinc in depletion media, which is likely to lead to a non-functional protein, may either directly affect expression of FBPA, or alternatively, non-zinc loaded FBPA may be degraded/turned over more rapidly, which may lead to overall decreased protein abundance.

#### 4.4.2.3 ABC Transporter, Substrate Binding Protein, Phosphate

*Synechococcus* sp. WH8102 possesses several putative alkaline phosphatases, as well as four periplasmic phosphate-binding proteins that are part of ABC transporter systems (Palenik *et al.*, 2006; Scanlan *et al.*, 2009).

The phosphate ABC transporter found in this study belongs to the PstS family, which corresponds to the substrate-binding component of the ABC-type transporter complex PstSACB. The gene for this protein (PstS) is accompanied, generally in the same operon, by

the genes for an ATP- binding protein (PstB) and two permease proteins (PstC and PstA). This system is responsible for high affinity inorganic phosphate ( $P_i$ ) uptake (Surin *et al.*, 1985; Pitt *et al.*, 2010). Moreover, phosphorus accounts for about 2–4% of the dry weight of most cells (Ilikchyan *et al.*, 2009). Inorganic phosphate is an essential cellular component for DNA, RNA, nucleic acids, lipids, sugars (van Veen, 1997; Cox & Saito, 2013).

Evidence has been presented for the translocation of  $H_2PO_4^-$  and  $HPO_4^{2-}$ , but not of  $MeHPO_4$  (where Me is a divalent cation) *via* the Pst system (van Veen, 1997). However, previously *Synechococcus* sp. WH8102 show changes in global gene expression levels during the growth under P stress conditions (Tetu *et al.*, 2009; Ostrowski *et al.*, 2010), and the *pstS* gene was strongly upregulated in less than 24 hours (Ostrowski *et al.*, 2010). Moreover, it has been hypothesized that Zn(II) and phosphorus co-limitation could occur in oligotrophic regions based on laboratory experiments with the coccolithophore *Emiliana huxleyi* (Shaked *et al.*, 2006) and *Synechococcus* sp. WH8102 (Ostrowski *et al.*, 2010).

Recently, a proteomic study of P stress in *Synechococcus* sp. WH8102 indicated direct zinc-phosphate links (Cox & Saito, 2013). Thus, Zn(II) appears to be critical to the phosphate response in this organism, whilst bacterial metallothionein (SmtA) also appears correlated with phosphate-stress-associated proteins (Cox & Saito, 2013). However, these authors stated “Yet with no Zn(II) in this proteome experiment the phosphate response was quite different including the greater relative abundance of five hypothetical proteins with no increase in PstS”.

Surprisingly, the PstS protein also shows considerable affinity for Zn(II) by binding to an IMAC column charged with Zn(II) (Barnett *et al.*, 2014). Together, the observations suggest that Zn(II) nutritional levels are connected to the  $PO_4^{3-}$  response in this cyanobacterium, and consistent with the ideas that Zn(II) is beneficial for the functioning of alkaline phosphatase.

The apparent upregulation of PstS at high Zn(II) (2  $\mu$ M) detected in the present study may hint at either of two possibilities. Firstly, perhaps *Synechococcus* sp. WH8102 is making use of the high zinc availability (2  $\mu$ M) in replete cultures and that this acclimation to “luxury” Zn(II) concentrations, allows transport ZnHPO<sub>4</sub> into cell *via* this PstS family protein. Conversely, under zinc replete concentrations, PstS system may mediate Zn(II) efflux, or metal exchange (Keasling, 1997; Beard *et al.*, 2000).

## 4.5 Summary and Conclusion

The SDS-PAGE and growth data presented in this chapter strongly suggest that *Synechococcus* sp. WH8102 has the ability to sense and respond to changes in the external zinc concentration, at least within the range of concentrations tested in this study.

This suggests the possibility of a two-tier strategy in *Synechococcus* sp. WH8102: Fructose-1,6-bisphosphate aldolase (FBPA) and the periplasmic phosphate binding proteins PstS were upregulated under replete concentration of zinc that likely corresponds to a “luxury” situation. In contrast, the ATP-dependent Clp protease, Hsp 100, ATP-binding subunit ClpB was upregulated under zinc deplete conditions, possibly to recycle, repair, and/ or degrade zinc-requiring proteins.

The fact that *Synechococcus* sp. WH8102 can cope with deplete and replete conditions (0-2  $\mu$ M added zinc) suggests the existence of highly efficient mechanisms that control the levels of free zinc inside the cells.

At this point one may ask what regulates these genes. Significantly, *Synechococcus* sp. WH8102 has a putative gene (*synw\_2401*) encoding Zur protein. Given results obtained here, I hypothesise that under zinc replete conditions, FBPA, which contains zinc in its active site, is expressed normally. In contrast, under zinc depleted conditions, FBPA may be repressed

indirectly by Zur and then zinc will be released from FBPA to support the pool concentration. Moreover, zinc releasing may lead to unstable FBPA which will be degraded by Clp/Hsp 100 (Figure 4.13). Alternatively under zinc deplete conditions, FBPA may be expressed but cannot fold properly.

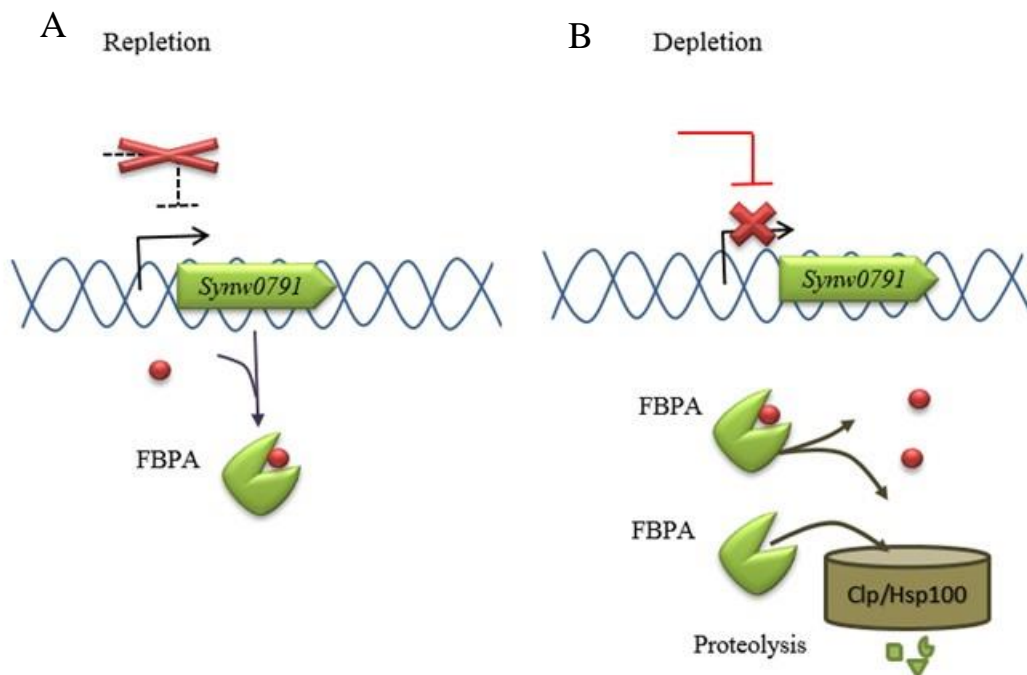


**Figure 4.13 Hypothetical modelling of expression of FBPA protein under Zur protein.**

(A) Protein de-repression of FBPA under zinc-repletion conditions, (B) Protein repression under zinc depletion conditions and proteolysis by Clp/Hsp100.

Also it was suggested that protein turnover may play a role in regulation of zinc homeostasis (Chivers, 2007; Pruteanu *et al.*, 2007). However, Zur protein may not regulate FBPA directly, and metalloregulation may not be the only possible explanation for increased/ decreased levels of a particular protein. Proteins could help to optimise zinc usage by rapid re-distribution between old and new proteins – a strategy that, for iron, has been dubbed as metal “hot-bunking” (Saito *et al.*, 2011).

In *Synechococcus* sp. WH8102, metallothionein appears to be regulated with alkaline phosphatase and PstS (Cox & Saito, 2013), suggesting a Zn-handling mechanism in which

metallothionein could be acting as a metal reservoir supplying alkaline phosphatase with Zn(II). However, the metallothionein SmtA was found to have Zur box in the RegPrecise ([http://regprecise.lbl.gov/RegPrecise/regulon.jsp?regulon\\_id=10736](http://regprecise.lbl.gov/RegPrecise/regulon.jsp?regulon_id=10736)), and it is possible that Zur regulate *smtA* directly (see Chapter 8) and may regulate PstS indirectly.

Despite this progress, we are still far from a complete picture, and certainly more work is required to investigate these hypotheses. In the first instance, the putative Zur from *Synechococcus* sp. WH8102 should be isolated and characterized (Chapter 5).

# Chapter 5

## Cloning, Expression, Purification and Identification of the Zinc Uptake Regulator (Zur) Protein from *Synechococcus* sp. WH8102

---

### 5.1 Introduction

As mentioned previously (see Section 1.9), BLAST searches of the genomes of marine cyanobacteria have retrieved members of the COG0735 family, including the Fur family that also contains sensor proteins for other metal ions (Barnett *et al.*, 2012). Genomic analysis of *Synechococcus* sp. WH8102 led to the identification of two Fur homologs assigned as Fur (*synw\_0865*) and Zur (*synw\_2401*).

Understanding the mechanism of zinc uptake regulatory, Zur protein, from *Synechococcus* sp. WH8102 will give new insights into zinc homeostasis in marine cyanobacteria. This knowledge requires an exhaustive study of the properties of Zur itself. However, an abundant supply of protein is required to achieve this analysis, so here the *synw\_2401* gene from *Synechococcus* sp. WH8102 was obtained as a codon-optimised synthetic gene, sub-cloned into a suitable *E. coli* expression vector, and has been over-expressed and purified by suitable techniques.

## 5.2 Flow Chart for this Study

The general steps for cloning, over-expression, optimizing the yield, purification and identification of the Zur protein from *Synechococcus* sp. WH8102 are described below in the flow chart (Figure 5.01).

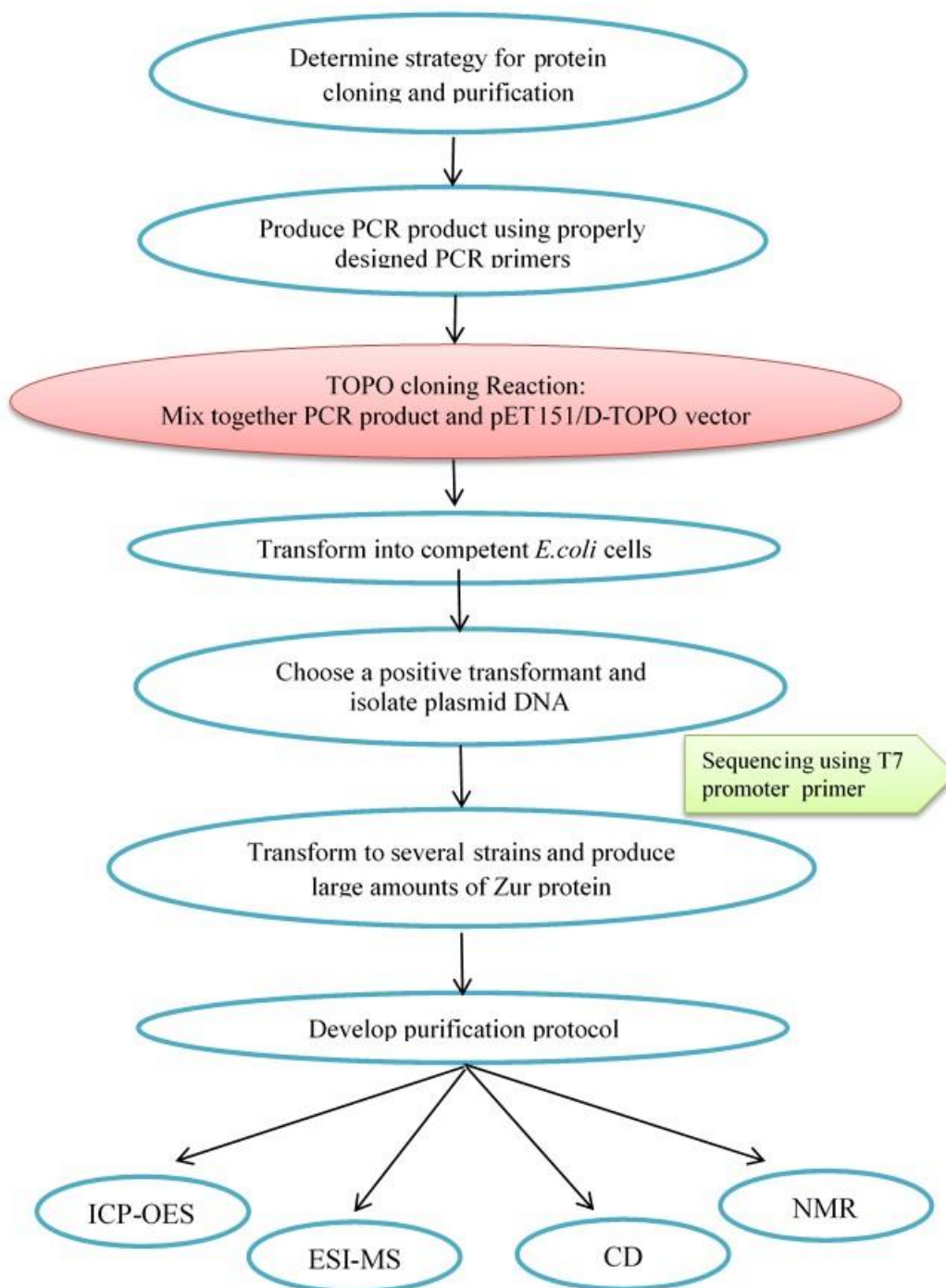


**Figure 5.01** General steps of cloning, over-expression and characterisations of the *Synechococcus* sp. WH8102 Zur protein, encoded by the *synw\_2401* gene.

### 5.3 Optimised *synw\_2401* Nucleotide Sequence

Codon usage in cyanobacteria differs from that in *E. coli*; therefore, it was decided to employ a codon-optimised synthetic gene (Figure 5.02).

The *synw\_2401* gene from *Synechococcus* sp. WH8102 was optimised by Gene Art® for *E. coli* nucleotide usage to improve translation efficiency (Sharp & Li, 1987). The codon adaptation index (CAI) was upgraded from 0.69 to 0.94 where a CAI of >0.8 is rated as good for expression in the desired expression organism, while 1.0 is considered to be perfect in the desired expression organism (Sharp & Li, 1987). The % GC content was adjusted from 51.37 to 59.13% according to Gen Script software, where the ideal percentage range of GC content is between 30-70%.

Original	ATGACTGGTTCCCTCCCTTGCTTTGAACGCCCGTCAACAGGCATTGCTGACGGCTCTCAAC	60
Optimised	ATGACCGGTAGCAGTCCGGCACTGAATGCACGTACGCAAGCACTGCTGACAGCCCTGAAT	60
Original	GCCTGTGGGGATGAAATGAGTGGTCAACAGCTGCATCGCAGCCTCGATGACGAGGCATCC	120
Optimised	GCATGTGGTGTGATGAAATGAGCGGTCAAGCAGCTGCATCGTAGCCTGGATGATGAAGCAAGC	120
Original	ATGGGACTGGCGACCGTTTTATCGCAATCTGCGGCAACTGCAGCAACGGGGCCTGGTGCGT	180
Optimised	ATGGGTCTGGCAACCGTTTTATCGTAATCTGCGTCAGCTGCAGCAGCGTGGTCTGGTTCGT	180
Original	TGTCGCCATCTGCCACCGGCGAAGCGCTCTACGCCCCCGTTGACCGGGATCGCCATCAC	240
Optimised	TGTCGTCATCTGCCGACCGGTGAAGCACTGTATGCACCGGTTGATCGTGTATCGTCATCAT	240
Original	CTCACCTGTGTGGACTGTGGAACGACGCAGGTGCTGGACCATTGCCCCATTCATGGCATC	300
Optimised	CTGACCTGTGTGATTTGTGGCACCAACCAGGTCTGGATCATTGTCCGATTTCATGGTATT	300
Original	GACGTGCCGTGCTGACAGTCGAGGGACTTCGAAATGTTGTTTTACACGCTTGAATTCTTT	360
Optimised	GATGTTCCGGCAGATAGCCGTGGTGAATTTGAACTGCTGTTTTCATACCCTGGAATTTTTT	360
Original	GGTTTCTGCAGCAGCTGTCTCCGCAGCGAAGCTCCAAACCATGA	405
Optimised	GGTTTGTGTAGCAGCTGTCTCCGCAGCGTAGCAGCAAACCGTAA	405

**Figure 5.02 Modified *synw\_2401* gene sequence for *Synechococcus* sp. WH8102.**

Original coding sequence of the *synw\_2401* gene from *Synechococcus* sp. WH8102, as well as the codon-optimised sequence for expression in *E. coli*. Bases in black indicate unchanged bases, and bases in red indicate modified bases.

## 5.4 Cloning of the Synthetic Gene *sync\_2401*

### 5.4.1 Amplification of *synw\_2401* Gene by PCR

The target gene was amplified by PCR from the synthetic gene (see Section 2.6.3). The specific primers were designed in this study, the reverse primer was designed to be a 20-base single-stranded sequence, while the forward primer was designed to be a very specific 20-base single-stranded sequence with a CACC overhang, to be used for cloning into the pET151/D-TOPO<sup>®</sup> vector (see Appendix E, Figure E.01). Two thermostable proofreading polymerases were used to produce the PCR product: Platinum<sup>®</sup>Pfx DNA polymerase (Invitrogen) and KAPA HiFi DNA polymerase (Kapa Biosystems) with several concentrations of magnesium (Figure 5.03).

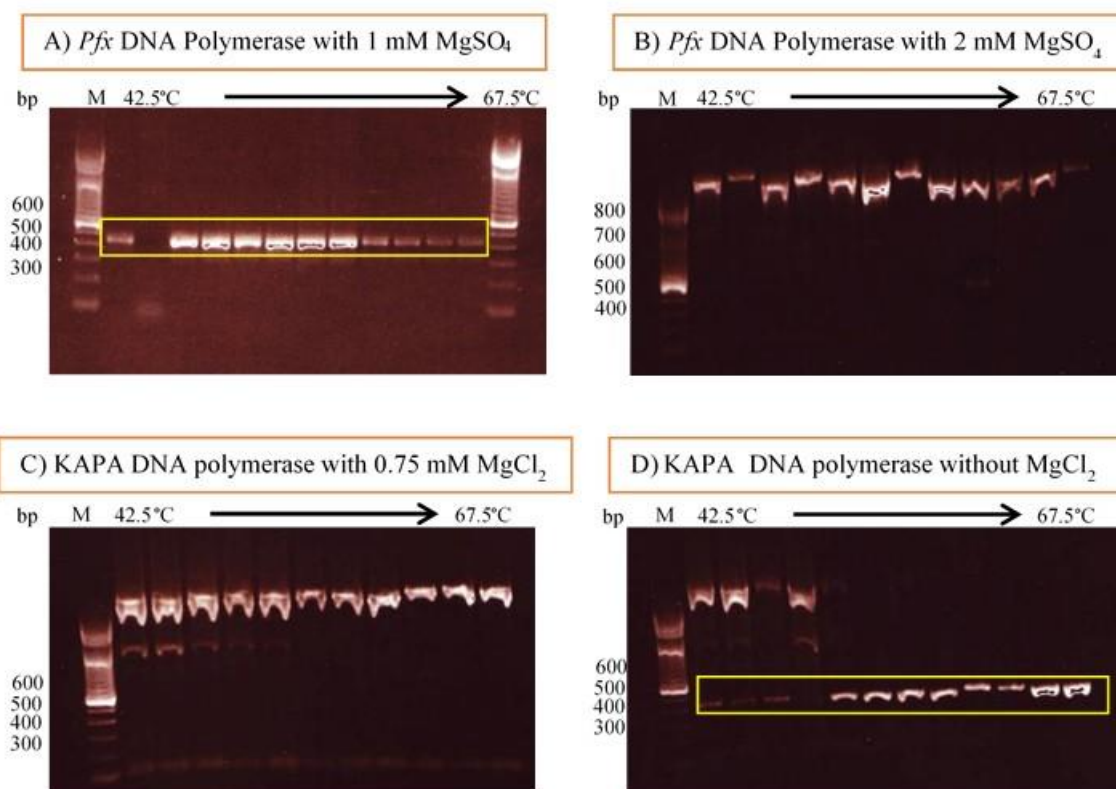


**Figure 5.03 Amplification of *synw\_2401* gene using two different thermostable proofreading polymerases.**

Analysis of PCR products by agarose gel electrophoresis. Platinum<sup>®</sup>Pfx DNA polymerase with 1 mM MgSO<sub>4</sub> (A) and 2 mM MgSO<sub>4</sub> (B). KAPA HiFi DNA polymerase with 0.75 mM MgCl<sub>2</sub> (C) and without adding MgCl<sub>2</sub> (D). 100 bp DNA ladder was used as markers (Invitrogen), and the *synw\_2401* gene provides a band at 405 bp.

PCR products were subjected to agarose gel electrophoresis to ensure that target gene products of the correct size, 405 bp, were present (Figure 5.03). Successful amplification of the *synw\_2401* gene was achieved by Platinum<sup>®</sup>Pfx DNA polymerase with 1 mM MgSO<sub>4</sub> and KAPA HiFi DNA polymerase without adding MgCl<sub>2</sub> (Figure 5.03).

## 5.4.2 Cloning of Target Gene using the TOPO Cloning System

PCR products from two reactions, using Platinum<sup>®</sup>Pfx and KAPA HiFi DNA polymerases, corresponding to the expected size of *synw\_2401*, were subsequently extracted from the gel and inserted into the pET151/D-TOPO<sup>®</sup> cloning vector (Invitrogen), to give full length for *synw\_2401* protein with an N-terminal His<sub>6</sub>-fusion tag, including a V5 epitope and a TEV-protease cleavage site (see Appendix E, Figure E.01). Although there are disadvantages of using His<sub>6</sub>-tag technology for metal binding proteins due to the affinity of histidine residues for metals and the potential degradation and co-elution of proteins that naturally have two or more adjacent histidine residues, His<sub>6</sub>-tag technology was used here for several reasons; (i) His<sub>6</sub>-tag was placed on the N-terminus of the protein which is known to improve the yield of recombinant proteins by providing a reliable context for efficient translation initiation (Waugh, 2005); (ii) His<sub>6</sub>-tag can easily be removed; (iii) polyhistidine tags, on an IMAC column, can bind proteins under both native and denaturing conditions.

### 5.4.2.1 Why pET151/D-TOPO<sup>®</sup>

The pET151/D TOPO<sup>®</sup> system utilizes a highly efficient T7-regulated expression in *E. coli* (see Appendix E, Figure E.01) with 5-minute cloning strategy. The cloning in this system is directed at greater than 90% efficiency, with no ligase, post-PCR procedures, or restriction enzymes required.

The key of TOPO cloning is the DNA enzyme Topoisomerase I which plays a role as a ligase and restriction enzymes. Topoisomerase I from *Vaccinia* virus binds to duplex DNA at specific sites and cleaves the phosphodiester backbone after 5'-CCCTT-3' in one strand (Shuman, 1991) (Figure 5.04). The obtained energy from the broken phosphodiester backbone is conserved by formation of a covalent bond between the 3' phosphate of the cleaved strand and a tyrosyl residue (Tyr-274) of topoisomerase I (Figure 5.04).

Directional joining of double-strand DNA using TOPO<sup>®</sup>-charged oligonucleotides occurs by adding four bases (GTGG) to the 3' single-stranded end (Figure 5.04). At the same time, PCR products should be cloned by adding four bases to the forward primer (CACC). The overhang in the cloning vector (GTGG) invades the 5' end of the PCR product, anneals to the added bases, and stabilizes the PCR product in the correct orientation.

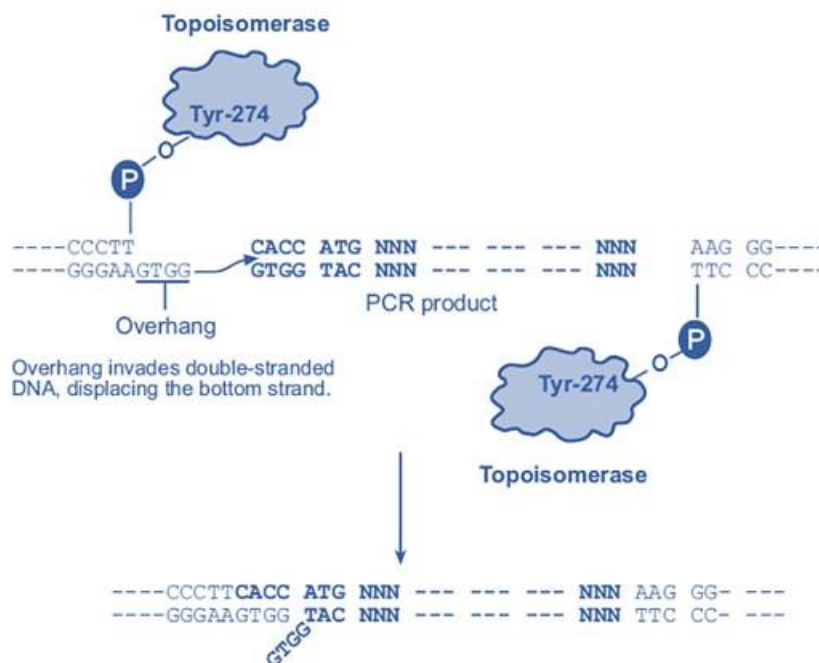


**Figure 5.04 TOPO vector mechanisms.**

Taken from ([http://xray.bmc.uu.se/Courses/MPC/literature\\_files/pettopo\\_man.pdf](http://xray.bmc.uu.se/Courses/MPC/literature_files/pettopo_man.pdf)).

The pET expression system uses elements from bacteriophage T7 to control expression of heterologous genes in *E. coli* and, in theory, enables the quick production of a large quantity of

any desired protein (Campbell, 2003). Ideally, the gene of interest is not transcribed unless the T7 RNA polymerase is present (Campbell, 2003) by lactose or a molecule similar to lactose such as IPTG, isopropyl  $\beta$ -D-1-thiogalactopyranoside (Blaber, 1998) (see Appendix E, Figure E.02).

### 5.4.3 Identifying Positive Colonies by PCR and DNA Sequencing

The pET151/D TOPO<sup>®</sup> cloning reaction with *synw\_2401* was carried out, and One Shot<sup>®</sup> TOP10 with DH5 $\alpha$ <sup>™</sup> competent cells were transformed with the resulting plasmid (see Section 2.6.7). Surprisingly, TOP10 cells did not work while DH5 $\alpha$ <sup>™</sup> worked successfully.

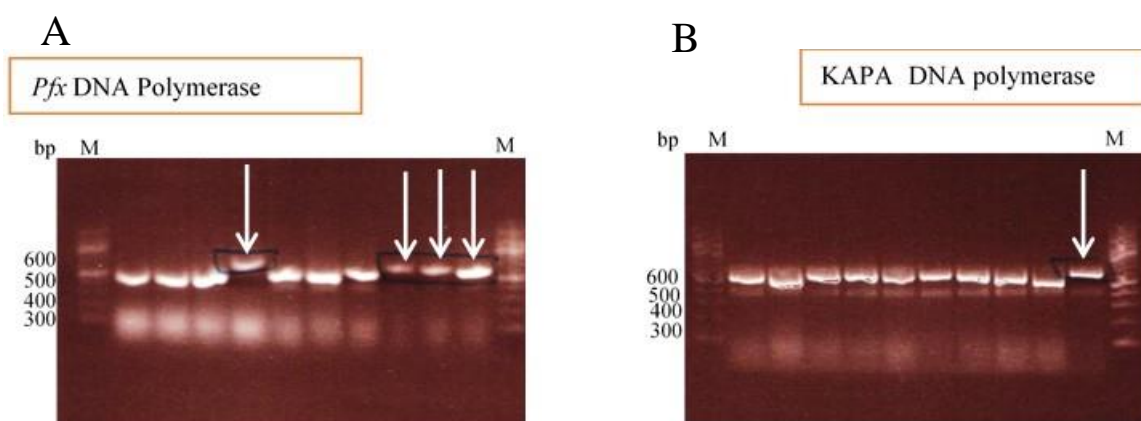


**Figure 5.05 PCR products for positive colonies.**

10 colonies from DH5 $\alpha$ <sup>™</sup> *E. coli* in two cases, (A) Platinum<sup>®</sup>Pfx and (B) KAPA HiFi DNA polymerase. Arrows indicate the correct product, 540 bp, after sequencing.

Ampicillin-resistant DH5 $\alpha$ <sup>™</sup> *E. coli* colonies appearing on LB agar plates were inoculated both onto a fresh agar plate and into LB medium containing ampicillin and then incubated at 37°C with shaking (180 rpm) overnight. Next day, 10 colonies for two DNA polymerases cases, platinum<sup>®</sup>Pfx and KAPA HiFi DNA polymerase<sup>®</sup>, were analysed using PCR (Figure 5.05).

Several constructs of the correct size were sequenced to confirm that the *synw\_2401* gene was in the correct reading frame with the appropriate N-terminal tag using T7 forward and reverse

primers as the sequencing primers (see Section 2.6.7). Five sequenced constructs (Figure 5.05) were 100 % matched with the correct frame in SeqMan software (see Appendix E, Figure E.03).

## 5.5 Over-expression of *Synechococcus* sp. WH8102 Zur protein

After confirming the correct insertion of the *synw\_2401* gene into the pET151/D-TOPO<sup>®</sup> vector (see Section 2.6.7), the construct was transformed into several types of competent cells: BL21 Star<sup>™</sup>(DE3), Rosetta<sup>™</sup> 2(DE3) pLysS and Takara competent cells. In small-scale expression studies, different growth and induction conditions over several hours were explored to establish the optimal expression conditions to maximize the yield of recombinant Zur protein. Induction was initiated at OD<sub>600</sub> of 0.8 for BL21 Star<sup>™</sup>(DE3) and Rosetta<sup>™</sup> 2(DE3) pLysS, and at OD<sub>600</sub> of 0.5 for Takara cells, using different concentrations of IPTG (see Section 2.7.1). Additionally, cells were cultured with and without 0.5 mM ZnSO<sub>4</sub>.

### 5.5.1 Over-expression using BL21 Star<sup>™</sup> (DE3) and Rosetta<sup>™</sup> 2(DE3)pLysS

There is no doubt that the production of recombinant proteins in microbial systems has revolutionized biochemistry. *E. coli*, Gram-negative bacterium, is a popular choice for the production of recombinant proteins. It grows to high cell densities on inexpensive substrates, its genetics have been heavily researched and are generally well understood, and a large number of cloning vectors engineered to achieve the high-level synthesis and facilitate the purification of recombinant gene products (Rosano & Ceccarelli, 2014).

In our study, the competent cells of *E. coli* strains BL21 Star<sup>™</sup> (DE3) (Invitrogen) and Rosetta<sup>™</sup> 2(DE3) pLysS (Novagen) were used as a host for Zur over-expression. Several growth curves at different IPTG concentrations were achieved (see Appendix E, Figure E.04 and Figure E.05).

In the absence of 0.5 mM ZnSO<sub>4</sub>, inserting *synw\_2401* gene affected the Rosetta™ 2(DE3) pLysS (see Appendix E, Figure E.05), while no affect was observed for BL21 Star™ (DE3) (see Appendix E, Figure E.04). However, in the presence of 0.5 mM ZnSO<sub>4</sub> and after inducing with IPTG, the growth of these strains were significantly slower than the growth in the absence of 0.5 mM ZnSO<sub>4</sub> (see Appendix E, Figure E.04 and Figure E.05).

Moreover, it was reported that if the recombinant strain is slower compared to an empty-vector bearing strain, a control one, then two causes may explain the phenotype: gene toxicity and basal expression of the toxic mRNA/protein (Rosano & Ceccarelli, 2014).

Pre and post induction of protein expression levels were checked by silver-stained SDS-PAGE for both strains (see Appendix E, Figure E.06 and Figure E.07) and solubility of the over-expressed protein was summarized in Table 5.01. The presence of the *Synechococcus* sp. WH8102 Zur protein under some over-expression conditions, even in the absence of inducer, suggested leaky expression, whilst when inducer was added Zur was present in the insoluble fraction.

**Table 5.01 Summary of Zur protein over-expression in BL21 Star™ (DE3) and Rosetta™ 2(DE3) pLysS strains.**

BL21 Star™ (DE3)	Growth curve	Zur in soluble fraction	Zur in insoluble fraction	Rosetta™ 2(DE3) pLysS	Growth curve	Zur in soluble fraction	Zur in insoluble fraction
BL21+Zur	-			Rosetta+Zur	√		
BL21+Zur+0.3 mM IPTG	-	No	No	Rosetta +Zur+0.3 mM IPTG	√	Yes, leaking	No
BL21+Zur+0.3 mM IPTG+0.5 mM ZnSO <sub>4</sub>	√	No	Yes	Rosetta +Zur+0.3 mM IPTG+0.5 mM ZnSO <sub>4</sub>	√	No	Yes
BL21+Zur	-			Rosetta +Zur	√		
BL21+Zur+0.5 mM IPTG	-	Yes, Leaking	No	Rosetta +Zur+0.5 mM IPTG	√	Yes, Low	No
BL21+Zur+0.5 mM IPTG+0.5 mM ZnSO <sub>4</sub>	√	No	Yes	Rosetta +Zur+0.5 mM IPTG+0.5 mM ZnSO <sub>4</sub>	√	No	Yes
BL21+Zur	-			Rosetta +Zur	√		
BL21+Zur+0.7 mM IPTG	√	Yes, Leaking	No	Rosetta +Zur+0.7 mM IPTG	√	No	No
BL21+Zur+0.7 mM IPTG+0.5 mM ZnSO <sub>4</sub>	√	No	Yes	Rosetta +Zur+0.7 mM IPTG+0.5 mM ZnSO <sub>4</sub>	√	No	Yes

“-” Empty cells indicate no effect on growth curve, “√” indicates an effect on growth curve. “Yes” indicates expression of the Zur protein. “No” indicates no expression of Zur protein.

Remarkably, when a foreign gene is introduced in *E. coli*, spatio-temporal control of its expression is lost in some cases. The newly synthesized recombinant polypeptide expressed in the microenvironment of *E. coli* may differ from that of the original source in terms of pH, osmolality, redox potential, cofactors and folding mechanisms (Rosano & Ceccarelli, 2014). These build-ups of protein aggregates are known as IBs, inclusion bodies, and resulted from an unbalanced equilibrium between protein aggregation and solubilisation (Rosano & Ceccarelli, 2014).

The phenomenon of leaking for Zur protein was also observed previously with most protein ending in the IBs (Patzner & Hantke, 2000). However, the induction of Zur at different temperatures and different media in BL21 did not increase the solubility of Zur protein (Patzner & Hantke, 2000). Although it was reported that adding zinc to the culture during the expression increased the solubility of Zur protein (Gabriel *et al.*, 2008). In our expression, supplementing zinc to the culture ending Zur protein in an inclusion body.

However, overexpression of recombinant proteins is not often well tolerated by bacteria and it is common for overexpressed polypeptides to accumulate within the cell as biologically inactive aggregates, inclusion bodies, or to be proteolytically degraded (Thomas *et al.*, 1997). Refolding the protein from inclusion bodies is technically possible, but yields can be variable and not be readily amenable to scale-up. Instead, co-expression of a molecular chaperone can help to refold and solubilize the protein (Thomas *et al.*, 1997; Nishihara *et al.*, 2000; Hoffmann *et al.*, 2006), and this approach was used here.

### **5.5.2 Over-expression of Zur protein using Takara system**

In all organisms, nascent proteins leaving the ribosome are assisted by a variety of general and specific cytosolic chaperones (Nishihara *et al.*, 2000; Hoffmann *et al.*, 2006). In eubacteria, the

general chaperones include trigger factor, the DnaK/DnaJ/GrpE complex and the GroEL/GroES complex.

Trigger factor, TF, is a protein that binds to ribosomes and nascent polypeptide chains. TF acts as a general co-translational folding catalyst and stabilizes nascent proteins before their transfer to chaperones (Thomas *et al.*, 1997; Nishihara *et al.*, 2000).

Downstream of TF, the DnaK-DnaJ-GrpE and GroEL-GroES chaperone systems assist further folding steps to the native state (Hoffmann *et al.*, 2006) (Figure 5.06). In the DnaK/DnaJ/GrpE complex, DnJ binds to nascent polypeptides emerging from the ribosome, and targets newly synthesized protein chains for recognition by DnaK (Figure 5.06). DnaK/DnaJ shield exposed hydrophobic stretches in the polypeptide chain, thus preventing unproductive interactions with other folding intermediates and cellular components. Binding of the GrpE nucleotide exchange factor to DanK catalyzes the release of the bound protein substrate which may fold into the native conformation; undergo additional cycles of DanK-DnaJ-GrpE binding and release, be transferred to the GroEL-GroES chaperon system, or misfold and aggregate.

The GroE chaperone system is believed to facilitate the productive isomerization of proteins that have reached a compact intermediate conformation. If the protein discharged from the GroE complex unable to fold into its native conformation, it may undergo another cycle of interaction with either chaperon system or aggregate. If proper folding cannot be achieved after several cycles of chaperon interaction, DnaK-DnJ-GrpE or GroEl-GroES, may present their substrates to the cellular protease machinery (Thomas *et al.*, 1997; Hartl & Hayer-Hartl, 2002) (Figure 5.10). Together these chaperones form a folding network of considerable robustness (Hoffmann *et al.*, 2006).

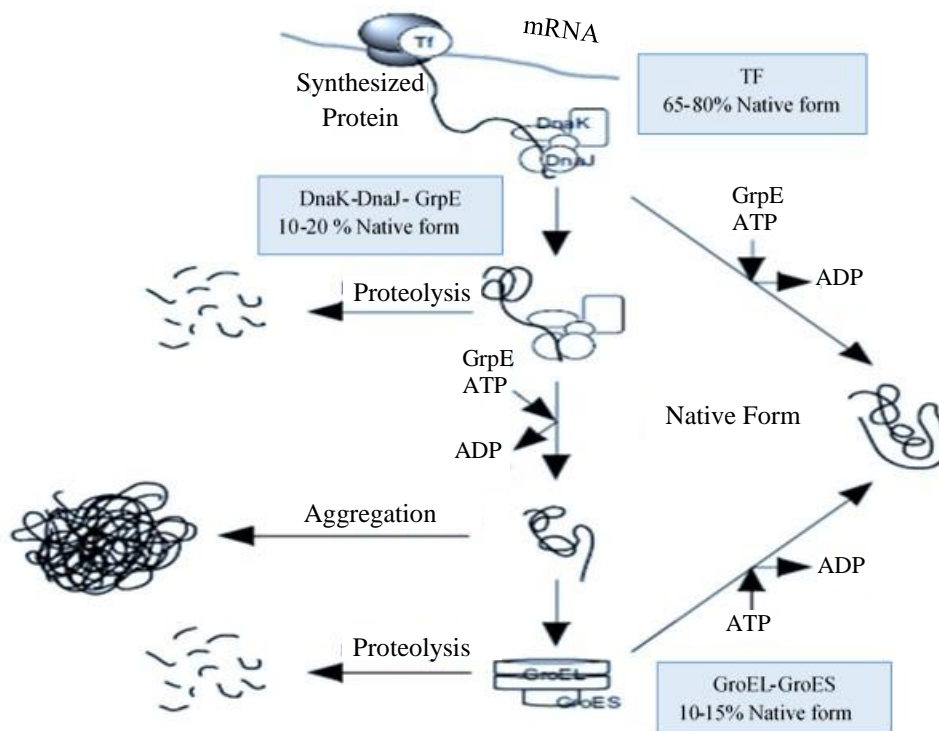


**Figure 5.06 Model of protein folding in the cytosol with the assistant of chaperones.**

Nascent chains probably interact generally with trigger factor (TF), and most small proteins (~65-80 % of total) may fold rapidly upon synthesis without more assistance. Longer chains interact subsequently with DnaK-DnaJ-GrpE and fold upon one or several cycles of ATP-driven binding and release (~10-20% of total). About 10-15 % of chains transit the GroES chaperone system for folding the native protein. Taken from ([http://www.ibt.unam.mx/computo/cepas/manual\\_Chaperone\\_plasmid\\_set.pdf](http://www.ibt.unam.mx/computo/cepas/manual_Chaperone_plasmid_set.pdf)).

Under these conditions, an increase in the intracellular concentration of molecular chaperon that are limiting for folding would be expected to lessen the formation of protein in the inclusion body and can significantly improve the recovery yields of many aggregation prone recombinant proteins, without changing protein folding pathways (Thomas *et al.*, 1997).

The commercially available Takara chaperone system containing plasmid pG-Tf2 (Figure 5.07) was used for co-expression with the Zur protein from *Synechococcus* sp.WH8102 in *E. coli*. This chaperone plasmid carries an origin of replication derived from pACYC and a chloramphenicol resistance gene (Cm<sup>r</sup>). The chaperone genes are downstream of the *Pzt-1* (*tet*) promoter that is induced by tetracycline. It was previously reported that *E. coli* cells harbouring

this plasmid could produce TF and GroEL-GroES at levels that were up to 10 times the levels produced by wild type *E. coli* cells (Nishihara *et al.*, 2000). Here, then expression of the chaperones, TF and GroEL- GroES, and our target protein are induced individually by tetracycline and IPTG, respectively.

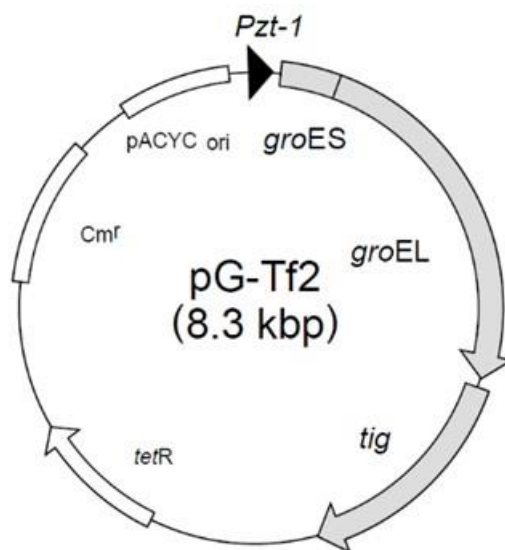


**Figure 5.07 A map of chaperon plasmid pG-Tf2.**

pG-Tf2 plasmid contains *Tig*: a trigger factor (TF); GroEL-GroES chaperon; *tetR*: a repressor gene; *Pzt-1*: a promoter gene; *ori*: replication region of pACYC; *Cm<sup>r</sup>*: a chloramphenicol resistance gene.

The pET/151-*synw\_2401* construct together with pG-Tf2 plasmid were transformed into *E. coli* BL21, and the resulting recombinant *E. coli* strain grown either in MagicMedia™ (MM) and Luria Broth (LB) to assess the optimal conditons for Zur protein over-expression.

### 5.5.2.1 Over-expression of Zur using pG-Tf2 in MagicMedia™

MagicMedia™ promotes a high growth yield of *E. coli* and high-level, T7 regulated, protein expression. Unlike traditional LB-IPTG induction systems, MagicMedia™ allows the regulation of expression without time consuming steps such as monitoring optical density (OD) or adding induction components such as IPTG.

*E. coli* BL21 containing pET/151-*synw\_2401* construct together with the chaperone plasmid pG-Tf2 was inoculated into 10 ml LB medium overnight, then this starter culture was transferred into 200 ml MagicMedia™ (Invitrogen), an auto induction medium (see Section 2.7.1). This *E. coli* strain was grown in MagicMedia™ at both 37°C and 30°C to assess the effect of temperature on Zur protein over-expression and solubility (see Appendix E, Figure E.08).

Unfortunately, whilst Zur expression in MagicMedia™ resulted in protein over-expression in the soluble fraction the size of the protein induced did not correspond to Zur protein, whilst in addition protein abundance did not increase with time. Including zinc in this medium did not change the expression level or assist in obtaining over-expression of the correct size of the protein (see Appendix E, Figure E.08).

### 5.5.2.2 Overexpression of Zur using pG-Tf2 in LB Medium

*E. coli* BL21 containing the pET/151-*synw\_2401* construct together with the chaperone plasmid pG-Tf2 was inoculated into 10 ml LB medium overnight, then this starter culture was transferred into 200 ml LB medium (see Section 2.7.1). In the presence and absence of 0.5 mM ZnSO<sub>4</sub>, the growth of this strain was also significantly slower than the growth of the wild-type at 37°C and 30°C (see Appendix E, Figure E.09 and Figure E.10).

Finally, the putative Zur protein (ca. 18.6 kDa in size) was induced in the soluble fraction after 2 hours, with a gradual increase in induction after 4 and 6 hours at three concentrations of IPTG (0.3 mM, 0.5 mM, and 0.7 mM) in the absence of 0.5 mM ZnSO<sub>4</sub> at 37°C (Figure 5.08A, C and E) and at 30°C (Figure 5.09A, C and E).

Thus, Zur protein over-expression in the soluble fractions appears to be greatly assisted by co-expression of chaperone proteins, and in sufficient quantities for large scale purification.

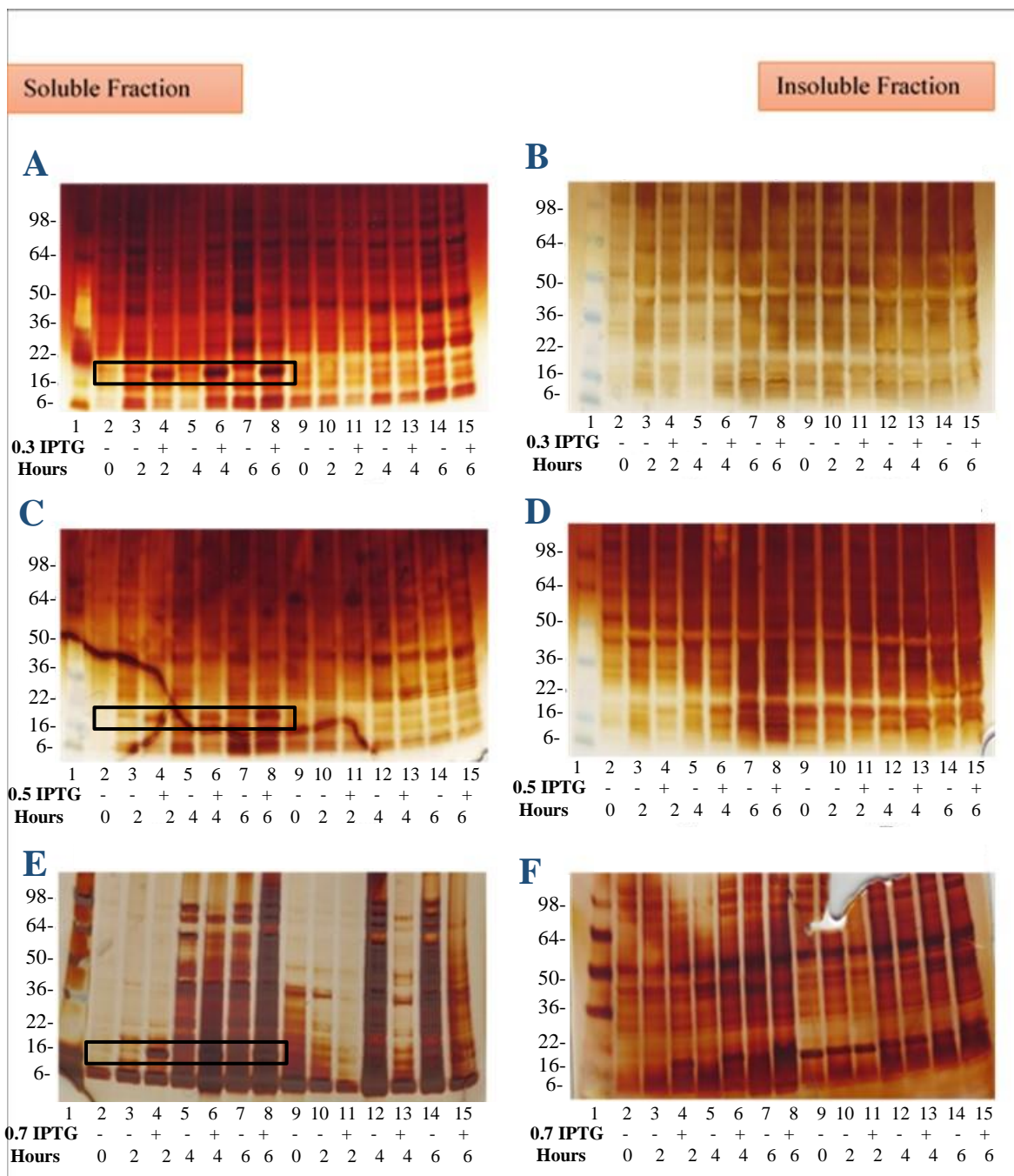


**Figure 5.08 Over-expression of the *Synechococcus* sp. WH8102 Zur protein using the Takara system at 37°C using silver staining.**

(A), (C), and (E) are soluble fractions, supernatants. (B), (D), and (F) are insoluble fractions, cell debris. (A) and (B) Zur protein was induced by 0.3 mM, (C) and (D) Zur protein was induced by 0.5 mM, and (E) and (F) Zur protein was induced by 0.7 mM. Lane 1 marker; Lane 2-8 cultures without zinc supplement; Lane 9-15 cultures with 0.5 mM ZnSO<sub>4</sub> supplement. Lane 2 and 9: t = 0 h induced with IPTG; Lane 3 and 10: t = 2 h un-induced with IPTG; Lane 4 and 11: t = 2 h induced with IPTG; Lane 5 and 12: t = 4 h un-induced with IPTG; Lane 6 and 13: t = 4 h induced with IPTG; Lane 7 and 14: t = 6 h un-induced with IPTG; Lane 8 and 15: t = 6 h induced with IPTG.

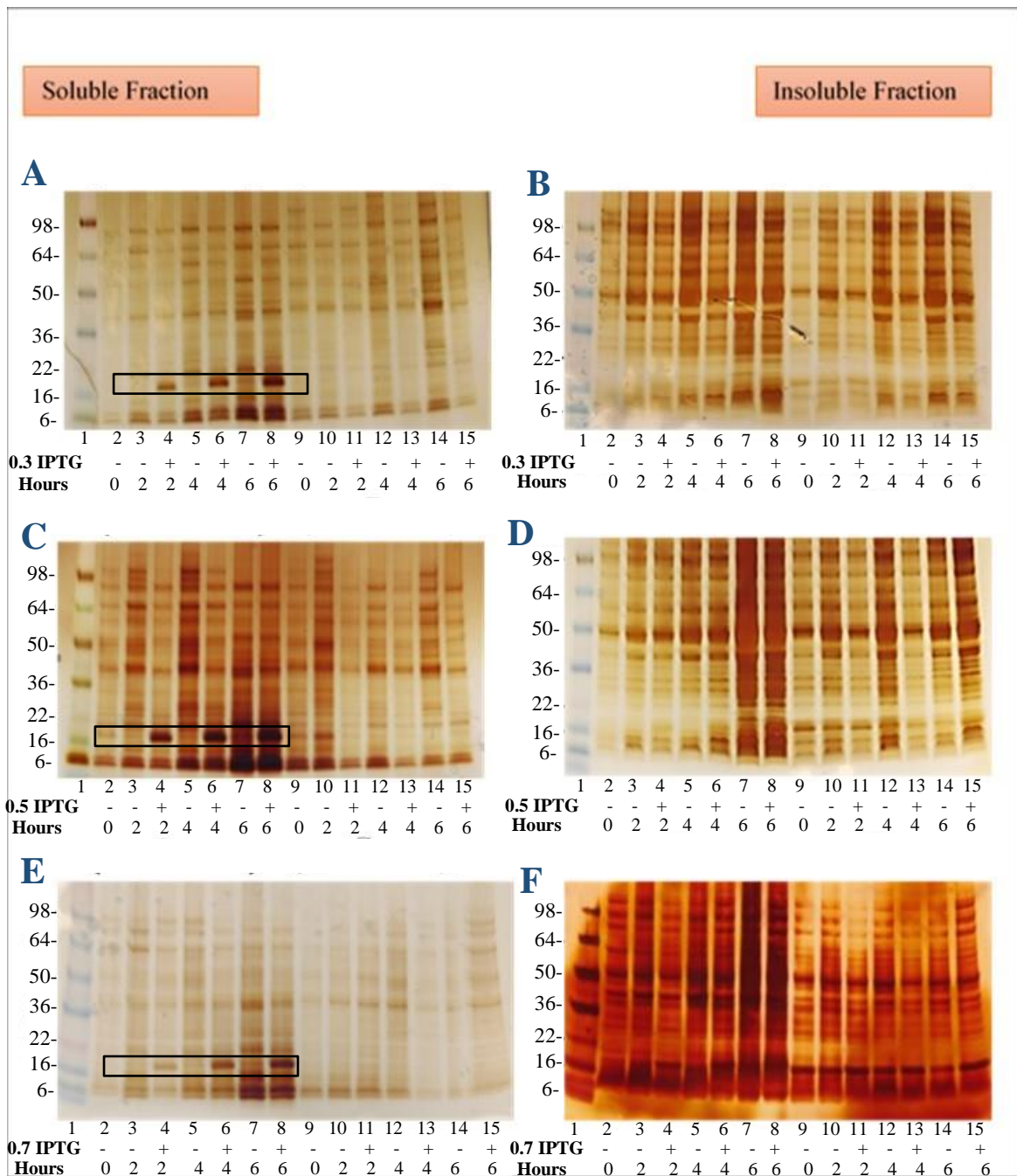


**Figure 5.09 Over-expression of the *Synechococcus* sp. WH8102 Zur protein using the Takara system at 30°C using silver staining.**

(A), (C), and (E) are soluble fractions, supernatants. (B), (D), and (F) are insoluble fractions, cell debris. (A) and (B) Zur protein was induced by 0.3 mM, (C) and (D) Zur protein was induced by 0.5 mM, and (E) and (F) Zur protein was induced by 0.7 mM. Lane 1 marker; Lane 2-8 cultures without zinc supplement; Lane 9-15 cultures with 0.5 mM ZnSO<sub>4</sub> supplement. Lane 2 and 9: t = 0 h induced with IPTG; Lane 3 and 10: t = 2 h un-induced with IPTG; Lane 4 and 11: t = 2 h induced with IPTG; Lane 5 and 12: t = 4 h un-induced with IPTG; Lane 6 and 13: t = 4 h induced with IPTG; Lane 7 and 14: t = 6 h un-induced with IPTG; Lane 8 and 15: t = 6 h induced with IPTG.

### 5.5.3 Western Blotting Confirmation of Over-expressed Zur Protein

Western blotting, known as immunoblotting or protein blotting, is one of the most prevalent laboratory procedures in use today due to inexpensive technique. It is used to detect the presence of a specific protein in a complex mixture extracted from the cells. Western blotting depends on three keys to visualize the specific protein; the separation of protein mixture by using gel electrophoresis; the efficient transfer of separated proteins to a solid support membrane; and the specific detection of a target protein by appropriately matched antibodies.

To confirm detection of the over-expressed protein as His<sub>6</sub>-tag Zur, a western blotting approach was investigated using rabbit anti-His antibodies (AbD Serotec, Bio-Rad, UK) (see Section 2.8.3). Figure 5.10 shows a polypeptide of the correct size (~18.6 kDa) as the Zur protein in the soluble fraction.

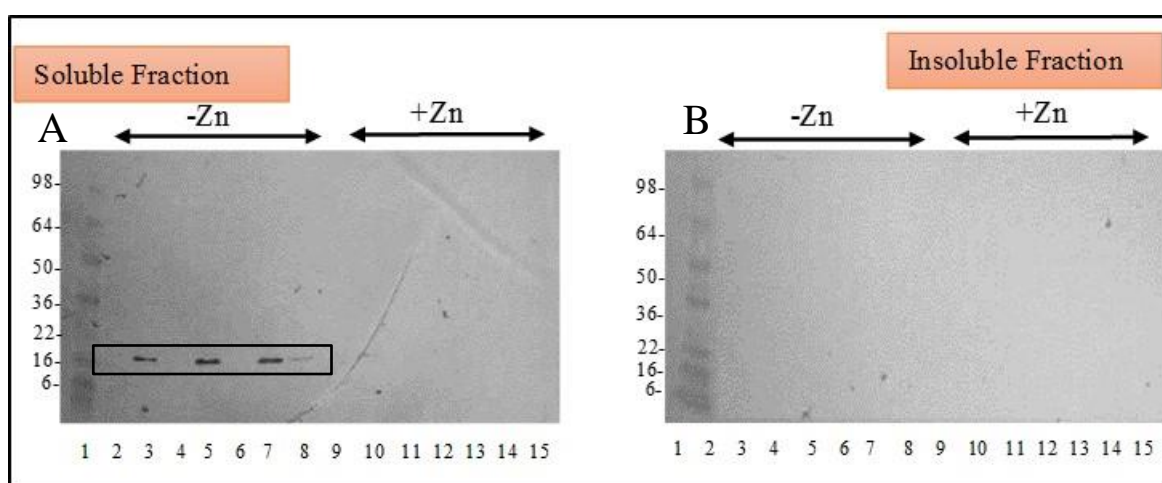


**Figure 5.10 Western blotting of the putative Zur protein.**

Western blot showing detection of Zur protein (~ 18.6 kDa) using Rabbit anti His<sub>6</sub>-tag antibodies from induced and un-induced using *E. coli* pET/151-*synw\_2401*/pG-Tf2 Takara strain and using 0.5 mM IPTG in the soluble fraction (A), and in the insoluble fraction (B). Lane 1 marker; Lane 2-8 cultures without zinc supplement; Lane 9-15 cultures with 0.5 mM ZnSO<sub>4</sub> supplement. Lane 2 and 9: t = 0 h induced with IPTG; Lane 3 and 10: t = 2 h induced with IPTG; Lane 4 and 11: t = 2 h un-induced with IPTG; Lane 5 and 12: t = 4 h induced with IPTG; Lane 6 and 13: t = 4 h un-induced with IPTG; Lane 7 and 14: t = 6 h induced with IPTG; Lane 8 and 15: t = 6 h un-induced with IPTG.

## 5.6 Purification of *Synechococcus* sp. WH8102 Zur Protein

The *Synechococcus* sp. WH8102 Zur protein was over-expressed in soluble form using *E. coli* pET/151-*synw\_2401*/pG-Tf2 Takara strain at 30°C induced with 0.5 mM IPTG. Purification and cleavage of the His<sub>6</sub>-tag were achieved in two steps, see below, which resulted in a good yield of Zur protein (see Section 2.7.2 and Section 2.7.3).

No zinc was supplemented to any buffer used in this study, with the idea to obtain *Synechococcus* sp. WH8102 Zur protein in the native form and to prevent non-specific metal ion binding to the protein. Because of the presence of the His<sub>6</sub>-tag, Zur protein was purified by immobilized metal affinity chromatography.

### 5.6.1 Immobilized Metal Affinity Chromatography

Immobilized metal affinity chromatography (IMAC) is a powerful purification technique that depends on a molecule's affinity for certain metals immobilized onto a chelating surface. Iminodiacetic acid (IDA) serves as the chelating ligand for di- or tri-valent metal ions. The structure of this resin offers selective binding of recombinant His<sub>6</sub>-tagged proteins when charged with Ni<sup>2+</sup> or other transition metals.

The efficacy of protein purification by IMAC is not only dependent on the number of histidine, tryptophan, and cysteine residues presence on a protein's surface but also the number of coordination sites of the immobilized metal that are not occupied by the chelating ligand, which are then free to interact with proteins. In the case of Ni- charged IDA resin, Ni<sup>2+</sup> ions, which have six coordination sites, bound to this tridentate chelator, will expose three coordination sites to the environment (Figure 5.11).

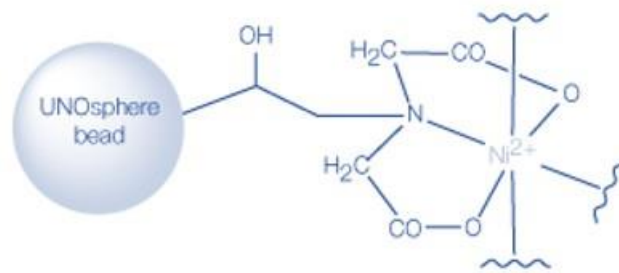


**Figure 5.11 Partial structure of IDA resin charged with Ni<sup>2+</sup>.**

Taken from ([http://www.bio-rad.com/webroot/web/pdf/lst/literature/Bulletin\\_3193.pdf](http://www.bio-rad.com/webroot/web/pdf/lst/literature/Bulletin_3193.pdf)).

Using IMAC to separate an expressed recombinant protein that has a His<sub>6</sub>-tag was demonstrated to yield a highly purified protein in a single chromatographic step (Hochuli *et al.*, 1988).

The crude extract, obtained following sonication, was loaded onto an IMAC column charged with nickel sulphate. The profile for loading of crude extract and elution of proteins was monitored by absorbance at 280 nm (aromatic residues) and 215 or 220 nm (peptide bonds) (Figure 5.12).

Whilst the crude extract was loaded onto the column, the absorbance at 280 was high at around 3300 units. This UV absorbance comes from proteins which have no affinity for Ni<sup>2+</sup> and therefore pass straight through the column. However the 220 nm was saturated and no useful information can be obtained from this absorbance. Bound proteins were eluted with an imidazole gradient (0-100% buffer B: 50 mM NaH<sub>2</sub>PO<sub>4</sub>, 300 mM NaCl, 250 mM imidazole) for 30 min and isocratically for another 30 min (Figure 5.12).

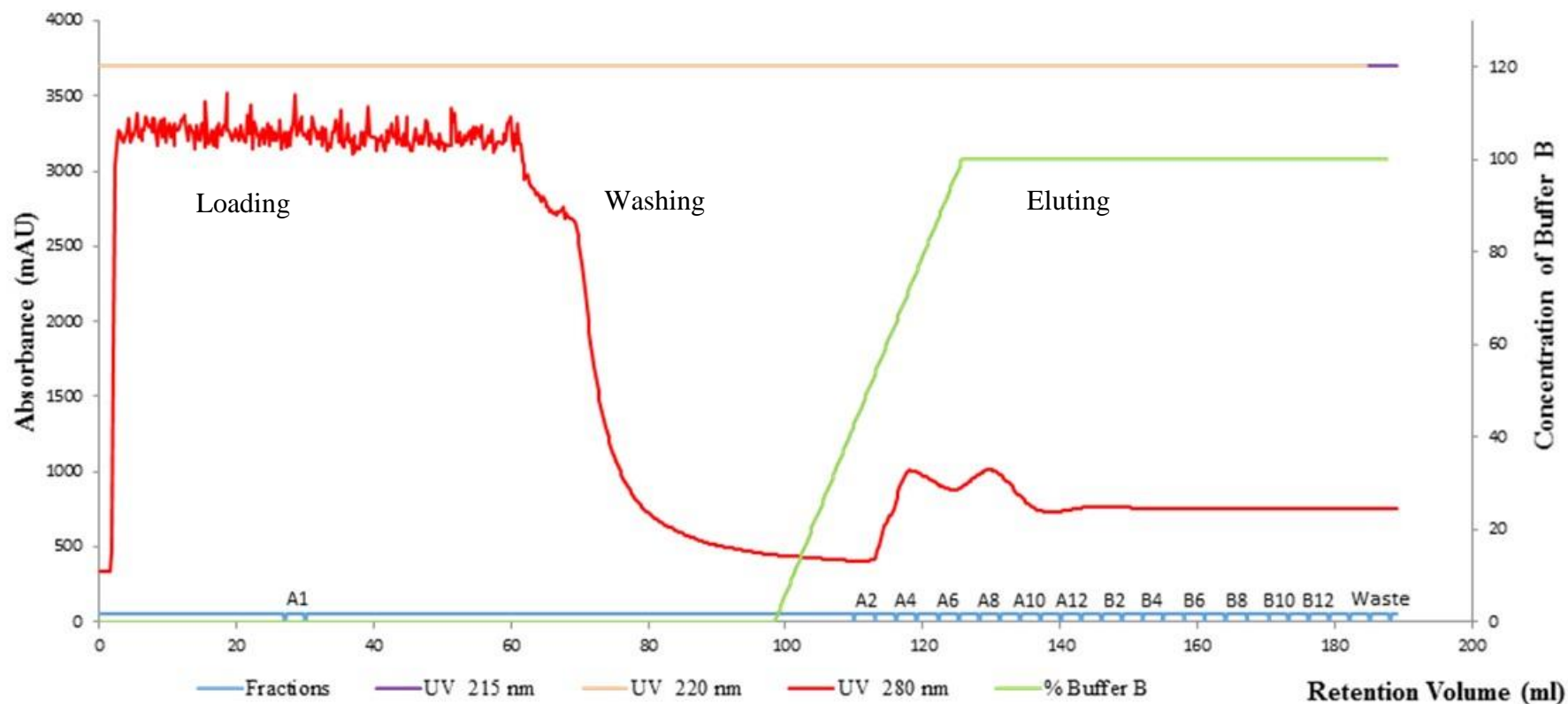


**Figure 5.12 The elution profile of crude extract proteins from the Ni-IMAC column.**

Loading and elution were monitored at three wavelengths, 215 nm (purple), 220 nm (orange) and 280nm (red). Proteins with high affinity for  $\text{Ni}^{2+}$  were eluted using an imidazole gradient (buffer B: 50 mM  $\text{NaH}_2\text{PO}_4$ , 300 mM NaCl, 250 mM imidazole) for 30 min and isocratically with buffer B for another 30 min (green). 3 ml fractions were collected in the elution.

Use of imidazole in the elution buffer at increasing concentration competes with proteins binding to the Ni-IMAC column resulting in elution of proteins that have lower affinity for the column at a specific imidazole concentration. This method yielded two relatively well resolved peaks (A2-A5) and (A6-A10) as shown in Figure 5.12 with absorbance of approximately 1100 units each.

The collected fractions across the elution profile were run on an SDS-PAGE gel (Figure 5.13). The elution profile and the SDS-PAGE gel, fraction A1, show that a high quantity of crude extract proteins have no affinity to Ni-IMAC.

The Coomassie-stained SDS-PAGE gel revealed a band with a molecular mass of 18.6 kDa which is consistent with the molecular mass of Zur protein with His<sub>6</sub>-tag in the second peak (A6-A10) and there was protein also in fractions A11 and A12 as well (Figure 5.13). Interestingly, in fractions A3-A5, several other proteins were present as well as the Zur protein. Fractions in the second peak (A6-A10) exhibited absorbance at 280 nm due to the presence of Zur protein with aromatic groups (13 His (H), 3 Tyr (Y), 7 Phe (F), and 6 Pro (P)).

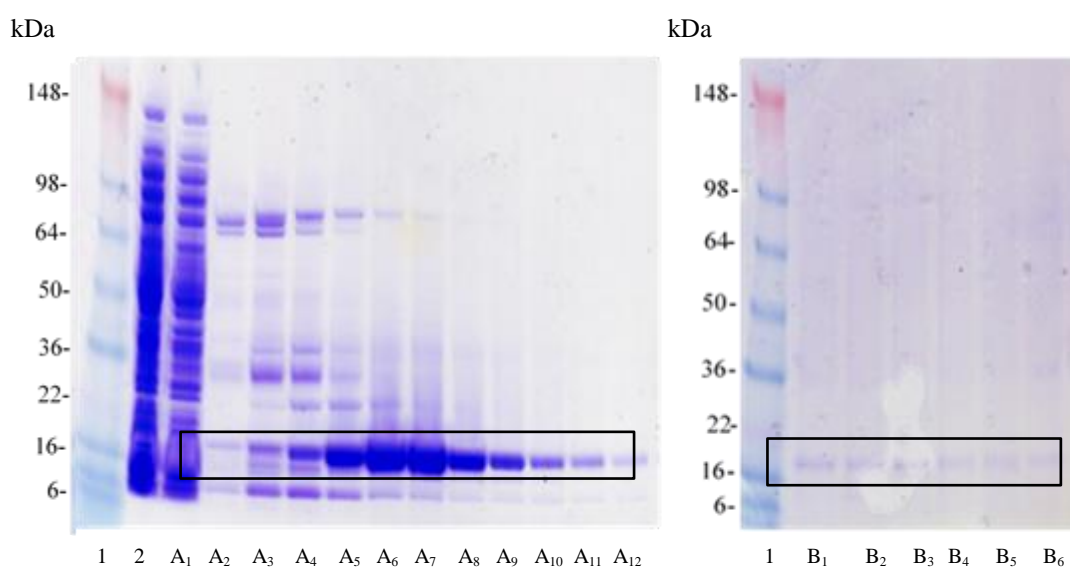


**Figure 5.13 SDS-PAGE analysis of protein fractions collected from the Ni-IMAC column.**

Lane 1: Pre-stained molecular weight markers. Lane 2: crude extract. Lane A<sub>1</sub>: flow through, proteins with no affinity for IMAC column. The subsequent lanes are from fractions eluted from the column at increasing imidazole concentration. Proteins were separated by SDS-PAGE and visualized by staining with Coomassie brilliant blue.

These results reveal that the *Synechococcus* sp. WH8102 Zur protein containing a His<sub>6</sub>-tag had sufficient affinity to the Ni-IMAC column to allow direct purification in one step, if fractions A6-A12 are collected.

## 5.6.2 Cleaving the Zur Protein with TEV Protease

Using His<sub>6</sub>-tag has recently become a widespread practice in the production of recombinant proteins. In spite of having been originally designed to facilitate the detection and purification of proteins, subsequently it has become clear that this tag can also increase the yield of their fusion partners, protect them from intracellular proteolysis, enhance their solubility and even facilitate their folding (Tropea *et al.*, 2009). However, the presence of this tag has the potential to interfere with the biological activity of a protein and may impede its crystallization (Tropea *et al.*, 2009). In the case of a metal-binding protein such as Zur, it is self-evident that a His-tag absolutely must be removed, as it will have metal-binding capacity, and therefore will distort any metal-binding stoichiometry and affinity experiments. Therefore, it is generally advisable to remove the tag at some stage.

It has become clear that certain viral proteases, such as that encoded by the tobacco etch virus (TEV), have much greater stringency (Parks *et al.*, 1994; Tropea *et al.*, 2009) than the other protease enzymes such as Factor Xa, enterokinase (enteropeptidase) and thrombin. TEV protease specifically recognizes a seven amino acid sequence (Glu-Asn-Leu-Tyr-Phe-Gln-Gly, cleaving between Gln and Gly), making it useful for removing affinity tags from fusion proteins.

His-tagged TEV protease was over-expressed in *E. coli* BL21 (DE3) CodonPlus-RIL cells (Stratagene, La Jolla, CA, USA) using the TEV protease expression vector pRK793 (see Appendix E, Figure E.11). A large-scale production was achieved at 15°C overnight (see Section 2.7.3).

The TEV protease protein was purified following loading of crude extracts onto HisPur Ni-NTA resin (Fisher Scientific, UK) exactly as performed for the Zur protein above. The induction of pRK793 with IPTG produces an MBP<sup>21</sup> fusion protein (see Appendix E, Figure E.12) that self-cleaves *in vivo* to generate a soluble His<sub>6</sub>-TEV(S219V)-Arg<sub>5</sub> protease. Then this protein was purified by a second round of batch purification using (see Appendix E, Figure E.12).

Purified *Synechococcus* sp. WH8102 His<sub>6</sub>-Zur protein from the first IMAC column (see Section 5.6.1) was incubated overnight at room temperature with TEV protease at a ratio of 2:1.

After incubating overnight, the TEV protease with the His-tag is easily removed from the cleavage reaction by a second IMAC column to obtain a pure and cleaved Zur protein that has no affinity for the column. Coomassie-stained SDS-PAGE revealed a single band ca.15.6 kDa in size, which is consistent with the expected size of the Zur protein without the His<sub>6</sub>-tag (Figure 5.14).

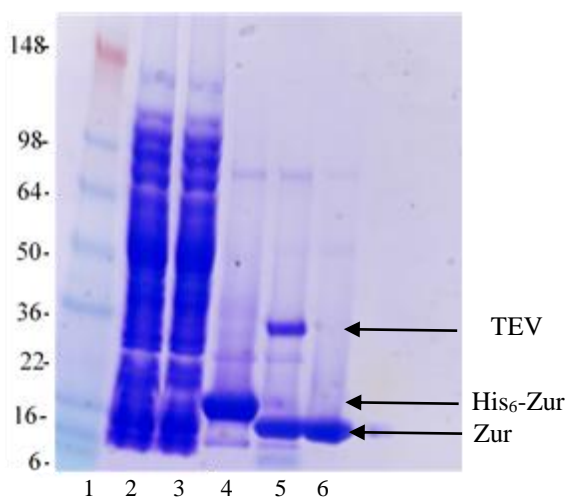


**Figure 5.14 SDS-PAGE analysis of the cleaved His<sub>6</sub>-tag from the Zur protein.**

Lane 1: Marker. Lane 2: crude extract. Lane 3: flow through from the first IMAC column. Lane 4: Purified Zur protein with His<sub>6</sub>-tag (first IMAC column). Lane 5: His<sub>6</sub>-Zur digested with TEV protease. Lane 6: Zur after cleavage of the His<sub>6</sub>-tag, flow-through of second IMAC column. The gel was stained with Coomassie brilliant blue.

<sup>21</sup> MBP is a maltose binding protein.

After cleaving the His<sub>6</sub>-tag from the Zur protein using a second IMAC column, the Zur protein was concentrated and average pure protein yields were recorded as 4-7 mg L<sup>-1</sup> culture, sufficient for further biophysical studies using mass spectrometry, circular dichroism, and nuclear magnetic resonance.

## 5.7 Characterization of Zur Protein

### 5.7.1 Mass Spectrometry under Denaturing Conditions: Apo-Zur

The purified *Synechococcus* sp. WH8102 Zur protein was analysed by electrospray mass spectrometry (ESI-MS) to identify this protein.

The sample obtained after the second IMAC column was desalted using a PD10 desalting column and buffer exchanged into 10 mM ammonium bicarbonate (pH 7.6) (see Section 2.10.1).

To obtain the apo-protein, or zinc-free Zur, 2 % (v/v) formic acid was added to samples (~pH 2.3), and then the mixture was infused directly onto the mass spectrometer (Figure 5.15). To avoid confusion, we suggest that the term ‘apo-Zur’ be applied to protein stripped of all transition metals, especially that Zn<sub>1</sub>PerR from *Bacillus subtilis* and Zn<sub>1</sub>Zur from *Streptomyces coelicolor* have been designated previously as apo protein (Traoré *et al.*, 2006; Jacquamet *et al.*, 2009; Shin *et al.*, 2011).

The large charge state distribution is typical of a denatured protein in electrospray ionisation mass spectrometry. The multiple charging of protein ions in ESI-MS is determined by their solvent-exposed area. However, fully unstructured protein molecules should be able to accommodate a significantly higher number of charges due to an increased surface area (and exposed proton groups) resulting from a protein losing its compactness (Kaltashov *et al.*, 2013).

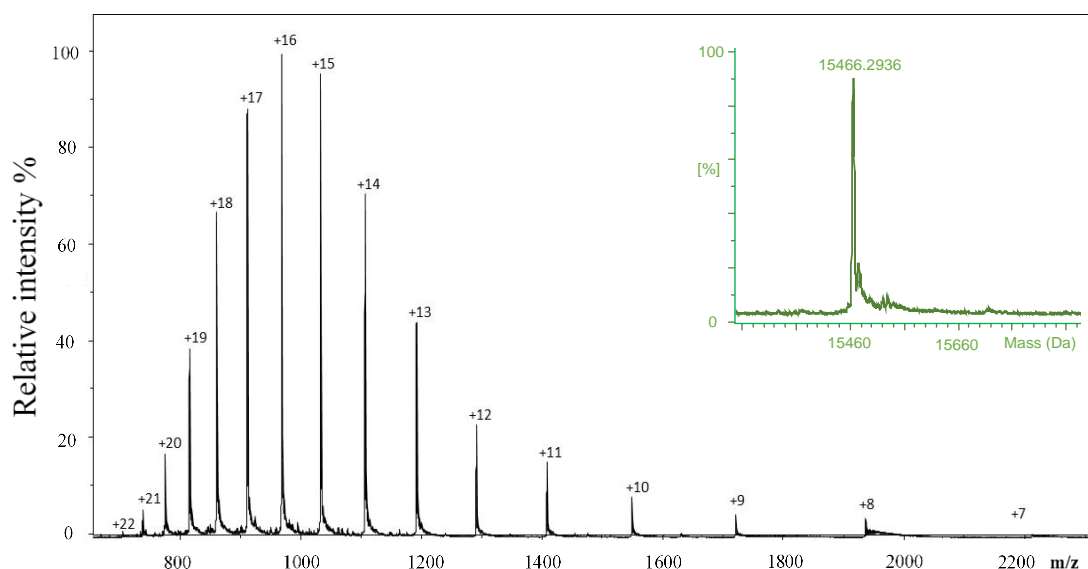


**Figure 5.15 Identification of the non-native Zur protein by ESI-MS.**

The concentration of Zur protein was 12  $\mu$ M in 10 mM ammonium bicarbonate with 10% methanol and 2% formic acid. The green insert shows the deconvoluted mass.

The primary sequence of the Zur protein, as deposited in Cyanobase, consists of 134 amino acids. The signal with a mass of 15466.29 Da in Figure 5.15 corresponds to the expected GIDPFT-Zur (theoretical mass 15466.4 Da) after cleavage of the His<sub>6</sub>-tag (Figure 5.16). This result indicates the successful cleavage of the His<sub>6</sub>-tag in the right place, as well as the correct protein composition.

**GIDPFT**MTGSSPALNARQQALLTALNACGDEMSGQQLHRSLDDEASMGL  
 ATVYRNLRQLQQRGLVRCRHLPTGEALYAPVDRDRHHLTCVDCGTTQV  
 LDHCPHIGIDVPADSRGDFELLFHTLEFFGFCSSCRPQRSSKP

**Figure 5.16 *Synechococcus* sp. WH8102 Zur protein amino acid in black with six additional amino acids (GIDPFT) in red resulting from sub-cloning.**

## 5.7.2 Determination of Protein Concentration

A number of methods were used to calculate the concentration of the protein within the samples produced (Table 5.02).

**Table 5.02 Comparison of three different techniques for the determination of protein concentration**

Sample	Zur concentration by each method ( $\mu\text{M}$ )		
	Bradford assay	Cysteine assay	ICP-OES
1	582.30	750.42	1027.06
2	450.70	693.56	939.15
3	491.59	603.12	978.34

Three samples were used to compare three techniques (Table 5.02), where in each case a higher concentration was found in ICP-OES comparing with the cysteine and Bradford assay.

The low concentration in the Bradford assay is not unexpected. The Bradford assay is based on binding between Coomassie brilliant blue and the protein. There is a striking correlation between the response of Coomassie dyes and the basicity of a protein which depends on the number of lysine, histidine and arginine residues, and also depending on the  $\text{NH}^+$ -terminal amino group (Tal *et al.*, 1985). If the protein has a large amount of positive charges on its surface, 17 positive charges in the case of Zur, this will reduce the possibility of binding the protein to the Coomassie dye (Tal *et al.*, 1985).

Cysteine residues play a key role in metal binding to proteins (Hernandez *et al.*, 2002; Gilston *et al.*, 2014). Although the Zur protein from *Synechococcus* sp. WH8102 has seven cysteine residues in its sequence some of the cysteines were not reactive to DTNB even in the presence of EDTA, which is expected to remove bound metal ions, providing the sites are accessible to this reagent. However, it became clear (see Chapter 7) that complete modification of the seven cysteines of Zur requires unfolding of the protein, such as achieved by the presence of the strong acid  $\text{HNO}_3$ , as used in ICP-OES.

The same phenomenon was deduced for the Fur protein from *Anabaena*, where AnaFur has five cysteines, but not all of them were accessible to DTNB in the presence of EDTA, and a strong

strong disulfide reducing agent, sodium borohydride, was required to access the five cysteines (Hernandez *et al.*, 2002).

### 5.7.3 Molar Extinction Coefficient

The theoretical value of the molar extinction coefficient for Zur was calculated based on the number of Trp, Tyr and Cys residues (Gill & Von Hippel, 1989) (Equation 5.01).

$$\epsilon_P = a \epsilon_{P, \text{Tyr}} + b \epsilon_{P, \text{Trp}} + c \epsilon_{P, \text{Cys}} \quad \text{Equation 5.01}$$

Where  $\epsilon_{P, \text{Tyr}}$ ,  $\epsilon_{P, \text{Trp}}$ , and  $\epsilon_{P, \text{Cys}}$  are the molar extinction coefficients of tyrosine, tryptophan, and cysteine residues at 280 nm wavelength, as follow: 1280 M<sup>-1</sup>cm<sup>-1</sup>, 5690 M<sup>-1</sup> cm<sup>-1</sup> and 120 M<sup>-1</sup>cm<sup>-1</sup>, respectively (Gill & Von Hippel, 1989).  $a$ ,  $b$  and  $c$  are the numbers of each type of residue per molecule of protein. The molar extinction coefficient for *Synechococcus* sp. WH8102 Zur protein was calculated as 3400 M<sup>-1</sup> cm<sup>-1</sup>. However, this relatively low value is expected since the protein sequence is devoid of Trp.

Using the protein concentration determined by ICP-OES, the extinction coefficient of the Zur protein from *Synechococcus* sp. WH8102 was calculated to be 4354± 5.6 M<sup>-1</sup> cm<sup>-1</sup>. This value is close to the extinction coefficient for Zur from *E. coli* (4380 M<sup>-1</sup> cm<sup>-1</sup>) (Outten *et al.*, 2001), but far from the extinction coefficient for Zur from *Bacillus subtilis* 13,785 M<sup>-1</sup>cm<sup>-1</sup> (Ma *et al.*, 2011). We caution however that the latter value may be incorrect due to use of the zinc-sensitive dye (PAR (4-(2-pyridylazo)-resorcinol) in calculating the protein concentration (Ma *et al.*, 2011).

In summary, results from the ICP-OES should be considered as the most reliable data on protein concentration, and are suitable to experimentally deduce an accurate value for the molar extinction coefficient, which was subsequently used for establishing protein concentrations.

### 5.7.4 Native ESI Mass Spectrometry of Zur Protein

The native state for Zur protein from *Synechococcus* sp. WH8102 (will be designated here as SynZur) was analysed by ESI-MS under native conditions (i.e., in largely aqueous solutions kept at neutral pH) (Figure 5.17).

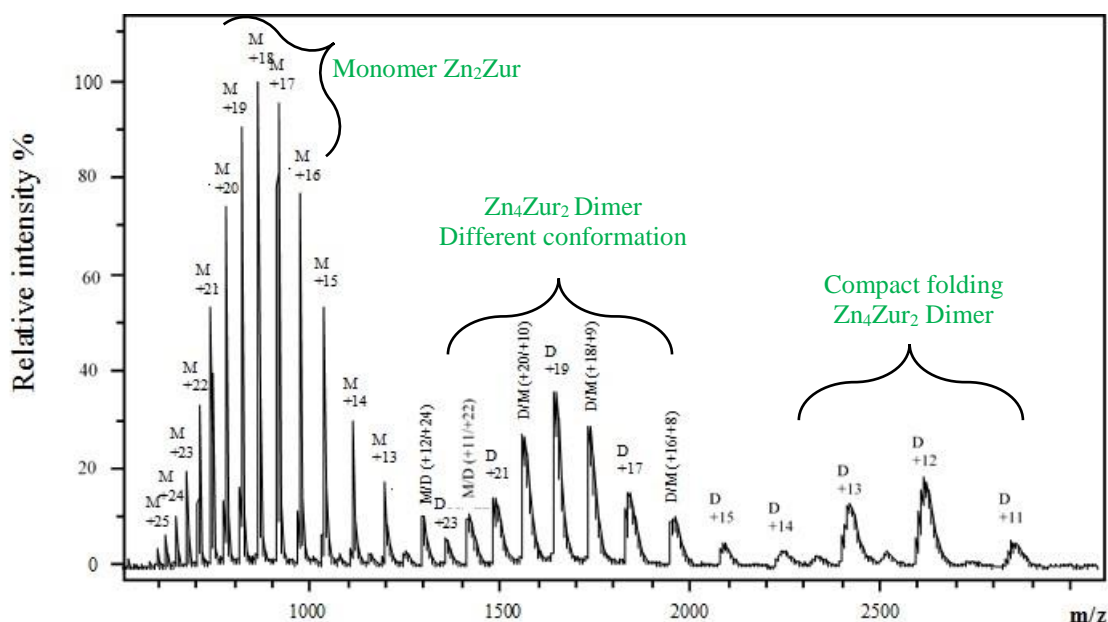


**Figure 5.17 ESI-MS analyses of the native state of SynZur.**

12  $\mu$ M of SynZur protein in 10 mM ammonium bicarbonate at pH 7.8 with 10 % methanol was used to record the native state of Zur protein from *Synechococcus* sp. WH8102 on ESI-MS.

The raw ESI mass spectrum of the holo-form of the protein revealed that SynZur is present as a mixture of at least three different species, including the monomer, dimer and compact folding of dimer (Figure 5.17). The multiply charged ions observed in the spectrum are produced as a result of proton attachment to available basic sites in the protein molecule (Chowdhury *et al.*, 1990). However, SynZur in its monomeric form binds to two zinc ions, giving Zn<sub>2</sub>Zur, and in

its dimeric form binds to four zinc ions,  $Zn_4Zur_2$ . Moreover, it was reported that Zur from *Bacillus subtilis* was purified as  $Zn_2Zur_2$  (Ma *et al.*, 2011), and this may be due to the presence of EDTA and DDT in buffers during purification (this will be discussed in more detail in chapter 7). Recently, *E. coli* Zur was reported to occur as  $Zn_4Zur_2$  (Gilston *et al.*, 2014).

Although it was reported that some Zur proteins contain three zinc ions per monomer (Lucarelli *et al.*, 2007; Shin *et al.*, 2011), no evidence for the occupation of further binding sites was observed from either ICP-OES or mass spectrometry. The ratio between zinc ions and protein was calculated by ICP-OES to be 2.1:1 with respect to the monomer. Also, a number of other first-row divalent transition-metal cations including Fe(III), Co(II), Cd(II) and Ni(II) were analysed by ICP-OES, but none of the mentioned metal was detectable. ESI-MS of the monomer gave a calculated mass of  $15592.9 \pm 0.3$  Da which is in excellent agreement with the theoretical mass of 15593.3 Da calculated from its amino acid composition plus two Zn(II) ions. The deconvoluted dimer mass was  $31186.3 \pm 0.9$  Da, which is very close to the theoretical mass of 31186.6 Da for  $Zn_4Zur_2$ . Additionally,  $Zn_1Zur$  and apo-species were also found in the monomeric state. The differences between the theoretical masses and observed mass for all species are recorded in Table 5.03.

**Table 5.03 The mass differences for the observed species for SynZur protein.**

Oligomer state	Theoretical mass (Da)	Observed mass (Da)	Mass difference
<i>Monomeric Zur</i>			
<b><math>Zn_2Zur</math></b>	15593.3	15592.9	-0.4
<b><math>Zn_1Zur</math></b>	15529.3	15529.4	0.1
<b>Apo-Zur</b>	15466.4	15465.7	-0.6
<i>Dimeric Zur</i>			
<b><math>Zn_4Zur_2</math></b>	31186.3	31186.6	0.3

To gain further insights into the oligomeric state of the recombinant protein, SynZur was studied by native gel electrophoresis (i.e., in aqueous solutions kept at neutral pH in the absence of denaturants) (see Section 2.8.2) (Figure 5.18).

Under non-reducing conditions, two bands were observed with molecular mass 15.5 kDa and 31.2 kDa representing the monomer and dimer respectively, with the dimer being most abundant (Figure 5.18).

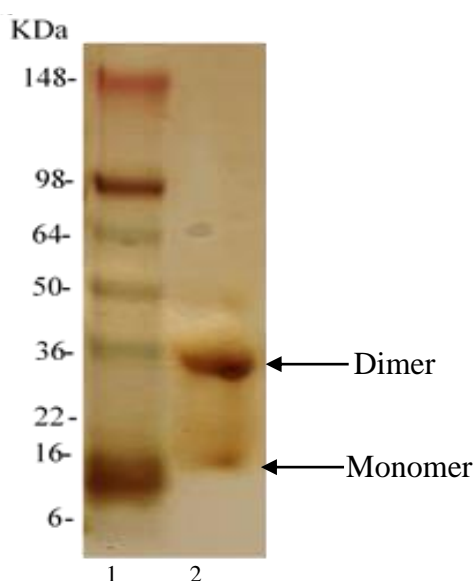


**Figure 5.18 Non-denaturing PAGE analysis of the SynZur protein.**

Lane 1: Marker. Lane 2: purified SynZur protein. Purified SynZur was separated by non-denaturing PAGE in the absence of denaturants and visualized by silver staining. Arrows indicate the estimated molecular masses of the monomer and dimer.

It has been reported that under native conditions Zur from *E. coli* is present as a monomer, dimer and trimer, with the dimer being the most abundant species (Patzner & Hantke, 2000; Gilston *et al.*, 2014). Similarly, Fur from *Anabaena* also showed several oligomerization states including the monomer, dimer, trimer and a small amount of the tetramer forms, but with the monomeric form being predominant (Hernandez *et al.*, 2002). Fur from *E. coli* can also present as dimeric, tetrameric and hexameric species, with the dimeric species being the most abundant one (D'Autréaux *et al.*, 2007).

Using a high ionic strength (300 mM NaCl) in the buffer during purification helped to strongly retain SynZur as an oligomer protein. The same observation was made for Zur from *E. coli* (Patzner & Hantke, 2000) and Fur from *Anabaena* (Hernandez *et al.*, 2002). Although it was stated that presenting high ionic strength in the buffer promotes the appearance of high-molecular-mass species (trimers and tetramers) held together by hydrophobic interactions (Hernandez *et al.*, 2002), in our case we did not observe this phenomenon.

### 5.7.5 Influence of Freezing on SynZur

In order to investigate the influence of storage and freezing conditions on SynZur, a sample of purified protein was analyzed by mass spectrometry after freezing at  $-80^{\circ}\text{C}$  for seven days and compared with the native state for zinc-loaded SynZur and the denatured state for zinc-free SynZur, apo-SynZur (Figure 5.19).

Inspection of the mass spectra (Figure 5.19B) reveals that there are dramatic differences in the charge state distribution, oligomer abundance, and folding of the monomer and dimer after a single freeze-thaw cycle. The mass spectrum for SynZur after freezing indicates the presence of two states belonging to the monomer and dimer, where monomer is more dominant than the dimer. However, these two states are different from zinc-free SynZur, apo-SynZur (Figure 5.19C). At the same time the charge state for the monomer was shifted to a higher  $m/z$  suggesting a better folding species.

Freezing/thawing to promote oligomerization has been studied in other proteins, showing that this treatment can affect the distribution of oligomer sizes (Steere & Eisenberg, 2000). Althaus and colleagues pointed out that thawing *E. coli* Zur protein (named as  $\text{Zn}_2\text{Fur}$ ) from the freezer led to only 50% of protein remaining intact with only one proteolytic fragment at 16 kDa (Althaus *et al.*, 1999), while the oligomerization pattern of the Fur protein from *Anabaena* PCC7119 did not change after storage at  $-80^{\circ}\text{C}$  (Hernandez *et al.*, 2002).

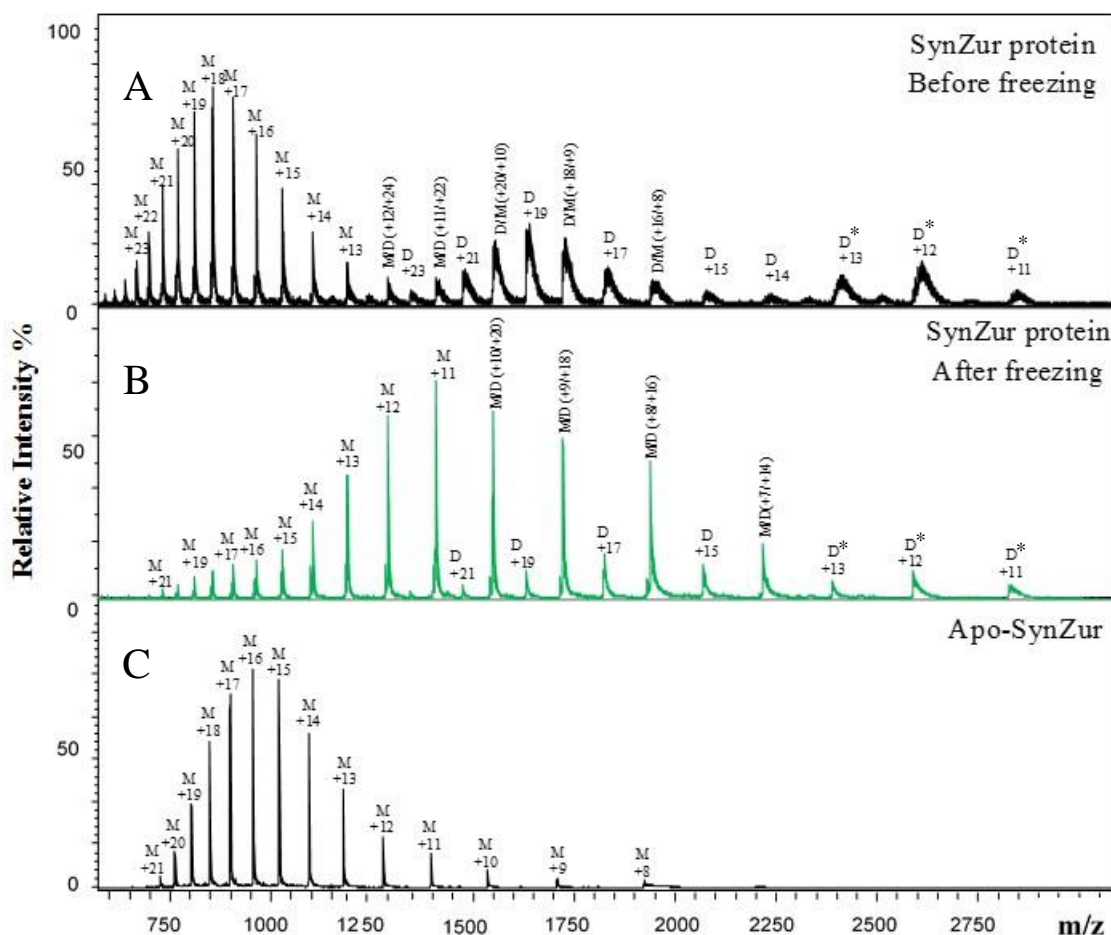


**Figure 5.19 Influence of freezing on SynZur charge state distribution.**

Mass spectrum of zinc-loaded SynZur protein before freezing (A), zinc-loaded SynZur protein after freezing (B), zinc-free SynZur protein after stripping the metal ions at low pH (C). Charge states corresponding to monomer (M), dimer (D) and compact folding of dimer (D\*) are labelled. Protein samples for mass spectrometry were 34  $\mu\text{M}$  of SynZur in 10 mM ammonium bicarbonate at pH= 7.8 for zinc-loaded SynZur protein and at pH= 2.1 for zinc-free SynZur protein.

To gain further insights into the monomer/dimer state, one signal from a monomer charge state, +15, and one signal from a dimer charge state, +19, were chosen to visualize the effects of freezing on the metallation degree of zinc-loaded SynZur (Figure 5.20).

For the monomeric state, zinc-loaded SynZur, as purified, was present as  $\text{Zn}_2\text{Zur}$  with low or negligible amount of  $\text{Zn}_1\text{Zur}$  species. However, after freezing, more species were seen, including  $\text{Zn}_3\text{Zur}$  and  $\text{Zn}_4\text{Zur}$ , besides  $\text{Zn}_2\text{Zur}$  and  $\text{Zn}_1\text{Zur}$  species (Figure 5.20A).  $\text{Zn}_3\text{Zur}$  was the most abundant species in this spectrum while  $\text{Zn}_4\text{Zur}$  species was present at low abundance.

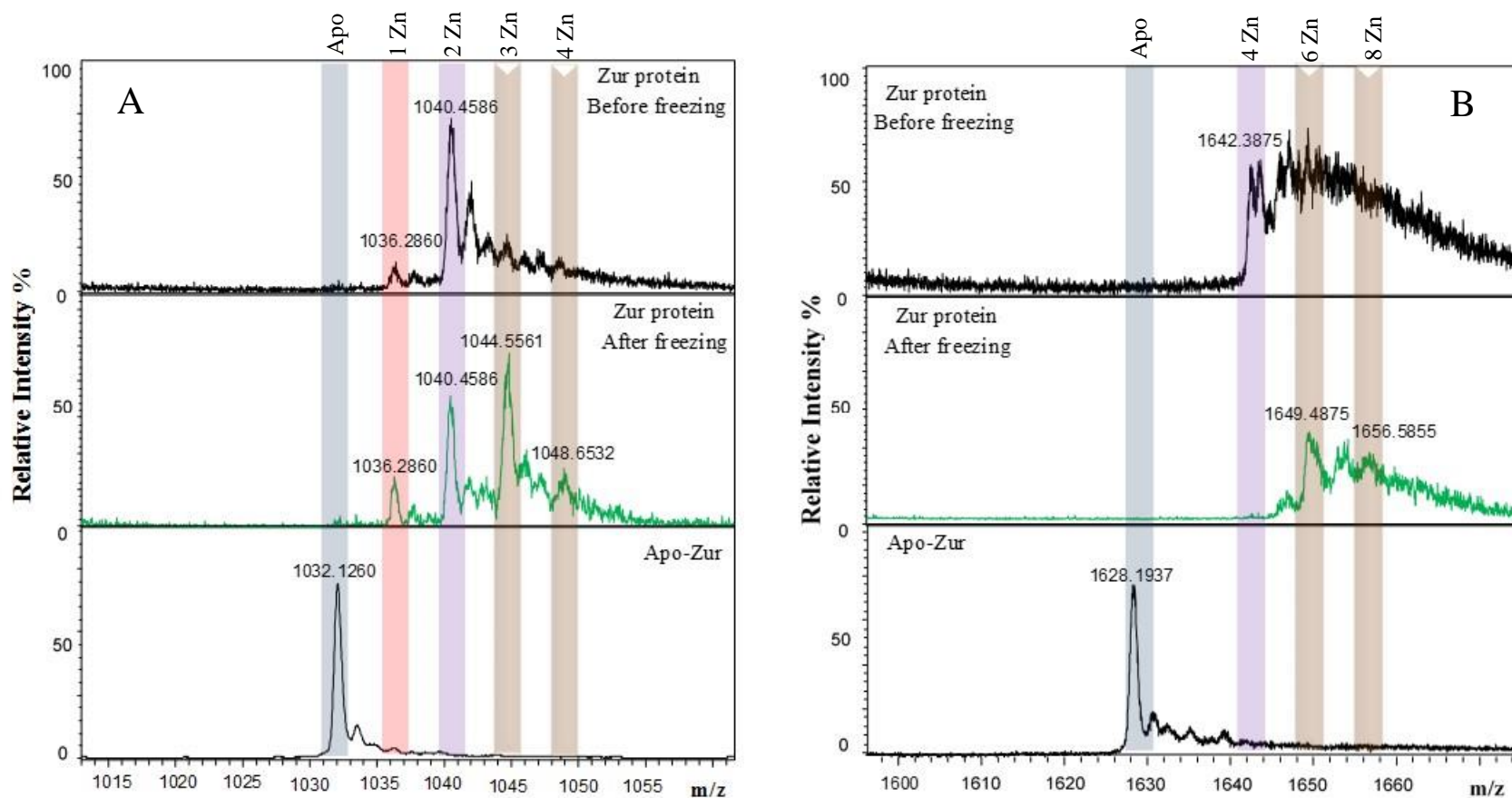


**Figure 5.20 Influence of freezing on selected monomer/dimer charge states for SynZur.**

(A) The speciation of the +15 charge state for the monomer. (B) The speciation of the +19 charge state for the dimer. The species are coloured as follows: Purple = 2 Zn(II) for monomer and 4 Zn(II) for dimer, Pink = 1 Zn(II) for monomer, Cyan = Apo, Brown = the new species including: 3 Zn(II) and 4 Zn(II) for monomer and 6 Zn(II) and 8 Zn(II) for dimer. Protein samples for mass spectrometry were 34  $\mu$ M of SynZur in 10 mM ammonium bicarbonate at pH = 7.8 for zinc-loaded SynZur protein, and at pH = 2.1 for zinc-free SynZur protein.

Moving to the dimeric state, zinc-loaded SynZur was present as  $Zn_4Zur_2$  species before freezing, then, after freezing, new species were observed including  $Zn_6Zur_2$  and  $Zn_8Zur_2$  with a remarkable disappearance of the  $Zn_4Zur_2$  species (Figure 5.20B). No zinc-free SynZur species were observed either in the monomeric state or in the dimeric state in the sample after freezing.

From the pre-dominance of the “over-metallated”  $Zn_3Zur$  and  $Zn_6Zur_2$  species, it appears that the zinc: protein ratio has increased. The origin of the “extra” zinc for formation of these species is unclear.

Taken together, these results establish that freezing SynZur can affect not only the oligomerization equilibrium but also the metal speciation. Thus, this is an important practical point for the correct handling and storage of the Zur protein from *Synechococcus* sp. WH8102 for future experiments and thus SynZur will be handling directly without freezing.

### 5.7.6 Circular Dichroism Spectroscopy

Circular dichroism spectroscopy is a fast, quantitative and non-destructive photometric technique that can help answer an array of common questions about the folding, conformational changes, and especially secondary structures of proteins (Wallace *et al.*, 2003). In general, this technique measures the difference in the absorption of left-handed circularly polarised light (L-CPL) and right-handed circularly polarised light (R-CPL) occurred when a molecule contains one or more chiral chromophores (light-absorbing groups).

Chiral molecules exist as pairs of mirror-image isomers and these pairs are not super-imposable and known as enantiomers. The physical and chemical properties of a pair of enantiomers are identical with two exceptions: the way that they interact with polarised light and the way that they interact with other chiral molecules.

When the molecule contains chiral chromophores, one CPL state will be absorbed to a greater extent than the other and the CD signal over the corresponding wavelengths will be non-zero. A circular dichroism signal can be positive or negative, depending on whether L-CPL is absorbed to a greater extent than R-CPL (CD signal positive) or to a lesser extent (CD signal negative).

In general, the polarised light states can be described as a sum of two linearly polarised lights, vertically and horizontally polarised light, states at right angles to each other (Figure 5.21).

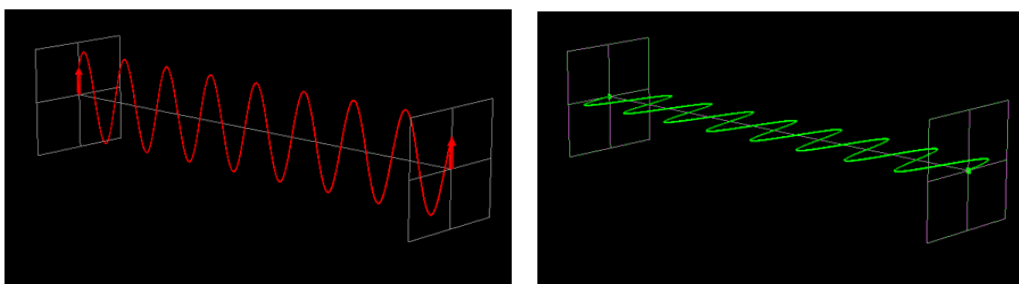


**Figure 5.21 Schematic diagram showing the vertically linearly polarized light (left panel) and horizontally linearly polarized light (right panel).**

If the two polarisation states are out of phase, the resultant wave ceases to be linearly polarised. For example, if one of the polarised states is out of phase with the other by a quarter-wave, the resultant will be a helix and is known as circularly polarised light (CPL). The helices can be either right-handed (R-CPL) or left-handed (L-CPL) and are non-superimposable mirror images (Figure 5.22) (Kelly *et al.*, 2005; Greenfield, 2006).

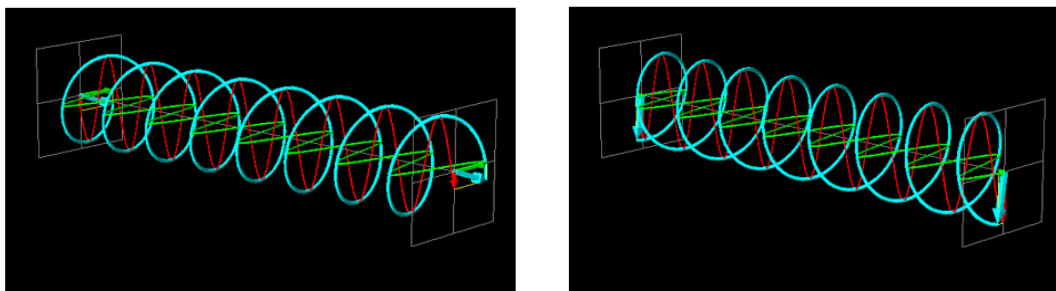


**Figure 5.22 Schematic diagram showing the left-hand circularly polarised light (left panel) and right-hand circularly polarised light (right panel).**

Usually the circular dichroism is used to detect the secondary structural elements of proteins. In protein, the chromophore is the peptide bond, and the signal arises when it is located in a regular and folded environment. The generated spectrum in circular dichroism normally allows us to distinguish between the main secondary structure elements of the protein, including  $\alpha$ -helices,  $\beta$ -sheets and random coils or unfolded (Figure 5.23).

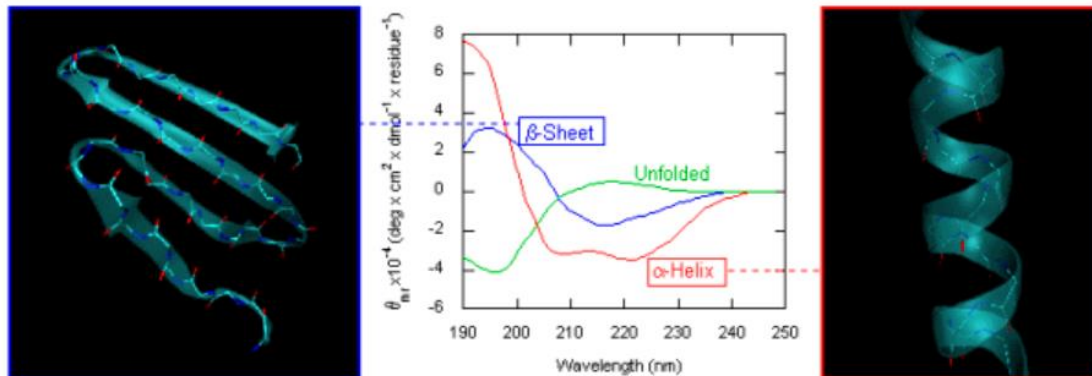


**Figure 5.23 The CD spectra of protein structural elements with the secondary structure conformation.**

Left panel is the conformation of a peptide in a  $\beta$ -sheet and the right panel is the conformation of a peptide in a  $\alpha$ -helix. The center panel is the associated CD spectra for these different conformations (<https://www.photophysics.com/resources/tutorials/circular-dichroism-cd-spectroscopy>).

CD analysis of the SynZur protein showed clear minima at 208 nm and 222 nm (Figure 5.24). This is characteristic of proteins rich in  $\alpha$ -helices and  $\beta$ -sheets. The same shape for the Zur protein was also observed in *Bacillus subtilis* (Ma *et al.*, 2011) and in the Fur protein from *E. coli* (D'Autréaux *et al.*, 2007).

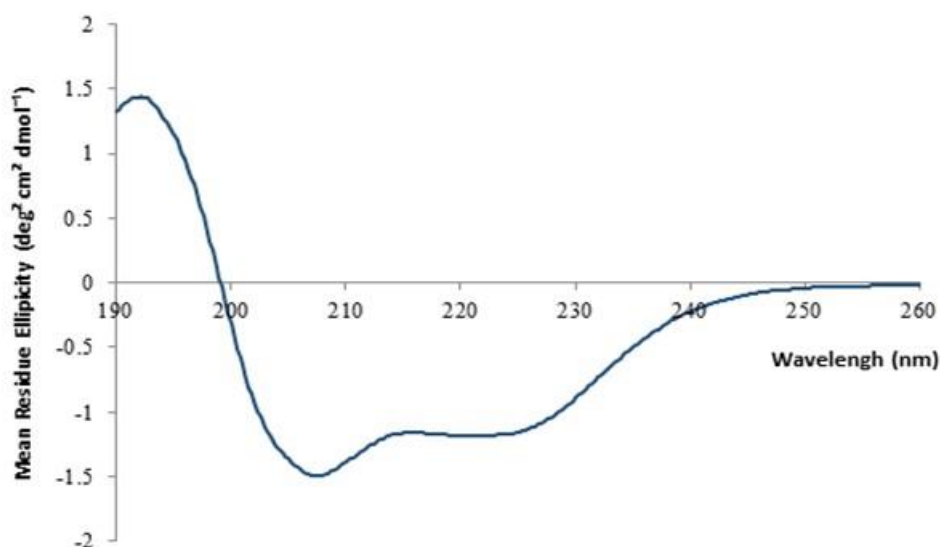


**Figure 5.24 Circular dichroism analyses of the *Synechococcus* sp. WH8102 Zur protein.**

Purified SynZur protein was used to obtain a CD spectrum over 200-260 nm using a Jasco J-815 spectrometer. The spectrum shown is an average taken from 8 consecutive scans.

Secondary structure analysis of SynZur in different softwares revealed the presence of the following; 45.5%  $\alpha$ -helices, 21.7%  $\beta$ -sheets and 32.8% random coils in I-TASSER software (Zhang, 2008; Roy *et al.*, 2010); 35%  $\alpha$ -helices, 33%  $\beta$ -sheets and 22.5% random coils in SELCON software (Sreerama *et al.*, 2000); 24%  $\alpha$ -helices, 35%  $\beta$ -sheets and 41% random coils in CONTIN software (Sreerama *et al.*, 2000); and 45 %  $\alpha$ -helices, 17.5%  $\beta$ -sheets and 34.2% random coils in RAUSSENS software (Raussens *et al.*, 2003) (Table 5.04). The calculated secondary structure from I-TASSER software for  $\alpha$ -helices,  $\beta$ -sheets and random coils are in good agreement with the predictions from RAUSSENS Web server (Raussens *et al.*, 2003) (Table 5.04).

**Table 5.04 Estimation of secondary structure proportions for SynZur using different algorithms.**

<b>Internet service</b>	<b><math>\alpha</math>-helices %</b>	<b><math>\beta</math>-sheets %</b>	<b>random coils %</b>
I-TASSER	45.5	21.7	32.8
SELCON	35	33	22.5
CONTIN	24	35	41
RAUSSENS	45	17.5	34.2

## 5.8 Summary and Conclusions

Although bacterial Fur proteins have been studied directly for nearly 15 years, the number of cases for which the details are fully understood is still limited, the same situation also accounts for Zur proteins.

To achieve a better understanding of SynZur functions in *Synechococcus* sp. WH8102, the *synw\_2401* gene was cloned into plasmid pET151/D using TOPO cloning. By optimizing the protein yield and solubility, the most promising expression method was found to be in the presence of the GroES-GroEL-Tig chaperones expressed from the pG-Tf2 plasmid in LB medium. Using IMAC chromatography and cleavage of the His<sub>6</sub>-tag with TEV protease allowed to obtain a pure cleaved SynZur protein.

Mass spectrometry confirmed that the recombinant SynZur protein was produced with good agreement between experimental and theoretical masses for both the apo and metal loaded form. SynZur at neutral pH (~pH 7.8) presented as a mixture of species, including a monomer with two zinc ions bound and dimers with four zinc ions bound. The presence of monomers and dimers was also confirmed by native gel electrophoresis. Its CD spectrum gave evidence that the protein is rich in  $\alpha$ -helices and  $\beta$ -sheets, as expected.

# Chapter 6

## Towards the Three Dimensional Structure of Zur Protein from *Synechococcus* sp. WH8102

---

### 6.1 Introduction

Structural analysis of known Zur proteins has revealed that they are homodimeric (Lucarelli *et al.*, 2007; An *et al.*, 2009; Jacquamet *et al.*, 2009; Sheikh & Taylor, 2009; Ma *et al.*, 2011; Shin *et al.*, 2011; Gilston *et al.*, 2014), and that each monomer consists of an N-terminal DNA binding (DB) domain, a C-terminal dimerization (D) domain, and a hinge loop between the two domains with two or three metal binding sites. In order to gain further understanding of the structure and protein folding of SynZur from *Synechococcus* sp. WH8102 a 3D structure is required.

In the present chapter, the optimisation of conditions for protein NMR studies is described in more detail. After that a homology model is created for SynZur in the absence of a complete 3D structure.

## 6.2 Nuclear Magnetic Resonance (NMR) Spectroscopy

### <sup>1</sup>H 1-Dimensional NMR Spectroscopy

Nuclear magnetic resonance spectroscopy is a powerful and theoretically complex analytical tool. The NMR phenomenon is based on the fact that nuclei of atoms have magnetic properties that can be utilized to yield the chemical information. All nuclei which do not contain an even number of protons and neutrons possess the quantum mechanical property called spin angular momentum ( $I$ ). Moreover, atoms that possess an angular momentum will produce a magnetic dipole moment ( $\mu$ ) which is proportional to the spin angular momentum moment (Equation 6.01).

$$\mu = \gamma \hbar \sqrt{I(I + 1)} \quad \text{Equation 6.01}$$

Where  $\mu$  is dipole moment,  $\hbar$  is Planck's constant,  $\gamma$  is gyromagnetic ratio, and  $I$  is spin angular momentum.

Of the NMR active nuclei, the most commonly used is the spin  $\frac{1}{2}$  hydrogen nucleus. A spin-half nucleus can interact with a magnetic field and gives rise to two energy levels,  $(2I + 1)$ , and these are characterised by another quantum number  $m$  which is restricted to the values  $-I$  to  $+I$  ( $m = \frac{1}{2}$  and  $m = -\frac{1}{2}$ ) (Figure 6.01).

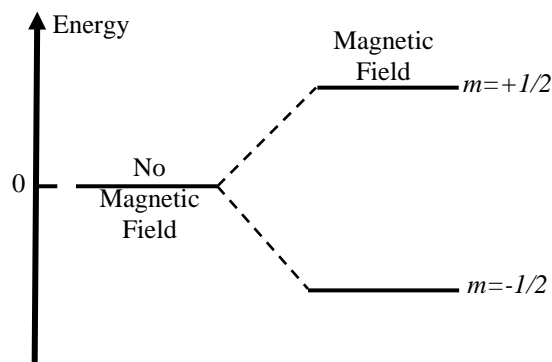


**Figure 6.01 Quantum model of NMR visualising the two spin states.**

A nucleus with spin  $1/2$  will have two possible orientations. In the absence of an external magnetic field, these orientations are of equal energy. If a magnetic field is applied, the energy levels will be split to two levels and each level will give a magnetic quantum number,  $m$ .

At thermal equilibrium, the nuclei will be orientated isotropically (Figure 6.02A). Applying an external magnetic field ( $B_0$ ), the equilibrium will shift and the nuclei will orient themselves one parallel and the other antiparallel to the applied an external magnetic field ( $B_0$ ) (Figure 6.02B). Moreover, the greater population of nuclei will reside in the lower energy state aligned with the external magnetic field and resulting in a net macroscopic magnetization ( $M_0$ ) (Figure 6.02B).

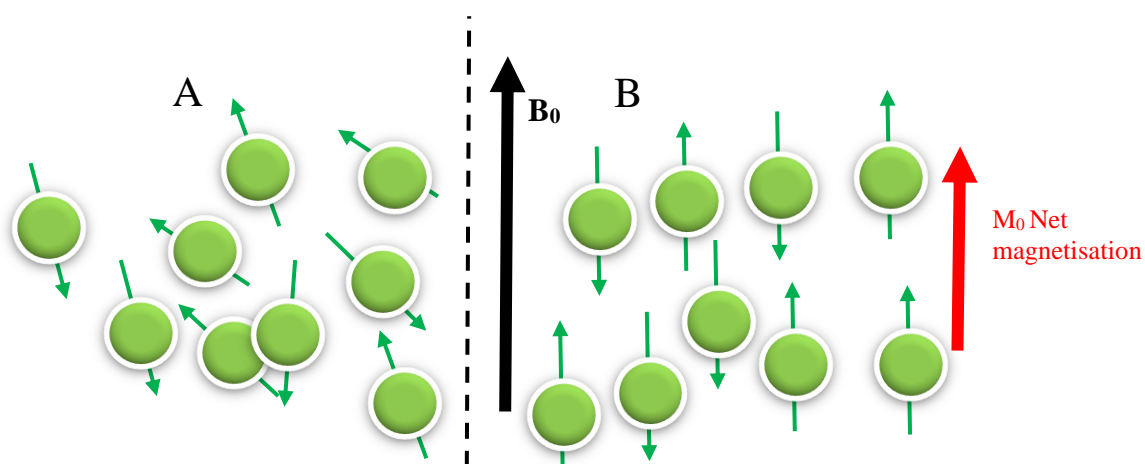


**Figure 6.02 Distribution of spin  $1/2$  nuclei in the absence and in the present of the external magnetic field ( $B_0$ ).**

(A) In the absence of an external magnetic field the spins are orientated isotropically. (B) Applying an external magnetic field ( $B_0$ ) leading to oriented the spin  $1/2$  nuclei in the parallel and antiparallel to the magnetic field. A small excess in the parallel spins resulting in a net magnetization ( $M_0$ ).

In the case of applying an external magnetic field along the z-axis, the nuclear magnetic moments will precess around the same axis (Figure 6.03A and B), and the rate of the precession is known as the Larmor frequency. Applying a radio frequency (RF) pulse perpendicular to the external magnetic field at the Larmor frequency will lead to rotate the equilibrium magnetization around  $xy$ -plane (Figure 6.03C) which will induce an electrical current that can be measured by receiver coil and the NMR spectrum is recorded as a free induction decay (FID) signal.

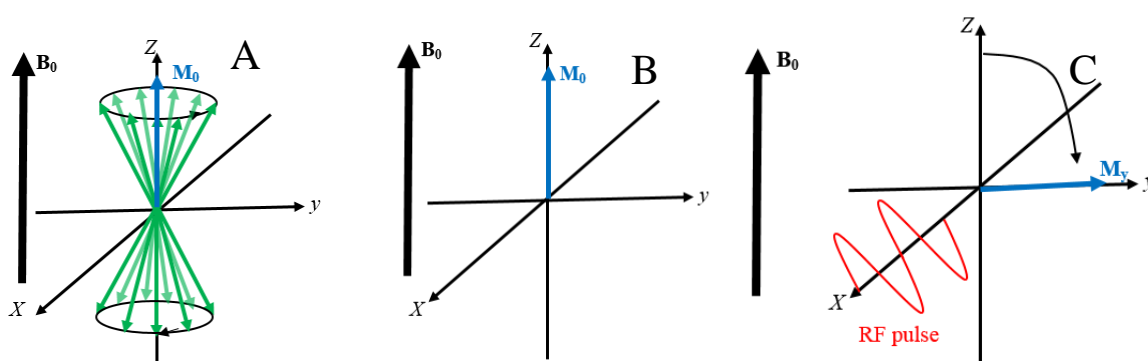


**Figure 6.03 A spin precessing about the magnetic field in the absence and present of radio frequency (RF) pulse.**

(A) Applying an external magnetic field ( $B_0$ ) along the z-axis will cause the nuclear spins to precess around the z-axis. (B) Simplify the net magnetization ( $M_0$ ) that is parallel to the external magnetic field ( $B_0$ ). (C) Applying RF pulse perpendicular to the external magnetic in the x-axis at larmor frequency will cause the net magnetization to rotate in the  $xy$ -plane inducing the electrical current measured by receiver coil.

Because each nucleus in the magnetic field possesses its own intrinsic magnetic field which can oppose the external field, these intrinsic fields will slightly affect the neighbouring nuclei (Keeler, 2011). For example, the magnetic field produced by the electron shell surrounding a nucleus acts as a shield from the external magnetic field causing the nuclei to be at a lower resonance frequency in the NMR spectrum. In contrast, presence of the electronegative groups near the nucleus will de-shield and the nucleus will appear in the downfield, at a higher resonance frequency in the NMR spectrum. As a result, the magnetic field experienced by each

nucleus is different causing each nucleus to precess at a different frequency resulting in separation of the signals in the NMR spectrum (chemical shift). The chemical shift allows to distinguish between different chemical structures and determines the folding state of protein.

One-dimensional  $^1\text{H}$  NMR spectroscopy is routinely used to characterize the folded state of protein targets (Page *et al.*, 2005). Like all protein NMR spectra, the 1D  $^1\text{H}$  NMR spectrum for SynZur displays three distinct areas of peaks (Figure 6.04). One area comprises aliphatic side-chain protons in the region of 0.3-3.8 ppm which are likely to belong to methyl and methylene groups (Hernandez *et al.*, 2002). A second set consist of  $\text{H}_\alpha$  proton which resonate between chemical shifts of 3.5-6 ppm (Saito *et al.*, 1991), and a third set includes backbone and side-chain amide (NH and  $\text{NH}_2$ ) as well as aromatic protons, which resonate in the downfield region with chemical shifts between 6 and 10 ppm (Figure 6.04).

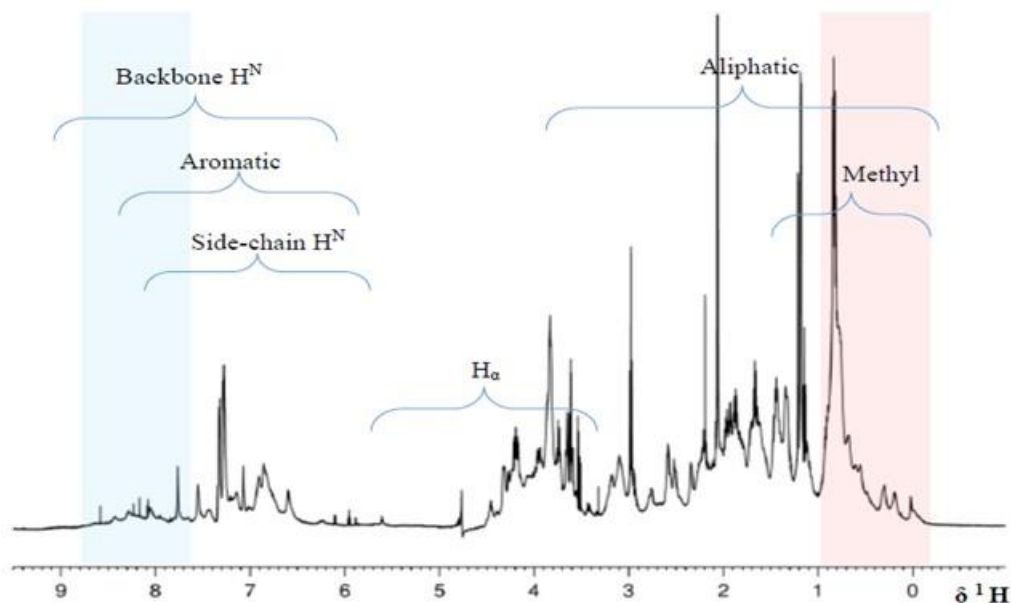


**Figure 6.04 One-dimensional  $^1\text{H}$  NMR spectrum of *Synechococcus* sp. WH8102 Zur.**

0.6 mM SynZur was prepared in 20 mM ammonium bicarbonate with 10%  $\text{D}_2\text{O}$  at pH 7.8. The spectrum was recorded on a 700 MHz spectrometer (Bruker Avance 700).

In the 1D  $^1\text{H}$  NMR spectrum, the dispersion of the NMR signals in the three regions can provide the main indicators of folded globular proteins (Page *et al.*, 2005). Large proteins have long

rotational correlation times, and the reliability of 1D  $^1\text{H}$  NMR to verify the folded state is therefore limited by protein size and possibly by the multimerization state (Page *et al.*, 2005). However, the 1D  $^1\text{H}$  NMR spectrum for SynZur yielded a significant dispersion of resonance lines in the three spectral regions. These resonances are well separated, with at least some lines in the region of the methyl protons (0.5 to 1.5 ppm) and  $\alpha$  protons (3.5–6 ppm) being relatively sharp, while there was only a small number of dispersed resonance lines in the amide proton region (6–10 ppm). However, improvements in the amide proton region (6–10 ppm) will be investigated in more detail in the next section.

### 6.3 Optimization of Conditions for NMR

1D  $^1\text{H}$  NMR spectra can be used to verify the folded protein state (Page *et al.*, 2005). The dispersion of signals in the proton NMR can be divided into three regions including: methyl protons (-0.5 to 1.5 ppm),  $\alpha$ -protons (3.5 to 6 ppm), and amide protons (6 to 10 ppm). Furthermore, the 1D  $^1\text{H}$  NMR spectra can be grouped into four groups from “A” to “D” according to their spectral quality (Page *et al.*, 2005). In group “A”, the resonances for proteins are well separated, display sharp lines, and the intensities represent the entire population of protein molecules, whereas in group “B”, the shapes and intensities of the dispersed resonance lines do not quite meet the stringent criteria for group A classification (Page *et al.*, 2005). In group “C”, the chemical shift dispersion is obvious in the region between 1.0 to 2.0 ppm, with line broadening over the entire spectrum due to intrinsic large size, aggregation, or oligomerization. In group “D”, there are no resolved resonance lines in the spectral regions from 0.5 to 6.5 ppm, indicating unfolded protein with only narrow chemical shift dispersion in the amide proton region (Page *et al.*, 2005).

The 1D  $^1\text{H}$  NMR spectrum for SynZur yielded a significant dispersion of resonance lines in the three spectral regions (see Section 6.2). Some resonances are well separated, with at least some

lines in the region of the methyl protons (-0.5 to 1.5 ppm) and  $\alpha$  protons (3.5 to 6 ppm) being relatively sharp, while there was only a small number of dispersed resonance lines in the amide proton region (6–10 ppm) which may be limited due to the oligomerisation state of our protein. However the 1D  $^1\text{H}$  NMR spectrum for SynZur can be classified as group “B” or “C” or between them. Therefore, in an attempt to improve the quality of the NMR spectra for the SynZur protein, the influence of variation in temperature and salt concentrations was investigated (see also 7.2.3. for the influence of pH) by recording the 1D  $^1\text{H}$  NMR spectra under different conditions.

### 6.3.1 Effect of Temperature on SynZur

To establish whether changes in temperature may cause a significant sharpening (or broadening) effect on NMR proton signals or affect the chemical shift dispersion of peaks, 1D  $^1\text{H}$  NMR spectra of a freshly purified sample of zinc-loaded SynZur were recorded at various temperatures ranging from 288K to 318K (in increments of 5K) (Figure 6.05).

Bearing in mind the concern that high temperature may significantly decrease the lifetime of the protein, no higher temperature above 318K was tested. Previously, it was reported that temperature may directly affect protein folding and hence may have effects on the tumbling rate and the transverse  $T_2$  relaxation time (Rule & Hitchens, 2006). It is apparent that variation in temperature has led to minor improvements in the fingerprint region (Figure 6.05A) and significant improvements in the aliphatic region (Figure 6.05C).

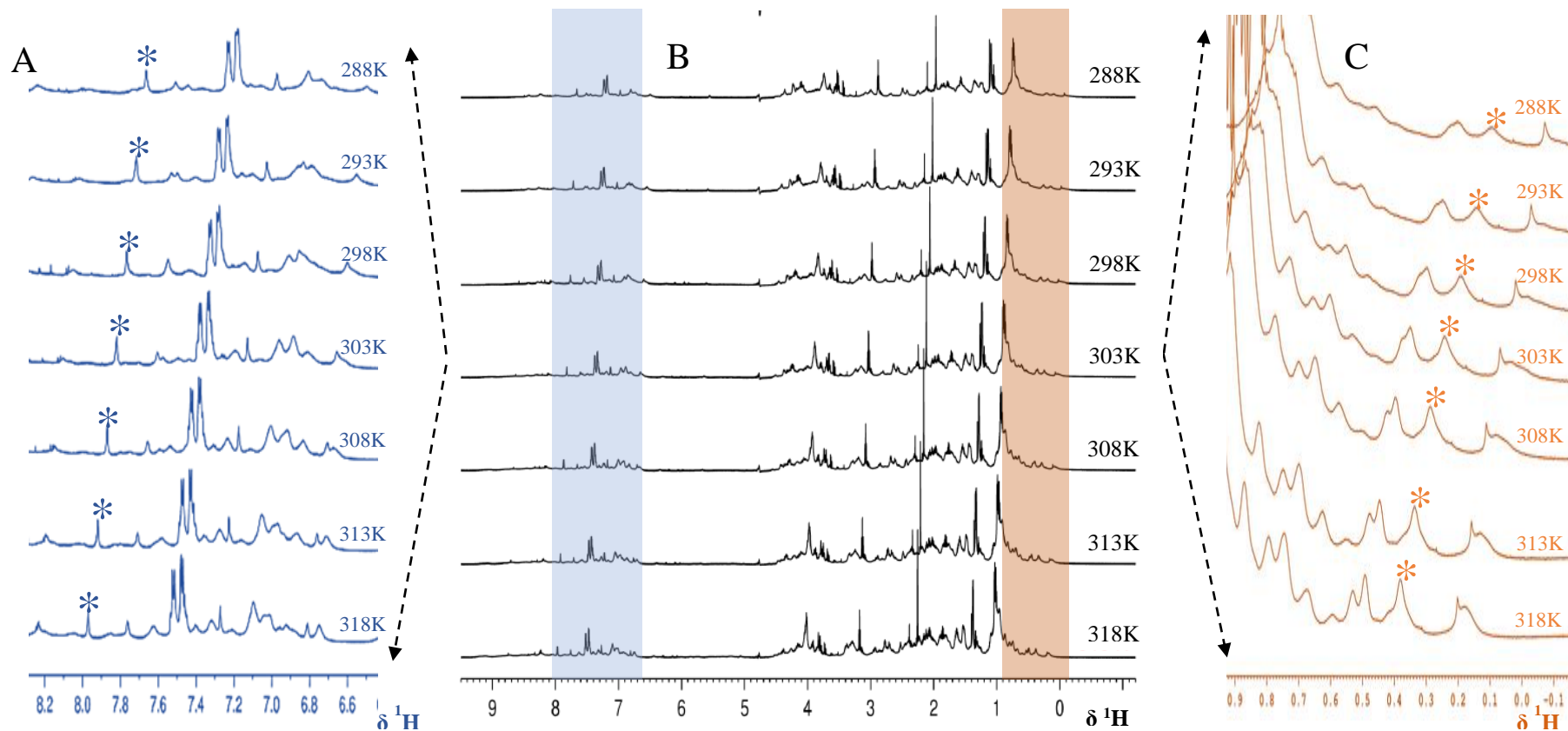


**Figure 6.05 Stacked plot of 1D  $^1\text{H}$  NMR spectra at various temperatures for SynZur.**

The effect of temperature on the full SynZur spectra, middle panel (black) (B), on the fingerprint region, left panel (blue) (A), on the aliphatic region, right panel (orange) (C). Protein samples of SynZur (600  $\mu\text{M}$ , 20 mM ammonium bicarbonate, 10%  $\text{D}_2\text{O}$ , pH  $\sim 7.4$ ) were subjected to various temperatures from 288K to 318K and the spectra were recorded on 700.24 MHz Spectrometer (Bruker Avance 700). Asterisks illustrate a shifting in the low-field and up-field regions.

To determine an optimum temperature, a peak in the fingerprint region (7.62 ppm) at 288K was chosen. Due to the isolated nature of the 7.62 ppm peak, it was useful to use this peak for monitoring the effect of changing temperature on SynZur spectra. At 288K, small number of dispersed resonance lines in the backbone NH signals were detected for SynZur with the peak width at half height ~ 8.97 Hz for the selected peak, 7.62 ppm. With increasing the temperature from 288K to 303K improvements in the number of peaks and in the resolution were achieved (Figure 6.05A). Hence, the peak width at half height of the selected peak was 7.13 Hz, and new peaks appeared at around 6.83 ppm, 6.9 ppm and 7.27 ppm. On the other hand, some peaks at 6.77 ppm, 7 ppm and 7.2 ppm became sharper. Further increase in temperature to 308K led to the appearance of a new peak at 6.67 ppm with the peak width at half height of selected peak ~ 7.05 Hz. Increasing the temperature above 308K appeared to give no significant benefit in spectral dispersion, resolution, and peak width at half height.

Despite these improvements in the fingerprint region, major improvements in the up-field region (where high-field-shifted methyl groups can be used as an indication for folding state) were spotted. In the aliphatic region, a peak (0.095 ppm) was chosen at 288K. With increasing the temperature from 288K to 303K, improvements in the number of peaks and in the resolution were observed (Figure 6.05C). The peak width at half height of the selected peak was 29.57 Hz, 26.37 Hz, 24.77 Hz and 22.37 Hz at 288K, 293K, 298K and 303K, respectively. However, increasing the temperature to 308K led to the appearance of new peaks with the peak width at half height of selected peak ~ 20.78 Hz. Further increasing in temperature above 308K, no significant improvements were achieved (Figure 6.05C). Therefore, the temperature at 308 K was selected as best temperature for Zur protein from *Synechococcus* sp. WH8102.

### 6.3.2 Effect of Salt on SynZur

Early studies have reported that variation of the ionic strength in the buffer can help to improve the 1D  $^1\text{H}$  NMR spectrum and stabilize protein structure in the case of the oligomeric state (Patel *et al.*, 1979; Narayanan & Reif, 2005; D'Autréaux *et al.*, 2007).

Protein surfaces, in principle, are heterogeneously composed of positively and negatively charged polar and nonpolar amino acid residues. Intermolecular interactions between protein molecules can have different origins, such as electrostatic, hydrophobic, van der Waals and hydrogen bonding. Sodium chloride acts as counter-ions which can significantly perturb and reduce intermolecular interactions (Zhang, 2012).

Thus, in order to improve the resolution of the 1D  $^1\text{H}$  NMR spectrum for SynZur protein, various concentrations of NaCl were investigated. Significant improvements in the up- and down-field regions, fingerprint and aliphatic regions, for SynZur spectra were achieved at higher NaCl concentrations (Figure 6.06).

Without NaCl, it was observed that there was less dispersion in both the up- and down-field regions at 298K (Figure 6.06). Increasing the salt concentration from 0 mM to 150 mM caused no improvement at 298K, with only small changes in the chemical shifts of some resonances in the down-field region. Moreover, after increasing the temperature to the optimum 308K (see Section 6.3.1), improvements in spectral dispersion and resolution were achieved in both up- and down-field regions (Figure 6.06). Therefore, 150 mM NaCl with 308K were selected as the best conditions for the SynZur protein. Regarding the fact that there are still broad lines at 150 mM salt, higher salt concentrations must be avoided in NMR spectroscopy due to spectral noise being generated by ions.

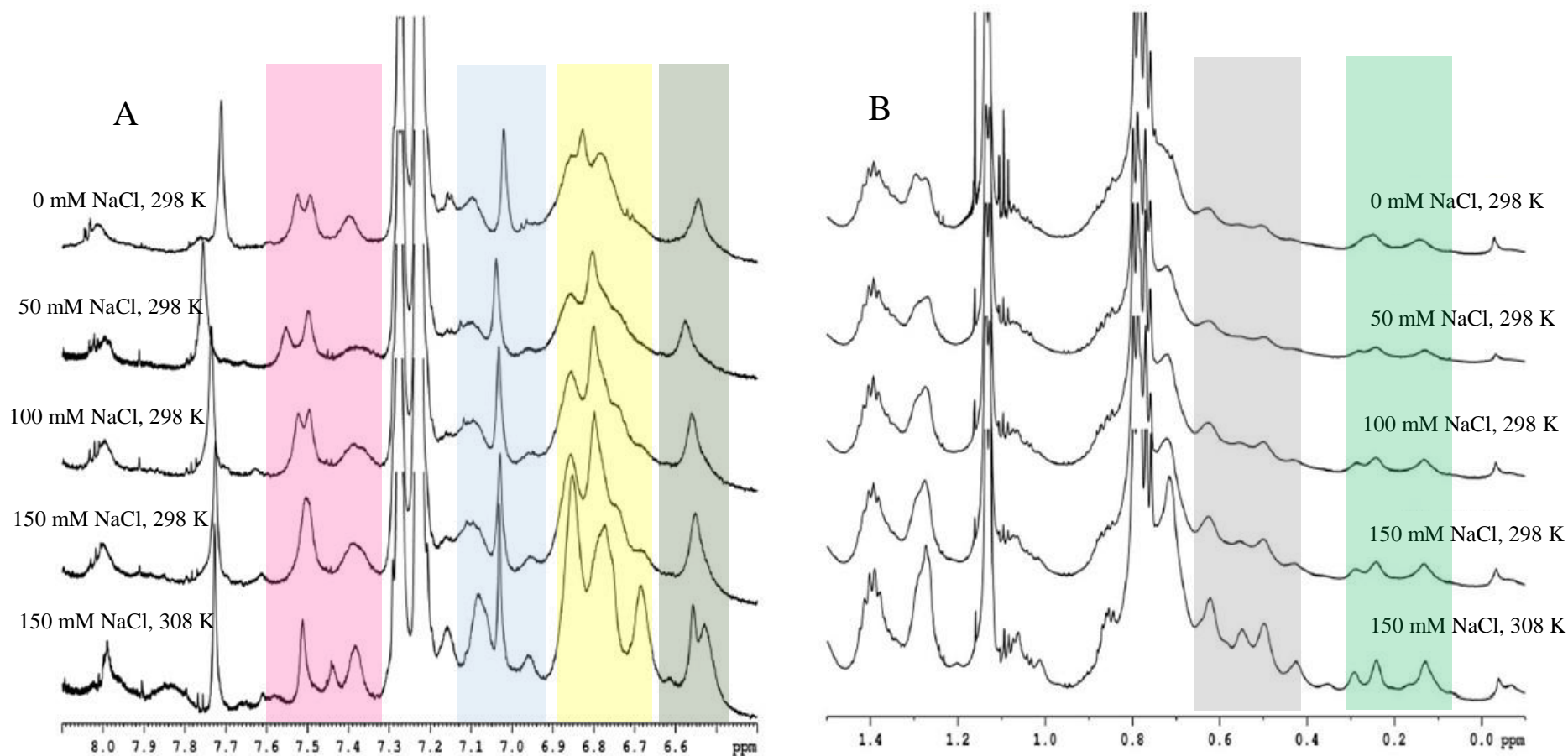


**Figure 6.06 Stacked plot of 1D  $^1\text{H}$  NMR spectra for SynZur at different salt concentration.**

The effect of NaCl on the SynZur spectra in the fingerprint region (A), and in the aliphatic region (B). Protein samples of SynZur (600  $\mu\text{M}$ , 20 mM ammonium bicarbonate, 10%  $\text{D}_2\text{O}$ , pH  $\sim 7.4$ ) were subjected to various concentration of NaCl: 0 mM, 50 mM, 100 mM and 150 mM respectively. 1D  $^1\text{H}$  spectra were recorded at 700.24 MHz on a Bruker Avance 700 Spectrometer equipped with a cryoprobe, using two different temperatures, 298K and 308K. The coloured boxes indicate the improvements in resolution.

In 2007, it was pointed out that the concentration of Fur family proteins plays an important role in the oligomerization state (D'Autréaux et al. 2007). For instance, at a low concentration, 0.2 mM, the Fur protein from *E. coli* was present as a dimer while at a higher concentration, 1.5 mM, Fur was present in higher-order oligomeric states as a hexamer, tetramer and dimer (D'Autréaux et al. 2007). Larger oligomers were also observed by SDS-PAGE analysis and MALDI-TOF mass spectrometry for the Fur protein from *Anabaena* PCC 7119, where even at only 125  $\mu$ M, Fur was present in several oligomerization states including monomeric, dimeric, trimeric and tetrameric forms (Hernandez *et al.*, 2002). Most recently higher-order oligomer states, tetramer forms, have also been observed for (PaFur) *P. aeruginosa*, (LpFur) *L. pneumophila* and (FtFur) *F. tularensis* using size exclusion chromatography (Pérard *et al.*, 2016). The higher-order oligomeric states can be formed due to inter-subunit salt bridges; thus, the tendency to form the higher oligomers can be reduced by using high monocation concentrations (D'Autréaux *et al.*, 2007; Pérard *et al.*, 2016). The oligomerisation state of the Fur protein from *E. coli* was resolved from hexameric and tetrameric states to the dimeric state at high ionic forces (D'Autréaux et al. 2007). Considering that  $\text{Na}^+$  is a monocation presenting usually at high concentrations in bacteria (Zinchenko & Yoshikawa, 2005), and in even larger amounts in bacteria living in the open ocean such as *Synechococcus*, the addition of salt may also reduce the tendency of SynZur to form higher oligomeric states. In principle, these lower oligomeric states, the monomeric and dimeric forms, should have narrower lines in the NMR spectra than any higher oligomeric (trimeric and tetrameric) forms.

Whilst it was clear that 150 mM NaCl at 308K temperature gave the best NMR spectrum, it was still evident that the NMR lines were too broad. Since it wasn't clear at this stage whether broadness was due to dynamic events on an intermediate timescale or due to the presence of higher oligomers, therefore, 2-Dimensional NMR technique that can give NH signals for very large assemblies, will be attempted.

## 6.4 Two Dimensional NMR Spectroscopy

However due to the size of the SynZur, 140 amino acids, the 1D- $^1\text{H}$  spectrum is far too complex for interpretation as most of the signals are heavily overlapping, and therefore applying an additional spectral dimensions will be useful to obtain extra information. Normally, 2D NMR spectroscopy forms provide correlations between proton (or other NMR-active nuclei) signals based on some interaction between them, most frequently J-coupling or dipolar coupling.

The most common type of 2D experiments is HSQC, Heteronuclear Single Quantum Coherence, which permits to obtain a 2D heteronuclear chemical shift correlation map between directly-bonded  $^1\text{H}$  and X-heteronuclei (commonly,  $^{13}\text{C}$  and  $^{15}\text{N}$ ). HSQC works by transferring magnetization from the *I* nucleus, usually the proton, to the *S* nucleus, usually the heteroatom, because the proton has a greater equilibrium magnetization. Then the magnetization evolves and transfers back to the *I* nucleus for observation.

The 2D  $^1\text{H}/^{15}\text{N}$  correlation, where each amino acid residue is normally represented by one signal from its amide group, is probably the most often used type of spectra in protein NMR (Golovanov et al. 2007). Homo-oligomeric proteins often have identical NMR spectra for their monomers, and thus the number of amino acid residues per monomer determines the total number of resonances (Fernández & Wider, 2003). Normally  $^1\text{H}-^{15}\text{N}$  HSQC spectrum shows coupling between hydrogen and nitrogen atoms in amide functional groups found in the protein backbone and side-chains (Figure 6.07).



$$\tau_c \propto 1/T_2$$

Equation 6.02

The larger the molecular mass, the larger the correlation time, the faster the transverse relaxation rates, and the broader the lines will be in the spectrum (Fernández & Wider, 2003) (Figure 6.08). In addition, for large molecules, relaxation is active during data acquisition resulting in a much weaker and more rapidly decaying NMR signal for large molecules (Figure 6.08).

In an attempt to solve these problems, advances have been achieved with the TROSY NMR technique (transverse relaxation-optimized spectroscopy) (Wider & Wüthrich, 1999; Zhu *et al.*, 2000). TROSY NMR, in combination with higher magnetic fields and cryogenic probes, has helped to generate spectra for large proteins with better resolution and sensitivity (Xu & Matthews, 2013).

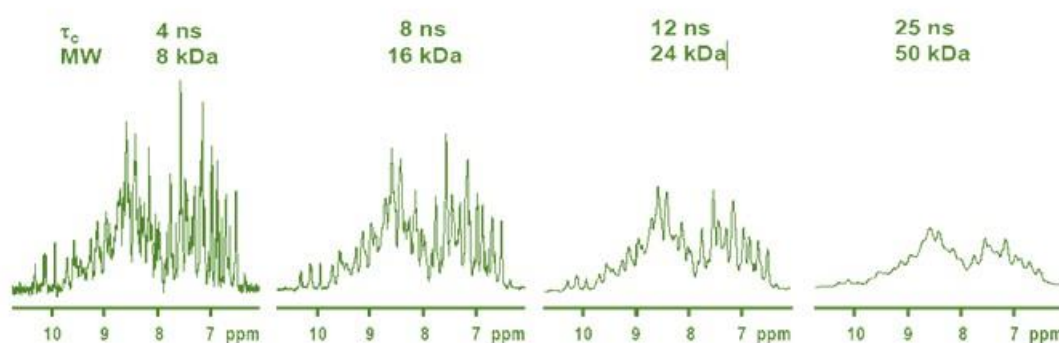


**Figure 6.08 Impact of protein size and rotational correlation on linewidths in 1D  $^1\text{H}$  NMR spectra.**

Taken from ([http://cwp.embo.org/wpc09-07/sattler\\_embo2009\\_large\\_proteins.pdf](http://cwp.embo.org/wpc09-07/sattler_embo2009_large_proteins.pdf)).

#### 6.4.1.1 Technical Background for TROSY NMR

Transverse-relaxation optimized spectroscopy (TROSY), as its name suggests, seeks to optimize and minimize the relaxation of transverse signals (Xu & Matthews, 2013). Typically, the transverse  $T_2$  relaxation for large proteins at high magnetic field is often dominated by

chemical shift anisotropy (CSA) of  $^1\text{H}$  and  $^{15}\text{N}$ , and dipolar coupling between  $^{15}\text{N}$  and  $^1\text{H}$ . Usually, both the  $^{15}\text{N}$  and the  $^1\text{H}$  nuclei have two possible spin states in a magnetic field, with one pointing in the same direction as the magnetic field and the other pointing in the opposite direction. The direction of dipole–dipole interaction depends on the spin states of both nuclei involved, while the direction of CSA depends only on the spin state of the nucleus itself (Wider & Wüthrich, 1999). Therefore, in non-decoupled 2D heteronuclear  $[^1\text{H},^{15}\text{N}]$  HSQC experiments, the NMR signal of each nucleus is split into two components by the scalar spin-spin coupling, allowing to observe four peaks in the spectrum (Figure 6.09A).

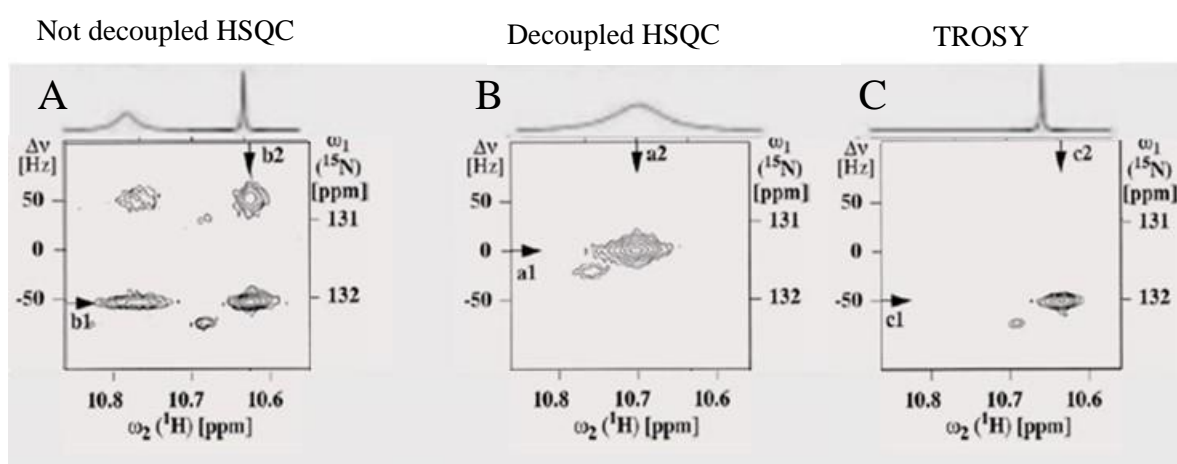


**Figure 6.09** Contour plots of  $[^1\text{H},^{15}\text{N}]$  correlation spectra for an example  $^1\text{H}$ ,  $^{15}\text{N}$  spin system.

(A) Conventional  $[^1\text{H},^{15}\text{N}]$  HSQC spectrum recorded without decoupling. (B) Conventional  $[^1\text{H},^{15}\text{N}]$  HSQC spectrum recorded with decoupling. (C)  $[^1\text{H},^{15}\text{N}]$  HSQC-TROSY spectrum. When no decoupling is applied in a  $[^1\text{H},^{15}\text{N}]$  HSQC for a large system at high field, the different relaxation properties can be seen on the multiplets, (A). The other three components experience different relaxation rates due to the dipole–dipole and chemical shift anisotropy mechanism effects. When decoupling is applied in a  $[^1\text{H},^{15}\text{N}]$  HSQC, the four components are collapsed into one due to the decoupling on the  $^{15}\text{N}$  nuclei during acquisition and decoupling of  $^1\text{H}$  during  $^{15}\text{N}$  evolution, (B). The  $[^1\text{H},^{15}\text{N}]$  HSQC-TROSY experiment selects only the narrowest component, where the CSA and dipole–dipole relaxation mechanisms cancel out, (C). Adapted from (Pervushin *et al.*, 1997).

With the advent of modern 2D NMR,  $[^1\text{H},^{15}\text{N}]$  HSQC with “decoupling”, the splitting of the resonance peaks is removed during the pulse sequence and the result is a single peak that is the average chemical shift of the four in the multiplet (Figure 6.09B) with the expectation of

obtaining a simplified spectrum with improved sensitivity. However, for the large molecules, the signal from decoupling [ $^1\text{H}$ ,  $^{15}\text{N}$ ] HSQC may be very much attenuated because of the contribution from the more rapidly relaxing resonance line (Fernández & Wider, 2003).

In large proteins and at higher magnetic field, the difference in relaxation rates can be seen from the different widths of the four components of an amide peak (Figure 6.09A). Using the TROSY technique, the multiplet structure is not decoupled and only the narrowest, most slowly relaxing line of each multiplet is retained (Xu & Matthews, 2013) (Figure 6.09C). By exploiting the constructive interference between dipole–dipole coupling and CSA relaxation, TROSY actually uses CSA relaxation at higher fields to cancel field-independent dipolar relaxation (Wider & Wüthrich, 1999; Fernández & Wider, 2003; Xu & Matthews, 2013). In [ $^1\text{H}$ ,  $^{15}\text{N}$ ] HSQC-TROSY experiments, there is no  $^1\text{H}$  decoupling during  $^{15}\text{N}$  evolution and no  $^{15}\text{N}$  decoupling during the acquisition.

It is worth noting that in special cases, sensitivity may be lost as a result of using only one component out of four multiplet components (Wider and Wüthrich 1999).

### 6.4.2 Impact of TROSY on [ $^1\text{H}$ , $^{15}\text{N}$ ] HSQC Spectra for SynZur

In the first instance to obtain more information, we have created and tested two types of  $^1\text{H}$ - $^{15}\text{N}$  correlation experiments, one based on the standard HSQC experiment with decoupling, and another based on the TROSY principle (Figure 6.10).

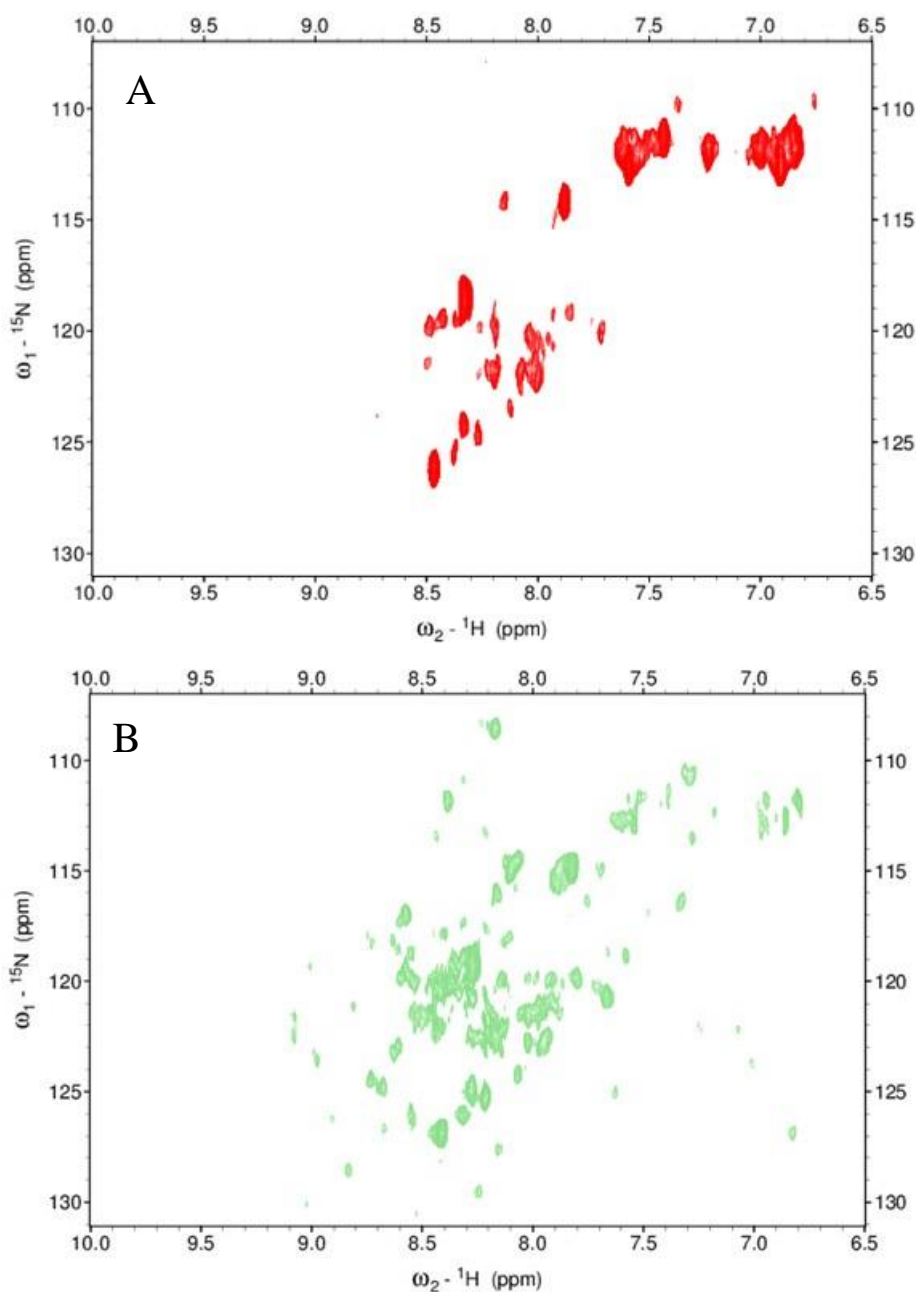


**Figure 6.10 Contour plots of [ $^1\text{H}$ , $^{15}\text{N}$ ] correlation spectra for SynZur.**

(A) Conventional [ $^1\text{H}$ , $^{15}\text{N}$ ] HSQC spectrum. (B) [ $^1\text{H}$ , $^{15}\text{N}$ ] HSQC-TROSY spectrum. Both spectra are plotted at the same levels with contour spacing being 1.2 and measured at a proton resonance frequency of 700.24 MHz using a 450  $\mu\text{M}$  sample of  $^{15}\text{N}$ -labelled SynZur protein in 20 mM ammonium bicarbonate at 308 K, 10%  $\text{D}_2\text{O}$ , 150 mM NaCl and pH~6.2 using 32 scans per transient.

Clearly, it is advantageous to use the TROSY technique on the SynZur protein rather than the conventional HSQC (Figure 6.10). The HSQC spectrum of SynZur displays only a very small number of peaks, less than 30 peaks, and poor signal-to-noise ratio (Figure 6.10A), with the strongest signals observed for side-chain amide protons. In contrast, with a TROSY experiment,

significant improvements in sensitivity and dispersion were achieved, as indicated by a dramatically increased number of backbone NH peaks – including a number of peaks above 8.5 ppm. This may suggest that the broadness of lines as observed in the 1D  $^1\text{H}$  spectra (section 6.2) was due to some extent to the molecular size of the assemblies in solution under the NMR conditions used. The line broadening, which is a manifestation of increased transverse relaxation rates that also cause deterioration of the sensitivity in the  $[\text{}^1\text{H}, \text{}^{15}\text{N}]$  HSQC spectrum, has been largely suppressed in the  $[\text{}^1\text{H}, \text{}^{15}\text{N}]$  HSQC-TROSY spectrum (Figure 6.10).

The  $[\text{}^1\text{H}, \text{}^{15}\text{N}]$  HSQC-TROSY spectrum of SynZur has moderately well-dispersed signals indicating that the uniformly labelled protein was largely well-folded (Figure 6.10B). Although the resolution in the  $[\text{}^1\text{H}, \text{}^{15}\text{N}]$  HSQC-TROSY spectrum is improved, the intensity of resonances is very variable from peak to peak, suggesting that there is differential mobility within the protein. A similar phenomenon was also observed for Fur from *E. coli* (Saito *et al.*, 1991).

In spite of progress in this part of the study, our conditions still require further optimisation. At this point, it was not clear whether it was even possible to find suitable conditions with the major problem appearing to be the formation of higher oligomers.

## 6.5 3D Structural Prediction for SynZur

In parallel to the NMR studies, crystallization trials were investigated resulting in the production of some promising conditions (see Appendix F, Figure F.01). However, within the timeframe of this project, full optimization of crystal conditions to obtain a sufficient size for structural determination was not possible. Hence, 3D homology modelling was performed. Structural prediction on the basis of known 3D structures (templates) of a homologous protein is still the only plausible method to obtain structural information based on sequential information. To enable the inspection of SynZur for the three dimensional prediction, the

*synw\_2401* amino acid sequence was provided in FASTA format to the I-TASSER server, an internet service system (Zhang, 2008; Roy *et al.*, 2010).

Prediction of the 3D structure of the SynZur protein gave two prediction models, SynWH\_Zur1 and SynWH\_Zur2 (Figure 6.11). However, both structures had five  $\alpha$ -helix and five  $\beta$ -sheets. Secondary structure analysis of SynZur revealed the presence of 45.5 %  $\alpha$ -helices, 21.7 %  $\beta$ -sheets and 32.8% random coils.

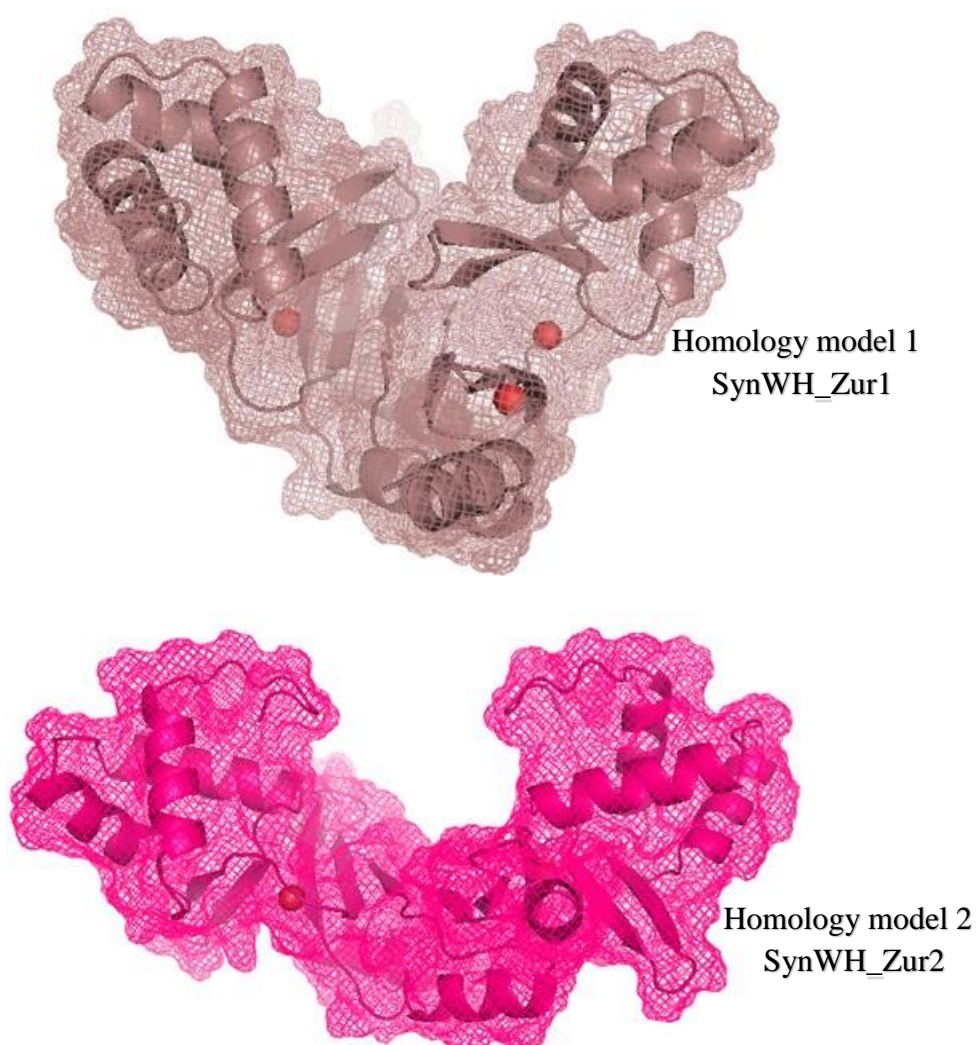


**Figure 6.11 Two 3D structural predictions for the SynZur protein.**

Models were created in I-TASSER service using the three templates Zur from *E. coli* ((Gilston *et al.*, 2014); pdb 4MTE), Zur from *S. coelicolor* ((Shin *et al.*, 2011); pdb 3MWM), and Zur from *M. tuberculosis* ((Lucarelli *et al.*, 2007); pdb 2O03). Figures were prepared using PyMOL.

Three criteria (C-Score<sup>22</sup>, TM score<sup>23</sup> and RMSD values) were employed to compare the quality of predicted models to choose the most suitable between the SynWH\_Zur1 and SynWH\_Zur2 homology models. SynWH\_Zur1 was predicted to have a C-Score of 0.04, which was comparatively better than the SynWH\_Zur2 with a C-Score of -4.54. The estimated computational TM score ( $0.72 \pm 0.11$ ) and RMSD ( $4.4 \pm 2.9\text{\AA}$ ) of SynWH\_Zur1 was also found to be better than the values obtained for the SynWH\_Zur2 model. SynWH\_Zur1 expeditiously signified all three criteria as the best quality model.

### 6.5.1 Structure Validation

After three-fold refining of the SynWH\_Zur1 using i3Drefine software (Bhattacharya & Cheng, 2013), the final refined model for SynWH\_Zur1 was verified by the Structural Analysis and Verification Server (SAVES) to evaluate its stereo-chemical quality (<http://services.mbi.ucla.edu/SAVES/>). After optimization, most residues fall within the allowed regions of the Ramachandran plot (Laskowski *et al.*, 1993; Kleywegt & Jones, 1996) as defined by the PROCHECK<sup>24</sup> program. PROCHECK showed that 92.2% of the residues were present in the most favoured regions (A, B, L); 6.9% of the residues were in additional allowed regions (a, b, l, p); and 0.9% of the residues were in generously allowed regions (~a, ~b, ~l, ~p); no residues were present in disallowed regions (see Appendix F, Figure F.02A). ERRAT<sup>25</sup> analysis showed the overall structural quality of the predicted structure to be 96.83,

---

<sup>22</sup>C-score is a confidence score for estimating the quality of predicted models by I-TASSER. This score calculated based on the threading template alignments and the convergence parameters of the structure assembly simulations.

<sup>23</sup>TM-score is a proposed scale for measuring the structural similarity between two structures.

<sup>24</sup>PROCHECK: Checks the stereo-chemical quality of a protein structure by analysing residue-by-residue geometry and overall structural geometry calculated by analysis of the phi ( $\Phi$ ) and psi ( $\psi$ ) torsion angles as determined by Ramachandran plot statistics.

<sup>25</sup>ERRAT: Analyses the statistics of non-bonded interactions between different atom types and plots the value of the error function *versus* the position of a 9-residue sliding window calculated by a comparison with statistics from highly refined structures.

which is very good both experimentally and computationally (see Appendix F, Figure F.02B). VERIFY\_3D<sup>26</sup> analysis showed that 85.10% of residues gave an average 3D-1D score  $\geq 0.2$ , showing good primary sequence to tertiary structure compatibility (see Appendix F, Figure F.02C).

In order to assess the reliability of the modelled structures, the root mean square deviation (RMSD) for the two homology models and other known available structures for Zur proteins were calculated. Although a range of structural data are available for the Fur family, only the structures for three Zurs are known to date i.e., MtZur from *Mycobacterium tuberculosis* (Lucarelli *et al.*, 2007), ScZur from *Streptomyces coelicolor* (Shin *et al.*, 2011) and EcZur from *E. coli* (Gilston *et al.*, 2014). To assess how close the topology of the initial structure for SynWH\_Zur1 was to MTZur (33.3%), ScZur (28.6%) and EcZur (26.4%), the backbone of SynWH\_Zur1 was superimposed with three known Zurs (Figure 6.12, and see Appendix F, Table F.01).

The superposition was performed using the Superpose program (Maiti *et al.*, 2004) and Pymol software, in which a low RMSD value corresponds to similarity in the structure of the two proteins. Use of the structural alignment program SuperPose (Maiti *et al.*, 2004) indicates that if the superposition value is  $< 1.6 \text{ \AA}$ , RMSD for the  $\alpha$ -carbons, this provides an indication that there is a strong agreement between the two selected structures, while if the superposition value is RMSD  $> 3.0 \text{ \AA}$ , this will indicate poorer agreement. RMSD values between SynWH\_Zur1 and ScZur gave the smallest values  $\sim 1.1 \text{ \AA}$  and  $2.97 \text{ \AA}$  in SuperPose and Pymol, respectively. At the same time SynWH\_Zur1 and EcZur gave  $\sim 2.1 \text{ \AA}$  and  $3.17 \text{ \AA}$  in SuperPose and Pymol,

---

<sup>26</sup> VERIFY\_3D: Determines the compatibility of an atomic model (3D) with its own amino acid sequence (1D) by assigning a structural class based on its location and environment (alpha, beta, loop, polar, nonpolar etc) and comparing the results to good structures.

respectively, while SynWH\_Zur1 and MtZur were  $\sim 6.2 \text{ \AA}$  and  $5.55 \text{ \AA}$ . Remarkably, SynWH\_Zur2 and MtZur are  $\sim 1.93 \text{ \AA}$  in Pymol (see Appendix F, Table F.01).

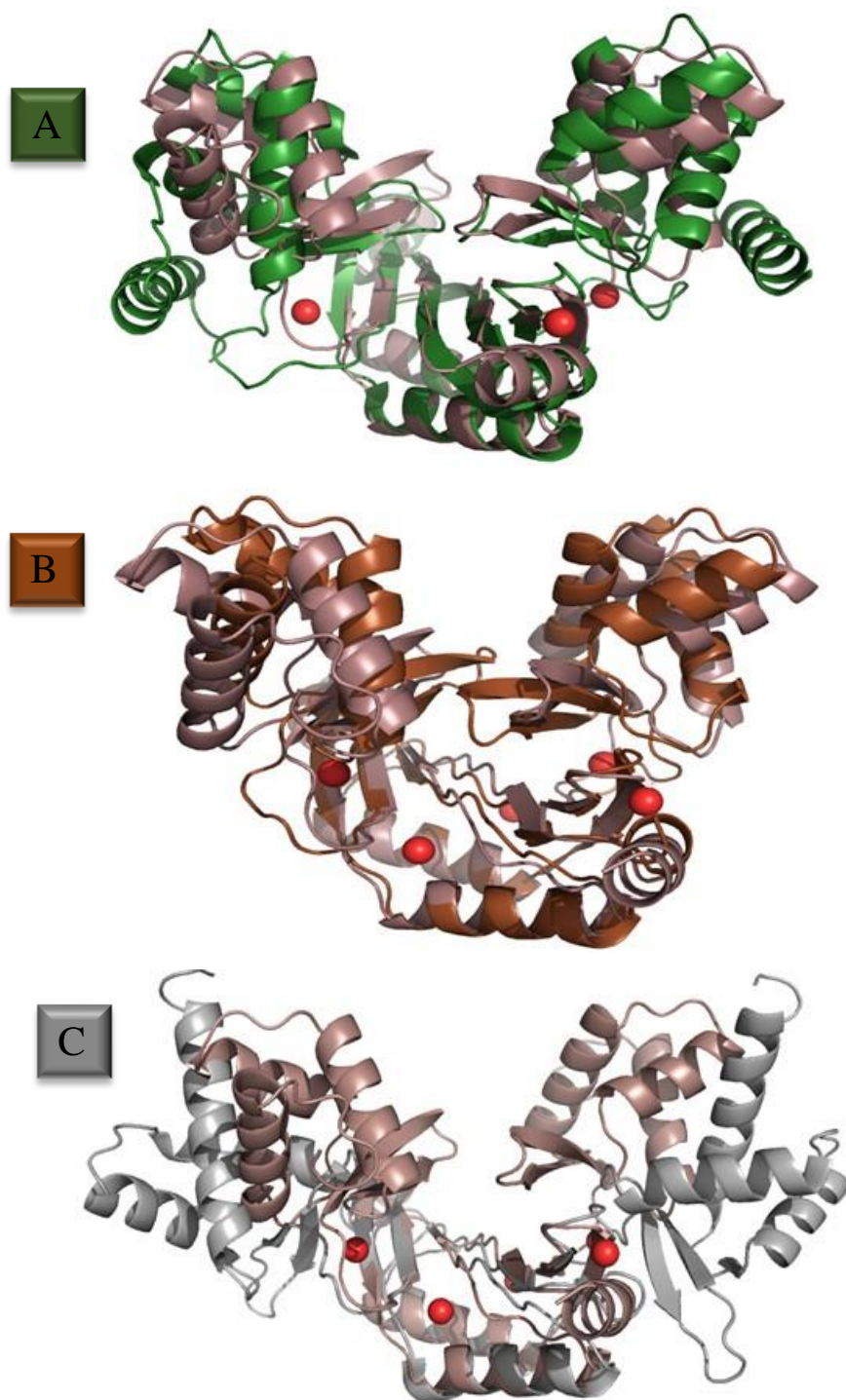


**Figure 6.12 Superimposition of SynWH\_Zur1 with three known Zur proteins.**

Ribbons represent the superposition of the C-terminal dimerization domain for homology model SynWH\_Zur1 from *Synechococcus* sp. WH8102 (salmon) with (A) EcZur from *E. coli* ((Gilston *et al.*, 2014); pdb 4MTE, green), (B) ScZur from *S. coelicolor* ((Shin *et al.*, 2011); pdb 3MWM, brown) and (C) MtZur from *M. tuberculosis* ((Lucarelli *et al.*, 2007), pdb 2O03, grey).

These comparisons reveal that SynWH\_Zur1 aligns with a reasonable degree of similarity to EcZur and ScZur. Moreover, it was reported that ScZur from *Streptomyces coelicolor* (Shin *et al.*, 2011) and EcZur from *E. coli* (Gilston *et al.*, 2014) are found in the closed conformation, while MtZur from *Mycobacterium tuberculosis* (Lucarelli *et al.*, 2007) is thought to correspond to the open conformation. We have compared SynWH\_Zur1 to the MtZur open conformation, which shows a good agreement across the C-terminal dimerization domains, but differs significantly in the relative positioning of the N-terminal DNA binding domains (Figure 6.12C). The “open” conformation is postulated to have a low affinity for DNA, as the N-terminal DNA-binding domains are too far apart to interact with a DNA molecule (Figure 6.12C). Structures thought to be determined in the closed conformation, ScZur (Shin *et al.*, 2011) and EcZur (Gilston *et al.*, 2014), proposed to both correspond to the fully metal-loaded form of the repressor and to have a high affinity for DNA, showed good agreement across the C-terminal dimerization domains and the N-terminal DNA binding domains (Figure 6.12A and B).

The overall structure of SynWH\_Zur1 with low RMSD values corresponds to protein structures in the “closed” state which may be capable of binding to their respective operator DNA.

SynZur is a homodimer with a modular architecture similar to previously determined Fur-family members, especially ScZur (Shin *et al.*, 2011) and EcZur (Gilston *et al.*, 2014). The three dimensional model for SynWH\_Zur1 has a DNA-binding domain (residues 1–76) and a C-terminal dimerization domain (residues 77–134). The DNA binding domain is composed of three helices followed by a two-stranded antiparallel sheet ( $\beta$ 1 and  $\beta$ 2). This domain exhibits the typical winged helix motif with three helices bundles ( $\alpha$ 1,  $\alpha$ 2 and  $\alpha$ 3), where the helix  $\alpha$ 1 and  $\alpha$ 3 may be the putative DNA recognition region (residues 9–22 for  $\alpha$ 1 and 43–56 for  $\alpha$ 3). The dimerization domain comprises three antiparallel strands ( $\beta$ 3,  $\beta$ 4 and  $\beta$ 5) and two helices ( $\alpha$ 4 and  $\alpha$ 5) stabilized by one of the metal-binding sites. The DNA-binding domains of SynWH\_Zur1 and (EcZur, ScZur) share the same basic fold, with one important difference

when superimposed. EcZur contains an additional N-terminal helix (residues 4-20) that may be involved in DNA recognition (Figure 6.12A). Four cysteine residues (Cys-83 and Cys-86, Cys-124, Cys-126) cluster to form a high-affinity Zn(II) binding site (Cys<sub>4</sub>Zn) this is the structural site 1 (Figure 6.13). Another four residues (Asp-77, His-79, Cys-95, His-115) are candidate ligands for the sensory site 2 (Figure 6.13).

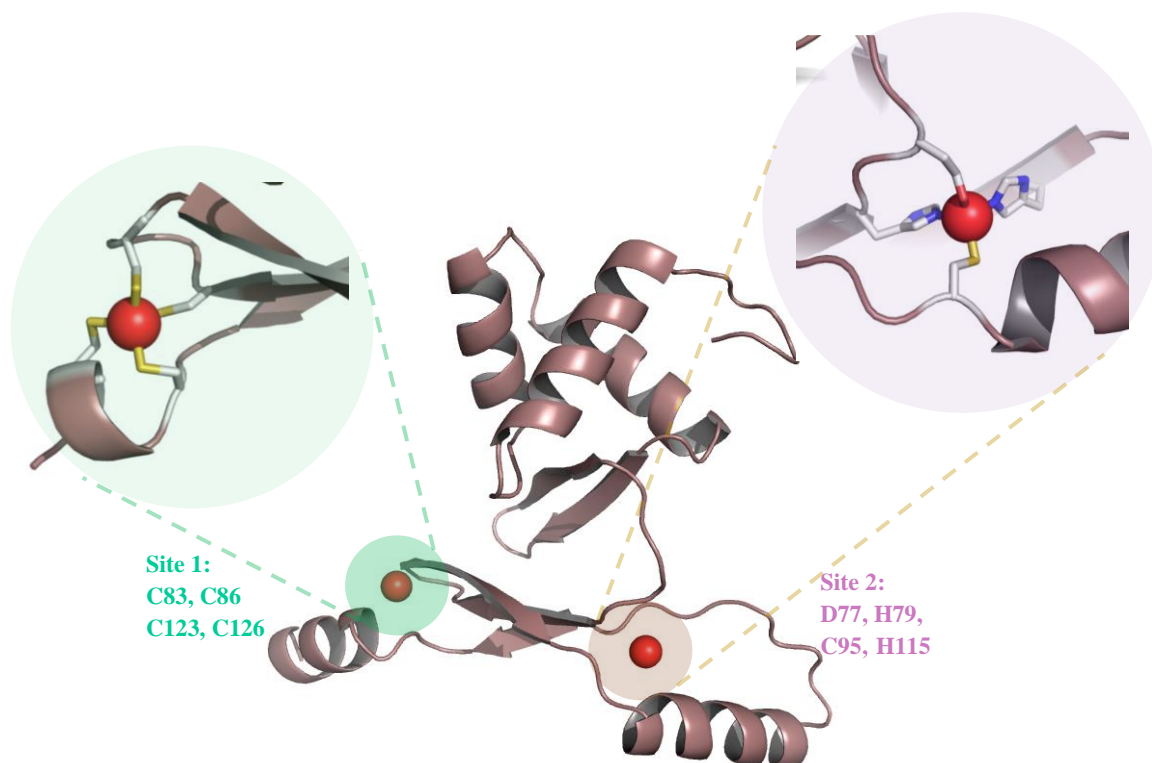


**Figure 6.13 Structural features for SynZur monomer form.**

Homology model for the SynZur protein, encoded by the *synw\_2401* gene, from *Synechococcus* sp. WH8102; only one monomer is shown, with putative ligands from the structural site 1 (Green) and the sensory site 2 (Purple) highlighted. SynZur is shown in salmon and zinc ions as red spheres.

The electrostatic charge distribution over the SynZur monomer is shown in Figure 6.14, and reveals a predominantly positive charge for the helical regions predicted to be involved in DNA recognition, particularly helix  $\alpha$ 1 and  $\alpha$ 3.

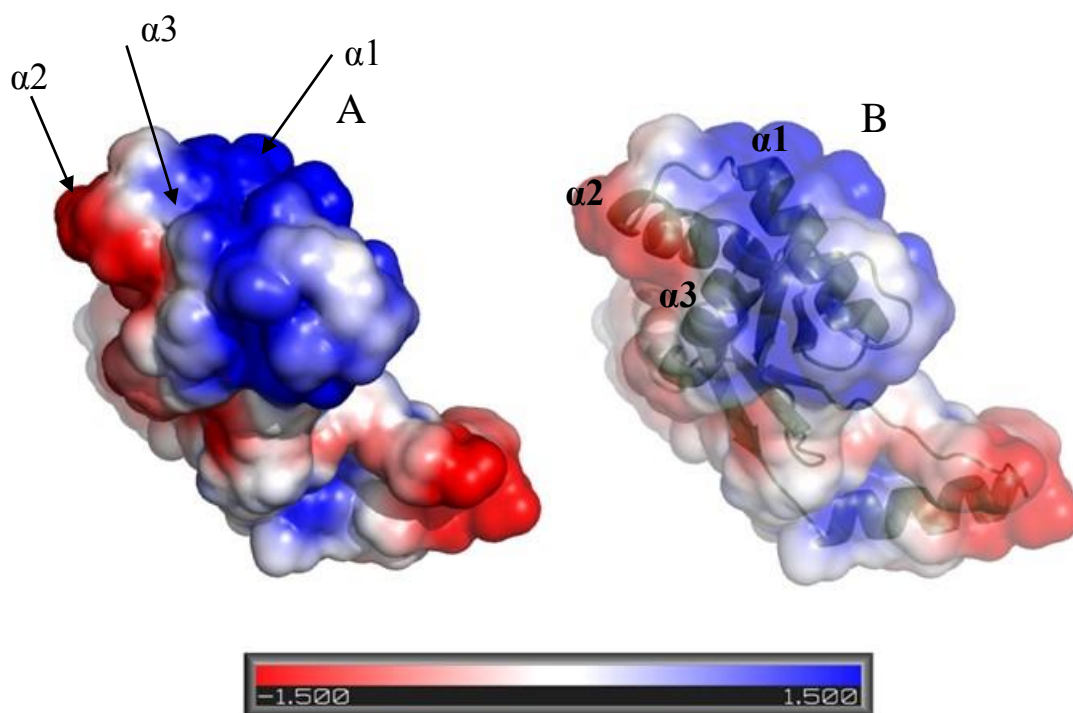


**Figure 6.14 Electrostatic potential map of the predicted SynZur protein.**

The electrostatic surfaces for SynZur monomer calculated using Adaptive Poisson-Boltzmann Solver (APBS) (Baker *et al.*, 2001) generated using the PyMOL software (DeLano, 2007). The electrostatic surface of the SynZur monomer (A) and with 40% transparency for the surface (B). A colour gradient from blue to white to red is used to colour the molecular surface where red, white and blue are for negative, neutral, and positive potentials, respectively. The arrow on the blue surface indicate the DNA binding domain.

## 6.6 Summary and Conclusion

Optimisation of conditions for protein NMR studies revealed that 150 mM NaCl at a temperature of 308K gave the best conditions for SynZur. In addition, a significant improvement in sensitivity and dispersion was achieved using the TROSY technique on the SynZur protein rather than the conventional HSQC.

However, because a good homology model can be an important step towards determining functional annotation for a protein, a 3D homology model for SynZur was created. Moreover, it was found that SynZur is a homodimer with a modular architecture similar to that determined for other Fur-family members.

# Chapter 7

## Monitoring Protein Conformational Changes and Dynamic Studies

---

### 7.1 Introduction

Research on Zur sensor proteins has burgeoned in the past decade and significant progress has been made (Lucarelli *et al.*, 2007; Shin *et al.*, 2011; Gilston *et al.*, 2014). Zur, as a member of the Fur family, is a homodimeric protein that has two or three metal sites per monomer. In all published structures, there is agreement that site 2 plays a critical role as the major sensory site, while site 1 is a structural site (see Section 1.7).

One of the major discoveries about Fur family proteins concerns the fact that the metal in the sensory site is labile and can easily be released and re-added (Althaus *et al.*, 1999; D'Autréaux *et al.*, 2007; Shin *et al.*, 2011). To check whether the Zur protein from *Synechococcus* sp. WH8102 also behaves in a similar manner, a series of dynamic studies on the SynZur protein using the metal chelator EDTA (Ethylenediamine-N,N,N',N'-tetraacetic acid) were initiated, and will be discussed in this chapter. Also the effect of pH on zinc release from SynZur protein will be discussed in more detail.

## 7.2 Observations of Zinc Release from SynZur

To achieve a better understanding for the relationship between the zinc binding chemistry of the SynZur protein and its biological functions in *Synechococcus* sp. WH8102 during zinc depletion/repletion conditions, it was necessary to characterise some of its zinc binding properties. However, the first step towards this endeavour was to study the effect of zinc depletion on SynZur by investigating the competition reaction with EDTA. The second step was to detect the effect of zinc repletion by investigating the effect of the zinc re-adding procedure. Investigation of the reactivity of SynZur protein with hydrogen ions was the last step in this endeavour.

To obtain more information about these reactions, different approaches including UV-Visible spectroscopy, circular dichroism spectroscopy, mass spectrometry, and nuclear magnetic resonance spectroscopy have been used in this part of the study.

### 7.2.1 Competition Reactions with EDTA

From a practical point of view, metal ions in a metalloprotein can be removed by chemical manipulation. If the metalloprotein is incubated with a suitable concentration of competitive chemical sequentially, the metal can be removed from the protein (Bertini *et al.*, 2007), providing its accessibility to the ligand and its affinity for the metal.

Ethylenediamine-N,N,N',N'-tetraacetic acid, EDTA, has been used as a chelator for a wide range of metal ions including zinc, cadmium, copper and iron (Li *et al.*, 1980; Ebright *et al.*, 1992). Furthermore, it is a multidentate ligand containing amine and carboxyl groups such as one finds in biological systems (Li *et al.*, 1980). It has therefore often been used to mimick the transfer of metal ions from one protein to another – a reaction that is thought to be particularly important for proteins involved in metal ion homeostasis.

### 7.2.1.1 Competition Reaction using UV-Visible Spectroscopy

Due to the poor amenability of the  $d^{10}$  zinc ion to most of the common spectroscopies (Leszczyszyn & Blindauer, 2010), it is not trivial to study the kinetics and mechanistic details of zinc release from metalloproteins. In the case of zinc bound to cysteines, the Zn–S charge transfer band at 220 nm can, in principle, be used to observe the changes in protein-bound zinc. However, caution should be applied in the data interpretation, as the backbone amide bonds also strongly absorb in this region with the maximum of the absorption at 215 nm (Leszczyszyn & Blindauer, 2010).

To probe the propensity of EDTA to strip metal ions from SynZur at pH~7.8, a fixed concentration of zinc-loaded SynZur (~2.1 zinc ions per monomer) protein was incubated with different concentrations of chelator including two, four and ten equivalents of EDTA (with respect to protein monomer concentration), and the reaction was monitored by the absorbance at 220 nm for twenty four hours (Figure 7.01).

Figure 7.01 clearly indicates that the incubation of SynZur with different concentrations of EDTA leads to a decrease in absorbance suggesting that changes to the Zn-S charge-transfer band have occurred. Under our conditions, it was also observed that removing zinc ions from SynZur was dependent on the EDTA concentration. Incubating the SynZur protein with 10 equivalents of EDTA led to faster completion (ca. 7 hours) of the reaction than the reactions with 4 (ca. 15 hours) or 2 (ca. 24 hours) equivalents.

Although direct comparison of the curves is not possible due to the fact that EDTA also absorbs at 220 nm (explaining the different absorbance after completion of the reactions), it is clear that a reaction occurs, which is likely metal release from SynZur. The dependence on EDTA concentration indicates that this reaction is bimolecular, and requires direct interaction between the protein and EDTA.

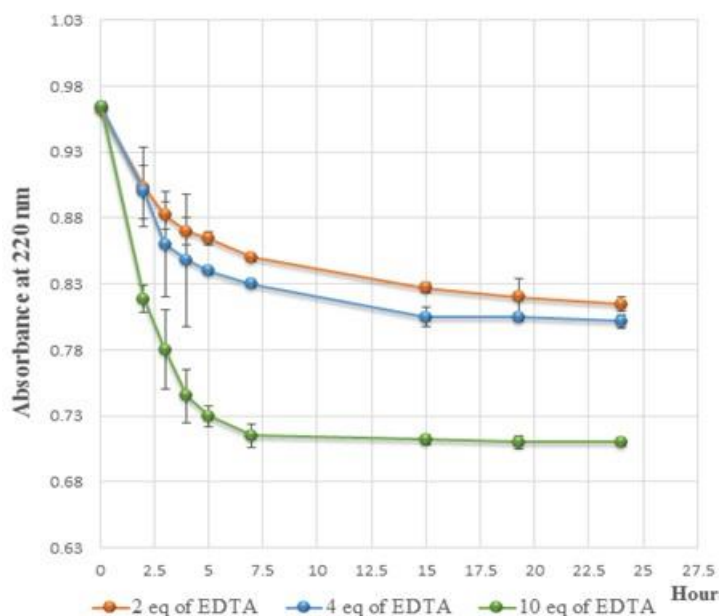


**Figure 7.01 Monitoring the competition reaction of SynZur with EDTA using UV-Visible spectroscopy.**

Comparison of time courses for the incubation of zinc-loaded SynZur protein with 2, 4 and 10 equivalents of EDTA (with respect to protein concentration). Protein samples of SynZur (12.4  $\mu\text{M}$ , 1 mM Tris-Cl buffer, pH~7.8) were incubated with 24.8  $\mu\text{M}$ , 29.6  $\mu\text{M}$  and 124  $\mu\text{M}$  EDTA. The error bars indicate standard error of the mean between three experimental replicates.

Despite the benefits of using UV-Visible spectroscopy (low sample requirements, cheap instrumentation), the information that can be gained is limited and several intriguing questions arise. For example, can EDTA remove the zinc ions from both the structural and the sensory site in SynZur? If so - from which site is the metal released first? What is the effect of metal release on the secondary, tertiary, and quaternary structure for SynZur? To answer all these questions other techniques were applied.

### 7.2.1.2 Competition Reaction using CD Spectroscopy

To gain further insights into the conformational changes of the secondary structure during the competition reaction with EDTA, CD spectroscopy was employed.

Similar to UV-Visible spectroscopy experiments, three different concentrations of EDTA (2, 4 and 10 equivalents (with respect to protein concentration), respectively) were incubated with SynZur and the time course was recorded for 24 hours (Figure 7.02).

The far-UV CD spectra of SynZur showed strong negative bands at 208 nm and 222 nm, thus indicating that the  $\alpha$ -helix and  $\beta$ -strands conformations provide a relevant contribution to the overall secondary structure of this protein (Figure 7.02). After incubating SynZur with different concentrations of EDTA, small changes in the CD spectra were noted. The intensity of the negative maxima at 208 nm was increased while the intensity of the second negative maxima at 222 nm was slightly flattened. The overall picture from Figure 7.02 is that SynZur is still folded after releasing zinc ions from the protein. To obtain more information about the secondary structure fractions, several online programmes for interpretation of CD data were employed.

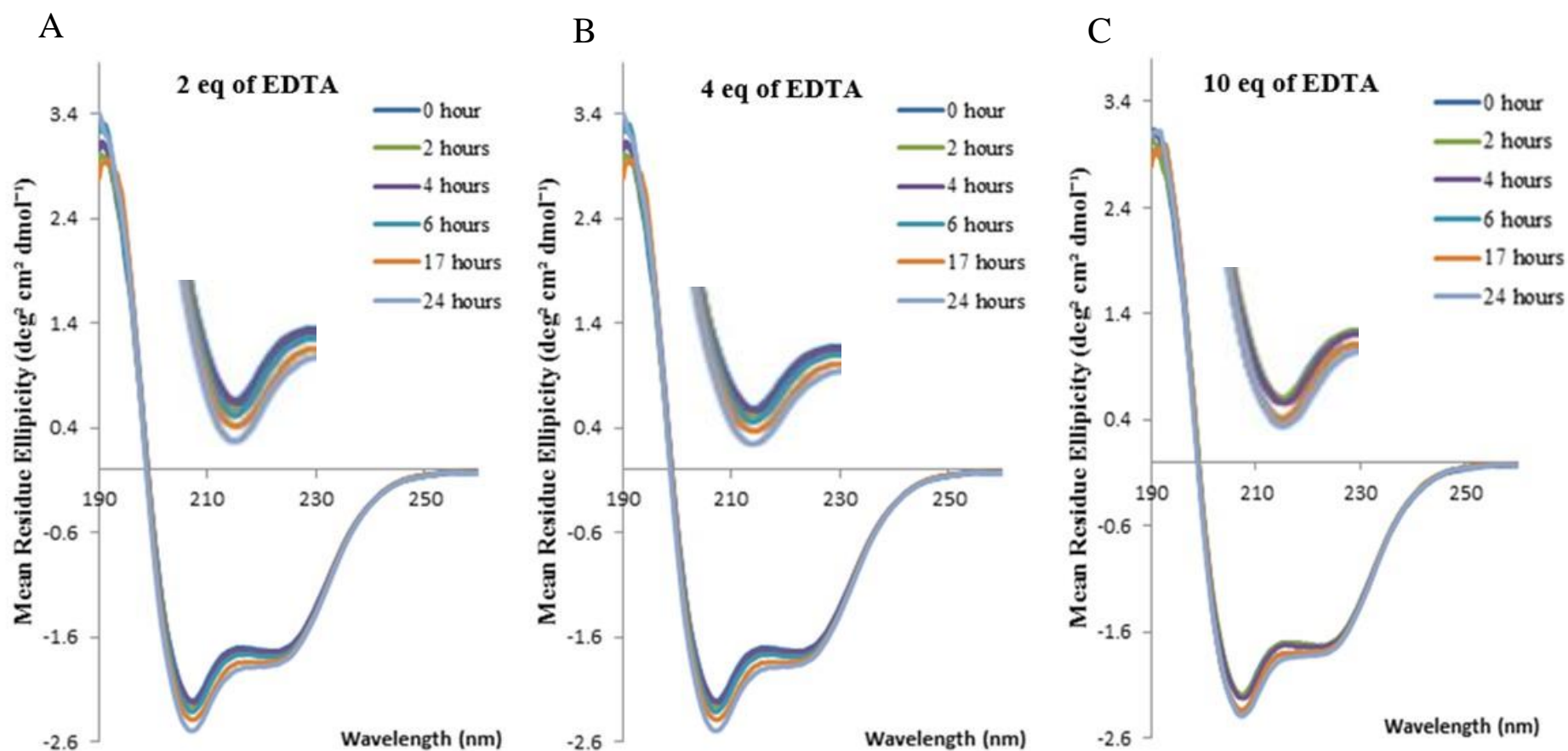


**Figure 7.02 Monitoring the competition reaction of SynZur with EDTA using CD spectroscopy.**

Far-UV circular dichroism (CD) spectra expressed in  $\Delta\epsilon$  units (mean residue ellipticity,  $\text{deg}^2 \text{cm}^2 \text{dmol}^{-1}$ ) for SynZur incubated with three different concentrations of EDTA including 2 equivalents (A), 4 equivalents (B) and 10 equivalents (C) (with respect for protein concentration) for 24 hours and the time course was recorded after 0, 2, 4, 6, 17 and 24 hours, respectively. Protein samples of SynZur ( $25.9 \mu\text{M}$ ,  $5 \text{mM}$  Tris-Cl buffer,  $\text{pH} \sim 7.8$ ) were incubated with  $51.8 \mu\text{M}$ ,  $103.6 \mu\text{M}$ , and  $259 \mu\text{M}$  EDTA. Spectra were recorded between 190-260 nm on a Jasco J-815 instrument with  $2 \text{nm}$  band width,  $100 \text{nm ml}^{-1}$  for scanning speed and 8 for accumulations. Inserts indicate the signal at 208 nm.

### 7.2.1.2.1 Prediction of Secondary Structure Fractions

Several methods that use CD data to predict the secondary structural content of proteins have been developed and improved over the last two decades (Sreerama *et al.*, 2000; Raussens *et al.*, 2003; Perez-Iratxeta & Andrade-Navarro, 2008). These methods use a variety of computational approaches from singular value decomposition to optimization algorithms, regression or neural networks (Sreerama *et al.*, 2000; Raussens *et al.*, 2003).

In this part of the study, three different programmes, SELCON and CONTIN software from the DICHROWEB Web server (Sreerama *et al.*, 2000), and RASUSSENS software from the RAUSSENS Web server (Raussens *et al.*, 2003) were used to estimate the secondary structure composition (i.e., fractions of  $\alpha$ -helices,  $\beta$ -strands and unordered contents) of SynZur before, during, and after incubation with EDTA (Figure 7.03).

Interestingly, the composition fractions for  $\alpha$ -helices,  $\beta$ -strands and unordered were different using the three different programmes (Figure 7.03). After the incubation with 10 equivalents of EDTA, only small changes in these compositions were observed in SELCON and RASUSSENS software and the changes were less than  $\sim 4\%$  for the secondary structure composition, these changes in the secondary structure are not significant. In contrast, no changings were observed in CONTIN software (Figure 7.03B).

From the data obtained above, it is likely that the slight changes in CD spectra following EDTA incubation (Figure 7.02) are due to metal releasing and changing in the oligomer distribution, monomer/dimer conversion, but not due to changes in the secondary composition fractions.

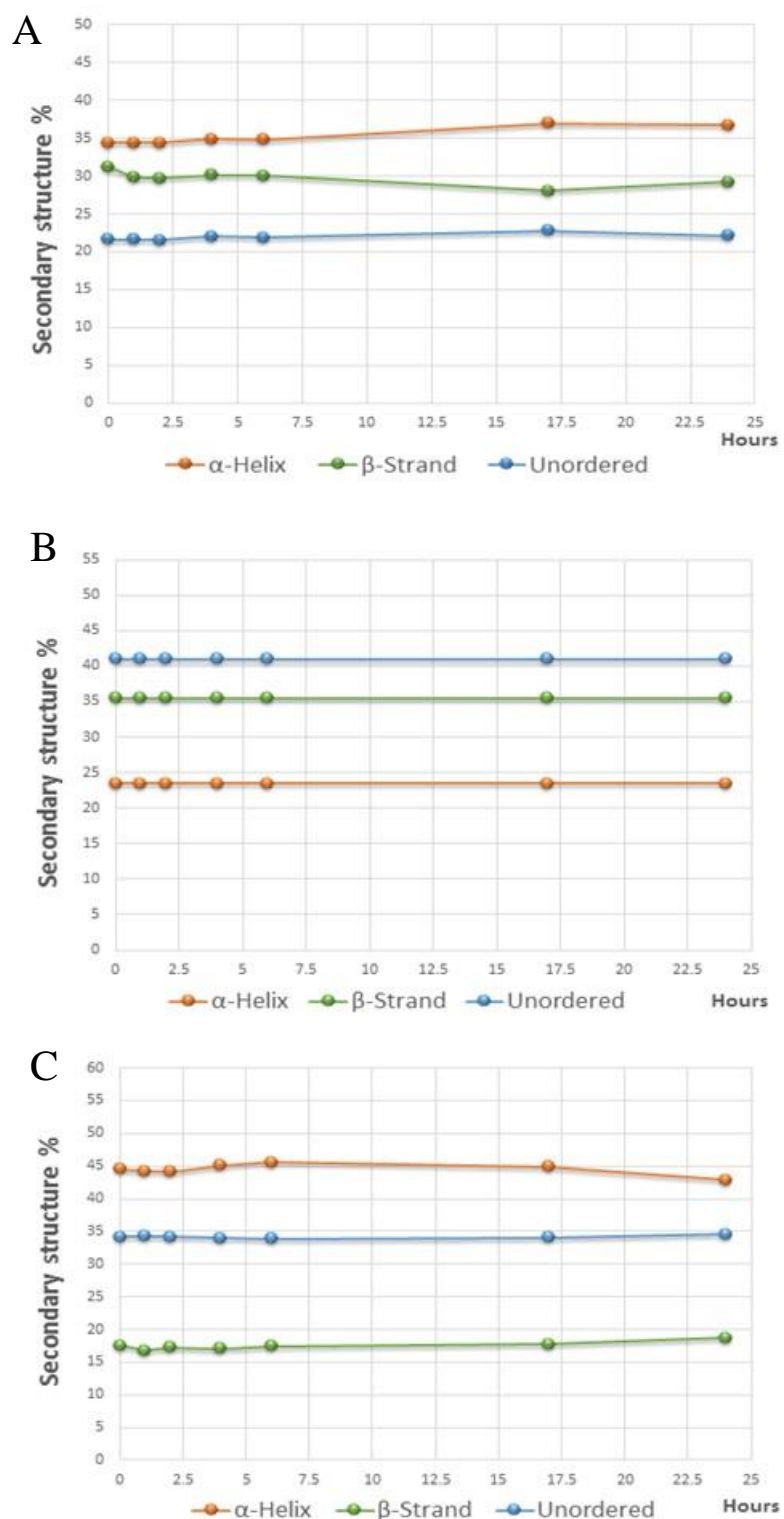


**Figure 7.03 Estimation of secondary structure fractions for SynZur.**

Prediction of secondary structure fractions for the SynZur protein, where  $\alpha$ -helices (Orange line),  $\beta$ -strands (Green line) and unordered (Blue line) are indicated from the CD spectra following incubation of the SynZur protein with 10 equivalents of EDTA by using three different programmes; (A) SELCON software, (B) CONTIN software from the DICHROWEB Web server (Sreerama *et al.*, 2000), and (C) RAUSSENS software from the RAUSSENS Web server (Raussens *et al.*, 2003).

A similar view has also been expressed for Zur and Fur proteins from *E. coli* and the Zur protein from *B. subtilis* (Althaus *et al.*, 1999; D'Autréaux *et al.*, 2007; Shin *et al.*, 2011). Using EDTA with DTT did not cause significant changes in the secondary structure of *E. coli* Fur (D'Autréaux *et al.*, 2007). However, it was stated that slight changes in CD spectra after zinc release may be due to partially losing dimerization of the *B. subtilis* Zur (Shin *et al.*, 2011).

The same phenomenon has also been observed for another kind of repressor CmtR, which is a cadmium-detecting transcriptional repressor. Under native conditions, this protein is present as a dimer containing two cadmium atoms (Banci *et al.*, 2007). The secondary structure content of CmtR also did not change upon cadmium removal or re-addition (Banci *et al.*, 2007).

Whilst UV-Vis and CD spectroscopy techniques, in principle, can give access to kinetic data, they provide only limited information on how metal releasing proceeds. These techniques are not able to clearly identify monomer/dimer conversion, distinguish between differential metallo-species, or report the effects on protein tertiary structure. So, it is impossible to attribute specific processes using the optical spectroscopy methods employed above. Furthermore, a combination of ESI-MS and NMR approaches can offer complementary access to complete speciation during zinc release.

### **7.2.1.3 Competition Reaction using ESI-MS**

The conformation of the protein in solution will govern the availability of ionisable basic sites. A tightly folded protein will have fewer basic sites available for protonation compared to the same protein in an unfolded conformation (Chowdhury *et al.*, 1990). Then, the charge states of the gas-phase ions observed in the electrospray mass spectrum will reflect the charge states of the protein in solution which will be displayed in the spectrum (Chowdhury *et al.*, 1990).

Native ESI-MS has been used in this study to investigate the structural changes related to monomer/dimer conversion and the distribution of metallo-species that may be present during the incubation of zinc-loaded SynZur protein with EDTA. Typically, mass spectrometry has the advantage of allowing all species within a sample to be observed (Kondrat *et al.*, 2013).

Zinc-loaded SynZur protein as purified contained  $2.1 \pm 0.2$  Zn(II) atoms per monomer (see Section 5.7.4) indicating that SynZur accumulates zinc inside the *E. coli* cell prior to purification. To investigate further details of the transfer/release of zinc ions from the SynZur protein, zinc-loaded SynZur was incubated with 2 equivalents of EDTA and the time course of this incubation recorded over time using native ESI-MS (Figure 7.04).

In the absence of EDTA at pH  $\sim 7.8$ , zinc-loaded SynZur exists in equilibrium between monomeric, dimeric and compact dimeric form (well-folded dimeric form) (Figure 7.04). Upon incubation at room temperature with 2 molar equivalents of EDTA, the proportion of monomeric to dimeric species changed, so that there was a notable increase in the amount of monomer with a shifting charge state to a higher m/z. This suggests that the removal of zinc ions causes the monomer to move to a better folded species. In spite this shifting of monomeric species, which was the most dominant one, no shifting of dimeric species, present at a lower relative percentage after 24 hours of incubation, was observed (Figure 7.04). Given this evidence, zinc release may affect the stability of the dimer.

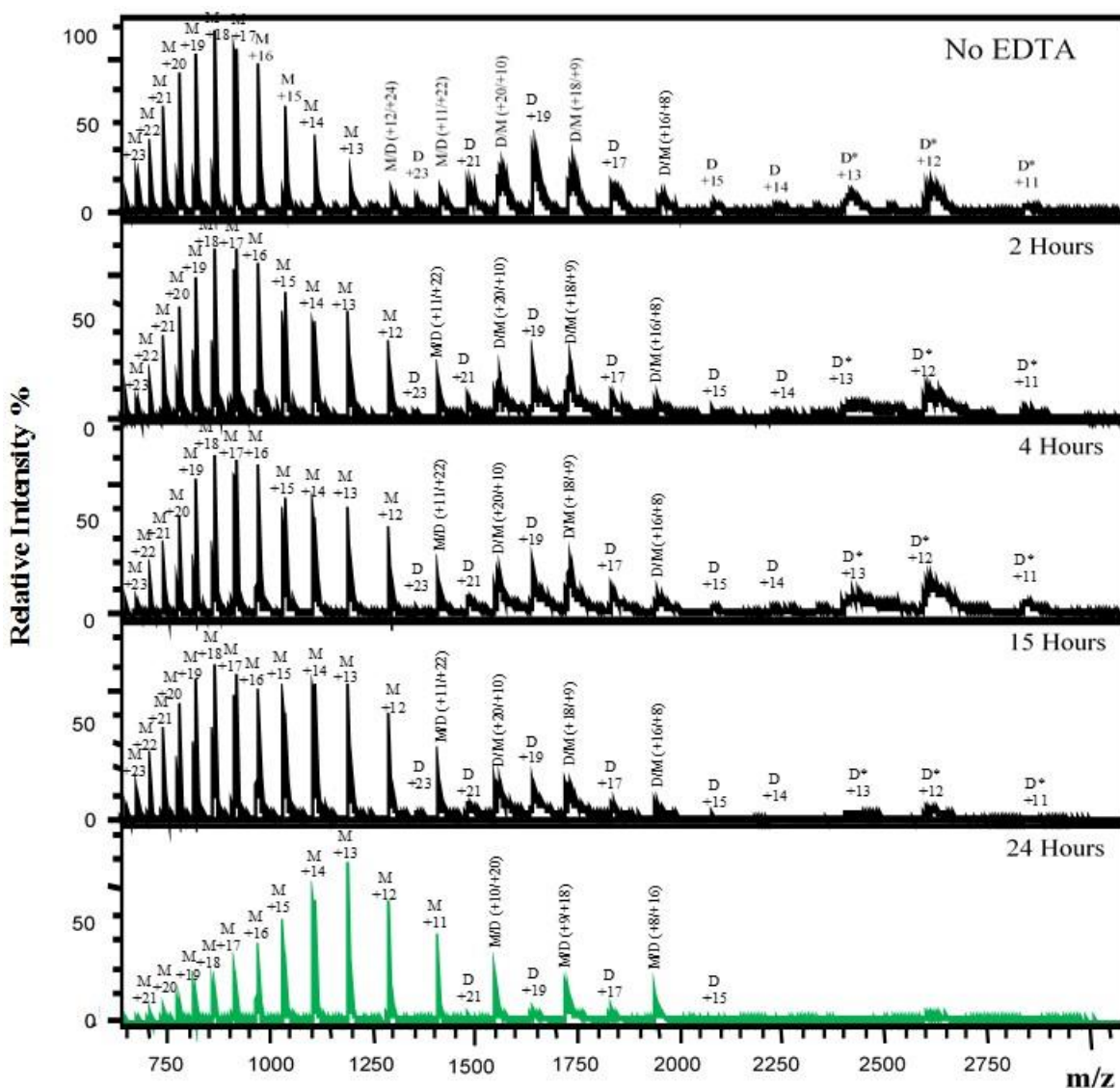


**Figure 7.04 Monitoring the competition reaction of SynZur using ESI-MS.**

Mass spectra for SynZur before and after incubation with EDTA. Charge states corresponding to monomer, dimer and well folded dimer are labelled, monomer (M), dimeric (D) and compact folding dimer (D\*). SynZur protein (32  $\mu\text{M}$ , 10 mM ammonium bicarbonate, pH= 7.8, 10% MeOH) was incubated with 64  $\mu\text{M}$  EDTA and the spectra were recorded on a Bruker MicroTOF spectrometer after 0, 2, 4, 15 and 24 hours, respectively.

To gain more insight about zinc speciation for the monomer and dimer states, one signal from the monomer charge state, +15 M, and another signal from the dimer charge state, +19 D, were chosen to visualize the effect of EDTA incubation on metallation, and data are displayed in qualitative and semi-quantitative plots (Figure 7.05 and Figure 7.06). Regarding the compact folding dimer, the intensity, resolution, and spectral quality were too low to allow a similar analysis.

Focusing on the +15 M charge state, the initial relative percentage for the monomeric state was determined as 92.6% for the  $Zn_2Zur$  species and 7.4% for the  $Zn_1Zur$  species (Figure 7.05). After 2 hours of EDTA incubation, the shifting towards the  $Zn_1Zur$  species can be clearly observed with this species increasing to 40%, while the relative percentage of the  $Zn_2Zur$  species dropped to approximately 56%, and the apo-SynZur was observed at 4%. Upon 4 hours incubation with EDTA, the relative percentage of the  $Zn_2Zur$  species slightly decreased to 52%, with a slight increase in the  $Zn_1Zur$  species to ~ 45%. Following 15 hours incubation with EDTA, the shifts towards the  $Zn_1Zur$  species were much more obvious (~ 62%) and this shifting continued as the sample was incubated overnight for 24 hours to 68% with a concomitant decrease in the  $Zn_2Zur$  species to ~ 27.6% (Figure 7.05). Meanwhile, under these incubation conditions, the apo-SynZur species was first noted in the spectra after two hours of EDTA incubation with a relative percentage of ~ 4% which remained constant even after 24 hours of incubation.

Moving to the dimeric state, the +19 charge state was chosen as it is an exclusively dimeric peak and present in high abundance before incubation with EDTA (Figure 7.04). Focusing on an odd-number dimeric charge state prevents monomeric interference affecting the abundance of certain species, especially when the abundance of monomeric species increases at the latter end of the EDTA time course. Similar to the monomer, all species present during incubation with EDTA were visualised and converted into a relative abundance plot (Figure 7.06).

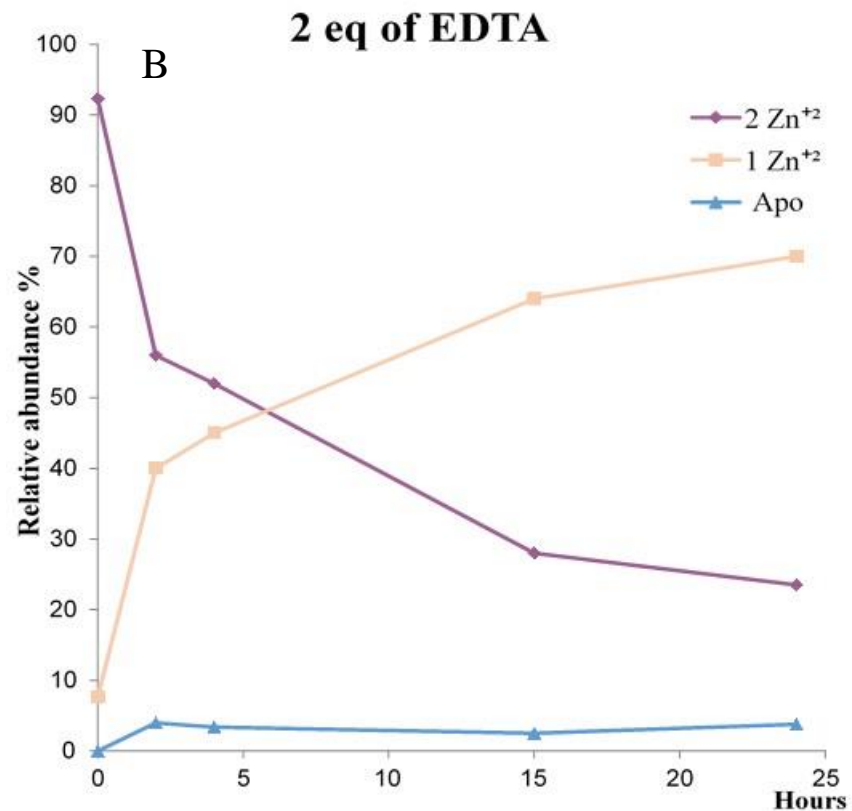
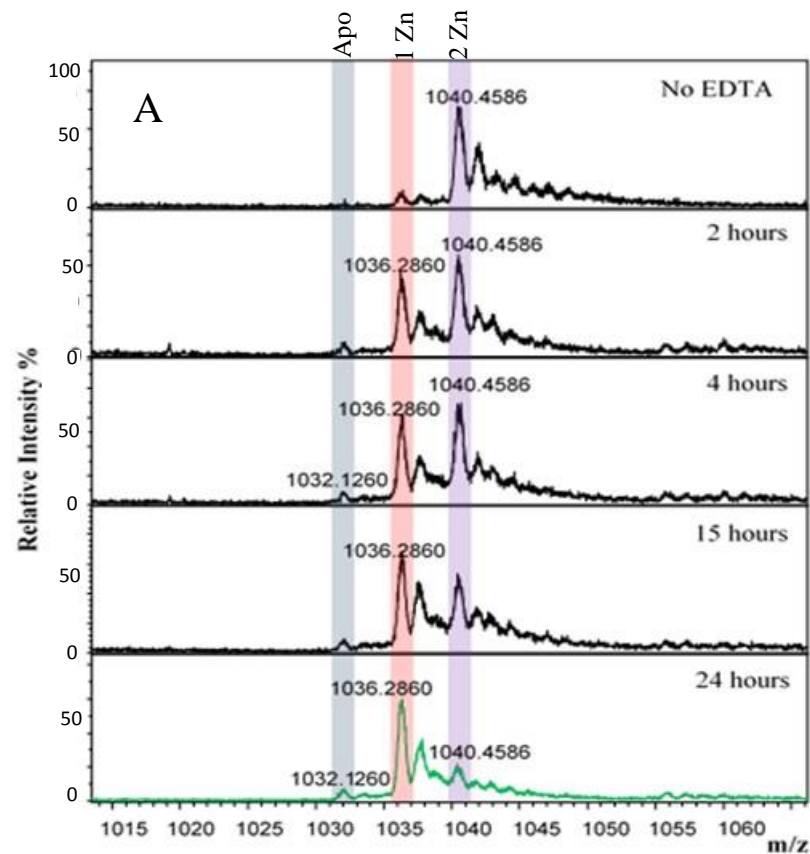


**Figure 7.05 The speciation of the +15 charge state from monomeric SynZur during the competition reaction with EDTA.**

(A) The mass spectra for the +15 charge state of monomeric SynZur before and after EDTA incubation. SynZur protein (32  $\mu\text{M}$ , 10 mM ammonium bicarbonate, pH= 7.8) was incubated with 64  $\mu\text{M}$  EDTA and the spectra were recorded on a Bruker MicroTOF spectrometer after 0, 2, 4, 15 and 24 hours, respectively. (B) Semi-quantitative plot for metallo-species from SynZur before and after incubation with EDTA. The relative abundance of each species was estimated from the intensity as a percentage of total intensity. The species are colour-coded as follows: Purple = 2 Zn(II), Pink = 1 Zn(II), Cyan = Apo.

Initially, the relative percentage of dimeric states was determined as 100% for the  $Zn_4Zur_2$  species (Figure 7.06). Surprisingly, the release of zinc ions from the dimeric zinc-loaded SynZur did not occur straight away, as was the case for the monomer. After two hours of EDTA incubation, SynZur in the dimeric state was still stable and present as the  $Zn_4Zur_2$  species. However, after 4 hours EDTA incubation, the  $Zn_2Zur_2$  species appeared beside the  $Zn_4Zur_2$  species with a relative percentage of ~ 35%. After 15 hours of EDTA incubation, the  $Zn_2Zur_2$  species increased to 39%, and to 43% after 24 hours. Concomitant with the build-up of the  $Zn_2Zur_2$  species, the  $Zn_4Zur_2$  species decreased in the raw spectra, being present only in low amounts after 24 hours (~9%).

Remarkably, in the dimeric state, no apo-SynZur species or  $Zn_1Zur_2$  species were observed in the raw mass spectra while the  $Zn_3Zur_2$  species was present at very low amounts during each time point ~ 5-3%. One of the interesting features of these experiments was that spectra taken after more than 28 hours did not show any further differences (data not shown). Noting that EDTA had been added at equimolar amounts with respect to zinc, this indicates that SynZur can release only half of its zinc ions in the presence of EDTA. SynZur, as purified, typically contained  $2.1 \pm 0.2$  zinc atoms per monomer. Treatment with the strong Zn(II) chelating agent EDTA (1:1 EDTA to Zn(II)) yielded  $0.9 \pm 0.3$  zinc atoms per monomer (according to ICP-OES). Notably, the  $Zn_4Zur_2$  species appeared to be more stable than the  $Zn_2Zur_2$  species during the competition reaction with EDTA.

Upon zinc ion removal from one site, it was noticed that the proportion of dimeric to monomeric species changed and this led to an increase in the amount of monomeric state with the  $Zn_1Zur_2$  species as the most dominant one in the raw spectrum (Figure 7.04). The monomeric SynZur sample was stable with time and only showed some proteolytic degradation after several days at 4°C. The same phenomenon has also been observed for the Fur protein from *E. coli*, whereas a higher yield of the monomeric species was obtained by incubating the protein with EDTA (Pecqueur *et al.*, 2006; D'Autréaux *et al.*, 2007).

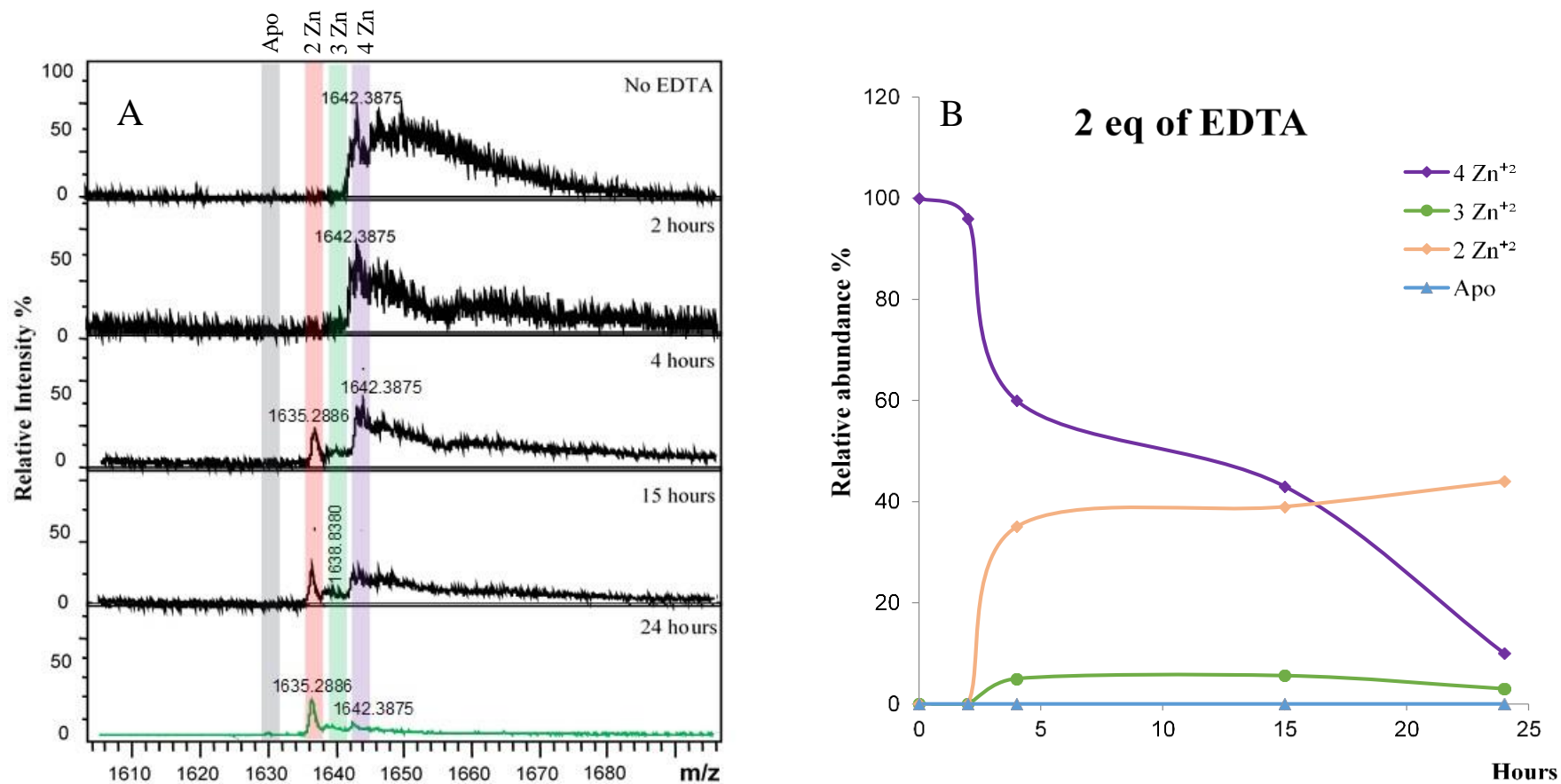


**Figure 7.06 The speciation of the +19 charge state of dimeric SynZur during the competition reaction with EDTA.**

(A) The mass spectra for the +19 charge state of dimeric SynZur before and after EDTA incubation. SynZur protein (32  $\mu\text{M}$ , 10 mM ammonium bicarbonate, pH= 7.8) was incubated with 64  $\mu\text{M}$  EDTA and the spectra were recorded on a Bruker MicroTOF spectrometer after 0, 2, 4, 15 and 24 hours, respectively. (B) Semi-quantitative plot for metallo-species from SynZur after incubation with EDTA. The relative abundance of each species was estimated from the intensity as a percentage of total intensity. The species are colour-coded as follows: Purple = 4 Zn(II), Green = 3 Zn(II), Pink = 2 Zn(II), Cyan = Apo.

These results highlight the fact that SynZur has two metal sites; one tightly bound and/or kinetically inert, and one more weakly bound/kinetically labile and EDTA has a propensity to remove zinc from one site which should be the sensory site 2. In agreement with this suggestion, it was reported that to remove almost all of the zinc from the protein, treatment with urea (which will denature the protein), coupled with extensive incubation with chelating agents was necessary (Outten & O'Halloran, 2001). Given this evidence, the MS data also indicates that zinc in the sensory site may affect the stability of the dimer.

Consistent with UV-Visible data (see Section 7.2.1.1), releasing zinc ion from SynZur was also dependent on the EDTA concentration (Figure 7.07). The proportion of dimeric to monomeric species can obviously change more rapidly by incubating with 10 equivalents of EDTA (with respect to protein concentration), and the new cluster peak of monomer,  $Zn_1Zur$  was completely achieved only after 6 hours (Figure 7.07).

The data presented in this section are in good agreement with recent discoveries about Fur family proteins. An early study on the Zur protein from *E. coli* (designated as  $Zn_2Fur$ , although it is now known as a zinc metalloprotein) showed that the protein contains 2.1 zinc atoms per monomer. However, one atom of zinc could easily be removed upon dialysis against EDTA, nitrilotriacetate (NTA), dipicolinate, and TPEN yielding a  $Zn_1Fur$  species (Althaus *et al.*, 1999; Outten & O'Halloran, 2001; Outten *et al.*, 2001). The same view has also been expressed for the Fur protein from *E. coli* by using EDTA and DTT (D'Autréaux *et al.*, 2007). In addition, using EDTA with DTNB for Fur from *Anabaena* PCC7119 did not help either to remove all metal ions (Hernandez *et al.*, 2002), and this explains the difficulty that we faced during our study to determine the correct concentration for SynZur protein using the Cysteine assay (see Section 5.7.2).

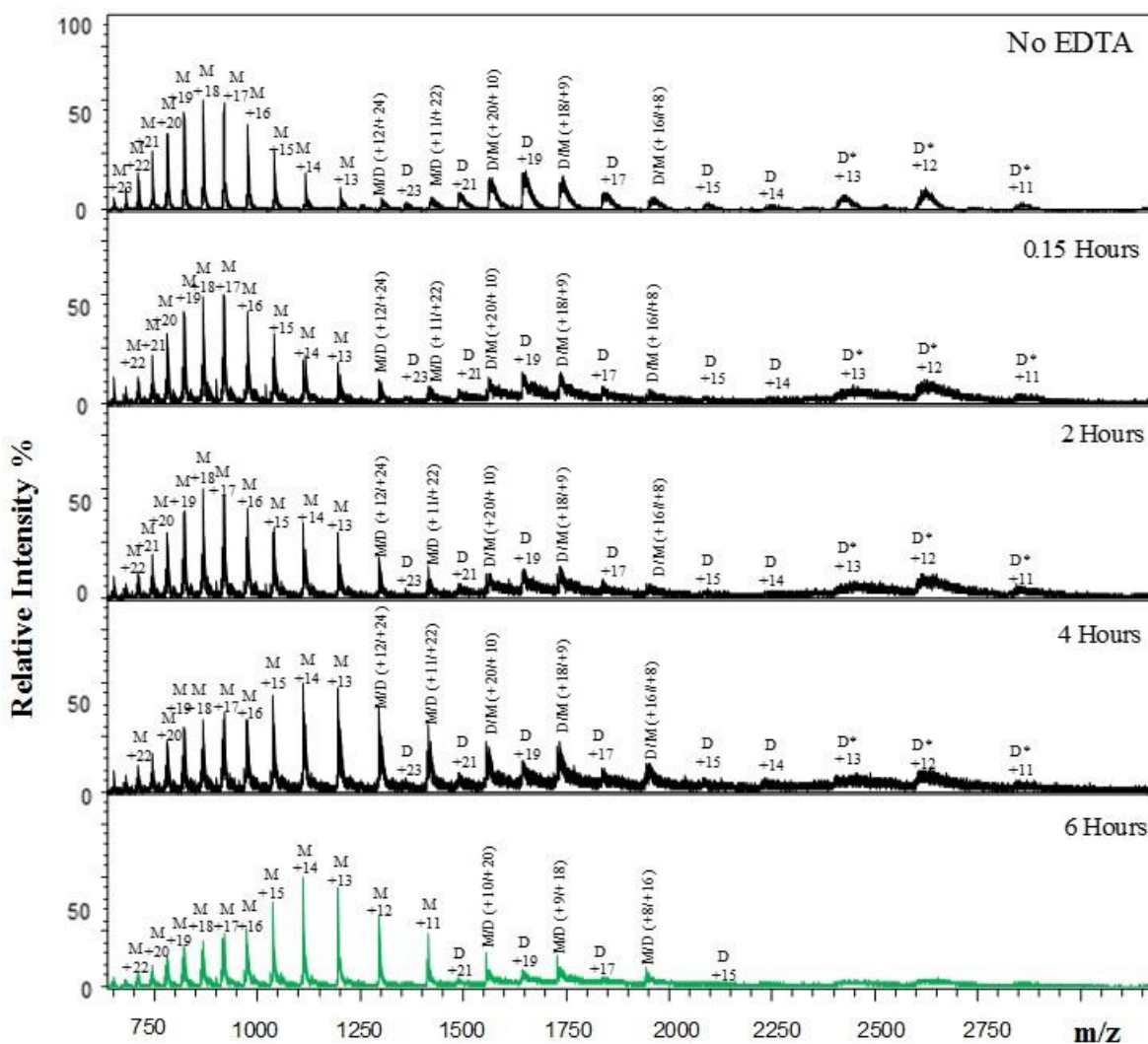


**Figure 7.07 Monitoring the competition reaction of SynZur with EDTA using ESI-MS.**

Mass spectra for SynZur before and after incubation with EDTA. Charge states corresponding to monomer, dimer and well folded dimer are labelled, monomer (M), dimeric (D) and compact folding dimer (D\*). SynZur protein (32  $\mu$ M, 10 mM ammonium bicarbonate, pH= 7.8, 10% MeOH) was incubated with 320  $\mu$ M EDTA and the spectra were recorded on a Bruker MicroTOF spectrometer after 0, 0.15, 2, 4 and 6 hours, respectively.

Furthermore, treating the Zur protein from *Streptomyces coelicolor*, which was purified as the  $Zn_3$ Zur species, with EDTA yielded 1.2 zinc atoms per monomer (Shin *et al.*, 2011), while treating the Zur protein from *Bacillus subtilis* yielded 0.5-0.8 Zn(II) per monomer (Ma *et al.*, 2011). A more recent study on Zur from the cyanobacterium *Synechocystis* sp. PCC 6803 indicated that treating the protein with EDTA yielded  $1.02 \pm 0.15$  zinc atoms per monomer (Tottey *et al.*, 2012).

It is worth mentioning that this phenomenon applies not only to Zur and Fur proteins, but also for other proteins from the Fur family such as PerR from *Bacillus subtilis* (Traoré *et al.*, 2006) and Mur from *Rhizobium leguminosarum* (Bellini & Hemmings, 2006). It is therefore important to appreciate that the use of EDTA at any point in the preparation or assay may result in significant partial Zn(II) chelation that may lead to potentially erroneous results.

Although the metal ion binding sites within the Zur protein are known to have a high affinity for zinc ions among Fur family proteins (Lucarelli *et al.*, 2007; Shin *et al.*, 2011; Gilston *et al.*, 2014), little knowledge is available surrounding the kinetics of zinc ions from each site. It is unlikely that structural site 1, which has two CXXC motifs (Cys-83 and Cys-86, Cys-124, Cys-126), in the SynZur protein is the sensory site, since incubation of Fur protein from *Vibrio cholerae*, which lacks the two CXXC motif, with EDTA could easily remove all metal ions from the protein and only 0.1 Zn(II) atom per monomer was detected by ICP-MS after incubation (Sheikh & Taylor, 2009). Furthermore, it appears to be generally true that if two CXXC motifs are present in a given Fur family protein, one zinc ion will remain bound to the protein after EDTA treatment (Traoré *et al.*, 2006; Lucarelli *et al.*, 2007; Jacquamet *et al.*, 2009; Shin *et al.*, 2011; Gilston *et al.*, 2014). A good example from the literature is the PerR protein from *Bacillus subtilis*, where a zinc ion in the Zn<sub>1</sub>PerR species was present as ZnCys<sub>4</sub> in the crystal structure (Traoré *et al.*, 2006). Additionally, a strong band for metal-sulfur coordination was found in the zinc-EXAFS spectrum for the Zur protein from *Mycobacterium tuberculosis* after treatment with EDTA (Lucarelli *et al.*, 2007), confirming that the recalcitrant site is the Cys<sub>4</sub> site. As a structural cofactor, the zinc ion could be buried in the protein interior, lacking contact with the buffer solution (Outten *et al.*, 2001). This would explain the difficulty encountered in attempting to remove zinc from the structural site 1.

But, however, what about electrostatic interactions? The electrostatic charge distribution over the SynZur monomer is shown in Figure 7.08 and reveals that structural site 1 is not accessible

(Figure 7.08C and D) due to electrostatic repulsion between the negatively charged EDTA and the negatively charged environment around structural site 1. On the other hand, sensory site 2 is accessible due to the negatively charged EDTA and positively charged environment around the sensory site 2 (Figure 7.08E and F).

Interestingly, the data produced from the EDTA time course indicated that the kinetics of zinc ion removal from the sensory site is surprisingly slow. High zinc affinity coupled with a slow rate for zinc removal may constitute a potential benefit for the zinc homeostatic system in *Synechococcus* sp. WH8102. On the other hand, the formation of a high amount of monomer under depletion conditions could prevent dimerization and DNA binding, and thus allow the constant expression of ZnuABC under zinc depletion conditions.

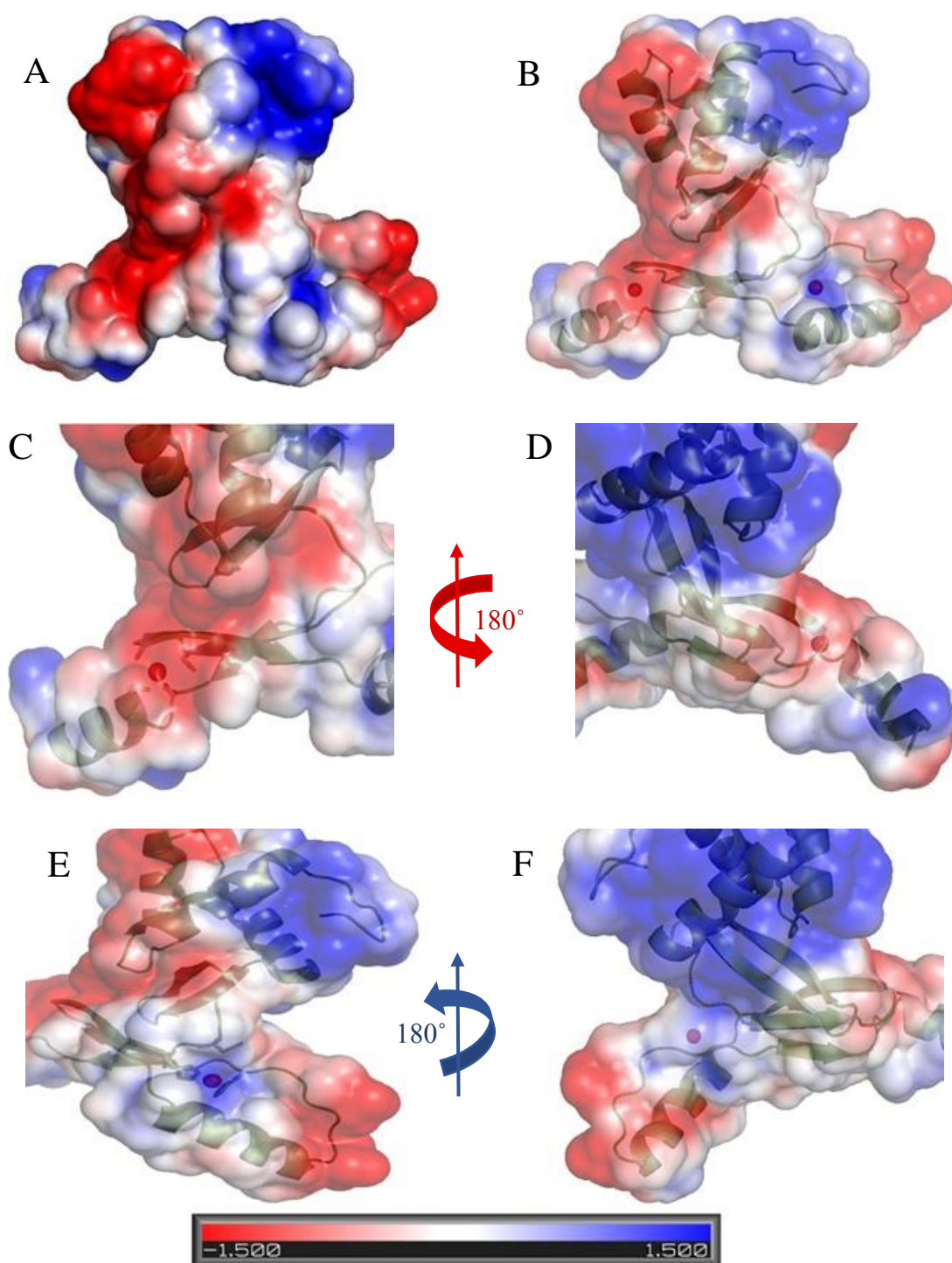


**Figure 7.08 Electrostatic potential map of the predicted SynZur protein.**

The electrostatic surfaces of the SynZur monomer calculated using Adaptive Poisson-Boltzmann Solver (APBS) (Baker *et al.*, 2001) generated using the PyMOL software (DeLano, 2007). The electrostatic surface of the Zur monomer with two zinc sites (A) and with 40% transparency for the surface (B). The surface electrostatic potential for structural site 1 (C), and after 180° rotation around a vertical axis (D). The surface electrostatic potential for sensory site 2 (E) and after 180° rotation around a vertical axis (F). A colour gradient from blue to white to red is used to colour the molecular surface where red, white, and blue are for negative, neutral, and positive potentials, respectively.

Combining the ESI-MS data (see Section 7.2.1.3) with the CD data (see Section 7.2.1.2) it can be concluded that there is no large difference in the secondary structure between the metallo-species of the SynZur protein, i.e. the  $Zn_2Zur/Zn_1Zur$  species of the monomer and the  $Zn_4Zur_2/Zn_2Zur_2$  species of the dimer. To further understand the effects of zinc loss on protein folding, the SynZur protein was incubated with 2 equivalents of EDTA and the effects were monitored by 1D  $^1H$  NMR.

#### 7.2.1.4 Competition Reaction using 1D $^1H$ NMR

In the last few years, nuclear magnetic resonance (NMR) spectroscopy has become a versatile and powerful method to investigate protein-ligand interactions. Particularly, EDTA has been widely used as chelating agent in NMR studies (Gennaro *et al.*, 1983; Han *et al.*, 2007; Barton *et al.*, 2010).

For the relatively slow and simple release of zinc from SynZur during incubation with EDTA, it was possible to follow the zinc transfer reaction also by 1D  $^1H$  NMR spectroscopy in a time-dependent manner. In principle, this technique also allowed the facile detection of both free and Zn(II)-bound EDTA simultaneously, and crucially could give time-dependent information on protein folding.

It is worth mentioning that the experimental concentrations and time frames used in UV-Visible, CD spectroscopy and mass spectrometry experiments are not suitable for NMR investigations, but considerable information can be gained by combining information from these techniques. ESI-MS revealed that the monomeric state with the  $Zn_1Zur$  species is the most dominant species after incubation with EDTA; therefore, it can be assumed that NMR spectra may also pertain to have one dominating species at later times of incubation with EDTA.

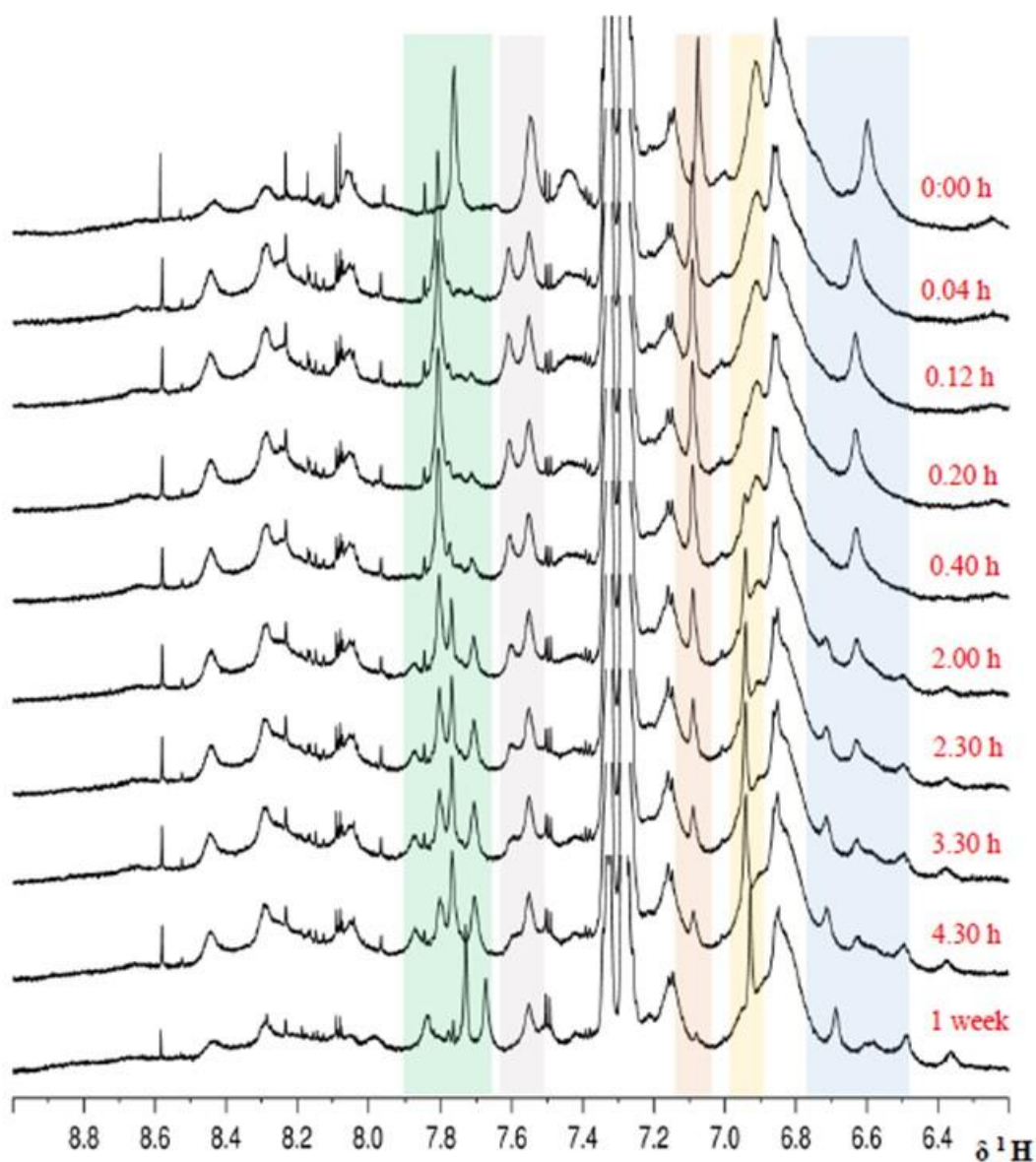


**Figure 7.09 Monitoring the competition reaction of SynZur using 1D  $^1\text{H}$  NMR.**

The effect of EDTA on the SynZur spectra in the fingerprint region. SynZur protein (600  $\mu\text{M}$ , 20 mM  $\text{NH}_4\text{HCO}_3$ , 10%  $\text{D}_2\text{O}$ , pH 7.4, 308K) was incubated with 1.2 mM EDTA and 1D  $^1\text{H}$  NMR spectra were recorded at 700.24 MHz using a Bruker Avance 700 Spectrometer equipped with a cryoprobe at various timepoints. Coloured boxes show the shifting, appearance, or disappearance of peaks during incubation with EDTA.

Zinc-loaded SynZur protein was incubated with 2 molar equivalents of EDTA and 1D  $^1\text{H}$  NMR spectra were acquired at suitable time intervals. The backbone NH region of the resulting spectra is shown in Figure 7.09.

Interestingly, Figure 7.09 shows further evidence of the competition reaction between SynZur and EDTA. Incubation with EDTA has a discernible impact on the appearance or disappearance of new peaks in the low-field NMR region or fingerprint region for SynZur spectra (Figure 7.09), while no significant changes were detected in the up-field region (data not shown).

Pronounced changes in the SynZur spectrum began to appear after 4 min of EDTA incubation, with shifting for some peaks and a new peak appearing at ~ 7.6 ppm (Figure 7.09). However, this new peak disappeared again at later incubation times. The intensity of a peak at 6.62 ppm was decreased after 40 min. Another example was noticed for the peak at 7.7 ppm, where this peak appeared after 20 min of incubation and its intensity was increased during the time course of the incubation. Some other chemical shifts values illustrating the effect of EDTA on SynZur in the fingerprint region are displayed in Appendix G and Table G.01. Between 3.30 hours to 4.30 hours, no further changes were identified. Later, up to 1 week, no significant differences in the resonances were detected. Hence, the remaining peaks in the low-field region suggest that the protein was still folded to at least some degree, which supports conclusions from ESI-MS and CD data, which had indicated that the Zn<sub>1</sub>Zur species can be stable for a long time. However, the changes in the fingerprint region of the 1D NMR spectra may belong to His residues (Saito & Williams, 1991; Saito *et al.*, 1991), amide side chain protons and aromatic side chains.

Crucially, with an <sup>1</sup>H NMR approach, it is not only possible to monitor the impact of zinc depletion on protein folding, but also to simultaneously observe the formation of the Zn(II)-EDTA complex. The analysis of data is aided by the fact that Zn(II)-bound EDTA and free EDTA are in slow exchange on the NMR time scale, and the resonances for these species can easily be distinguished due to their sharpness and good separation (Leszczyszyn *et al.*, 2007). Therefore, such data allows the quantification of both species at any time of the reaction.

Free EDTA gives rise to two sharp singlet peaks due to acetate-methylene and amine-methylene protons (Han *et al.*, 2007). Zinc binding to EDTA causes splitting of the acetate-methylene proton peak to an AB pattern at room temperature (Han *et al.*, 2007; Barton *et al.*, 2010). Meanwhile, the singlet from the amine-methylene protons will remain as a singlet. In the Zn(II)-bound EDTA form, both peaks will be shifted with respect to the free EDTA chemical shifts.

Figure 7.10 shows the aliphatic region of the 1D  $^1\text{H}$  NMR spectrum for the SynZur protein, where the chemical shifts for free and Zn(II)-bound EDTA are distinguishable. The singlets associated with free EDTA have chemical shifts of 3.19 and 3.59 ppm. After 4 min of EDTA incubation, a small proportion of signals corresponding to Zn(II)-bound EDTA were identified in the 1D  $^1\text{H}$  NMR spectrum. Regarding the Zn(II)-bound EDTA form, an AB multiplet was observed at 3.33 ppm for the protons of the N-CH<sub>2</sub>COO group and a singlet was noted at 2.83 ppm corresponding to the NCH<sub>2</sub>CH<sub>2</sub>N- protons. After 3.30 hours of incubation with EDTA, the intensity of peaks belonging to free EDTA decreased while the intensity for peaks belonging to the Zn(II)-bound EDTA increased (Figure 7.10).

However, after further incubation for one week, no further changes in the intensity were observed. A semi-quantitative evaluation plot of the  $^1\text{H}$  NMR data (Figure 7.10C) also shows the slow pace of the reaction at the EDTA concentration used. Moreover, even after one week of incubation, free EDTA and Zn(II)-bound EDTA have reached only half the total EDTA concentration, ca. 0.6 mM, which indicates that one zinc atom was removed from SynZur protein (Figure 7.10C). Crucially, the intensity of the signal for the Zn<sub>1</sub>Zur species reached the concentration of protein (ca. 0.6 mM) after only a few hours, while the intensity of the Zn(II)-loaded SynZur decreased to zero (Figure 7.10C).

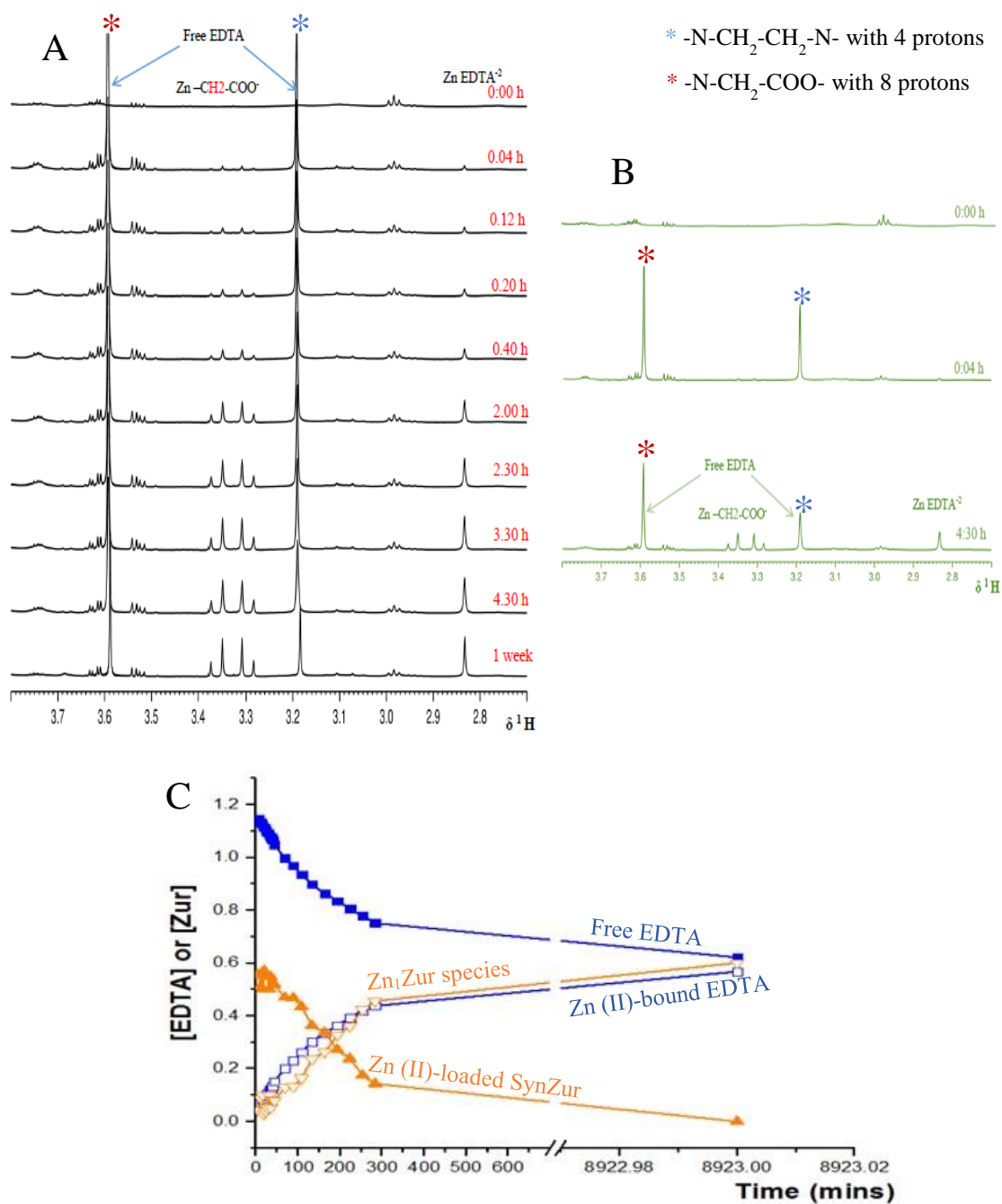


**Figure 7.10 Stacked plot of the EDTA time course with SynZur.**

(A) Up-field region of 1D <sup>1</sup>H NMR spectra acquired during the incubation of SynZur with EDTA. SynZur protein (600 μM, 20 mM NH<sub>4</sub>HCO<sub>3</sub>, 10% D<sub>2</sub>O, pH 7.4, 308K) was incubated with 1.2 mM EDTA and spectra were recorded at 700.24 MHz using a Bruker Avance 700 spectrometer at various timepoints. Marked peaks correspond to free EDTA resonances. (B) The green insert shows the time-course incubation after 0, 0.04 and 4.30 hours, respectively. (C) Time course plot of the reaction between SynZur and EDTA followed by changes in the integrals of selected signals in <sup>1</sup>H NMR spectra. The abundance of Zn(II)-bound EDTA and free EDTA are derived from the integration of the eight methylene protons empty and filled blue square, respectively; those for the protein are followed by changes in the intensity of 6.94 ppm and 7.12 ppm species as a Zn<sub>1</sub>Zur species and Zn(II)-loaded SynZur protein empty and filled orange triangle, respectively.

Therefore, this indicates that the SynZur protein, Zn(II)-bound EDTA, and free EDTA have reached a thermodynamic equilibrium. On this basis, it may be inferred that ca. half of the EDTA is still free in solution. These data also support the conclusion from ESI-MS data that incubating SynZur with EDTA for a long time did not remove zinc ions from structural site 1 of the protein.

### 7.2.1.5 Competition Reaction using [ $^1\text{H}$ , $^{15}\text{N}$ ] TROSY

Probably the most detailed information about protein behaviour in complexes can be obtained by [ $^1\text{H}$ ,  $^{15}\text{N}$ ] heteronuclear experiments. The protein is usually labelled isotopically with  $^{15}\text{N}$  and mixed with unlabelled ligands. Typically, the changes in the fingerprint  $^1\text{H}$ - $^{15}\text{N}$  correlation spectra caused by the unlabelled ligand result in changes in the chemical shifts of backbone protons and nitrogen atoms (Golovanov *et al.*, 2007) which can give information about protein folding.

#### 7.2.1.5.1 Chemical Shift Perturbation

Chemical shift perturbation (CSP), also known as chemical shift mapping or complexation-induced changes in chemical shift (CIS), is a very useful technique for studying the binding of small molecules to proteins.

Ligand (or indeed metal) binding or releasing can lead to structural changes. If the structural changes occur between two environments (bound and free protein) this will lead to change in the chemical shifts. When a spin exchanges between environments and its chemical shift is different in each environment, its spectral properties will change too (Rule and Hitchens 2006). Notably, backbone atoms are very sensitive to any structural changes which can be observed using heteronuclear experiments (Figure 7.11). Moreover, this phenomenon is often referred to as *chemical exchange* (Rule & Hitchens, 2006).

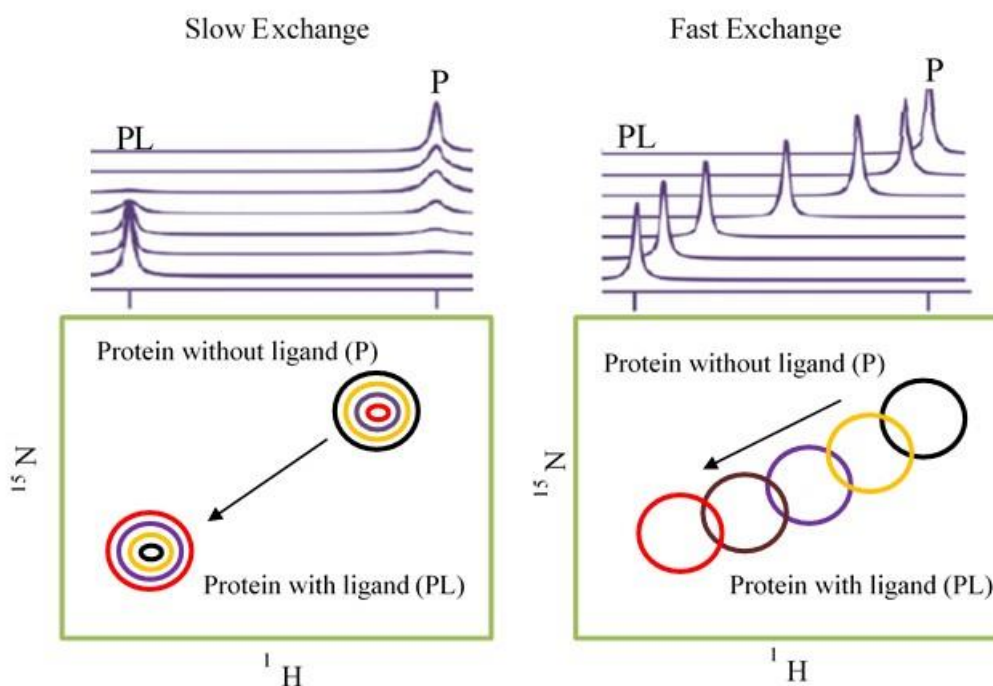


**Figure 7.11 Description of chemical shift perturbations in slow and fast exchange rate.**

Slow exchange: the free protein peak P (black) decreases in intensity or disappears as the bound protein PL peak (red) increases, left panel. Fast exchange: peaks move smoothly from free protein P (black) to bound protein PL (red), Right panel. In the limit of very fast exchange, peaks have the same shape throughout, while in the slow exchange regime, they do not. Partially adapted from (Williamson, 2013).

Usually, the unlabelled ligand, L, is incubated with the  $^{15}\text{N}$  labelled protein, P, and the titration or time course is monitored at each stage by acquiring a 2D NMR spectrum. Consequently, the signal for a particular proton may become faint or disappear with the appearance of a new signal which indicates slow or intermediate exchange between the original and the new species (Golovanov *et al.*, 2007; Williamson, 2013) (Figure 7.11). On the other hand, a particular proton may move smoothly from its original position to the new position with the possibility of presence of the resonance at each point of incubation which indicates fast exchange (Golovanov *et al.*, 2007; Williamson, 2013) (Figure 7.11).

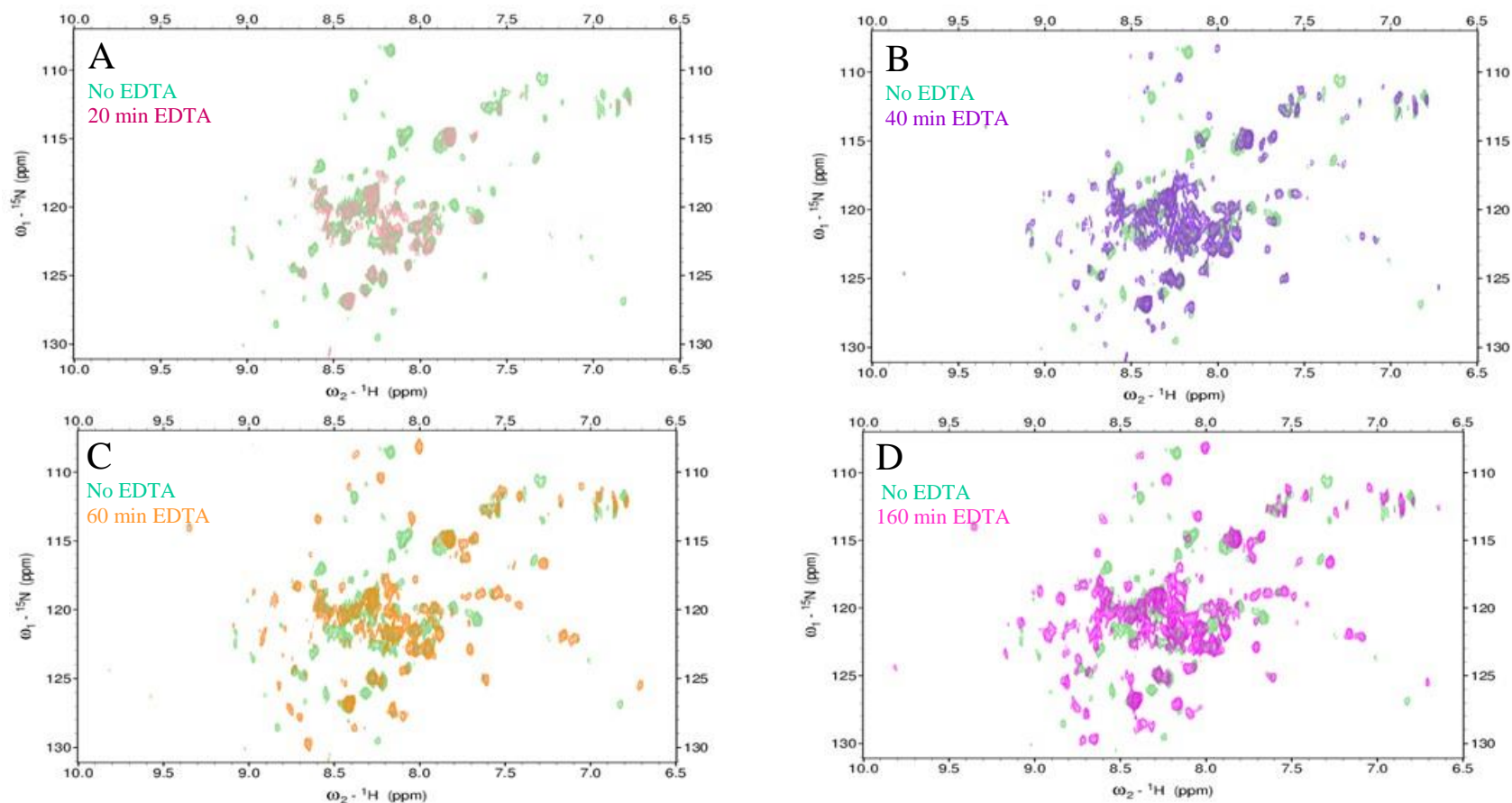


**Figure 7.12 Monitoring the competition reaction of SynZur using 2D [ $^1\text{H}$ ,  $^{15}\text{N}$ ] HSQC-TROSY spectroscopy.**

Superimposed [ $^1\text{H}$ ,  $^{15}\text{N}$ ] HSQC-TROSY spectra for zinc-loaded SynZur in the absence of EDTA (Light green) and in the presence of EDTA at various time intervals (shown in different colours). (A) At 20 min after incubation (Light red), (B) At 40 min after incubation (Purple), (C) At 60 min after incubation (Yellow), and (D) At 160 min after incubation (Pink). 900  $\mu\text{M}$  EDTA was incubated with 450  $\mu\text{M}$  of  $^{15}\text{N}$ -labelled SynZur protein in 20 mM ammonium bicarbonate at 308 K, 10%  $\text{D}_2\text{O}$ , 150 mM NaCl and pH-6.2, using 32 scans and 32 increments. The spectra were recorded at 700.24 MHz on a Bruker Avance 700 spectrometer equipped with a cryoprobe.

In order to gain insights into the nature of changes between SynZur and zinc ions (ligand), 2D [ $^1\text{H}$ ,  $^{15}\text{N}$ ] HSQC-TROSY, due to its sensitivity for the backbone changes (see Section 6.4), was employed after incubation of SynZur with EDTA. [ $^1\text{H}$ ,  $^{15}\text{N}$ ] HSQC-TROSY spectra were recorded at each point during the competition reaction making it possible to detect some chemical shift changes (Figure 7.12).

The fact that the TROSY spectrum for zinc-loaded SynZur is not the same as the spectrum after incubation with EDTA indicates that the competition reaction is taking place (Figure 7.12). Incubation with EDTA caused the shifting, appearance, or disappearance of some peaks within the first 20 min (Figure 7.12A). Following the next 2.40 hours (Figure 7.12), it was observed that most peaks completed their shifting due to no observed changes after this time.

[ $^1\text{H}$ ,  $^{15}\text{N}$ ] HSQC-TROSY spectra for SynZur before and after incubation with EDTA are overlaid in Figure 7.13 with the expectation that the final spectrum refers to a  $\text{Zn}_1\text{Zur}$  species. Both spectra for zinc-loaded SynZur and  $\text{Zn}_1\text{Zur}$  species indicate that protein before and after EDTA treatment is folded with well dispersed amide signals. The spectrum of the SynZur protein before incubation with EDTA shows ~ 93 peaks. Moreover, the missing peaks may indicate that the protein undergoes conformational exchange (Pecqueur *et al.*, 2006). After incubation with EDTA, the spectrum shows ~ 101 peaks (Figure 7.13).

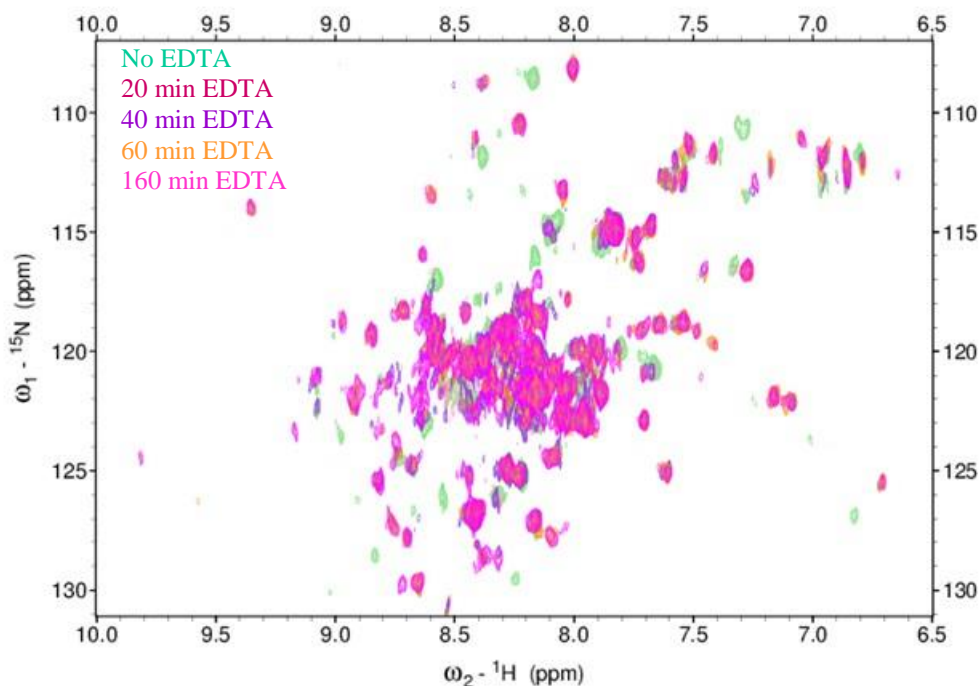


**Figure 7.13 Overlay of 2D [ $^1\text{H}$ ,  $^{15}\text{N}$ ] HSQC-TROSY for SynZur during the EDTA time course.**

Superimposed [ $^1\text{H}$ ,  $^{15}\text{N}$ ] HSQC-TROSY spectra for zinc-loaded SynZur in absence of EDTA (Light green) and presence of EDTA at 20 min (Light red), 40 min (Purple), 60 min (Yellow), and 160 min (Pink). 900  $\mu\text{M}$  EDTA was incubated with 450  $\mu\text{M}$   $^{15}\text{N}$ -labelled SynZur protein in 20 mM ammonium bicarbonate at 308 K, 10%  $\text{D}_2\text{O}$ , 150 mM NaCl and pH~6.2, using 32 scans and 32 increments. The spectra were recorded at 700.24 MHz on a Bruker Avance 700 spectrometer equipped with a cryoprobe.

It is clear that there are conformational/dynamic changes occurring during incubation with EDTA. As a result of incubation, many chemical shifts are perturbed (Figure 7.14). Notably, the peaks in [ $^1\text{H}$ ,  $^{15}\text{N}$ ] HSQC-TROSY spectra have different intensities which may be due to minor conformational exchange dynamics in a slow-intermediate exchange timescale.

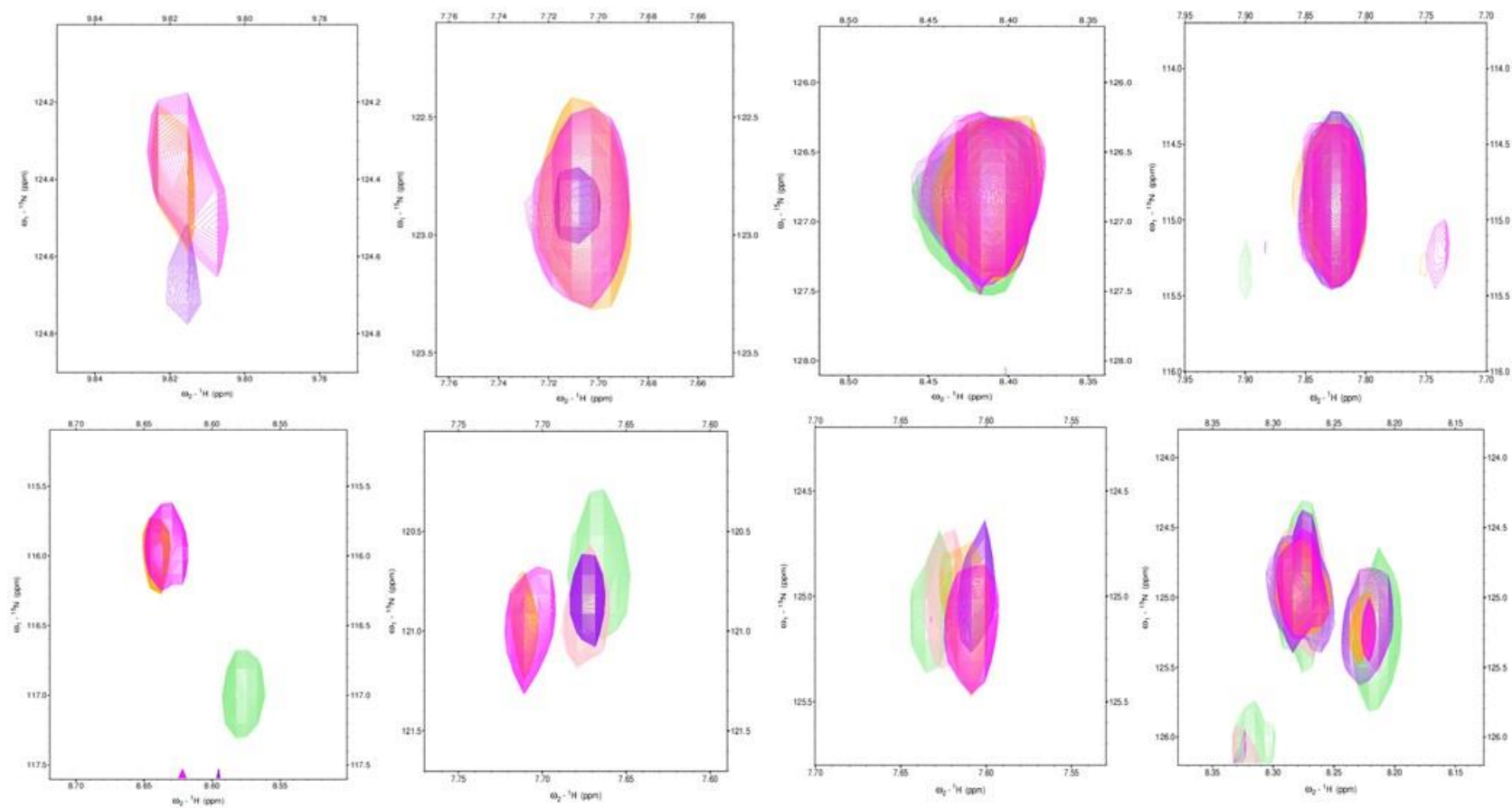


**Figure 7.14 Chemical shift perturbation, close-up, of  $[^1\text{H},^{15}\text{N}]$  HSQC-TROSY spectra for SynZur during the EDTA time course.**

Sub-spectral regions highlight the chemical shift changes of the backbone amide groups in the absence of EDTA (Light green contour) and presence of EDTA at 20 min (Light red contour), 40 min (Purple contour), 60 min (Yellow contour), and 160 min (Pink contour) after incubation with EDTA. 900  $\mu\text{M}$  EDTA was incubated with 450  $\mu\text{M}$   $^{15}\text{N}$ -labelled Zur protein in 20 mM ammonium bicarbonate at 308 K, 10%  $\text{D}_2\text{O}$ , 150 mM NaCl and pH~6.2, using 32 scans and 32 increments. The spectra were recorded at 700.24 MHz on a Bruker Avance 700 spectrometer equipped with a cryoprobe.

Pecqueur and colleagues pointed out that the NMR spectrum of the monomeric Fur from *E. coli* is less extended both in the proton and in the nitrogen dimension, indicating a lower degree of structuralization of the monomer compared with the dimer (Pecqueur *et al.*, 2006). However, Figure 7.12 and Figure 7.13 show that the spectrum for the monomeric state, Zn<sub>1</sub>Zur species, is more extended both in the proton and in the nitrogen dimension than the fully zinc-loaded SynZur.

The time-course spectra were each acquired within 20 min to enable the capture of as many time points as possible during the fastest stage of the reaction. Thus their resolution and sensitivity is relatively low. Therefore, the pre-incubation and final spectra were also recorded with a higher number of increments (TD=64) in the nitrogen dimension, to improve the resolution. As can be seen, a significant improvement in resolution was achieved by increasing the number of scans from 32 increments (Figure 7.13) to 64 increments (Figure 7.15).

By increasing the number of increments to 64, the NH signals significantly narrowed in the <sup>15</sup>N dimension, and the number of detected NH signals increased from 93 to 103 for the zinc-loaded SynZur spectrum (Figure 7.15). Difficulties in counting the number of peaks was not only faced for SynZur protein in our study but has also been observed for another repressor family protein such as CmtR, which is a cadmium-detecting transcriptional repressor (Banci *et al.*, 2007).

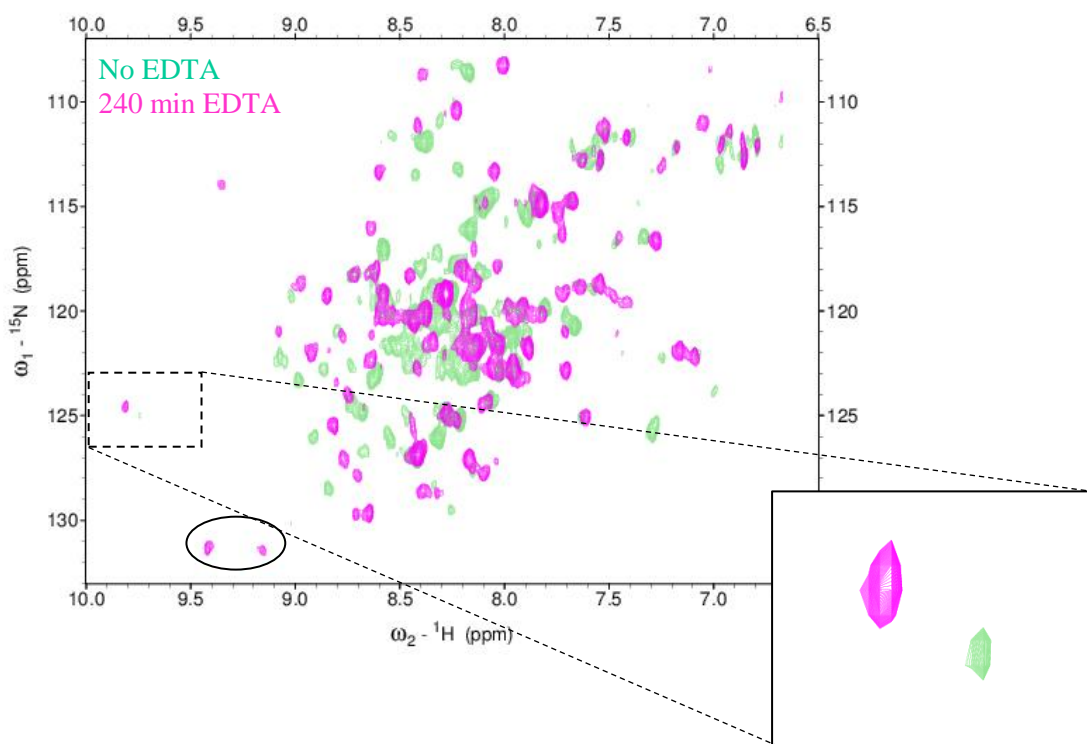


**Figure 7.15 Overlay of  $[^1\text{H},^{15}\text{N}]$  HSQC-TROSY before and after EDTA incubation.**

Superimposed  $[^1\text{H}, ^{15}\text{N}]$  HSQC-TROSY spectra of zinc-loaded SynZur in the absence of EDTA (Light green) and after incubation with EDTA for 240 min using higher increments 64 (Pink). 900  $\mu\text{M}$  EDTA was incubated with 450  $\mu\text{M}$  of  $^{15}\text{N}$ -labelled Zur protein in 20 mM ammonium bicarbonate at 308 K, 10%  $\text{D}_2\text{O}$ , 150 mM NaCl and pH-6.2, using 32 scans. The spectra were recorded at 700.24 MHz on a Bruker Avance 700 spectrometer equipped with a cryoprobe. Insert panel highlights the chemical shift perturbation by zooming into  $[^1\text{H}, ^{15}\text{N}]$  HSQC-TROSY spectrum. Circle indicates appearing the new peaks that was not detected at lower increments 32.

Unfortunately, further structural investigations of the SynZur protein using NMR were impossible due to the overall insufficient quality of the NMR spectra, issues with intermediate exchange. It was deemed that attempting to further improve spectral quality would prove either impossible or too time consuming. Difficulties in studying metallo-repressor proteins by 2D NMR were previously described in the literature (Pecqueur *et al.*, 2006; Banci *et al.*, 2007). Only about 40% of the side chain resonances could confidently be assigned for Fur protein from *E. coli* and attempts to obtain additional structural information from  $^{13}\text{C}$ -edited NOESY spectra failed (Pecqueur *et al.*, 2006). In another study, the amide resonances for the N-terminal region

were missing (Banci et al. 2007). Pecqueur and colleagues stated the most significant changes in the 2D spectrum belonged to the C-terminal part (Pecqueur *et al.*, 2006).

## 7.2.2 Re-addition of Zinc Ions to the Zn<sub>1</sub>Zur Species

To gain further information about the ability of SynZur to sense zinc ions, and whether the dissociation into the monomer, Zn<sub>1</sub>Zur species, was reversible, the re-addition of zinc to the Zn<sub>1</sub>Zur species was investigated.

ESI-MS and NMR data for EDTA-treated SynZur indicated that half of the added EDTA was still free in solution (see Section 7.2.1.3 and Section 7.2.1.4). Hence, the addition of a stoichiometric concentration of zinc ions is required to complete the saturation of the free EDTA, and to achieve occupation of the sensory binding site in the protein. Therefore to detect conformational changes in 1D NMR, SynZur was incubated with 2 equivalents of EDTA (with respect to protein concentration) (see Section 7.2.1.4) and then 4 equivalents of zinc acetate were added anaerobically. The backbone NH regions of the resulting spectra are shown in Figure 7.16.

Interestingly, Figure 7.16 shows that zinc release from the sensory site is reversible. The re-addition of zinc ion to EDTA-treated SynZur yielded a 1D <sup>1</sup>H NMR spectrum identical to the native SynZur before incubation with EDTA. Some chemical shifts showing the effects of EDTA on SynZur and re-addition of zinc ions to the EDTA-treated SynZur are described elsewhere (see Appendix G, Table G.02).

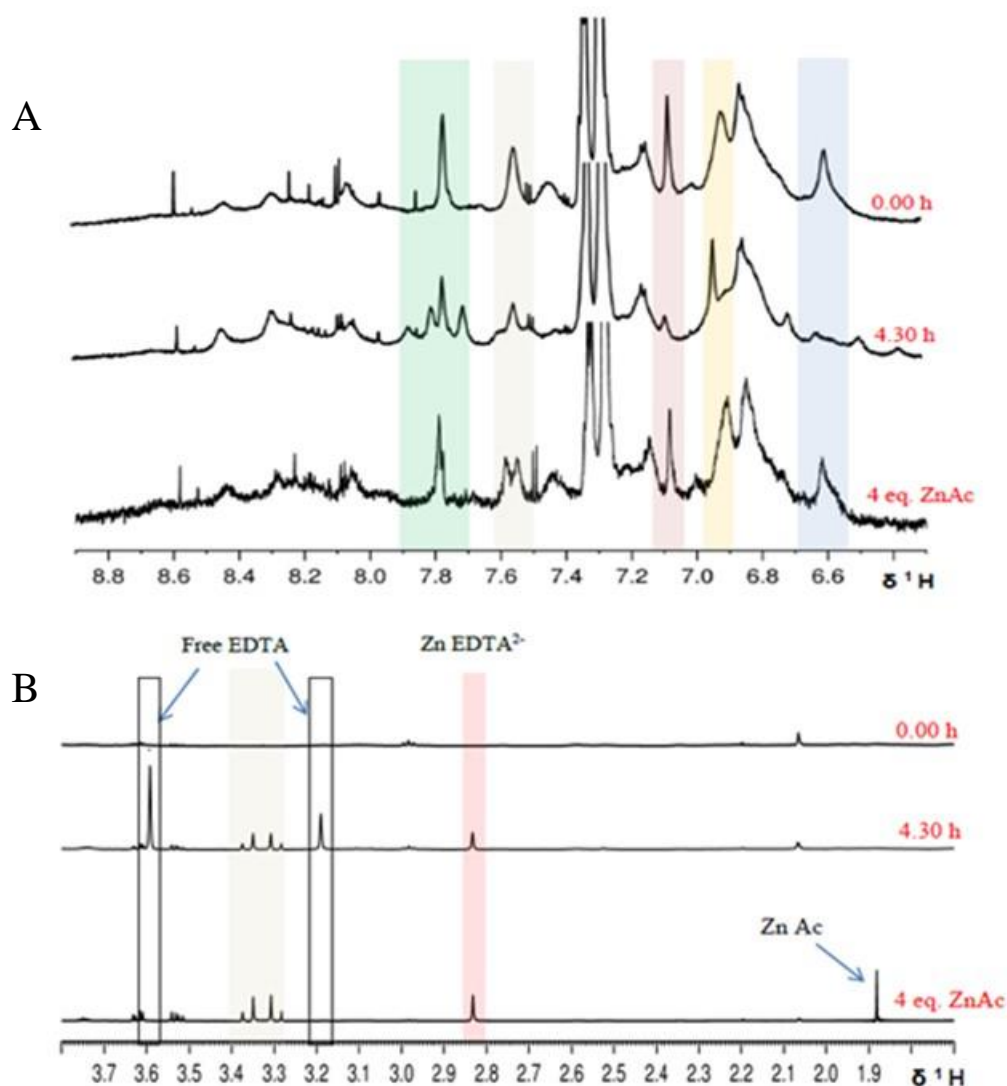


**Figure 7.16 Stacked plot of the 1D  $^1\text{H}$  NMR spectra for SynZur before and after EDTA treatment, as well as after zinc ion re-addition.**

1D  $^1\text{H}$  NMR spectra for SynZur in the fingerprint region (A), and in the aliphatic region (B), before incubation with EDTA, after incubation with 2 equivalents of EDTA for 4.30 hours, and after re-addition of 4 zinc ion equivalents. SynZur protein (600  $\mu\text{M}$ , 20 mM  $\text{NH}_4\text{HCO}_3$ , 10%  $\text{D}_2\text{O}$ , pH 7.4, 308 K) was incubated with 1.2 mM EDTA for 4.30 hours then 2.4 mM zinc acetate was added. 1D  $^1\text{H}$  NMR spectra were recorded at 700.24 MHz (Bruker Avance 700 Spectrometer). Coloured boxes show the shifting, appearance, or disappearance of peaks during incubation with EDTA and after re-addition of zinc acetate in the fingerprint region, upper panel. Empty and brown coloured boxes correspond to free and Zn(II)-bound EDTA resonances in the aliphatic region, lower panel.

This 1D  $^1\text{H}$  NMR approach gave us the ability to monitor the impact of zinc depletion not only on resonances shifting back and protein folding (Figure 7.16A), but also to observe the

saturation of the remaining free EDTA (Figure 7.16B). The two singlets associated with free EDTA, which have chemical shifts of 3.19 and 3.59 ppm were noticed to have disappeared after zinc addition. On the other hand, the intensities of the Zn(II)-bound EDTA, the AB multiplet at 3.33 ppm and a singlet at 2.83 ppm, increased (Figure 7.16B), whilst a new peak for zinc acetate appeared at 1.88 ppm. The evidence seems to indicate that the amount of zinc acetate added was sufficient to complete saturation of the remaining free EDTA, and to complete occupation of the sensory binding site in the SynZur protein.

To gain more knowledge about monomer/dimer conversion, mass spectrometry was employed. SynZur was incubated with 2 equivalents of EDTA for 24 hours (see Section 7.2.1.3), and then 4 equivalents of zinc acetate was added to the EDTA-treated SynZur,  $Zn_1Zur$  species, anaerobically. The mass spectrum after re-addition of zinc ions to the  $Zn_1Zur$  species is comparable to that of the native protein before EDTA incubation (Figure 7.17).

The new spectrum also yielded a monomer, dimer as well as a well folded dimer with  $1.9 \pm 0.4$  of Zn(II) atoms per monomer measured by ICP-OES after 15 min of zinc acetate re-addition. Remarkably, the  $Zn_1Zur$  species was returned to negligible amounts after only 15 min. This would ensure a faster response to an increase in cytosolic Zn(II) concentration.

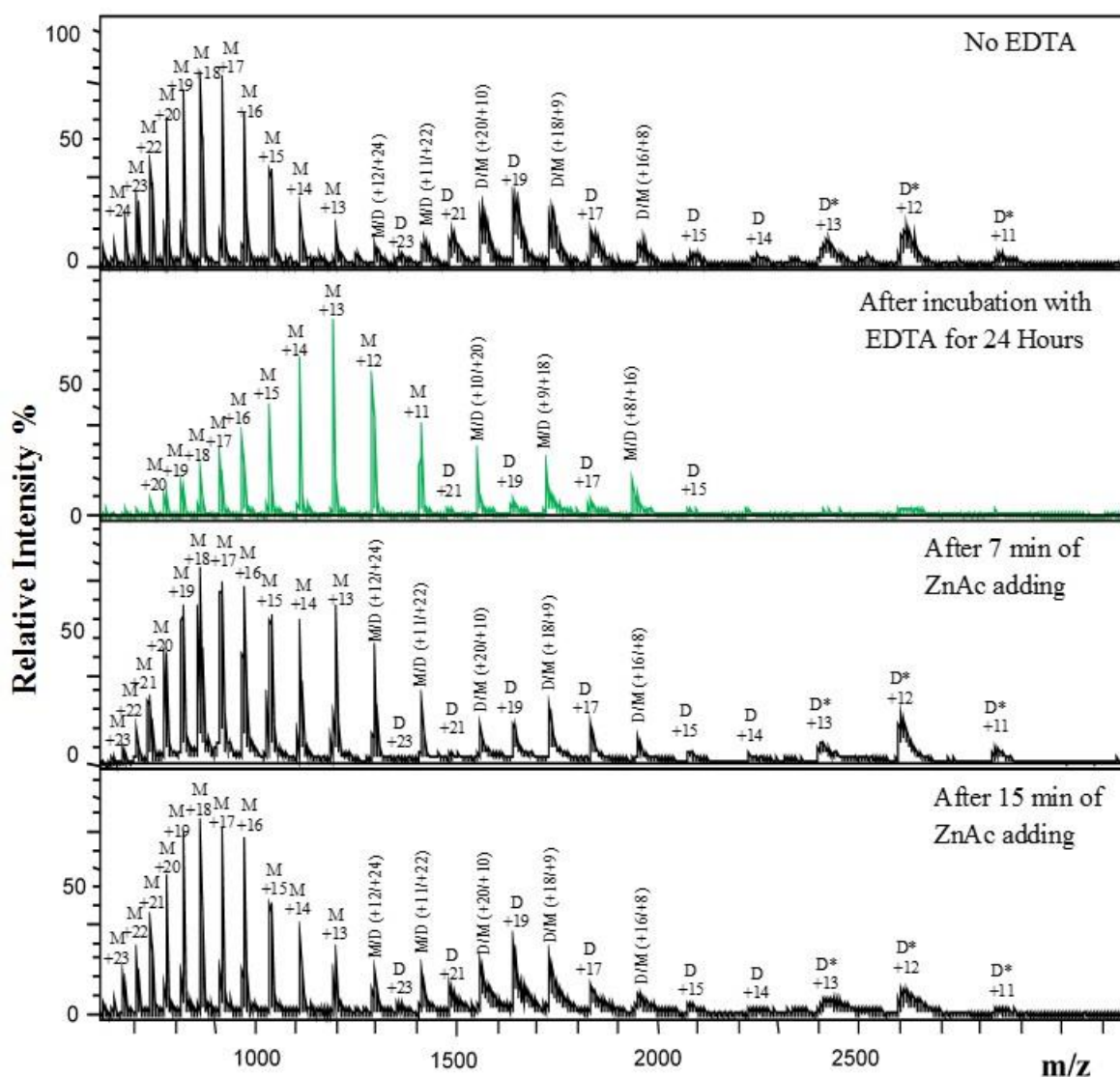


**Figure 7.17 Re-addition of zinc ions to the EDTA-treated SynZur, Zn<sub>1</sub>Zur species.**

Mass spectra for SynZur before incubation with EDTA, after 24 hours incubation with 2 equivalents of EDTA, and after re-addition of 4 equivalents of zinc acetate for 7 min and 15 min. Charge states corresponding to monomer (M), dimer (D) and compact folding dimer (D\*) are labelled. SynZur protein (32  $\mu$ M, 10 mM ammonium bicarbonate, pH= 7.8, 10% MeOH) was incubated with 64  $\mu$ M EDTA for 24 hours and then 128  $\mu$ M zinc acetate was re-added.

Furthermore, monomer/dimer conversion was deduced and +15/+19 charge states are displayed (Figure 7.18 and Figure 7.19). Before EDTA incubation, the Zn<sub>2</sub>Zur species was dominant in the monomeric state. However, after incubation with 2 equivalents of EDTA for 24 hours, the Zn<sub>1</sub>Zur species became dominant (Figure 7.18). After 7 min of adding 4 equivalents of zinc acetate, Zn<sub>2</sub>Zur was observed again as the major species in the spectrum (Figure 7.18). Whilst the relative intensity of the Zn<sub>2</sub>Zur species was around ~85% before incubation, this dropped

to ~ 28% after incubation with EDTA. After that it rose to ~ 65% upon zinc acetate addition. Moreover, the relative intensity before EDTA addition was around 15% for the  $Zn_1Zur$  species then the value increased to 60% after incubation with EDTA, then decreased to ~ 23% after addition of zinc acetate (Figure 7.18). Interestingly, in this set of experiments, the apo-Zur species was formed during incubation with EDTA at low amounts (~ 12%), this portion of the sample did not change even after re-addition of zinc acetate and remained at ~ 12%. It is possible that this fraction of the protein somehow became fully denatured and was unable to refold.

Moving to the +19 dimeric charge state, Figure 7.19 shows that after formation of  $Zn_2Zur_2$ , resulted from EDTA incubation, the  $Zn_4Zur_2$  species can be (re-)formed by Zn(II) addition. Before incubation with EDTA, the  $Zn_4Zur_2$  species was dominant. After incubation with the metal chelator, the relative intensity of the  $Zn_4Zur_2$  species was dramatically decreased to ~ 23% with the emergence of the new dominant  $Zn_2Zur_2$  species. Re-addition of zinc acetate caused the  $Zn_4Zur_2$  species to reappear with a relative intensity of ~ 88% after only 7 min, and to cause a decrease in the intensity of the  $Zn_2Zur_2$  species to ~ 12%.

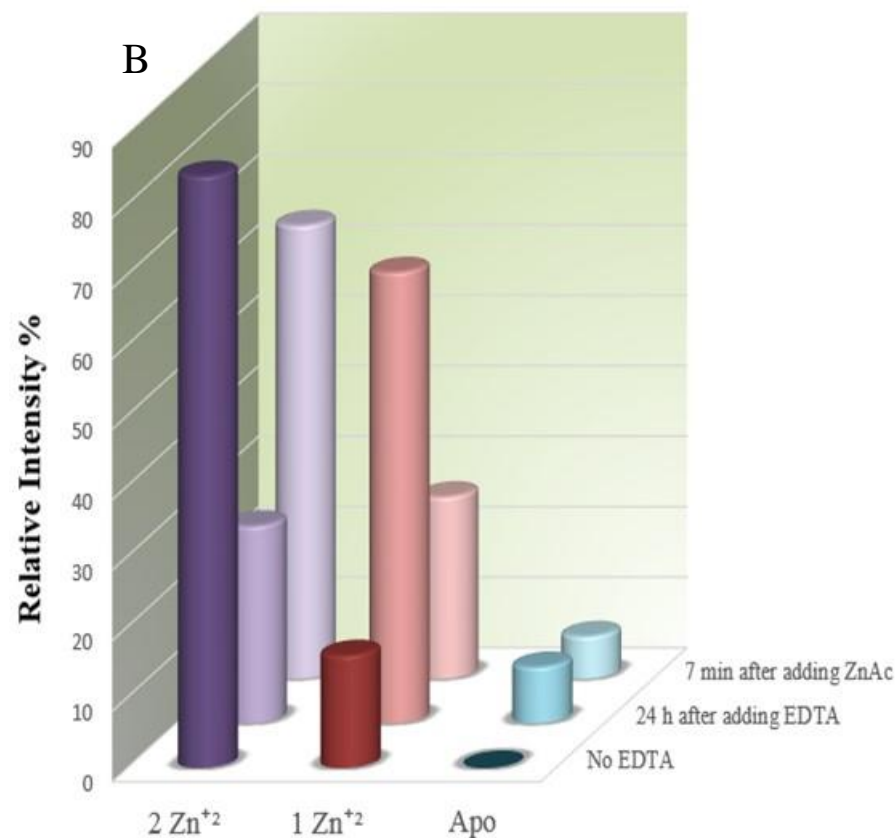
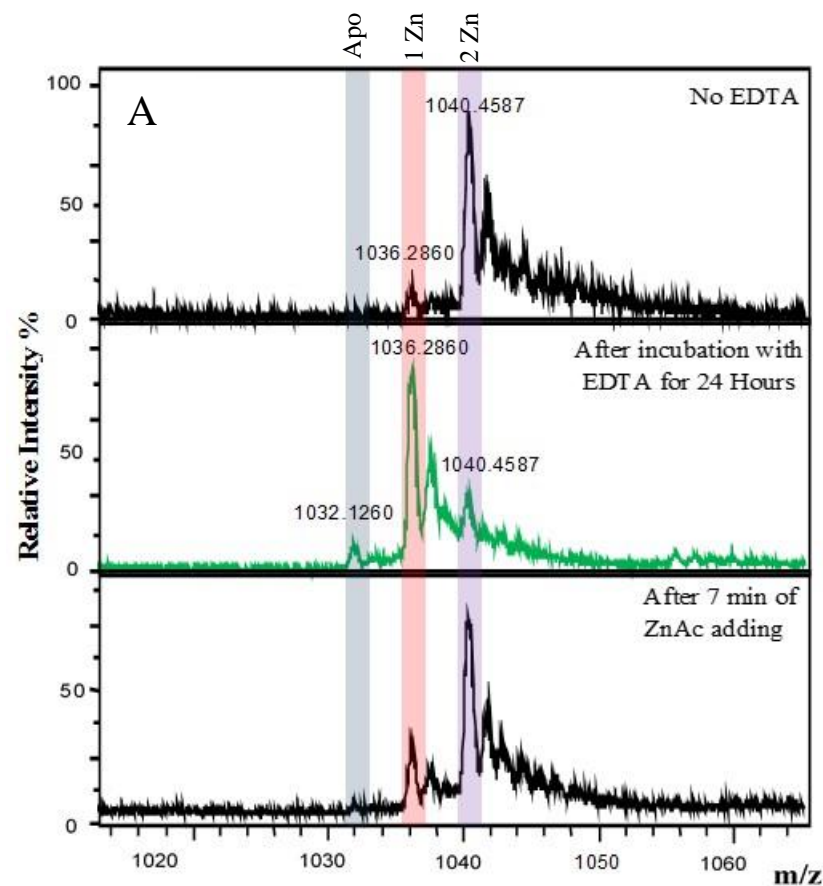


**Figure 7.18 +15 charge state of the SynZur monomer before EDTA treatment, after EDTA treatment, and after zinc ion re-addition.**

(A) The mass spectra of the +15 charge state for the monomeric SynZur before incubation with EDTA, after incubation with 2 equivalents of EDTA for 24 hours, and after re-addition of 4 zinc equivalents. SynZur protein (32  $\mu\text{M}$ , 10 mM ammonium bicarbonate, pH= 7.8, 10 % MeOH) was incubated with 64  $\mu\text{M}$  EDTA for 24 hours and then 128  $\mu\text{M}$  zinc acetate was re-added. (B) Semi-quantitative plot of metallo-species from the SynZur protein after incubation with EDTA and re-addition of zinc acetate. The relative abundance of each species was estimated from the intensity as a percentage of total intensity. The species are colour-coded as follows: Purple = 2 Zn(II), Pink = 1 Zn(II), Cyan = Apo.

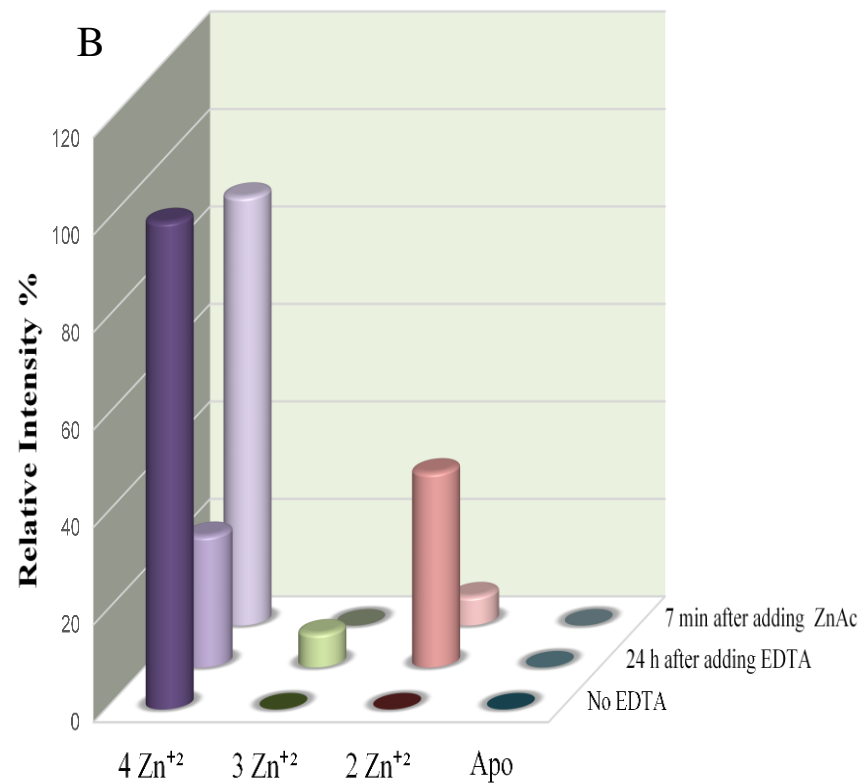
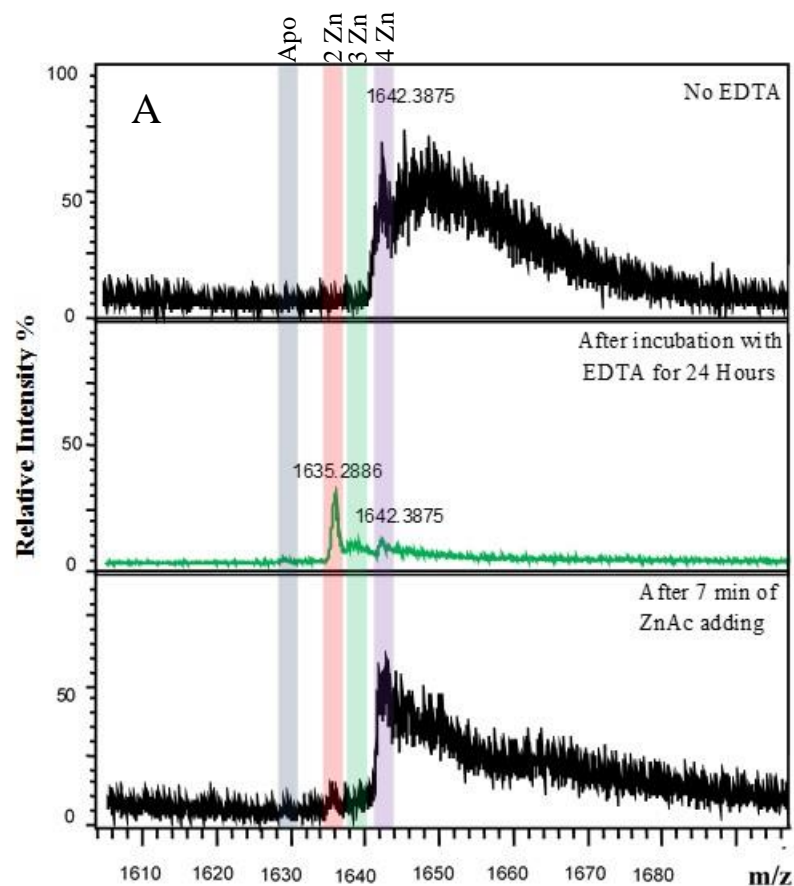


**Figure 7.19 +19 charge state of the SynZur dimer before EDTA treatment, after EDTA treatment, and after zinc ion re-addition.**

(A) The mass spectra of the +19 charge state for the dimeric SynZur before incubation with EDTA, after incubation with 2 equivalents of EDTA for 24 hours, and after re-addition of 4 zinc equivalents. SynZur protein (32  $\mu$ M, 10 mM ammonium bicarbonate, pH= 7.8, 10 % MeOH) was incubated with 64  $\mu$ M EDTA for 24 hours and then 128  $\mu$ M zinc acetate was re-added. (B) Semi-quantitative plot of metallo-species from the SynZur protein after incubation with EDTA and re-addition of zinc acetate. The relative abundance of each species was estimated from the intensity as a percentage of total intensity. The species are colour-coded as follows: Purple = 4 Zn(II), Green = 3 Zn(II), Pink = 2 Zn(II), Cyan = Apo.

Figure 7.18 and Figure 7.19 reveal the fact that the majority of the metallo-species within the SynZur spectrum after zinc ion re-addition are for  $Zn_2Zur$  (15591.7 Da) in the monomeric state and  $Zn_4Zur_2$  in the dimeric state (31184.9 Da). All experiments in this part of the study were run under anaerobic conditions, differences of  $\sim 1.6$ - $1.4$  Da between the observed and the theoretical masses were observed (see Section 5.7.4), which may indicate some degree of oxidation. Nevertheless, the evidence seems to be strong that zinc removal from the sensory site is fully reversible, and relatively rapid.

Ma and colleagues have proposed a stepwise activation of the Zur protein from *Bacillus subtilis* (Ma *et al.*, 2011). The  $Zn_2Zur_2$  species will be activated to an asymmetric dimer,  $Zn_3Zur_2$ , with moderate DNA binding activity and finally to the fully zinc-loaded protein, a high affinity DNA-binding species  $Zn_4Zur_2$  (Ma *et al.*, 2011). However, during the re-addition of zinc ions, no significant amount of the  $Zn_3Zur_2$  species was observed ( $\sim 7\%$  in our data Figure 7.19), therefore, our data do not support their hypothesis.

Although work by Patzer and Hantke supported the hypothesis that dimerization is independent of metal ions in the Zur protein from *E. coli* (Patzer & Hantke, 2000), our results, together with other studies (Althaus *et al.*, 1999; Pecqueur *et al.*, 2006; D'Autréaux *et al.*, 2007), did not support this hypothesis. The free zinc concentration required to activate Zur has been measured *in vitro* as  $2.0 \times 10^{-16}$  (Outten & O'Halloran, 2001). Re-addition of zinc ions to the monomer species (treated with EDTA) for the Fur protein from *E. coli* led to formation of the dimers in  $<10$  min using size exclusion chromatography whereas the newly formed dimer was identical to the native dimeric protein (Pecqueur *et al.*, 2006; D'Autréaux *et al.*, 2007). Althaus and colleagues pointed out that addition of excess zinc ions to  $Zn_1Zur$  yielded a dimer with four zinc atoms per dimer (Althaus *et al.*, 1999). Meanwhile, the data presented in this section supports the idea that the presence of zinc ions in the sensory site helps dimerization and re-establishes the monomer-dimer equilibrium.

Finally, data reported in this section indicates that zinc binding to SynZur in two sites is more than just an artefact of the purification procedure of SynZur, whilst zinc in structural site 1 is a “resting state” of the protein. Structural site 1 and sensory site 2 have different dynamic properties where one site is accessible to EDTA (labile), but the other is not. Zinc ions in the sensory site may be ligated with four residues (Asp-77, His-79, Cys-95, His-115) (see Section 6.5.1), thus, re-binding zinc ion to the  $Zn_1Zur$  species will lead to dimerization and conformational change that leads, in principle, to an altered orientation of the DNA-binding domains in SynZur. However, removing zinc from the sensory site for SynZur is fully reversible and this results not only in re-establishment of a (2:1) Zn: protein ratio but also very similar spectra.

### 7.2.3 Hydrogen Ions as a Probe for SynZur Protein

Nyborg and Peersen stated that EDTA can bind zinc with extremely high affinity and low dissociation constant  $K_d$  of approx.  $10^{-16}$  M (Nyborg & Peersen, 2004). As results indicated in the previous section, EDTA was able to effectively remove zinc ions from the sensory site. Therefore, removal of zinc ions completely from both sites might be achieved by another method.

In general, exposing the protein to changes in pH can be a suitable method to investigate the stability and metal binding affinity. Hence, low pH, i.e. a high concentration of protons in solution, can affect the “foldedness” of proteins, protonate certain residues, and the protons can compete for interactions. At the same time, protons can also compete with the metal ions for binding sites, leading to dissociation of the metal ions from their sites. In the case of more than one metal binding site with different affinities, such as is the case with SynZur, different concentrations of protons might be needed to cause metal ion dissociation from different sites or even to cause protein unfolding.

In an attempt to investigate the effect of pH on zinc-loaded SynZur, its reactivity towards hydrogen ions was studied, and several techniques were employed.

### 7.2.3.1 Reactivity with Hydrogen Ions using UV-Visible Spectroscopy

In general, protons can compete for lone pairs of ligand atoms, causing the release of metal ions from their binding sites. The presence of zinc-sulfur bonds in SynZur can be monitored easily using UV-Visible spectroscopy by observing the characteristic ligand-to-zinc charge transfer (LMCT) bands of the Zn(II)-thiolate bonds at 220-230 nm.

Using the data obtained from the pH titration observed by UV-Visible spectroscopy, a pH of half dissociation can be calculated. The pH of half dissociation expressed as a  $pK_a$  value is defined as the pH value at half maximum UV absorbance of the respective ligand to metal-charge transfer band (Equation 7.01), where half of protein metal binding sites are occupied.

$$pK_a = \frac{1}{2}(A_{max} + A_{min}) \quad \text{Equation 7.01}$$

For determining the half-dissociation constants for SynZur, the absorbance at 220 nm was plotted against pH (Figure 7.20). From the plot, two  $pK_a$  values may be found ( $pK_{a1} = 4.8$ , and  $pK_{a2} = 6.24$ ) for SynZur. It was noticed that the protein and bound metals are stable down to pH 6.5, and then a very sudden drop in absorbance occurs between pH 6.5 and 5.7, with a further less steep drop between pH 5.5 and 4.3 (Figure 7.20). The absorbance of the first step dropped from 0.92 to 0.82 and from 0.81 to 0.71 for the second step. Unfortunately, the half-dissociation constant has not been determined for other Fur family proteins. Therefore, we were able to compare the obtained data in this section with other data from Fur family protein.

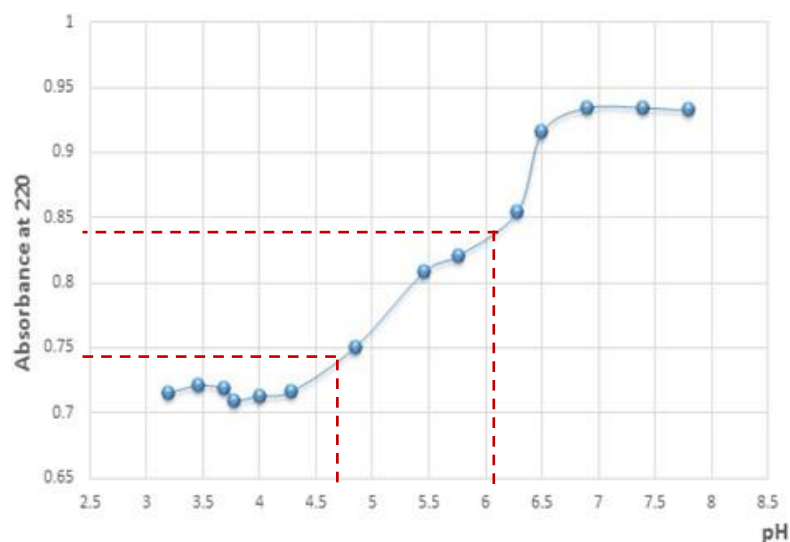


**Figure 7.20 Influence of pH on SynZur using UV-Visible spectroscopy.**

Absorbance changes at 220 nm for the Zn(II)-thiolate bond in SynZur at different pH values (7.8-3.1). Zinc-loaded SynZur (5.2  $\mu$ M, 1 mM Tris-Cl buffer, pH~7.8) was subjected to pH titration using different concentrations of hydrochloric acid. The pHs of half dissociation are displayed by the red dashed lines.

### 7.2.3.2 Reactivity with Hydrogen Ions using CD

In order to identify changes in SynZur secondary structure during the reaction with protons, CD spectroscopy was again employed (Figure 7.21).

Data in Figure (7.21A and B) illustrate that changing the pH has substantial effects on the secondary structure of SynZur. Dropping the pH from 7.8 to 6.5 did not lead to changes (data not shown) on the far UV-CD spectrum. However, dropping the pH to ~ 5.20 yielded a major effect on the secondary structure of the SynZur protein, where the intensity for both bands at 220 nm and 208 nm was decreased with more flattening in the 222 nm band. Further reduction in pH to ~3.60, caused the intensity of both bands to increase, while at pH ~ 3.15 the whole spectrum was shifted towards the lower far UV field. A dramatic shift in the CD spectrum and a lowering in intensity of both bands was observed at pH 2.71 (Figure 7.21A and B).

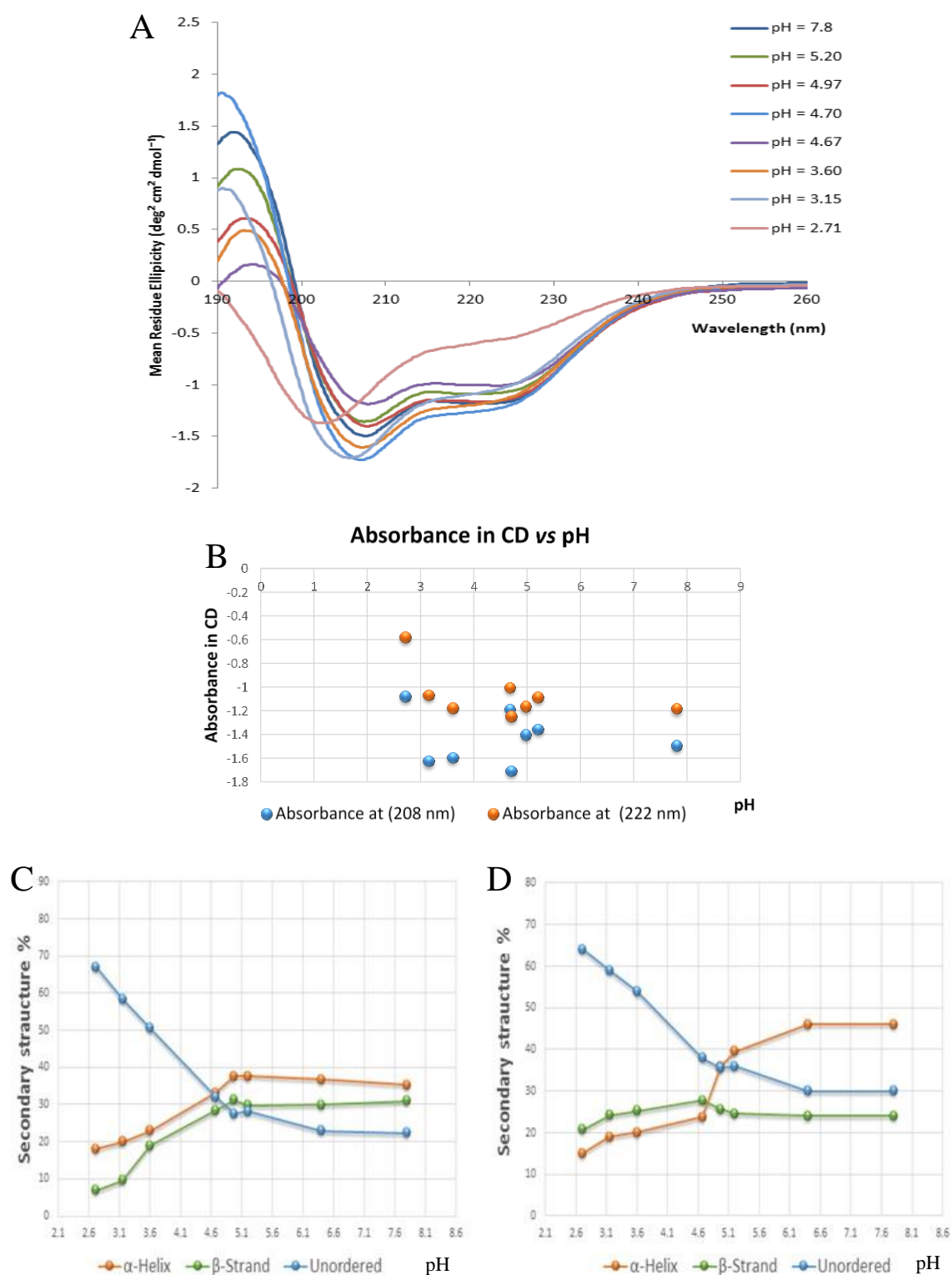


**Figure 7.21 Influence of pH on SynZur using CD spectroscopy.**

(A) Far-UV circular dichroism spectra expressed in  $\Delta\epsilon$  units (mean residue ellipticity,  $\text{deg}^2 \text{cm}^2 \text{dmol}^{-1}$ ) for SynZur recorded between 190-260 nm at pH values varying from 7.8 to 2.71. SynZur (25.9  $\mu\text{M}$ , 5 mM Tris-Cl buffer, pH~7.8) was subjected to pH titration using different concentrations of hydrochloric acid. (B) Absorbance at 208 nm and 222 nm vs pH. Prediction of secondary structure fractions for SynZur, with  $\alpha$ -helices (Orange line),  $\beta$ -strands (Green line), and unordered (Blue line) from CD spectra using (C) SELCON software from the DICHROWEB Web server (Sreerama *et al.*, 2000), and (D) RAUSSENS software from the RAUSSENS Web server (Raussens *et al.*, 2003).

Using SELCON software from the DICHROWEB Web server (Sreerama *et al.*, 2000), the compositions values measured from the deconvolution of the CD spectrum for SynZur at pH=7.8 were 35%, 33% and 22.5% for  $\alpha$ -helices,  $\beta$ -strands and unordered, respectively (Figure 7.21C). After decreasing the pH to  $\sim 5.2$ , changes were noted in the secondary structure composition, where  $\alpha$ -helices were slightly increased to 39%,  $\beta$ -strands remained at 33%, and unordered increased to 27%. Dramatic changes were observed by dropping the pH to 2.71, where the compositional fractions were 17.2%, 8.7%, and 68.7% for  $\alpha$ -helices,  $\beta$ -strands and unordered, respectively. The same observations were also noted using RAUSSENS software from the RAUSSENS Web server (Raussens *et al.*, 2003) (Figure 7.21D). The composition values measured from the deconvolution of the CD spectrum for SynZur at pH=7.8 were 45%, 17.5% and 34.2% for  $\alpha$ -helices,  $\beta$ -strands and unordered, respectively (Figure 7.21D). After dropping the pH to  $\sim 2.71$ , the composition fractions were 14.4%, 20.4% and 63.1% for  $\alpha$ -helices,  $\beta$ -strands and unordered, respectively.

It is clear therefore that dropping the pH and releasing zinc ions from their sites have effects both on the secondary structure and the foldedness of the SynZur protein.

### 7.2.3.2 Reactivity with Hydrogen Ions by NMR

To gain mechanistic insights into the nature of proton attack on the SynZur protein, 1D  $^1\text{H}$  NMR spectra were recorded at various pH values. The effect of protons on protein folding is illustrated in Figure 7.22.

At high and neutral pH, the SynZur protein is folded and shows both sharp and broad peaks in the down- and up-field regions (Figure 7.22). Using the optimised conditions for NMR (see Section 6.3) with acidic conditions at pH 4.60, more peaks appeared with sharper resonances in the down-field region which may be due to the unfoldedness of the protein (Figure 7.22A).

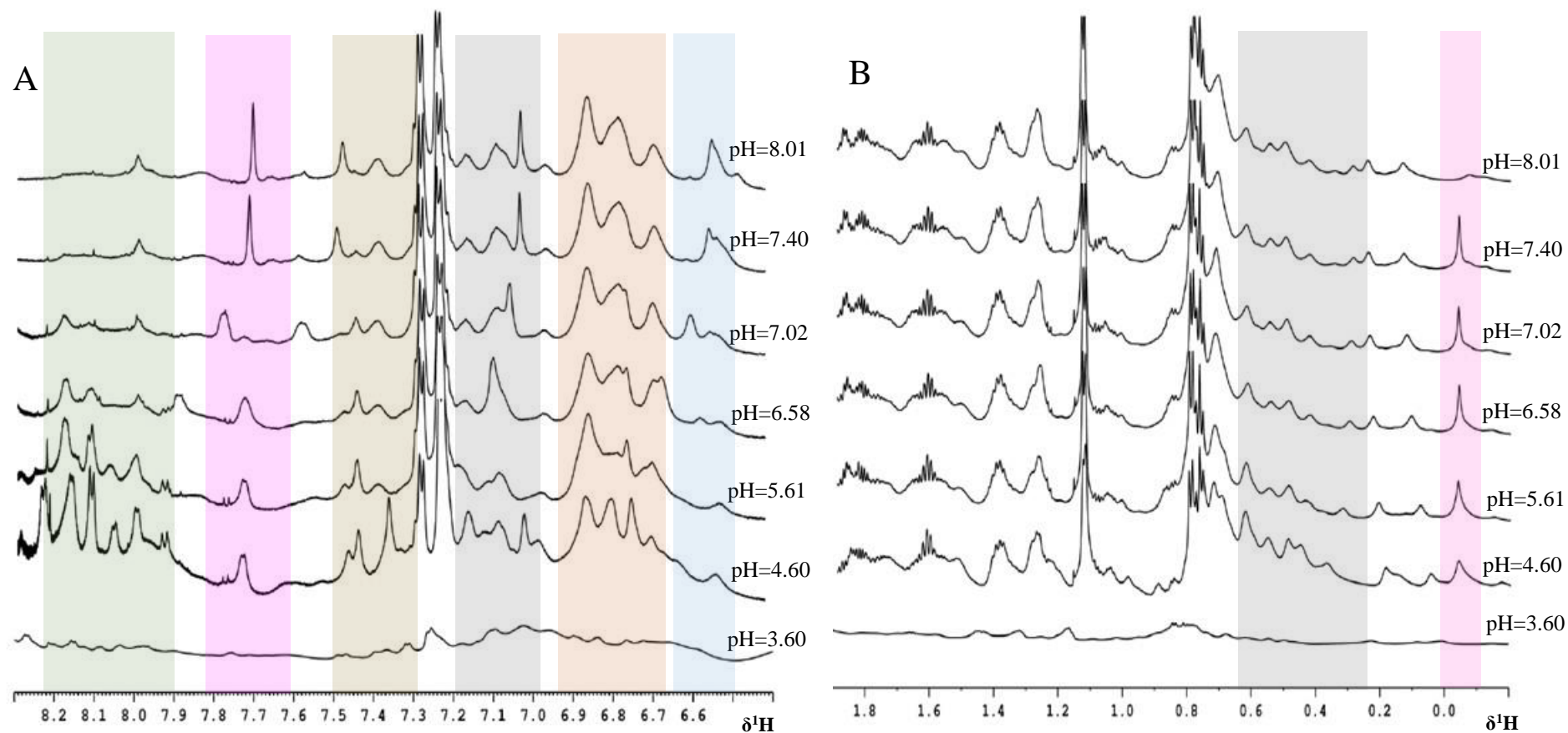


**Figure 7.22 Monitoring the influence of pH on SynZur by 1D  $^1\text{H}$  NMR.**

1D  $^1\text{H}$  NMR spectra acquired at different pH values for zinc-loaded SynZur in the finger print region (A), and aliphatic region (B). SynZur protein (600 mM, 20 mM  $\text{NH}_4\text{HCO}_3$ , 10%  $\text{D}_2\text{O}$ , pH 8.01, 150 mM NaCl, 308 K) was subjected to pH titration using different concentrations of hydrochloric acid and the spectra were recorded at 700.24 MHz on a Bruker Avance 700 Spectrometer. The pH values at each point are shown for each spectrum. Coloured boxes show the shift, appearance, or disappearance of peaks during the pH titration.

On the other hand, no significant changes in the up-field region were observed (Figure 7.22B). The evolution of more signals appearing at lower pH is most likely due to the more favourable exchange regimes imposed on the backbone protons under this condition. Upon further reduction in pH to 3.60, no protein was found and some aggregation was noticed in the solution. Further chemical shifts assessing the effect of protons on SynZur are displayed in Appendix G and Table G.03.

These results seem to indicate that SynZur was at least partially folded until pH 4.60, then became aggregated at pH 3.60. A similar observation was also made for Fur from *Anabaena* PCC 7119, where a one-dimensional NMR experiment indicated that Fur protein was folded at pH 4 with some aggregation (Hernandez *et al.*, 2002).

### 7.2.3.3 Reactivity with Hydrogen Ions using ESI-MS

To better understand the role of protons on monomer/dimer conversion during proton competition, and also to identify the most abundant metallo-species at different pH values, mass spectrometry was used. The mass spectra obtained for SynZur at a range of pH values (8.01 - 4.25) provides clear evidence of the protein's reactivity with protons and zinc release from its binding sites (Figure 7.23).

At pH ~8.01, as normal, the oligomeric protein was present as a monomer, dimer and compact folding dimer (Figure 7.23). No difference in the SynZur spectrum was noted at pH 7.80. Interestingly, at pH ~ 6.97, the proportion of monomer/dimer was observed to shift toward the dimeric state and surprisingly, this shifting was even more pronounced at pH ~ 5.61 (Figure 7.23). At pH ~ 5.61, it was obvious that the dimeric state was more dominant in the spectrum. Whilst this phenomenon is highly unexpected, there is some precedent in the literature. Early in 2007, it was stated that the oligomerization state of the *E. coli* Fur protein was sensitive to pH (D'Autréaux *et al.*, 2007). At low pH the protein favoured formation of higher-order

oligomers (D'Autr aux *et al.*, 2007). The strong influence of pH on oligomerization can have its origin in protonation, causing neutralization of repulsive charges or leading to additional attractive forces (D'Autr aux *et al.*, 2007). However, upon further reduction to pH 5.45 and pH 4.25, a new species was observed (Figure 7.23).

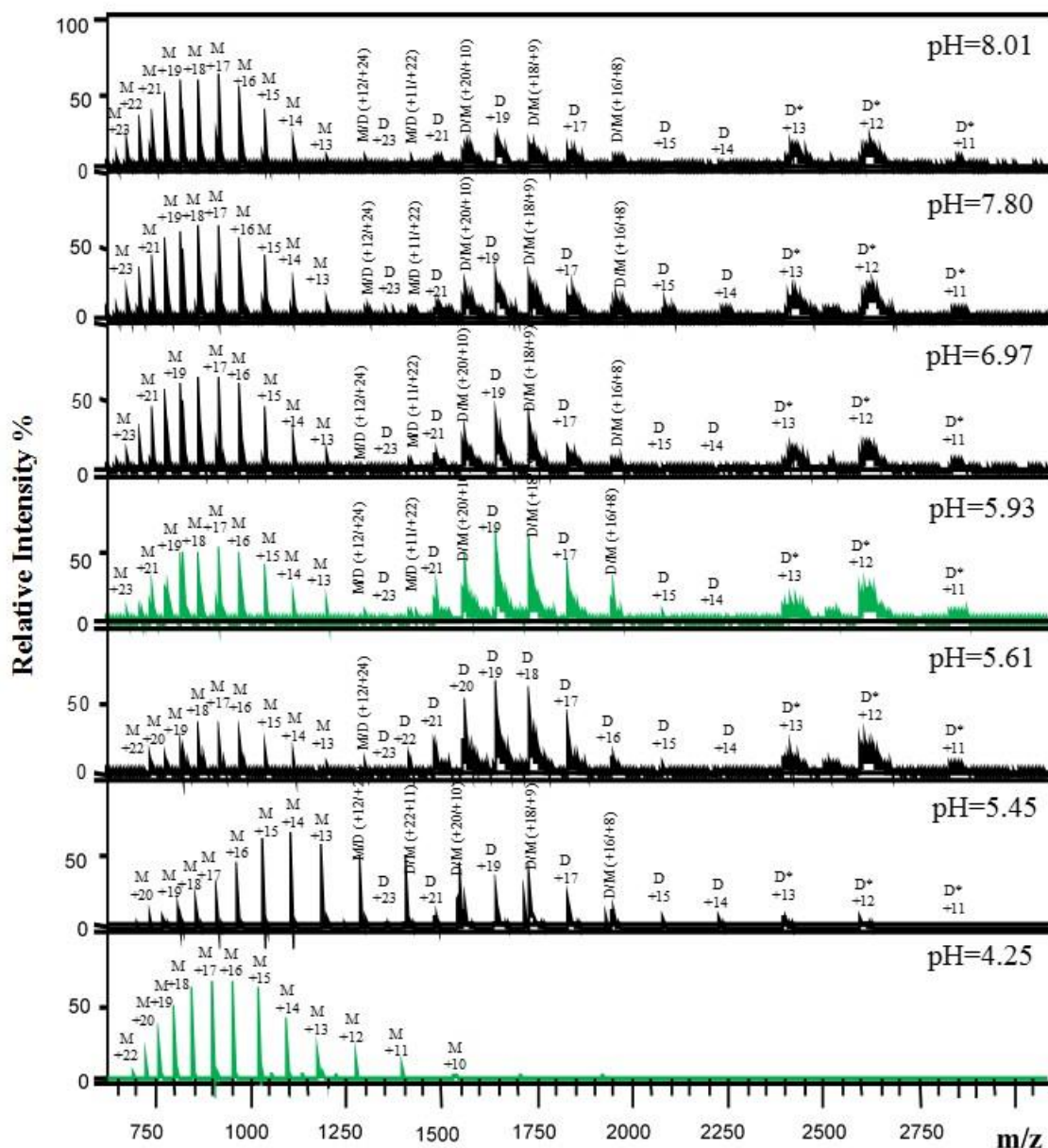


**Figure 7.23 Monitoring the influence of pH on SynZur using ESI-MS.**

Mass spectra for SynZur recorded at different pH values. Charge states corresponding to monomer (M), dimer (D) and compact folding dimer (D\*) are labelled. SynZur protein (35  $\mu$ M, 10 mM ammonium bicarbonate, pH~8.01, 10% MeOH) was subjected to pH titration using different concentrations of hydrochloric acid.

To gain more insights about metal speciation of monomer/dimer conversion and the new species, again one single monomeric charge state, +15 M, and one single dimeric charge state, +19 D, were chosen to visualize the effect of pH on SynZur and the data are displayed in qualitative and semi-quantitative plots (Figure 7.24 and Figure 7.25).

Initially, the relative percentage of  $Zn_2Zur$  and  $Zn_1Zur$  at pH 8.01 was 85% and 15%, respectively (Figure 7.24). The abundance of both species was unchanged upon dropping the pH to 7.80. Upon further reduction to pH 6.97, the relative percentages of  $Zn_2Zur$  and  $Zn_1Zur$  species were slightly decreased. Significant changes were observed at pH 5.93, where the relative percentage of  $Zn_2Zur$  dropped to 55% with an increase in the  $Zn_1Zur$  species to 33% and the emergence of the apo-SynZur species to 12%. Upon further reduction in pH to 5.61, the relative percentage of the  $Zn_2Zur$  species dropped to 31% but with a remarkable decrease in the  $Zn_1Zur$  species to 5% and an increase in the apo-Zur species to 64% at the same time. Dropping the pH from 5.61 to 5.45 and then to 4.25, resulted in a complete disappearance of the  $Zn_2Zur$  and  $Zn_1Zur$  species with the apo-SynZur species then dominating (Figure 7.24).

Turning to the dimeric state, around pH 8.01 the  $Zn_4Zur_2$  species was dominant, with the relative percentage approximately 100% (Figure 7.25). After a reduction in pH to 7.80 and 6.97, no changes were observed. Reduction in pH to 5.93,  $Zn_4Zur_2$  species was still observed with an emergence of the  $Zn_2Zur_2$  and apo-SynZur species ~ 7%. Upon acidification to pH 5.61,  $Zn_4Zur_2$  was still the most dominated one in the spectrum, and the apo-SynZur species increased to 20% (Figure 7.25). Further dropping in pH to 5.45, the relative intensity of  $Zn_4Zur_2$  dropped to ~ 55% with an increase of the apo-SynZur to ~ 43%. Finally, dropping the pH to 4.25, led to the total disappearance of  $Zn_4Zur_2$  with the apo-SynZur species then dominating (Figure 7.25).

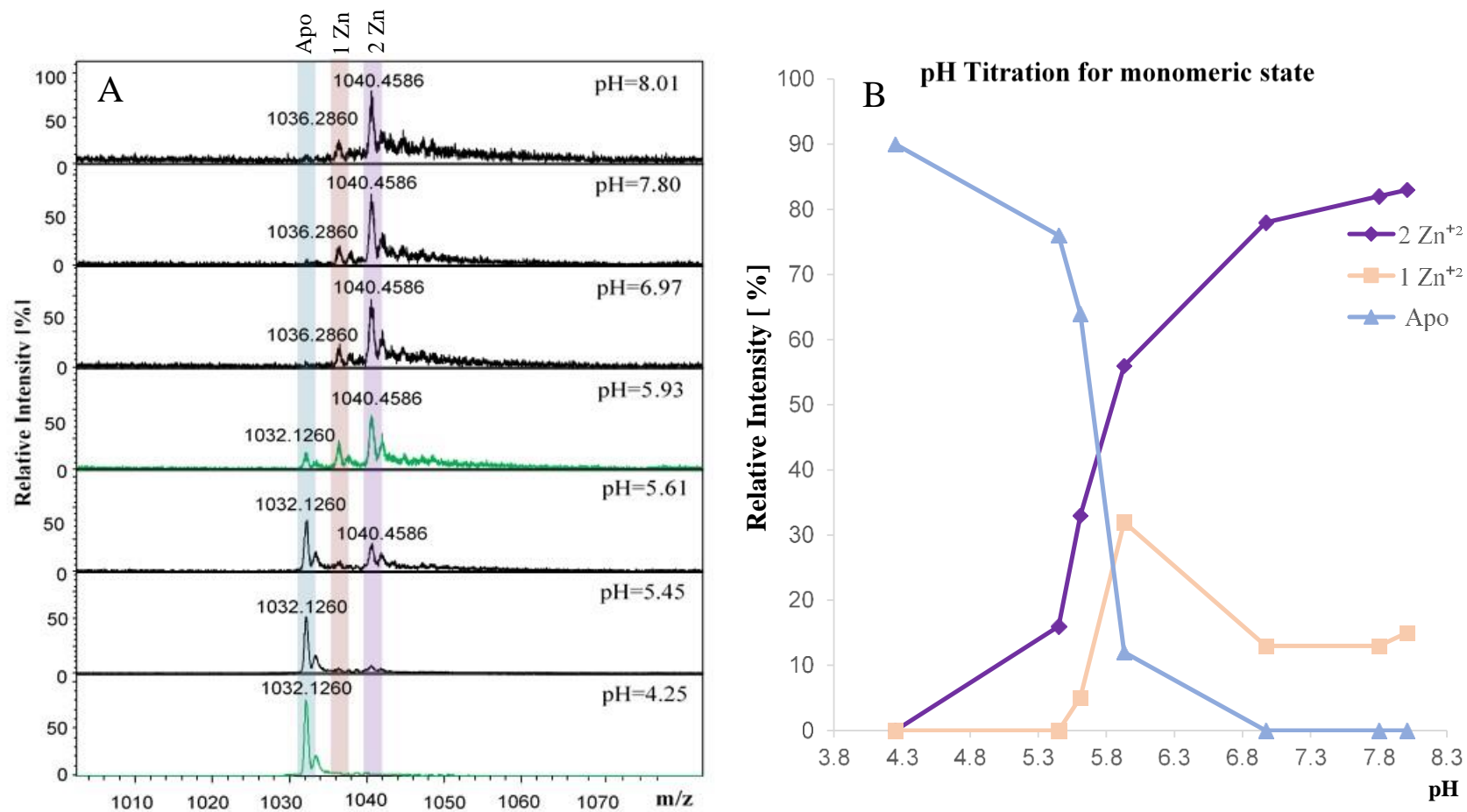


**Figure 7.24 The speciation of the +15 charge state for monomeric SynZur during pH titration.**

(A) Mass spectra of the +15 charge state from monomeric SynZur recorded at various pH values. SynZur protein (35  $\mu$ M, 10 mM ammonium bicarbonate, pH~8.01, 10 % MeOH) was subjected to pH titration using different concentrations of hydrochloric acid. (B) Semi-quantitative plot for metallo-species from SynZur protein during pH titration. The relative abundance of each species was estimated from the intensity as a percentage of total intensity. The species are coloured as follows: Purple =2 Zn(II), Pink= 1 Zn(II), Cyan = Apo.

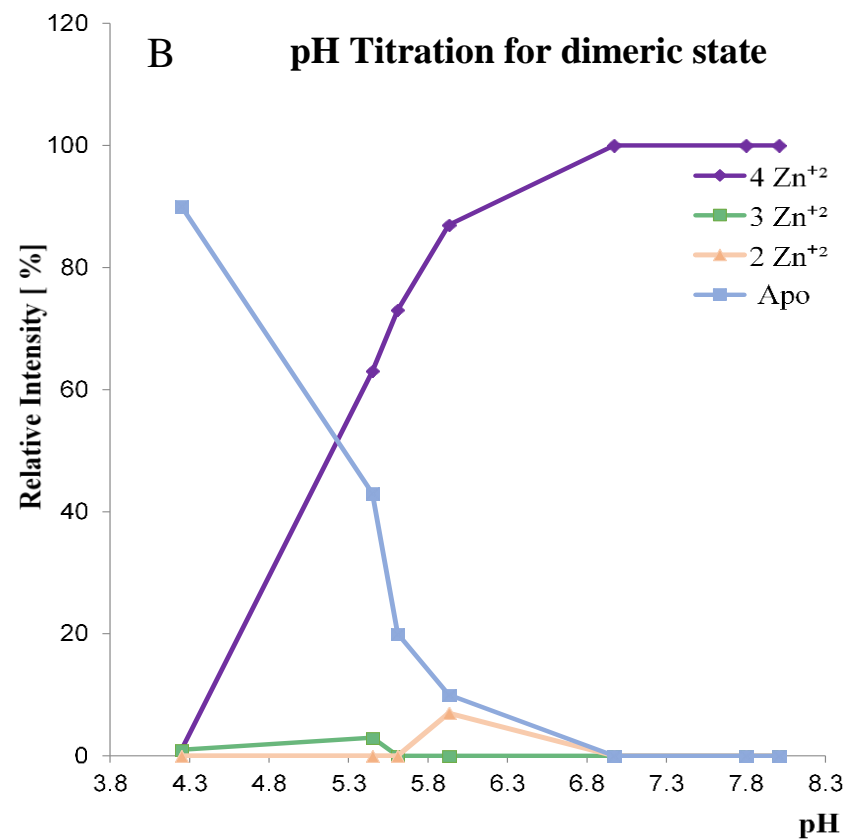
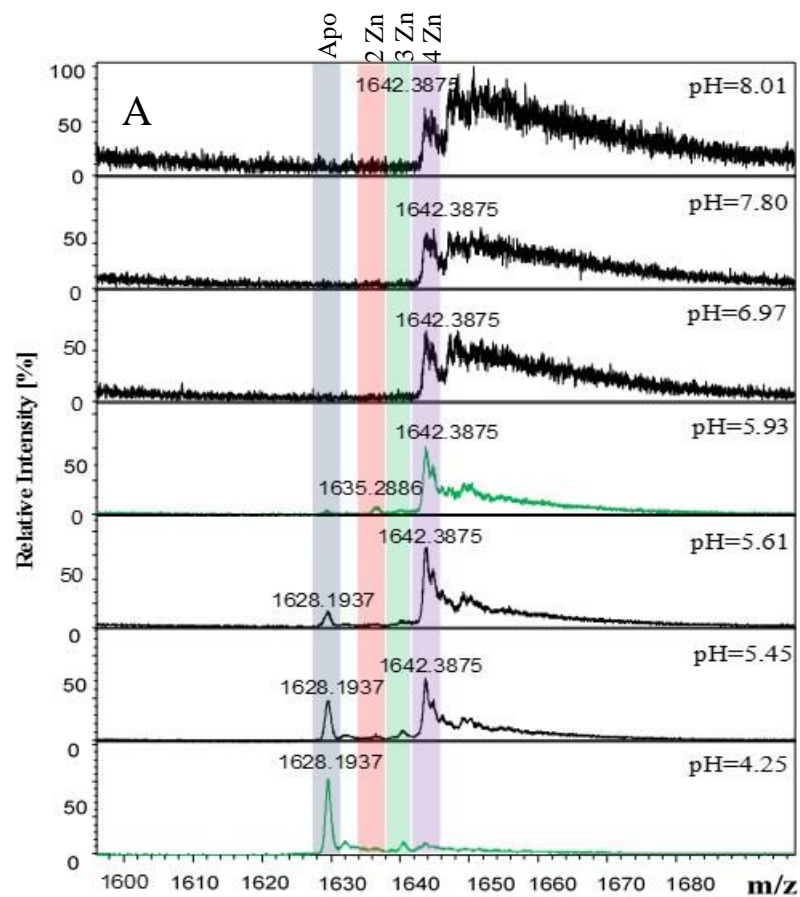


**Figure 7.25 The speciation of the +19 charge state for dimeric Zur during pH titration.**

(A) Mass spectra of the +19 charge state from dimeric SynZur recorded at various pH values. SynZur protein (35  $\mu$ M, 10 mM ammonium bicarbonate, pH~8.01, 10 % MeOH) was subjected to pH titration using different concentrations of hydrochloric acid. (B) Semi-quantitative plot for metallo-species from SynZur protein during pH titration. The relative abundance of each species was estimated from the intensity as a percentage of total intensity. The species are coloured as follows: Purple = 4 Zn(II), Green = 3 Zn(II), Pink = 2 Zn(II), Cyan = Apo.

These results show that a lower pH can remove zinc ions from both monomeric and dimeric species. The most exciting observation is the stability of the  $Zn_4Zur_2$  species at low pH  $\sim 5.45$ . Comparing the monomer with the dimer at pH 5.93, the  $Zn_1Zur$  species, present in the monomeric state, looks more stable than  $Zn_2Zur_2$  which is present in negligible amounts in the spectrum while  $Zn_2Zur$  and  $Zn_4Zur_2$  were both abundant at this pH. Dropping the pH to 5.61 resulted in a small amount of apo-SynZur from the dimeric state while apo-SynZur from the monomeric state is most dominant in this spectrum. Further dropping the pH to 5.45 showed the  $Zn_4Zur_2$  species was still dominant in the dimeric spectrum, while  $Zn_2Zur$  had vanished from the spectrum suggesting that the dimeric state is perhaps more stable than the monomeric state under this condition. Upon acidification to pH 4.25, all zinc ions were stripped from the monomer and dimer states with apo-Zur the dominating species in the spectrum. These data are in good agreement with those for the Zur protein from *E. coli*, where zinc ions in the Zur protein could be totally stripped at pH 4.8 (Althaus *et al.*, 1999).

On this basis, it could be concluded that a lower pH, less than 4.25, can efficiently release zinc from both sites of the SynZur protein resulting in a reduced proportion of  $\alpha$ -helices and  $\beta$ -strands with increasing the unordered composition. These results lead us to propose that the zinc ion in structural site 1,  $Zn_{Cys_4}$ , plays an important role in maintaining the foldedness of the protein and, hence, loss of this metal leads to aggregation of the protein.

### 7.3 Summary and Conclusion

While the precise metal binding characteristics of Fur family proteins remains controversial, the work described in this chapter provides the first insight into structural changes upon zinc release and re-binding in a Zur protein from a marine cyanobacteria, *Synechococcus* sp. WH8102.

Our results indicate that zinc binding to SynZur in two sites is more than an artefact of the purification procedure, and zinc in structural site 1 is in a “resting state” in the protein. SynZur as purified typically contains  $2.1 \pm 0.2$  of Zn(II) atom per monomer; however, treating SynZur protein with a strong Zn(II) chelating agent such as EDTA resulted in efficient removal zinc ions from one site, the regulatory site, giving  $0.9 \pm 0.3$  Zn(II) atoms per monomer. Surprisingly, during incubation with EDTA, the monomer/dimer equilibrium was shifted towards the monomeric state and the  $Zn_1Zur$  species was the most dominant one in the spectrum. Moreover, ESI-MS and NMR data indicate that  $Zn_1Zur$  species was stable for long time. Adding back zinc ions to the EDTA-treated SynZur,  $Zn_1Zur$  species, yielded a comparable spectra in NMR and ESI-MS to the native one in less than 15 min, indicating a fast response of *Synechococcus* sp. WH8102 Zur protein to an increase in cytosolic Zn(II) concentration. The new spectrum also displayed monomer, dimer and a well-folded dimer form containing  $1.9 \pm 0.4$  Zn(II) atoms per monomer (using ICP-OES measurements).

The slight changes observed in CD spectra upon incubating SynZur protein with EDTA were due to the zinc releasing from sensory site and changing in the oligomer distribution, monomer/dimer conversion, but not due to the changes in the secondary structure compositions for SynZur protein. This, sequentially, indicates that no large difference in the secondary structure between the metallo-species of the SynZur protein, i.e. the  $Zn_2Zur$ / $Zn_1Zur$  species of the monomer and the  $Zn_4Zur_2$ / $Zn_2Zur_2$  species of the dimer.

Although, EDTA could effectively remove zinc ions from the sensory site, the removal of zinc ions completely from both sites required dropping in pH. Moreover, the interesting view which was noted during the dropping in pH is the proportion of monomer/dimer which was shifted toward the dimeric state at lower pH  $\sim 6.97$ - $5.61$  and  $Zn_4Zur_2$  species was the most dominant one in the spectrum, suggesting that the dimeric state is perhaps more stable than the monomeric state under lower pHs. Upon dropping in pH to 4.25, all zinc ions were stripped from the

monomeric and dimeric states with apo-Zur the dominating species in the spectrum. Several lines of evidence lead us to propose that the zinc ion in structural site 1, plays an important role in maintaining the foldedness of the protein.

While the results presented in this study give some interesting insights regarding the SynZur protein, they are, due to difficulties with the NMR experiments, not comprehensive and further work is required to achieve deeper insights into the mechanisms of zinc release from the sensory site. It would be desirable to attempt further optimisations of NMR conditions, which ultimately might allow sequential assignments for multidimensional NMR studies, and to enable conclusive chemical shift perturbation experiments.

# Chapter 8

## Identification of Target Genes for the SynZur Protein

---

### 8.1 Introduction

Zur is a member of the Fur family (Gilston *et al.*, 2014; Sein-Echaluce *et al.*, 2014), regulating zinc homeostasis, which although well characterized in a variety of bacteria has received little attention in cyanobacteria so far. The high degree of conservation between different members of the Fur family and the presence of multiple homologues per genome complicates the determination of the DNA binding specificity of these proteins from sequence data alone.

Based on our results, the SynZur protein, encoded by the *synw\_2401* gene from *Synechococcus* sp. WH8102, plays an important role in zinc sensing (see Chapter 7) and hence may maintain intracellular zinc homeostasis in this cyanobacterium. Zur usually binds to the promoter of the *znuABC* genes that encode a high-affinity zinc uptake system comprising the ZnuB channel, the ZnuC ATPase component, which provides the energy necessary for Zn(II) ion transport through the inner membrane, and ZnuA, a soluble protein that captures Zn(II) in the periplasm with high efficiency and delivers it to ZnuB (Patzner and Hantke, 1998) (Figure 8.01). In principle, as zinc levels increase, the Zur protein directly ‘senses’ the concentration of intracellular zinc ions, which in turn influences its ability to bind to DNA and repress target

gene expression. On the other hand, when zinc levels decrease, the Zur proteins directly repress their target genes.

The ZnuABC transporters have been studied in a number of bacteria, including *Escherichia coli* (Patzner & Hantke, 1998; Chandra *et al.*, 2007), *Streptococcus pneumoniae* (Dintilhac & Claverys, 1997), *Salmonella enterica* (Campoy *et al.*, 2002) and *Yersinia pestis* (Desrosiers *et al.*, 2010), in addition to cyanobacteria such as *Synechococcus* sp. PCC7942 (Phung *et al.*, 1994), *Nostoc punctiforme* (Hudek *et al.*, 2013a), *Synechocystis* sp. PCC6803 (Tottey *et al.*, 2012), and *Anabaena* sp. PCC 7120 (Napolitano *et al.*, 2012).

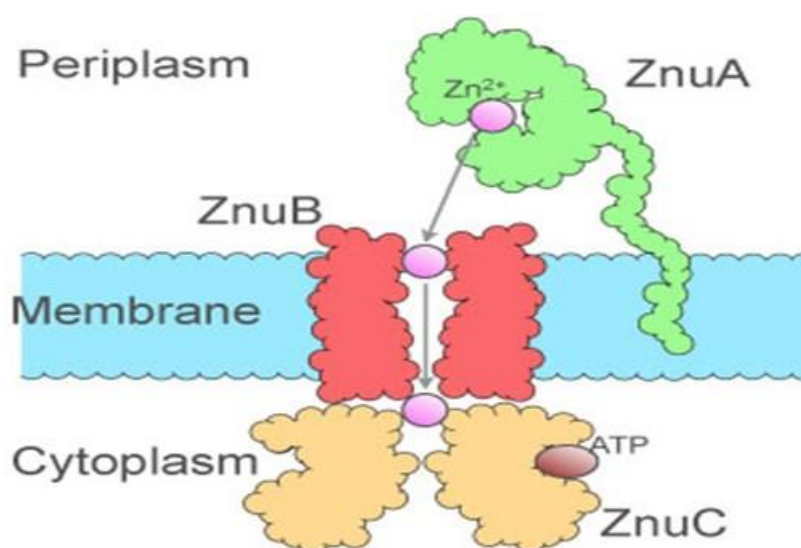


**Figure 8.01 The Zn(II)-uptake transporter, ZnuABC system.**

Znu transporters belong to cluster 9 of the ABC family and mainly transport metal ions. These transporters consist of an ATP-binding protein (ZnuC), a permease (ZnuB) and a plasma membrane or periplasmic substrate-binding protein (ZnuA), usually all encoded at the same locus. The soluble binding protein (ZnuA) associates with its substrate in the periplasm for delivery to the cognate membrane-permease (ZnuB) thus facilitating import *via* ATP-hydrolysis (ZnuC). Taken from (<https://www.danforthcenter.org/scientists-research/principal-investigators/thomas-smith/projects/zinc---znu>).

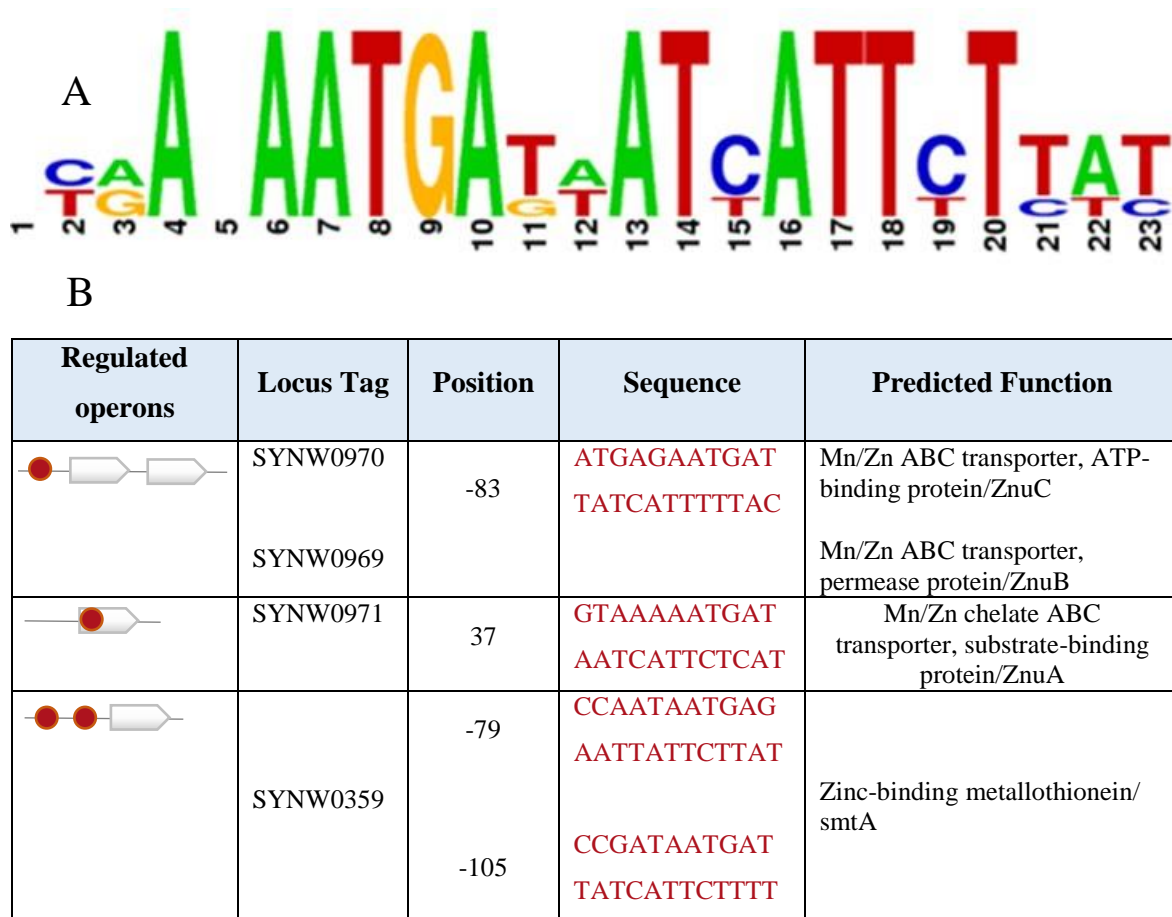


**Figure 8.02 Zur boxes in *Synechococcus* sp. WH8102.**

(A) Logo consensus sequence of the four predicted Zur boxes from the *Synechococcus* sp. WH8102 genomes (Novichkov *et al.*, 2009). (B) The table indicates the four predicted Zur boxes in the *Synechococcus* sp. WH8102 genome with the location, sequence and predicted function of these genes indicated.

During the last ten years a number of advances have been made in the identification of Zur regulons in cyanobacteria (Novichkov *et al.*, 2009; Napolitano *et al.*, 2012). Bioinformatic prediction of Zur-binding motifs in *Synechococcus* sp. WH8102 has indicated the presence of three Zur boxes in the RegPrecise database (Figure 8.02A): two Zur boxes for a *znuABC* system (one for *znuA* and another for *znuC*) and, surprisingly, two boxes for *smtA*, a metallothionein protein. These latter two boxes for *smtA* will be termed Zur box-1 and Zur box-2 in this study (Figure 8.02B). Also, the *znuA* and *znuC* promoters reside in the same DNA region only differing in their direction of action. For more details see Appendix H, Figure H.01.

Inspection of the *Synechococcus* sp. WH8102 genome revealed two sets of genes with a likely role in Zn(II) uptake processes. The consecutive genes *synw\_2479*, *synw\_2480* and *synw\_2481* are predicted to encode the first ZnuABC transporter (Barnett *et al.*, 2012; Barnett *et al.*, 2014) (Predicted in Cyanobase, designated in this study as ZnuABC system 1), and the second ZnuABC transporter genes, including *synw\_0969*, *synw\_0970* and *synw\_0971* (Predicted in RegPrecise, designated in this study as ZnuABC system 2). The *synw\_0971* and *synw\_2481* genes encode the periplasmic binding protein ZnuA; the *synw\_0970* and *synw\_2480* genes encode ZnuC (ATPase); and the *synw\_0969* and *synw\_2479* genes encode ZnuB, the inner membrane permease. However, bioinformatic analysis revealed that Zur boxes are only found for the ZnuABC system 2 operon but not for the ZnuABC system 1 operon.

In the present chapter, an endeavour was made to assess DNA binding of the SynZur protein to the predicted promoters, including those for *znuABC* system 1, *znuABC* system 2, *smtA*, *zur* itself and *ntcA* (a nitrogen regulatory protein, as a negative control). To better understand the role of SynZur in gene regulation, gel electrophoretic mobility shift assays (EMSA), using zinc-loaded SynZur, and EDTA-treated SynZur were studied.

## 8.2 Correcting the Start Codon for *synw\_0971*

It was noticed that the Zur box for the *synw\_0971* gene, ZnuA, was located in Genbank after the ATG start codon at position 37 (Figure 8.02B and for more detail see Appendix H, Figure H.01). Knowledge of the exact position of the start of translation of an mRNA molecule is crucial for identification of the upstream regulatory regions.

Sequence comparisons between the *synw\_0971* gene from *Synechococcus* sp. WH8102 and other ABC transporter systems from different bacteria revealed that the start codon determined in Genbank for *synw\_0971* was not correct (see Appendix H, Figure H.02). Moreover, the true ZnuA protein can often be distinguished by the presence of a His-rich loop, whereas the putative

ZnuA from *Synechococcus* sp. WH8102 is unusual in that it does not contain this loop. Instead, it contains three strictly conserved His residues which may be involved in forming the major metal-binding site (Barnett *et al.*, 2014). The same phenomenon has also been observed for ZnuAs from other cyanobacteria (see Appendix H, Figure H.02).

Given ZnuA is a 'secreted' protein i.e. is being transported across the cytoplasmic membrane, evidence for a signal sequence was sought. Two distinct pathways are present in bacteria for the export of proteins across the cytoplasmic membrane. The majority of proteins translocated across the cytoplasmic membrane occur in the unfolded state *via* the Sec translocon, or in the folded state *via* the twin-arginine translocation (Tat) pathway (Natale *et al.*, 2008; Barnett *et al.*, 2011; Singh *et al.*, 2013). Proteins which are exported through the Sec translocon contain a hydrophobic signal peptide sequence at their N-terminus. The signal peptide plays a key role in targeting and membrane insertion of secretory material in both prokaryotes and eukaryotes (Singh *et al.*, 2013). After membrane insertion, signal sequences are cleaved by the membrane-bound signal peptidases. In general, the signal sequences have a common tripartite structure consisting of a positively charged N-terminus (N-region), a stretch of 18-30 hydrophobic residues, and a more polar region containing proline and glycine residues (Mergulhao *et al.*, 2005; Natale *et al.*, 2008). However the signal peptide sequence is distinct for a periplasmic protein.

The SignalP 4.1 server (Petersen *et al.*, 2011) was used in the present study to detect the signal peptide in the amino acid sequence of ZnuA, *synw\_0971* (Figure 8.03). The method incorporates a prediction of cleavage sites and a signal peptide/non-signal peptide prediction based on a combination of a number of artificial neural networks (Petersen *et al.*, 2011).

The SignalP 4.1 server gave further evidence that the translation start site predicted by genomic studies in Genbank was incorrect, where the score for the presence of a signal peptide in *synw\_0971* was very low  $\sim 0.24$  according to the Y score (score of the cleavage site) (Figure

8.03A). Moreover, the newly identified start codon, predicted in this study, gave a higher score for the signal peptide, ~ 0.65 according to the Y score, and the predicted Zur box was located at position -32 as expected (Figure 8.03 B and C).

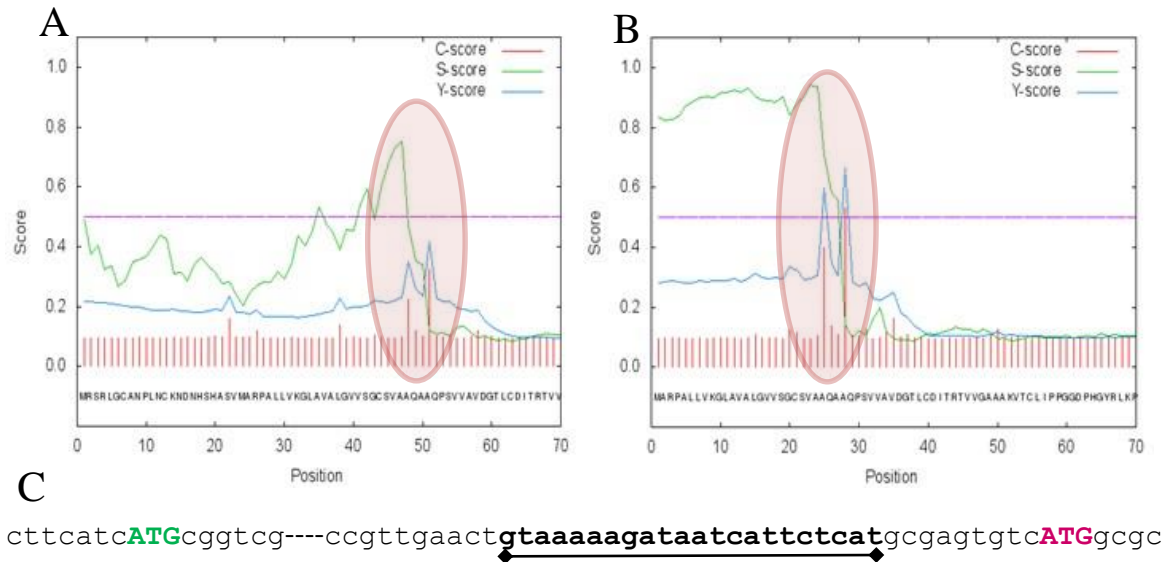


**Figure 8.03 Analysis of the signal peptide sequence in *synw\_0971*.**

The N-terminal signal sequence, signal peptide, of *synw\_0971* was analysed before correcting the start codon as predicted by genomic studies (A) and after correcting the start codon as predicted in our study (B) using SignalP 4.1 web-server. The X axis shows the residual positions of the protein, and the Y axis indicates the scores for the cleavage site. ‘C-score’ is the predicted cleavage site value, the raw cleavage site score. ‘S-score’, the signal peptide score, is the predicted signal peptide value. ‘Y-score’ is a combination of C- and S-scores, a combined cleavage site score. The predicted cleavage site is between position 27 and 28 with the local sequence context “AQA-AQ.” (C) Start codon for *synw\_0971* before (Green line) and after (Pink line) correcting the start codon. The predicted Zur binding box is underlined (Black bold line) at position -32 before the new starting codon.

### 8.3 Transcription Factor Elements, -10 and -35

In bacteria, a core promoter sequence must be present for RNA polymerase in order to initiate transcription. The promoter usually contains two short sequence elements -10 and -35 nucleotides at approximately -30, -75, or -90 base pairs upstream from the transcription start site (TSS). In *E. coli*, the sequence at -10 (the -10 element) has the consensus sequence TATAAT, and TTGACA for the -35 element. However, in most promoters these consensus

sequences are not found intact. On average, only three to four of the six base pairs in each consensus sequence may be found in any given promoter. In an attempt to predict the DNA sequence features associated with promoter recognition for RNA polymerase (RNAP) in *Synechococcus* sp. WH8102, the SoftBerry online program was used.

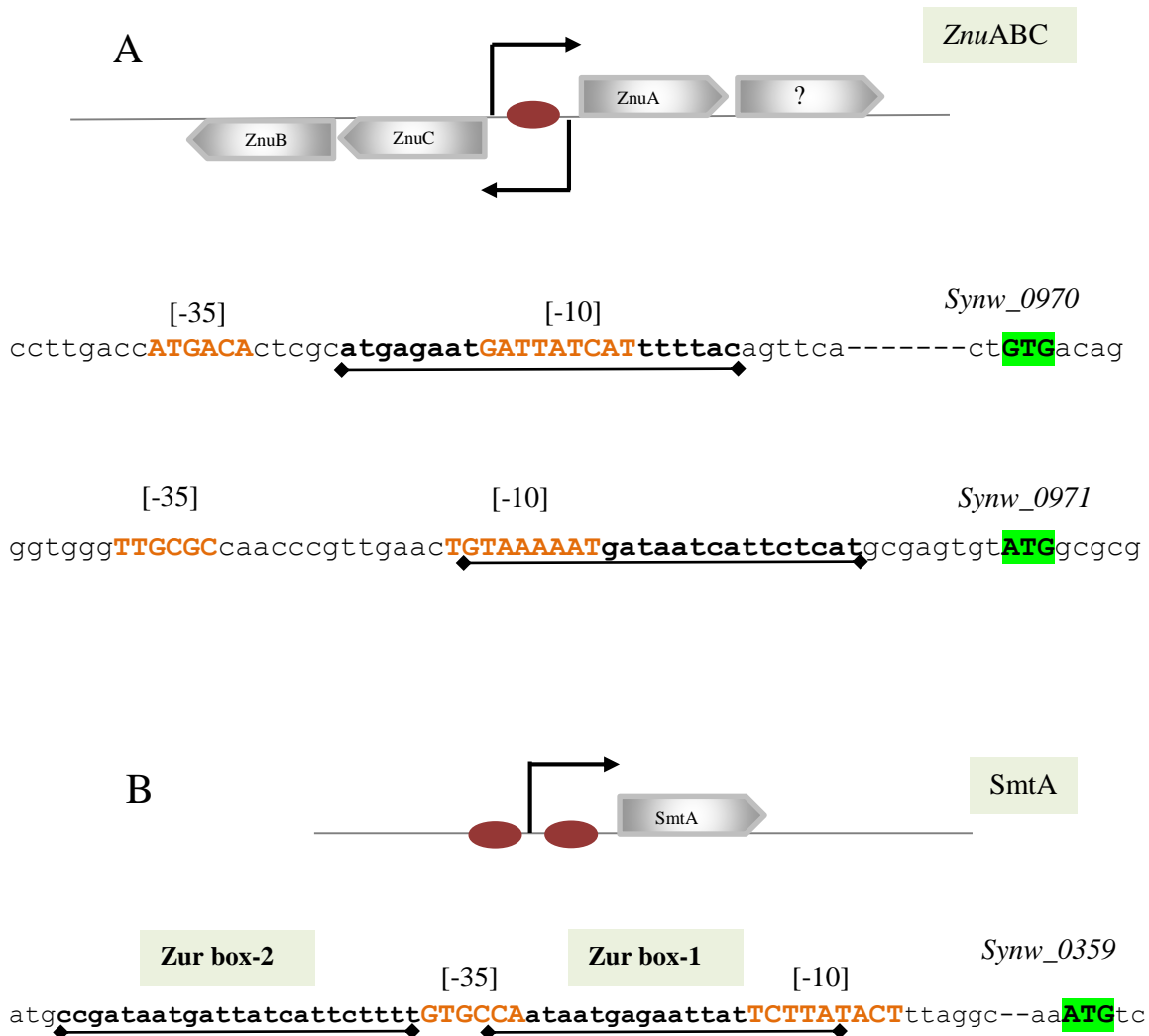


**Figure 8.04 The upstream region of the *znuABC* transporter and *smtA* genes.**

The *znuABC* transporter (A) and *smtA*, metallothionein, (B) gene promoter and operator regions from *Synechococcus* sp. WH8102. Open reading frames are indicated by an open pentagon, transcription start sites are indicated by bent arrows, and Zur boxes are indicated by closed red circles. Sequences of the four Zur-controlled promoters are underlined and shown as recognition sites (Black bold) while the -10 and -35 promoter elements are shown in orange bold. Start codons are highlighted in green.

Using the SoftBerry online program (Solovyev & Salamov, 2011), the consensus sequences of the -10 and -35 regions were found in the 5'-upstream region of the *znuC*, *znuA* and *smtA* genes.

The -10 and -35 sequences were located at position (-75 and -94) for *synw\_0970*, (-32 and -51) for *synw\_0971*, and (-62 and -82) for *synw\_0359*, respectively, where the -10 sequence was present as a nonamer, and the -35 sequence as a hexamer according to the SoftBerry program (Figure 8.04).

The Zur boxes overlap the putative -10 region of both the *znuC* and *znuA* genes (Figure 8.04A), while for *smtA*, the consensus sequence of the -10 box was located at the beginning of a putative Zur box (Zur box-1) and the -35 consensus sequence was located between the two Zur boxes (Figure 8.04B). These data suggest that SynZur may play a critical role for RNA polymerase binding and expressing these target genes. Additionally, it was found that the Zur box for *znuA* is complementary to the Zur box in *znuC* which may indicate that SynZur can repress the components of the *znuABC* transporter in one place.

In order to assess the ability of the SynZur protein to bind to the predicted Zur boxes, ~250-bp upstream regions of each promoter were amplified by PCR and gel shift assays were carried out (see Section 2.13).

## 8.4 Electrophoretic Mobility Shift Assays (EMSA).

The electrophoretic mobility shift assay (EMSA), also known as gel retardation assay, is a system regularly used to detect protein-nucleic acid interactions. It is the core technology underlying a wide range of quantitative purposes, including the determination of binding affinities, kinetics and stoichiometry (Garner & Revzin, 1981; Hellman & Fried, 2007). In the classical assay, solutions of protein and nucleic acid are combined and the resulting mixtures are subjected to electrophoresis under native conditions through polyacrylamide or agarose gel. After electrophoresis, the distribution of species containing nucleic acid can be determined, usually by autoradiography of <sup>32</sup>P-labeled nucleic acid, labelled protein or possibly even by using high concentration of DNA and protein without labelling. In the case of a DNA–protein

complex, the presence of a given DNA-binding protein will cause the DNA to migrate in a characteristic manner, usually more slowly than the free DNA, and will thus cause a change or shift in DNA mobility visible upon detection (Figure 8.05).

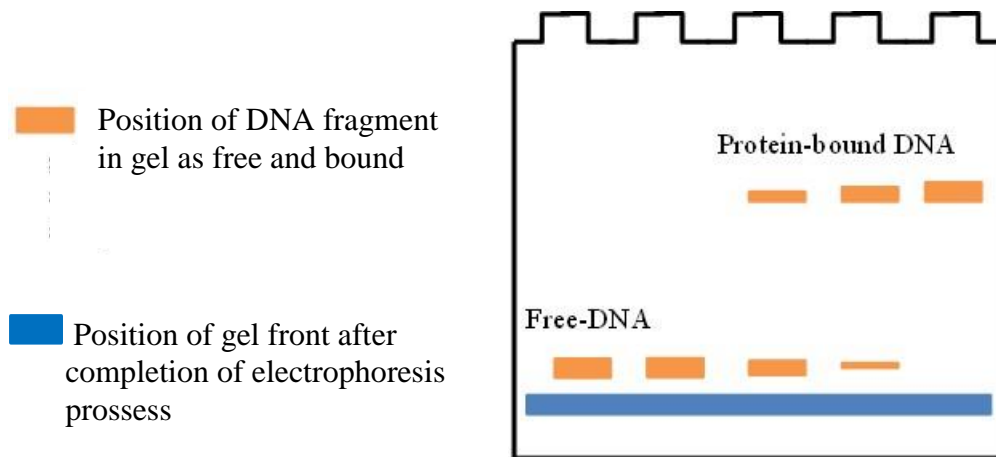


**Figure 8.05 Principles of electrophoretic mobility shift assay.**

DNA can migrate more rapidly through the gel matrix close to the gel front when not bound to protein. In contrast, DNA bound to a specific protein will show retardation on the gel matrix and move more slowly.

### 8.4.1 Detection Limit in EMSA

To assess the detection limit, native gel shift experiments were used to evaluate the detection limit for a DNA probe using a 6% polyacrylamide gel (Figure 8.06).

The lower detection limit for a DNA probe was shown to be 1 ng while 0.1 ng and 0.01 ng could not be detected on a 6% polyacrylamide gel (Figure 8.06). The optimal concentration for the DNA probe was therefore chosen as 5 ng for the remaining experiments.

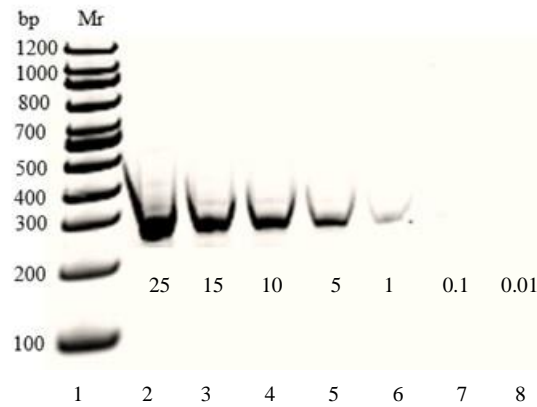


**Figure 8.06 Determining the detection limit for a DNA probe using SYBR-Green dye.**

The detection limit for 256-bp DNA fragment, the *znuC* promoter, on a 6% polyacrylamide gel. Lane 1: DNA Marker, Lanes 2, 3, 4, 5, 6, 7 and 8 are the DNA probe with concentrations 25, 15, 10, 5, 1, 0.1 and 0.01 ng, respectively.

### 8.4.2 Zinc-loaded SynZur Binds Specifically to its Promoters

To examine the DNA binding activity *in vitro*, the SynZur protein was expressed in *E. coli* and purified using IMAC (see Section 2.7.2). DNA fragments of the promoter regions (~250-bp upstream of the start codon) of *synw\_0970*, *synw\_0971* and *synw\_0359* were amplified by PCR using chromosomal DNA from *Synechococcus* sp. WH8102 as the template (see Section 2.13).

Electrophoretic mobility shift assays (EMSA) were carried out for the SynZur protein following incubation with DNA fragments containing the putative upstream regulatory regions of *synw\_0970*, *synw\_0971* and *synw\_0359*. Samples were then run on a native polyacrylamide gel (Figure 8.07) for 4-6 hours, to allow unbound DNA fragments to migrate some distance from the top of the gel. Bound fragments remained higher in the gel about 1-2 cm from the top. The SynZur protein reduced the electrophoretic mobility of the chosen DNA fragments, where the SynZur-DNA complex formation increased with increasing the concentrations of the SynZur protein up to 1  $\mu$ M (Figure 8.07). Beyond this concentration it was observed that the Zur-DNA complex began to aggregate.

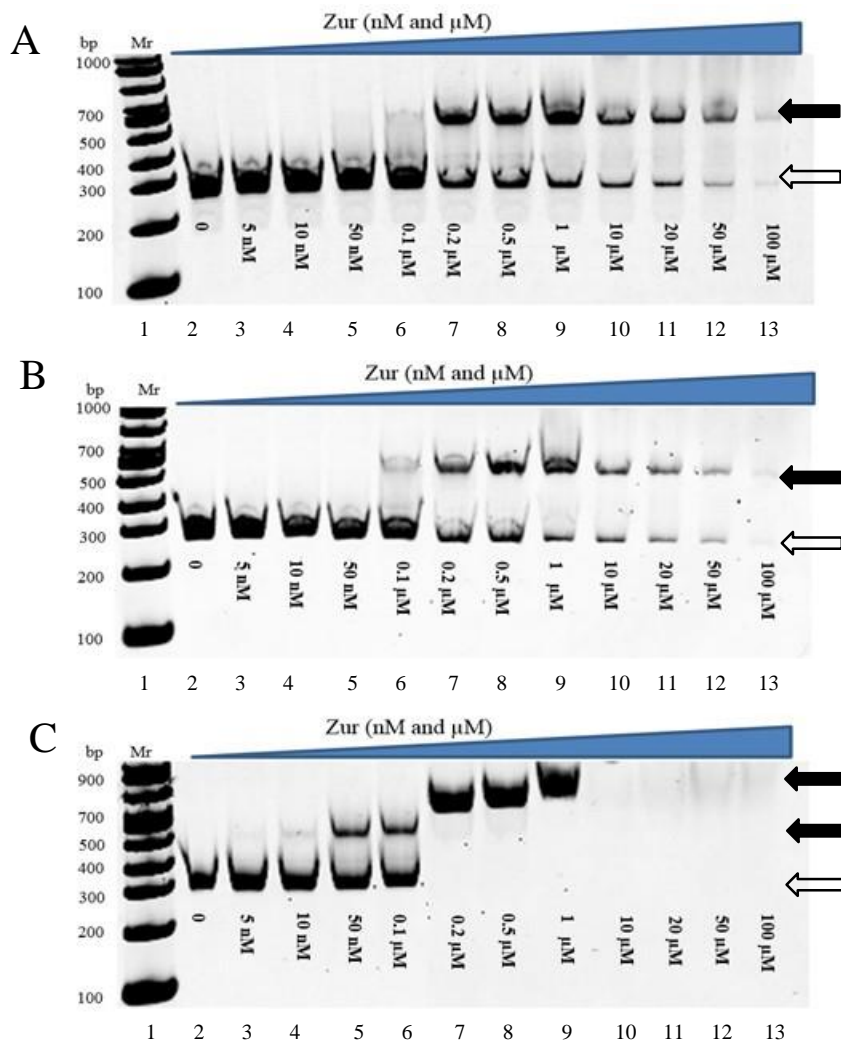


**Figure 8.07 Titration of the *znuA*, *znuC* and *smtA* upstream DNA fragments with the SynZur protein.**

*In vitro* binding of SynZur to the 246-bp *znuC*, *synw\_0970*, promoter (A), the 256-bp *znuA*, *synw\_0971*, promoter (B), and the 250-bp *smtA*, *synw\_0359*, promoter (C) regions. All samples contained 5 ng of the DNA probe. Lane 1: DNA marker, Lanes 2, 3, 4, 5, 6, 7, 8, 9, 10, 11, 12 and 13 contained 0, 5 nM, 10 nM, 50 nM, 0.1  $\mu$ M, 0.2  $\mu$ M, 0.5  $\mu$ M, 1  $\mu$ M, 10  $\mu$ M, 20  $\mu$ M, 50  $\mu$ M and 100  $\mu$ M SynZur protein, respectively. The DNA-protein mixture was supplemented with 10 mM ZnSO<sub>4</sub>. The binding buffer contained 20 mM Tris (pH 8 at 23°C), 50 mM KCl, 100  $\mu$ g/mL bovine serum albumin, 5% v/v glycerol and 3 mM spermidine. Samples were resolved on a 6% w/v polyacrylamide gel cast and run at room temperature (23  $\pm$  2°C) in running buffer (40 mM Tris-acetate, 1 mM EDTA, 1 mM MgCl<sub>2</sub>). Free DNA and the SynZur-DNA complexes are indicated by white and black arrowheads, respectively.

Recently, it has been reported that Zur from *Anabaena* sp. PCC 7120 plays a dual role, depending on the protein concentration in the cell (Sein-Echaluce *et al.*, 2014). At low concentrations, Zur works as a transcriptional regulator binding to the promoters of target genes

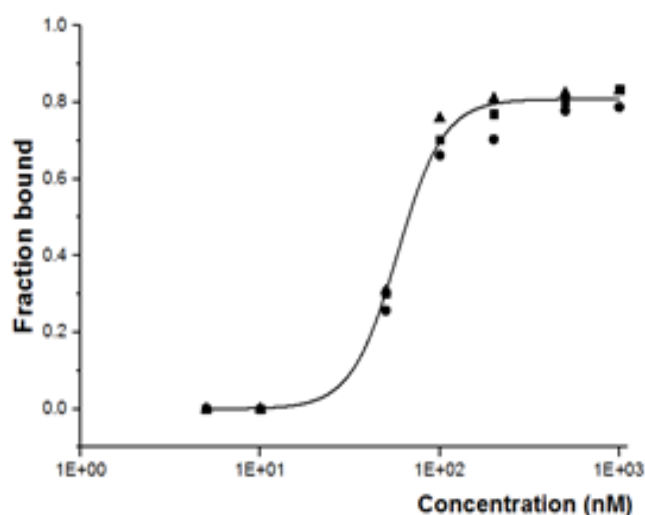
in a specific manner, whereas at higher protein concentration Zur binds non-specifically to DNA, protecting it from oxidative damage (Sein-Echaluce *et al.*, 2014) or polymerises on DNA to create extended arrays of bound repressor (Baichoo & Helmann, 2002; Gabriel *et al.*, 2008). Therefore, in this study, higher SynZur concentrations were avoided.

Figure 8.07 shows the retardation of gel migration due to SynZur protein binding to the chosen probes which expected to be DNA:dimer 1:1. The *smtA* promoter, *synw\_0359*, forms stable complexes with the SynZur protein at a significantly smaller protein-DNA ratio than observed for the other Zur regulon promoters such as *synw\_0970* and *synw\_0971*. At low concentrations of protein (0-50 nM), SynZur did not bind to either the *synw\_0970* or the *synw\_0971* promoter, but at 0.1  $\mu$ M, retarded fragments were observed at  $\sim$ 550-bp<sup>27</sup> for both promoters (Figure 8.07 A and B). For *synw\_0359*, binding started at 10 nM with a retarded fragment at 550-bp, and this fragment began to shift at around 0.2  $\mu$ M to a new position  $\sim$  (800-850 bp) (Figure 8.07C). This potentially indicates that both Zur boxes for *smtA* can be occupied simultaneously. The *znuA* and *znuC* promoters behave reproducibly because the *znuA* and *znuC* promoters reside on the same stretch of DNA though directing transcription in different directions. Interestingly, in freshwater *Synechococcus*, *smtA* has previously been shown to be regulated by the SmtB repressor that up-regulates *smtA* expression in response to excess zinc (Morby *et al.*, 1993; Osman & Cavet, 2010). However, as far as is known, this is the first reported instance of regulation of a metallothionein gene by a Zur sensor.

In an attempt to calculate a dissociation constant  $K_d$  for *znuA* promoter, the data points obtained from the integral of the bands using Aida/2D Densitometry software in Figure 8.07 were subjected to OriginPro 9.1 software (Figure 8.08).

---

<sup>27</sup> The (bp) ladder cannot be directly converted into a molecular weight for the complexes.



**Figure 8.08 Binding affinity curve for *Zur-P<sub>znuA</sub>*.**

Graphical representation of the fractions of bound DNA *versus* the concentration of the SynZur protein. The data points presented in the graph are representative of three separate gel shift experiments. A binding isotherm fitted to a Hill-type equation in OriginPro 9.1 software gave a protein-DNA dissociation constant of  $K_d = 58.29 \pm 1.68$  nM.

The Hill equation in OriginPro 9.1 software gave a dissociation constant of  $K_d = 58.29 \pm 1.68$  nM for the *Zur-P<sub>znuA</sub>* promoter complex (Figure 8.08) which is comparable with protein-DNA dissociation constants ( $K_d$ ) measured for other Zur proteins: 20 nM for Zur from *E. coli* (Althaus *et al.*, 1999), and 2.5 nM to 7 nM for Zur from *Anabaena* sp. PCC7120 (Napolitano *et al.*, 2012). However, SynZur may bind as a single dimer at 550-bp to *znuABC*. In the case of *smtA*, the presence of two bands may indicate that one dimer per DNA binds at 550-bp, an intermediate complex, and that two dimers bind per DNA at 800-850 bp. However, insufficient data points were obtained for *smtA* to derive a binding affinity curve.

To ensure the specificity of the SynZur-DNA interactions, the promoter region of the *synw\_0275* gene, encoding the NtcA protein, a nitrogen regulatory protein in *Synechococcus* sp. WH8102, was used as a negative control. In contrast to the DNA sequences containing putative Zur boxes (Figure 8.07), the mobility of the *ntcA* promoter region was essentially unaffected by the presence of the SynZur protein (Figure 8.09A).

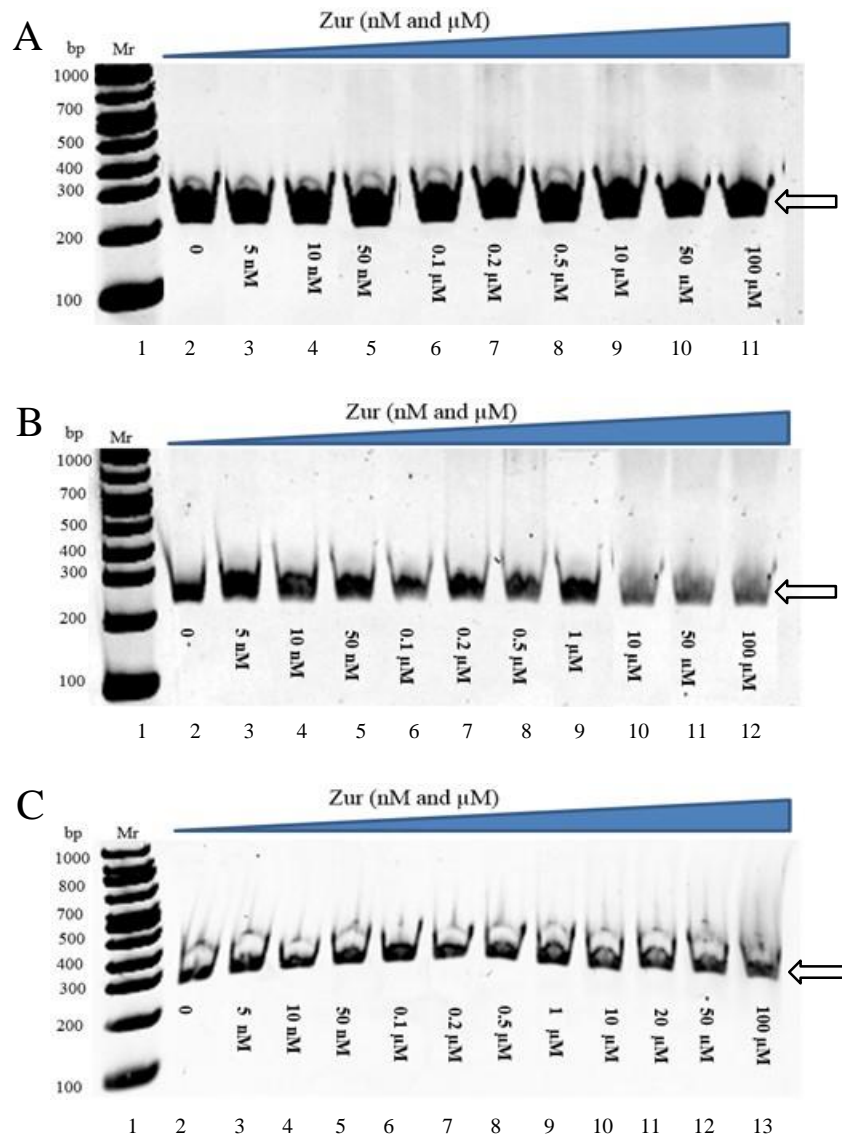


**Figure 8.09 Titration of *ntcA*, *znuA* from system 1 and *zur* promoter regions with the SynZur protein.**

In *vitro* non-specific binding of SynZur to the 201-bp *ntcA* promoter (*synw\_0275*) (A), the 220-bp *zur* promoter (*synw\_2401*) (B), and the 252-bp *znuA* promoter (*synw\_2481*) (C), regions. All samples contained 5 ng of the respective DNA probe. Lane 1: DNA marker, Lanes 2, 3, 4, 5, 6, 7, 8, 9, 10, 11, 12 and 13 contained 0, 5 nM, 10 nM, 50 nM, 0.1 μM, 0.2 μM, 0.5 μM, 1 μM, 10 μM, 20 μM, 50 μM and 100 μM from SynZur protein, respectively. The DNA-protein mixture was supplemented with 10 mM ZnSO<sub>4</sub>. The binding buffer contained 20 mM Tris (pH 8 at 23°C), 50 mM KCl, 100 μg/mL bovine serum albumin, 5% v/v glycerol and 3 mM spermidine. Samples were resolved on a 6% w/v polyacrylamide gel cast and run at room temperature (23 ± 2°C) in running buffer (40 mM Tris-acetate, 1 mM EDTA, 1 mM MgCl<sub>2</sub>). Free DNA is indicated by white arrowheads.

Some metalloregulatory transcription factors also control their own expression (Cavet *et al.*, 2003). Therefore, the possibility that the *synw\_2401* gene, encoding the SynZur protein, is

regulated by SynZur itself was also investigated by studying SynZur binding to the *synw\_2401* promoter region. EMSA showed that SynZur did not bind to this promoter region *in vitro*, suggesting that it does not regulate its own expression (Figure 8.09B). Furthermore, the promoter region of the second putative ZnuABC system (system 1, upstream region of *synw\_2481*) was studied by EMSA. Surprisingly, no apparent direct regulation by SynZur for the ZnuABC system 1 was observed by EMSA (Figure 8.09C).

The above results indicate that SynZur binds to the *znuABC* and *smtA* promoter regions in a sequence-specific manner. However, these experiments were conducted in the presence of 10 mM ZnCl<sub>2</sub>, and it was noticed that zinc-loaded SynZur was also able to bind to these promoters in the absence of zinc ions (data not shown). This suggests that on activation purified SynZur is able to bind to its target promoters, and this phenomenon may be due to the presence of zinc ions in sensory site 2. Additionally, the binding might also be due to zinc contamination from other sources, such as the running buffer, the gel matrix, or even the glass plates.

To examine the effect of the presence or absence of Zn(II) in the sensory site on DNA:protein complex formation, further experiments were conducted after treating SynZur with 2 molar equivalents of EDTA for 24 hours under anaerobic conditions (see Section 2.13).

### 8.4.3 EDTA-Treated SynZur

By using the metal chelator EDTA, zinc was removed with great efficiency from the sensory site (see Section 7.2.1.3). The risk of thiol oxidation was reduced since all reactions were conducted in an anaerobic workstation (see Section 2.13).

The SynZur protein caused retardation of the chosen probe, *synw\_0970*, in the presence of Zn(II) (Figure 8.10A), whereas no clear effect was observed in the absence of Zn(II) in the binding reaction (Figure 8.10B). At the same time it was noticed that protein-DNA complex

increased with increasing concentration of the protein (Figure 8.10). Similar observations were also made for *synw\_0971* (Figure 8.10C and D).

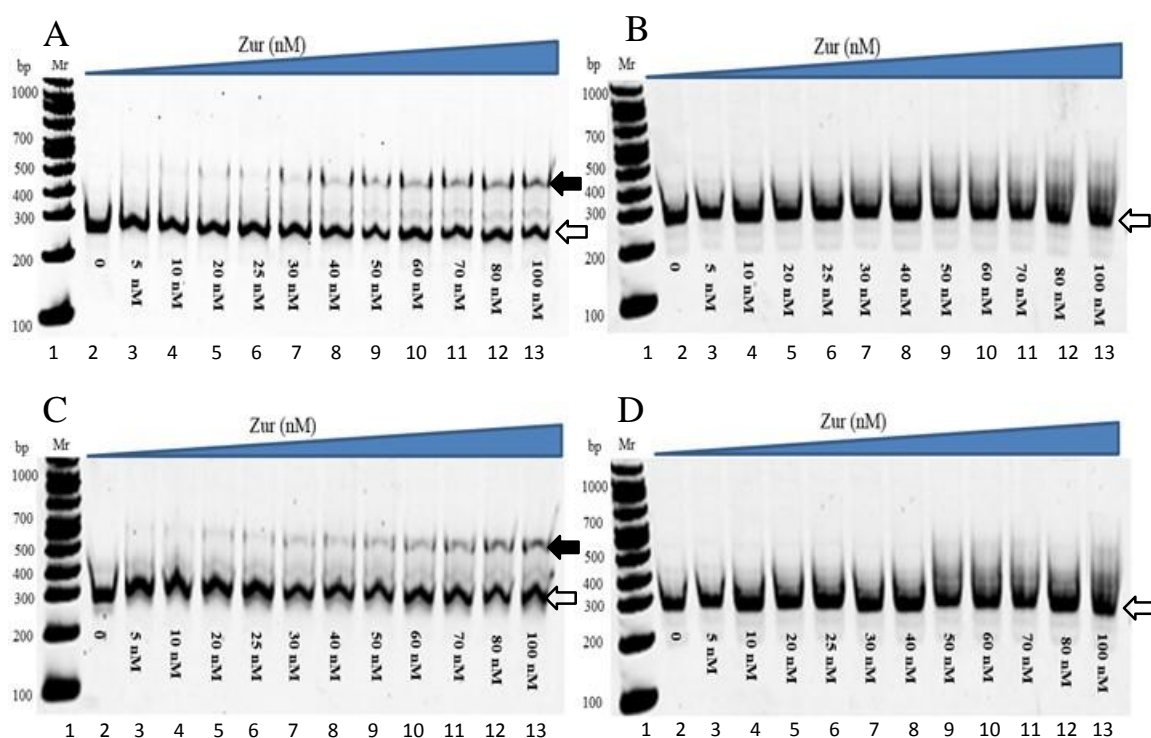


**Figure 8.10 Titration of the *znuA* and *znuC* promoters with EDTA-treated SynZur.**

*In vitro* titration of EDTA-treated SynZur to the 246-bp *znuC*, *synw\_0970*, promoter in presence of Zn(II) (A), absence of Zn(II) (B), and titration of EDTA-treated SynZur to the 256-bp *znuA*, *synw\_0971*, promoter in presence of Zn(II) (C), absence of Zn(II) (D). All samples contained 5 ng of the DNA probe. Lane 1: DNA marker, Lanes 2, 3, 4, 5, 6, 7, 8, 9, 10, 11, 12 and 13 contained 0 nM, 5 nM, 10 nM, 20 nM, 25 nM, 30 nM, 40 nM, 50 nM, 60 nM, 70 nM, 80 nM and 100 nM EDTA-treated SynZur, respectively. The DNA-protein mixture was supplemented with and without 10 mM ZnSO<sub>4</sub>. The binding buffer contained 20 mM Tris (pH 8 at 23°C), 50 mM KCl, 100 µg/mL bovine serum albumin, 5% v/v glycerol and 3 mM spermidine. Samples were resolved on a 6% w/v polyacrylamide gel cast and run at room temperature (23 ± 2°C) in running buffer (40 mM Tris-acetate, 1 mM EDTA, 1 mM MgCl<sub>2</sub>). Free DNA and the DNA-protein complexes are indicated by white and black arrowheads, respectively.

The Hill equation in OriginPro 9.1 software gave a dissociation constant of  $K_d = 62.65 \pm 1.47$  nM for the *SynZur-P<sub>znuA</sub>* promoter (Figure 8.11).

Figure 8.10 shows a very faint band at ca. 400-bp and a strong band at 550-bp which may indicate the relative ability of monomer (faint band) and dimer (strong band) for binding and

this may be due to the presence of SynZur as an oligomeric protein in solution (see Section 5.7.4). The Fur protein from *Anabaena* PCC 7119 has also been observed to bind as a dimer with a strong band and as a monomer with very faint band, indicating lower affinity (Hernandez *et al.*, 2002). The ability of the monomer to bind to DNA with low affinity has also been observed in a number of other studies (Althaus *et al.*, 1999; Pecqueur *et al.*, 2006; Sheikh & Taylor, 2009).

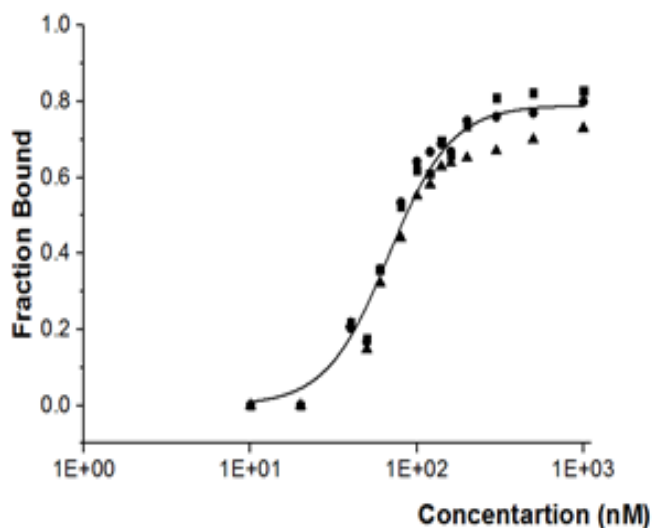


**Figure 8.11** Binding affinity curve for *SynZur-P<sub>znuA</sub>*.

Graphical representation of the fraction of bound DNA *versus* the concentration of EDTA-treated SynZur. The data points presented in the graph are representative of three separate gel shift experiments. A binding isotherm fitted to Hill equation in OriginPro 9.1 software gave a protein-DNA dissociation constant of  $K_d = 62.65 \pm 1.47$  nM.

Mixtures containing SynZur-DNA complexes, using the probes for *synw\_0970* or *synw\_0971*, were subsequently treated with increasing concentrations of  $ZnCl_2$  or the metal chelator EDTA (Figure 8.12).

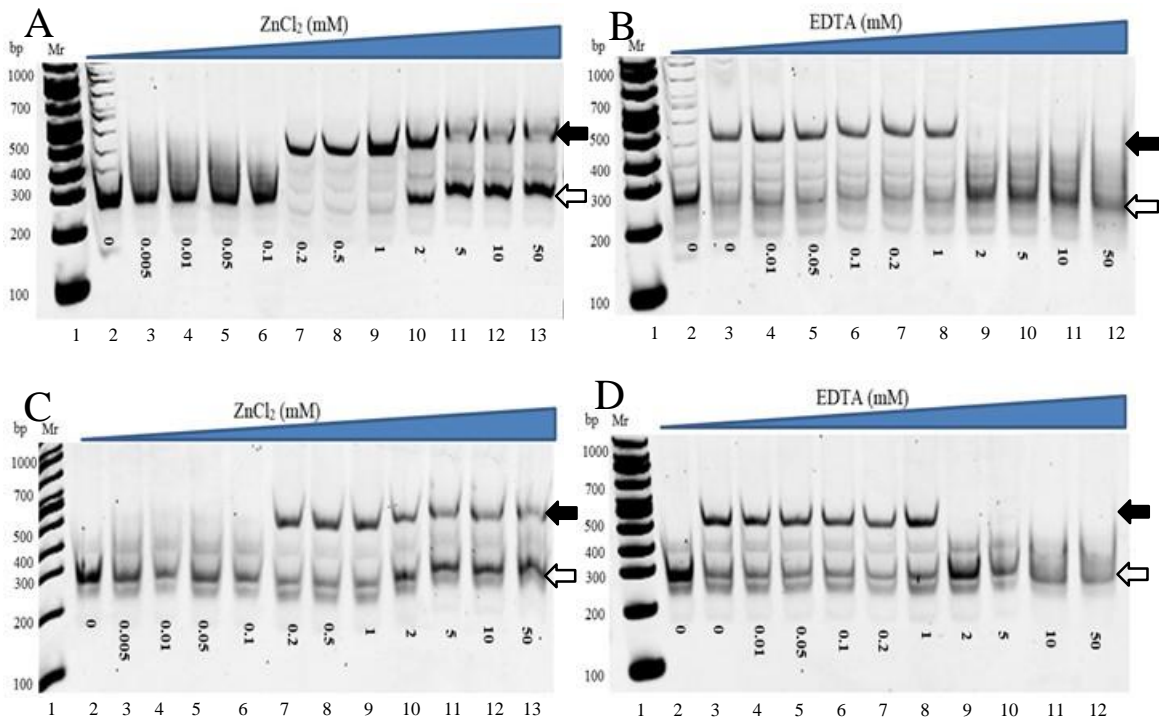


**Figure 8.12 Effects of Zn(II) and EDTA on *SynZur-znuA* and *SynZur-znuC* complexes.**

The effect of  $\text{ZnCl}_2$  on *SynZur-znuC* complex (A), and on *SynZur-znuA* complex (C). The effect of EDTA on *SynZur-znuC* complex (B), and on *SynZur-znuA* complex (D). (A) and (C) Lane 1: DNA ladder, Lane 2 is 5 ng promoter with no EDTA-treated SynZur, Lanes 3, 4, 5, 6, 7, 8, 9, 10, 11, 12 and 13 are 5 ng promoter with 70 nM EDTA-treated SynZur and different  $\text{ZnCl}_2$  0, 0.005, 0.01, 0.05, 0.1, 0.2, 0.5, 1, 2, 5, 10 and 50 mM, respectively. (B) and (D) Lane 1: DNA ladder, Lane 2 is 5 ng promoter without EDTA-treated SynZur, Lanes 3, 4, 5, 6, 7, 8, 9, 10, 11 and 12 are 5 ng promoter with 70 nM EDTA-treated SynZur and 1 mM  $\text{ZnCl}_2$  at different EDTA concentrations: 0, 0.01, 0.05, 0.1, 0.2, 1, 2, 5, 10 and 50 mM, respectively. The binding buffer contained 20 mM Tris (pH 8 at 23°C), 50 mM KCl, 100  $\mu\text{g}/\text{mL}$  bovine serum albumin, 5% v/v glycerol, and 3 mM spermidine. Samples were resolved on a 6% w/v polyacrylamide gel cast and run at room temperature ( $23 \pm 2^\circ\text{C}$ ) in running buffer (40 mM Tris-acetate, 1 mM EDTA, 1 mM  $\text{MgCl}_2$ ). Free DNA and the SynZur-DNA complexes are indicated by white and black arrowheads, respectively.

At 0.2 mM  $\text{ZnCl}_2$ , EDTA-treated SynZur starts to bind to its promoters *synw\_0970* and *synw\_0971*, while in the presence of 2 mM  $\text{ZnCl}_2$  binding begins to be inhibited (Figure 8.12A and C). We suggest that in our case moderate (i.e., milimolar) EDTA concentrations can directly interfere with these protein-DNA interactions. EDTA-treated SynZur binds to DNA in the presence of 1 mM EDTA and 1 mM Zn(II), but that the DNA-binding affinity of SynZur is totally inhibited at higher EDTA concentrations (i.e., 2 mM) (Figure 8.12B and D), suggesting

that an anionic EDTA molecule can again remove Zn(II) from the sensory site of the SynZur protein and disrupt protein-DNA interactions. Inhibition of SynZur binding to DNA confirms the importance of Zn(II) and provides evidence that the binding of SynZur with its DNA targets requires Zn(II) as a cofactor. The same type of inhibition has been found for Zur from *Anabaena* sp. PCC7120 using TPEN (Huang *et al.*, 2008; Napolitano *et al.*, 2012) and DTT/EDTA (González *et al.*, 2010) as the chelators.

Using the WEBMAXC STANDARD online service to calculate the equilibrium levels of free zinc<sup>28</sup> as sensed by SynZur with ZnuABC, it was found that the free zinc concentration was in the femtomolar range  $\sim 1.78 \times 10^{-15}$  M, which is in good agreement with data using the Zur protein from *E. coli* (Outten & O'Halloran, 2001) and *Bacillus subtilis* (Gabriel *et al.*, 2008).

To further investigate binding specificity to the *smtA* promoter, *synw\_0359* was also assessed as a binding target using EDTA-treated SynZur (Figure 8.13). EDTA-treated SynZur reduced the electrophoretic mobility of the *synw\_0359* probe only in the presence of Zn(II) (Figure 8.13A). No retardation of dsDNA was evident in the absence of Zn(II) (Figure 8.13B). In the presence of Zn(II), again two bands were observed, one at 550-bp and another at  $\sim 800$ -850 bp (Figure 8.13A).

To assess the dependence of Zn(II) on binding, EMSA experiments were performed in the presence of Zn(II) (Figure 8.13C) and EDTA (Figure 8.13D). At 0.1 mM ZnCl<sub>2</sub>, the protein started binding to the *synw\_0359* promoter with one band at 550-bp, while at 0.5 mM ZnCl<sub>2</sub>, the shift resulted in a band at 800-850 bp (Figure 8.13C). However, it has previously been reported that Zur can bind to its target promoters in differing ways (Teramoto *et al.*, 2012; Gilston *et al.*, 2014). The molecular basis of metal ion recognition and the nature of the metal-

---

<sup>28</sup> The equilibrium levels of free zinc were calculated using the results in Figure 8.12B and D by applying the following parameters: Temperature: 23°C, pH= 8, Chelator EDTA= 2 mM, Metal Zn(II) total= 1mM.

induced conformational changes in the protein, which in turn affect gene expression, are fundamental issues in this system (Althaus *et al.*, 1999).

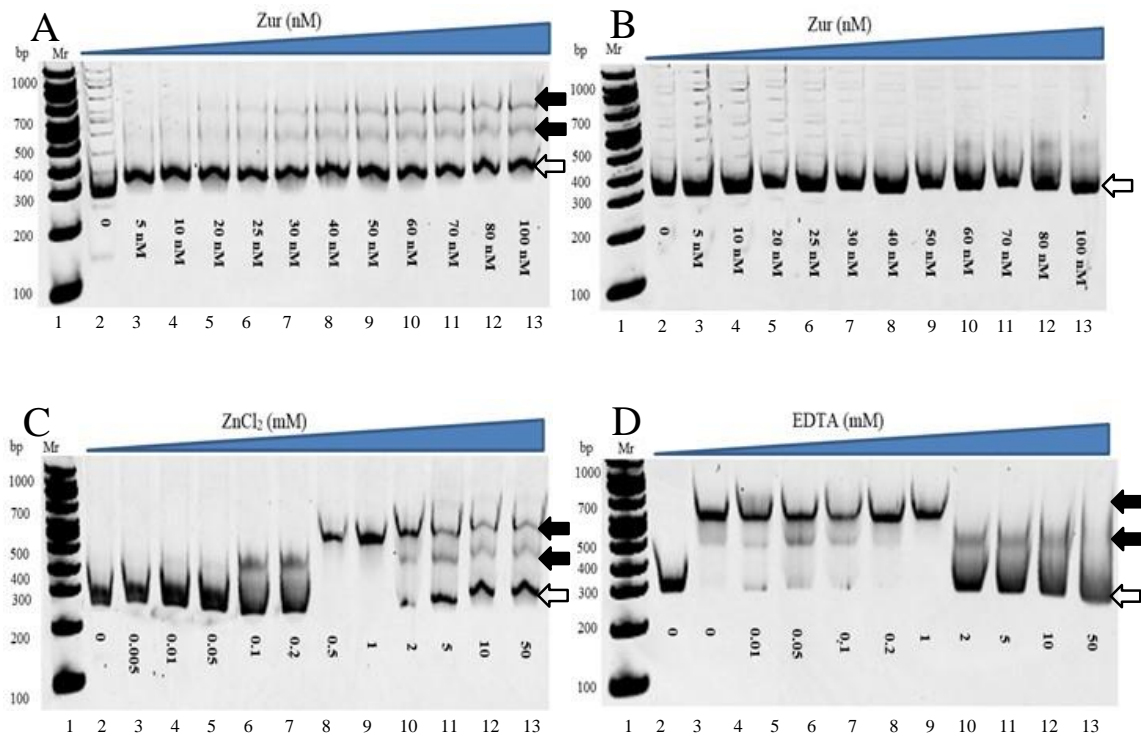


**Figure 8.13 Titration of the *smtA* promoter with EDTA-treated SynZur, in the presence of both Zn(II) and EDTA.**

*In vitro* titration of EDTA-treated SynZur with the 250-bp *smtA*, *synw\_0359*, promoter in the presence of Zn(II) (A), absence of Zn(II) (B). The effect of ZnCl<sub>2</sub> and EDTA on SynZur-*smtA* complexes (C) and (D), respectively. All samples contained 5 ng of the DNA probe. (A) and (B) Lane 1: DNA marker, Lanes 2, 3, 4, 5, 6, 7, 8, 9, 10, 11, 12 and 13 contained 0 nM, 5 nM, 10 nM, 20 nM, 25 nM, 30 nM, 40 nM, 50 nM, 60 nM, 70 nM, 80 nM and 100 nM EDTA-treated SynZur, respectively. The protein-DNA mixture was supplemented with 10 mM ZnSO<sub>4</sub> (A) and without (B). (C) Lane 1: DNA ladder, Lane 2 is 5 ng promoter with no EDTA-treated SynZur, Lanes 3, 4, 5, 6, 7, 8, 9, 10, 11, 12 and 13 are 5 ng promoter with 70 nM EDTA-treated SynZur and different ZnCl<sub>2</sub> concentrations: 0, 0.005, 0.01, 0.05, 0.1, 0.2, 0.5, 1, 2, 5, 10 and 50 mM, respectively. (D) Lane 1: DNA ladder, Lane 2 is 5 ng promoter without EDTA-treated SynZur, Lanes 3, 4, 5, 6, 7, 8, 9, 10, 11 and 12 are 5 ng promoter with 70 nM EDTA-treated SynZur protein and 1 mM ZnCl<sub>2</sub> at different EDTA concentrations: 0, 0.01, 0.05, 0.1, 0.2, 1, 2, 5, 10 and 50 mM, respectively. The binding buffer contained 20 mM Tris (pH 8 at 23°C), 50 mM KCl, 100 µg/mL bovine serum albumin, 5% v/v glycerol, and 3 mM spermidine. Samples were resolved on a 6% w/v polyacrylamide gel cast and run at room temperature (23 ± 2°C) in running buffer (40 mM Tris-acetate, 1 mM EDTA, 1 mM MgCl<sub>2</sub>). Free DNA and protein-DNA complexes are indicated by white and black arrowheads, respectively.

However, above 1 mM EDTA, protein-DNA complexes moved to another position and the band at 800-850 bp totally disappeared, and an intermediate species was observed at 550-pb (Figure 8.13D). In this case, 50 mM EDTA was required to totally block SynZur from binding to the *synw\_0359* promoter. These data provide evidence that the binding of SynZur with its *synw\_0359* promoter requires Zn(II) as a cofactor.

These findings underscore the principle that Zn(II) occupancy in the sensory site is important in inducing or stabilising the DNA binding conformation of SynZur. Accordingly, mutations in either structural site or sensory site in Zur proteins from *E. coli* led to a complete loss of Zur-regulated transcription *in vivo* and loss of their ability to bind to DNA even at high concentration of DNA (Gilston *et al.*, 2014). These results indicate that the Zur protein from *Synechococcus* sp. WH8102 behaves in similar way to other Zur proteins: *S. coelicolor* (ScZur) (Shin *et al.*, 2011); *B. subtilis* (BsZur) (Ma *et al.*, 2011); and *E. coli* (EcZur) (Gilston *et al.*, 2014).

Meanwhile, no binding was observed between the EDTA-treated SynZur species and *znuABC* system 1 promoter (*synw\_2481*), *ntcA* promoter (*synw\_0275*), or the *zur* promoter (*synw\_2401*), either in the presence or in the absence of zinc ions (see Appendix H, Figure H.03).

Using the WEBMAXC STANDARD online service to calculate the equilibrium levels of free zinc<sup>29</sup> as sensed by SynZur in *smtA* for the two bands, it was found that the free zinc concentration was in the femtomolar range  $\sim 1.78 \times 10^{-15}$  M for the band at 800-850 bp and  $\sim 1.98 \times 10^{-16}$  M for the band at 550-bp.

Using OriginPro 9.1 software the Hill equation gave a dissociation constant  $K_d = 61.76 \pm 2.42$  nM for the *SynZur-P<sub>smtA</sub>* promoter (Figure 8.14A). Subsequently, a semi-empirical description

---

<sup>29</sup> The equilibrium levels of free zinc were calculated using the results in Figure 8.13D by applying the following parameters: Temperature: 23°C, pH= 8, Metal Zn(II) total= 1mM, and Chelator EDTA= 2 mM for the first band at (800-850) pb and 10 mM for the second band at 550-pb.

was used (Hill, 1910) to detect the presence of cooperative<sup>30</sup> or non-cooperative binding for the *znuA* promoter (Figure 8.14B). The parameter  $\alpha_H$  is known as the Hill constant or coefficient, in which  $1 \leq \alpha_H \leq n$ . When  $\alpha_H = 1$ , this implies no cooperativity between the protein and its promoter. On the other hand, when  $\alpha_H = n$ , this indicates that there is cooperativity between the protein and its promoter. In the case of *SynZur-P<sub>smtA</sub>*, the Hill constant was  $\alpha_H = 1.47$  (Figure 8.14B), indicating cooperativity and possibly Zur binds as two dimers to the *smtA* promoter at 800-850 bp and as one dimer at 550-bp.

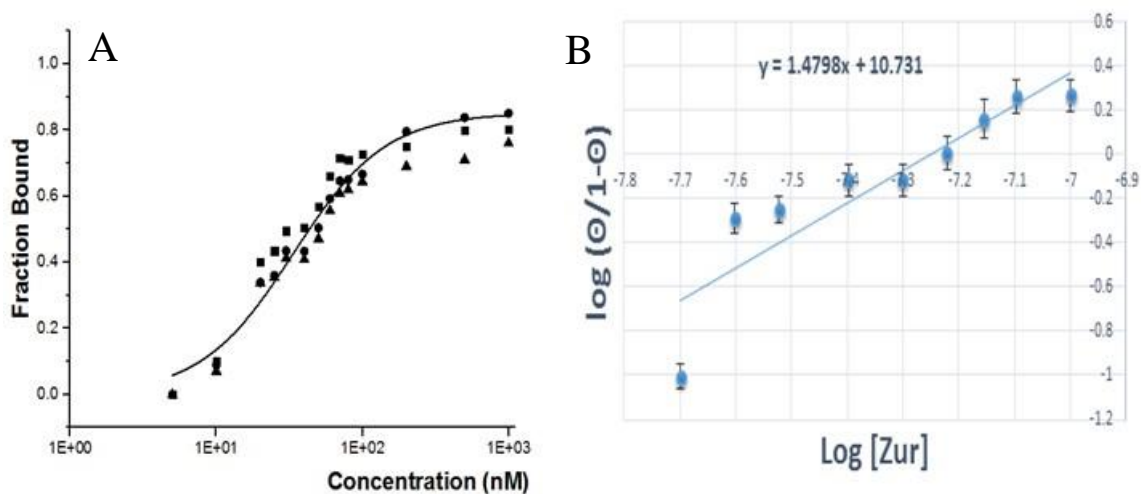


**Figure 8.14 Binding affinity curve and Hill plot for *SynZur-P<sub>smtA</sub>*.**

(A) Graphical representation of the fraction of bound DNA *versus* the concentration of EDTA-treated SynZur. The data points presented in the graph are representative of three separate gel shift experiments. A binding isotherm fitted to Hill equation in OriginPro 9.1 software gave a protein-DNA dissociation constant of  $K_d = 61.76 \pm 2.42$  nM. (B) Hill plot measures the central portion of *SynZur-P<sub>smtA</sub>* gel shifts between EDTA-treated SynZur and *P<sub>smtA</sub>* operator whereas theta,  $\Theta$ , is the fraction bound. Using the slope from the line of best fit, the Hill coefficient ( $\alpha_H$ ) can be estimated to be  $\sim 1.47$  correspond to a cooperative binding interaction, as appropriate for a 1:2 complex.

Early studies confirmed that Fur can bind cooperatively at some promoter regions and generates helical arrays spiralling around the DNA duplex suggesting that two dimers bind per 19-bp Fur box (Escolar *et al.*, 1998; Baichoo & Helmann, 2002; Pohl *et al.*, 2003).

<sup>30</sup> Cooperativity describes the situation in which more than one protein binds to the promoter (Rippe, 1997).

A study on the Mur protein from *Rhizobium leguminosarum* also revealed that Mur can bind as one or two homo-dimers to its regulator, presenting two bands on gels, where a band of lower mass belongs to one dimer and the higher mass band to two dimers bound (Bellini & Hemmings, 2006). Similar phenomena were reported for Zur from *E. coli* (Gilston *et al.*, 2014) and Nur from *Streptomyces coelicolor* (An *et al.*, 2009).

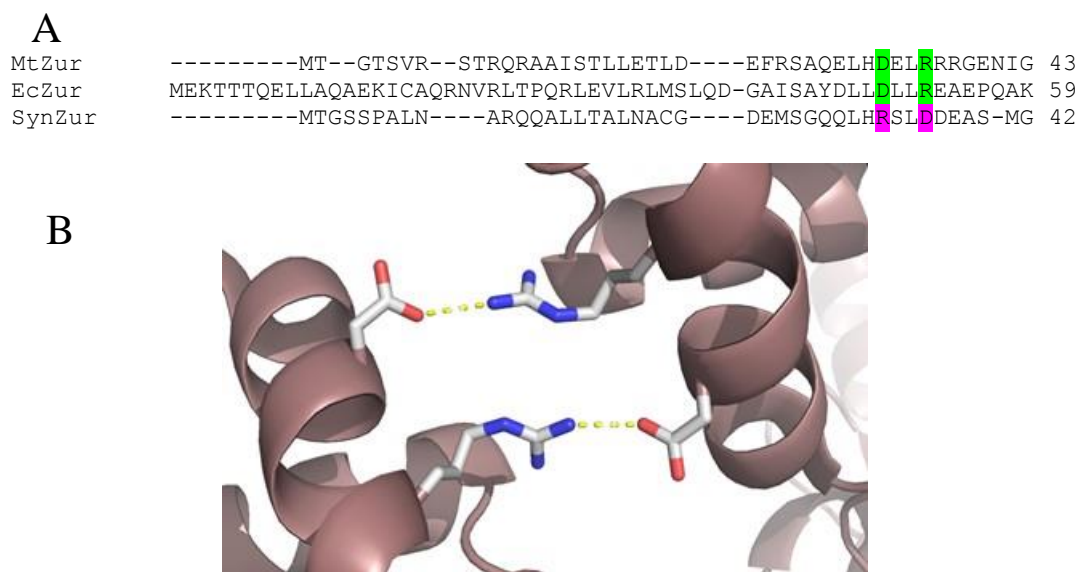


**Figure 8.15 Sequential alignment of SynZur with other Zur proteins.**

(A) Sequence alignment of SynZur from *Synechococcus* sp. WH8102 with MtZur from *M. tuberculosis* (Lucarelli *et al.*, 2007) and EcZur from *E. coli* (Gilston *et al.*, 2014). The two residues forming salt bridges are marked in green for MtZur and EcZur, presenting as Asp33XXArg36 and Asp49XXArg52 for MtZur and EcZur, respectively. The predicted two salt-bridge forming residues are marked in pink for SynZur, presenting as Arg33XXAsp36. (B) Ribbons represent the predicted two salt bridges in *Synechococcus* sp. WH8102.

Gilston and colleagues have recently addressed the observation that in a  $(Zur_2)_2$ -DNA complex, the two dimers are able to communicate with each other through two salt bridges between Asp49 from monomer A in dimer 1 to Arg52 of monomer B in dimer 2 and *vice versa* (Gilston *et al.*, 2014). Mutant forms of Zur in which the salt bridge is removed (D49A or R52A) retain their tight DNA binding activity but do not exhibit the highly cooperative binding observed for the WT protein and it has been proposed that these pairs of salt bridges act as a “cooperativity linker” (Gilston *et al.*, 2014). The sequential alignment between MtZur, EcZur and SynZur

shown in Figure 8.15 demonstrates that although these two residues are not conserved in *Synechococcus* sp. WH8102, they are replaced by Arg33 and Asp36; thus it is possible that they play a similar role in forming two salt bridges between two dimers (Figure 8.15).

## 8.5 Defining the Recognition Motif

### 8.5.1 (6-1-6) Motif

The mode of interaction of the Fur-family with DNA has been controversial over a long period of time (Escolar *et al.*, 1998; Baichoo & Helmann, 2002; Fuangthong & Helmann, 2003). Since the Fur-family protein is usually a dimer, it was originally assumed that one dimer would bind to a 19-bp inverted repeat sequence, known as the Fur box (Figure 8.16A). However, this model could not easily be reconciled with the observation that Fur protein tends to polymerise at a number of operator sites to generate footprints which are not easy to interpret in terms of a single dimer. An early study by Escolar and colleagues proposed a reinterpretation of the Fur box in terms of three GATAAT repeated hexamers in a head-to-head-to-tail (6-6-1-6) orientation (Escolar *et al.*, 1998) (Figure 8.16B). According to this model, Fur binding requires three repeats of a simple 6 bp sequence in either direct or indirect repeats. However, this interpretation is not also easy to reconcile with the dimeric state of Fur and it is not clear whether each 6 bp motif represents the proposed binding site for one dimer or two dimers. Later, following the observation that Fur binds cooperatively to some promoter regions and generates helical arrays spiralling around the DNA duplex, Baichoo and colleagues had proposed a [(7-1-7)<sub>2</sub>] heptamer motif, closely related to the hexamer motif (Baichoo & Helmann, 2002) (Figure 8.16C). According to this model, the classic 19 bp Fur box is recognised by two Fur dimers, each interacting with one of two overlapping 7-1-7 motifs from opposite faces of the helix.

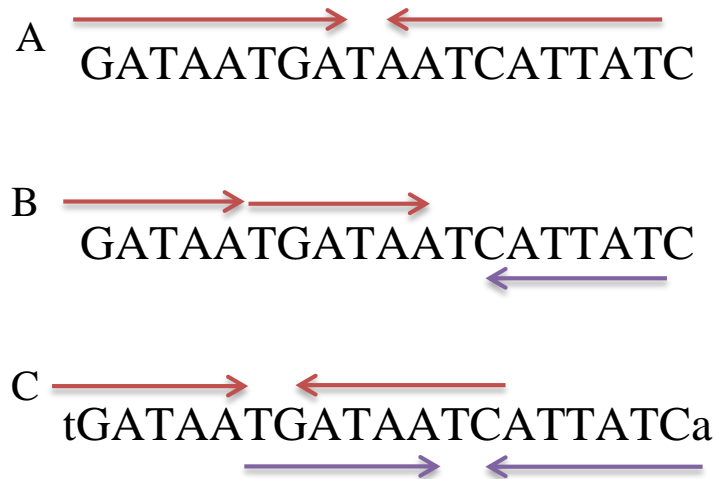


**Figure 8.16 Comparison of models explaining the Fur box consensus sequence.**

(A) The Fur box is classically defined as a 19-bp inverted repeat sequence, originally envisioned to bind a single Fur dimer. (B) An alternative view proposed that Fur binds to repeated arrays of three or more copies of the hexamer GATAAT (Escolar *et al.*, 1998). According to this model, the classic Fur box is the result of three GATAAT motifs in a head-to-head-to-tail (6-6-1-6) arrangement, but this would not explain how one or two Fur dimers could bind. (C) A further alternative suggested that the 19-bp Fur box resulted from two overlapping inverted heptamer repeats [(7-1-7)<sub>2</sub>] (Baichoo & Helmann, 2002). According to this model, two Fur dimers can bind to the Fur box [(7-1-7)<sub>2</sub>].

Recent studies of Zur proteins have recognised several alternative motifs including: a 10-1-10 palindromic inverted repeat motif (Tottey *et al.*, 2012), a 7-1-7 palindromic inverted repeat motif (Napolitano *et al.*, 2012), a 6-3-6 palindromic inverted repeat sequence motif (Pawlik *et al.*, 2012) and a 10-1-10 direct repeat sequence motif (Teramoto *et al.*, 2012).

Applying the classical motif to Zur boxes from *Synechococcus* sp. WH8102, it appears that the newly identified Zur binding motif is a 6-1-6, or even a 9-1-9 palindromic inverted repeat (Figure 8.17A). Interestingly, the predicted Zur in *Synechococcus* sp. WH8102 promoters are AT rich. To further define the DNA sequences required for recognition by the SynZur protein in cyanobacteria (see Appendix H, Table H.01), multiple sequence alignments reveal a 8-1-8 motif palindromic inverted repeat, with a conserved core sequence of a hexamer inverted repeat (6-1-6) (Figure 8.17B).

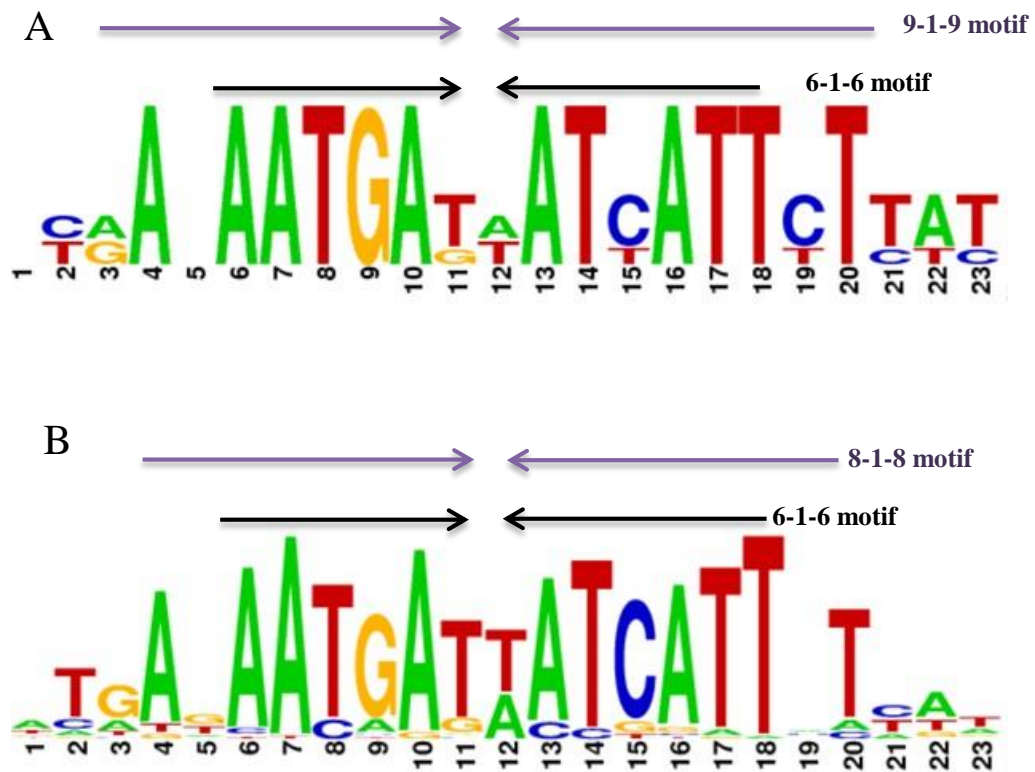


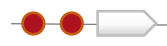
**Figure 8.17 Motifs prediction for Zur boxes in cyanobacteria.**

(A) Nucleotide sequence alignment for the putative Zur boxes in *Synechococcus* sp. WH8102 with the predicted 9-1-9 and 6-1-6 motif palindromic inverted repeat. (B) Nucleotide sequence alignment for the putative Zur boxes located in RegPrecise for cyanobacteria including: *Synechococcus* sp. WH8102, *Synechococcus* sp. PCC7002, *Synechococcus elongatus* PCC7942, *Synechococcus* sp. JA-3-3Ab, *Synechocystis* sp. PCC6803, *Prochlorococcus marinus* str. MIT9313, *Gloeobacter violaceus* PCC7421, *Microcystis aeruginosa* NIES-843 and *Cyanothece* sp. PCC 7425. These exhibit 8-1-8 motif palindromic inverted repeat head to tail and the conserved core 6-1-6.

However, the classical model does not help to explain whether in our case one or two dimers were binding, and we therefore adopted the alternative view proposed by Baichoo and Helmann (2002). It was noticed that the 6-1-6 palindromic inverted repeat head to tail (AATGAT) motif is conserved in the Zur box of the *synw\_0970* and *synw\_0971* genes, while the scenario for *synw\_0359* is probably different (Table 8.01). It was noticed that the operator for Zur box1 did not provide a perfect match for the 6-1-6 motif, where four of six residues are matched. It is also interesting to note that the operator in Zur box 2 gave a perfect 6-1-6 (AATGAT) match, and surprisingly, another 6-1-6 (GATAAT) motif was identified which was not observed for the other three Zur boxes (Table 8.01). These results support the notion that a 6-1-6 palindromic

inverted repeat head to tail may bind one dimer in the case of *synw\_0970* and *synw\_0971* genes, as well as for Zur box 1 on *synw\_0359*. On the other hand, (6-1-6)<sub>2</sub> site may bind two dimers such as is the case for the second Zur box, Zur box 2, for *synw\_0359*. This may explain the presence of one band for *synw\_0970* and *synw\_0971* genes and two bands for *synw\_0359* gene. These findings are in good agreement with the Hill equation measurements given in Section 8.4.3.

**Table 8.01 Zur boxes in *Synechococcus* sp. WH8102 with their sequences, location, (6-1-6) motif, and [(6-1-6)<sub>2</sub>] motifs.**

Regulated operons	Number	Sequence
 SYNW0970	Zur box 1	 ATGAGAATGATTATCATTTTAC
 SYNW0971	Zur box 1	 GTAAAAATGATAATCATTCTCAT
 SYNW0359	Zur box 1 Zur box 2	 CCAATAATGAGAATTATTCTTAT  CCGATAATGATTATCATTCTTT

## 8.5.2 Purine-N-N-N-N-Pyrimidine Motif

Gilston and colleagues have recently demonstrated, by determining the crystal structure of a Zur-DNA complex, that Zur from *E. coli* binds to DNA as two dimers to its regulatory target region and they suggested that each promoter contains multiple interrupted purine-N-N-N-N-pyrimidine binding motifs which are recognized by Zur monomers (Gilston *et al.*, 2014). In each promoter they found two purine-N-N-N-N-pyrimidine motifs separated by three residues, to give RNNNYxxxRNNNY, which serves as the core recognition element for one Zur dimer

(Figure 8.18A). The binding of two dimers at overlapping RNNNY sites gives rise to a skeletal structure-based dimer-dimer recognition motif: **RNNNYRNNRYNNYRNNY**, in which R is purine (R=A or G), and Y is pyrimidine (Y= T or C) and N is indeterminate (N= T, A, G, or C) (Figure 8.18A).

It is obvious that the sequence for the Zur-DNA recognition in *E. coli* is different from Zur-DNA recognition in *Synechococcus* sp. WH8102 (Figure 8.18B). Searching for the same sequence in the identified Zur boxes in *Synechococcus* sp. WH8102 gives the motif of (**RNNNNYRNNNRYNRNYNNY**) (Figure 7.18B). Within each promoter I find two purine-N-N-N-N-pyrimidine motifs. The first motif is separated by four residues, to give **RNNNNYxxxxRNNNNY**, which may serve as the core recognition element for one Zur dimer while the second motif is separated by one residue to give **YNNNNR<sub>x</sub>YNNNNR** which may be able to bind to the second dimer (Figure 7.18A). Including one more nucleotide, I find alternative one (Figure 8.18C). The first motif is still separated by four residues (**RNNNNYxxxxRNNNNY**) which may serve as the core recognition for one Zur dimer while the second motif is separated by four residues to give **YNNNNR<sub>x</sub>xxxxYNNNNR** which may be able to bind to the second dimer which gives the motif of (**RNNNNYRNNNRYNNNYYNNNNR**) (Figure 8.18C).

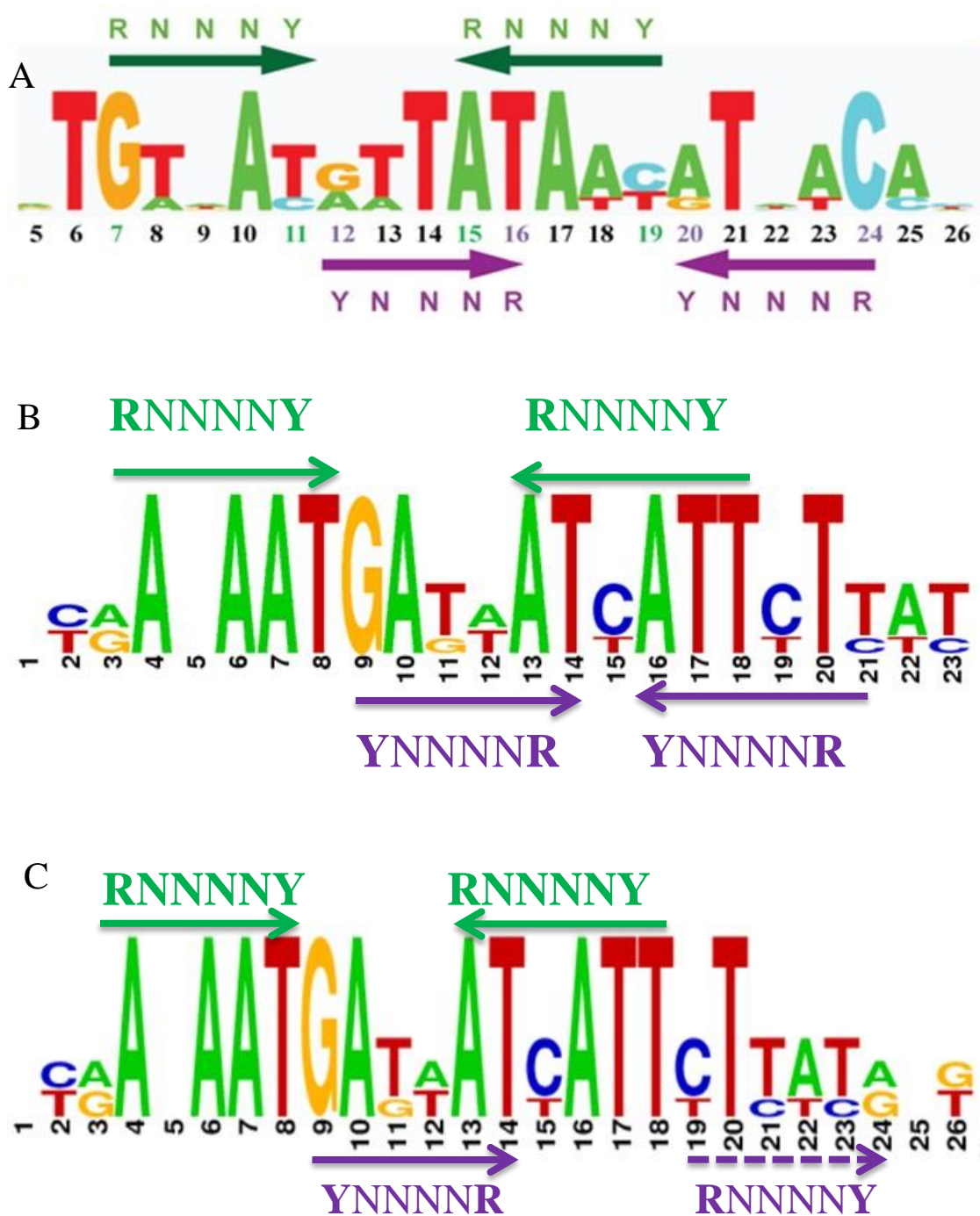


**Figure 8.18 Sequence logo representation for RNNNNY motifs.**

Sequence logo representation of the template strand in Zur-DNA recognition (A) for *E. coli* Zur (Gilston *et al.*, 2014), (B) and (C) for the three known Zur operators (*synw\_0970*, *synw\_0971* and *synw\_0359*) in *Synechococcus* sp. WH8102. The bases in the motif which may be recognized by one dimer, and these are highlighted in green line as **RNNNNYxxxRNNNNY** motif, while for the second dimer are highlighted in purple line as **YNNNRxYNNNNR** (B) or **YNNNRxxxRNNNNY** (C). The purine-N-N-N-N-pyrimidine (i.e., R-N-N-N-N-Y) motif is conserved within all operators regulated by SynZur and created a skeletal structure-based dimer-dimer recognition motif: (B) for the first motif (**RNNNNYRNNNRYNRNYNNY**), and (C) for the second motif (**RNNNNYRNNNRYNNNYYNNNR**).

However, it is obvious that the first dimer can be easily recognized with strong interaction while the second dimer cannot be recognized and may have a weak interaction. Moreover, DNA footprinting which is a method of investigating the sequence specificity of DNA-binding protein may solve this puzzle.

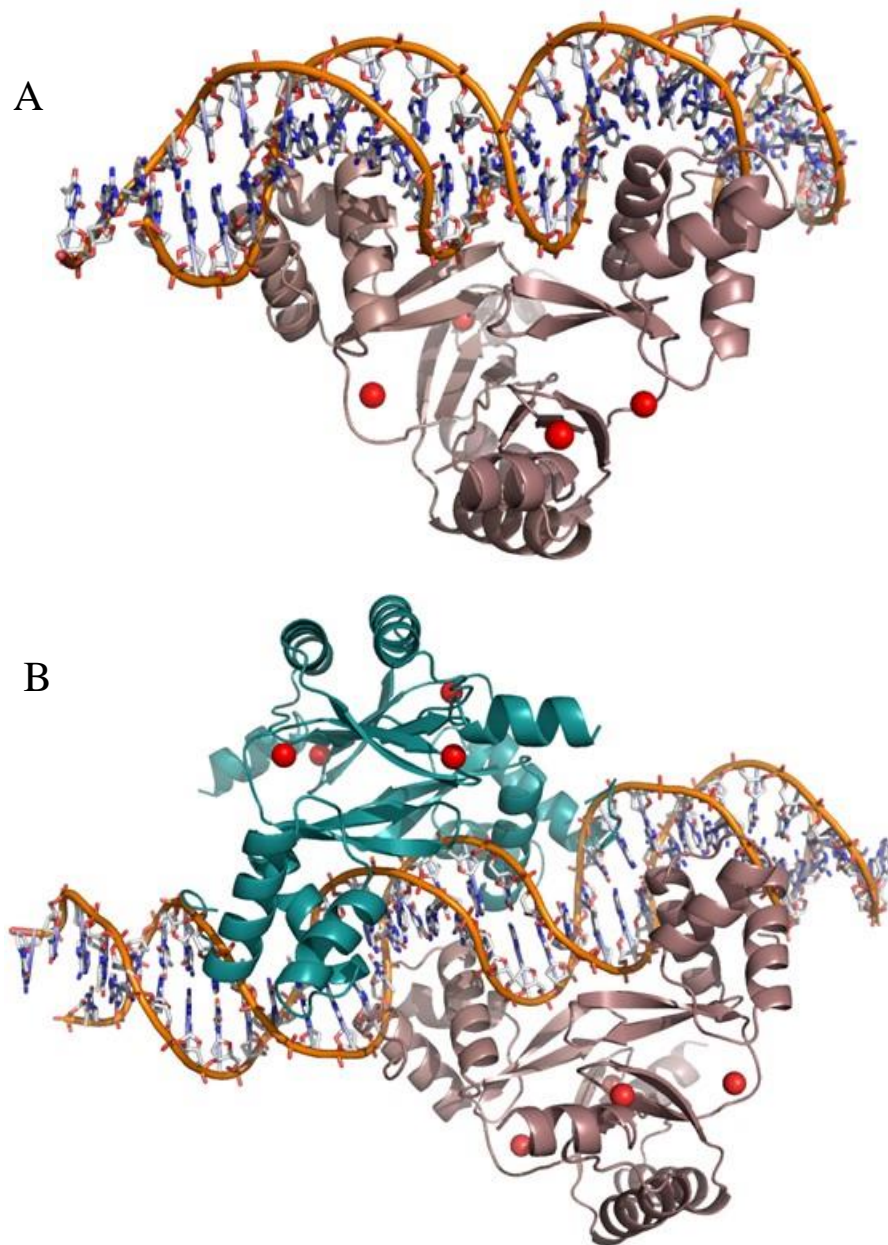


**Figure 8.19 Model of one and two SynZur dimers bound to a Zur box.**

Homology model of SynZur binding to the *znuABC* promoter as one dimer (A) and binding to the *smtA* promoter as two dimers (B). The two dimers are highlighted as salmon and purple ribbons, DNA strands are shown in orange and zinc ions as red spheres.

I next addressed whether the sequence, **RNNNNYRNNNRYNRNYYNY**, could be applied to the other predicted Zur boxes from cyanobacteria (see Appendix H, Figure H.02), and sequence comparison exhibited a favourable agreement with the structure-based Zur recognition motif. Although this represented a degree of progress, it was unable to distinguish whether Zur could bind to its promoters either as one or two dimers.

Based on our observations and results, I postulate a simplified model for SynZur when it is bound as one dimer to *znuABC*, or when it binds as a two dimers to *smtA* (Figure 8.19).

## 8.6 Why does ZnuABC System 1 (*synw\_2481*) Lack a Zur Box?

The ZnuA component (*synw\_2481*) of a putative ZnuABC zinc uptake transporter was identified in the Zn-IMAC eluate, confirming its expression, and supporting the hypothesis that this system could operate in zinc uptake in *Synechococcus* sp. WH8102 (Barnett *et al.*, 2014). Our data did not show any binding to this promoter, however, indicating that this system may be under the control of a different sensor rather than the Zur protein.

*B. subtilis* has three identified zinc uptake systems (*yciABC*, *yedHI-yceA* and *zosA*), where *yciABC* and *yedHI-yceA* are under the control of Zur but *zosA* is not (Gaballa *et al.*, 2002). The *zosA* gene is not repressed by zinc and is expressed under the regulation of the peroxide-sensing repressor PerR rather than Zur (Gaballa *et al.*, 2002; Gabriel *et al.*, 2008). Increased zinc uptake under conditions of oxidative stress has been postulated as helping to protect cells against metal-catalyzed oxidation reactions by displacing redox-active metals from adventitious binding sites (Gaballa *et al.*, 2002).

The ZnuABC system 1 (*synw\_2481*) may therefore be a zinc uptake system regulated by different sensors or perhaps it is constitutively expressed. In addition, it is in principle still possible that it is not involved in zinc uptake at all.

## 8.7 Why does *smtA* Promoter (*synw\_0359*) have a Zur Box?

Tight control of zinc is essential for redox homeostasis. Depending on its availability, zinc can be cytoprotective as a pro-antioxidant or cytotoxic as a pro-oxidant (Maret, 2006). Metallothioneins (MTs) are low-molecular weight proteins possessing a very high sulfur content. Typically, the combined metal and sulfur content of fully metallated metallothioneins ranges between ca. 10–20% of total protein mass (Blindauer & Leszczyszyn, 2010).

Metallothioneins can in principle bind a variety of metal ions, but the most important *in vivo* binding partners are Zn(II), Cu(I) and Cd(II). These clusters have been evaluated as being thermodynamically stable, although kinetically labile (Wu *et al.*, 2007; Babula *et al.*, 2012; Leszczyszyn *et al.*, 2013). As a result, metallothioneins are able to donate zinc to apo-proteins or other ligands providing a labile pool of zinc available for other functions as needed (Barnett *et al.*, 2012; Choi & Bird, 2014). On the other hand, metallothionein gene expression increases when zinc is in excess, one of its functions being to bind excess zinc and protect cells from zinc toxicity (Kelly *et al.*, 1996).

Genomic studies have indicated the presence of *smtA* genes in some marine *Synechococcus* strains, encoding cysteine-rich proteins grouped as bacterial metallothioneins (*bmtA* or *smtA*) (Figure 8.20B), which at least in freshwater *Synechococcus* strains appear to contain Zn(II) as the preferred metal ion *in vivo* (Cavet *et al.*, 2003). This points strongly to the existence of mechanisms for dealing with Zn(II) homeostasis in these organisms (Scanlan *et al.*, 2009). Transcription from the *smtA* operator is maximally induced by zinc rather than other metal ions (Huckle *et al.*, 1993), and is mediated by zinc-sensing SmtB, a DNA binding repressor (Cavet *et al.*, 2003). SmtB, which like Zur is a homodimeric protein, binds in its apo form to the promoter region and acts as a repressor of *smtA* transcription. If the cells are challenged by elevated levels of Zn(II), zinc-binding to SmtB induces conformational changes in SmtB, which

lead to de-repression and hence the production of SmtA protein able to bind the excess zinc (Blindauer, 2011). In addition to sequestering excess zinc, it has been suggested that SmtA also has a role in controlling the zinc status of zinc-requiring proteins, such as DNA primase (Cavet *et al.*, 2003).

A

Species/ Strain	Zur	SmtA/BmtA	SmtB
<i>Synechococcus</i> PCC7002	√	√	√
<i>Cyanothece</i> ATCC51142	?	√	-
<i>Synechococcus</i> PCC7942	?	√	√
<i>Synechococcus</i> CC9311	√	√	-
<i>Synechococcus</i> WH8102	√	√	-

B

SmtA/BmtA from Cyanobacteria

```

PCC7002      --MVTVTQMKCAGESCLCIVDLNSAIQKEGKSYCSQACADGHPAGSEGCGHGGETCHQ-- 56
ATCC51142    MTSATVTQMKCACPSCNCIVSISDAVQKEGKYYCGDACANGHPNGS-GCSHHGECHA-- 57
PCC6301      --MTSTTLVKCACEPCLONVDPKAIDRNGLYYCSEACADGHTGGSKGCGHTSGNCHG-- 56
PCC7942      --MTSTTLVKCACEPCLONVDPKAIDRNGLYYCSEACADGHTGGSKGCGHTSGNCHG-- 56
CC9311       --MATSNQV-GACDPCSCAVSVESAVQKDGKVYCSQPCADGHS-GSDECKKS-QDCC--- 52
WH8102       ----MSTAIKCACPKCTOMVAEESAIVLQGKFFCSTSCSTGHANNEPCHGEGSCGKCGE 56
  
```

**Figure 8.20 Multiple sequence alignments for SmtA/BmtAs from cyanobacteria.**

(A) The presence of Zur, SmtA/ BmtAs and SmtB genes predicted to be involved in zinc homeostasis in some cyanobacterial genomes. “-” Empty cells indicate absence of a recognizable zinc-related homologs, “?” indicates the presence of homologs with unclear metal specificity, and “√” indicates the presence of homologues in the genome. (B) The primary sequences for SmtA/ BmtAs are from *Synechococcus elongatus* PCC7942, *Synechococcus* sp. WH8102, *Synechococcus* sp. PCC7002, *Synechococcus* sp. CC9311, *Synechococcus* sp. PCC6301 and *Cyanothece* sp. ATCC51142. Residues known to be metal-binding ligands in SmtA and/or conserved in other sequences are shaded green (cysteines) and light grey (histidines), and other potential metal-binding residues are shaded in cyan.

Although some cyanobacteria have *bmtA* homologs, no obvious SmtB orthologs have been found in marine *Synechococcus* strains that possess *bmtA/smtA* (Figure 8.20A) suggesting an alternative method of regulation, different to that in freshwater strains, may exist. For instance,

*Synechococcus* sp. WH8102 is a marine strain that possesses an *smtA* gene, but no gene encoding a SmtB/ZiaR family zinc sensor (Figure 8.20A) (Barnett *et al.*, 2012).

Recent work by a colleague on the coastal cyanobacterium *Synechococcus* sp. CC9311 reveals that this bacterium possesses four metallothionein genes (*sync\_0853*, *sync\_1081*, *sync\_2379* and *sync\_2426*) (Chu, 2013). Of these, *sync\_0853* and *sync\_1081* exhibited the highest expression levels in response to zinc depletion, suggesting that these two genes might participate in zinc scavenging. There was no change in expression level for *sync\_2379* when this bacterium was exposed either to Zn(II) shock or Zn(II) starvation. In contrast, *sync\_2426* was the only metallothionein gene induced by zinc shock, and was markedly shut down following zinc starvation, suggesting that this gene may play a key role in zinc homeostasis in this organism (Chu, 2013). Surprisingly, *Synechococcus* sp. CC9311 does not possess SmtB either, but it was found to possess a Zur homolog (*sync\_2831*). The alignment of the product of the *synw\_0359* gene from *Synechococcus* sp. WH8102 with BmtAs from *Synechococcus* sp. CC9311 indicates that *synw\_0359* has 68.5% similarity to *sync\_1081*, which might act in a similar way (see Appendix H, Table H.03).

A greater understanding of the regulation of *smtA* by the SynZur protein in *Synechococcus* sp. WH8102 will provide a clear insight into other processes that require zinc or are affected by changes in zinc levels. In the absence of an *in vivo* study (such as qPCR), two possible scenarios could account for the regulation of *smtA* by SynZur, either the repression or the activation at high levels of Zn(II) for *smtA*. Next, the two scenarios will be discussed in more detail.

### 8.7.1 SynZur May Repress *smtA* at High Levels of Zn(II)

Zinc deficiency increases oxidative stress by increasing the production of nitrogen reactive species (RNS) and reactive oxygen species (ROS<sup>31</sup>), including hydroxyl radicals ( $\bullet\text{OH}$ ) and hydrogen peroxide ( $\text{H}_2\text{O}_2$ ) (Oteiza *et al.*, 2000; Wu *et al.*, 2007; Song *et al.*, 2009; Eide, 2011; Günther *et al.*, 2012; Parente *et al.*, 2013; Glover-Cutter *et al.*, 2014). Moreover, zinc deficiency can activate an unfolded protein response (UPR), indicating that protein misfolding is occurring; this might also be mediated through oxidative stress (Eide, 2011). MTs can function as antioxidants against reactive oxygen and nitrogen species (Eide, 2011; Ruttkay-Nedecky *et al.*, 2013). Inasmuch as MTs contain a high number of Cys residues, these proteins have been shown *in vitro* to scavenge hydroxyl radicals, due to their cysteinyl thiolate groups (Ruttkay-Nedecky *et al.*, 2013). For example, under oxidative stress conditions, MT was up-regulated in transgenic mouse hearts (Kang, 1999), whilst zinc deficiency in normal PrEC prostate epithelial cells results in up-regulated MT-1 gene expression (Yan *et al.*, 2008).

According to our first hypothesis, SynZur may repress and block the Zn-inducible gene *smtA* at high Zn(II) concentration and de-repress the *smtA* promoter at lower concentrations. This means that *smtA* from *Synechococcus* sp. WH8102 will be up-regulated under zinc-deficient conditions. The low-zinc environment and high-zinc requirements of cyanobacteria may suggest that the *Synechococcus* sp. WH8102 SmtA protein functions in zinc uptake and protects the cells from the oxidative stress that may face the cells under low Zn(II) concentration. Cyanobacteria are known to survive in zinc-deficient environments, but the manner in which they acquire and handle Zn(II) are not completely understood (Barnett *et al.*, 2014).

---

<sup>31</sup> Reactive oxygen species (ROS) such as hydroxyl radical ( $\text{HO}\bullet$ ), superoxide radical ( $\text{O}_2^{\bullet-}$ ) or hydrogen peroxide ( $\text{H}_2\text{O}_2$ ) can overwhelm the intrinsic antioxidant defences of cells, resulting in a condition known as “oxidative stress”.

Recently, it has been pointed out that two Zn-inducible transporter genes: *cgR\_1359* (designated as *zrf*, encoding a member of the cation diffusion facilitator CDF) and *cgR\_0148* (designated as *zra*, encoding a putative metal-translocating P-type ATPase), both of which are involved in Zn(II) resistance in *Corynebacterium glutamicum*, are up-regulated under zinc-deficient conditions and both are repressed by the Zur protein under high zinc conditions (Teramoto *et al.*, 2012).

In another example, Fur from *Synechocystis* sp. PCC6803, under iron-deficient conditions, a novel gene *sll1263* encoding a putative cation diffusion facilitator protein (CDF) (Jiang *et al.*, 2012) was up-regulated under low-iron conditions, hence, the high iron requirements of cyanobacteria lead to the functioning of CDF protein in iron uptake rather than efflux (Jiang *et al.*, 2012).

### 8.7.2 SynZur May Activate *smtA* at High Levels of Zn(II)

In most bacteria, the ferric uptake regulator (Fur) is a global regulator for iron homeostasis and other cellular processes such as combatting oxidative stress (Carpenter *et al.*, 2009; Da Silva Neto *et al.*, 2009). Apart from its role as a direct repressor of bacterial iron uptake systems, Fur can also activate genes encoding iron-requiring proteins in *E. coli* (SdhCDAB, AcnA, FumA, FtnA, and Bfr), often by an indirect mechanism (Da Silva Neto *et al.*, 2009).

Recent evidence also suggests that some Fur proteins can act as a direct transcriptional activator for a small RNA (sRNA<sup>32</sup>) named RyhB<sup>33</sup> (Hantke, 2001b; Altuvia, 2004; Masse *et al.*, 2007). Fur from *Neisseria meningitidis* mediates the classical iron-dependent repression of some genes (e.g. the transferrin receptor gene *tbp2*), where it performs as an activator for others

---

<sup>32</sup> A non-coding RNA (ncRNA) is a functional RNA molecule that is not translated into a protein.

<sup>33</sup> RyhB, The 90 nt-small regulatory RNA, downregulates a large number of transcripts encoding iron-using proteins, resulting in redistribution of the intracellular iron.

(e.g. *norB*, *panI* and *nuoABCDE*) (Delany *et al.*, 2004). Fur from the human pathogen *Helicobacter pylori* can directly regulate iron-co-factored superoxide dismutase *sodB*, which is essential for defence against toxic superoxide radicals under iron-replete conditions (with Fe), while there is no expression of *sodB* in iron-restricted conditions (without Fe) (Ernst *et al.*, 2005). Iron-loaded Fur appears to be an activator in the presence of FeSO<sub>4</sub> for the *nifS* gene involved in Fe-S cluster formation (Alamuri *et al.*, 2006), and the *Pfr* gene involved in iron storage ferritin (Delany *et al.*, 2001). Remarkably, iron-loaded Fur, as an activator, can bind to two DNA binding sites (Alamuri *et al.*, 2006).

Mur from *Deinococcus radiodurans* serves as a positive regulator, in other words an activator, of the manganese efflux pump gene *mntE* (*dr1236*), and as a negative regulator of MunABC transporter genes, in the presence Mn(II) (Shah *et al.*, 2014). Irr from *Bradyrhizobium japonicum* functions when cellular iron levels are low, and can serve as either a repressor for the heme uptake system or as an activator for bacterioferritin and rubrerythrin homologues in iron replete medium (Rudolph *et al.*, 2006).

Recently, it was demonstrated, both *in vivo* and *in vitro*, that in addition to acting as a repressor of putative Zn(II)-uptake systems, Zur from the bacterial phytopathogen *Xanthomonas campestris* pathovar *campestris* (Xcc) acts as an activator of a Zn(II) efflux pump (Huang *et al.*, 2008). XccZur binds to a similar Zur-box with a ~30-bp AT-rich sequence in the promoters of the genes encoding putative Zn(II)-uptake systems, but a 59-bp GC-rich sequence with a 20-bp inverted repeat overlapping the promoters -35 to -10 sequence of the gene encoding a Zn(II)-export system (Huang *et al.*, 2008). This revealed that XccZur functions as both a repressor and an activator of putative zinc homeostasis genes through the recognizing of two distinct sequences within its target promoters (Huang *et al.*, 2008). In our case, a similar phenomenon occurred for SmtA. SynZur binds to a similar Zur-box with ~23-bp AT-rich sequence in the

promoters of the genes encoding putative Zn(II)-uptake systems, ZnuABC transporter, but a 49-bp AT-rich sequence overlapping the promoters -35 to -10 sequence of *smtA*.

According to our second hypothesis, SynZur may activate *smtA* at high Zn(II) concentration by facilitating the binding of RNA polymerase. In the human pathogen *Streptococcus pneumoniae*, there is evidence that the regulation of zinc-uptake and zinc-efflux occurs at distinct zinc concentrations, with repression of uptake genes occurring at lower total zinc relative to de-repression/activation of export genes (Jacobsen *et al.*, 2011; Braymer & Giedroc, 2014). This could explain why SynZur may be bound to both *znuABC* and *smtA* promoters at the same time.

However, up-regulating metallothionein could have a dual role in protection against zinc excess, and at the same time providing a source of zinc that can be brought into use during periods of zinc limitation. It was pointed out that MT could function as a zinc chaperone to transfer zinc directly to acceptor proteins in order to make zinc available specifically on the demand of the zinc-binding proteins (Feng *et al.*, 2005) such as is the case of apo-carbonic anhydrase (Mason *et al.*, 2004) and mitochondrial aconitase (Feng *et al.*, 2005). However, up-regulation of *smtA* at high zinc levels is the more likely scenario than at low zinc levels in our case.

It is clear from the examples presented in this section that Zur activation does not occur in a similar manner to Zur repression. How might SynZur binding contribute to up-regulating transcription? Does the binding of Zur alter the structure of DNA to allow the binding of RNA polymerase? All these questions are waiting to be answered. In the most probable scenario, SynZur may be able to change the overall structure of the DNA by distorting the operator DNA sequence. A hypothesis will next be presented regarding the role of SynZur as a transcriptional activator.

### 8.7.2.1 SynZur as a Transcriptional Activator of *smtA*

$\beta\beta'\alpha_2\omega$  is the core enzyme subunit composition in RNA polymerase. This form of polymerase is capable of DNA-dependent RNA synthesis, but is unable to locate promoters and direct specific transcript initiation (Lee *et al.*, 2012) (Figure 8.21). The key factor for specific transcript initiation at promoters is the  $\sigma$  subunit (Lee *et al.*, 2012). This contains four distinct domains, and has three main functions. Firstly, it ensures the recognition of specific promoter sequences; Secondly, it ensures the position of RNA polymerase holoenzyme,  $\beta\beta'\alpha_2\omega\sigma$ , at a target promoter; and finally, it facilitates the unwinding of the DNA duplex near the transcription start site (Browning & Busby, 2004). Cyanobacteria have additionally unique composition of the RNA polymerase (RNAP) core due to splitting of the  $\beta'$  subunit to N-terminal  $\gamma$  and C-terminal  $\beta''$  subunits (Gunnelius *et al.*, 2014).

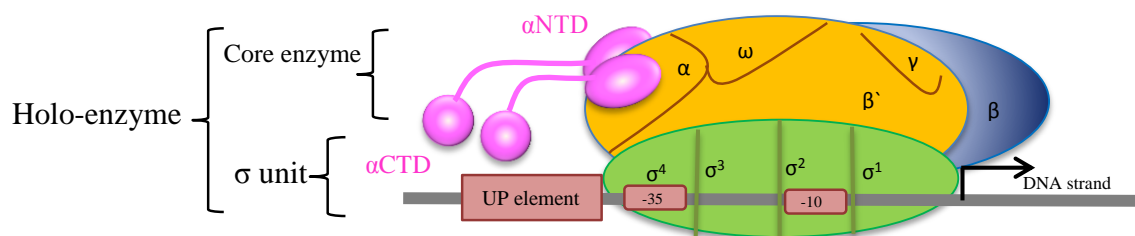


**Figure 8.21 A schematic representation of the Holo-enzyme for RNA polymerase.**

Interactions of the holo-enzyme of RNA polymerase, which consists of  $\beta\beta'\alpha_2\omega\sigma\gamma$  with its promoter in cyanobacteria. The location of the transcription start site is indicated by the bent arrow. NTD is a N-terminal domain, CTD is a C-terminal domain, and UP is an upstream of DNA. Adapted from (Lee *et al.*, 2012).

The main promoter elements that facilitate specific transcript initiation by RNA polymerase are the UP (upstream) element, the -35 element and the -10 element (Murakami & Darst, 2003; Lee *et al.*, 2012). Additional promoter recognition determinants are provided by the C-terminal domains of the two RNA polymerase  $\alpha$  subunits ( $\alpha$ CTDs) that interact with UP elements,

located upstream of the -35 element (Figure 8.21).  $\alpha$ CTDs are separated from the  $\alpha$  subunit N-terminal domain ( $\alpha$ NTD) by an unstructured linker, and it has been observed that  $\alpha$ CTDs operate as antennae for RNA polymerase (Lee *et al.*, 2012).

In principle there are two mechanisms for transcriptional activation. The activator might alter the conformation of the promoter DNA to improve its quality, or the activator could interact directly with RNA polymerase to compensate for the defects in a promoter (Browning & Busby, 2004; Lee *et al.*, 2012).

Three general mechanisms are used for 'simple' activation described as Class I, Class II and Class III. In class I activation, the activator binds to a target that is located upstream of the promoter -35 element and recruits RNA polymerase to the promoter by directly interacting with the RNA polymerase  $\alpha$ CTD. In Class II activation, the activator binds to a target that overlaps the promoter -35 element and contacts domain 4 of the RNA polymerase  $\sigma$  subunit (Browning & Busby, 2004). In Class III activation, the activator binds to the promoter both as Class I and Class II (Browning & Busby, 2004; Lee *et al.*, 2012). Another mechanism for simple activation is found in cases where the activator alters the conformation of the target promoter to enable the interaction of RNA polymerase with the promoter -10 and/or -35 elements. This requires the activator to bind at, or very close to, the promoter elements (Brown *et al.*, 2003; Browning & Busby, 2004).

For example, a nice story is told by Lee and colleagues showed that the CRP protein, the global regulator of genes for carbon source utilization in the absence of glucose, functions as a dimer and is the best-studied prokaryotic transcription factor that operates as an activator (Lee *et al.*, 2012). CRP binds DNA as a dimer and has two binding sites in some promoters where it works both as an activator and repressor (Zheng *et al.*, 2004; Shimada *et al.*, 2011; Lee *et al.*, 2012). This leads to an interesting question: is there any similarity between CRP and SynZur, when

the SynZur protein from *Synechococcus* sp. WH8102 may work as an activator, our second hypothesis? (see Section 8.7.2).

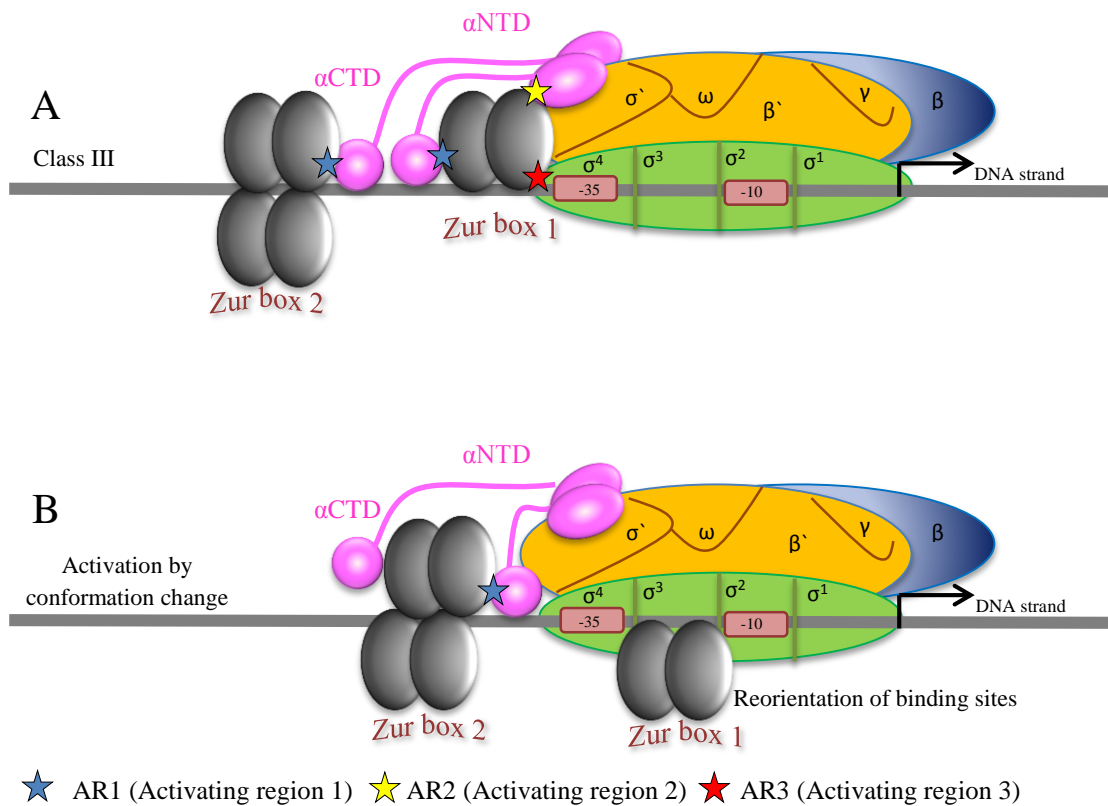


**Figure 8.22 Hypothetical mechanism for SynZur as an activator for the *smtA* promoter.**

The above figure illustrates our hypothesis about the organisation of RNA polymerase subunits and the SynZur protein during activation at a *smtA* promoter. (A) Activation of a *smtA* promoter by SynZur dimers at a Class III position, where SynZur in Zur box 2 interacts with the C-terminal domain of the RNA polymerase  $\alpha$  subunit via AR1 (blue star) (Class I) as two dimers, while in Zur box 1, SynZur binds adjacent to RNA polymerase and interacts with different polymerase subunits: AR2 (yellow star) interacts with  $\alpha$ CTD, AR1 interacts with an  $\alpha$  subunit N-terminal domain (NTD), and AR3 (red star) interacts with  $\sigma$  domain 4 (Class II) as one dimer. (B) Activation of *smtA* promoter by two SynZur dimers as a Class I in the Zur box 2 and as a conformational change in the Zur box 1 with one dimer. SynZur dimer binds upstream of RNA polymerase and contacts one or both  $\alpha$  subunit C-terminal domains (CTDs) via AR1 (activating region 1) (blue star). SynZur dimer is shown in grey; the -10 and -35 elements are indicated by red boxes. This hypothesis depends on CRP, a dimer protein which performs as an activator (Lee *et al.*, 2012).

Depending on CRPs mechanism as an activator and our results demonstrating two DNA fragments retarded on the gel (Figure 8.07C) as well as my conclusion from the 6-1-6 motif (Section 8.5.1), I postulate that SynZur may bind to *smtA* at a Class III position (Figure 8.22A)

or *via* a conformational change (Figure 8.22B). In the proposed Class III scenario, SynZur may bind adjacent to RNA polymerase and interacts with different polymerase subunits, whereas one SynZur dimer interacts with the  $\alpha$  subunit N-terminal domain (NTD) *via* AR2 (activating region 2), and  $\sigma$  domain 4 *via* AR3 (activating region 3) for RNA in Zur box 1(class II), whereas in Zur box 2, two SynZur dimers may interact with  $\alpha$  subunit C-terminal domain (CTD) *via* AR1 (activating region 1) (class I) (Figure 8.22A). In the conformational change scenario, SynZur dimers may bind as Class I in Zur box 2 and as a conformational change in Zur box 1 with one dimer (Figure 8.22B). However, depending on the location of the -10 and -35 elements (Section 8.3), the most probable mechanism is supported by the second hypothesis (Figure 8.22B).

## 8.9 Summary and Conclusion

Metalloregulatory proteins serve as a direct link between intracellular metal ion levels and the expression of metal uptake, efflux, and storage systems (Dennis, 2007; Giedroc & Arunkumar, 2007). These proteins allow organisms to adapt quickly to either excess or scarcity of a particular metal ion in their micro-environment, thus avoiding toxicity or deprivation. The regulatory ion-binding (sensing) sites of metalloregulatory sensor proteins should have a quick reaction for rapid reversible uptake of the target metal ion (Bellini & Hemmings, 2006).

The previous chapter has shown that the zinc ion in sensory site 2 is labile and that binding and release are reversible. SynZur contains essentially two Zn(II) ions per monomer. Zinc-loaded SynZur exhibited an ability to bind to the zur-box of specific DNA probes irrespective of the presence of further zinc ions. Moreover, treating the SynZur protein with the strong Zn(II) chelating agent, EDTA, had the effect of removing zinc ion efficiently from one site, likely the sensory site, forming a Zn<sub>1</sub>Zur species. This species was not able to bind to the same promoters in the absence of zinc ions. Back titration of Zn<sub>1</sub>Zur species with zinc ion under anaerobic

conditions confirmed the ability of SynZur to re-form the dimeric  $Zn_4(Zur)_2$  species, and to re-bind to the zur-box containing promoter sequences.

Our data imply a complicated interplay between the Zn(II) uptake system (ZnuABC) and (SmtA) under the control of SynZur. It is interesting to note that in *Synechococcus* sp. WH8102, SynZur may play a dual role both as an activator or repressor. *In vitro* studies show that SynZur binds specifically to a Zur box located between the divergently transcribed *znuCB* and *znuA* genes. At the same time SynZur binds specifically to a 49-bp region presenting as two Zur boxes and activates or represses the expression of the *synw\_0359* gene, *smtA*. To our knowledge, this is the first evidence of direct interaction between a Zur protein and a gene for a bacterial metallothionein.

These findings open the door to understanding how zinc availability and occupancy in the sensory sites can fine tune gene expression across the promoters. Despite this significant development in our study, the molecular details of the distinctive Zn(II)-responsive binding modes of SynZur remain an interesting subject for future studies.

# Chapter 9

## General Discussion, Recommendations and Conclusions

---

### 9.1 Introduction

Zinc is involved in a huge number of biological processes and its chemical properties make this metal ion act as a structural element which helps to maintain the conformation of particular protein domains. Additionally, it is a catalytic cofactor in the active site of a variety of enzymes such as those involved in respiration, CO<sub>2</sub> fixation and photosynthesis (Morel *et al.*, 1994; Cohen & Gurevitz, 2006).

Therefore, it is essential for bacteria to maintain zinc ion homeostasis, and to achieve this they have evolved sophisticated systems for controlling the uptake and efflux of this ion (Patzner & Hantke, 1998; Kondrat *et al.*, 2013; Prusic *et al.*, 2015).

In general, the proteins that transduce metal ion signals into changes in gene or protein expression are designated as “metallo-regulatory” sensing proteins (Dennis, 2007; Giedroc & Arunkumar, 2007). These proteins allow the organisms to adapt quickly to toxicity or deprivation, due to either excess or depletion of metal ions in their environment. These sensing proteins have evolved metal coordination sites able to “sense” specific metals ion(s) by forming

specific coordination complexes which in turn either activate or inhibit DNA binding, thereby controlling the expression of genes (Giedroc & Arunkumar, 2007).

Zur, the zinc uptake regulator protein which is a member of the Fur family of proteins, is a metallo-regulatory sensing protein which senses zinc ions and controls the expression of zinc transport systems that maintain zinc homeostasis.

Marine picocyanobacteria are the most abundant photosynthetic organisms on Earth, with only two genera, *Prochlorococcus* and *Synechococcus*, numerically dominating most oceanic waters. *Synechococcus* are abundant and widely distributed (Partensky *et al.*, 1999) in the oligotrophic gyres, coastal regions, and upwelling zones where availability of zinc can limit growth and thus primary production (Morel *et al.*, 1991; Morel *et al.*, 1994; Hong *et al.*, 1996). *Synechococcus* strains are usually limited to the upper 100 m of the water column (Partensky *et al.*, 1999) and less abundant in very oligotrophic environments, but they have a broad global distribution, including in HNLC regions (high nutrient, low chlorophyll) (Zwirgmaier *et al.*, 2008; Scanlan *et al.*, 2009).

Remarkably, *Synechococcus* strains have the ability to acquire major nutrients and trace metals at the submicromolar concentrations found in the oligotrophic open seas (Palenik *et al.*, 2003). This has led to a strong selective pressure towards adaptations that aid survival during periods of nutrient limitation (Blindauer, 2008; Tetu *et al.*, 2009). Indeed, the availability of zinc can lead to changes in the composition and structure of marine planktonic communities (Sunda & Huntsman, 1995; Saito & Goepfert, 2008). If zinc can affect marine planktonic community structure, does this mean that all *Synechococcus* species require zinc?

In *Synechococcus* species, zinc is likely to be important for CO<sub>2</sub> fixation *via* the enzyme carbonic anhydrase, which is part of the CO<sub>2</sub>-concentrating mechanism, usually using a zinc co-factor for catalysis (Duursma & Dawson, 1981). Despite the obvious environmental

importance of marine cyanobacteria, only a few experimental studies have been achieved regarding zinc homeostasis in these bacteria and related organisms (Morby *et al.*, 1993; Sunda & Huntsman, 1995; Cavet *et al.*, 2003; Napolitano *et al.*, 2012; Kondrat *et al.*, 2013; Mahadev *et al.*, 2013; Barnett *et al.*, 2014). Moreover, understanding modes of acquisition and homeostasis of the micronutrient zinc by cyanobacteria is of key importance, given their global role in the biogeochemical cycling of elements.

*Synechococcus* sp. WH8102 is a strain from Clade III of the marine *Synechococcus* lineage which was isolated from oligotrophic regions (Waterbury *et al.*, 1986), where zinc is thought to be limited and zinc organic speciation is dominated (Jakuba *et al.*, 2008a). This strain acquires zinc even under extremely low zinc concentrations (Barnett *et al.*, 2014), indicating that *Synechococcus* sp. WH8102 possesses effective mechanisms both for zinc acquisition and zinc homeostasis. Moreover, bioinformatics analyses of *Synechococcus* sp. WH8102 strongly indicated that this strain contains a Fur homologue likely to be Zur (SYNW2401) (<http://genome.kazusa.or.jp/cyanobase>).

These early findings and publications set the stage for my PhD study and established several questions that needed to be answered: Does *Synechococcus* sp. WH8102 responsible for a zincophore-mediated zinc system, dominated in its area, similar to siderophore-mediated iron and chalkophore-mediated copper systems? Is the Fur homologue SYNW2401 a real zinc uptake regulator protein? Therefore, in an attempt to answer these questions, work has been performed in this study to understand zinc network and homeostasis in *Synechococcus* sp. WH8102.

## 9.2 Key Findings

Regarding the existence of zincophores produced by *Synechococcus* sp. WH8102 (**Chapter 3**), it seems likely that this marine cyanobacterium produces, in axenic culture, ligands that can bind to zinc under zinc-depleted conditions (80 nM) but not under zinc replete conditions (2  $\mu$ M). The identity of the putative zincophore(s) unfortunately remained elusive.

Furthermore, proteomic analysis provided evidence that *Synechococcus* sp. WH8102 possesses an adaptive response to different zinc concentrations (**Chapter 4**). Thus, *Synechococcus* sp. WH8102 grew not only in medium that closely matches its *in situ* environment i.e. in medium containing 80 nM zinc (zinc-deplete medium), but also in media that are far from its *in situ* environment i.e. in medium containing 2  $\mu$ M zinc (zinc-replete medium), and had the ability to adapt to its environment by altering the expression of several proteins under zinc-deplete/replete conditions.

Genomic analysis of *Synechococcus* sp. WH8102 suggested that the gene *synw\_2401* encodes a Zur protein (Barnett *et al.*, 2012), designated SynZur in this study. To begin to understand the mode of action of this protein in *Synechococcus* sp. WH8102, studies on recombinantly expressed SynZur were performed. The *synw\_2401* gene was cloned into pET151/D plasmid using TOPO cloning and SynZur was expressed as a His<sub>6</sub>-tag fusion protein in different strains of *E. coli* (**Chapter 5**). The most promising expression method was found to be in the presence of the GroES-GroEL-Tig chaperones expressed from the pG-Tf2 plasmid in LB medium. Immobilized metal affinity chromatography (IMAC), followed by cleavage of the His<sub>6</sub>-tag with TEV protease were powerful techniques to obtain significant quantities of pure, untagged SynZur protein. SynZur was produced with good agreement between experimental and theoretical masses for both the apo and metal loaded forms. SynZur, at neutral pH (~pH 7.8) presented as a mixture of species, including a monomer with two zinc ions bound, a dimer with

four zinc ions bound, and another well folded Zur<sub>2</sub>Zn<sub>4</sub> dimer. The ESI-MS data were corroborated by ICP-OES data which indicated that SynZur as isolated contained  $2.1 \pm 0.2$  Zn(II) ions per monomer.

The 1D <sup>1</sup>H NMR spectrum for SynZur yielded a significant dispersion of resonance lines in three spectral regions of interest. Some resonances were well separated in the region of the methyl protons (-0.5 to 1.5 ppm) and the resonances were relatively sharp in the α proton region (3.5 to 6 ppm), while there was only a small number of dispersed resonance lines in the amide proton region (6–10 ppm). Moreover, variation in temperature and salt concentrations were found to be useful to modestly improve the 1D <sup>1</sup>H NMR spectrum for SynZur. In addition, a significant improvement in sensitivity and observation of dispersed signals for 2D <sup>1</sup>H, <sup>15</sup>N NMR spectra was achieved using the [<sup>1</sup>H, <sup>15</sup>N] HSQC-TROSY technique rather than the conventional [<sup>1</sup>H, <sup>15</sup>N] HSQC (**Chapter 6**), although the spectral quality was not sufficient for structural studies. Further optimisations may be possible, but were not pursued; instead, crystallisation trials were initiated and resulted in some promising conditions that may allow the structure of SynZur to be solved in the future.

A major feature of Fur family proteins concerns the fact that the metal in the sensory site is labile (Althaus *et al.*, 1999; D'Autréaux *et al.*, 2007; Shin *et al.*, 2011). To assess this feature in SynZur, the metal chelator EDTA was employed, essentially mimicking a drop in available cellular zinc as may be expected in zinc-deplete conditions. Only one of the two metal ions bound per monomer was removed by EDTA from the SynZur protein, giving  $0.9 \pm 0.3$  Zn(II) atoms per monomer. It is thought that the labile metal ion corresponds to the sensory site, whilst the inert site corresponds to a structural Cys<sub>4</sub> site that is present in most Fur family proteins. Surprisingly, during incubation with EDTA, the monomer/dimer equilibrium was shifted towards the monomeric state and the Zn<sub>1</sub>Zur species was the dominant one in the spectrum (**Chapter 7**). Moreover, ESI-MS and NMR data indicate that the Zn<sub>1</sub>Zur species was stable for

a long time. Upon incubation of SynZur protein with EDTA, slight changes were observed in CD spectra which were due to the zinc being released from the sensory site and changes in the oligomer distribution suggesting no large difference in the secondary structure between the metallo-species of the SynZur protein.

SynZur was also found to behave in a similar manner to previously studied Fur family proteins, in that zinc removal from the sensory site is fully reversible. SynZur has the ability to re-establish a (2:1) Zn(II):protein ratio giving very similar spectra to the native ones, in less than 15 min, containing: monomer, dimer, and well-folded dimer, with  $1.9 \pm 0.4$  Zn(II) atoms per monomer, which is very close to the native ratio,  $2.1 \pm 0.2$  Zn(II) ions per monomer. This gave an idea how fast the response of *Synechococcus* sp. WH8102 Zur protein to increase in the cytosolic Zn(II) concentration might be.

Although EDTA could effectively remove zinc ions from the sensory site, the removal of zinc ions completely from both sites required dropping in the pH. At lower pHs  $\sim 6.97$ - $5.61$ , it was observed that the proportion of monomer/dimer was shifted toward the dimeric state and  $Zn_4Zur_2$  species was the most dominant one in the spectrum, suggesting that the dimeric state is perhaps more stable than the monomeric state at lower pH. Upon dropping in pH to 4.25, all zinc ions were stripped from the monomer and dimer, with apo-Zur the dominating species in the spectrum. However, during pH titration, it was noted that Zn(II) at the structural Cys<sub>4</sub> site in the SynZur protein plays an important role in maintaining the integrity of the protein structure and, hence, losing the metal ion from this site led to partial unfolding and/or aggregation, as observed by NMR and CD data.

Taken together these observations give us the opportunity to present a hypothesis in Figure 9.01. At low levels of Zn(II), the zinc ion will be removed from sensory sites in  $Zn_4Zur_2$  and this will cause the DNA-binding domain to swing around the hinge region with respect to the dimerization-domain, from closed (swung-in) to an open (swung-out) conformation and form

a  $Zn_2Zur_2$  dimer. However, the newly formed species,  $Zn_2Zur_2$ , is unstable at low levels of  $Zn(II)$  and dissociates into two  $Zn_1Zur$  species (Figure 9.01).

In turn, when  $Zn(II)$  levels increase, a zinc ion will re-bind to the sensory site, and this will lead to dimerization of two monomers to form the swung-in  $Zn_4Zur_2$  species that has a high DNA-binding affinity.

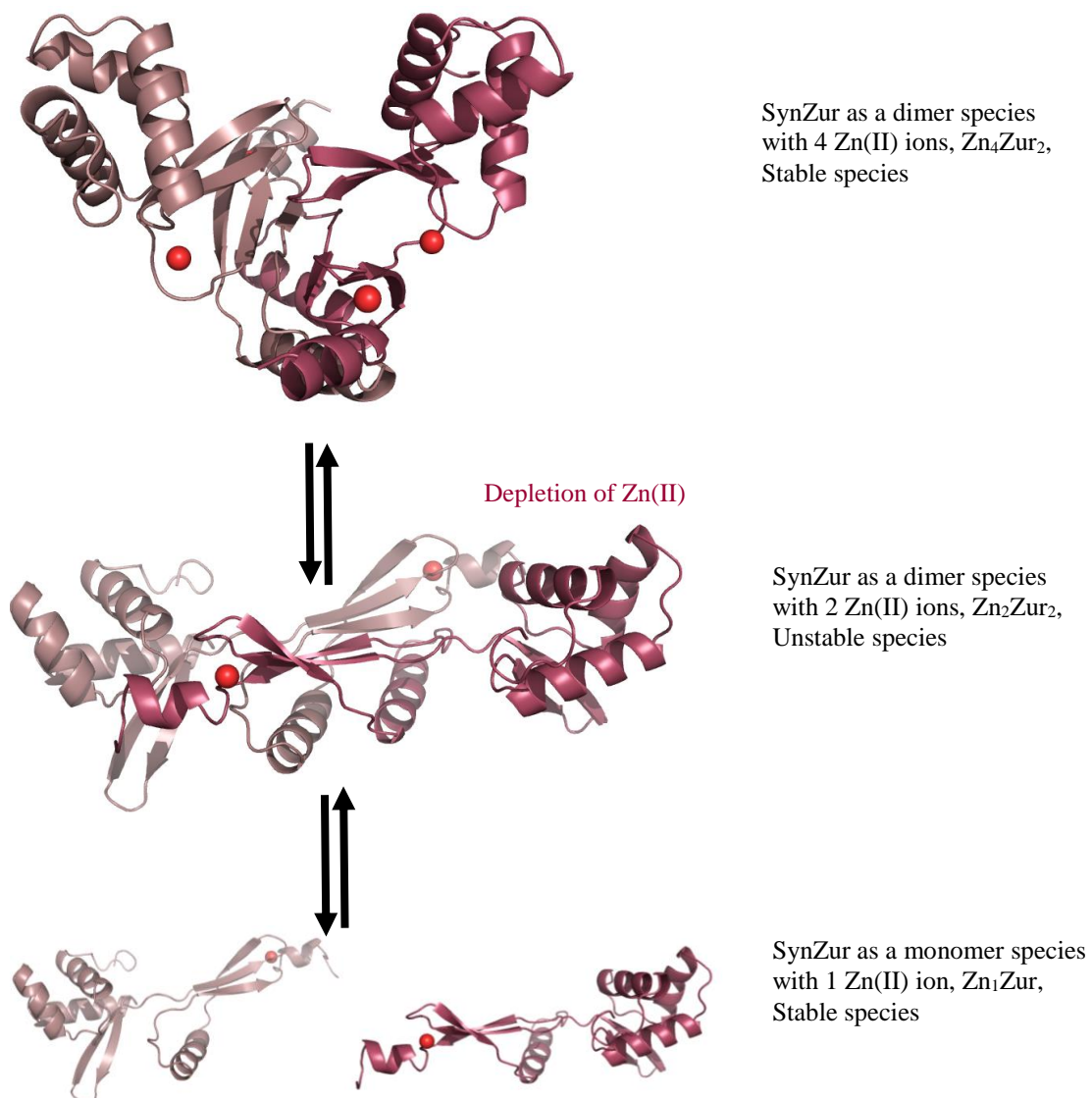


**Figure 9.01 Allosteric structural changes in SynZur in low levels of  $Zn(II)$ .**

Suggested allosteric structural changes for the Zur protein from *Synechococcus* sp. WH8102 induced by changes in the  $Zn_4Zur_2$  species under low levels of  $Zn(II)$ .  $Zn(II)$  ions are in red. Ribbon representation of the  $Zn_4Zur_2$ ,  $Zn_2Zur_2$  and  $Zn_1Zur$  species are in light and dark salmon.

Bioinformatic prediction of Zur-binding motifs in *Synechococcus* sp. WH8102 using the RegPrecise database indicated the presence of three Zur boxes including one Zur box for a *znuABC* transport system, and two adjacent boxes for *smtA*, a metallothionein. Therefore, EMSAs were employed to investigate binding of SynZur to these predicted promoters. In light of our *in vitro* EMSA studies, SynZur was shown to bind specifically to the AT-rich Zur box located between the divergently transcribed *znuCB* and *znuA* genes and is thus predicted to repress the transcription of *znuABC* (**Chapter 8**). The Zur boxes overlap the putative -35 region of the target genes, suggesting that the binding of SynZur prevents RNA polymerase from interacting with the promoter. At the same time SynZur binds specifically to a 49-bp region comprising two Zur boxes, Zur box-1 and Zur box-2, to regulate the expression of the *synw\_0359* gene, *smtA*. To our knowledge, this is the first description of regulation of a bacterial metallothionein by a Zur sensor protein.

The “free” zinc concentrations that trigger transcription of *znuABC* and *smtA* were found to be extremely low and falling into the femtomolar range, suggesting that *Synechococcus* sp. WH8102 may exert tight control over cytosolic metal concentrations, even for relatively low-toxicity metals such as zinc. The dissociation constant was  $\sim 62.65 \pm 1.47$  nM and  $61.76 \pm 2.42$  nM for *SynZur-P<sub>znuA</sub>* promoter and *SynZur-P<sub>smtA</sub>* complexes, respectively. The Hill constant,  $\alpha_H = 1.47$ , indicated the presence of cooperativity in the case of *SynZur-P<sub>smtA</sub>* complexes which may suggest that SynZur can bind as two dimers to the *smtA* promoter.

Moreover, the presence of EDTA, presumably leading to the removal of the sensory zinc as shown in Chapter 7, impaired the ability of the SynZur protein to bind to the same promoters. Back titration of the  $Zn_1Zur$  species with zinc ions under anaerobic conditions confirmed the ability of SynZur to re-form a DNA-binding species, likely the dimeric  $Zn_4(Zur)_2$  species characterised in Chapter 7, giving the same protein-DNA complexes as observed for the untreated protein.

These findings open the door to understanding how zinc availability and occupancy at the sensory site in the sensor protein can fine-tune gene expression across the promoters. Despite this significant development in this study, many molecular details of the mechanisms of zinc homeostasis in *Synechococcus* sp. WH8102 are still to be elucidated, even though these are of particular interest for environments in which the concentration of essential zinc is extremely low such as oligotrophic oceans. Many questions remain and further work is required to establish the zinc transport network in these marine cyanobacteria.

### 9.3 Recommendations

Solid phase extraction with liquid chromatography/mass spectrometry gave indications for the presence of zincophore(s) in *Synechococcus* sp. WH8102 culture supernatants. However, further optimization – e.g. different solid phase extraction with lower zinc concentrations – may be required to obtain sufficiently large amounts of this compound to enable MS and NMR characterisation. Additionally, microarrays or RNA-Seq analysis will give a more complete picture of the genes up- and down-regulated in *Synechococcus* sp. WH8102 during zinc deplete/replete conditions.

Despite the identification of some promising conditions (see Section 6.5), due to time constraints, full optimisation of crystallization conditions was not possible. Hence, further work is required to obtain crystals of a sufficient size for structural determination.

Whilst it was clear that 150 mM NaCl 308 K and [<sup>1</sup>H,<sup>15</sup>N] HSQC-TROSY improve the NMR spectra, these conditions still require further optimisation. TROSY NMR or even solid state NMR may provide more information that might allow sequential assignments through multidimensional NMR studies. This may enable determination of the (solution) structure for both Zn<sub>1</sub>Zur species and fully metallated dimer, and conclusive chemical shift perturbation experiments.

Knocking out the *synw\_2401* gene may also provide information about the role of this gene in zinc homeostasis; however, genetic manipulation of *Synechococcus* sp. WH8102 is challenging and extremely time-consuming, so was outside the scope of the current project. Site-directed mutagenesis of the *synw\_2401* gene may also be employed to explore the role of the two metal ion binding sites individually. Studying the binding affinity of Zn(II) for SynZur as well as such mutant proteins using a zinc-sensitive fluorescent dye with fluorescence spectroscopy will provide quantitative binding affinity data.

Evidence has been reported that, in addition to repressing *znuABC*, Zur can also repress a number of genes encoding homologues of ribosomal proteins (Panina *et al.*, 2003; Gilston *et al.*, 2014). For example, the genetic response to zinc limitation in *B. subtilis* (Panina *et al.*, 2003), *S. coelicolor* (Shin *et al.*, 2007), *M. tuberculosis* (Prisic *et al.*, 2015) and *E. coli* K-12 (Hantke, 2005; Gilston *et al.*, 2014) includes several ribosomal protein (r-protein) paralogs (L31 (*rpmE* and *ytiA*), L33 (*rpmGA*, *rpmGB* and *rpmGC*), S14 (*rpsN* and *yhzA*) and L36). Significantly, *Synechococcus* sp. WH8102 contains homologues for all the ribosomal protein mentioned above (L31 (*synw\_2095*), L33 (*synw\_1226*), L36 (*synw\_2087*) and S14 (*synw\_1896*)). Therefore, it would be interesting to assess if these particular genes are also under the control of Zur in *Synechococcus* sp. WH8102.

Although other divalent cations could trigger the dimerization of the Zur protein, zinc seems to be favoured for Zur proteins *in vivo* due to its high affinity for zinc rather than other cations (Foster *et al.*, 2012; Tottey *et al.*, 2012). A question remains if this is also the case for SynZur from *Synechococcus* sp. WH8102.

Further study is required to check whether SynZur is a repressor or activator for *smtA* (for example using qPCR). A complete understanding still awaits the elucidation of Zur–DNA complexes by carrying out DNA footprinting studies.

## 9.4 Conclusions

Overall, research presented in this thesis investigating selected members of the putative zinc network in *Synechococcus* sp. WH8102, including the SynZur protein and zincophores, has extended our knowledge about the importance of Zn(II) in this cyanobacterium. Additionally, these investigations give us the insights into the role that the micronutrient zinc plays in natural marine *Synechococcus* populations occupying large tracts of the global oligotrophic ocean and that play a key role in global carbon cycling.

# Bibliography

- Ahn, B. E., J. Cha, E. J. Lee, A. R. Han, C. J. Thompson and J. H. Roe.** 2006. Nur, a nickel-responsive regulator of the Fur family, regulates superoxide dismutases and nickel transport in *Streptomyces coelicolor*. *Mol. Microbiol.* **59**(6): 1848-1858.
- Akanuma, G., H. Nanamiya, Y. Natori, N. Nomura and F. Kawamura.** 2006. Liberation of zinc-containing L31 (RpmE) from ribosomes by its paralogous gene product, YtiA, in *Bacillus subtilis*. *J. Bacteriol.* **188**(7): 2715-2720.
- Alamuri, P., N. Mehta, A. Burk and R. J. Maier.** 2006. Regulation of the *Helicobacter pylori* Fe-S cluster synthesis protein *NifS* by iron, oxidative stress conditions, and Fur. *J. Bacteriol.* **188**(14): 5325-5330.
- Althaus, W. E., C. E. Outten, K. E. Olson, H. Cao and T. V. O'Halloran.** 1999. The ferric uptake regulation (Fur) repressor is a zinc metalloprotein. *Biochemistry* **38**(20): 6559-6569.
- Altuvia, S.** 2004. Regulatory small RNAs: the key to coordinating global regulatory circuits. *J. Bacteriol.* **186**(20): 6679-6680.
- An, Y. J., B. E. Ahn, A. R. Han, H. M. Kim, K. M. Chung, J. H. Shin, et al.** 2009. Structural basis for the specialization of Nur, a nickel-specific Fur homolog, in metal sensing and DNA recognition. *Nucleic Acids Res.* **37**(10): 3442-3451.
- Anderson, E. S., J. T. Paulley, D. A. Martinson, J. M. Gaines, K. H. Steele and M. R. Roop.** 2011. The iron-responsive regulator Irr is required for wild-type expression of the gene encoding the heme transporter BhuA in *Brucella abortus* 2308. *J. Bacteriol.* **193**(19): 5359-5364.
- Andreini, C., L. Banci, I. Bertini and A. Rosato.** 2006. Zinc through the three domains of life. *J. Proteome. Res.* **5**(11): 3173-3178.
- Andreini, C., I. Bertini and A. Rosato.** 2009. Metalloproteomes: a bioinformatic approach. *Acc. Chem. Res.* **42**(10): 1471-1479.
- Anton, A., A. Weltrowski, C. J. Haney, S. Franke, G. Grass, C. Rensing, et al.** 2004. Characteristics of zinc transport by two bacterial cation diffusion facilitators from *Ralstonia metallidurans* CH34 and *Escherichia coli*. *J. Bacteriol.* **186**(22): 7499-7507.
- Aristilde, L., Y. Xu and F. M. Morel.** 2012. Weak organic ligands enhance zinc uptake in marine phytoplankton. *Environ. Sci. Technol.* **46**(10): 5438-5445.

- Baars, O. and P. L. Croot.** 2011. The speciation of dissolved zinc in the Atlantic Sector of the Southern Ocean. *Deep Sea Res. Part II: Topical Studies Oceanogra.* **58**(25-26): 2720-2732.
- Babula, P., M. Masarik, V. Adam, T. Eckschlager, M. Stiborova, L. Trnkova, et al.** 2012. Mammalian metallothioneins: properties and functions. *Metallomics* **4**(8): 739-750.
- Baichoo, N. and J. D. Helmann.** 2002. Recognition of DNA by Fur: A reinterpretation of the Fur box consensus sequence. *J. Bacteriol.* **184**(21): 5826-5832.
- Baker, A. N., D. Sept, S. Joseph, M. J. Holst and J. A. McCammon.** 2001. Electrostatics of nanosystems: application to microtubules and the ribosome. *Proc. Natl. Acad. Sci.* **98**(18): 10037-10041.
- Banci, L., I. Bertini, F. Cantini, S. Ciofi-Baffoni, J. S. Cavet, C. Dennison, et al.** 2007. NMR structural analysis of cadmium sensing by winged helix repressor CmtR. *J. Biol. Chem.* **282**(41): 30181-30188.
- Banci, L., I. Bertini, S. Ciofi-Baffoni, L. A. Finney, C. E. Outten and T. V. O'Halloran.** 2002. A new zinc-protein coordination site in intracellular metal trafficking: solution structure of the apo and Zn (II) forms of ZntA. *J. Mol. Biol.* **323**(5): 883-897.
- Barnett, J. P., A. Millard, A. Z. Ksibe, D. J. Scanlan, R. Schmid and C. A. Blindauer.** 2012. Mining genomes of marine cyanobacteria for elements of zinc homeostasis. *Front. Microbiol.* **3**: 142.
- Barnett, J. P., C. Robinson, D. J. Scanlan and C. A. Blindauer.** 2011. The Tat protein export pathway and its role in cyanobacterial metalloprotein biosynthesis. *FEMS Microbiol. Ecol.* **325**(1): 1-9.
- Barnett, J. P., D. J. Scanlan and C. A. Blindauer.** 2014. Identification of major zinc-binding proteins from a marine cyanobacterium: insight into metal uptake in oligotrophic environments. *Metallomics* **6**(7): 1254-1268.
- Barton, R. H., D. Waterman, F. W. Bonner, E. Holmes, R. Clarke, J. K. Nicholson, et al.** 2010. The influence of EDTA and citrate anticoagulant addition to human plasma on information recovery from NMR-based metabolic profiling studies. *Mol. BioSyst.* **6**(1): 215-224.
- Beard, S. J., R. Hashim, G. Wu, M. B. Binet, M. N. Hughes and R. K. Poole.** 2000. Evidence for the transport of zinc (II) ions *via* the pit inorganic phosphate transport system in *Escherichia coli*. *FEMS Microbiol. Lett.* **184**(2): 231-235.
- Bellini, P. and A. M. Hemmings.** 2006. *In vitro* characterization of a bacterial manganese uptake regulator of the Fur superfamily. *Biochemistry* **45**(8): 2686-2698.

- Bentley, D. S., K. F. Chater, A. M. Cerdeno-Tarraga, G. L. Challis, N. R. Thomson, K. D. James, et al.** 2002. Complete genome sequence of the model actinomycete *Streptomyces Coelicolor* A3(2). *Nature* **417**(1): 141-147.
- Berry, A. and K. E. Marshall.** 1993. Identification of zinc-binding ligands in the class II fructose- 1,6-bisphosphate aldolase of *Escherichia coli*. *FEBS Lett.* **318**(1): 11-16.
- Bertini, I., P. Turano, H. B. Gray, E. I. Stiefel and S. J. Valentine.** 2007. Metal Ions and Proteins: Binding, Stability, and Folding. In: I. Bertini, H.B. Gray, E.I. Stiefel and J.S. Valentine (Eds), *Biological Inorganic Chemistry Structure and Reactivity*, p. 31-41. University Science Books, Sausalito-California, USA, USA.
- Bhattacharya, D. and J. Cheng.** 2013. i3Drefine software for protein 3D structure refinement and its assessment in CASP10. *Plos One* **8**(7): e69648.
- Blindauer, C. A.** 2008. Zinc-handling in cyanobacteria: An update. *Chem. Biodiversi.* **5**(10): 1990-2013.
- Blindauer, C. A.** 2011. Bacterial metallothioneins: past, present, and questions for the future. *J. Biol. Inorg. Chem.* **16**(7): 1011-1024.
- Blindauer, C. A.** 2015. Advances in the molecular understanding of biological zinc transport. *Chem. Commun.* **51**(22): 4544-4563.
- Blindauer, C. A. and O. I. Leszczyszyn.** 2010. Metallothioneins: unparalleled diversity in structures and functions for metal ion homeostasis and more. *Nat. Prod. Rep.* **27**(5): 720-741.
- Bozym, R., A., F. Chimienti, L. Giblin, J., G. Gross, W., I. Korichneva, Y. Li, et al.** 2010. Free zinc ions outside a narrow concentration range are toxic to a variety of cells *in vitro*. *Exp. Biol. Med.* **235**(6): 741-750.
- Bradford, M. M.** 1976. A rapid and sensitive method for the quantitation of microgram quantities of protein utilizing the principle of protein-dye binding. *Anal. Biochem.* **72**(1-2): 248-254.
- Brand, L. E., W. G. Sunda and R. L. Guillard.** 1983. Limitation of marine phytoplankton reproductive rates by zinc, manganese, and iron. *Limnol. Oceanogr.* **28**(6): 1182-1198.
- Braymer, J. J. and D. P. Giedroc.** 2014. Recent developments in copper and zinc homeostasis in bacterial pathogens. *Curr. Opin. Chem. Biol.* **19**(1): 59-66.
- Brocklehurst, K. R., J. L. Hobman, B. Lawley, L. Blank, S. J. Marshall, N. L. Brown, et al.** 1999. ZntR is a Zn(II)-responsive MerR-like transcriptional regulator of ZntA in *Escherichia coli*. *Mol. Microbiol.* **31**(3): 893-902.
- Brown, N. L., J. V. Stoyanov, S. P. Kidd and J. L. Hobman.** 2003. The MerR family of transcriptional regulators. *FEMS Microbiol. Rev.* **27**(2-3): 145-163.

- Browning, D. F. and S. W. Busby.** 2004. The regulation of bacterial transcription initiation. *Nat. Rev. Microbiol.* **2**(1): 57-65.
- Bruland, K. W.** 1989. Complexation of zinc by natural organic ligands in the central North Pacific. *Limnol. Oceanogr.* **34**(2): 269-285.
- Bruland, K. W., J. R. Donat and D. A. Hutchins.** 1991. Interactive influences of bioactive trace metals on biological production in oceanic waters. *Limnol. Oceanogr.* **36**(8): 1555-1577.
- Bruland, W. K. and M. C. Lohan.** 2006. Controls on trace metals in seawater. In: H. Elderfield (Ed.), *The Oceans and Marine Geochemistry: Treatise on Geochemistry, Volume 6*, p. 23-47. Elsevier Ltd., Oxford, UK.
- Campoy, S., M. Jara, N. Busquets, A. M. de Rozas, I. Badiola and J. Barbé.** 2002. Role of the high-affinity zinc uptake *znuABC* system in *Salmonella enterica* serovar typhimurium virulence. *Infect. Immun.* **70**(8): 4721-4725.
- Carpenter, B. M., J. M. Whitmire and S. D. Merrell.** 2009. This is not your mother's repressor: the complex role of Fur in pathogenesis. *Infect. Immun.* **77**(7): 2590-2601.
- Cavet, J. S., G. M. Borrelly and N. J. Robinson.** 2003. Zn, Cu and Co in cyanobacteria: selective control of metal availability. *FEMS Microbiol. Rev.* **27**(2-3): 165-181.
- Cerasi, M., J. Liu, Z., S. Ammendola, A. Poe, J., P. Petrarca, M. Pesciaroli, et al.** 2014. The ZupT transporter plays an important role in zinc homeostasis and contributes to *Salmonella enterica* virulence. *Metallomics* **6**(4): 845-853.
- Chandra, R. B., M. Yogavel and A. Sharma.** 2007. Structural analysis of ABC-family periplasmic zinc binding protein provides new insights into mechanism of ligand uptake and release. *J. Mol. Biol.* **367**(4): 970-982.
- Cheryl, O. Y., C. M. Gillen, T. C. Barnett, M. J. Walker and A. G. McEwan.** 2014. An antimicrobial role for zinc in innate immune defense against group A *Streptococcus*. *J. Infect. Dis.* **209**(10): 1500-1508.
- Chivers, P. T.** 2007. A galvanizing story—protein stability and zinc homeostasis. *J. Bacteriol.* **189**(8): 2953-2954.
- Choi, S. and A. J. Bird.** 2014. Zinc'ing sensibly: controlling zinc homeostasis at the transcriptional level. *Metallomics* **6**(7): 1198-1215.
- Chowdhury, S. K., V. Katta and B. T. Chait.** 1990. Probing conformational changes in proteins by mass spectrometry. *J. Am. Chem. Soc.* **112**(24): 9012-9013.
- Chu, J.** 2013. Towards an understanding of multiple paralogues for metalhandling genes in a coastal cyanobacterium, PhD thesis submitted to Chemistry Department, University of Warwick . UK.

- Citiulo, F., I. D. Jacobsen, P. Miramón, L. Schild, S. Brunke, P. Zipfel, et al.** 2012. *Candida albicans* scavenges host zinc via Pra1 during endothelial invasion. *Plos One* **8**(6): e1002777.
- Clarke, A. K.** 1996. Variations on a theme: combined molecular chaperone and proteolysis functions in Clp/HSP100 proteins. *J. bioscience* **21**(2): 161-177.
- Cohen, Y. and M. Gurevitz.** 2006. The cyanobacteria-ecology, physiology and molecular genetics. In: M. Dworkin, S. Falkow, E. Rosenberg, K.-H. Schleifer and E. Stackebrandt (Eds), *The Prokaryotes; A Handbook on the Biology of Bacteria: Bacteria, Firmicutes, Cyanobacteria*, p. 1074-1098. Springer Science+Business Media, LLC., New York, USA.
- Conroy, O., E. H. Kim, M. M. McEvoy and C. Rensing.** 2010. Differing ability to transport nonmetal substrates by two RND-type metal exporters. *FEMS Microbiol. lett.* **308**(2): 115-122.
- Cooper, S. J., G. A. Leonard, S. M. McSweeney, A. W. Thompson, J. H. Naismith, S. Qamar, et al.** 1996. The crystal structure of a class II fructose-1, 6-bisphosphate aldolase shows a novel binuclear metal-binding active site embedded in a familiar fold. *Structure* **4**(11): 1303-1315.
- Cox, A. D. and M. A. Saito.** 2013. Proteomic responses of oceanic *Synechococcus* WH8102 to phosphate and zinc scarcity and cadmium additions. *Front. Microbiol.* **4**(387).
- D'Autréaux, B., L. Pecqueur, A. Gonzalez de Peredo, R. M. Diederix, C. Caux-Thang, L. Tabet, et al.** 2007. Reversible redox- and zinc-dependent dimerization of the *Escherichia coli* Fur protein. *Biochemistry* **46**(5): 1329-1342.
- Da Silva Neto, J. F., V. S. Braz, V. S. Italiani and M. V. Marques.** 2009. Fur controls iron homeostasis and oxidative stress defense in the oligotrophic alpha-proteobacterium *Caulobacter crescentus*. *Nucleic Acids Res.* **37**(14): 4812-4825.
- De Angelis, F., J. K. Lee, J. D. O'Connell, L. W. Miercke, K. H. Verschueren, V. Srinivasan, et al.** 2010. Metal-induced conformational changes in ZneB suggest an active role of membrane fusion proteins in efflux resistance systems. *Proc. Natl. Acad. Sci.* **107**(24): 11038-11043.
- DeLano, W. L.** 2007. The PyMOL Molecular Graphics System, Version 1.8 Schrödinger, LLC. DeLano Scientific, Palo Alto-CA, USA.
- Delany, I., R. Rappuoli and V. Scarlato.** 2004. Fur functions as an activator and as a repressor of putative virulence genes in *Neisseria meningitidis*. *Mol. Microbiol.* **52**(4): 1081-1090.
- Delany, I., G. Spohn, R. Rappuoli and V. Scarlato.** 2001. The Fur repressor controls transcription of iron-activated and-repressed genes in *Helicobacter pylori*. *Mol. Microbiol.* **42**(5): 1297-1309.

- Dennis, W. R.** 2007. Metal ion receptors and signaling. In: I. Bertini, B.G. Harry, I.S. Edward and S.V. Joan (Eds), *Biological Inorganic Chemistry Structure and Reactivity*, p. University Science Books., USA.
- Desrosiers, D. C., S. W. Bearden, I. Mier, J. Abney, J. T. Paulley, J. D. Fetherston, et al.** 2010. Znu is the predominant zinc importer in *Yersinia pestis* during *in vitro* growth but is not essential for virulence. *Infect. Immun.* **78**(12): 5163-5177.
- Diaz-Mireles, E., M. Wexler, G. Sawers, D. Bellini, J. D. Todd and A. B. Johnston.** 2004. The fur-like protein Mur of *Rhizobium leguminosarum* is a Mn<sup>2+</sup>-responsive transcriptional regulator. *Microbiol.* **150**(5): 1447-1456.
- Dintilhac, A. and J. P. Claverys.** 1997. The *adc* locus, which affects competence for genetic transformation in *Streptococcus pneumoniae*, encodes an ABC transporter with a putative lipoprotein homologous to a family of *Streptococcal adhesins*. *Res. Microbiol.* **148**(2): 119-131.
- Donat, R. J. and K. W. Bruland.** 1990 A comparison of two voltammetric techniques for determining zinc speciation in Northeast Pacific Ocean Waters. *Mar. Chem.* **28**: 301-323.
- Doyle, S. M. and S. Wickner.** 2009. Hsp104 and ClpB: protein disaggregating machines. *Trends. Biochem. Sci.* **34**(1): 40-48.
- Duursma, E. K. and R. Dawson.** 1981. *Marine Organic Chemistry: Evolution, Composition, Interactions and Chemistry of Organic Matter in Seawater, Elsevier Oceanography Series, 3 I.* Elsevier Scientific Publishing Company. The Netherlands, pp. 521.
- Ebright, Y. W., Y. Chen, S. P. Pendergrast and R. H. Ebright.** 1992. Incorporation of an EDTA-metal complex at a rationally selected site within a protein: application to EDTA-iron DNA affinity cleaving with catabolite gene activator protein (CAP) and Cro. *Biochemistry* **31**(44): 10664-10670.
- Eide, D. J.** 2006. Zinc transporters and the cellular trafficking of zinc. *BBA. Mol. Cell. Res.* **1763**(7): 711-722.
- Eide, D. J.** 2011. The oxidative stress of zinc deficiency. *Metallomics* **3**(11): 1124-1129.
- Ellman, G. L.** 1958. A colorimetric method for determining low concentrations of mercaptans. *Arch. Biochem. Biophys.* **74**(2): 443-450.
- Ellwood, M. J.** 2004. Zinc and cadmium speciation in subantarctic waters east of new zealand. *Mar. Chem.* **87**: 37-58.
- Ellwood, M. J. and C. G. Van den Berg.** 2000. Zinc speciation in the Northeastern Atlantic Ocean. *Mar. Chem.* **68**(4): 295-306.

- Ernst, F. D., G. Homuth, J. Stoof, U. Mäder, B. Waidner, E. J. Kuipers, et al.** 2005. Iron-responsive regulation of the *Helicobacter pylori* iron-cofactored superoxide dismutase *SodB* is mediated by Fur. *J. Bacteriol.* **187**(11): 3687-3692.
- Escolar, L., J. Pérez-Martín and V. de Lorenzo.** 1998. Binding of the Fur (ferric uptake regulator) repressor of *Escherichia coli* to arrays of the GATAAT sequence. *J. Mol. Biol.* **283**(3): 537-547.
- Feng, W., J. Cai, W. M. Pierce, R. B. Franklin, W. Maret, F. W. Benz, et al.** 2005. Metallothionein transfers zinc to mitochondrial aconitase through a direct interaction in mouse hearts. *Biochem. Biophys. Res. Commun.* **332**(3): 853-858.
- Fernández, C. and G. Wider.** 2003. TROSY in NMR studies of the structure and function of large biological macromolecules. *Curr. Opin. Struct. Biol.* **13**(5): 570-580.
- Forchhammer, G.** 1862. On the constitution of sea-water, at different depths, and in different latitudes. *Journal of the Franklin Institute* **74**(6): 401-403.
- Foster, A. W., C. J. Patterson, R. Pernil, C. R. Hess and N. J. Robinson.** 2012. Cytosolic Ni (II) sensor in cyanobacterium; nickel detection follows nickel across four families of metal sensors. *J. Biol. Chem.* **287**(15): 12142-12151.
- Fuangthong, M. and J. D. Helmann.** 2003. Recognition of DNA by three ferric uptake regulator (Fur) homologs in *Bacillus subtilis*. *J. Bacteriol.* **185**(21): 6348-6357.
- Fuszard, M. A., Y. S. Ow, S. C. Gan, J. Noirel, N. G. Ternan, G. McMullan, et al.** 2013. The quantitative proteomic response of *Synechocystis* sp. PCC6803 to phosphate acclimation. *Aquatic biosystems* **9**(1): 1-12.
- Gaballa, A., T. Wang, Y. W. Rick and J. D. Helmann.** 2002. Functional analysis of the *Bacillus subtilis* Zur regulon. *J. Bacteriol.* **184**(23): 6508-6514.
- Gabriel, S. E., F. Miyagi, A. Gaballa and J. D. Helmann.** 2008. Regulation of the *Bacillus subtilis* *yciC* gene and insights into the DNA-binding specificity of the zinc-sensing metalloregulator Zur. *J. Bacteriol.* **190**(10): 3482-3488.
- Gaither, A. L. and D. J. Eide.** 2001. Eukaryotic zinc transporters and their regulation. *Biometals* **14**(3): 251-270.
- Galkin, A., L. Kulakova, E. Melamud, L. Li, C. Wu, P. Mariano, et al.** 2007. Characterization, kinetics, and crystal structures of fructose-1, 6-bisphosphate aldolase from the human parasite, *Giardia lamblia*. *J. Biol. Chem.* **282**(7): 4859-4867.
- Galkin, A., Z. Li, L. Li, L. Kulakova, L. R. Pal, M. Dunaway, D., et al.** 2009. Structural insights into the substrate binding and stereoselectivity of giardia Fructose-1, 6-bisphosphate aldolase. *Biochemistry* **48**(14): 3186-3196.

- Garner, M. M. and A. Revzin.** 1981. A gel electrophoresis method for quantifying the binding of proteins to specific DNA regions: application to components of the *Escherichia coli* lactose operon regulatory system. *Nucleic Acids Res.* **9**(13): 3047-3060.
- Gennaro, M. C., P. Mirti and C. Casalino.** 1983. NMR study of intramolecular processes in EDTA metal complexes. *Polyhedron* **2**(1): 13-18.
- Giedroc, D. P.** 2009. Hydrogen peroxide sensing in *Bacillus subtilis*: it is all about the (metallo) regulator. *Mol. Microbiol.* **73**(1): 1-4.
- Giedroc, D. P. and A. I. Arunkumar.** 2007. Metal sensor proteins: nature's metalloregulated allosteric switches. *Dalton Trans.*(29): 3107-3120.
- Gill, S. C. and P. H. Von Hippel.** 1989. Calculation of protein extinction coefficients from amino acid sequence data. *Anal. Biochem.* **182**(2): 319-326.
- Gilston, B. A., S. Wang, M. D. Marcus, M. A. Canalizo-Hernández, E. P. Swindell, Y. Xue, et al.** 2014. Structural and mechanistic basis of zinc regulation across the *E. coli* Zur regulon. *Plos One* **12**(11): e1001987.
- Glover-Cutter, K. M., S. Alderman, J. E. Dombrowski and R. C. Martin.** 2014. Enhanced oxidative stress resistance through activation of a zinc deficiency transcription factor in *Brachypodium distachyon*. *Plant. Physiol.* **166**(3): 1492-1505.
- Glusker, J. P., A. K. Katz and C. W. bock.** 1999. Metal ions in biological systems *The Rigaku J.* **16**(2): 8-17.
- Goldberg, E. D.** 1963. The ocean as a chemical system. In: M.N. Hill (Ed.), *The sea: The Composition of Sea-water Comparative and Descriptive Oceanography, Volume 2*, p. 3-25 John Willey & sons, Inc. , USA.
- Goldberg, M., T. Pribyl, S. Juhnke and D. H. Nies.** 1999. Energetics and topology of CzcA, a cation/proton antiporter of the resistance-nodulation-cell division protein family. *J. Biol. Chem.* **274**(37): 26065-26070.
- Golovanov, A. P., R. T. Blankley, J. M. Avis and W. Bermel.** 2007. Isotopically discriminated NMR spectroscopy: a tool for investigating complex protein interactions in vitro. *J. Am. Chem. Soc.* **129**(20): 6528-6535.
- González, A., M. T. Bes, F. Barja, M. L. Peleato and M. F. Fillat.** 2010. Overexpression of FurA in *Anabaena* sp. PCC 7120 reveals new targets for this regulator involved in photosynthesis, iron uptake and cellular morphology. *Plant Cell Physiol.* **51**(11): 1900-1914.
- Grass, G., B. Fan, B. P. Rosen, S. Franke, D. H. Nies and C. Rensing.** 2001. ZitB (YbgR), a member of the cation diffusion facilitator family, is an additional zinc transporter in *Escherichia coli*. *J. Bacteriol.* **183**(15): 4664-4667.

- Grass, G., M. D. Wong, B. P. Rosen, R. L. Smith and C. Rensing.** 2002. ZupT is a Zn (II) uptake system in *Escherichia coli*. *J. Bacteriol.* **184**(3): 864-866.
- Green, R. T., J. D. Todd and A. W. B. Johnston.** 2013. Manganese uptake in marine bacteria; the novel MntX transporter is widespread in Roseobacters, Vibrios, Alteromonadales and the SAR11 and SAR116 clades. *ISME J.* **7**(3): 581-591.
- Greenfield, N. J.** 2006. Using circular dichroism spectra to estimate protein secondary structure. *Nature protocols.* **1**(6): 2876-2890.
- Guerinot, M. L.** 2000. The ZIP family of metal transporters. *BBA-Biomembranes.* **1465**(1): 190-198.
- Guerra, A. J., C. E. Dann and D. P. Giedroc.** 2011. Crystal structure of the zinc-dependent MarR family transcriptional regulator AdcR in the Zn (II)-bound state. *J. Am. Chem. Soc.* **133**(49): 19614-19617.
- Gunnelius, L., K. Hakkila, J. Kurkela, H. Wada, E. Tyystjärvi and T. Tyystjärvi.** 2014. The omega subunit of the RNA polymerase core directs transcription efficiency in cyanobacteria. *Nucleic Acids Res.*(1-9).
- Günther, V., U. Lindert and W. Schaffner.** 2012. The taste of heavy metals: gene regulation by MTF-1. *Biochim. Biophysica. Acta.* **1823**(9): 1416-1425.
- Hamza, I., S. Chauhan, R. Hassett and M. R. O'Brian.** 1998. The bacterial Irr protein is required for coordination of heme biosynthesis with iron availability. *J. Biol. Chem.* **273**(34): 21669-21674.
- Han, S., E. V. Mathias and Y. Ba.** 2007. Proton NMR determination of Mg<sup>2+</sup> and Ca<sup>2+</sup> concentrations using tetrasodium EDTA complexes. *J. Chem.* **1**: 1-5.
- Hantke, K.** 2001a. Bacterial zinc transporters and regulators. *Biometals* **14**(3): 239-249.
- Hantke, K.** 2001b. Iron and metal regulation in bacteria. *Curr. Opin. Microbiol.* **4**(2): 172-177.
- Hantke, K.** 2005. Bacterial zinc uptake and regulators. *Curr. Opin. Microbiol.* **8**(2): 196-202.
- Hartl, U. F. and M. Hayer-Hartl.** 2002. Molecular chaperones in the cytosol: from nascent chain to folded protein. *Science* **295**(5561): 1852-1858.
- Hellman, L. M. and M. G. Fried.** 2007. Electrophoretic mobility shift assay (EMSA) for detecting protein–nucleic acid interactions. *Nat. Prot.* **2**(8): 1849-1861.
- Henley, J. W. and Y. Yin.** 1998. Growth and photosynthesis of marine *Synechococcus* (cyanophyceae) under iron stress. *J. Physiol.* **34**(1): 94-103.
- Hernandez, J., M. Bes, M. Fillat, J. Neira and M. Peleato.** 2002. Biochemical analysis of the recombinant Fur (ferric uptake regulator) rotein from *Anabaena* PCC 7119: factors Affecting its oligomerization state. *J. Biochem.* **366**: 315-322.

- Hider, R. C. and X. Kong.** 2010. Chemistry and biology of siderophores. *Nat. Prod. Rep.* **27**: 637-657.
- Hill, A. V.** 1910. The possible effects of the aggregation of the molecules of haemoglobin on its dissociation curves. *J. Physiol.* **40**: 4-7.
- Hochuli, E., W. Bannwarth, H. Döbeli, R. Gentz and D. Stüber.** 1988. Genetic approach to facilitate purification of recombinant proteins with a novel metal chelate adsorbent. *Nat. Biol.* **6**(11): 1321-1325.
- Hoffmann, A., F. Merz, A. Rutkowska, B. Zachmann-Brand, E. Deuerling and B. Bukau.** 2006. Trigger factor forms a protective shield for nascent polypeptides at the ribosome. *J. Biol. Chem.* **281**(10): 6539-6545.
- Holt, D. P., R. R. Reid, B. L. Lewis, G. W. Luther and A. Butler.** 2005. Iron (III) coordination chemistry of alterobactin A: a siderophore from the marine bacterium *Alteromonas luteoviolacea*. *Inorg. Chem.* **44**(21): 7671-7677.
- Hong, S., J. P. Candelone, C. Turetta and C. F. Boutron.** 1996. Changes in natural lead, copper, zinc and cadmium concentrations in central greenland ice from 8250 to 149,100 years ago: their association with climatic changes and resultant variations of dominant source contributions. *Earth. Planet. Sci. Lett.* **143**(1): 233-244.
- Hood, I. M., B. L. Mortensen, J. L. Moore, Y. Zhang, T. E. Kehl-Fie, N. Sugitani, et al.** 2012. Identification of an *Acinetobacter baumannii* zinc acquisition system that facilitates resistance to calprotectin-mediated zinc sequestration. *Plos One* **8**(12).
- Hou, Z. and B. Mitra.** 2003. The metal specificity and selectivity of ZntA from *Escherichia coli* using the acylphosphate intermediate. *J. Biol. Chem.* **278**(31): 28455-28461.
- Huang, D. L., D. J. Tang, Q. Liao, H. C. Li, Q. Chen, Y. Q. He, et al.** 2008. The Zur of *Xanthomonas campestris* functions as a repressor and an activator of putative zinc homeostasis genes *via* recognizing two distinct sequences within its target promoters. *Nucleic Acids Res.* **36**(13): 4295-4309.
- Huckle, J. W., A. P. Morby, J. S. Turner and N. J. Robinson.** 1993. Isolation of a prokaryotic metallothionein locus and analysis of transcriptional control by trace metal ions. *Mol. Microbiol.* **7**(2): 177-187.
- Hudek, L., A. Michalczk, B. A. Neilan and L. M. Ackland.** 2013a. Zinc homeostasis in cyanobacteria. In: A.K. Srivastava, A.N. Rai and B.A. Neilan (Eds), *Stress Biology of Cyanobacteria: Molecular Mechanisms to Cellular Responses*, p. 245-254. CRC Press, Taylor & Francis Group LLC., Boca Raton, London, New York.
- Hudek, L., L. A. Pearson, A. Michalczyk, B. A. Neilan and L. M. Ackland.** 2013b. Molecular and cellular characterisation of the zinc uptake (Znu) system of *Nostoc punctiforme*. *FEMS Microbiol. Ecol.* **86**(2): 149-171.

- Hudek, L., L. C. Rai, D. Freestone, A. Michalczyk, M. Gibson, Y. F. Song, et al.** 2009. Bioinformatic and expression analyses of genes mediating zinc homeostasis in *Nostoc punctiforme*. *Appl. Environ. Microbiol.* **75**(3): 784-791.
- Huffman, J. L. and R. G. Brennan.** 2002. Prokaryotic transcription regulators: more than just the helix-turn-helix motif. *Curr. Opin. Struct. Biol.* **12**(1): 98-106.
- Hwang, T. L. and A. J. Shaka.** 1995. Water suppression that works. Excitation sculpting using arbitrary wave-forms and pulsed-field gradients. *J. Magn. Reson. Ser. A.* **112**(2): 275-279.
- Ilikchyan, I. N., M. L. McKay, J. P. Zehr, S. T. Dyrman and G. S. Bullerjahn.** 2009. Detection and expression of the phosphonate transporter gene *phnD* in marine and freshwater picocyanobacteria. *Environ. Microbiol.* **11**(5): 1314-1324.
- Jacobsen, F. E., K. M. Kazmierczak, J. P. Lisher, M. E. Winkler and D. P. Giedroc.** 2011. Interplay between manganese and zinc homeostasis in the human pathogen *Streptococcus pneumoniae*. *Metallomics* **3**(1): 38-41.
- Jacquamet, L., D. A. Traore, J. L. Ferrer, O. Proux, D. Testemale, J. L. Hazemann, et al.** 2009. Structural characterization of the active form of PerR: insights into the metal-induced activation of PerR and Fur proteins for DNA binding. *Mol. Microbiol.* **73**(1): 20-31.
- Jakuba, R. W., J. W. Moffett and M. Saito, A.** 2008a. Use of a modified, high-sensitivity, anodic stripping voltammetry method for determination of zinc speciation in the North Atlantic Ocean. *Anal. Chim. Acta.* **614**(2): 143-152.
- Jakuba, W. R., J. W. Moffett and S. T. Dyrman.** 2008b. Evidence for the linked biogeochemical cycling of zinc, cobalt, and phosphorus in the western North Atlantic Ocean. *Glob. Biogeochem. Cycles.* **22**(4): 1-13.
- Jakuba, W. R., M. A. Saito, J. W. Moffett and Y. Xu.** 2012. Dissolved zinc in the subarctic North Pacific and Bering Sea: Its distribution, speciation, and importance to primary producers. *Glob. Biogeochem. Cycles* **26**(2): 1-15.
- Jardillier, L., M. V. Zubkov, J. Pearman and D. J. Scanlan.** 2010. Significant CO<sub>2</sub> fixation by small prymnesiophytes in the subtropical and tropical Northeast Atlantic Ocean. *ISME J.* **4**(9): 1180-1192.
- Jiang, B. L., W. J. Lou, H. Y. Du, N. M. Price and B. S. Qiu.** 2012. Sll1263, A unique cation diffusion facilitator protein that promotes iron uptake in the cyanobacterium *Synechocystis* sp. strain PCC 6803. *Plant Cell Physiol.* **53**(8): 1404-1417.
- Kallifidas, D., B. Pascoe, G. A. Owen, C. M. Strain-Damerell, H. J. Hong and M. S. Paget.** 2010. The zinc-responsive regulator Zur controls expression of the coelibactin gene cluster in *Streptomyces coelicolor*. *J. Bacteriol.* **192**(2): 608-611.

- Kaltashov, I. A., C. E. Bobst and R. R. Abzalimov.** 2013. Mass spectrometry-based methods to study protein architecture and dynamics. *Prot. Sci.* **22**(5): 530-544.
- Kang, J. Y.** 1999. The antioxidant function of metallothionein in the heart. *Exp. Biol. Med.* **222**(3): 263-273.
- Kanoh, K., K. Kamino, G. Leleo, K. Adachi and Y. Shizuri.** 2003. Pseudoalterobactin A and B, new siderophores excreted by marine bacterium *Pseudoalteromonas* sp. KP20-4. *J. Antibiot.* **56**(10): 871-875.
- Keasling, D. J.** 1997. Regulation of intracellular toxic metals and other cations by hydrolysis of polyphosphate. *Ann. N. Y. Acad. Sci.* **829**(1): 242-249.
- Keeler, J.** 2011. *Understanding NMR spectroscopy*. Second Edition ed. 2010 vols. Hoboken, USA: Wiley-Blackwell. pp.
- Kelly, E. J., C. J. Quaife, G. J. Froelick and R. D. Palmiter.** 1996. Metallothionein I and II protect against zinc deficiency and zinc toxicity in mice. *J. Nutr.* **126**(7): 1782.
- Kelly, S. M., T. J. Jess and N. C. Price.** 2005. How to study proteins by circular dichroism. *Biochim. Biophysica. Acta.* **1751**(2): 119-139.
- Kim, E. H., D. H. Nies, M. M. McEvoy and C. Rensing.** 2011. Switch or funnel: how RND-type transport systems control periplasmic metal homeostasis. *J. Bacteriol.* **193**(10): 2381-2387.
- Kim, J. H., D. W. Graham, A. A. DiSpirito, M. A. Alterman, N. Galeva, C. K. Larive, et al.** 2004. Methanobactin, a copper-acquisition compound from methane-oxidizing bacteria. *Science* 305(5690): 1612-1615.
- Klein, J. S. and O. Lewinson.** 2011. Bacterial ATP-driven transporters of transition metals: physiological roles, mechanisms of action, and roles in bacterial virulence. *Metallomics* **3**(11): 1098-1108.
- Kleywegt, G. J. and A. T. Jones.** 1996. Phi/psi-chology: Ramachandran rsevisited. *Structure* **4**(12): 1395-1400.
- Kondrat, F. D., G. R. Kowald, C. A. Scarff, J. H. Scrivens and C. A. Blindauer.** 2013. Resolution of a paradox by native mass spectrometry: facile occupation of all four metal binding sites in the dimeric zinc sensor SmtB. *Chem. Commun.* **49**(8): 813-815.
- Kozelka, B. P. and K. W. Bruland** 1998. Chemical speciation of dissolved Cu, Zn, Cd, Pb in Narragansett Bay, Rhode Island. *Mar. Chem.* **60**: 267-282.
- Ksibe, A. Z.** 2011. Analytical method development for metallomics, MSc thesis submitted to Chemistry Department, Warwick University, UK.

- Laskowski, R. A., M. W. MacArthur, D. S. Moss and J. M. Thornton.** 1993. PROCHECK: A program to check the stereochemical quality of protein structures. *J. Appl. Crystallogr.* **26**(2): 283-291.
- Lebrette, H., E. Borezée-Durant, L. Martin, P. Richaud, E. Erba, B. and C. Cavazza.** 2015. Novel insights into nickel import in *Staphylococcus aureus*: the positive role of free histidine and structural characterization of a new thiazolidine-type nickel chelator. *Metallomics* **7**(4): 613-621.
- Lee, D. J., S. D. Minchin and S. W. Busby.** 2012. Activating transcription in bacteria. *Annu. Rev. Microbiol.* **66**: 125-152.
- Lee, J. W. and J. D. Helmann.** 2006. Biochemical characterization of the structural Zn<sup>2+</sup> site in the *Bacillus subtilis* peroxide sensor PerR. *J. Biol. Chem.* **281**(33): 23567-23578.
- Lee, J. W. and J. D. Helmann.** 2007. Functional specialization within the Fur family of metalloregulators. *Biometals* **20**(3-4): 485-499.
- Lennartson, A.** 2014. Zinc of unsuspected worth. *Nat. Chem.* **6**(2): 166-166.
- Leszczyszyn, O. I. and C. A. Blindauer.** 2010. Zinc transfer from the embryo-specific metallothionein EC from wheat: a case study. *Phys. Chem. Chem. Phys.* **12**(41): 13408-13418.
- Leszczyszyn, O. I., C. D. Evans, S. E. Keiper, G. Z. L. Warren and C. A. Blindauer.** 2007. Differential reactivity of individual zinc ions in clusters from bacterial metallothioneins. *Inorg. Chim. Acta.* **360**(1): 3-13.
- Leszczyszyn, O. I., H. T. Imam and C. A. Blindauer.** 2013. Diversity and distribution of plant metallothioneins: a review of structure, properties and functions. *Metallomics* **5**(9): 1146-1169.
- Li, Y. T., A. J. Kraker, F. C. Shaw and D. H. Petering.** 1980. Ligand substitution reactions of metallothioneins with EDTA and apo-carbonic anhydrase. *Proc. Natl. Acad. Sci.* **77**(11): 6334-6338.
- Lim, C. K., K. A. Hassan, A. Penesyan, J. E. Loper and I. T. Paulsen.** 2013. The effect of zinc limitation on the transcriptome of *Pseudomonas protegens* Pf-5. *Environ. Microbiol.* **15**(3): 702-715.
- Linton, J. K. and C. F. Higgins.** 2007. Structure and function of ABC transporters: the ATP switch provides flexible control. *J. Physiol.* **453**(5): 555-567.
- Liu, T., S. Nakashima, K. Hirose, M. Shibasaka, M. Katsuhara, B. Ezaki, et al.** 2004. A novel cyanobacterial SmtB/ArsR family repressor regulates the expression of a CPx-ATPase and a metallothionein in response to both Cu (I)/Ag (I) and Zn (II)/Cd (II). *J. Biol. Chem.* **279**(17): 17810-17818.

- Lu, M. and D. Fu.** 2007. Structure of the zinc transporter YiiP. *Science* **317**(5845): 1746-1748.
- Lucarelli, D., S. Russo, E. Garman, A. Milano, W. Meyer-Klaucke and E. Pohl.** 2007. Crystal structure and function of the zinc uptake regulator FurB from *Mycobacterium tuberculosis*. *J. Biol. Chem.* **282**(13): 9914-9922.
- Lyons, J. T. and J. D. Eide.** 2007. Transport and storage of metal ions in biology. In: I. Bertini, H.B. Gray, E.I. Stiefel and J.S. Valentine (Eds), *Biological Inorganic Chemistry Structure and Reactivity*, p. 57-77. University Science Books, Sausalito-California, USA.
- Ma, Z., S. E. Gabriel and J. D. Helmann.** 2011. Sequential binding and sensing of Zn (II) by *Bacillus subtilis* Zur. *Nucleic Acids Res.* **39**(21): 9130-9138.
- Ma, Z., F. E. Jacobsen and D. P. Giedroc.** 2009. Coordination chemistry of bacterial metal transport and sensing. *Chem. Rev.* **109**(10): 4644-4681.
- MacDiarmid, C. W., A. L. Gaither and D. Eide.** 2000. Zinc transporters that regulate vacuolar zinc storage in *Saccharomyces cerevisiae*. *EMBO J.* **19**(12): 2845-2855.
- Mahadev, R. S., H. Hayashi, T. Ikegami, S. Abe and H. E. Morita.** 2013. Improved protein overexpression and purification strategies for structural studies of cyanobacterial metal-responsive transcription factor, SmtB from marine *Synechococcus* sp. PCC7002. *Proteins* **32**(8): 626-634.
- Maiti, R., G. H. Van Domselaar, H. Zhang and D. S. Wishart.** 2004. SuperPose: a simple server for sophisticated structural superposition. *Nucleic Acids Res.* **32**(suppl 2): 590-594.
- Maret, W.** 2006. Zinc coordination environments in proteins as redox sensors and signal transducers. *Antioxid. Redox. Signal* **8**(9-10): 1419-1441.
- Maret, W.** 2013. Zinc biochemistry: from a single zinc enzyme to a key element of life. *Adv. Nutr.* **4**(1): 82-91.
- Martin, J. D., Y. Ito, V. V. Homann, M. G. Haygood and A. Butler.** 2006. Structure and membrane affinity of new amphiphilic siderophores produced by *Ochrobactrum* sp. SP18. *J. Biol. Inorg. Chem.* **11**(5): 633-641.
- Martin, J. H., K. H. Coale, K. S. Johnson, S. E. Fitzwater, R. M. Gordon, S. J. Tanner, et al.** 1994. Testing the iron hypothesis in ecosystems of the equatorial pacific ocean. *Nature* **371**(123 - 129).
- Martin, J. H. and S. E. Fitzwater.** 1988. Iron deficiency limits phytoplankton growth in the North-East Pacific subarctic. *Nature* **331**: 947-975.

- Mason, A. Z., N. Perico, R. Moeller, K. Thrippleton, T. Potter and D. Lloyd.** 2004. Metal donation and apo-metalloenzyme activation by stable isotopically labeled metallothionein. *Mar. Environ. Res.* **58**(2): 371-375.
- Masse, E., H. Salvail, G. Desnoyers and M. Arguin.** 2007. Small RNAs controlling iron metabolism. *Curr. Opin. Microbiol.* **10**(2): 140-145.
- Matthijs, S., N. Brandt, M. Ongena, W. Achouak, J. M. Meyer and H. Budzikiewicz.** 2016. Pyoverdine and histocorrugatin-mediated iron acquisition in *Pseudomonas thivervalensis*. *Biometals* **29**(3): 467-485.
- McCormack, P., P. J. Worsfold and M. Gledhill.** 2003. Separation and detection of siderophores produced by marine bacterioplankton using high-performance liquid chromatography with electrospray ionization mass spectrometry. *Anal. Chem.* **75**(11): 2647-2652.
- Merchant, S. S. and J. D. Helmann.** 2012. Elemental economy: microbial strategies for optimizing growth in the face of nutrient limitation. In: R.K. Poole (Ed.), *Advances in microbial physiology*, p. 91-210. Academic Press
- Mergulhao, M. F., D. K. Summers and G. A. Monteiro.** 2005. Recombinant protein secretion in *Escherichia coli*. *Biotechnology. Adv.* **23**(3): 177-202.
- Moffett, J. W. and L. E. Brand.** 1996. Production of strong, extracellular Cu chelators by marine cyanobacteria in response to Cu stress. *Limnol. Oceanogr.* **41**(3): 388-395.
- Morby, A. P., J. S. Turner, J. W. Huckle and N. J. Robinson.** 1993. SmtB is a metal-dependent repressor of the cyanobacterial metallothionein gene *smtA*: identification of a Zn inhibited DNA-protein complex. *Nucleic Acids Res.* **21**(4): 921-925.
- Morel, F. M., R. J. Hudson and N. M. Price.** 1991. Limitation of productivity by trace metals in the sea. *Limnol. Oceanogr.*(8): 1742-1755.
- Morel, F. M., A. J. Milligan and M. A. Saito.** 2006. Marine bioinorganic chemistry: The role of trace metals in the oceanic cycles of major nutrients. In: H. Elderfield (Ed.), *The Oceans and Marine Geochemistry: Treatise on Geochemistry, Volume 6*, p. 113-143. Elsevier Ltd., Oxford, UK.
- Morel, F. M., R. Reinfelder, S. B. Roberts, C. P. Chamberlain, L. J. G. and Y. D.** 1994. Zinc and carbon co-limitation of marine phytoplankton. *Nature* **369**(6483): 740-742.
- Murakami, K. S. and S. A. Darst.** 2003. Bacterial RNA polymerases: the whole story. *Curr. Opin. Struct. Biol.* **13**(1): 31-39.
- Napolitano, M., A. M. Rubio, J. Santamaría-Gómez, E. Olmedo-Verd, N. J. Robinson and I. Luque.** 2012. Characterization of the response to zinc deficiency in the cyanobacterium *Anabaena* sp. strain PCC 7120. *J. Bacteriol.* **194**(10): 2426-2436.

- Narayanan, S. and B. Reif.** 2005. Characterization of chemical exchange between soluble and aggregated states of  $\beta$ -amyloid by solution-state NMR upon variation of salt conditions. *Biochemistry* **44**(5): 1444-1452.
- Natale, P., T. Brüser and A. M. Driessen.** 2008. Sec-and Tat-mediated protein secretion across the bacterial cytoplasmic membrane—distinct translocases and mechanisms. *Biochim. Biophysica. Acta.* **1778**(9): 1735-1756.
- Neilands, B. J.** 1981. Microbial iron compounds. *Annu. Rev. Biochem.* **50**(1): 715-731.
- Neis, D. H.** 2007. How cells control zinc homeostasis. *Science* **317**: 1695–1696.
- Nienhuis, H. P.** 1981. Distribution of organic matter in living marine organisms. In: K.E. Duursma and R. Dawson (Eds), *Marine Organic Chemistry: Evolution, Composition, Interactions and Chemistry of Organic Matter in Seawater, Elsevier Oceanography Series 31*, p. 31-68. Elsevier Scientific Publishing Company, The Netherlands.
- Nies, D. H.** 2012. Zinc starvation response in a cyanobacterium revealed. *J. Bacteriol.* **194**(10): 2407-2412.
- Nishihara, K., M. Kanemori, H. Yanagi and T. Yura.** 2000. Overexpression of trigger factor prevents aggregation of recombinant proteins in *Escherichia coli*. *Appl. Environ. Microbiol.* **66**(3): 884-889.
- Novichkov, P. S., O. N. Laikova, E. S. Novichkova, M. S. Gelfand, A. P. Arkin, I. Dubchak, et al.** 2009. RegPrecise: a database of curated genomic inferences of transcriptional regulatory interactions in prokaryotes. *Nucleic Acids Res.* **38**(suppl 1): 111-118.
- Nyborg, J. and O. Peersen.** 2004. That zincing feeling: the effects of EDTA on the behaviour of zinc-binding transcriptional regulators. *Biochem, J.* **381**(3): e3-e4.
- Okujo, N., M. Saito, S. Yamamoto, T. Yoshida, S. Miyoshi and S. Shinoda.** 1994. Structure of vulnibactin, a new polyamine-containing siderophore from *Vibrio vulnificus*. *Biometals* **7**(2): 109-116.
- Osman, D. and J. S. Cavet.** 2010. Bacterial metal-sensing proteins exemplified by ArsR–SmtB family repressors. *Nature* **27**(5): 668-680.
- Ostrowski, M., S. Mazard, S. G. Tetu, K. Phillippy, A. Johnson, B. Palenik, et al.** 2010. PtrA is required for coordinate regulation of gene expression during phosphate stress in a marine *Synechococcus*. *ISME J.* **4**(7): 908-921.
- Oteiza, I. P., M. S. Clegg, P. M. Zago and C. L. Keen.** 2000. Zinc deficiency induces oxidative stress and AP-1 activation in 3T3 cells. *Free. Radical. Biol. Med.* **28**(7): 1091-1099.
- Outten, C. E. and T. V. O'Halloran.** 2001. Femtomolar sensitivity of metalloregulatory proteins controlling zinc homeostasis. *Science* **292**: 2488-2492.

- Outten, C. E., D. A. Tobin, J. E. Penner-Hahn and T. V. O'Halloran.** 2001. Characterization of the metal receptor sites in *Escherichia coli* Zur, an ultrasensitive zinc (II) metalloregulatory protein. *Biochemistry* **40**(35): 10417-10423.
- Page, R., W. Peti, I. A. Wilson, R. C. Stevens and K. Wüthrich.** 2005. NMR screening and crystal quality of bacterially expressed prokaryotic and eukaryotic proteins in a structural genomics pipeline. *Proc. Natl. Acad. Sci.* **102**(6): 1901-1905.
- Pak, E. J., N. E. Ekendé, E. G. Kifle, D. J. O'Connell, F. De Angelis, M. B. Tessema, et al.** 2013. Structures of intermediate transport states of ZneA, a Zn (II)/proton antiporter. *Proc. Natl. Acad. Sci.* **110**(46): 18484-18489.
- Palenik, B., B. Brahamsha, F. W. Larimer, M. Land, L. Hauser, P. Chain, et al.** 2003. The genome of a motile marine *Synechococcus*. *Nature* **424**(6952): 1037-1042.
- Palenik, B., Q. Ren, C. L. Dupont, G. S. Myers, J. F. Heidelberg, J. H. Badger, et al.** 2006. Genome sequence of *Synechococcus* CC9311: insights into adaptation to a coastal environment. *Proc. Natl. Acad. Sci.* **103**(36): 13555-13559.
- Palmiter, R. D. and L. Huang.** 2004. Efflux and compartmentalization of zinc by members of the SLC30 family of solute carriers. *Pflügers Archiv* **447**(5): 744-751.
- Panina, E. M., A. A. Mironov and M. S. Gelfand.** 2003. Comparative genomics of bacterial zinc regulons: enhanced ion transport, pathogenesis, and rearrangement of ribosomal proteins. *Proc. Natl. Acad. Sci.* **100**(17): 9912-9917.
- Parente, F. A., C. T. de Rezende, P. K. De Castro, M. A. Bailão, A. J. Parente, L. C. Borges, et al.** 2013. A Proteomic view of the response of *Paracoccidioides* yeast cells to zinc deprivation. *Fungal Biol.* **117**(6): 399-410.
- Parks, D. T., K. K. Leuther, E. D. Howard, S. A. Johnston and W. G. Dougherty.** 1994. Release of proteins and peptides from fusion proteins using a recombinant plant virus proteinase. *Anal. Biochem.* **216**(2): 413-417.
- Parsell, D. A., A. S. Kowal, M. A. Singer and S. Lindquist.** 1994. Protein disaggregation mediated by heat-shock protein Hsp104. *Nature* **372**(6505): 475-478.
- Partensky, F., J. Blanchot and V. D.** 1999. Differential distribution and ecology of *Prochlorococcus* and *Synechococcus* in oceanic waters: a review. In: L. Charpy and A. Larkum (Eds), *Marine Cyanobacteria*, p. 457-475. Musée Océanographique, Monaco, France.
- Patel, D. J., L. L. Canuel and F. M. Pohl.** 1979. " Alternating B-DNA" conformation for the oligo (dG-dC) duplex in high-salt solution. *Proc. Natl. Acad. Sci.* **76**(6): 2508-2511.
- Patzer, S. I. and K. Hantke.** 1998. The ZnuABC high-affinity zinc uptake system and its regulator Zur in *Escherichia coli*. *Mol. Microbiol.* **28**(6): 1199-1210.

- Patzer, S. I. and K. Hantke.** 2000. The zinc-responsive regulator Zur and Its control of the *znu* gene cluster encoding the ZnuABC zinc uptake system in *Escherichia coli*. *J. Biol. Chem.* **275**(32): 24321-24332.
- Pawlik, C. M., K. Hubert, B. Joseph, H. Claus, C. Schoen and U. Vogel.** 2012. The zinc-responsive regulon of *Neisseria meningitidis* comprises 17 genes under control of a Zur element. *J. Bacteriol.* **194**(23): 6594-6603.
- Pecqueur, L., B. D'Autréaux, J. Dupuy, Y. Nicolet, L. Jacquamet, B. Brutscher, et al.** 2006. Structural changes of *Escherichia coli* ferric uptake regulator during metal-dependent dimerization and activation explored by NMR and X-ray crystallography. *J. Biol. Chem.* **281**(30): 21286-21295.
- Pegan, D. S., K. Rukseree, S. G. Franzblau and A. D. Mesecar.** 2009. Structural basis for catalysis of a tetrameric class IIa fructose 1, 6-bisphosphate aldolase from *Mycobacterium tuberculosis*. *J. Mol. Biol.* **386**(4): 1038-1053.
- Pegan, S. D., K. Rukseree, G. G. Capodagli, E. A. Baker, O. Krasnykh, S. G. Franzblau, et al.** 2013. Active site loop dynamics of a class IIa Fructose 1, 6-bisphosphate Aldolase from *Mycobacterium tuberculosis*. *Biochemistry* **52**(5): 912-925.
- Pérard, J., J. Covès, M. Castellan, C. Solard, M. Savard, R. Miras, et al.** 2016. Quaternary structure of Fur proteins, a new subfamily of tetrameric proteins. *Biochemistry* **55**(13): 1503-1515.
- Perez-Iratxeta, C. and M. A. Andrade-Navarro.** 2008. K2D2: estimation of protein secondary structure from circular dichroism spectra. *BMC Struct. Biol.* **8**(1): 25.
- Pervushin, K., R. Riek, G. Wider and K. Wüthrich.** 1997. Attenuated T2 relaxation by mutual cancellation of dipole–dipole coupling and chemical shift anisotropy indicates an avenue to NMR structures of very large biological macromolecules in solution. *Proc. Natl. Acad. Sci.* **94**(23): 12366-12371.
- Petersen, T. N., S. Brunak, G. von Heijne and H. Nielsen.** 2011. SignalP 4.0: discriminating signal peptides from transmembrane regions. *Nature* **8**(10): 785-786.
- Phung, L. T., G. Ajlani and R. Haselkorn.** 1994. P-type ATPase from the cyanobacterium *Synechococcus* 7942 related to the human menkes and wilson disease gene products. *Proc. Natl. Acad. Sci.* **91**(20): 9651-9654.
- Pitt, F. D., S. Mazard, L. Humphreys and D. J. Scanlan.** 2010. Functional characterization of *Synechocystis* sp. strain PCC 6803 *pst1* and *pst2* gene clusters reveals a novel strategy for phosphate uptake in a freshwater cyanobacterium. *J. Bacteriol.* **192**(13): 3512-3523.
- Pohl, E., J. C. Haller, A. Mijovilovich, W. Meyer-Klaucke, E. Garman and M. L. Vasil.** 2003. Architecture of a protein central to iron homeostasis: crystal structure and spectroscopic analysis of the ferric uptake regulator. *Mol. Microbiol.* **47**(4): 903-915.

- Prisic, S., H. Hwang, A. Dow, O. Barnaby, T. S. Pan, J. A. Lonzanida, et al.** 2015. Zinc regulates a switch between primary and alternative S18 ribosomal proteins in *Mycobacterium tuberculosis*. *Mol. Microbiol.* **97**(2): 263-280.
- Pruteanu, M., S. B. Neher and T. A. Baker.** 2007. Ligand-controlled proteolysis of the *Escherichia coli* transcriptional regulator ZntR. *J. Bacteriol.* **189**(8): 3017-3025.
- Raussens, V., J. M. Ruyschaert and E. Goormaghtigh.** 2003. Protein concentration is not an absolute prerequisite for the determination of secondary structure from circular dichroism spectra: a new scaling method. *Anal. Biochem.* **319**(1): 114-121.
- Reid, R. T., D. H. Live, J. D. Faulkner and A. Butler.** 1993. A siderophore from a marine bacterium with an exceptional ferric ion affinity constant. *Nature* **366**: 455- 458.
- Rensing, C., B. Mitra and B. P. Rosen.** 1997. The *zntA* gene of *Escherichia coli* encodes a Zn (II)-translocating P-type ATPase. *Proc. Natl. Acad. Sci.* **94**(26): 14326-14331.
- Reyes-Caballero, H., A. J. Guerra, F. E. Jacobsen, K. M. Kazmierczak, D. Cowart, U. M. Koppolu, et al.** 2010. The metalloregulatory zinc site in *Streptococcus pneumoniae* AdcR, a zinc-activated MarR family repressor. *J. Mol. Biol.* **403**(2): 197-216.
- Rippe, K.** 1997. Analysis of protein-DNA binding at equilibrium. *BIF futura.* **12**(1): 20-26.
- Ritchie, R. J.** 2006. Consistent sets of spectrophotometric chlorophyll equations for acetone, methanol and ethanol solvents. *Photosynth. Res.* **89**(1): 27-41.
- Rogers, B. M., Nicola. J. Patron and P. J. Keeling.** 2007. Horizontal Transfer of a Eukaryotic Plastid-targeted Protein Gene to Cyanobacteria. *BMC Biology.* **5**.
- Rosano, G. L. and E. A. Ceccarelli.** 2014. Recombinant protein expression in *Escherichia coli*: advances and challenges. *Front. Microbiol.* **5**: 172.
- Rosenzweig, A. C. and R. Balasubramanian.** 2008. Copper methanobactin: a molecule whose time has come. *Curr. Opin. Chem. Biol.* **1**: 245-249.
- Roy, A., A. Kucukural and Y. Zhang.** 2010. I-TASSER: a unified platform for automated protein structure and function prediction. *Nat. Prot.* **5**(4): 725-738.
- Rudolph, G., G. Semini, F. Hauser, A. Lindemann, M. Friberg, H. Hennecke, et al.** 2006. The iron control element, acting in positive and negative control of iron-regulated *Bradyrhizobium japonicum* genes, is a target for the Irr protein. *J. Bacteriol.* **188**(2): 733-744.
- Rule, G. S. and T. K. Hitchens.** 2006. *Fundamentals of Protein NMR Spectroscopy, Volume 5.* Vol. **5**. Springer Science+Business Media B.V. The Netherlands, pp.
- Ruttkey-Nedecky, B., L. Nejdil, J. Gumulec, O. Zitka, M. Masarik, T. Eckschlager, et al.** 2013. The role of metallothionein in oxidative stress. *Int. J. Mol. Sci.* **14**(3): 6044-6066.

- Saito, M. A., E. M. Bertrand, S. Dutkiewicz, V. V. Bulygin, D. M. Moran, F. M. Monteiro, et al.** 2011. Iron conservation by reduction of metalloenzyme inventories in the marine Diazotroph *Crocospaera watsonii*. *Proc. Natl. Acad. Sci.* **108**(6): 2184-2189.
- Saito, M. A. and T. J. Goepfert.** 2008. Zinc-cobalt colimitation of *Phaeocystis antarctica*. *Limnol. Oceanogr.* **53**(1): 266-275.
- Saito, T. and R. J. Williams.** 1991. The binding of the ferric uptake regulation protein to a DNA fragment. *J. Biochem.* **197**(1): 43-47.
- Saito, T., M. R. Wormald and R. J. Williams.** 1991. Some structural features of the iron-uptake regulation protein. *J. Biochem.* **197**(1): 29-38.
- Sanchez, Y. and S. L. Lindquist.** 1990. HSP104 required for induced thermotolerance. *Science* **248**(4959): 1112-1115.
- Sanchez, Y., J. Taulien, K. A. Borkovich and S. Lindquist.** 1992. Hsp104 is required for tolerance to many forms of stress. *EMBO J.* **11**(6): 2357.
- Sanson, M., N. Makthal, A. R. Flores, R. J. Olsen, J. M. Musser and M. Kumaraswami.** 2015. Adhesin competence repressor (AdcR) from *Streptococcus pyogenes* controls adaptive responses to zinc limitation and contributes to virulence. *Nucleic Acids Res.* **43**(1): 418-432.
- Scanlan, D. J., M. Ostrowski, S. Mazard, A. Dufresne, L. Garczarek, W. R. Hess, et al.** 2009. Ecological genomics of marine picocyanobacteria. *Microbiol. Mol. Biol. Rev.* **73**(2): 249-299.
- Schelin, J., F. Lindmark and A. K. Clarke.** 2002. The clpP multigene family for the ATP-dependent Clp protease in the cyanobacterium *Synechococcus*. *Microbiol.* **148**(7): 2255-2265.
- Sein-Echaluze, V. C., A. González, M. Napolitano, I. Luque, F. Barja, L. M. Peleato, et al.** 2014. Zur (FurB) is a key factor in the control of the oxidative stress response in *Anabaena* sp. PCC 7120. *Environ. Microbiol.* **17**(6): 2006-2017.
- Shah, A. M., Y. Zhao, Y. Wang, G. Yan, Q. Zhang, L. Wang, et al.** 2014. A Mur regulator protein in the extremophilic bacterium *Deinococcus radiodurans*. *Plos One* **9**(9): e106341.
- Shaked, Y., Y. Xu, K. Leblanc and F. M. Morel.** 2006. Zinc availability and alkaline phosphatase activity in *Emiliana huxleyi* : implications for Zn-P co-limitation in the ocean. *Limnol. Oceanogr.* **51**(1): 299-309.
- Sharp, P. M. and W. H. Li.** 1987. The codon adaptation index—a measure of directional synonymous codon usage bias, and its potential applications. *Nucleic Acids Res.* **15**(3): 1281-1295.

- Shcolnick, S. and N. Keren.** 2006. Metal homeostasis in cyanobacteria and chloroplasts. balancing benefits and risks to the photosynthetic apparatus. *Plant Physiol.* 141(3): 805-810.
- Sheikh, M. A. and G. L. Taylor.** 2009. Crystal structure of the *Vibrio cholerae* ferric uptake regulator (Fur) reveals insights into metal co-ordination. *Mol. Microbiol.* **72**(5): 1208-1220.
- Shimada, T., N. Fujita, K. Yamamoto and A. Ishihama.** 2011. Novel roles of cAMP receptor protein (CRP) in regulation of transport and metabolism of carbon sources. *Plos One* 6(6).
- Shin, J. H., H. J. Jung, Y. J. An, Y. B. Cho, S. S. Cha and J. H. Roe.** 2011. Graded Expression of Zinc-responsive Genes Through Two Regulatory Zinc-binding Sites in *Zur*. *Proc. Natl. Acad. Sci.* 108(12): 5045-5050.
- Shin, J. H., S. Y. Oh, S. J. Kim and J. H. Roe.** 2007. The zinc-responsive regulator *Zur* controls a zinc uptake system and some ribosomal proteins in *Streptomyces coelicolor* A3 (2). *J. Bacteriol.* **189**(11): 4070-4077.
- Sigman, D. M. and E. A. Boyle.** 2000. Glacial/interglacial variations in atmospheric carbon dioxide. *Nature* **407**(6806): 859-869.
- Singh, D. P. and S. P. Singh.** 1987. Action of heavy metals on hill activity and O<sub>2</sub> evolution in *Anacystis nidulans*. *Plant Physiol.* **83**(1): 12-14.
- Singh, P., L. Sharma, S. R. Kulothungan, V. B. Adkar, R. S. Prajapati, P. Ali, et al.** 2013. Effect of signal peptide on stability and folding of *Escherichia coli* thioredoxin. *Plos One* **8**(5): e63442.
- So, A. K. and G. S. Espie.** 1998. Cloning, characterization and expression of carbonic anhydrase from the cyanobacterium *Synechocystis* PCC6803. *Plant. Mol. Biol.* **37**(2): 205-215.
- Solovyev, V. and A. Salamov.** 2011. Automatic annotation of microbial genomes and metagenomic sequences. In: R.W. Li (Ed.), *Metagenomics and its Applications in Agriculture, Biomedicine and Environmental Studies* p. p. 61-78 Nova Science Publishers, Agricultural Research Service, USA.
- Song, Y. F., S. W. Leonard, M. G. Traber and E. Ho.** 2009. Zinc deficiency affects DNA damage, oxidative stress, antioxidant defenses, and DNA repair in rats. *J. Nutr.* **139**(9): 1626-1631.
- Sreerama, N., S. Y. Venyaminov and R. W. Woody.** 2000. Estimation of protein secondary structure from circular dichroism spectra: inclusion of denatured proteins with native proteins in the analysis. *Anal. Biochem.* **287**(2): 243-251.

- Steere, B. and D. Eisenberg.** 2000. Characterization of high-order diphtheria toxin oligomers. *Biochemistry* **39**(51): 15901-15909.
- Stork, M., M. P. Bos, I. Jongerius, N. de Kok, I. Schilders, V. E. Weynants, et al.** 2010. An outer membrane receptor of *Neisseria meningitidis* involved in zinc acquisition with vaccine potential. *Plos One* **6**(7): e1000969.
- Sunda, W., N. Price and F. M. Morel.** 2005. Trace metal ion buffers and their use in culture studies. In: A.R. Andersen (Ed.), *Algal culturing techniques*, p. Elsevier., Burlington. USA.
- Sunda, W. G. and S. A. Huntsman.** 1995. Cobalt and zinc interreplacement in marine phytoplankton: biological and geochemical implications. *Limnol. Oceanogr.* **40**(8): 1404-1417.
- Surin, P. B., H. Rosenberg and G. B. Cox.** 1985. Phosphate-specific transport system of *Escherichia coli*: nucleotide sequence and gene-polypeptide relationships. *J. Bacteriol.* **161**(1): 189-198.
- Suzuki, I., W. J. Simon and A. R. Slabas.** 2006. The heat shock response of *Synechocystis* sp. PCC 6803 analysed by transcriptomics and proteomics. *J. Exp. Bot.* **57**(7): 1573-1578.
- Tal, M., A. Silberstein and E. Nusser.** 1985. Why does coomassie brilliant blue R interact differently with different proteins? A partial answer. *J. Biol. Chem.* **260**(18): 9976-9980.
- Taudte, N. and G. Grass.** 2010. Point mutations change specificity and kinetics of metal uptake by ZupT from *Escherichia coli*. *Biometals* **23**(4): 643-656.
- Teramoto, H., M. Inui and H. Yukawa.** 2012. *Corynebacterium glutamicum* Zur acts as a zinc-sensing transcriptional repressor of both zinc-inducible and zinc-repressible genes involved in zinc homeostasis. *FEBS J.* **279**(23): 4385-4397.
- Tetu, S. G., B. Brahamsha, D. A. Johnson, V. Tai, K. Phillippy, B. Palenik, et al.** 2009. Microarray analysis of phosphate regulation in the marine cyanobacterium *Synechococcus* sp. WH8102. *ISME J.* **3**(7): 835-849.
- Thelwell, C., N. J. Robinson and J. S. Turner-Cavet.** 1998. An SmtB-like repressor from *Synechocystis* PCC 6803 regulates a zinc exporter. *Proc. Natl. Acad. Sci.* **95**(18): 10728-10733.
- Thomas, J. G., A. Ayling and F. Baneyx.** 1997. Molecular chaperones, folding catalysts, and the recovery of active recombinant proteins from *E. coli*. *Appl. Biochem. Biotechnology.* **66**(3): 197-238.
- Totter, S., C. J. Patterson, L. Banci, I. Bertini, I. C. Felli, A. Pavelkova, et al.** 2012. Cyanobacterial metallochaperone inhibits deleterious side reactions of copper. *Proc. Natl. Acad. Sci.* **109**(1): 95-100.

- Totley, S., K. J. Waldron, S. J. Firbank, B. Reale, C. Bessant, K. Sato, et al.** 2008. Protein-folding location can regulate manganese-binding versus copper-or zinc-binding. *Nature* **455**(7216): 1138-1142.
- Towbin, H., T. Staehelin and J. Gordon.** 1979. Electrophoretic transfer of proteins from polyacrylamide gels to nitrocellulose sheets: procedure and some applications. *Proc. Natl. Acad. Sci.* **76**(9): 4350-4354.
- Traoré, D. A., A. El Ghazouani, S. Ilango, J. Dupuy, L. Jacquamet, J. L. Ferrer, et al.** 2006. Crystal structure of the apo-PerR-Zn protein from *Bacillus subtilis*. *Mol. Microbiol.* **61**(5): 1211-1219.
- Tropea, E. J., S. Cherry and D. S. Waugh.** 2009. Expression and purification of soluble His<sub>6</sub>-tagged TEV protease. In: S.A. Doyle (Ed.), *High Throughput Protein Expression and Purification*, p. USA,
- Van den Berg, C. G., A. A. Merksb and E. K. Duursmab.** 1987. Organic complexation and its control of the dissolved concentrations of copper and zinc in the Scheldt Estuary. *Coastal. Shelf. Sci.* **24**: 785-797.
- van Veen, H. W.** 1997. Phosphate transport in prokaryotes: molecules, mediators and mechanisms. *Antonie Van Leeuwenhoek.* **72**(4): 299-315.
- Velasquez, I. B., G. S. Jacinto and F. S. Valera.** 2002. The speciation of dissolved copper, cadmium and zinc in manila bay, philippines. *Mar. Pollut. Bull.* **45**(1): 210-217.
- Waldron, K. J. and N. J. Robinson.** 2009. How do bacterial cells ensure that metalloproteins get the correct metal? *Nat. Rev. Microbiol.* **7**(1): 25-35.
- Wallace, B. A., J. G. Lees, J. W. Orry, A. Lobley and R. W. Janes.** 2003. Analyses of circular dichroism spectra of membrane proteins. *Protein science* **12**(4): 875-884.
- Waterbury, B. J., S. W. Watson, F. W. Valois and D. G. Franks.** 1986. Biological and ecological characterization of the marine unicellular cyanobacterium *Synechococcus*. . *Can. Bull. Fish. Aquat. Sci.* **214**: 71-120.
- Waugh, D. S.** 2005. Making the most of affinity tags. *Trends Biotechnol.* **23**(6): 316-320.
- Wider, G. and K. Wüthrich.** 1999. NMR spectroscopy of large molecules and multimolecular assemblies in solution. *Curr. Opin. Struct. Biol.* **9**(5): 594-601.
- Wilhelm, S. W. and C. G. Trick.** 1995. Physiological profiles of *Synechococcus* (cyanophyceae) in iron-limiting continuous cultures. *J. Phycol.* **31**(1): 79-85.
- Williamson, M. P.** 2013. Using chemical shift perturbation to characterise ligand binding. *Prog. Nucl. Magn. Reson. Spectrosc.* **73**: 1-16.

- Wiramanaden, E. C., J. T. Cullen, A. S. Ross and K. J. Orians.** 2008. Cyanobacterial copper-binding ligands isolated from artificial seawater cultures. *Mar. Chem.* 110(1): 28-41.
- Wu, C. Y., A. J. Bird, D. R. Winge and D. J. Eide.** 2007. Regulation of the yeast TSA1 peroxiredoxin by ZAP1 is an adaptive response to the oxidative stress of zinc deficiency. *J. Biol. Chem.* 282(4): 2184-2195.
- Xu, Y. and S. Matthews.** 2013. TROSY NMR spectroscopy of large soluble proteins. *Top. Curr. Chem.* 335: 97-119.
- Yan, M., Y. Song, C. P. Wong, K. Hardin and E. Ho.** 2008. Zinc deficiency alters DNA damage response genes in normal human prostate epithelial cells. *J. Nutr.* 138(4): 667-673.
- Yoon, S., A. A. DiSpirito, S. M. Kraemer and J. D. Semrau.** 2011. A simple assay for screening microorganisms for chalkophore production. *Method. Enzymol.* 495: 247-258.
- Yoon, S., S. M. Kraemer, A. A. DiSpirito and J. D. Semrau.** 2010. An assay for screening microbial cultures for chalkophore production. *Environ. Microbiol.* 2(2): 295-303.
- Zhang, J.** 2012. Protein-protein interactions in salt solutions. In: W. Cai and H. Hong (Eds), *Protein-Protein Interactions - Computational and Experimental Tools*, p. 472. InTech., USA.
- Zhang, Y.** 2008. I-TASSER server for protein 3D structure prediction. *BMC bioinformatics* 9(1): 40.
- Zhao, B., S. C. Moody, R. C. Hider, L. Lei, L. Steven, S. L. Kelly, et al.** 2012. Structural analysis of cytochrome P450 105N1 involved in the biosynthesis of the zincophore, Coelibactin. *J. Mol. Sci.* 13(7): 8500-8513.
- Zhao, H. and D. Eide.** 1996. The yeast ZRT1 gene encodes the zinc transporter protein of a high-affinity uptake system induced by zinc limitation. *Proc. Natl. Acad. Sci.* 93(6): 2454-2458.
- Zheng, D., C. Constantinidou, J. L. Hobman and S. D. Minchin.** 2004. Identification of the CRP regulon using *in vitro* and *in vivo* transcriptional profiling. *Nucleic Acids Res.* 32(19): 5874-5893.
- Zhou, X. and P. J. Wangersky.** 1989. Production of copper-complexing organic ligands by the marine diatom *Phaeodactylum tricornutum* in a cage culture turbidostat. *Mar. Chem.* 26(3): 239-259.
- Zhu, G., Y. Xia, L. K. Nicholson and K. H. Sze.** 2000. Protein dynamics measurements by TROSY-based NMR experiments. *J. Magn. Reson.* 143(2): 423-426.

- Zinchenko, A. A. and K. Yoshikawa.** 2005. Na<sup>+</sup> shows a markedly higher potential than K<sup>+</sup> in DNA compaction in a crowded environment. *J. Biophysical.* **88**(6): 4118-4123.
- Zwicker, N., U. Theobald, H. Zahner and H. P. Fiedler.** 1997. Optimization of fermentation conditions for the production of ethylene-diamine-disuccinic acid by *amycolatopsis orientalis*. *J. Ind. Microbiol. Biot.* **19**: 280–285
- Zwirgmaier, K., L. Jardillier, M. Ostrowski, S. Mazard, L. Garczarek, D. Vault, et al.** 2008. Global phylogeography of marine *Synechococcus* and *Prochlorococcus* reveals a distinct partitioning of lineages among oceanic biomes. *Environ. Microbiol.* **10**(1): 147-161.

# Appendices

## Appendix A

**Table A.01 The function of elements in the microbial cells.** Taken from (Merchant & Helmann, 2012).

<b>Element (symbol)</b>	<b>Major function and uses in microbial cells</b>
<i>Macronutrients</i>	<i>Essential elements required for all cells</i>
C	Basis of all organic molecules
H	H <sub>2</sub> O, organic molecules
N	Organic molecules, especially proteins and nucleic acids
O	H <sub>2</sub> O, organic molecules
P	Nucleic acids, NTPs, metabolites, phospholipids
S	Proteins, glutathione, thiols, biotin, lipoic acid thiamine
<i>Major cation</i>	<i>Most abundant element in the cells</i>
Mg	Major cation, cofactor for phosphotransferase reaction
Zn	Enzyme cofactor, protein folding
<i>Macronutrients</i>	<i>Elements required for all cells</i>
K	Major cation, common in cells
Ca	Major cation, required by many eukaryotes
Fe	Heme, iron-sulfur cluster, nonheme enzymes
Cu	Enzyme cofactor, electron carrier, respiration, SOD
Mn	Enzyme cofactor, ribonucleotide reductase, SOD
Co	Enzyme cofactor, B12-dependent enzymes
Mo	Cofactor enzymes
<i>Other elements</i>	<i>Elements required for special function in some cells</i>
Cd	Cofactor for carbonic anhydrase (CA)
Ni	Urease, SOD (SodN), glyoxalase
Na	Used for ion potential in halophiles
Se	Selenocysteine in proteins
Si	Some plant cell wall
B	Plant cell wall
V	Nitrogenase, haloperoxidases
W	Tungstoenzymes

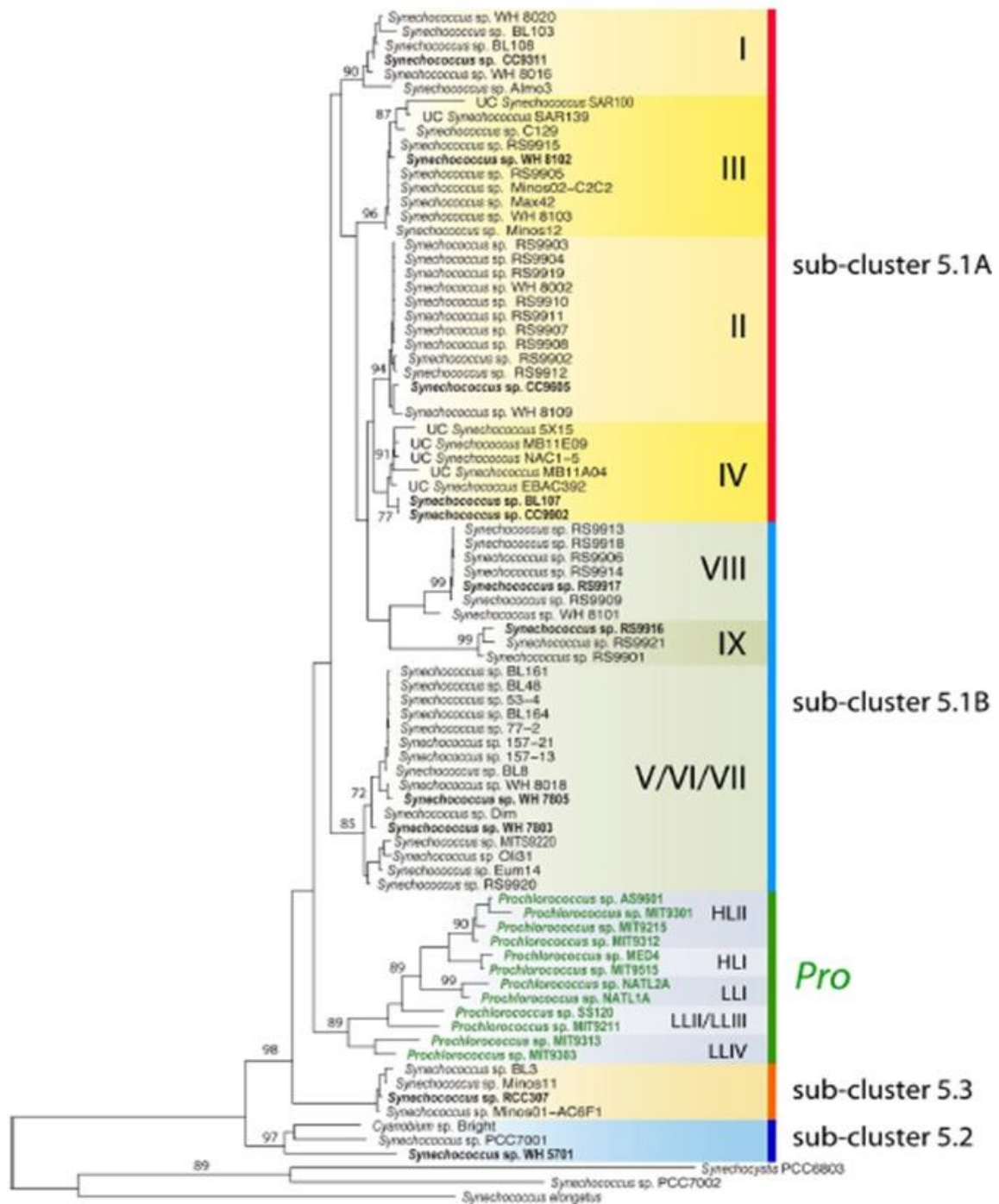


**Figure A.01 Phylogenetic relationships of *Synechococcus* and *Prochlorococcus* based on 16S rRNA gene sequences.**

Roman numerals indicate different clades and boldface indicates strains with sequenced genomes. Taken from (Scanlan *et al.*, 2009).

# Appendix B

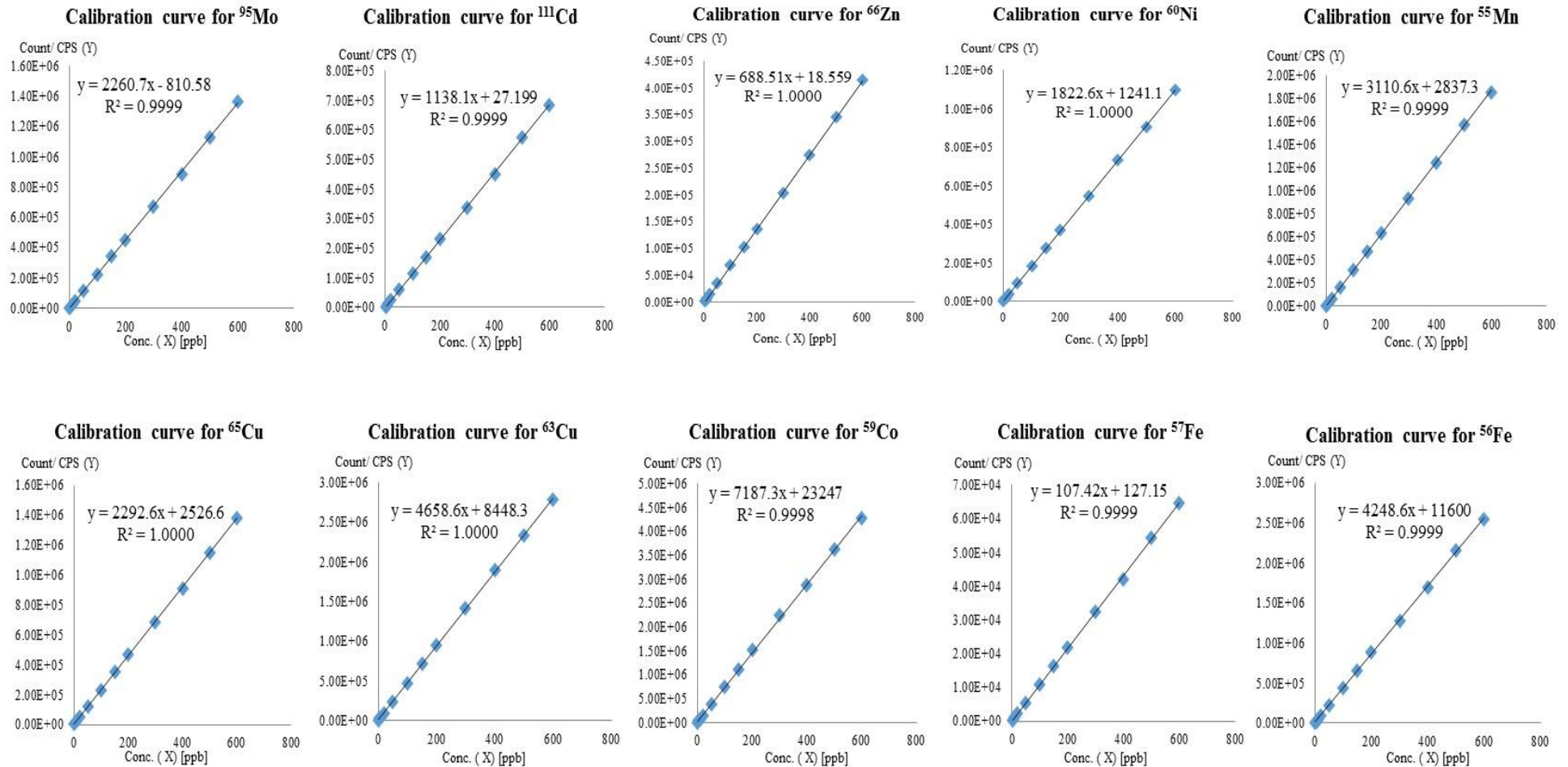


**Figure B.01 Calibration curves in ICP-MS for isotopic elements.**

Calibration curves for  $^{56}\text{Fe}$ ,  $^{57}\text{Fe}$ ,  $^{59}\text{Co}$ ,  $^{60}\text{Ni}$ ,  $^{63}\text{Cu}$ ,  $^{65}\text{Cu}$ ,  $^{66}\text{Zn}$ ,  $^{111}\text{Cd}$ ,  $^{95}\text{Mo}$  and  $^{55}\text{Mn}$  as external standards (0-600 ppb).

# Appendix C

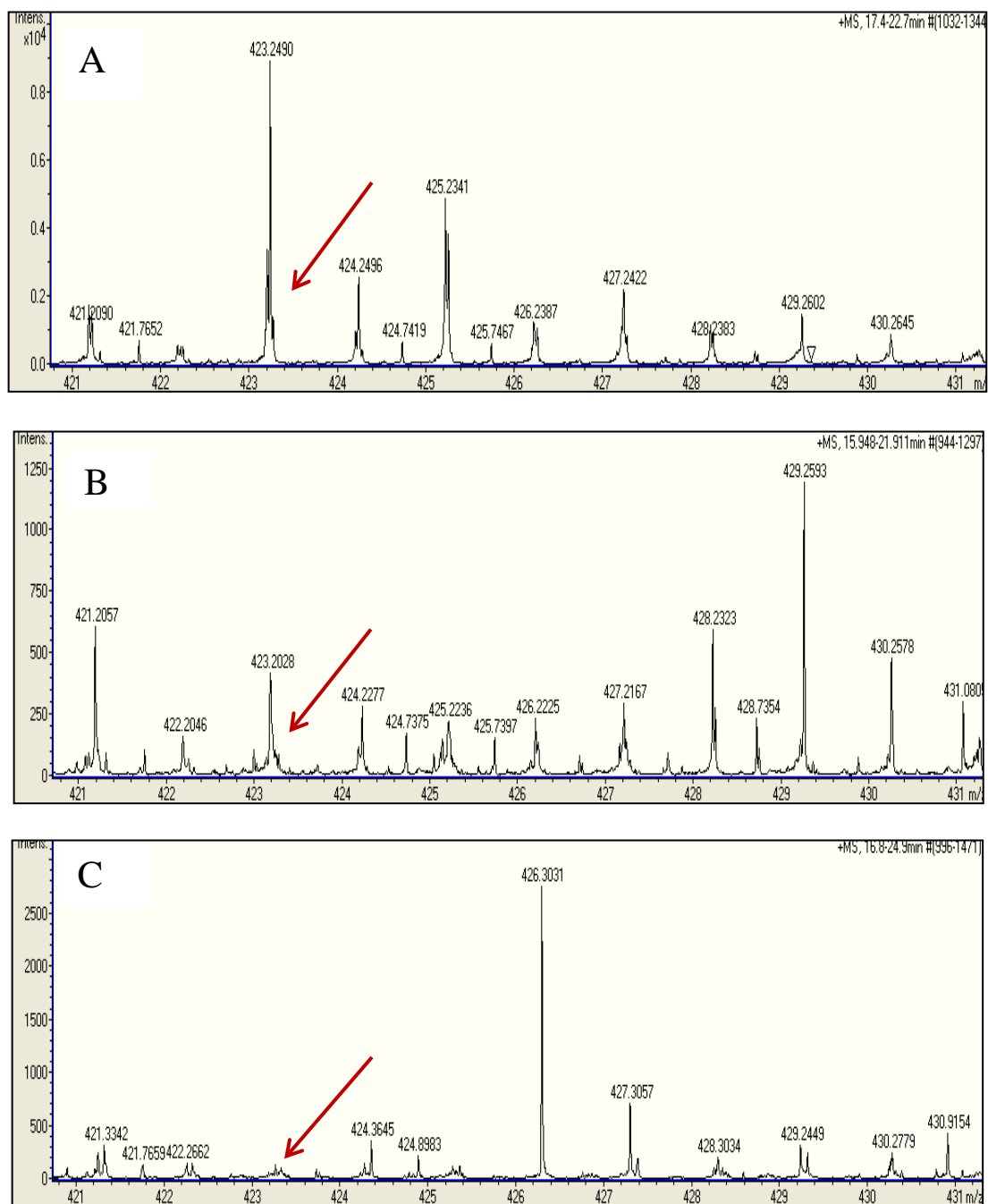


**Figure C.01 UHPLC/Q-TOF-MS Spectra.**

*Synechococcus* sp. WH8102 was grown in Pro99 medium containing natural seawater. (A) Incubated seawater sample (culture supernatant); (B) Control sample (uncultured medium); (C) Milli-Q water (without any addition). Taken from (Ksibe, 2011).

# Appendix D

**Table D.01 Assignment some peaks for fructose-1,6-bisphosphate aldolase.**

Measured mass m/z	Calculated mass m/z	Assignment
839.1026658	839.4966	[y9+3H <sup>+</sup> ]
848.4923296	848.5553	[b8-CO <sub>2</sub> -H <sup>+</sup> ]
854.4467446	854.4862	[y9+H <sub>2</sub> O]
855.0602348	855.4932	[y9+H <sub>2</sub> O+H <sup>+</sup> ]
869.4820196	869.4995	[b8-H <sub>2</sub> O-6H <sup>+</sup> ]
877.0535516	877.53335	[b8-NH <sub>2</sub> <sup>+</sup> ]
1043.535912	1043.694	[b9+CO <sub>2</sub> + 9H <sup>+</sup> ]
1066.083799	1066.6482	[y12-CO+2H <sup>+</sup> ]
1082.561392	1082.786	[b10-CO <sub>2</sub> +7H <sup>+</sup> ]
1094.611754	1094.6451	[y12+2H <sup>+</sup> ]
1104.534934	1104.7093	[b10-NH <sup>+</sup> ]
1170.659636	1170.621	[y13+NH <sup>+</sup> -8H <sup>+</sup> ]
1210.541299	1210.694	[b11-H <sub>2</sub> O+6H <sup>+</sup> ]
1272.672986	1272.676	[y14-CO <sub>2</sub> -10H <sup>+</sup> ]
1330.678211	1330.757	[y14+4H <sup>+</sup> ]
1370.61919	1370.793	[b12-H <sup>+</sup> ]
1417.706465	1417.8692	[b13-CO+3H <sup>+</sup> ]
1420.580138	1420.796	[y15-H <sub>2</sub> O-H <sup>+</sup> ]
1479.686144	1479.8323	[y16]
1503.68486	1503.9135	[b14-NH <sub>2</sub> <sup>+</sup> +6H <sup>+</sup> ]
1579.717833	1579.8629	[y 17+NH <sub>2</sub> -4H <sup>+</sup> ]
1586.802196	1586.8897	[y 17+H <sub>2</sub> O+H <sup>+</sup> ]
1591.808748	1591.8391	[y 17+CO-4H <sup>+</sup> ]
1634.749066	1634.866 <b>OR</b> 1634.9823	[b15-8H <sup>+</sup> ] <b>OR</b> [b15-H <sub>2</sub> O+10H <sup>+</sup> ]
1650.80873	1650.885	[b15-NH <sub>2</sub> <sup>+</sup> -8H <sup>+</sup> ]
1660.789837	1660.9334	[b15+H <sub>2</sub> O]
1671.683073	1671.9247	[b15+CO+H <sup>+</sup> ]
1688.745363	1688.9597	[y18-CO <sub>2</sub> +2H <sup>+</sup> ]
1756.8409	1756.9164 <b>OR</b> 1756.9658	[y18+CO-2H <sup>+</sup> ] <b>OR</b> [b16]
1773.836409	1773.9694	[b16+H <sub>2</sub> O-H <sup>+</sup> ]
1795.819487	1795.9767	[b17-H <sub>2</sub> O <sup>+</sup> ]
1800.757016	1800.95564	[b16+CO <sub>2</sub> ]
1805.825733	1805.9906	[b16+CO <sub>2</sub> +5H <sup>+</sup> ]
1877.854976	1877.9802	[y19-NH <sub>2</sub> <sup>+</sup> ]
1896.889361	1896.0128	[y19+2H <sup>+</sup> ]
1903.939078	1903.9517	[y19-NH <sub>2</sub> <sup>+</sup> -6H <sup>+</sup> ]

2054.975492	2054.0456	[y20+CO <sub>2</sub> +2H <sup>+</sup> ]
2087.957108	2087.0889	[y21-CO-6H <sup>+</sup> ]
2196.065123	2196.10696	[y22-H <sub>2</sub> O-8H <sup>+</sup> ]
2251.030047	2251.1754	[y22+CO+H <sup>+</sup> ]
2262.0577	2262.2194	[b21+H <sub>2</sub> O]
2265.033592	2265.24045	[b21+H <sub>2</sub> O+3H <sup>+</sup> ]
2339.011694	2339.2492 <b>OR</b> 2339.2129	[y23-NH <sup>+</sup> +4H <sup>+</sup> ] <b>OR</b> [b22+CO-4H <sup>+</sup> ]
2494.192399	2494.33733	[b23+CO+4H <sup>+</sup> ]

**Table D.02 Assignment some peaks for ABC transporter, substrate binding protein, phosphate.**

Measured mass m/z	Calculated mass m/z	Assignment
850.4692034	850.5082	[b8-CO+2H <sup>+</sup> ]
855.0740164	855.4575	[b8-H <sub>2</sub> O-3H <sup>+</sup> ]
861.0962889	861.47824	[b8-NH <sup>+</sup> ]
877.0656488	877.4961	[b8+H <sup>+</sup> ]
1171.606819	1171.6456	[b11- 4H <sup>+</sup> ]
1218.597241	1218.7158	[b12-CO <sub>2</sub> ]
1389.723506	1389.769	[b13+CO]
1409.691856	1409.7919	[b13+CO <sub>2</sub> +4H <sup>+</sup> ]
1426.719351	1426.8855	[y14+H <sub>2</sub> O+2H <sup>+</sup> ]
1443.69263	1443.8422	[b14-CO-H <sup>+</sup> ]
1459.695213	1459.8473	[b14-NH <sup>+</sup> ]
1472.634828	1472.8441	[b14-2H <sup>+</sup> ]
1475.688444	1475.8651	[b14+H <sup>+</sup> ]
1481.680491	1481.813	[b14+NH <sup>+</sup> -8H <sup>+</sup> ]
1483.719137	1483.827	[b14+NH <sup>+</sup> -6H <sup>+</sup> ]
1620.729327	1620.0245 <b>OR</b> 1620.8852	[b16-CO <sub>2</sub> +5H <sup>+</sup> ] <b>OR</b> [y16+CO <sub>2</sub> -2H <sup>+</sup> ]
1666.862485	1666.0355	[y17-CO <sub>2</sub> +3H <sup>+</sup> ]
1730.722966	1730.9904	[b17+H <sub>2</sub> O-3H <sup>+</sup> ]
1748.798656	1748.9801	[y17+CO <sub>2</sub> -2H <sup>+</sup> ]
2050.860422	2050.1419	b21-NH+3H
2067.881259	2067.1668 <b>OR</b> 2067.2483	[b21+5H <sup>+</sup> ] <b>OR</b> [y20+CO <sub>2</sub> +7H <sup>+</sup> ]
2127.943419	2127.3441 <b>OR</b> 2127.1270	[y21-CO <sub>2</sub> +8H <sup>+</sup> ] <b>OR</b> [b22-6H <sup>+</sup> ]
2164.022517	2164.1849	[b22+CO+3H <sup>+</sup> ]
2178.080955	2178.1658	[b22+CO <sub>2</sub> +H <sup>+</sup> ]
2813.329528	2813.6167	[y28-H <sub>2</sub> O]

# Appendix E

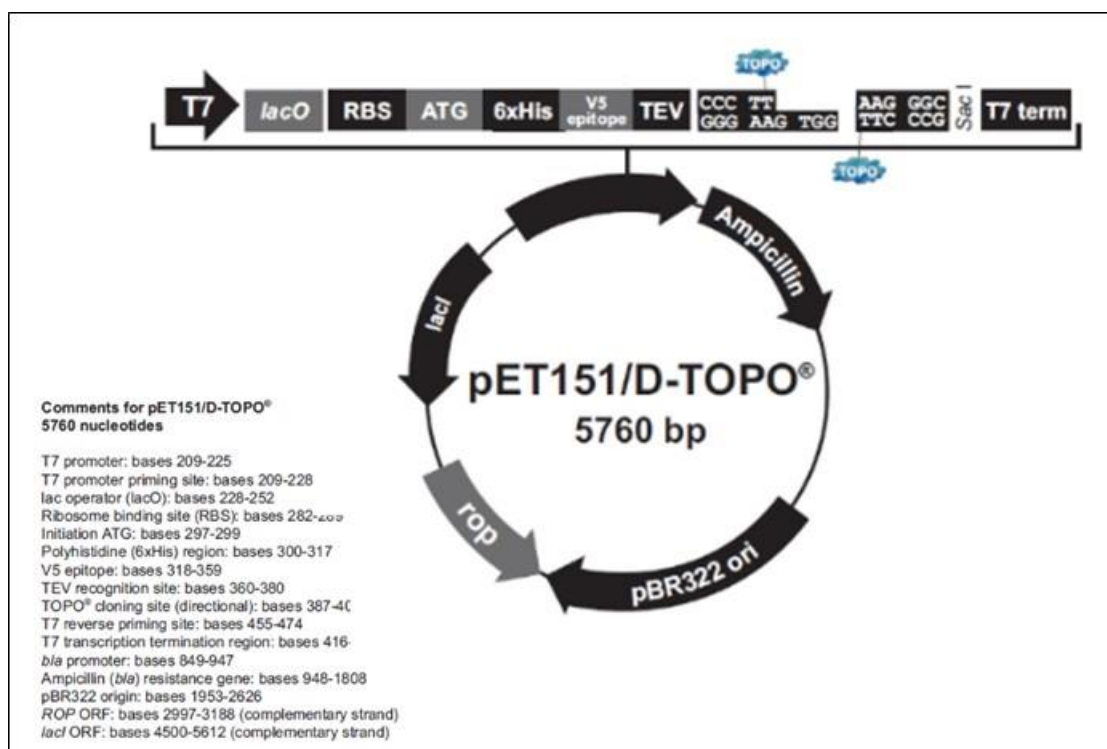


**Figure E.01 Features of the pET151/D-TOPO<sup>®</sup> (5760 bp) vector.**

pET151/D-TOPO vector carries a promoter called T7/*lac* containing T7 bacteriophage RNA polymerase and a *lac* operator. Schematic representation of pET151/D-TOPO (lower panel), and close-up of the T7 expression region of TOPO (top panel). Taken from ([http://biochem.web.utah.edu/hill/links/pet151dtopo\\_map.pdf](http://biochem.web.utah.edu/hill/links/pet151dtopo_map.pdf)).

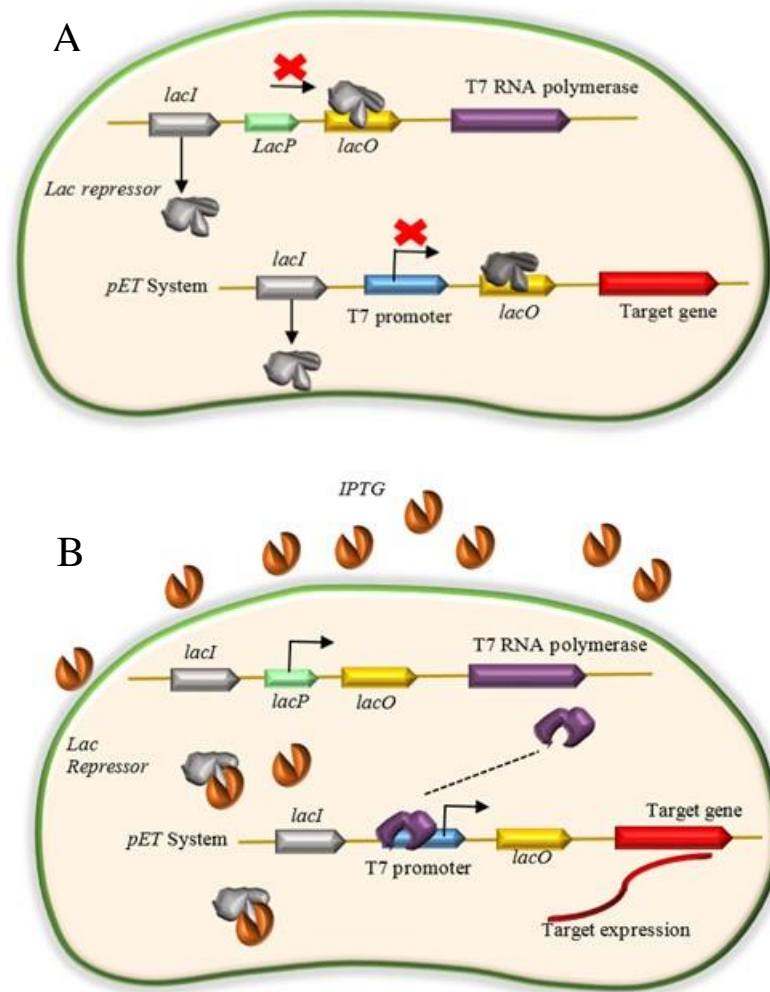


**Figure E.02 pET expression system in the host cell.**

In general prokaryotic cells do not produce T7 RNA polymerase, and therefore this system must be added. Moreover, pET plasmid contains several important elements including: a *lacI* gene which codes for the *lac* repressor protein, a T7 promoter which is specific to only T7 RNA polymerase, a *lac* operator which can block transcription. When lactose or IPTG is present inside the cell, transcription of the T7 RNA polymerase is activated. (A) In the absence of inducer, IPTG, the *lac* repressor binds to the *lac* operator (*LacO*) in both the pET system and in the host plasmid, and thereby preventing transcription the *lac* promoter by repressing. (B) In the presence of the inducer, IPTG will bind to *lac* repressor and dissociate from the operator, which permits the transcription of *lac* structural genes that contain T7 RNA polymerase. In this case T7 RNA polymerase can bind to T7 promoter and transcript the target gene.

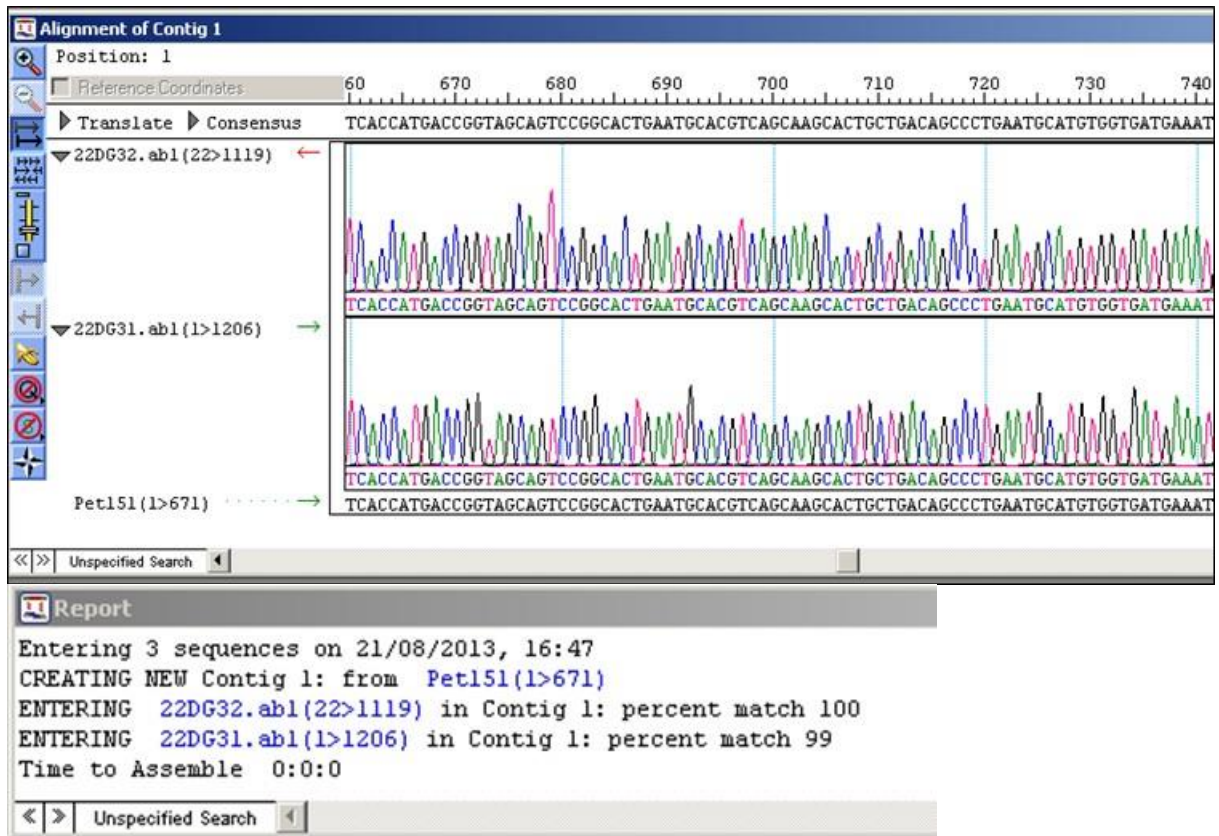


**Figure E.03 Construct sequencing using SeqMan software.**

Construct sequencing from one colony that has the correct size for *synw\_2401* gene in the TOPO vector with T7 reverse and forward primers using SeqMan software.

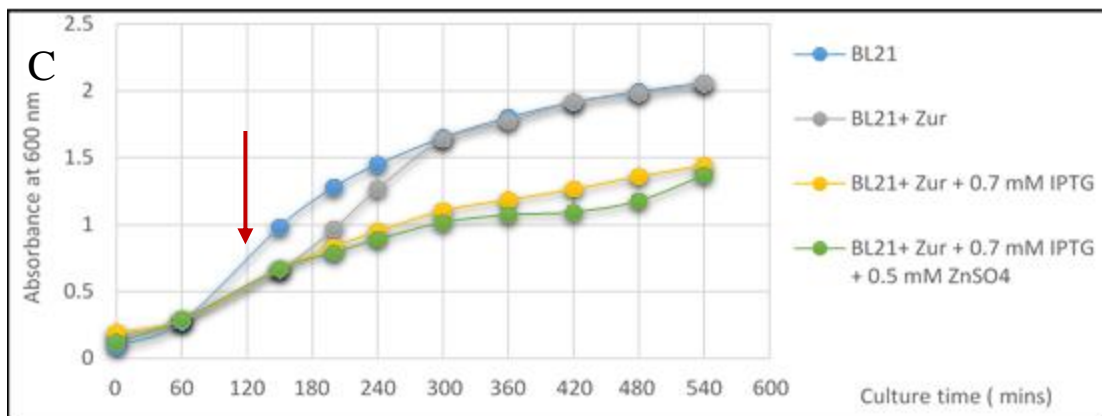
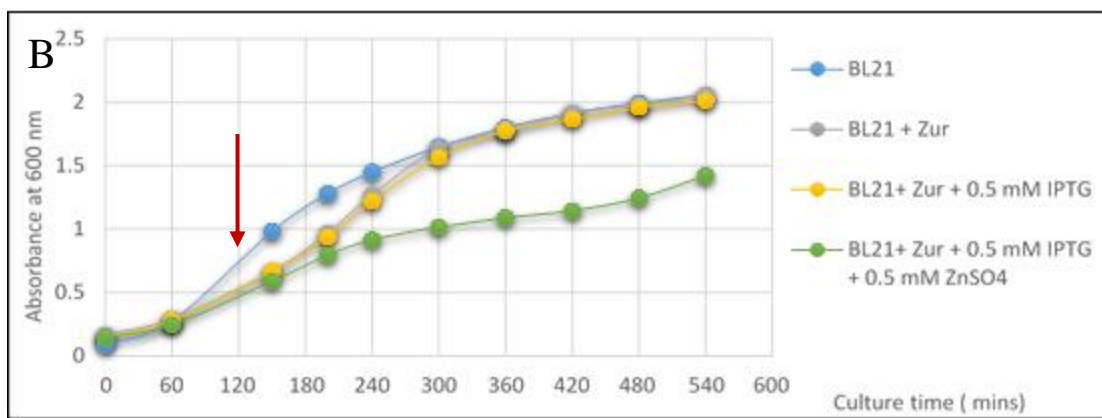
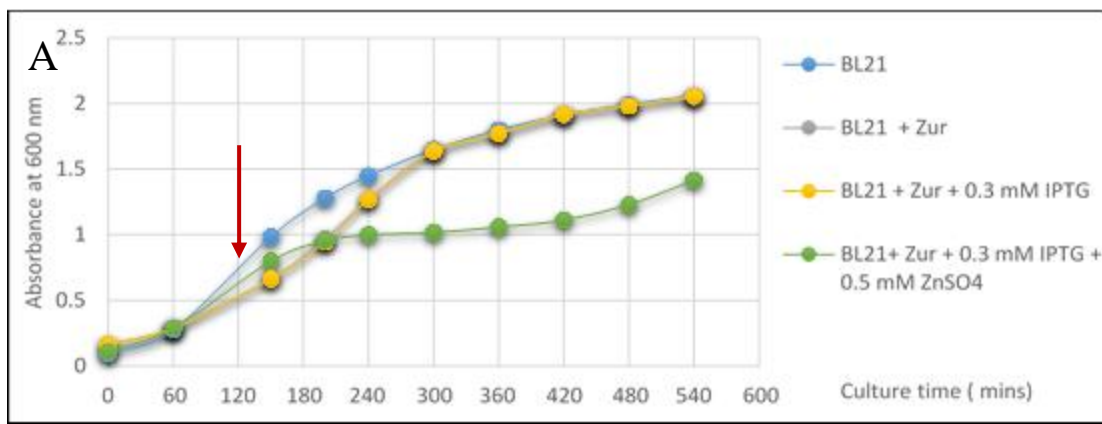


**Figure E.04 Growth curves of BL21 Star™ (DE3) induced at different IPTG.**

Growth curve showing  $OD_{600}$  of BL21 Star™ (DE3) for the induction at (A) 0.3 mM IPTG, (B) 0.5 mM IPTG, (C) 0.7 mM IPTG, for 9 hours of growth at 37°C. Blue line is culture of BL21 without *synw\_2401* gene as a control. Grey line is culture of BL21 with *synw\_2401* gene. Yellow line is culture of BL21 with *synw\_2401* gene and IPTG. Green line is culture of BL21 with *synw\_2401* gene, IPTG and 0.5 mM ZnSO<sub>4</sub>. Red arrows indicate the time of induction.

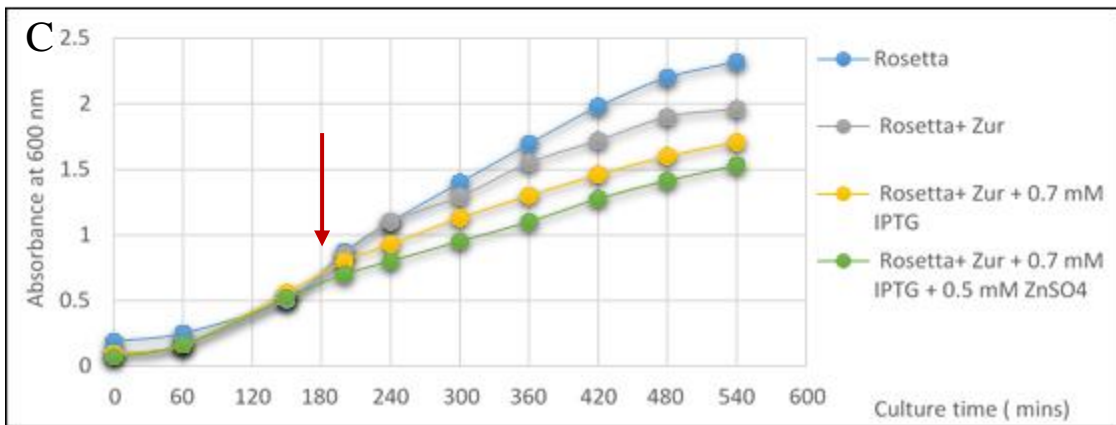
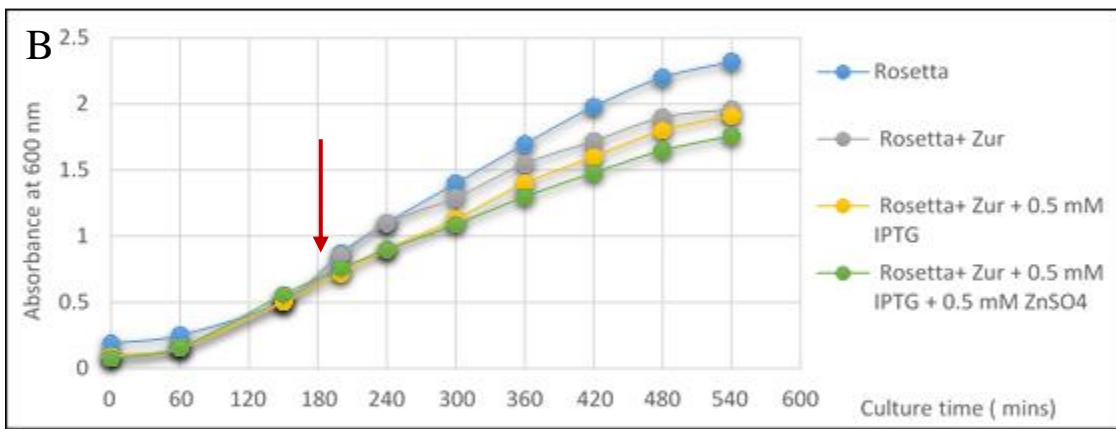
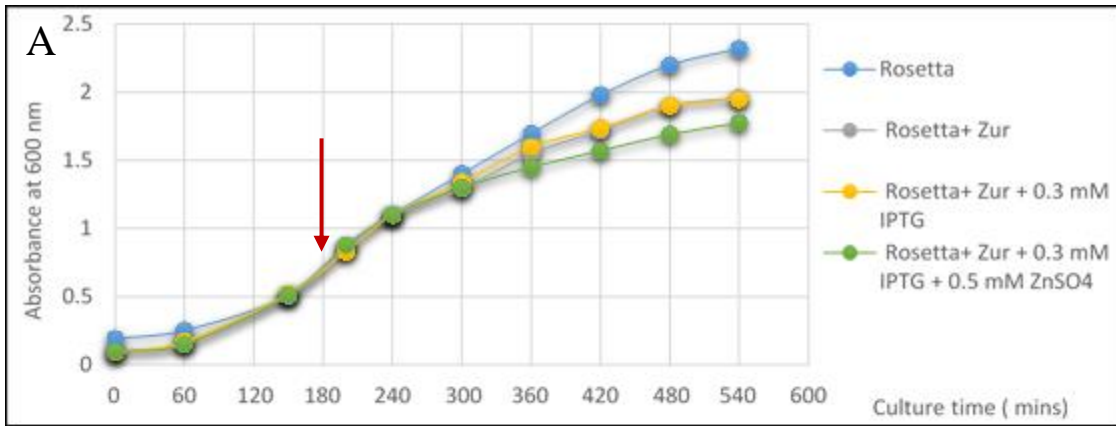


**Figure E.05 Growth curves of Rosetta™ 2(DE3) pLysS induced at different IPTG.**

Rosetta™ 2(DE3) pLysS was grown with three conditions of IPTG in the cultures 0.3 mM (A), 0.5 mM (B) and 0.7 mM (C). Blue line is culture of Rosetta without *synw\_2401* gene as a control. Grey line is culture of Rosetta with *synw\_2401* gene. Yellow line is culture of Rosetta with *synw\_2401* gene and IPTG. Green line is culture of Rosetta with *synw\_2401* gene, IPTG and 0.5 mM ZnSO<sub>4</sub>. Red arrows indicate the time of induction.

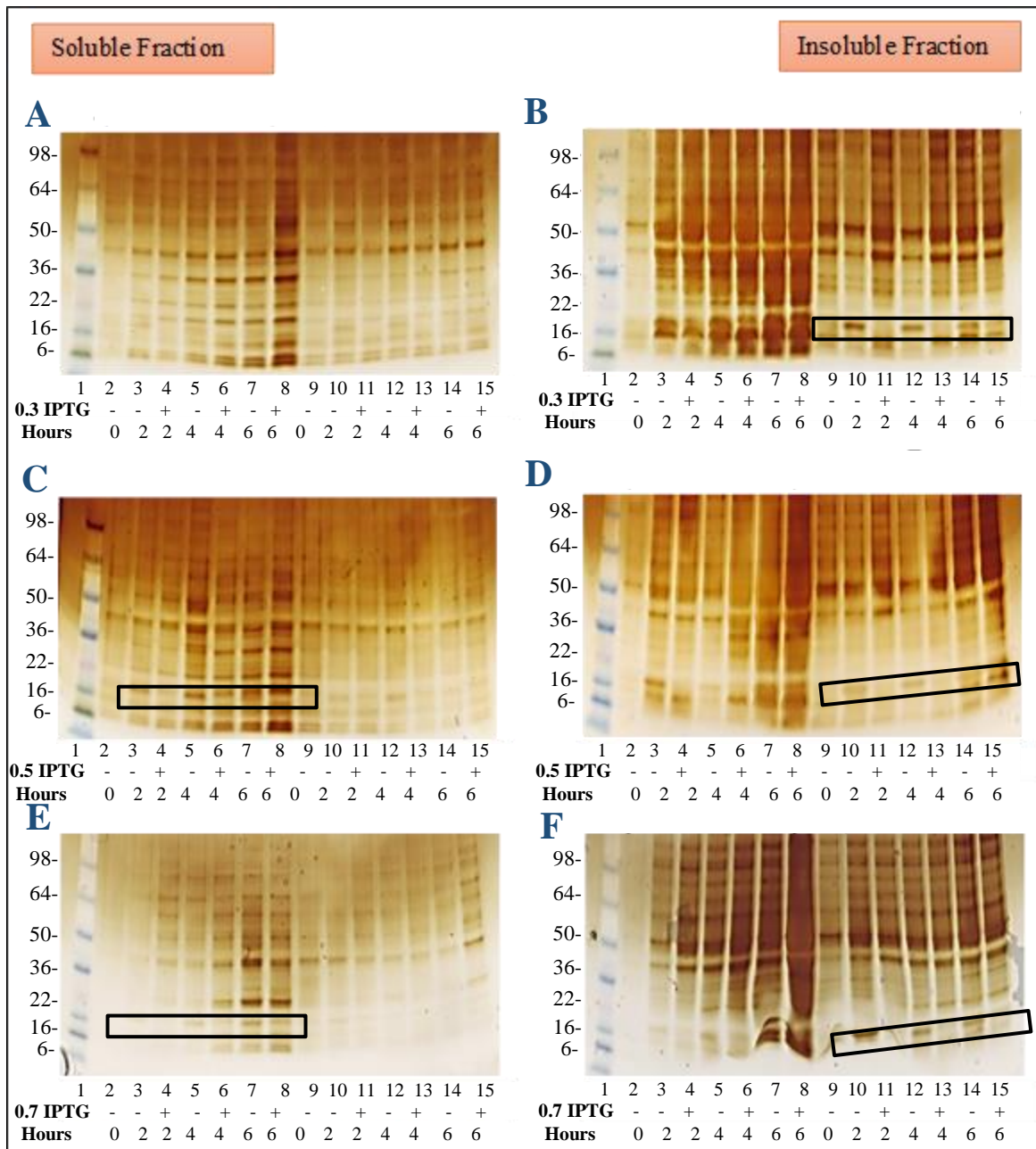


**Figure E.06 Over-expression of Zur protein in BL21 Star<sup>TM</sup> (DE3) at 37°C using silver staining.**

(A), (C) and (E) are soluble fractions, supernatants. (B), (D) and (F) are insoluble fractions, cell debris. Lane 1 marker; Lane 2-8 cultures without zinc supplement; Lane 9-15 cultures with 0.5 mM ZnSO<sub>4</sub> supplement. Lane 2 and 9: t = 0 h induced with IPTG; Lane 3 and 10: t = 2 h induced with IPTG; Lane 4 and 11: t = 2 h un-induced with IPTG; Lane 5 and 12: t = 4 h induced with IPTG; Lane 6 and 13: t = 4 h un-induced with IPTG; Lane 7 and 14: t = 6 h induced with IPTG; Lane 8 and 15: t = 6 h un-induced with IPTG.

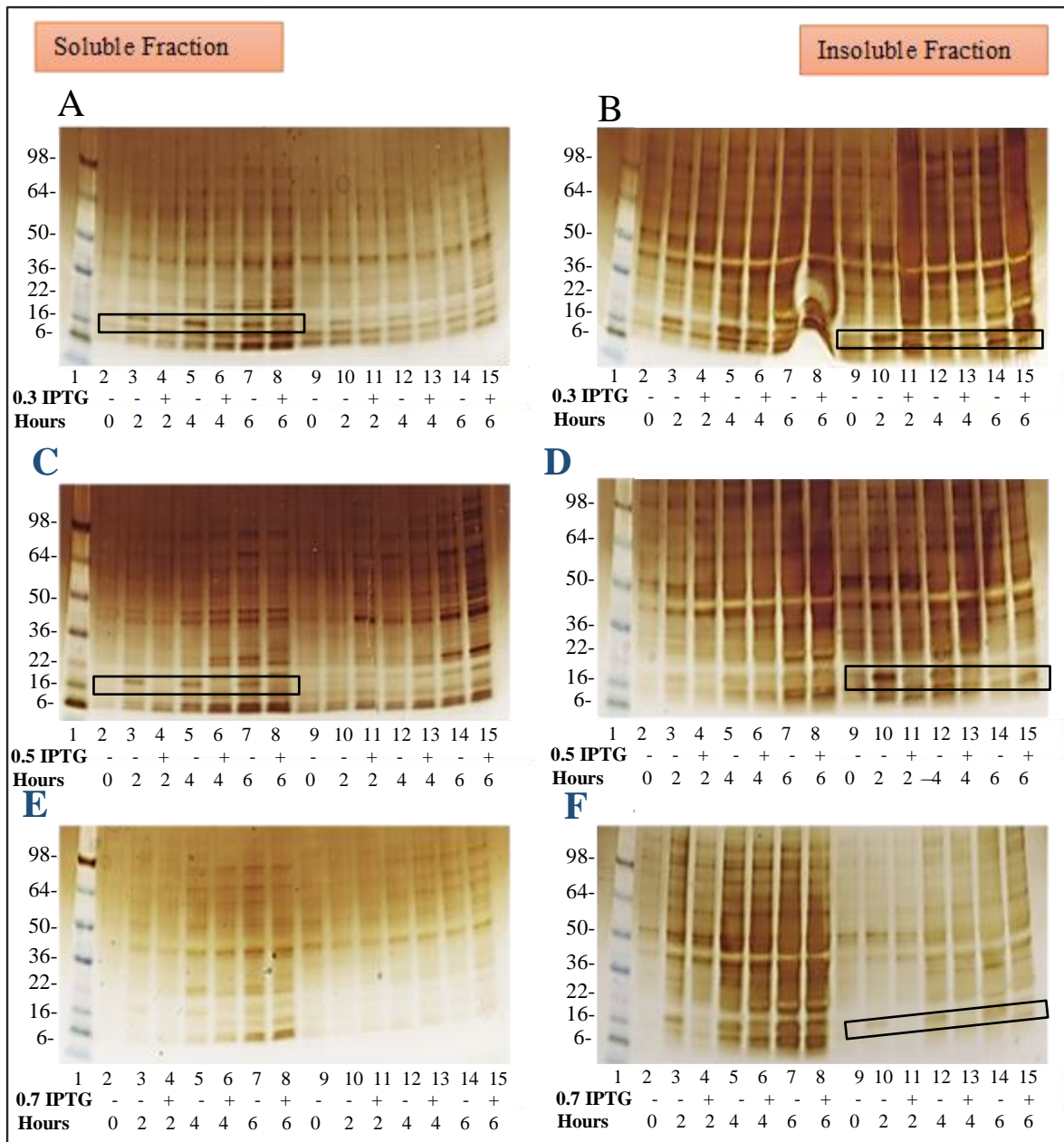


**Figure E.07 Over-expression of Zur protein in Rosetta™ 2(DE3) PLYS at 37°C using silver staining.**

(A), (C) and (E) are soluble fractions, supernatants. (B), (D) and (F) are insoluble fractions, cell debris. Lane 1 marker; Lane 2-8 cultures without zinc supplement; Lane 9-15 cultures with 0.5 mM ZnSO<sub>4</sub> supplement. Lane 2 and 9: t = 0 h induced with IPTG; Lane 3 and 10: t = 2 h induced with IPTG; Lane 4 and 11: t = 2 h un-induced with IPTG; Lane 5 and 12: t = 4 h induced with IPTG; Lane 6 and 13: t = 4 h un-induced with IPTG; Lane 7 and 14: t = 6 h induced with IPTG; Lane 8 and 15: t = 6 h un-induced with IPTG.

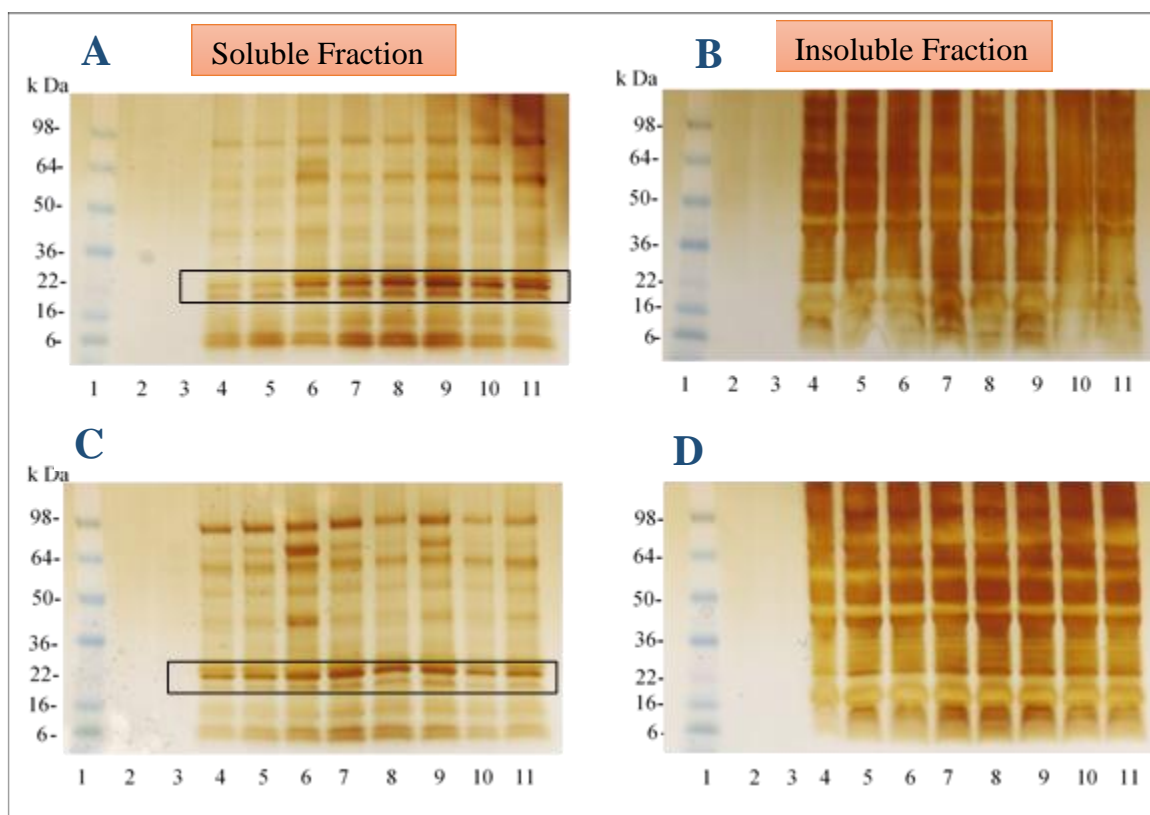


**Figure E.08 Over-expression of the *Synechococcus* sp. WH8102 Zur protein using the pG-Tf2 plasmid in MagicMedium™.**

Over-expression of the *Synechococcus* sp. WH8102 Zur protein in MagicMedium™ using the pG-Tf2 plasmid and the pET/151-synw\_2401 construct. (A) Soluble fraction at 30°C. (B) Insoluble fraction at 30°C. (C) Soluble fraction at 37°C. (D) Insoluble fraction at 37°C. Lane 1 marker, Lanes 2, 4, 6, 8 and 10 without adding zinc after 0, 2, 4, 6 and 18 hours, respectively. Lane 3, 5, 7, 9 and 11 with adding 0.5 mM ZnSO<sub>4</sub> after 0, 2, 4, 6 and 18 hours, respectively.

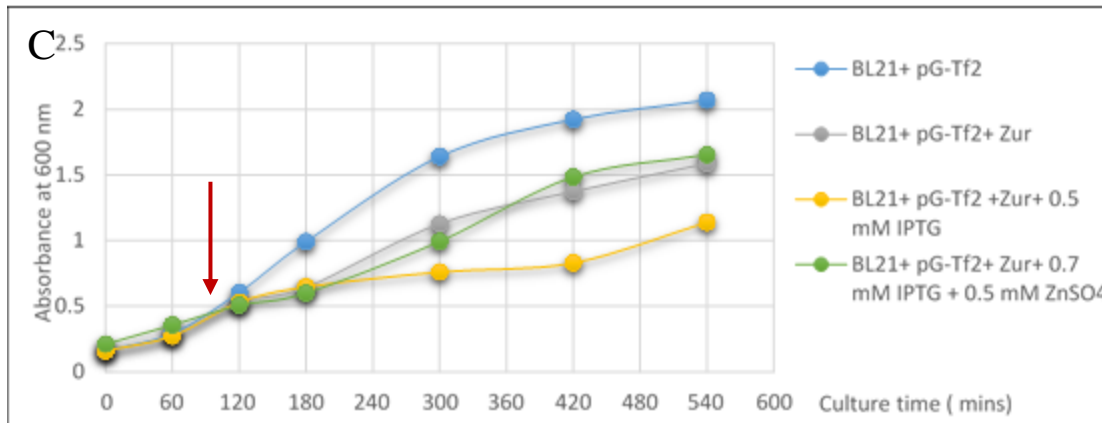
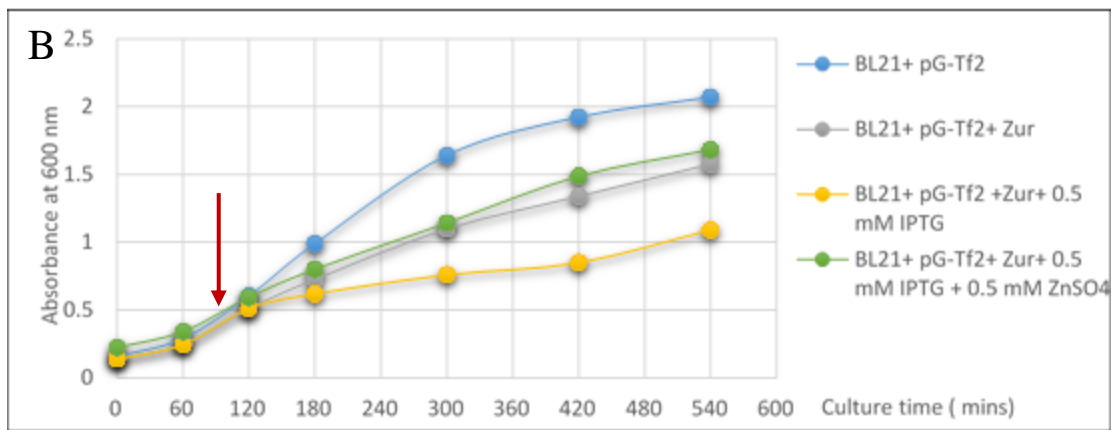
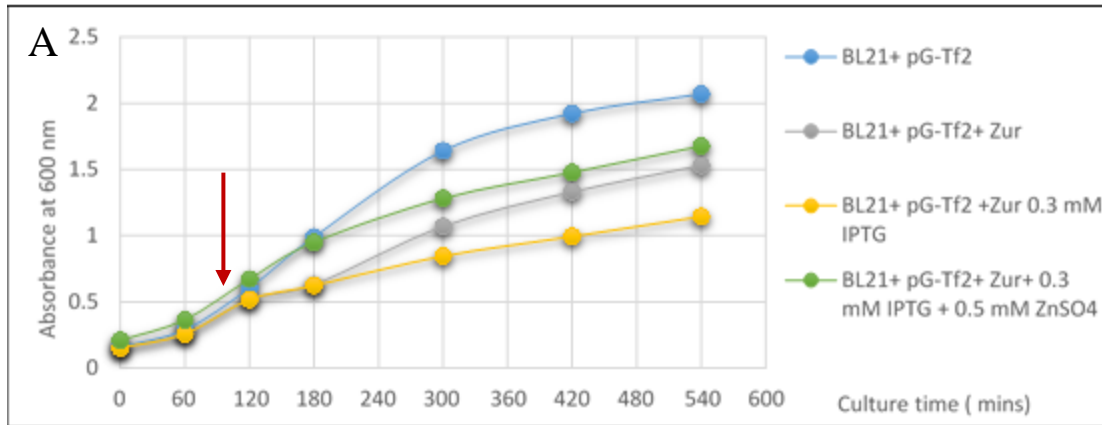


**Figure E.09 Growth curves of Takara strain induced at different IPTG at 37°C for 9 hours.**

Takara strain was grown with three different conditions of IPTG in the cultures 0.3 mM (A), 0.5 mM (B) and 0.7 mM (C). Blue line is culture of Takara strain without *synw\_2401* gene as a control. Grey line is culture of Takara strain with *synw\_2401* gene. Yellow line is culture of Takara strain with *synw\_2401* gene and IPTG. Green line is culture of Takara strain with *synw\_2401* gene, IPTG and 0.5 mM ZnSO<sub>4</sub>. Red arrows indicate the time of induction.

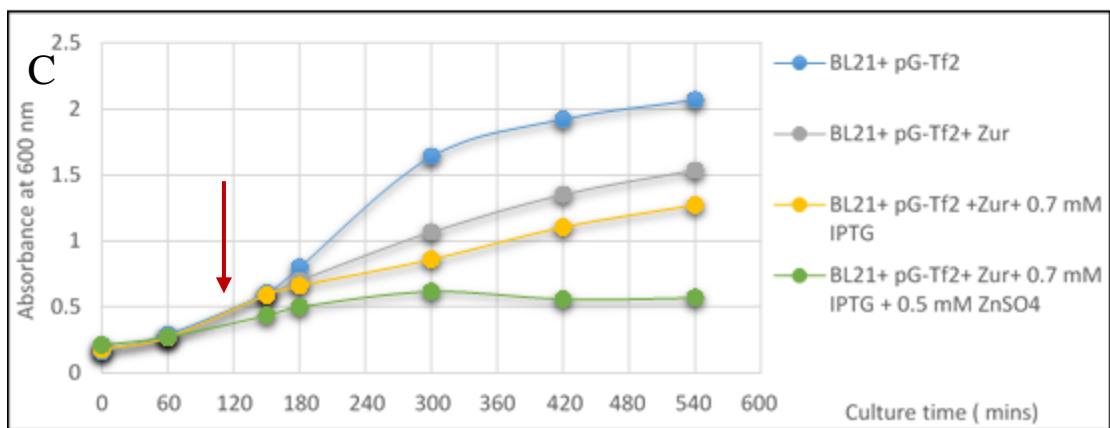
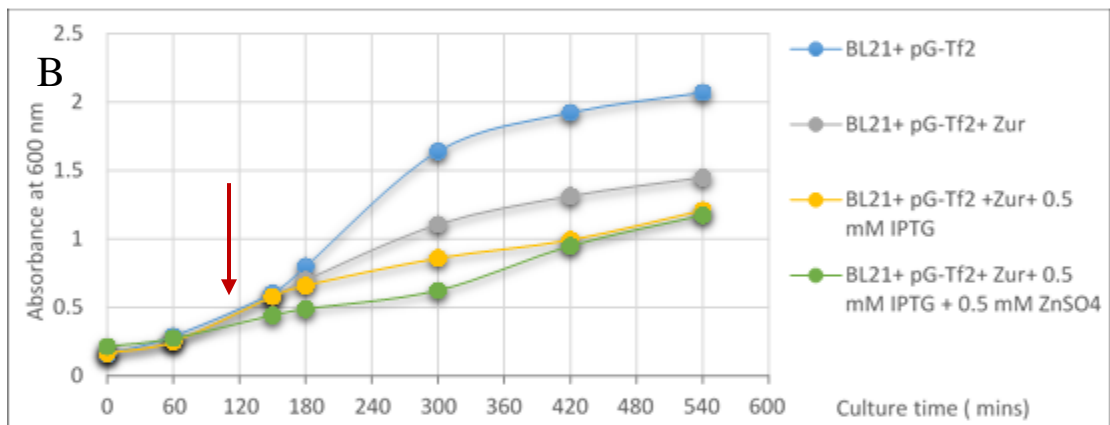
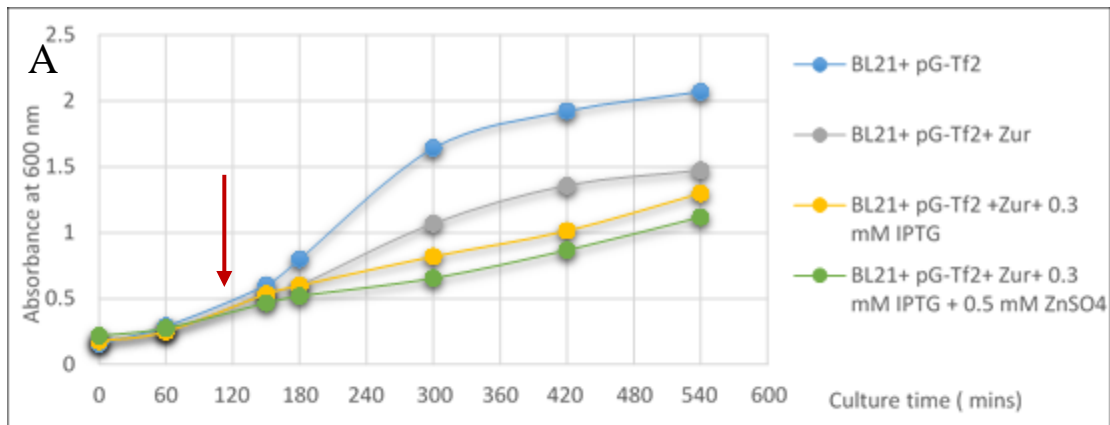


**Figure E.10 Growth curves of Takara strain induced at different IPTG at 30°C.**

Takara strain was grown with three conditions of IPTG in the cultures 0.3 mM (A), 0.5 mM (B) and 0.7 mM (C). Blue line is culture of Takara strain without *synw\_2401* gene as a control. Grey line is culture of Takara strain with *synw\_2401* gene. Yellow line is culture of Takara strain with *synw\_2401* gene and IPTG. Green line is culture of Takara strain with *synw\_2401* gene, IPTG and 0.5 mM ZnSO<sub>4</sub>. Red arrows indicate the time of induction.

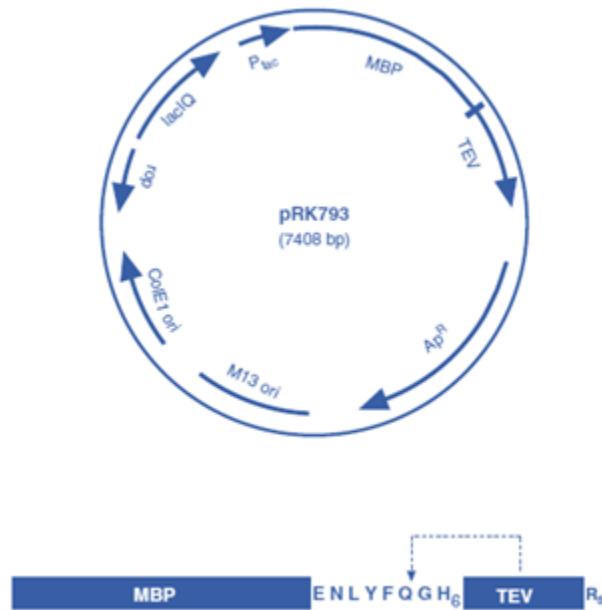


**Figure E.11 TEV protease expression vector pRK793.**

Schematic representation of the TEV protease expression vector pRK793 and its fusion protein product (Tropea *et al.*, 2009).

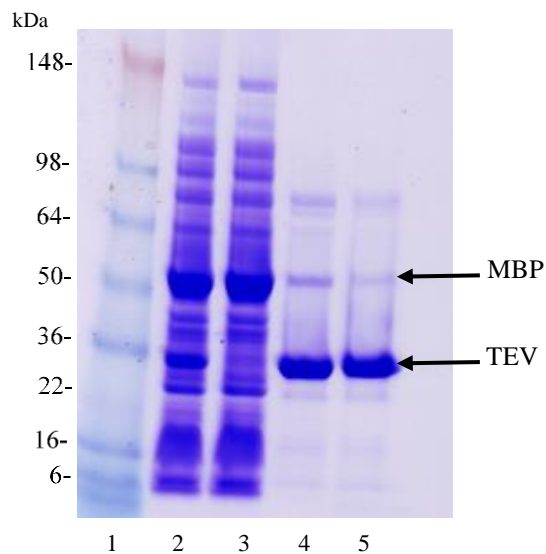


**Figure E.12 Purification of His<sub>6</sub>-TEV (S219V) protease monitored by SDS-PAGE gel.**

Lane 1: Marker. Lane 2: crude extract. Lane 3: flow through. Pooled fractions after first and second Ni-NTA resin purification Lane 4 and Lane 5, respectively. The purification product was separated by SDS-PAEG gel and visualized by staining with Coomassie brilliant blue.

# Appendix F

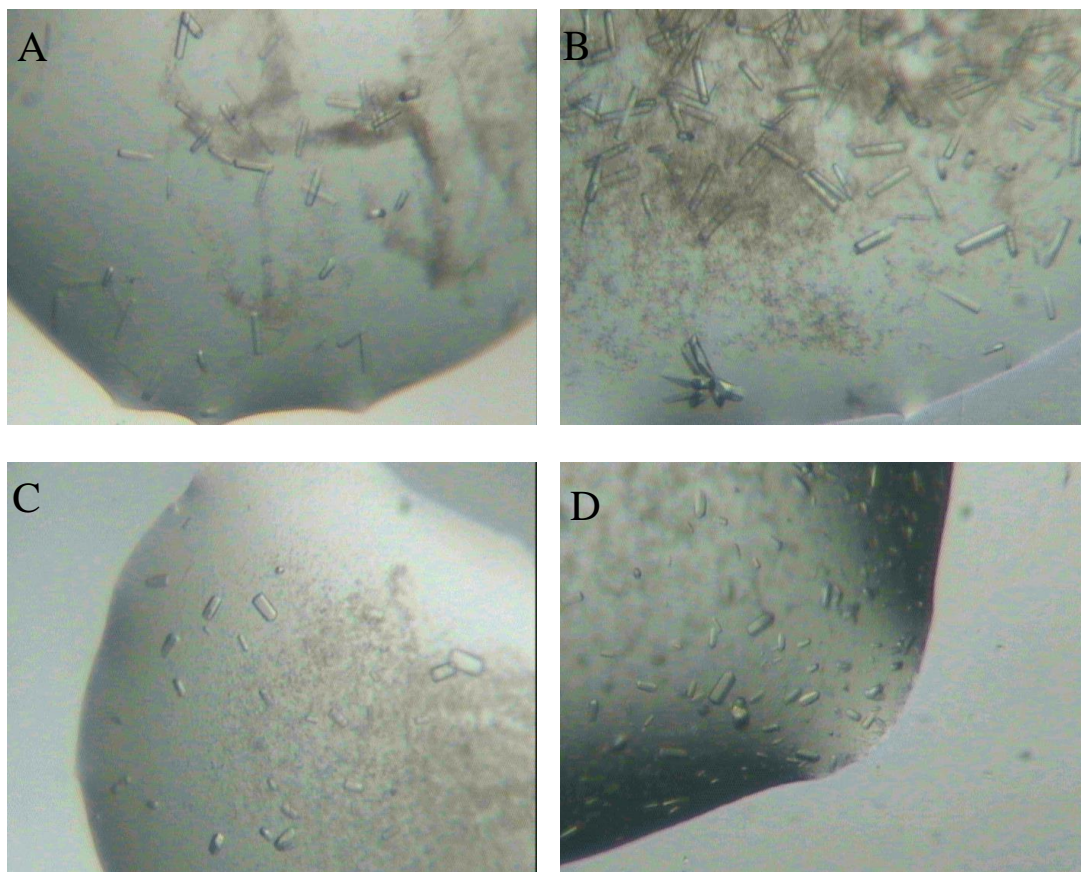


**Figure F.01 Microscopic images for SynZur crystals grown under different conditions.**

Small crystals for Zur protein from *Synechococcus* sp. WH8102 grown under different conditions using the hang drop method. (A) MORPHEUS buffer (10% PEG 4000, 20% glycerol, 0.03 M divalent cations, 0.1 M MES/Imidazole pH 6.5). (B) MORPHEUS buffer (10% w/v PEG 8000, 20% v/v ethylene glycol, 0.03 M divalent cations, 0.1 M MES/Imidazole pH 6.5). (C) JCSG buffer (40% PEG 400, 0.2 M  $\text{Li}_2\text{SO}_4$ , 0.1 M Tris pH 8.5). (D) PROPLEX buffer (15% PEG 400, 0.1 M LiCl, 0.1 M MES pH 6). 9 mg/ml of SynZur was in 10 mM Tris, pH 7.8.

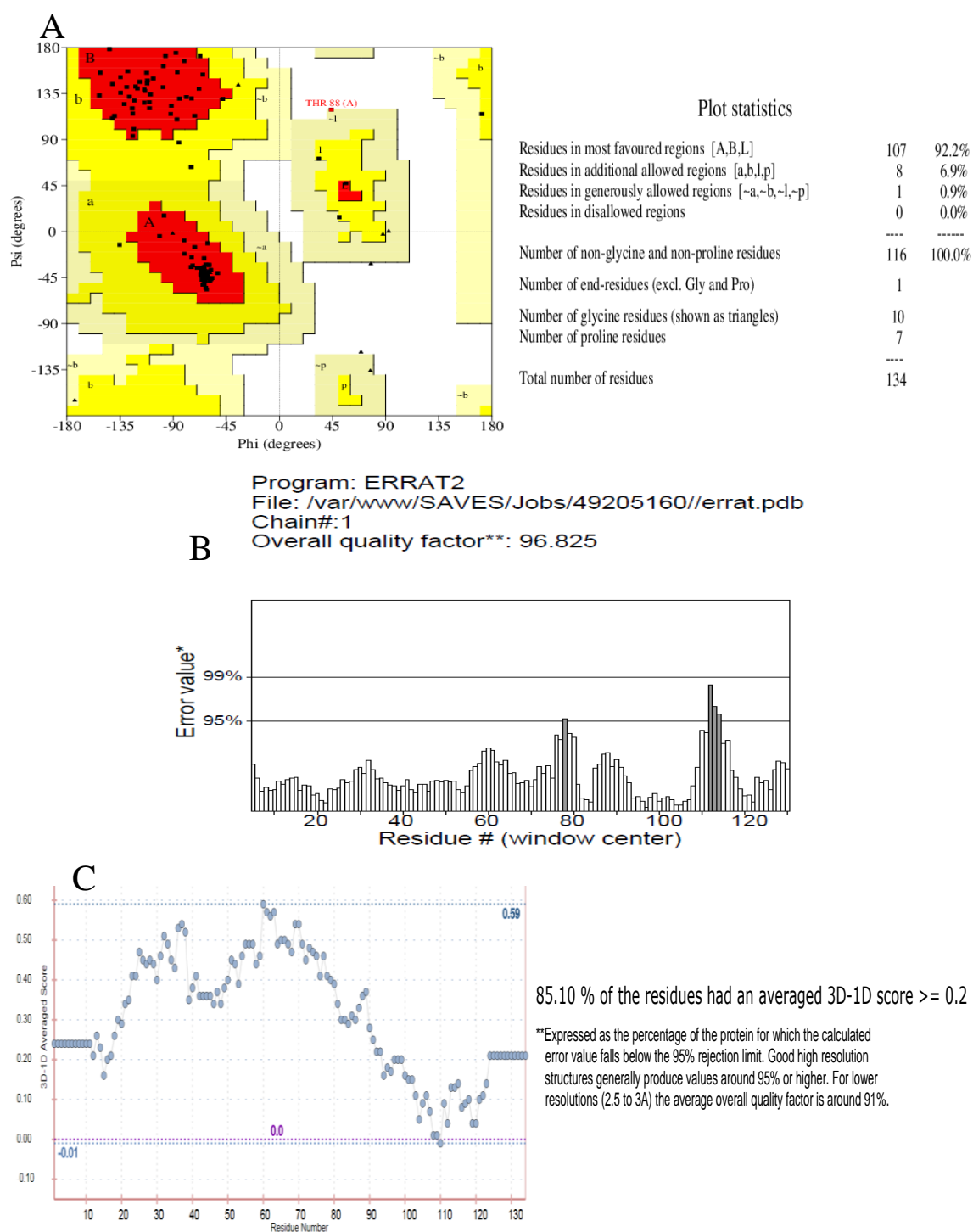


**Figure F.02 Stereo-chemical validation for the predicted SynWH\_Zur1.**

Stereo-chemical validation of the predicted SynWH\_Zur1 is shown above using Ramachandran plot and its statistics from PROCHECK (A), ERRAT plot (B) and Verify\_3D plot profile (C). All plots show reasonable scores for the predicted SynWH\_Zur1 from SAVES online service (Structural Analysis and Verification Server).

**Table F.01 Superposition of SynZur homologies 1 and 2 with known structure of Zur proteins.**

Crystal structure	SynZur Homologies	PyMOL RMSD Å	SuperPose RMSD* Å
<b>EcZur (pdb 4MTE)</b>	1	3.17	2.1
	2	7.99	3.0
<b>ScZur (pdb 3MWM)</b>	1	2.97	1.1
	2	7.41	3.4
<b>MtZur (pdb 2O03)</b>	1	5.55	6.2
	2	1.93	4.1
<b>EcZur (pdb 4MTE)</b>	ScZur (pdb 3MWM)	2.85	1.2
<b>EcZur (pdb 4MTE)</b>	MtZur (pdb 2O03)	6.48	3.0
<b>ScZur (pdb 3MWM)</b>	MtZur (pdb 2O03)	7.41	3.4

\* Superposition for SynZur homologies with known structure was performed using the Superpose program (Maiti *et al.*, 2004) and PyMOL software.

# Appendix G

**Table G.01 The effect of EDTA on resonances in the fingerprint region of SynZur.**

Chemical shift (ppm)	Comment
6.38	New peak
6.50	New peak
6.60	Peak shifts and intensity decreased
6.71	New peak
6.88	Peak disappeared
6.93	New peak
7.12	Peak shifts and intensity decreased
7.45	Peak intensity decreased
7.55	Peak intensity decreased
7.63	New peak and then disappeared
7.72	New peak
7.78	Peak shift and then disappeared
7.82	New peak
7.88	New peak

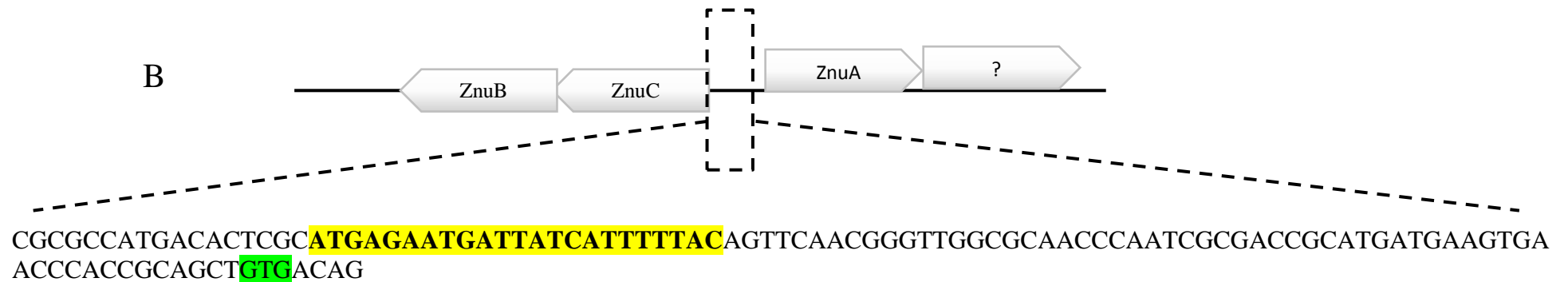
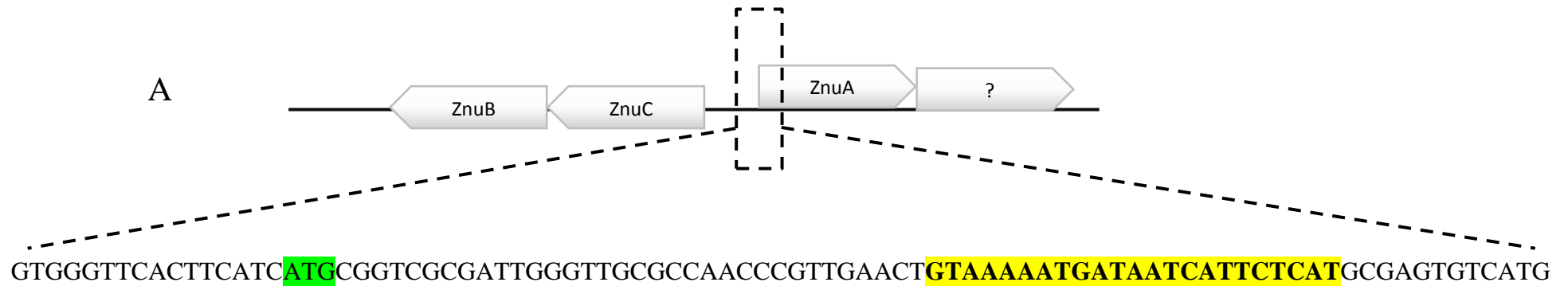
**Table G.02 The effect of EDTA and zinc re-addition on the fingerprint region of SynZur.**

Chemical shift (ppm)	Comment after incubation with 2 eq of EDTA	Comment after re-adding 4 eq of zinc acetate
6.38	New peak	Peak disappeared
6.50	New peak	Peak disappeared
6.60	Peak shift and intensity decreased	Peak shift and intensity increased
6.71	New peak	Peak disappeared
6.88	Peak disappeared	Peak appeared
6.93	New peak	Peak disappeared
7.12	Peak shift and intensity decreased	Peak shift and intensity increased
7.45	Peak intensity decreased	Peak intensity increased
7.55	Peak intensity decreased	Peak intensity increased and split
7.63	New peak and then disappeared	Peak disappeared
7.72	New peak	Peak disappeared
7.78	Peak shift and then disappeared	Peak appeared
7.82	New peak	Peak disappeared
7.88	New peak	Peak disappeared

**Table G.03 Effect of proton on 1D <sup>1</sup>H NMR spectra for SynZur in the up- and down-field regions.**

<b>Chemical shift (ppm)</b>	<b>Comment</b>
<b><i>up-field region</i></b>	
-0.1	New peak and then intensity decreased
<b><i>low-field region</i></b>	
6.5	Peak disappeared
6.6	New peak
6.7	Peak intensity decreased
6.75	Broad peak became sharp
6.8	New peak
7.05	Peak shift and then disappeared
7.1	Peak disappeared
7.14	The broad peak became sharp
7.35	New peak
7.43	New peak
7.48	Peak intensity decreased
7.55	New peak and then disappeared
7.73	Sharp peak became broad
8.06	New peak
8.1	New peak
8.15	New peak

# Appendix H



Continue-----

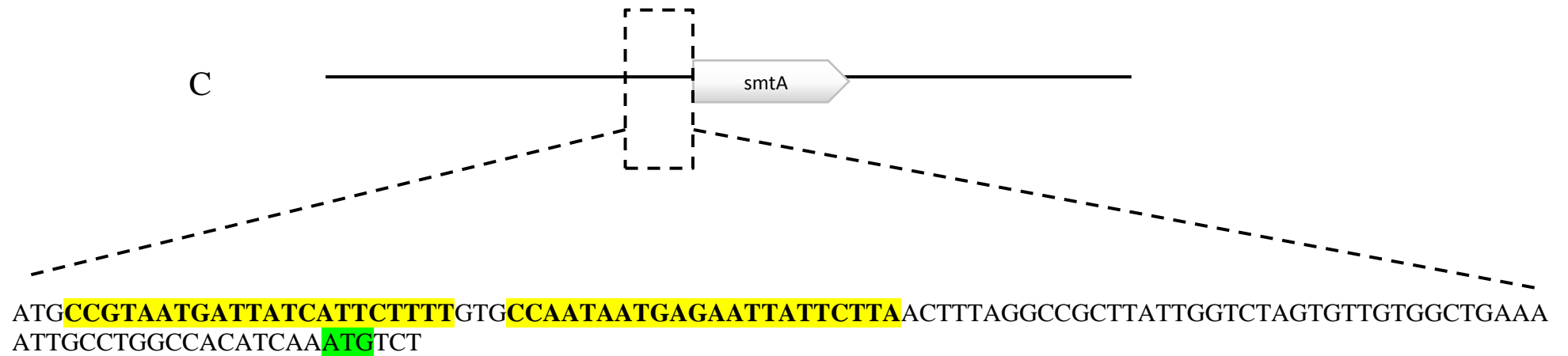


**Figure H.01 Maps of *znuABC* and *smtA* genes in *Synechococcus* sp. WH8102.**

Open reading frames are indicated by open pentagon which show the dimensions of the individual genes in the *znuABC* (A) and (B), and in *smtA* (C). The corresponding gene tags being *synw\_0971* and *synw\_0359* in direct direction while *synw\_0970*, and *synw\_0969* in complement direction. The middle section shows the sequence upstream of the ATG start of *znuA* (A), *znuC* (B) and *smtA* (C) with one Zur motif being boxed for *znuA* and *znuC* and two Zur motifs for *smtA*. The starting codon are highlighted in green, Zur boxes are highlighted in yellow.

CC9902 -----MRRSSWIALGSLPSL-----VAISLAHLPVQASQPSV 32  
 BL107 -----MRRSSWIARGSLTSL-----LAISLAQIPVQASQPSV 32  
 WH8102 **MRSRLGCANPLNCKNDNHSHASV**MARPALLVKGLAVAL-----GVVSGCSVAAQAAQPSV 55  
 RS9916 -----MKRSTSLAALCSGL-----VAGSLTP-AAHAAIPTV 31  
 JA-3-3Ab -----MKIKALFFAGRRLAVGFGLVIGGWLSLAGLAVARPRV 37  
 PCC7336 -----MNRFAVVVS----FAVN----LAFFTIGVAASSATPQV 30  
 2-WH8102 -----MVRFSKWATGSLASIFLVS--CGSLTTPPERSKKISI 35  
 F62 -----MKHLK-----LTL----IAALLATAATAAPLPVVT 26  
 K12 -----MLHKK-----TLLFAALSAALWGGATQAADA AVVA 30

CC9902 VAVDGTLCDLTRTLAATAVSVTCLIPPGDPHGYRLKPSDRQALSKADLVVHGFNLTPS 92  
 BL107 VAVDGTLCDLTRTLAATAVSVTCLIPPGDPHGYRLKPSDRQALSKADLVVHGFNLTPS 92  
 WH8102 VAVDGTLCDITRTVVGAAKVTCCLIPPGDPHGYRLKPSDRQAIATSAAVVHIGFGLTPA 115  
 RS9916 VAGDGVLCDLTRTVSGGATDVRCLIAAGADPHYYRLTPANRRDISQSKVVINGYGLTPT 91  
 JA-3-3Ab VVTTTLIADWVGQVQDRIQLSLLQPGVDPHVVYEPTADAAALEQADLVFYNGYNLEPG 97  
 PCC7336 ITTVAPITNIVSNIGGDRIEAI GIVPEGVNSHTFEPRPSDVLELLSEADLI IANGLFLEEP 90  
 2-WH8102 MTSFPLITLFAVARAGECGDVKALIPTNIGPHDFQSTPKDILSIGKADIFFINGLMETF 95  
 F62 SFSILGDVAKQIGGERVAVQSLVGANQDTHAYHMTSGDIKKIRSAKLVLLNGLGLEAADI 86  
 K12 SLKPVGFIASAIADGVTEVELLPDGA SEHDYSLRPSDVKRLQNADLVVWVGPEMEAFMQ 90

CC9902 AKQISVP-----GPVVAVGEVALP-----SYQGN-----PHVWHNPANSAAMTSVVA 135  
 BL107 AKDISVP-----APVVAVGEVALP-----SYRGN-----PHVWHD PANSAAMTSAIA 135  
 WH8102 ANEITSP-----GSVVAVGEQALP-----NYKGDD-----PHVWHD PANSAAMLSALS 158  
 RS9916 LARLSGS-----FSLVPVGEQAVP-----SNPSKD-----PHLWHSPTNTSAMAVVS 134  
 JA-3-3Ab LIRLIEAT-AQGARRVALAEILEP-----IVADEDGIPTDPHVWGNVENILMVEHIA 150  
 PCC7336 ILNLRASKPDETKIVLLGDETI SRDEWVDFSFPESGKPNPHLWVNPLYAMAYAELVA 150  
 2-WH8102 LDRLISS---ASTTLSVVDTSIGIKTISTDISNADS--DPNPHIWLDP IRAISQVETIK 150  
 F62 QRA---VEQSKVSYAEATKGIQPLKAE EGGHHHHDHHDHDEGHHHHDHGEYDPHVWN 143  
 K12 KPVSKLPEAKQVT-IAQLEDVKPLLMKSIHGDDDDHHA---EKSDEHHHGDFNMHLWL 146

CC9902 DRLSPL-LSGDASSFATRAARALSVLNDLGIWASVQFEKLPAKERVLVTDHQTYSHLAS 194  
 BL107 NRLSPL-LSGDARVAFASRAANAQSVLADLGTWASVQFAKLPANQRVLVTDHQTYSHLAN 194  
 WH8102 TALIPV-LPASETEAFKERATAAIAVFN DLGRWGAIQFETLSQPQRVIVTDHKTYSHLAD 217  
 RS9916 RTLQQLPISAESKAGLKRREQTVTSILRDLDAWNRRQIETIPSAHRALVSEHLAFGFFTD 194  
 JA-3-3Ab QELTEQ--VPNEA AFFQANAAAYRAELELHTWIGE QIPTIPPANRVLVTHDAFAYYTQ 208  
 PCC7336 TALQEL--DPSGRDYARNLNLYLAQLEALDRVTREVVASIPVENRKL LTYHDSWAYWGR 208  
 2-WH8102 DALAEL--NPACSEVYTLNASAYVDDLALHAEILSKLEPYQ--GKSFIAYHDFAPYFAE 206  
 F62 DPVMSDYAQNVAETLIKADPEGKVYY-QQRLGNYQMQLKKLHSDAQAAFNAVPAAKRKY 202  
 K12 SPEIARATAVAIHGKLVLMQPQRSAKL-DANLKD FEALASTET--QVGNELAPLKGKGY 203

CC9902 RYGLKEISMLDSYTTGGALKPSSLNAITRAVTGSGAKVIFSSYLPANKSLKRISKRSGLP 254  
 BL107 RYDLEEISMLDSYTTGGALKPSSLNAITKAVTDSGARVIFSSYLPANKSLRRISKRSGLP 254  
 WH8102 RYGVDEIAMLDSYTTGGVLRPSSLRRISKEIQSSGAKVIFTPSIPPNKTLRRISKSTGLP 277  
 RS9916 RYGLKQVAMIDDYATGGQLRPSSLKSI SNAVQASNTKVLFAEQPPSKTLRRISKRSKGP 254  
 JA-3-3Ab AYGLKMGSSLGISTEEQPSAQTVAQLVEEIRALGVPVFAETTLPALIQTVAAEAGVQ 268  
 PCC7336 EYGIEILGAIQPSDLSE-PSAREVAEIVDRVRETGVPAIFGSEVFPSRIAAQIARETGVK 267  
 2-WH8102 RYQLKAEYLVLDLPDINP--SPVDLQRVSNLVRDSDLKALLTEPQDGNNSFNSLARDLNIK 264  
 F62 LTGHDAFSYMGNRYNISFIAPQGVSSAEPSAKQ--VAAIIRQIKREGIKAVFTENIKDT 260  
 K12 FVFHDAYGYFEKQFGLTPLGHFTVNPEIQPGAQR--LHEIRTQLVEQKATCVFAEPQFRP 261

CC9902 IAST---PLYGEGIAPG-----ESAVSTATKNVCAILKGQATCDQAAATALANRWAS 304  
 BL107 IAST---PLYGEGIAPG-----ETAVSTATKNICAILKGQGASCDEAAANVLANRWAD 304  
 WH8102 IAPT---PLFGEGTAAG-----ETAISTAAINICTMVQGGGTCDKASAEALNDRWQA 327  
 RS9916 IASK---ILFADGVAPG-----KSLIETATANTCAVVNAQGGTCDQAGAKALQQRWET 304  
 JA-3-3Ab VAEQ---ELYSDSLGEAGSG---AETYVAMRLNTCTIVAALGGSPDCP----- 311  
 PCC7336 LDNTSDDDLPEGEGNANAVLNDNPEHTYVGMMAENLRIFAKNLGGDTSAIERLDVRNPIEA 327  
 2-WH8102 IALFNPIETISRDFVYD-----ESLYFDLMRDNLNLLSLGG----- 302  
 F62 RMVDRIAKETGVNVS-----GKLYSDALGNAPADTYIGMYRHNVKALTNA 305  
 K12 AVVESVARGTSVRMGTLDPLGTN---IKLGKTSYSEFLSQ-LANQYASCLKGD----- 310

CC9902 I----- 305  
 BL107 I----- 305  
 WH8102 IR----- 329  
 RS9916 VR----- 306  
 JA-3-3Ab -----

Continue-----

```

PCC7336          VLVEVLQEQ 336
2-WH8102         -----
F62              -----
K12              -----

```

**Figure H.02 Sequential alignment for ZnuA protein from different bacteria.**

Where (CC9902) *Synechococcus* sp. CC9902; (BL107) *Synechococcus* sp. BL107; (WH8102), *synw\_0791* gene from *Synechococcus* sp. WH8102; (2-WH8102), *synw\_2481* gene from *Synechococcus* sp. WH8102; (RS9916) *Synechococcus* sp. RS9916; (JA-3-3Ab) *Synechococcus* sp. JA-3-3Ab; (PCC 7336) *Synechococcus* sp. PCC 7336; (F62) *N. gonorrhoeae* F62 and (K12) *E.coli* K12. The three conserved His residues in cyanobacteria are highlighted in green.

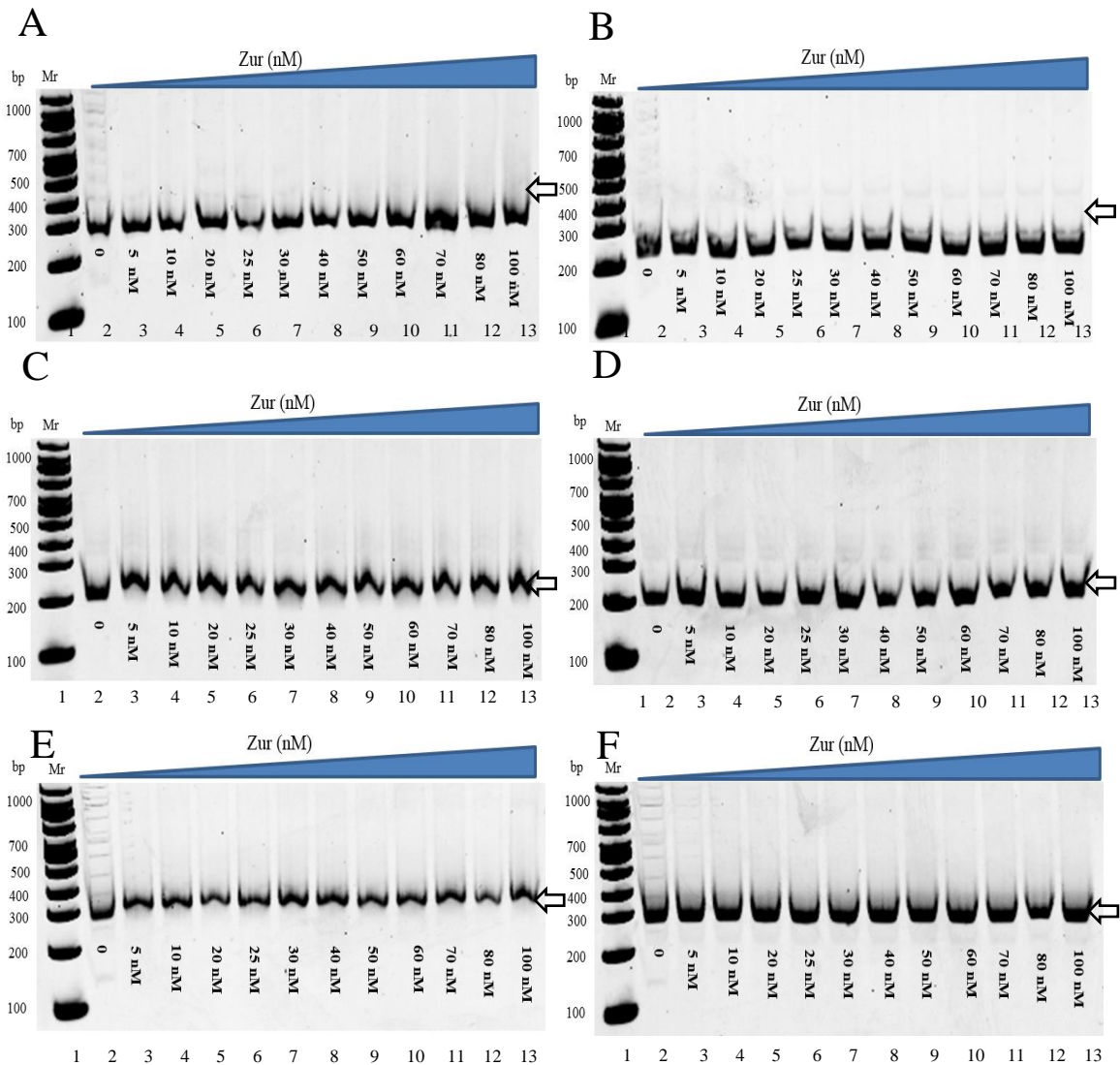


**Figure H.03 Titration of *ntcA*, *znuA* from system 1, and *zur* promoter with EDTA-treated SynZur.**

*In vitro* non-specific binding of EDTA-treated SynZur to the 201-bp *ntcA* promoter (*synw\_0275*) in presence of Zn(II) (A) and absence of Zn(II) (B); the 220-bp *zur* promoter (*synw\_2401*) in presence of Zn(II) (C) and absence of Zn(II) (D); and the 252-bp *znuA* promoter (*synw\_2481*) in presence of Zn(II) (E) and absence of Zn(II) (F). All samples contained 5 ng of the DNA probe. Lane 1: DNA marker, Lanes 2, 3, 4, 5, 6, 7, 8, 9, 10, 11, 12 and 13 contained 0 nM, 5 nM, 10 nM, 20 nM, 25 nM, 30 nM, 40 nM, 50 nM, 60 nM, 70 nM, 80 nM and 100 nM EDTA-treated SynZur, respectively. The DNA-protein mixture was supplemented with 10 mM ZnSO<sub>4</sub> for (A), (C), (F) and without 10 mM ZnSO<sub>4</sub> for (B), (D), and (F), respectively. The binding buffer contained 20 mM Tris (pH 8 at 23°C), 50 mM KCl, 100 µg/mL bovine serum albumin, 5% v/v glycerol and 3 mM spermidine. Samples were resolved on a 6% w/v polyacrylamide gel cast and run at room temperature (23 ± 2°C) in running buffer (40 mM Tris-acetate, 1 mM EDTA and 1 mM MgCl<sub>2</sub>). Free DNA is indicated by white arrowheads.

**Table H.01 Analysis of predicted occurring Zur boxes in cyanobacteria.**

Locus Tag	Name	Position	6-1-6 Consensus sites	
			AATGAT (L)	ATCATT (R)
<i>Synechococcus</i> sp. WH8102				
Synw0971	cce_1484	-32	GTAAAAATGATAATCATTCTCAT	
Synw0970	cce_1485	-83	ATGAGAATGATTATCATTTTTAC	
Synw0359	smtA	-105	CCGATAATGATTATCATTCTTTT	
Synw0359	smtA	-79	CCAATAATGAGAATTATTCTTAT	
<i>Synechococcus</i> sp. PCC 7002				
Synpcc7002_G0127	hemB2	-25	TCGAGAATGATTATCATTTTTTA	
Synpcc7002_G0132	PF07992	-70	TTGATAATAATTATCATTTTTAT	
Synpcc7002_A2501	znuA	-39	ATAAGAACGATTATCATTCAAG	
<i>Synechococcus elongatus</i> PCC 7942				
Synpcc7942_1316	cce_1484	-59	TAGGGAATGATAACGATTCTCAA	
Synpcc7942_1316	ompZ	-37	ATGAGAATAATAATCATTTTTAG	
slr2043	znuA	-84	ATGATAATGATTATCGTTTATTG	
<i>Synechococcus</i> sp. JA-3-3Ab				
Cya_2533	sufE	-39	TTATGATTGATTATCATTCTCAT	
<i>Synechocystis</i> sp. PCC 6803				
sll1550	ompZ	-118	ATGATAATGATTATCATTATTTA	
slr2043	znuA	-84	ATGATAATGATTATCATTATTTA	
sll1937	Zur	-45	CAATAAACGATAATCATTATCAT	
<i>Prochlorococcus marinus</i> str. MIT 9313				
PMT2202	cce_1485	-111	ATGAGAATGATTCCCATTTTAT	
PMT2203	cce_1484	-34	ATAAAAATGGGAATCATTCTCAT	
<i>Cyanothece</i> sp. PCC 7425				
Cyan7425_0794	cce_1485	-29	ATAAGAATTATCTCATTTTCAC	
Cyan7425_0822	cce_1484	-29	TTGAAAATGAGAATGGTTCTTAT	
Cyan7425_1909	yciC2	-41	TTGATAATGATTATCATTGTATA	
Cyan7425_1916	Cyn7425	-104	AAGGCAATGATAATCATTATCAT	
Cyan7425_1917	zur	-56	ATGATAATGATTATCATTGCCTT	
<i>Microcystis aeruginosa</i> NIES-843				
MAE_10010	ompZ	-40	CTGAGAACAATAATCATTCTTGT	
MAE_31590	thrS2	-34	GCTACAATGATAATCATTATCAT	
MAE_22860	folE2	-323	ATGATAACGATTATCATTCTAGG	
MAE_20780	znuA	-67	TTCAGAATGATAACGATTCTCAC	
MAE_31630	alr1197	-6	GCTAGAATGATTATCATTATCAC	
<i>Gloeobacter violaceus</i> PCC 7421				
glr1694	cce_1484	-6	TCTAGAATGAGAATCATTCTTGA	
gll1693	cce_1486	-56	TCAAGAATGATTCTCATTCTAGA	
glr0533	glr0533	-40	TTGAGAACGACTATCATTGTTAT	
<i>Thermosynechococcus elongatus</i> BP-1				
tlr1246	ompZ	-84	AGTAGAATGATAATCATTACAAT	
tlr2276	yciC	-36	ATGAGAATGATTCTCTTTTCTT	

tlr2062	znuA	-31	ATGAGAATGATTATCATTTCATCT
<i>Nostoc sp. PCC 7120</i>			
all4723	thrS2	-28	ATGATAACGATTCTCATTATTTA
all4725	hemB2	-31	ATGATAATGGTTATCAATCTTGT
all1751	yciC2	-44	GTGATAATGATTATCCGTATGGT
all0833	znuA	-110	ATGAGAATGAGAATTATTATAAT
all0833	znuA	-80	TGTACAATAAGTATCATTGTCAA
alr4028	Omp	-122	GTGATAATAATAATCATTATCTA
all3515	all3515	-52	CTGATTATGATAATCATATCCGG
alr1197	alr1197	-29	AACTGCATGAAAATGATTATCAT
alr1197	alr1197	-23	ATGAAAATGATTATCATTTAAAA
alr3242	alr3242	-260	ATGATAATCATATCAAAAAATG
alr3242	alr3242	-266	GTAAACATGATAATCATATCAA

**Table H.02 Analysis of predicted occurring Zur boxes in cyanobacteria.**

Locus Tag	Name	Position	RNNNNYRNNNRYNRYNNY
<i>Synechococcus sp. WH8102</i>			
Synw0971	cce_1484	-32	GTAAAAATGATAATCATTCTCAT
Synw0970	cce_1485	-83	ATGAGAATGATTATCATTTTTAC
Synw0359	smtA	-105	CCGATAATGATTATCATTCTTTT
Synw0359	smtA	-79	CCAATAATGAGAATTATTCTTAT
<i>Synechococcus sp. PCC 7002</i>			
Synpcc7002_G0127	hemB2	-25	TCGAGAATGATTATCATTTTTAA
Synpcc7002_G0132	PF07992	-70	TTGATAATAATTATCATTTTTAT
Synpcc7002_A2501	znuA	-39	ATAAGAACGATTATCATTTCACG
<i>Synechococcus elongatus PCC 7942</i>			
Synpcc7942_1316	cce_1484	-59	TAGGGAATGATAACGATTCTCAA
Synpcc7942_1316	ompZ	-37	ATGAGAATAATAATCATTTTTATG
slr2043	znuA	-84	ATGATAATGATTATCGTTTATTG
<i>Synechococcus sp. JA-3-3Ab</i>			
Cya_2533	sufE	-39	TTATGATTGATTATCATTCTCAT
<i>Synechocystis sp. PCC 6803</i>			
sll1550	ompZ	-118	ATGATAATGATTATCATTATTTA
slr2043	znuA	-84	ATGATAATGATTATCATTATTTA
sll1937	zur	-45	CAATAAACGATAATCATTATCAT
<i>Prochlorococcus marinus. MIT 9313</i>			
PMT2202	cce_1485	-111	ATGAGAATGATTCCATTTTTAT
PMT2203	cce_1484	-34	ATAAAAAATGGGAATCATTCTCAT
<i>Cyanothece sp. PCC 7425</i>			
Cyan7425_0794	cce_1485	-29	ATAAGAATTATTCTCATTTCAC

Cyan7425_0822	cce_1484	-29	TT <b>G</b> AAAAT <b>G</b> AGA <b>A</b> T <b>G</b> GT <b>T</b> CTTAT
Cyan7425_1909	yciC2	-41	TT <b>G</b> ATAAT <b>G</b> ATT <b>A</b> TC <b>A</b> TTGTATA
Cyan7425_1916	Cyn7425	-104	AA <b>G</b> GCAAT <b>G</b> ATA <b>A</b> TC <b>A</b> TTATCAT
Cyan7425_1917	zur	-56	AT <b>G</b> ATAAT <b>G</b> ATT <b>A</b> TC <b>A</b> TTGCCTT
<i>Microcystis aeruginosa</i> NIES-843			
MAE_10010	ompZ	-40	CT <b>G</b> AGA <b>A</b> CAATA <b>A</b> TC <b>A</b> TTCTTGT
MAE_31590	thrS2	-34	GCTACAAT <b>G</b> ATA <b>A</b> TC <b>A</b> TTATCAT
MAE_22860	folE2	-323	AT <b>G</b> ATA <b>A</b> CGATT <b>A</b> TC <b>A</b> TTCTAGG
MAE_20780	znuA	-67	TTCAGAAT <b>G</b> ATA <b>A</b> CG <b>A</b> TTCTCAC
MAE_31630	alr1197	-6	GCTAGAAT <b>G</b> ATT <b>A</b> TC <b>A</b> TTATCAC
<i>Gloeobacter violaceus</i> . PCC 7421			
glr1694	cce_1484	-6	TCTAGAAT <b>G</b> AGA <b>A</b> TC <b>A</b> TTCTTGA
gll1693	cce_1486	-56	TC <b>A</b> AGAAT <b>G</b> ATTCT <b>C</b> ATTCTAGA
glr0533	glr0533	-40	TT <b>G</b> AGA <b>A</b> CGACT <b>A</b> TC <b>A</b> TTGTTAT
<i>Thermosynechococcus elongatus</i> BP-1			
tlr1246	ompZ	-84	AGTAGAAT <b>G</b> ATA <b>A</b> TC <b>A</b> TTACAAT
tlr2276	yciC	-36	AT <b>G</b> AGAAT <b>G</b> ATTCT <b>C</b> TTTTTCTT
tlr2062	znuA	-31	AT <b>G</b> AGAAT <b>G</b> ATT <b>A</b> TC <b>A</b> TTCATCT
<i>Nostoc</i> sp. PCC 7120			
all4723	thrS2	-28	AT <b>G</b> ATA <b>A</b> CGATTCT <b>C</b> ATTATTTA
all4725	hemB2	-31	AT <b>G</b> ATAAT <b>G</b> GTT <b>A</b> TC <b>A</b> ATCTTGT
all1751	yciC2	-44	GT <b>G</b> ATAAT <b>G</b> ATT <b>A</b> TCCGTATGGT
all0833	znuA	-110	AT <b>G</b> AGAAT <b>G</b> AGA <b>A</b> TT <b>A</b> TTATAAT
all0833	znuA	-80	TGTACAAT <b>A</b> AGT <b>A</b> TC <b>A</b> TTGTCAA
alr4028	Omp	-122	GT <b>G</b> ATAAT <b>A</b> ATA <b>A</b> TC <b>A</b> TTATCTA
all3515	all3515	-52	CT <b>G</b> ATTAT <b>G</b> ATA <b>A</b> TC <b>A</b> TTATCGG
alr1197	alr1197	-29	AACTGCAT <b>G</b> AAA <b>A</b> T <b>G</b> ATTATCAT
alr1197	alr1197	-23	AT <b>G</b> AAAAT <b>G</b> ATT <b>A</b> TC <b>A</b> TTTAAAA
alr3242	alr3242	-260	AT <b>G</b> ATAAT <b>C</b> ATT <b>A</b> TC <b>A</b> AAAAATG
alr3242	alr3242	-266	GT <b>A</b> AACAT <b>G</b> ATA <b>A</b> TC <b>A</b> TTATCAA

**Table H.03 Identity and similarity of *synw\_0359* from *Synechococcus* sp. WH8102 with *bmtAs* genes from *Synechococcus* sp. CC9311.**

<b>bmtA from <i>Synechococcus</i> sp. WH8102</b>	<b>bmtAs from <i>Synechococcus</i> sp. CC9311</b>	<b>Identity %</b>	<b>Similarity%</b>
<i>synw_0359</i>	<i>sync_2426</i>	46.2	59.6
	<i>sync_2379</i>	43.5	60.9
	<i>sync_1081</i>	55.6	68.5
	<i>sync_0853</i>	49.0	57.1